

DISSERTATION

SYNTHESIS, CHARACTERIZATION AND CATALYTIC EVALUATION OF A ZIEGLER-
TYPE MODEL IRIDIUM HYDROGENATION CATALYST PLUS A NOVEL
TETRAIRIDIUM TETRAHYDRIDE COMPLEX

Submitted by

Isil Kayiran Hamdemir

Department of Chemistry

In partial fulfillment of the requirements

For the Degree of Doctor of Philosophy

Colorado State University

Fort Collins, Colorado

Summer 2013

Doctoral Committee:

Advisor: Richard G. Finke

Elliot R. Bernstein

Eugene Y.-X. Chen

C. Michael Elliott

David (Qiang) Wang

ABSTRACT

SYNTHESIS, CHARACTERIZATION AND CATALYTIC EVALUATION OF A ZIEGLER- TYPE MODEL IRIDIUM HYDROGENATION CATALYST PLUS A NOVEL TETRAIRIDIUM TETRAHYDRIDE COMPLEX

Following a critical review of the pertinent literature of Ziegler-type hydrogenation catalysts, the research presented herein is primarily focused on the synthesis, characterization and catalytic properties of a model Ziegler-type hydrogenation catalyst system made from $[\text{Ir}(1,5\text{-COD})(\mu\text{-O}_2\text{C}_8\text{H}_{15})]_2$ plus AlEt_3 . The studies include: (i) a critical review of the relevant literature, (ii) ranking the activity, lifetime and thermal stability of the resulting $\text{Ir}(0)_n$ Ziegler nanoparticles; (iii) characterization of the true stabilizer species for $\text{Ir}(0)_n$ Ziegler nanoparticles as a function of the initial Al/Ir ratio; and (iv) the synthesis and characterization of a novel $[\text{Ir}(1,5\text{-COD})(\mu\text{-H})]_4$ complex considered as a plausible intermediate en route to $\text{Ir}(0)_n$ Ziegler nanoparticles.

Studies evaluating and ranking the catalytic properties of Ziegler-type catalysts in the test reaction of cyclohexene hydrogenation reveal that the catalyst made with $[\text{Ir}(1,5\text{-COD})(\mu\text{-O}_2\text{C}_8\text{H}_{15})]_2$ plus AlEt_3 is a highly catalytically active, long-lived and thermally unusually stable nanoparticle catalyst. The catalytic lifetimes of the $\text{Ir}(0)_n$ Ziegler nanoparticles are higher than any known $\text{Ir}(0)_n$ nanoparticles in the extant literature.

The nature of the stabilizer species in the Ziegler-type catalyst system made with $[\text{Ir}(1,5\text{-COD})(\mu\text{-O}_2\text{C}_8\text{H}_{15})]_2$ plus AlEt_3 at Al/Ir ratios 1-3 is then investigated by comparing ^1H , ^{13}C , ^{27}Al NMR and IR data of the catalysts with those of individually-synthesized standards such as

$\text{AlEt}_2(\text{O}_2\text{C}_8\text{H}_{15})$, $[(n\text{-Bu})_4\text{N}][\text{AlEt}_3(\text{O}_2\text{C}_8\text{H}_{15})]$ and $[(n\text{-Bu})_2\text{Al}(\mu\text{-OH})]_3$. The results of the study shows that (i) $\text{AlEt}_2(\text{O}_2\text{C}_8\text{H}_{15})$ (Al/Ir=1, 2 and 3) and (iii) free AlEt_3 (Al/Ir=3) are present in the catalyst solution in this model Ziegler-type hydrogenation catalyst system made from $[\text{Ir}(1,5\text{-COD})(\mu\text{-O}_2\text{C}_8\text{H}_{15})]_2$ plus AlEt_3 . The spectroscopic and catalytic evidence provided in this study helps to rule out the initial hypotheses (iii) that anionic $[\text{AlEt}_3(\text{O}_2\text{C}_8\text{H}_{15})]^-$ stabilizer exists and provides DLVO-type, Coulombic-repulsion stabilization. Also ruled out is (iv) that the AlEt_3 -derived stabilizers are Al-O-Al containing alumoxanes.

In a separate study, a novel $[\text{Ir}(1,5\text{-COD})(\mu\text{-H})]_4$ complex is synthesized and characterized with the goal of (i) obtaining information on formation and stabilization mechanisms of Ziegler-type industrial hydrogenation model catalysts prepared from $[\text{Ir}(1,5\text{-COD})(\mu\text{-O}_2\text{C}_8\text{H}_{15})]_2$ plus AlEt_3 ; and with the goal of (ii) understanding the stabilization efficacies of various Al-based cocatalysts in the absence of any added carboxylate. The synthesis of the previously unavailable $[\text{Ir}(1,5\text{-COD})(\mu\text{-H})]_4$ complex in 55% recrystallized yield was accomplished starting with commercially available LiBEt_3H and $[\text{Ir}(1,5\text{-COD})(\mu\text{-Cl})]_2$ in the presence of excess 1,5-COD in THF. The resultant $[\text{Ir}(1,5\text{-COD})(\mu\text{-H})]_4$ was fully characterized by single-crystal XRD, XAFS, ESI-MS, UV-visible, IR, and NMR.

In addition to the four main chapters, two appendix chapters (in which Isil K. Hamdemir has significant contributions) are included in the current dissertation due to their relevancy to the research presented herein. The characterization studies showing the presence of $\text{Ir}_{\sim 4-15}$ subnanometer clusters and $\text{Ir}_{\sim 40-150}$ nanoparticles, before and after catalytic hydrogenation, respectively, in the Ziegler-type catalyst system made from $[\text{Ir}(1,5\text{-COD})(\mu\text{-O}_2\text{C}_8\text{H}_{15})]_2$ plus AlEt_3 catalyst solution has been published (William M. Alley, Isil K. Hamdemir, Qi Wang, Anatoly Frenkel, Long Li, Judith C. Yang, Laurent D. Menard, Ralph G. Nuzzo, Saim Özkar,

Kimberly Johnson, Richard G. Finke, “Iridium Ziegler-Type Hydrogenation Catalysts Made from [(1,5-COD)Ir(μ -O₂C₈H₁₅)₂ and AlEt₃: Spectroscopic and Kinetic Evidence for the Ir_n Species Present and for Nanoparticles as the Fastest Catalyst”). Additionally, a broad distribution of metal cluster sizes from subnanometer to nanometer scale particles was observed in industrial Ziegler-type hydrogenation catalysts made with Co(neodecanoate)₂ or Ni(2-ethylhexanoate)₂ plus AlEt₃ (William M. Alley, Isil K. Hamdemir, Qi Wang, Anatoly I. Frenkel, Long Li, Judith C. Yang, Laurent D. Menard, Ralph G. Nuzzo, Saim Özkar, Kimberly Johnson, Richard G. Finke, “Industrial Ziegler-type Hydrogenation Catalysts made from Co(neodecanoate)₂ or Ni(2-ethylhexanoate)₂, and AlEt₃: Evidence for Nanoclusters and Sub-Nanocluster or Larger Ziegler-Nanocluster Based Catalysis”). These two studies were published as two chapters in the dissertation of, graduate student co-worker, William M. Alley, a dissertation which acknowledges Isil Kayiran Hamdemir’s (I.K.H.) contributions.

ACKNOWLEDGMENTS

I dedicate this dissertation to my wonderful husband, Levent, whose endless support and encouragement helped me through many difficulties along the way. I am thankful to my advisor, Prof. Richard G. Finke, for his advice and supervision throughout this study. This dissertation would not have been possible without them. Special thanks and recognition has to go to my friends Hanife and Ercan for always being there, when I needed them. Finally, I would like to thank Finke group members for intellectual stimulation and scientific support.

Acknowledgments for Chapter II: Financial support was provided by NSF Grant CHE-0611588.

Acknowledgments for Chapter III: We thank Dr. JoAn S. Hudson of the Clemson University Electron Microscope Facility for obtaining TEM images. Financial support was provided by NSF Grant CHE-0611588.

Acknowledgments for Chapter IV: We thank Prof. Andrew Barron for his valuable insights regarding the synthesis of $[(t\text{-Bu})_2\text{Al}(\mu\text{-OH})]_3$, JoAn Hudson and her associates at Clemson University for TEM images, Prof. Eugene Chen for MMAO samples and valuable discussions and references regarding alumoxane chemistry, and Prof. Anatoly Frenkel of Yeshiva University and W. M. Alley (Colorado State University) for XAFS data and interpretations. Financial support at Colorado State University was provided by NSF Grant CHE-0611588.

Acknowledgments for Chapter V: We thank the following people working as part of the Colorado State University Central Instrumentation Facility: Stephanie Fiedler for the XRD data and Donald L. Dick for the ESI MS data. Financial support at Colorado State University was

provided by NSF Grant CHE-0611588 and at Yeshiva University by DOE BES Grant DE-FG02-03ER15476. Use of the NSLS was supported by the U.S. Department of Energy, Office of Science, Office of Basic Energy Sciences, under Contract No. DE-AC02-98CH10886. Beamline X19A at the NSLS is supported in part by the Synchrotron Catalysis Consortium, U.S. Department of Energy Grant No DE-FG02-05ER15688.

Acknowledgments for Appendix A: We thank J.-G. Wen, C.-H. Lei, and the user facilities at the CMM, UIUC. We thank JoAn Hudson of Clemson University for bright field TEM and HRTEM imaging. Mass spectra were obtained with the expert assistance of Phil Ryan (now deceased) of the Macromolecular Resources Lab at CSU. XPS was accomplished thanks to the help of Patrick McCurdy at CSU. This work was supported by NSF Grant CHE-0611588 at Colorado State University. We thank Nebojsa Marinkovic and Syed Khalid at the NSLS. AIF, JCY and RGN acknowledge support by DOE BES Grant DE-FG02-03ER15476. Use of the NSLS was supported by the U.S. Department of Energy, Office of Science, Office of Basic Energy Sciences, under Contract No. DE-AC02-98CH10886. Beamline X18B at the NSLS is supported in part by the Synchrotron Catalysis Consortium, U.S. Department of Energy Grant No DE-FG02-05ER15688. Special thanks go to five reviewers and the editor, each of whose careful readings and constructive criticisms helped improve the final manuscript.

Acknowledgments for Appendix B: Work was supported by NSF Grant CHE-0611588 at Colorado State University. MALDI MS were obtained with the expert assistance of Phil Ryan (now deceased) of the Macromolecular Resources Lab at CSU. AIF, JCY and RGN acknowledge support by DOE BES Grant DE-FG02-03ER15476. We thank Nebojsa Marinkovic and Syed Khalid at the NSLS, the use of which was supported by the U.S. Department of Energy, Office of Science, Office of Basic Energy Sciences, under Contract No.

DE-AC02-98CH10886. Beamline X18B at the NSLS is supported in part by the Synchrotron Catalysis Consortium, U. S. Department of Energy Grant No DE-FG02-05ER15688. We thank JoAn Hudson of Clemson University for the additional TEM imaging.

TABLE OF CONTENTS

CHAPTER I:	INTRODUCTION.....	1
CHAPTER II:	ZIEGLER-TYPE HYDROGENATION CATALYSTS MADE FROM GROUP 8-10 TRANSITION METAL PRECATALYSTS AND AIR ₃ COCATALYSTS: A CRITICAL REVIEW OF THE LITERATURE	4
	Synopsis	5
	Introduction.....	5
	Polymer Hydrogenation	6
	An Important Distinction: Ziegler-type Hydrogenation Catalysts versus Ziegler-Natta Polymerization Catalysts.....	7
	Overview of the Main Sections of This Review	10
	Studies of Ziegler-type Hydrogenation Catalysts	11
	Effect of Preparation Variables on Ziegler-type Hydrogenation Catalysts.....	11
	The Nature and Mechanism of Formation of Ziegler-type Hydrogenation Catalysts.....	27
	A Closer Look at the More General Homogeneous versus Heterogeneous Catalysis Question	66
	Summary	73
	References.....	89
SUPPORTING INFORMATION_A:	SUPPORTING INFORMATION FOR: ZIEGLER-TYPE HYDROGENATION CATALYSTS MADE FROM GROUP 8-10 TRANSITION METAL PRECATALYSTS AND AIR ₃ COCATALYSTS: A CRITICAL REVIEW OF THE LITERATURE.....	96
CHAPTER III:	HYDROCARBON-SOLUBLE, ISOLABLE ZIEGLER-TYPE Ir(0) _n NANOPARTICLE CATALYSTS MADE FROM [(1,5-COD)Ir(μ-O ₂ C ₈ H ₁₅)] ₂ AND 2-5 EQUIVALENTS OF AlEt ₃ -DEPENDENT, EXCEPTIONAL, 200 °C THERMAL STABILITY.....	110
	Synopsis	111
	Introduction.....	111
	Results and Discussion	115
	Summary and Conclusions	126
	Experimental.....	128
	References.....	136
SUPPORTING INFORMATION_B:	SUPPORTING INFORMATION FOR:	

HYDROCARBON-SOLUBLE, ISOLABLE ZIEGLER-TYPE Ir(0) _n NANOPARTICLE CATALYSTS MADE FROM [(1,5-COD)Ir(μ-O ₂ C ₈ H ₁₅) ₂] AND 2-5 EQUIVALENTS OF AlEt ₃ -DEPENDENT, EXCEPTIONAL, 200 °C THERMAL STABILITY	143
CHAPTER IV: EXCEPTIONALLY THERMALLY STABLE, HYDROCARBON SOLUBLE ZIEGLER- TYPE Ir(0) _n NANOPARTICLE CATALYSTS MADE FROM [Ir(1,5-COD)(μ-O ₂ C ₈ H ₁₅) ₂] PLUS AlEt ₃ : TESTS OF KEY HYPOTHESES FOR THEIR UNUSUAL STABILIZATION	158
Synopsis	160
Introduction.....	160
Results and Discussion	165
Summary and Conclusions	177
Experimental	178
References.....	193
SUPPORTING INFORMATION_C: SUPPORTING INFORMATION FOR: EXCEPTIONALLY THERMALLY STABLE, HYDROCARBON SOLUBLE ZIEGLER- TYPE Ir(0) _n NANOPARTICLE CATALYSTS MADE FROM [Ir(1,5-COD)(μ-O ₂ C ₈ H ₁₅) ₂] PLUS AlEt ₃ : TESTS OF KEY HYPOTHESES FOR THEIR UNUSUAL STABILIZATION.....	197
CHAPTER V: SYNTHESIS AND CHARACTERIZATION OF [(1,5- CYCLOOCTADIENE)Ir(μ-H)] ₄ : TETRAMETALLIC Ir ₄ H ₄ -CORE, COORDINATIVELY UNSATURATED CLUSTER.....	251
Synopsis	253
Introduction.....	253
Experimental	256
Results and Discussion	260
Summary and Possible Future Directions.....	269
References.....	272
SUPPORTING INFORMATION_D: SUPPORTING INFORMATION FOR: SYNTHESIS AND CHARACTERIZATION OF [(1,5-CYCLOOCTADIENE)Ir(μ-H)] ₄ : TETRAMETALLIC Ir ₄ H ₄ -CORE, COORDINATIVELY UNSATURATED CLUSTER.....	276
CHAPTER VI: SUMMARY	318
APPENDIX _A: IRIDIUM ZIEGLER-TYPE HYDROGENATION CATALYSTS MADE FROM [(1,5-COD)Ir(μ-O ₂ C ₈ H ₁₅) ₂] AND AlEt ₃ : SPECTROSCOPIC AND KINETIC EVIDENCE FOR THE Ir _n SPECIES PRESENT AND FOR NANOPARTICLES AS THE FASTEST CATALYST	320

APPENDIX_B:	INDUSTRIAL ZIEGLER-TYPE HYDROGENATION CATALYSTS MADE FROM $\text{Co}(\text{NEODECANOATE})_2$ OR $\text{Ni}(\text{2-ETHYLHEXANOATE})$ AND AlEt_3 : EVIDENCE FOR NANOCCLUSERS AND SUB-NANOCCLUSER OR LARGER ZIEGLER-NANOCCLUSER BASED CATALYSTS377
APPENDIX_C:	GENERAL STATEMENT ON “JOURNALS-FORMAT THESES”429

CHAPTER I

INTRODUCTION

The broad theme of this dissertation is the synthesis, characterization and catalytic evaluation of model Ziegler-type cyclohexene hydrogenation catalyst made from $[\text{Ir}(1,5\text{-COD})(\mu\text{-O}_2\text{C}_8\text{H}_{15})]_2$ plus AlEt_3 . This dissertation is written in the “journals-format” style (see Appendix A for a discussion of this type of dissertation). It is based on four separate publications written in a format set by the American Chemical Society. Additionally, a published literature review and a paper submitted for publication were written in the format of *Journal of Molecular Catalysis A: Chemical* (Elsevier). Consistency of this dissertation as a single document is achieved by (i) this introduction, (ii) the use of bridging paragraphs at the beginning of each chapter, (iii) a final summary chapter and (iv) two appendix chapters consisting of published, co-authored papers, that are closely related to the main theme of this dissertation. Detailed accounts of contributions from each individual to this dissertation are given at the beginning of each chapter. A concise overview of each chapter’s contents is presented below.

Chapter II is a published literature review (W.M. Alley, I.K. Hamdemir, K.A. Johnson, R.G. Finke, *J. Mol. Catal. A.: Chem.* 315 (2010) 1-27) that critically analyzes the existing literature of Ziegler-type hydrogenation catalysts in the areas of (i) variables important in catalyst preparation, and (ii) the homogeneous versus heterogeneous nature of the active catalyst species. Additionally, the literature review briefly reports literature findings on nature of the AlEt_3 -derived species.

Chapter III is a publication (I.K. Hamdemir, S. Özkar, S.; K.-H. Yih, J.E. Mondloch, R.G. Finke, *ACS Catal.* 2 (2012) 632-641) that demonstrates the high activity, long lifetime and

unusually high thermal stability of the hydrocarbon-soluble, isolable and then redissolvable Ziegler-type hydrogenation catalysts made from $[\text{Ir}(1,5\text{-COD})(\mu\text{-O}_2\text{C}_8\text{H}_{15})]_2$ plus AlEt_3 at Al/Ir ratios of 1-5.

Chapter IV is a paper submitted for publication to *J. Mol. Catal. A: Chem* that investigates the true nature of the AlEt_3 -derived stabilizer species in the Ziegler-type catalyst solution made with $[\text{Ir}(1,5\text{-COD})(\mu\text{-O}_2\text{C}_8\text{H}_{15})]_2$ plus AlEt_3 at Al/Ir ratios of 1-3. This study reveals that $\text{AlEt}_2(\text{O}_2\text{C}_8\text{H}_{15})$ (Al/Ir=1, 2 and 3) and free AlEt_3 (Al/Ir=3) are present in the Ziegler-type hydrogenation catalyst solution starting with $[\text{Ir}(1,5\text{-COD})(\mu\text{-O}_2\text{C}_8\text{H}_{15})]_2$ plus AlEt_3 . The spectroscopic and catalytic evidence helps to rule out initial, literature-based, hypotheses (iii) that anionic $[\text{AlEt}_3(\text{O}_2\text{C}_8\text{H}_{15})]^-$ stabilizer exists and provides DLVO-type, Coulombic-repulsion stabilization, or (iv) that the AlEt_3 -derived stabilizers are Al-O-Al containing alumoxanes.

Chapter V is a publication (K.-H. Yih, I.K. Hamdemir, J.E. Mondloch, E. Bayram, S. Özkar, R. Vasić, A.I. Frenkel, O.P. Anderson, R.G. Finke, *Inorg. Chem.* 51 (2012) 3186-3183) that describes the synthesis of the previously unavailable $[\text{Ir}(1,5\text{-COD})(\mu\text{-H})]_4$ complex in 78% initial, and 55% recrystallized, yield starting with commercially available LiBEt_3H and $[\text{Ir}(1,5\text{-COD})(\mu\text{-Cl})]_2$ in the presence of excess 1,5-COD in THF. The resultant $[\text{Ir}(1,5\text{-COD})(\mu\text{-H})]_4$ complex is fully characterized by single-crystal XRD, XAFS, ESI-MS, UV-visible, IR, and NMR spectroscopies.

Chapter VI is a brief summary of the material presented in this dissertation.

Two appendix chapters (Appendix E and Appendix F) are also included in this dissertation. Appendix E is a publication (W.M. Alley, I.K. Hamdemir, Q. Wang, A.I. Frenkel, L. Li, J.S. Yang, L.D. Menard, R.G. Nuzzo, S. Özkar, K.A. Johnson, R.G. Finke, *Inorg. Chem.* 49 (2010) 8131-8147) that investigates the nature of the transition metal species in the catalyst

solution starting with $[\text{Ir}(1,5\text{-COD})(\mu\text{-O}_2\text{C}_8\text{H}_{15})]_2$ plus AlEt_3 . The results of this study show that the catalyst solutions contain Ir_n species ranging from mono-Ir compounds to $\text{Ir}_{\sim 4}$ to $\text{Ir}_{\sim 100}$ clusters. A transformation to $\text{Ir}(0)_{\sim 40-150}$ nanoclusters is observed in the $[\text{Ir}(1,5\text{-COD})(\mu\text{-O}_2\text{C}_8\text{H}_{15})]_2$ plus AlEt_3 catalyst solution under catalytic cyclohexene hydrogenation conditions.

Appendix F is a publication (W.M. Alley, I.K. Hamdemir, Q. Wang, A.I. Frenkel, L. Li, J.S. Yang, L.D. Menard, R.G. Nuzzo, S. Özkar, K.-H. Yih, K.A. Johnson, R.G. Finke, *Langmuir* 27 (2011) 6279-6294) that reports studies determining the nature of the transition metal component in the industrial Co- and Ni-based Ziegler-type hydrogenation catalysts. The results demonstrate that, both before and after catalytic cyclohexene hydrogenation, the species present comprise a broad distribution of metal cluster sizes from subnanometer to nanometer scale particles. The estimated mean cluster diameter is about 1 nm (ca. $\text{Co}_{\sim 4}$ and $\text{Ni}_{\sim 4}$) for both Co- and Ni-based Ziegler-type catalysts.

CHAPTER II

ZIEGLER–TYPE HYDROGENATION CATALYSTS MADE FROM GROUP 8–10

TRANSITION METAL PRECATALYSTS AND AIR₃ COCATALYSTS:

A CRITICAL REVIEW OF THE LITERATURE

This dissertation chapter consists of a review article published in the *Journal of Molecular Catalysis A: Chemical* **2010**, 315, 1–27. This chapter is a critical review of the extant literature on Ziegler–type hydrogenation catalysts in the main areas of the variables important in catalyst preparation, and the homogeneous versus heterogeneous nature of the active catalyst species. Additionally, the literature review briefly reports literature findings on nature of the AlEt₃-derived stabilizer species.

Contributions from each author to this review can be summarized as follows, details which agree with those given in Chapter II in the dissertation by William M. Alley: (i) the initial draft of the section on the homogeneous versus heterogeneous nature of Ziegler–type hydrogenation catalysts was written by Isil K. Hamdemir; (ii) the extant literature was compiled, the literature tables were prepared and then edited by both Isil K. Hamdemir and William M. Alley; (iii) permission to reprint figures and schemes from prior publications was obtained by Isil K. Hamdemir; and (iv) the figures and schemes were prepared by both Isil K. Hamdemir and William M. Alley. The other sections of the manuscript and subsequent drafts of the complete manuscript were written by William M. Alley with editing by Isil K. Hamdemir, Kimberly A. Johnson, and relatively light edits by Richard G. Finke (16 hours according to Prof. Finke).

Synopsis

Ziegler–type hydrogenation catalysts (group 8–10 transition metal precatalysts plus AlR_3 cocatalysts) are one of the most important families of industrial hydrogenation catalysts, especially for polymer hydrogenation. Despite their ~40 year history of industrial use, there is a need for improved fundamental understanding in order to make further, rationally directed improvements in these catalysts. This review examines the existing literature on Ziegler–type hydrogenation catalysts, specifically: (i) the variables important to catalyst synthesis, (ii) the catalyst formation reaction mechanism, (iii) the compositional and structural nature of the active catalyst species, and (iv) the mechanism of catalytic hydrogenation. This review also (v) discusses the current approaches to the homogeneous versus heterogeneous catalysis question, with the goal of identifying if Ziegler–type hydrogenation catalysts are homogeneous (e.g., monometallic) versus heterogeneous (e.g., nanoclusters) as the true catalyst(s). A summary of the main insights from each section of the review is also given.

1. Introduction

In 1953, while studying the polymerization of ethylene using trialkylaluminum (AlR_3), Ziegler and coworkers [1,2,3,4,5] discovered the “nickel effect”. When one experiment gave a majority of butene instead of the expected higher molecular weight polyethylene, a search for the cause of this unanticipated result revealed that small amounts of residual nickel salts, mostly $\text{Ni}(\text{acac})_2$, were present from having cleaned the metal autoclave with sulfuric acid. These nickel salts had reacted with AlEt_3 to cause the observed change in catalysis, and the phenomenon was therefore termed the “nickel effect” [4]. These and other investigations into catalysts and polymerization products led to the 1963 Nobel Prize shared by Karl Ziegler and Giulio Natta [5].

The industrial and technological potential of Ziegler–Natta¹ catalysts was subsequently realized with remarkable speed [5]. Interest in variations on these catalysts for their potential use in *hydrogenation, particularly for polymer hydrogenation*, was considerable (Appendix 2.A, Table 2.A.1), and began in the early 1960s [2,6].

1.1. *Polymer hydrogenation*

Diene polymers such as polyisoprene and polybutadiene, or styrenic block copolymers (SBCs, Scheme 2.1) that contain polyisoprene or polybutadiene blocks, have multiple commercial applications [6]. They possess the desired physical properties of high strength, wide range of hardness, and ease of processing. The olefins in these polymers allow them to undergo post-polymerization modification (including crosslinking, isomerization, cyclization, and hydrogenation) to create new polymers possessing desired physical and chemical properties [7]. Of the various desired types of modifications possible, hydrogenation is arguably the most important [6]. The primary purpose of polymer hydrogenation is to make the resultant polymer more resistant to the deleterious effects of thermal, oxidative, and ultraviolet radiation exposure. A main pathway for degradation of polymers containing olefinic groups occurs by autoxidation of allylic positions in the polymer to allylic –OOH groups and subsequent oxidation products [8]. Non-hydrogenated SBCs with their unsaturated olefinic midblock regions are prone to these effects.

SBCs were first produced in the early 1960s by Shell Chemical Co. with the trade name KRATONTM polymers [9]. Roughly one decade later, hydrogenated SBCs with improved thermal and oxidative stability were also being produced (see Appendix 2.A, Table 2.A.1).

¹ Early on, Karl Ziegler [5] referred to these catalysts generally as “organometallic mixed catalysts,” and preferred the specific title “Mülheim catalysts” because of where the original work was done. Giulio Natta named them Ziegler catalysts [1,5]. They are usually now called Ziegler–Natta catalysts in the case of polymerization (as opposed to hydrogenation) catalysts.

Without selective hydrogenation of the olefinic blocks of SBCs, the polymers become yellow, brittle, and of little use in many applications where exposure to heat, air, and light are unavoidable. Hydrogenated SBCs would have found wider application shortly after their introduction were it not for their relatively high cost due to the extra expense of the hydrogenation step [6]. Development of more economically favorable catalytic hydrogenation processes has, and continues to, alleviate this added expense. The use of homogeneous (soluble)² [10,11,12,13,14,15,16,17,18,19] hydrogenation catalysts has helped by allowing for more complete polymer hydrogenation [6]. Ziegler–type hydrogenation catalysts, the focus of this review, are one of the most important families of soluble catalyst commonly used for the purpose of polymer hydrogenation. Consequently, the timeline for the industrial development of Ziegler–type hydrogenation catalysts mirrors that of hydrogenated styrenic block copolymers (SBCs) [9].

1.2. An Important Distinction: Ziegler–type hydrogenation catalysts vs. Ziegler–Natta polymerization catalysts

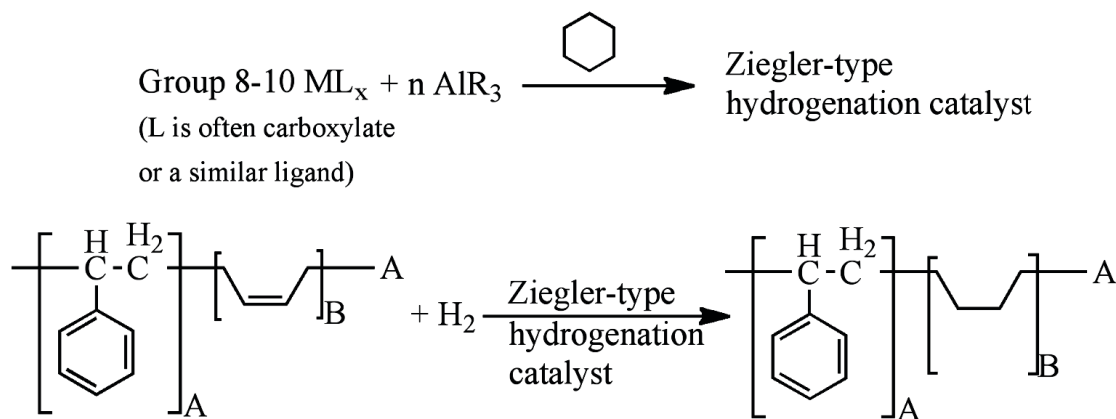
A broad definition of Ziegler–Natta catalysts includes any catalyst formed by reaction between a transition metal compound precatalyst and a group 1, 2, 13 or 14 alkyl or aryl halide cocatalyst [6,20,21]. It is important to make a distinction between the late-metal *Ziegler–type hydrogenation catalysts* of interest herein versus the currently popular *Ziegler–Natta*

² See the references listed [10–19] for a more in-depth discussion of the terminology of “heterogeneous vs. homogeneous” catalysts, and the problem of distinguishing between the two. Briefly, the classic use of the terms heterogeneous and homogeneous is in reference to the phase of catalyst and substrate. If the substrate is in solution, as is typical for hydrogenation reactions such as polymer hydrogenation, a homogeneous catalyst would be soluble whereas a heterogeneous catalyst would not. However, the true catalytically active species in catalyst systems formed of a transition metal complex under reducing conditions may be soluble metal complexes, films, powders, or nanoscale colloids formed in-situ [10]. The latter is soluble, but it shares characteristics with heterogeneous catalysts due to the heterogeneity in its active sites [11]. Such a catalyst is also sometimes called “microheterogeneous” [19]. For the sake of clarity in this review, the terms “soluble” and “insoluble” will hereafter refer to the phase of the catalyst. The terms “homogeneous” and “heterogeneous” will refer to whether the catalyst species has, respectively, only one or multiple types of active sites [16].

polymerization catalysts. Classic Ziegler–Natta olefin polymerization catalysts are formed by the reaction between early metals such as TiCl_3 plus Et_2AlCl and are heterogeneous catalysts with active sites on TiCl_3 crystallites [20,22]. Homogeneous variants of Ziegler–Natta polymerization catalysts have been developed using metallocene compounds such as $[\text{Cp}_2\text{MX}_2]$ (Cp = cyclopentadiene, M = Ti or Zr, and X = Cl or CH_3) [21,22,23,24,25,26]. At first these precursors were tested with AlR_3 cocatalysts, but the discovery that small amounts of water had an activating effect led to their use with methylalumoxane (MAO), a historically enigmatic cocatalyst formed by incomplete reaction between AlMe_3 and water [20,21,26,27,28,29,30,31,32,33,34,35]. Metallocene compounds of early transition metals dominate the field of homogeneous Ziegler–Natta polymerization catalysis, although rare-earth metals have been used as well [21,22,36]. The bulk of research on Ziegler–Natta catalysts has been focused on *polymerization*; the term “*Ziegler–Natta catalyst*” is, therefore, practically synonymous with “*polymerization catalyst*” [5,20].

However, herein we consider a different type of Ziegler-based catalyst made from non-zero-valent group 8–10 transition metal (M) precatalysts plus AlR_3 cocatalysts, and used for hydrogenations. Therefore, for the purposes of this review, the term “*Ziegler–type hydrogenation catalysts*” will be reserved for catalysts prepared from group 8–10 transition metals plus AlR_3 . Such Ziegler–type catalysts have found wide use [37], including the hydrogenation [38] of a variety of compounds such as olefins, aromatics [2,39], and diene-based polymers as already mentioned [6,9]. The catalysts most commonly used for such industrial hydrogenation reactions are derived from first row, group 8–10 transition metal compounds [6,9]. The most frequently encountered are Co or Ni chelate compounds such as the divalent acetylacetonate (acac) or carboxylate salts, combined with AlR_3 cocatalysts. It is reasonable to

suspect differences between this family of late transition metal Ziegler–type hydrogenation catalysts and the broader family of Ziegler–Natta catalysts based on early, high-valent transition metals [23,34], others having previously noted that the nature of these catalysts “probably is different when nickel salts, for instance, are replaced by titanium complexes or when AlEtCl_2 is substituted for AlEt_3 ” [40]. Furthermore, we have largely excluded from discussion herein those systems which contain additives or ligands that coordinate through P or N atoms such as PPh_3 or $[(\text{CH}_3)_2\text{N}]_3\text{PO}$ [41,42,43,44,45]. Our focus herein is on what is understood, and especially on what remains unknown, about *Ziegler–type hydrogenation catalysts* based on a careful, critical examination of the existing literature.



Scheme 2.1. A Ziegler–type hydrogenation catalyst is formed by combination of a group 8–10 transition metal precatalyst and a trialkylaluminum cocatalyst in a hydrocarbon solvent. Ziegler–type hydrogenation catalysts are employed for the hydrogenation of olefins, aromatics, and polymers, for example the industrially important process of selective styrenic block copolymer (SBC) hydrogenation shown here. Ziegler–Natta or other *polymerization* catalysts are *not* a subject of this review.

1.3. Overview of the main sections of this review

Despite the history of the industrial application of Ziegler–type hydrogenation catalysts, opportunities remain for further improvements in hydrogenation rates, selectivity, stability, and

applicability in hydrogenation of a wider range of materials [2,6,46]. Surprisingly little fundamental understanding of Ziegler–type hydrogenation catalysts exists [9,37]. Increased fundamental understanding of Ziegler–type hydrogenation catalysts would allow for *rationaly-directed* improvements [9,37,47,48]. Consequently, increased knowledge of Ziegler–type hydrogenation catalysts is highly desirable [9,37].

Published research papers seeking greater knowledge of Ziegler–type hydrogenation catalysts have generally investigated one or more of four basic issues: (i) the variables important to catalyst synthesis and their effect on catalyst properties, particularly the catalyst’s hydrogenation activity; (ii) the reaction between the transition metal precatalyst and cocatalyst components; (iii) the compositional and structural nature of the active catalyst species; and (iv) the postulated mechanism of catalytic hydrogenation. Our examination of the literature in this review is organized according to these four basic categories.

The first section of this review examines the *effects of variables* in the preparation of Ziegler–type hydrogenation catalysts, especially in terms of how they influence the resulting catalyst activity. The most important variables of catalyst preparation appear to be the: (i) identities of the transition metal precatalyst and the AlR_3 cocatalyst; (ii) ratio of these two components and the role of impurities, particularly H_2O ; (iii) solvent; (iv) identity of the substrate; (v) details of component addition (such as order and rate, presence of substrate, atmosphere, and temperature); and (vi) aging of the prepared catalyst before use in hydrogenation reactions.

The second section of this review evaluates what is known about the reaction between the catalyst precursors, and whether the resulting catalysts are homogeneous (e.g., single metal organometallics) or heterogeneous (e.g., nanoclusters). Specific questions in this regard include:

(i) how are the catalysts formed?; (ii) how many transition metal atoms constitute the active catalyst species?; (iii) what are their oxidation states?; (iv) what is the form and role of the cocatalyst?; and (v) what is known about the mechanism of the catalytic hydrogenations? This second section which follows is divided into two parts; studies that support a homogeneous catalyst hypothesis are examined first, and those that support a heterogeneous catalyst hypothesis are examined second. Many authors supporting a heterogeneous catalyst hypothesis have claimed formation of nanoclusters, for which we herein coin the term “Ziegler nanoclusters” [13,49,50].³

The third section of this review is a discussion of the future outlook for additional fundamental studies of Ziegler–type hydrogenation catalysts. Possible reasons why the desired depth of understanding of Ziegler–type hydrogenation catalysts has remained elusive—despite several decades of research on the topic—are presented, along with thoughts about and what can potentially be done to improve this situation and provide the desired, additional knowledge.

2. Studies of Ziegler–type hydrogenation catalysts

2.1. Effect of preparation variables on Ziegler–type hydrogenation catalysts

Because of their rapid adoption by industry [5], research in Ziegler–type hydrogenation catalysts initially focused on optimization of the processes for which they were used [47,48]. This included the catalyst synthesis step, for which a wide variety of possible starting components, methods, and conditions exist. Many observations on how variables of catalyst synthesis affected the activity of the resulting hydrogenation catalysts were made early on. Table 2.1 contains a concise summary of the relevant literature, and gives an overview of the breadth of systems explored.

³ See the references listed for a definition of the distinction between modern nanoclusters and traditional colloids [13,49,50].

Catalyst preparation variables have not been exhaustively investigated despite their importance. The paucity of “systematic order” in the literature [51]⁴ (i.e., which catalyst synthesis variables influence catalytic properties for which specific systems and why) is apparent in the many systems explored and the apparent contradictions among some of the findings (vide infra). This was noted recently by Shmidt and coworkers [19]: “contradictory published data on the interaction of catalytic system components do not allow us to interpret reliably the general concepts of the effect of the composition of the system on the properties of catalysts.” Therefore, gaining a better understanding of how variables in catalyst preparation affect the resulting catalytic properties is the first major goal of the field of Ziegler–type hydrogenation catalysts.

Table 2.1. Catalyst Preparation Variables

Authors	Catalyst Systems	Results	Ref.
Sloan, Matlack, and Breslow (1963)	Acac salts of Fe(III), Co(II and III), Ni(II), Ru(III), or Pd(II) (also Cr(III), Cu(II), Mn(II and III), Mo(VI), V(V), or Zr(IV)) + 1.2–12.6 Al(<i>i</i> -Bu) ₃ , AlH(<i>i</i> -Bu) ₂ , or AlEt ₃	Most active: Co(III) > Fe(III) > Cr(III). Cu(II) salts fail to form effective hydrogenation catalysts. Use of AlClEt ₂ , BEt ₃ SnEt ₄ , P(<i>n</i> -Bu) ₃ , ZnEt ₂ , or Mg(<i>n</i> -Bu)Br as cocatalysts results in either no reaction or an inactive ppt. at 30-50 °C and 3.7 atm H ₂ . Ketones, aldehydes, nitriles, nitro compounds, azo compounds, and esters are <i>not</i> hydrogenated.	57
Laporte and Schuett (1963)	Ni(2-ethylhexanoate) ₂ + AlEt ₃ , also Co, Fe, Cr, or Cu salts + AlEt ₃ for arene hydrogenation	The highest catalytic activity and amount of gas evolution (> 95% ethane) is at Al/Ni = 3–4. The activity for benzene hydrogenation decreases according to Ni ≥ Co > Fe > Cr > Cu. Catalytic activity is highly dependent on the anion of the Ni(II) precursor; carboxylates, especially 2-ethylhexanoate is good, but halides are poor. Benzene hydrogenation is poisoned by PPh ₃ .	39

⁴ We have found, paraphrasing what A.K. Galwey has written about a different area [51], that there is: little ability to carry out inductive prediction across ostensibly similar Ziegler–type hydrogenation catalyst systems, few established trends on which to expand, and therefore no coherent and generalized theory.

Authors	Catalyst Systems	Results	Ref.
Kroll (1969)	Fe(acac) ₃ , Co(acac) ₂ , or Ni(acac) ₂ + Al(i-Bu) ₃ or a <i>p</i> -dioxane adduct of Al(i-Bu) ₃	Relative catalytic activities are Co > Fe > Ni. The highest activities are achieved at Al/M = 6 for M(II), 8–10 for Fe(III). It is very difficult to properly adjust the Al/M ratio due to impurities such as oxygen and H ₂ O always present, even after careful purification. The poisoning action of excess Al cocatalyst can be overcome by making a <i>p</i> -dioxane adduct of Al(i-Bu) ₃ before catalyst synthesis. Improved kinetics are observed when the catalyst is allowed to age overnight.	75
Laporte (1969)	2-ethylhexanoate salts of Ni, Co, Fe, Cr + AlEt ₃	Activity order: Ni > Co > Fe > Cr. The anion of the Ni salt has a significant effect on the activity: 2-ethylhexanoate > benzoate > acac > acetate > chloride, mirroring solubility. Activities are equal for Ni(2-ethylhexanoate) ₂ + AlEt ₃ , Al(i-Bu) ₃ , or Al(C ₆ H ₁₃) ₃ catalysts. The highest catalytic activity is observed when Al/M=3–4 for M(II). The olefin affects the hydrogenation rate: monosubstituted > unsymmetrically disubstituted > cyclic > symmetrically disubstituted. Nitrobenzene and PPh ₃ act as catalyst poisons.	58
Shmidt et al. (1970)	Co(C ₁₇ H ₃₅ CO ₂) ₂ , Fe(C ₅ H ₇ O ₂) ₂ , Ni(C ₅ H ₇ O ₂) ₂ , Ni(C ₆ H ₆ NO) ₂ , Ni(C ₇ H ₆ NO ₂) ₂ , Ni(C ₉ H ₆ NO) ₂ , Ni(C ₄ H ₇ N ₂ O ₂) ₂ , or Ni(NO ₃) ₂ [P(C ₆ H ₅) ₃] ₂ (also Ti(C ₅ H ₅) ₂ Cl ₂ or Ti(OCH(CH ₃) ₂) ₄ + AlEt ₃	Activity as influenced by precatalyst anion: acac > <i>o</i> -aminophenoxide > salicylaloximate > 8-quinolinoxide > dimethylglyoximate, the same as the decreasing order of the ligand dissociation equilibrium constant of the precatalyst. Catalytic activity is improved if the AlEt ₃ is “added to the precatalyst in the absence of the acetylenic hydrocarbon, and if the catalyst solution absorbs hydrogen beforehand.” Various ligands are added to the prepared catalyst solutions.	42
Falk (1971)	Co(2-ethylhexanoate) ₂ or Ni(2-ethylhexanoate) ₂ + AlEt ₃ or (n-Bu)Li, cyclopentyllithium, phenyllithium, ethyllithium, or (sec-Bu)Li	Catalyst prepared by slowly adding (over 90 min) the Co or Ni solution to a solution of AlEt ₃ in a N ₂ atmosphere. Slight impurities affect activity and change the Al or Li(alkyl)/M ratios optimal for selectivity. Li alkyls are generally inferior to AlEt ₃ as cocatalyst. Catalyst solutions do not deteriorate after being stored for several months.	79

Authors	Catalyst Systems	Results	Ref.
Esselin et al. (1986)	Ni(acac) ₂ , Fe(acac) ₃ , Ni(octoate) ₂ , or Co(octoate) ₂ + 1, 3, or 6 AlEt ₃ or GaEt ₃	Catalytic activity trends: Ni > Fe, and AlEt ₃ > GaEt ₃ . Optimal activity occurs at Al/M = 3 for Ni catalysts and at Al/M = 6 for Fe catalysts. Catalyst preparation is done at room temperature. Ni(acac) ₂ •2H ₂ O dried to ≥ 80% to give, on average, (Ni(acac) ₂) ₃ .	40
Reguli and Staško (1987)	Ni(3,5-diisopropylsalicylate) ₂ , Ni(acac) ₂ , Ni(stearate) ₂ , or Ni(benzohydroxamate) ₂ + 1, 2, 3, 4, 5, or 6 AlEt ₃ , Al(<i>i</i> -Bu) ₃ or LiBu.	Catalytic activity by precatalyst anion: diisopropylsalicylate > acac > stearate > benzohydroxamate, which correlates well with the solubility sequence of corresponding Ni salts (activity is also dependent on the solvent). The Al/M ratio strongly influences activity, the optimum is 1.5–4 depending on the catalyst precursors. Traces of O-containing compounds, especially those with acidic H, poison the catalysis, but could be partially offset by additional cocatalyst. Ni precipitates in the presence of aromatic solvents resulting in loss of catalytic activity. Order of addition: solvent, precatalyst, and then cocatalyst. Catalyst was prepared both in the presence and absence of cyclohexene substrate; the presence of cyclohexene increases the resulting catalytic activity when AlEt ₃ or LiBu are the cocatalysts used, but the opposite effect is observed with Al(<i>i</i> -Bu) ₃ . Temperatures from 20–45 °C during the catalyst preparation reaction have no effect on optimal Al/M. The time of catalyst aging before use in hydrogenation, and Ar versus H ₂ preparation atmosphere have no influence on activity.	70
Alvanipour and Kispert (1988)	Co(stearate) ₂ + 2 AlEt ₃	Naphthalene, quinoline, isoquinoline, 6-methylquinoline and 2-methylquinoline can be hydrogenated with the catalyst employed, but dibenzothiophene nitroquinolines and 4-chloro-2-methylquinoline cannot. Compounds containing sulfur, nitro, and chlorine groups act as poisons.	67
Barrault et al. (1994)	Co(acac) ₂ + 0.5, 1.0, or 1.5 AlEt ₃	Higher Al/Co ratios give increased activity and lower selectivity. The catalyst is ~3 times more active for the hydrogenation of cinnamaldehyde than for 2-pentyl-2-nonenal. For 2-pentyl-2-nonenal, the catalyst is more active, but less selective at a given conversion when pre-treated with CO ₂ /H ₂ (syngas) than with just H ₂ . “The final catalytic properties... depend on the activation process.”	37

Authors	Catalyst Systems	Results	Ref.
James et al. (1998)	Ni(OAc) ₂ + 0.5 Zn(OAc) ₂ + 4.5 AlEt ₃	Hydrogenation of 2-methoxy-4-propylphenol with the catalyst at 90 °C under 50 atm H ₂ for 24 h gives a 65.2% conversion with 92.2% of the product being 2-methoxy-4-propylcyclohexanol. The catalyst is poisoned by Hg(0).	84
Šabata and Hetflejš (2002)	Ni(2-ethylhexanoate) ₂ or Ni(acac) ₂ + “Li-diene,” <i>n</i> -BuLi, or AlEt ₃	Catalytic activity trends: Ni(2-ethylhexanoate) ₂ > Ni(acac) ₂ , and “Li-diene” > BuLi, or AlEt ₃ . Catalytic activity depends on Li or Al/M ratio, temperature, and particular method used in catalyst formation, the optimal being: Li/Ni is 8–10, cocatalyst added rapidly to the Ni compound at 50 °C, and kept at that temperature for 10 min before allowing to cool. Batches of catalyst prepared fresh daily to avoid changes in activity due to aging.	69
Nindakova et al. (2006)	Co(acac) ₂ • <i>n</i> H ₂ O, <i>n</i> =0, 0.5, or 1.5; or Co(acac) ₃ + 2, 4, 6, 8, 12, or 16 AlEt ₃	AlEt ₃ added to the Co salt dropwise under an atmosphere of H ₂ before the introduction of substrate. Using Co(acac) ₂ • <i>n</i> H ₂ O, the optimum Al/Co ratio depends on <i>n</i> : <i>n</i> = 0, Al/Co = 3.5–4; <i>n</i> = 0.5, Al/Co = 8–10. The <i>n</i> = 0.5 catalyst has a higher hydrogenation activity than the <i>n</i> = 0 catalyst. As [Co] decreases the optimal Al/Co ratio increases. Higher activities are achieved in heptane solvent than in toluene.	19
Belykh et al. (2006)	Pd(acac) ₂ + 2, 4, 6, 8, 10, 15, or 16 AlEt ₃	AlEt ₃ is added dropwise under flowing H ₂ to Pd(acac) ₂ in the absence of substrate; the optimal Al/Pd is 4. When H ₂ O or O ₂ traces are present, no decrease in activity at high Al/Pd is observed up to Al/Pd = 80. Use of modifiers, such as PPh ₃ , OPPh ₃ , ethanol, the order of component addition, the substrate used, and catalyst loading affect the catalyst activity. The effect of modifiers is dependent on Al/Pd.	81, 114
Finke and coworkers (2009)	[(1,5-COD)Ir(μ-O ₂ C ₈ H ₁₅) ₂ , Co(neodecanoate) ₂ , or Ni(2-ethylhexanoate) ₂ + AlEt ₃	At room temperature, and under an N ₂ atmosphere, AlEt ₃ in cyclohexane is added to a cyclohexane solution of the transition metal precatalyst with 1000 rpm stirring in the absence of olefinic substrate. However, <i>simultaneous</i> addition of Co(neodecanoate) ₂ and AlEt ₃ , Al/Co = 2, results in higher hydrogenation activity. Alternatively, the hydrogenation activity of the catalyst is independent of the order of addition for Al/Co = 3. The optimal Al/Ir is 1, Al/Ni is 2, and Al/Co is from 2 to 4. AlEt ₃ was added rapidly to the Ir precatalyst and at rate of 1 drop every 5 sec for the Ni precatalyst. Rigorous drying of glassware	11, 12, 13, 14, 15

Authors	Catalyst Systems	Results	Ref.
		and solvents was performed throughout these studies; however, for the Co system intentionally added H ₂ O decreases hydrogenation activity. The following catalyst preparation variables have, at most, minor effects on hydrogenation activity of the Co system: (i) AlEt ₃ vs. Al(t-Bu) ₃ cocatalyst; (ii) temperature during mixing of catalyst components (e.g., 30 °C vs. 60 °C); (iii) individual vs. batch preparation; and (iv) use of neat AlEt ₃ added at a slower rate.	

2.1.1. Identities of the precursors

The first obvious variable in the synthesis of Ziegler–type hydrogenation catalysts is the identity of the specific transition metal precatalyst and AlR₃ cocatalyst employed. As expected, industry favors use of the inexpensive first row metals (Fe, Co, and Ni) rather than the more expensive second and third row metals in the same groups (i.e. Ru and Os, Rh and Ir, Pd and Pt) [2,6,22]. Early studies surveyed potential catalyst precursors to ascertain which were promising as useful catalysts resulting in similar sequences for the most active metals, Ni > Co > Fe > Cr > Cu [57,58]. Also, the catalytic activities of *soluble* Ni and Co Ziegler–type hydrogenation catalysts were found to be generally superior to pre-activated, *supported* Ni or Raney Co catalysts [58]. There is a lack of agreement about whether Ni or Co systems are the most active for polymer hydrogenation, a discrepancy caused at least in part by a lack of standardization in polymer feed quality [46], differences in properties of precursor solutions such as water content or level of acidity (which, of course, readily react with the AlR₃ component, thereby indirectly influencing catalytic activity) [40], or both. Whether the Ni and Co catalysts favored by industry have the absolute best activity, selectivity, and lifetime is arguable; however, the fact that they

are industrially favored signifies that they likely have an advantageous balance of low cost, ease of synthesis, and desirable catalytic properties.

Another aspect of the precursor identity is the anion in the transition metal salt. The literature has included claims of the use of alkoxides [59,60,61,62,63] or halides [43,44,45,64]. However, a catalyst poisoning effect of halides has also been reported [65,66,67]. A few patents have claimed the usefulness of sulfur-containing anions such as sulfonate, salts of sulfur-containing acids [60,68], $M(SO_x)_n$ (and partial esters thereof), and metal salts of sulfonic acids $M(RSO_3)_n$ [62]; however, those patents do not report the control of comparing the activity of catalysts containing S-element anions to the activities of those made from the more common, generally favored anions acac and carboxylate. Precatalyst compounds with inexpensive 2-ethylhexanoate ligands, as well as the catalysts made from them, tend to be soluble in the hydrocarbon solvents typically used. In one study, the anion in Ni salt precatalysts had a significant effect on the resulting catalytic activity in a sequence that corresponded to the solubility of the precatalysts: 2-ethylhexanoate > benzoate > acac > acetate > chloride [58]. Similar findings correlating precursor solubility and catalytic activity have been made by others [69,70]. However, whether the increased catalytic activity is the influence of solubility, a result of the formation of different amounts of catalyst, or due to catalyst species with different activities, is not clear.

The choice of alkyls in the AlR_3 cocatalyst has also been of much interest. In a 1968 patent, Kroll [64] stated that it was generally agreed, even as of 1968, that the choice of cocatalyst does affect the catalyst activity. Many studies appear to favor AlR_3 with relatively short alkyl chains such as $AlMe_3$ [71], $AlEt_3$ [46,63,44,72,73,74], or $Al(i-Bu)_3$ [57,70,75], but use of triarylaluminum [72,76,77] has also been reported. Lapporte [58] found with Ni(2-

ethylhexanoate)₂ that AlEt₃, Al(*i*-Bu)₃, and Al(C₆H₁₃)₃ were equivalent in the resulting catalytic activity of hydrogenation of a variety of substrates and at a variety of conditions. Some patents have described the preferred cocatalyst as R_{3-n}AlH_n where *n* = 0–2 [59,45,65,66]. In general, the preferred cocatalyst appears to vary with the particular system; therefore, the need remains for studies elucidating the roles of the cocatalyst in both the catalyst formation and substrate hydrogenation processes.

2.1.2. Molar ratio of the precursor components (precatalyst and cocatalyst) and the role of impurities, particularly H₂O

Several reports claim that the Al/M ratio (M = the transition metal of the precatalyst) was a key factor affecting the resulting catalyst [70,69,63]. It has been noted that when too little cocatalyst was used, it failed to adequately “activate” the catalyst, resulting in decreased activity [40]. On the other hand, it was also reported that when *too much* AlR₃ cocatalyst was used, it acted as a catalyst poison [75]. Most reports agree that there is an optimum Al/M. In general, the optimum Al/M seems to be highly dependent on the specific system used [57,78], and ranges from 1.5–4 are typical, at least with a Ni precatalyst [39,70].

The most important difficulty regarding optimization of Al/M appears to have been the presence of contaminants, especially those containing oxygen atoms, acidic protons, or both [75,79]. The most ubiquitous of these is almost surely H₂O. Despite the occasional claim that oxygen-containing species such as water were *not* important considerations in catalyst preparation [59,77], for most systems, water and other such species are generally thought to have a significant influence. This is as expected for a system employing a water-sensitive, AlR₃ cocatalyst [80].

The activity of Ziegler–type hydrogenation catalyst systems are often reduced by oxygen-containing contaminants, with water being the prime example [40,63,70,72]. Reguli and Staško [70] found that this poisoning effect could be offset by the addition of more cocatalyst, the additional AlR_3 ostensibly acting to scavenge contaminants. Esselin and coworkers opted to use acac salts instead of $\text{M}(\text{“octoate”})_2$ (M is Ni or Co) because solubilization of the “octoate” compounds required a variable amount of free acid in the precatalyst solution (the term “octoate” is industry jargon for a C_8 carboxylate, frequently 2-ethylhexanoate) [40]. Additional potential contaminants are residual polymerization catalyst and excess alcohol from termination of the polymerization reaction [65,73]. Overall, these studies report the effects of O-containing contaminants as detrimental to the activity of the Ziegler-type hydrogenation catalyst systems used.

However, in other Ziegler–type systems the reaction of oxygen-containing species with the cocatalyst has been exploited to *improve* the catalytic system. This has been done in two ways: (i) by simply stopping the poisoning effect of excess cocatalyst [64,75,77,81], or (ii) by actually increasing the activity of the resulting catalyst [19,61,78]. In US Patent 3,937,759, Baumgartner and Balas claim that addition of one mole of AlEt_3 per mole of Ni to an *active* hydrogenation reaction will halt the reaction. This effect was found to be reversible by addition of a sufficient amount of alcohol to react away the AlEt_3 that had been added to stop the reaction [82]. In such cases where water is used, one might expect a reaction between H_2O and the AlR_3 compound to form Al–O–Al bonded compounds known as alumoxanes [20,34,80]. Hoxmeier et al. [62], claimed that a catalyst prepared with alumoxanes was useful for hydrogenation reactions. However, the complicated effects of the interaction of the catalyst components with H_2O on the resulting catalyst properties is an important, yet still incompletely understood, aspect

of Ziegler–type hydrogenation catalysts, effects that depend on the AlR_3/M ratio of the catalyst, as well as the amount of H_2O (or ROH , etc.). The effects of H_2O , ROH , and other such compounds on Ziegler–type hydrogenation catalysts is another area that begs for a more detailed and fundamental understanding, one using carefully controlled conditions beginning from a definitively characterized precatalyst.

2.1.3. *Solvent*

Studies of Ziegler–type hydrogenation catalysts have tended to use inert hydrocarbons, mostly alkanes such as cyclohexane [70] or heptane [57], but also aromatic solvents like benzene, toluene, or xylenes [70]. Inert hydrocarbons are commonly used because they lack lone-pair electrons that would be reactive with the Lewis acidic AlR_3 cocatalyst [58,70,72]. The relative merits of such solvents have elicited only a little discussion in the literature. Catalytic activity is very dependent on solvent in the study by Reguli and Staško [70]; their NiL_2 plus AlR_3 or LiBu catalysts became less active in the order: cyclohexane \gg xylene $>$ toluene $>$ benzene $>$ chlorobenzene. The aromatic solvents resulted in an inactive Ni precipitate being formed [70]. Shmidt and coworkers [19] reported that with their $\text{Co}(\text{acac})_3$ plus 50 AlEt_3 catalyst, activity for the hydrogenation of 1-hexene was 17-fold higher in heptane instead of toluene. However, Sloan et al. [57] reported the hydrogenation of a wide variety of substrates with a wide range of catalysts in solutions of heptane or toluene, and made no mention of differences in hydrogenation rates or formation of precipitates based on which solvent was used. It is still unclear exactly how and why such prominent differences are seen with different solvents in some instances, but not others. In short, a further examination of solvents under

carefully controlled conditions is another aspect of Ziegler–type hydrogenation catalysts that merits additional attention.

2.1.4. *Identity of the hydrogenation substrate*

Numerous substrates have been tested with Ziegler–type hydrogenation catalysts, from simple olefins to various polymers, even those with polar, acidic, or oxygen-containing functionalities [58,61,69,76]. However, not all hydrogenation attempts with a variety of substrates have been successful [57,67]. In a 1988 paper, Alvanipour and Kispert hydrogenated naphthalene and some quinolines using a $\text{Co}(\text{stearate})_2$ plus AlEt_3 catalyst [67]. However, attempts to hydrogenate 4-chloro-2-methylquinoline, nitroquinolines, or dibenzothiophene failed [67]. They believed that substrates containing chloro, nitro, and sulfur groups acted as catalyst poisons by coordinating to the catalyst [67].

In general, and as one might expect, the rate of hydrogenation was found to have some dependence on the identity of the substrate [37]. Several reports revealed a decreasing hydrogenation rate with increasing substitution about the olefinic bond while using a variety of catalysts including $\text{Ni}(\text{2-ethylhexanoate})_2$ plus AlEt_3 [58], $\text{Ni}(\text{3,5-diisopropylsalicylate})_2$ plus $\text{Al}(i\text{-Bu})_3$ [70], and a non-Ziegler–type, but related $\text{Cr}(\text{acac})_3$ plus $\text{Al}(i\text{-Bu})_3$ catalyst [57]. The known exception to this trend was reported by Sloan et al., namely that the diallyl olefin cyclohexene is among the most rapidly hydrogenated olefins [57]. Overall, the catalyst activity is dependent on the identity of the substrate as one might expect. However, the details of the effects seen require further scrutiny and explanation, for example, what rate laws are seen for the different classes of olefins?

2.1.5. Other aspects of catalyst synthesis

The catalyst component addition order, rate of component addition, and whether or not the substrate should be present during catalyst synthesis have been points of concern in the literature. There is wide disagreement on these issues between researchers, and among different systems, as to the effects, if any, of the above-noted variables on catalysis [45,64]. Various reports have stated preferences for: (i) slow addition of the precatalyst solution to the cocatalyst solution [79]; (ii) addition in the opposite order, but still slowly [77]; or (iii) keeping Al/M molar ratios essentially constant during the reaction, either by simultaneous addition or by rapid addition of a solution of the cocatalyst to a solution of the transition metal precatalysts [63]. Likewise, different reports have expressed, oppositely, the benefits of preparing the catalyst in the presence of substrate [68], or in the absence of substrate [62]. In 1987 Reguli and Staško [70] observed that the presence of cyclohexene during the catalyst synthesis reaction increased the hydrogenation activity of the resulting catalyst when AlEt₃ or LiBu were used as cocatalysts, but that the presence of cyclohexene inexplicably had the *opposite* effect when Al(*i*-Bu)₃ was employed as the cocatalyst.

Another detail occasionally discussed is the gas present (i.e., N₂, Ar, or H₂) during catalyst synthesis. Shmidt and coworkers [42] obtained a higher activity if “the catalyst solution absorbs hydrogen beforehand.” However, Reguli and Staško [70] found that conducting their Ni(3,5-diisopropylsalicylate)₂ plus Al(*i*-Bu)₃ catalyst preparation in an atmosphere of either Ar or H₂ ultimately had no influence on the resulting catalyst activity. The question, then, is whether there is something special about using H₂ as opposed to the inert gasses N₂ or Ar (i.e., whether the key is just to provide an O₂ and H₂O-free atmosphere, or is H₂ acting as a reductant during the catalyst preparation). A subtlety here may be whether one is carrying out reactions in

solution under H₂ gas with the first row group 8–10 metals versus those with second or third row transition metals, since only the latter are reduced to metal zero compounds under an atmosphere of hydrogen and standard conditions [83].⁵ Overall, it appears that the primary purpose of the atmosphere employed is to ensure conditions free of O₂ and oxygen-containing impurities such as H₂O. That said, reduction/activation of the catalyst when H₂ is used has not been adequately tested via careful control experiments with and without H₂ in Ziegler–type hydrogenation catalyst systems.

The temperature of catalyst preparation is another variable occasionally mentioned in the literature [41], with different temperatures often being employed for different systems. For example, temperatures reported for optimal catalyst preparation range from 50 °C (followed by holding the solution at that temperature for 10 min before being allowed to cool [69]), to heating the catalyst after the synthesis reaction at 90 °C under 1 atm of N₂ for 2 hours [84]. In general, and despite various claims of reaction temperatures that lead to an optimal catalyst, activity as a function of reaction temperature has also not been systematically studied.

The effects that temperature and other variables in catalyst preparation (order and rate of precursor addition, presence of substrate, and atmosphere) have on the activity of the resulting catalysts appear to depend on the individual system used. It is clear that they have not been adequately studied, or even reported in some cases. Additionally, *how* these and other variables influence catalyst activity will not be fully understood without studying how these variables are

⁵ Standard reduction potentials (E°, 25 °C, 1 atm) vs. SHE in volts for Mⁿ⁺ + ne⁻ → M, where M is: Fe³⁺/Fe = -0.037, Fe²⁺/Fe = -0.447, Co²⁺/Co = -0.28, Ni²⁺/Ni = -0.257, Ru²⁺/Ru = 0.455, Rh²⁺/Rh = 0.600, Pd²⁺/Pd = 0.951, Ir³⁺/Ir = 1.156, Pt²⁺/Pt = 1.18, and 2H⁺/H₂ = 0.000. The most commonly used precatalysts of first row group 8–10 transition metals Fe, Co, and Ni therefore have unfavorable potentials for reduction by H₂ gas under standard conditions, unlike second and third row transition metals [83]. Hence, if a second or third row transition metal precatalyst was used, pretreatment by even 1 atm of H₂ at standard conditions could influence the catalyst formation reaction, at least from a thermodynamic perspective.

affecting first (i) the products of the catalyst synthesis reaction (i.e., the composition and structure of the resulting catalyst), and second (ii) the kinetics and mechanism of the catalysis.

2.1.6. Aging of prepared catalyst

Another factor that has garnered mention in the literature as potentially significant for the activity of Ziegler–type catalysts is the aging of prepared catalyst solutions. The issues of whether or not prepared catalyst solutions have a significant “shelf-life” before deactivation or precipitation is related to this topic. It has been noted for some systems that in the catalyst solution, a precipitate often formed if it was stored at a high temperature for long periods of time [68]. Šabata and Hetflejš [69] took the precaution of making fresh batches of catalyst daily to avoid changes in activity due to aging. In contrast, others have allowed the prepared catalyst to age overnight [67,75], claiming that it improved reproducibility of the kinetic experiments [75]. Reguli and Staško reported that the time of catalyst aging before use in hydrogenation had no influence on activity [70]. However, the actual experimental results, including what aging times were examined, were not reported [70]. Conclusions regarding the effects of catalyst aging cannot be drawn from this assortment of results for Ziegler–type hydrogenation catalysts as a group; the outcome is dependent on the individual system, requiring independent optimization of each set of conditions. Without a more detailed understanding of the fundamental chemistry involved, the contradictory results prevent the ability to develop a consistent picture of the phenomenology of Ziegler–type hydrogenation catalyst aging.

2.1.7. Conclusions for the section on catalyst preparation variables

The above survey of variables makes apparent that there are many important details involved in preparation of Ziegler–type hydrogenation catalysts, specifically: the identities of the

transition metal precatalyst and the AlR_3 cocatalyst; the ratio of these two components and the role of impurities, particularly H_2O ; the solvent; the identity of the substrate; the details of component addition such as order and rate, presence of substrate, atmosphere, and temperature; and any aging of the prepared catalyst before use in hydrogenation reactions. Furthermore, the question of *how* these variables have the effects they do is an open one. The ability to explain the effects of these variables in catalyst preparation is hampered by the fact that the effects themselves are often dissimilar for ostensibly similar, but ultimately somehow different, systems. Therefore, it is desired to perform studies of the catalysts under conditions that are either optimized, industrially relevant, or both if needed. Since these catalysts are used industrially, and since faster, longer lifetime, and more selective catalysts are always of interest, there is an incentive for additional studies, along with a host of the necessary control experiments—for example, comparing the best or other's catalysts to one's own catalyst, all under identical conditions.

When one considers the obstacles to understanding the effects of all possible variables in Ziegler-type catalyst preparation, it becomes easier to understand why this class of industrial catalysts has not been exhaustively investigated, and why contradictory data exist. Isolation of any single variable for study is difficult because of how many variables there are (*at least* 11), the possibility that additional, still-unidentified variables exist, and the indication [58,70] that many variables may be correlated with one another. A modern systematic and/or combinatorial study holds the potential of identifying superior industrial catalysts, for example.

Furthermore, accurate evaluation of catalyst activity, the indicator most often used for the effect on the catalyst, may be hindered by an H_2 gas-to-solution mass-transfer limitation (MTL)

[85,86,87,88].⁶ The presence of an H₂ gas-to-solution MTL in hydrogenations using Ziegler–type catalysts is especially likely because of their high catalytic activities—indeed, we have routinely run into such MTL issues in our own studies [55,56]. Additionally, when polymers are the substrate, adequate mixing is difficult to achieve in the viscous polymer solutions thereby increasing the chances that kinetics will be dominated by MTL. Despite this, *few studies discussed herein mentioned efforts to avoid MTL kinetics* [41,57,69,75]. It is possible that many of the kinetic results reported for Ziegler–type hydrogenation catalysts are questionable because their studies have fallen victim to MTL effects. Unless specifically ruled out, undetected MTL should be suspected for instances where there is disagreement about whether or not a given variable had any effect on the catalyst properties of a given system. For these reasons, all research, both the patent literature assembled in Appendix 2.A, Table 2.A.1, and other published studies shown in Table 2.1, should, in our opinion, be viewed with a critical eye and with possible MTL effects in mind.

Importantly, the effects that synthesis variables have on the catalytic properties of Ziegler-type hydrogenation catalysts (e.g., activity), are likely to be closely related to the effects of those variables on the *homogeneous or heterogeneous nature of the catalysts*. When catalyst formation of a non-Ziegler–type hydrogenation catalyst is carried out in-situ, “the lesson is that the nature of the true catalyst can change with the reaction conditions” [16]; this may be just as true for Ziegler–type hydrogenation catalysts pre-formed by the addition of AlR₃. Therefore, a way to look for answers as to *how* catalyst synthesis variables affect catalytic activity would be

⁶ See the references listed [85,86,87,88] for a more in-depth discussion of MTL effects and its consequences. MTL should be a concern for one attempting to measure the kinetics of any solution phase reaction where one of the reactants (H₂ in this case) is supplied as a gas. If the hydrogenation reaction of interest is fast relative to the mass transfer of H₂ gas into solution, then the overall reaction kinetics will be dominated by the slower mass-transfer step. In certain cases where there may be competing reactions, such as isomerization or olefin oligomerization [58] with Ziegler–type hydrogenation catalysts, the presence of significant MTL effects can also alter product ratios.

to study the composition and structure (i.e., the homogeneous or heterogeneous nature) of the resulting catalysts. Connecting these aspects of Ziegler–type hydrogenation catalysts—namely synthesis variables, catalytic properties, and homogeneous or heterogeneous nature—remains a, if not *the*, significant challenge for the field.

2.2. *The nature and mechanism of formation of Ziegler–type hydrogenation catalysts*

Because of the desire to make rationally-directed improvements to Ziegler–type hydrogenation catalysts, important topics include: the reaction between the precatalyst and the cocatalyst; the true nature of the active catalyst; and the identity of the cocatalyst species in the resulting catalyst solution. Specifically of interest are the homogeneous or heterogeneous nature of the true catalyst(s), the oxidation state of the transition metal, and the resultant form and role of the initially added, for example AlR_3 , cocatalyst species. A detailed mechanism of the reaction between catalyst precursor components is also desired, one that includes the compositions and structures of all intermediate species and the kinetics of constituent elementary steps [89]. However, this level of detail is still unrealized with Ziegler–type hydrogenation catalysts.

As noted above, a main question about Ziegler–type hydrogenation catalysts is whether they are homogeneous (e.g., single metal organometallics) or heterogeneous (e.g., nanoclusters). The patent literature (Appendix 2.A, Table 2.A.1) has given only cursory attention to the topic; uncertainty and disagreement exist [60,77,78]. This is understandable since determining the true nature of a catalyst is a classic, non-trivial problem [16,90]. A generalized methodology for addressing this problem does exist [12,13,14,15,16,17,18], and has been successful at distinguishing between heterogeneous and homogeneous catalysts; it has identified catalysts of

both types, even in a system where slight differences in conditions were a deciding factor [17]. One of the main ideas behind this approach is (i) to first address the question of what species are present that could be catalysts—that is, what are the main, resting forms of the (pre)catalyst, and then (ii) to *determine which species contribute to catalysis primarily via kinetic and quantitative poisoning experiments* [12,13,14,15,16,17,18]. In studying Ziegler–type hydrogenation catalyst systems, nearly all workers have struggled to answer the difficult question of what species are present (i.e., what are the products and the catalyst formation reaction stoichiometry?). The needed kinetic and poisoning experiments are only rarely present [57,58]; without definitive kinetic evidence, species identified in the following papers may or may not be related to the actual catalyst(s) [91].⁷ In many cases they might be “catalyst reservoir” species that actually are not in the catalytic cycle and therefore, may even detract from the overall rate. The classic example of this is the “catalyst reservoir” of five observable species identified in Halpern’s studies of Wilkinson’s hydrogenation (pre)catalyst; only the spectroscopically invisible, 16-electron $\text{RhClL}_2(\text{solvent})$ and subsequent species contribute to the observed hydrogenation catalysis [10].

2.2.1. The “Ziegler–type catalysts are homogeneous” hypothesis.

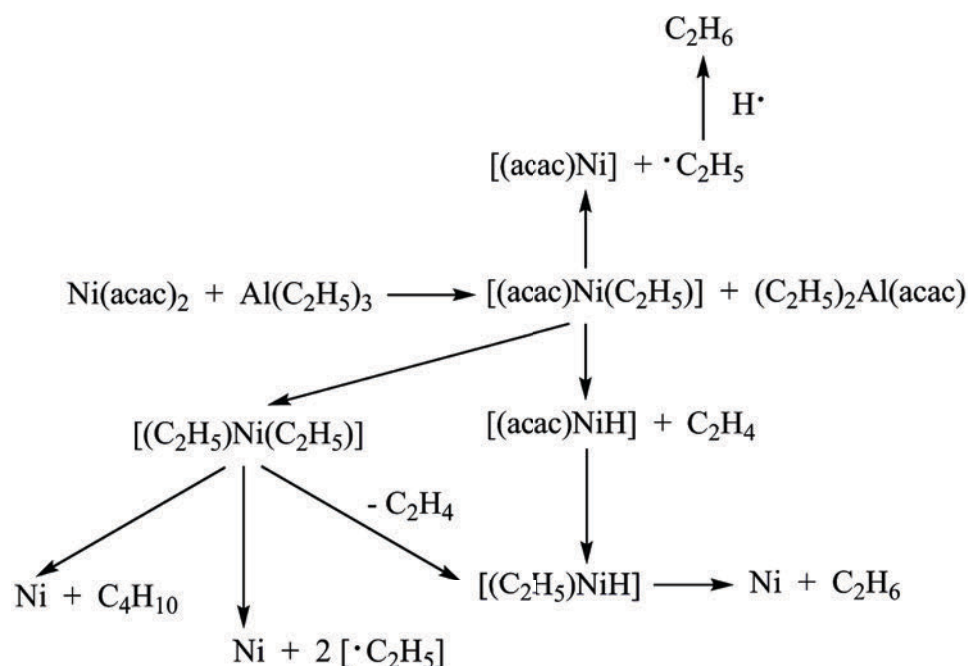
2.2.1.1. *Systems investigated by Wilke and coworkers [4]: $\text{Ni}(\text{acac})_2$ plus AlMe_3 , AlEt_3 , or $\text{Al}(i\text{-Bu})_3$.* When Karl Ziegler and coworkers first discovered the “Ni effect” in 1953, it was assumed that the Ni in the complexes took the form of a metal colloid which, in attempted ethylene *polymerizations*, was responsible for chain cleavage after each insertion step [1,2,3,4,5]. Wilke

⁷ This point is based on two basic principles in catalysis. The first is that the majority, or even all, of the observed catalysis could be due to a minority, but highly active species [10]. The second is Bergman’s formulation, somewhat tongue-in-cheek, of “Halpern’s Rules” for catalysis, which state, “if you can isolate it, it is probably not the catalyst; if it is metastable and you can detect it, it *could* be the catalyst; and if it is highly unstable and undetectable, then it probably *is* the catalyst!” [91].

and coworkers [4] have written that this assumption was based, at least in part, on the lack of knowledge at the time about metal π -complexes. Consequently, the work of Wilke and coworkers [4,92,93,94,95,96] was carried out with the different hypothesis that the Ni species responsible may be π -complexes, and *not* colloidal Ni. Wilke and coworkers [4] analyzed catalyst formation in two stages: (i) the reduction of the precatalyst by AlR_3 , and (ii) the subsequent reactions between the zero-valent transition metal, AlR_3 , and olefin.

The reduction of $\text{Ni}(\text{acac})_2$ by AlMe_3 , which resulted in the formation of $\text{Ni}(0)$, $\text{AlMe}_2(\text{acac})$, and methane and ethane gases, was thought to proceed by “homolysis of the Ni–C bond of an intermediate dimethylnickel species” [4]. The presence of intermediate dimethylnickel species was based on the isolation of crystalline $[(\alpha,\alpha'\text{-bipyridyl})\text{NiMe}_2]$ complex from a model system [4,94]. Methane and ethane formation were rationalized by homolysis of the Ni–C bond of the proposed NiMe_2 complexes, followed by either H-abstraction from AlMe_3 (disproportionation) or radical combination [4]. The reduction of $\text{Ni}(\text{acac})_2$ by AlEt_3 or $\text{Al}(i\text{-Bu})_3$ was described as “homolysis giving alkyl radicals, which H atoms, and the dimerization of alkyl groups, are accompanied by β -H elimination to give a Ni–H species and an olefin,” Scheme 2.2 [4]. Evidence for $[(\text{acac})\text{Ni-H}]$ was provided by the addition of 1,5-COD, then isolation and x-ray crystal structure determination of the 4-cyclooctenyl(acac)nickel formed [4].

The second stage of catalyst formation consisted of the subsequent reactions of $\text{Ni}(0)$ with AlR_3 and olefin. By analogy to reactions investigated in a variety of model systems, Wilke and coworkers suggested the formation of Ni–olefin π -complexes similar to $\text{Ni}(0)(\text{ethylene})_3$ [4,97]. This and other complexes, such as allyl–Ni species, similar to the Ni–olefin π -complexes, have been referred to as “bare” Ni atoms [93].



Scheme 2.2. A reconstruction of a reaction scheme for Ni(acac)₂ plus AlEt₃ proposed by Wilke and coworkers [4]. Redrawn with permission.

The π -complexes were thought to interact with AlR₃ via multicenter bonds comprised of Ni(0) plus Al and a bridging C atom. In Figure 2.1, from the work of Wilke and coworkers [4], one can see how the close proximity of the AlR₃ β -H atom to the olefinic double bond could permit an electrocyclic reorganization to give the proposed active catalyst species. A prominent feature of Wilke's proposed catalyst is the absence of Ni-H. Ni-olefin π -complexes were proposed as the active catalyst species in alkyl-olefin exchange reactions between Grignard reagents (RMgBr) and olefins by Marko and coworkers [98,99], in which H migration within the organonickel complex was suggested *without* formation of a definite Ni-H bond. However, others have studied similar Ni plus AlR₃ systems and their results do implicate Ni-H species as responsible for catalysis in olefin dimerization or oligomerization reactions [41,100]. It is important to emphasize that Wilke and coworkers were *not* investigating catalysts for hydrogenation reactions [4]. Hence, their postulation of an alkyl-olefin exchange reaction

without formation of Ni–H would seem to have little bearing on a mechanism of *hydrogenation* with similar systems.

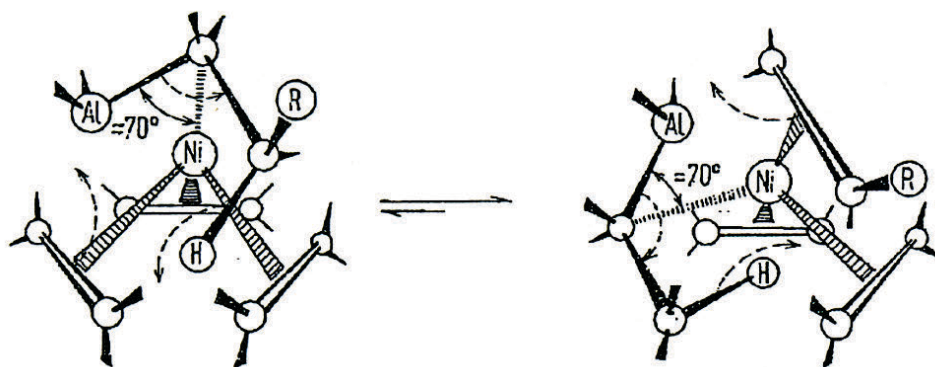


Figure 2.1. Ni(0)–olefin π -complexes proposed by Wilke and coworkers [4]. Interaction with AlR_3 is depicted as occurring through Ni–C–Al multicenter bonds. H migration is shown in a reorganization involving the AlR_3 β -H atom, and without forming a definite Ni–H species. Reproduced with permission.

Lardicci et al. [101], studied the effect of the transition metal precatalyst on the nature of the resulting catalyst. Their observation of a difference in catalytic activity using two different precatalysts, $\text{Ni}(\text{acac})_2$ and $\text{Ni}(\text{N-alkylsalicylaldimino})_2$ (plus AlR_3), lead them to the conclusion that the catalyst species formed are different in nature, thus ostensibly ruling out the “bare” Ni atoms concept [93]—that is, if the same “bare” Ni atoms were the catalyst in both systems, then the catalytic activity would have been the same, not different as observed. However, the expectation that the same catalyst would form when two different precursors are used seems flawed because the anion of the Ni precatalyst is expected to affect the catalysis as discussed previously in section 2.1.1 of this review.

Wilke and coworkers concluded that their true catalyst was likely a Ni(0) complex, although they did note that the colloidal catalyst hypothesis was impossible to disprove via their studies [4,102]. One of the important observations in the work of Wilke and coworkers [4] was that, “the extent to which a reaction follows a particular direction is dependent upon a number of

external factors (purity of Ni(acac)₂, hydride content of the Al(C₂H₅)₃, solvent, temperature, presence of ligands).” For that reason, confirmation of reactions, products, and intermediates, under exact reaction conditions—and without the use of trapping agents or non-Ziegler-type model systems [103]⁸—although difficult, would contribute considerably to our understanding of Ziegler-type hydrogenation catalyst formation and the nature of the true catalyst.

2.2.1.2. *Systems investigated by Sloan et al. [57]: M(acac)_n plus AlEt₃, Al(i-Bu)₃, or AlH(i-Bu)₂; M = Fe(III), Co(II and III), Ni(II), Ru(III), or Pd(II).* Sloan et al. [57] tested a wide variety of systems for potential catalytic hydrogenation activity, and observed similarities between the catalytic behavior of these soluble catalysts and their insoluble, heterogeneous counterparts such as Raney Ni. For example, Sloan et al. [57] reported kinetic experiments that indicated the reaction was first order in [H_{2,gas}]¹ and zero-order in [olefin]⁰, which “is the same rate behavior observed in many heterogeneous hydrogenations.” As mentioned in the previous section, they also found that, like the effects observed in heterogeneous catalysts such as Raney Ni, greater degrees of substitution on olefinic carbons generally led to slower hydrogenation. The research was conducted, in part, with the goal of being able to use soluble Ziegler-type and related hydrogenation catalysts as mechanistic models for heterogeneous hydrogenation by bulk or supported metal catalysts despite the author’s belief that the true catalysts are homogeneous [104].

In an effort to rule out either the homogeneous or heterogeneous catalyst hypothesis, the authors performed catalyst poisoning experiments—an important type of kinetics-based experiment. They observed that the addition of ethanol or acetone to the catalyst systems under

⁸ In the final analysis, the use of a model system that is available for study over another system rigorously only yields information about the model (as one would logically expect). Another noteworthy general comment on models is that “all models are wrong, but some are useful,” a quote attributed to George E. P. Box [103].

investigation killed the catalytic activity. They concluded that colloidal metal must therefore be absent and the catalysts must be homogeneous. However, another interpretation of this result is plausible, namely that the observed catalyst poisoning could be due to reaction of ethanol or acetone with the AlR_3 -derived components of the (heterogeneous) catalyst. Furthermore the result itself has been contradicted (albeit with other systems): Kroll [75], using a $Co(acac)_2$ plus $Al(i-Bu)_3$ -p-dioxane catalyst, found that the catalyst activity was decreased, but *not* killed by the addition of even a > 200 fold excess of butyl alcohol over the Al present. Schmidt and coworkers [114], studying a $Pd(acac)_2$ plus $AlEt_3$ system (discussed below), found that the addition of ethanol either enhanced or decreased the catalyst activity depending on the specific Al/Pd and EtOH/Al ratios used. Therefore, the Sloan et al. poisoning experiment alone cannot discern whether Ziegler-type hydrogenation catalysts are homogeneous or heterogeneous—they probably are reporting more on the AlR_3 -component of the catalyst than on the $(metal)_n$ nuclearity (n value) of the catalyst(s).

Sloan et al. proposed a generalized mechanistic scheme, shown below in Scheme 2.3, starting with the precursor components, showing both catalyst formation and hydrogenation of olefins. It was based on the concept that any such hydrogenation mechanism should be analogous to that of heterogeneous hydrogenation. This mechanistic scheme was noted by the authors as speculative and deliberately oversimplified, “since the structures of the various catalysts are largely uninvestigated” [57].

In the generalized mechanistic scheme, the transition metal precatalyst is first alkylated by the organoaluminum cocatalyst. Hydrogenolysis of the newly formed metal alkyl bond gives a metal hydride and an alkane. The authors mentioned elimination from the metal alkyl as an alternative way to generate the transition metal hydride. The reduction of transition metal and

the formation of transition-metal–Al and/or transition-metal–olefin complexes were given as other possibilities [38].⁹ The addition of the olefin substrate was shown as a single-step insertion into the Ni–H bond leading to a new metal alkyl, but it was mentioned that it is probably preceded by complex formation with the olefin π -bonded to the metal.¹⁰ Note that this equilibrium step (or steps) must lie to the far right in order to explain the observed zero-order olefin kinetics. The catalytic cycle is completed in this mechanism by hydrogenolysis of the M–R bond, either by molecular H₂ or by another molecule containing hydride followed by reduction, to give the saturated olefin and regenerate the M–H catalyst species.

The simple alternative explanation here is that the catalysts used by Sloan et al. are heterogeneous. Evidence for this alternative hypothesis are the similarities in catalytic behavior to known heterogeneous catalysts and the likely alternative interpretation of their poisoning experiment given above (i.e., that additions of ethanol or acetone react with the AlR₃-derived component). In short, while an important and early effort, one that included kinetic and poisoning experiments, the homogeneous versus heterogeneous nature of the true catalysts is uncertain despite these early studies.

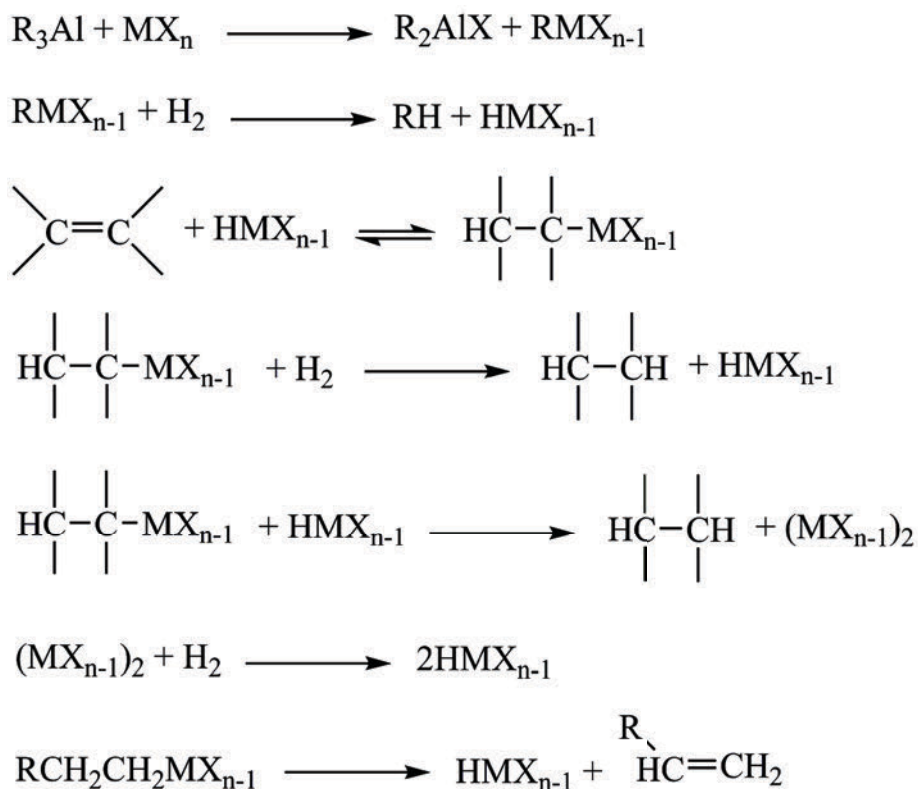
2.2.1.3. Systems investigated by Lapporte [58]: M(2-ethylhexanoate)₂ plus m AlEt₃, M= Ni or Co, m=3–4. Similar to the work of Sloan et al. [57], Lapporte [58] had observed that the rate behavior of his soluble catalysts bore similarity to heterogeneous catalysts.¹¹ Lapporte pointed

⁹ The timing of steps in a case like this is a standard mechanistic ambiguity; whether the addition of olefin occurs before or after H₂ enters and the formation of the metal hydride is possible, but often difficult, to ascertain [38].

¹⁰ To test part of the proposed scheme, a solution of a Cr(acac)₃ plus Al(*i*-Bu)₃ catalyst with 2-methyl-2-butene as substrate was treated with D₂ gas. Analysis of the reaction products by MS showed mono-, di-, and trideuterated species, explained by reversible olefin migratory insertion to a M–D(H).

¹¹ One exception, however, was that nitrobenzene, which is easily hydrogenated using non-AlR₃ containing heterogeneous Ni_n catalysts, showed only sparing conversion with the Ni Ziegler-type hydrogenation catalyst studied by Lapporte [58]. It is now known that nitrobenzene reduction is not a reliable indicator of heterogeneous catalysis [16].

out that the diminished hydrogenation activity when NiCl_2 was used as the Ziegler-type precatalyst was analogous to the diminished rate of hydrogenation when Cl^- was present using a Raney Ni catalyst. Also like Sloan et al., Lapporte was motivated by the prospect of using soluble Ziegler-type and related hydrogenation catalysts as models of heterogeneously catalyzed hydrogenation [104]. Therefore, it is no surprise that Lapporte gave a simplified mechanistic scheme (see Equations 6 and 9–11 detailed elsewhere [104]) that is quite similar to the scheme by Sloan et al.



Scheme 2.3. A reconstruction of a reaction scheme postulated by Sloan et al. [57]. The first step in this mechanism is alkylation of the transition metal precatalyst MX_n by the aluminum alkyl. Hydrogenolysis forming a metal hydride and olefin coordination follow. Elimination from the M-alkyl is shown as an alternative path to M-H formation (last line). Hydrogenolysis to give saturated olefin is shown as possibly involving either H_2 or another molecule of metal-hydride. Redrawn with permission.

One minor difference between the Sloan et al. and Lapporte schemes is that in the Lapporte scheme, reduction of the Ni(II) precatalyst with AlEt₃ to Ni(0) was shown proceeding via the formation of Ni–Et. Magnetic susceptibility measurements of the Al/Ni = 4 catalyst solutions at variable temperatures were interpreted as containing diamagnetic 3d¹⁰ Ni species, although binuclear Ni(I) species could not be ruled out. Another difference is that Ni–H was shown as generated by elimination from the metal alkyl, and metal–olefin π -complex formation was depicted before insertion into the Ni–H bond. Like Sloan et al., Lapporte observed substrate isomerization and carried out a deuterium labeling experiment. It was noted that the observation of 1,2-dideuteroethylene and HD are consistent with Ni–ethylene π -complex and Ni–H intermediates, and reversible addition of the Ni–H species to the olefin double bond. Further, more direct evidence for the presence of Ni–ethylene π -complex and Ni–H species was obtained from low temperature ¹H NMR spectra [58]. However, it was found that these signals irreversibly disappeared upon warming of the catalyst solutions to room temperature. The reasons and implications for this were not discussed, and it is not clear if the observed species are on, or off, the catalytically productive pathway. Lapporte’s NMR observations are, however, a great lead for someone to pursue to see if the observed species do (or do not) show the kinetics of a catalytically competent intermediate.

Lapporte also interpreted his observations in terms of the knowledge available at the time, that is, that the true catalyst was homogeneous. Lapporte cited the “bare” Ni atoms idea of Wilke and coworkers [93] in proposing the catalysts could be mononuclear Ni(0) species solubilized by labile –H, –R, solvent, or Al(Et)₂(2-ethylhexanoate) ligands that could be easily displaced by the unsaturated substrate. Additionally, Lapporte observed that gas evolution, apparently the products of reduction of the Ni(II) precatalyst by AlEt₃, was greatest at the same

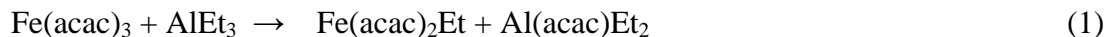
Al/Ni giving optimal catalytic activity, ostensibly suggesting a Ni(0) catalyst. However, like the work of Sloan et al., none of the results can be taken to rule out either homogenous or heterogeneous catalysts as the active species—indeed, we can be pretty sure now that it was pretty much impossible to solve the homogeneous versus heterogeneous catalysis question for these complex catalysts at that time [16]. The formation of a dark color upon hydrogenation of ketones to the corresponding alcohol was interpreted as “decomposition of at least some Ni to metal, albeit very finely dispersed” [58]. The black reaction mixture, though inseparable by ultracentrifugation, is consistent with M_n nanocluster formation [16], nanoparticles which are expected to be a potent hydrogenation catalyst in the presence of moderate amounts of AlR_3 and in hydrocarbon solvents under H_2 .

2.2.1.4. System investigated by Klinedinst and Boudart [105]: $Fe(acac)_3$ plus 6 $AlEt_3$.

Klinedinst and Boudart sought to determine the nature of Ziegler–type hydrogenation catalysts of especially Fe using IR and Mössbauer spectroscopy. An IR spectrum of the catalyst solution was similar to the superposition of spectra of $AlEt_3$ and $AlEt_2(acac)$ obtained separately for the sake of comparison. This qualitatively indicated that the catalyst formation reaction between precursor components involved the transfer of acac from $Fe(acac)_3$ to the cocatalyst. However, exchange of ethyl from Al to Fe could not be detected by IR because the band region characteristic of the C–H stretch in “ $FeEt_2$ ” was obscured by the same C–H stretch in $AlEt_3$.

The authors hoped that Mössbauer spectroscopy of the catalyst solutions would confirm the presence of metallic particles too small to be detected by X-ray diffraction. Catalyst samples were prepared for Mössbauer spectroscopy in toluene at 190 K and then rapidly quenched to 77 K. The spectra obtained indicated that high spin Fe(II) were the only Fe species present. A possible explanation offered was that the reaction of $Fe(acac)_3$ with $AlEt_3$ may be limited to a

one electron reduction at these temperatures. This is depicted in Equations (1) and (2) below, reproduced from the original publication [105]. However, evidence for the gaseous products H₂, ethane and/or ethylene was not provided as part of this study and would be useful for anyone interested in reinvestigating this Fe(acac)₂ plus AlEt₃ system.



When the catalyst sample was warmed to room temperature and then re-quenched to 77 K, it gave a Mössbauer spectrum identical to those of active catalyst samples prepared at room temperature. These Mössbauer spectra of activated catalysts showed that further reaction of the high spin Fe(II) had taken place. The most significant finding was that no metallic iron particles ≥ 1.7 nm were detected, which was taken to be consistent with a homogeneous catalyst hypothesis. The obvious alternative hypothesis is that the catalyst is heterogeneous, but consists entirely of particles smaller than 1.7 nm. Another possibility is that the catalysts are heterogeneous, but do not display the hyperfine pattern in Mössbauer spectra characteristic of metallic iron because they are amorphous [106,107], or are amorphous until exposed to high pressure H₂ [108] (these samples were not exposed to H₂). However, while it provides (negative) evidence against a crystalline heterogeneous Fe_n, catalyst of diameter ≥ 1.7 nm (which corresponds to Fe _{≥ 218} if it were close-packed Fe(0), [50]),¹² even this clever study by Klinedinst

¹² The number (N) of atoms in a metal nanocluster of diameter (D) can be estimated according to the equation: $N = (N_0\rho(4/3)\pi(D/2)^3)/M$, where $N_0 = 6.022 \times 10^{23} \text{ mol}^{-1}$, ρ = the room temperature density of the pure bulk metal, and M = atomic mass [50]. For Fe: $\rho = 7.87 \text{ g/cm}^3$ and $M = 55.845 \text{ g/mol}$ [83].

and Boudart was unable to answer the difficult homogeneous versus heterogeneous catalysis question.

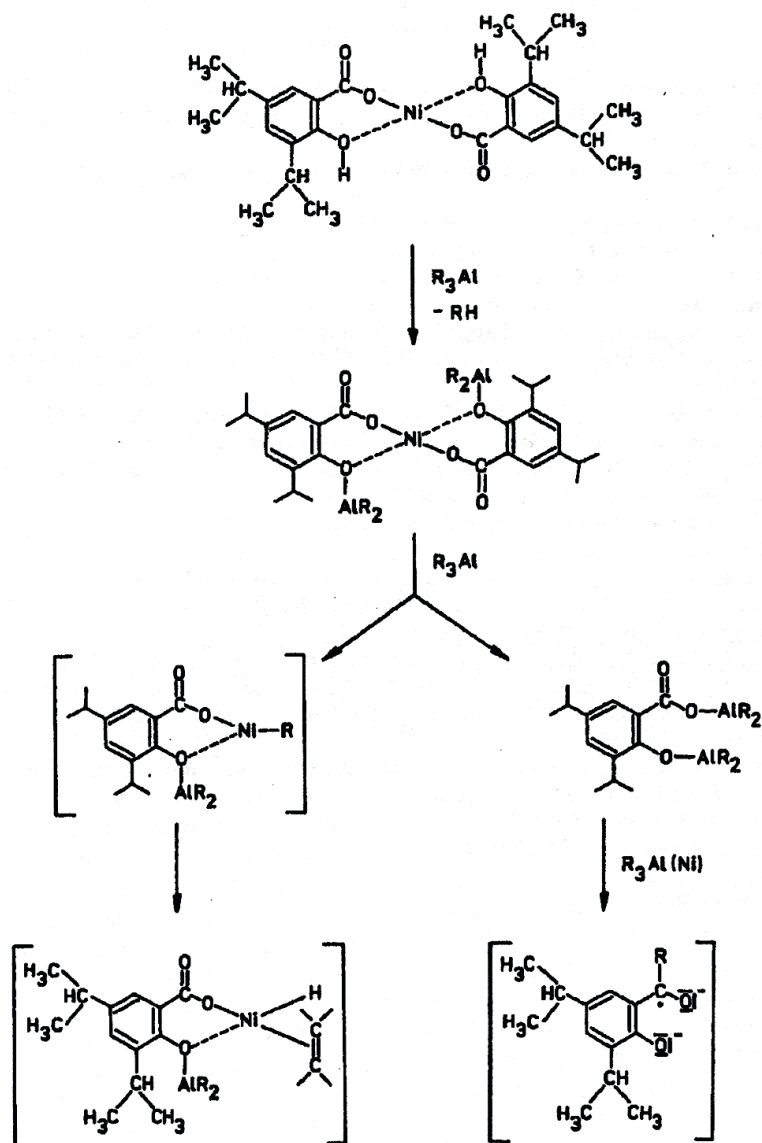
2.2.1.5. System investigated by Alvanipour and Kispert [67]: $\text{Co}(\text{stearate})_2$ plus 2 AlEt_3 .

Alvanipour and Kispert [67] concluded that Ziegler–type hydrogenation catalysts are most likely homogeneous metal hydride or π -complexes. Their basis for this conclusion is their own finding that “high speed” centrifugation was unable to induce a separation in a solution of the catalyst in their $\text{Co}(\text{stearate})_2$ plus 2 AlEt_3 system, and the absence of other evidence of metallic particles. In addition, they cited the results of others that suggested Ziegler–type hydrogenation catalysts are homogeneous: Wilke’s isolated $[(\text{P}(\text{Ph})_3)_2\text{Ni}(\text{C}_2\text{H}_4)]$ complex [92], the diamagnetic $3d^{10}$ Ni(0) catalyst species proposed by Lapporte [58], and the Mössbauer spectroscopy results of Klinedinst and Boudart [105]. However, their work did not include the kinetic studies required to identify the true catalyst(s).

2.2.1.6. Systems investigated by Reguli and Staško [70]: NiL_2 plus AlR_3 or BuLi ($L = 3,5$ -diisopropylsalicylate, acac, stearate, or benzohydroxamate; $R = \text{Et}$ or $i\text{-Bu}$).

The study by Reguli and Staško is noteworthy for its detailed examination of a range of variables in search of the optimum synthesis conditions for their Ziegler–type hydrogenation catalysts [70]. The authors also considered the nature of the catalyst preparation reaction and the resulting catalyst. In aliphatic solvent, EPR spectra indicated two paramagnetic species, interpreted as Ni(I), and ketylradicals ($\text{ArCO}^{\bullet}\text{R}$), which were thought to form during the last stage of reaction between the precursors. The (unquantitated) concentrations of these species increased with Al/Ni to a maximum at Al/Ni = 8–10, yet the catalytic activity was optimal at Al/Ni in the 2–4 range, providing an important disconnect between the EPR signals and the (kinetic) catalysis. Based on this observation, the active catalyst species were thought to be diamagnetic species of Ni(II)

formed by alkylation of the precatalyst, although these results do not necessarily mean the catalyst must be a homogeneous Ni(II) complex, only that the catalyst is not likely a Ni(I) species. A scheme depicting formation of the active catalyst species was proposed and is reproduced, Scheme 2.4.



Scheme 2.4. A speculative reaction scheme and structures proposed by Reguli and Staško for Ni(diisopropylsalicylate)₂ plus AlR₃ [70]. Reproduced with permission.

2.2.1.7. *System investigated by Barrault et al. [37]: Co(acac)₂ plus AlEt₃.* Studies by Barrault et al. investigated the catalyst formation reactions in a Co(acac)₂ plus AlEt₃ system using IR spectroscopy of the reaction solutions and GC analysis of the gas products. IR spectra at 25 min and 18 hours indicated that the timescale of reaction at room temperature was rapid, and GC showed completion of gas production after only three min of mixing. IR spectra were obtained at Al/Co = 0.5, 1.0, and 1.5. At lower Al/Co ratios they showed formation of Al(acac)₃. At Al/Co = 1.5, formation of Al(Et)₂(acac) and complete transfer of the acac ligands from the Co(acac)₂ precatalyst was observed. GC showing the production of ethane was interpreted as suggesting the disproportionation shown, Equation (3).



However, the observed ethane fraction was > 96% of the gas composition, whereas according to Equation 3 the reduction of Co(II) to Co(0) is expected to produce *equal amounts* of ethane and *ethylene*. Therefore, Barrault et al. postulated that either the disproportionation was not taking place, or that some of the ethylene was involved in π -binding interactions with soluble Co(0) complexes. The IR spectra obtained are at least consistent with such π -bonded Co(0)–ethylene complexes.

Carbonylation experiments were also carried out in which Al/Co = 1 catalyst samples were bubbled with a mixture of CO and H₂ gases, and monitored by IR spectroscopy. The highest $\nu(\text{CO})$ frequency observed indicated CO binding to Co(0) centers that were more electron-donating to the $2\pi^*$ orbital of CO than what had been previously observed for CO surface-bound to Co(0) particles. Mononuclear Co(0) species complexed by such ligands as π -bound CH₂=CH₂ were expected to be more electron rich than exposed Co(0) on the surface of metal particles. Therefore, this result was interpreted as evidence of such soluble mononuclear

species. However, the authors were correct to conclude that, despite the fact that the carbonylation experiments showed the *presence* of complexed Co(0) species, neither these nor Co(0)_n metal particles could be ruled out as the sole active catalyst.

2.2.1.8. *Systems investigated by Schmidt and coworkers: AlEt₃ plus Co(acac)₂ [109], Co(acac)₃ [110,111], Ni(acac)₂ [42,111], Fe(acac)₃, or Pd(acac)₂ [111].* The reactions of AlEt₃ with the above-listed metals and precursors were monitored using UV-Visible and IR spectroscopies. Transfer of acac ligands from the transition metal to Al was observed with the consequent formation of a mixture of Al(acac)₃ and AlEt₂(acac) for M = Fe, Co or Ni, and only AlEt₂(acac) at various Al/M ratios for M = Pd. Analysis of aromatic hydrocarbon solutions of the Co catalyst with EPR spectroscopy led the authors to propose a paramagnetic Co(0) complex as the active catalyst [109], which is shown in Figure 2.2; AlEt₂(acac) is proposed as a ligand of the Co(0) complex along with a molecule of the arene solvent, and AlR₃ bound through a carbon atom. It is understood, however, that “Et₂Al⁺” cations such as that in Figure 2.2 are normally stabilized through coordination by a Lewis base [112].

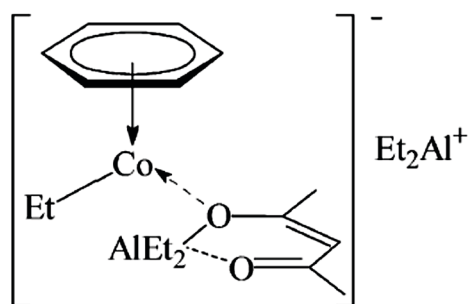


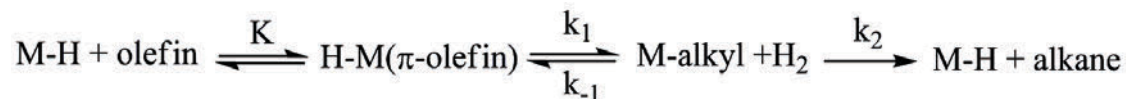
Figure 2.2. A Co(0) complex suggested as a possible active Ziegler–type hydrogenation catalyst species by Schmidt and coworkers [109,110,111]. In later work and based on additional evidence (*vide infra*), this species, whose presence was identified spectroscopically, was reinterpreted as the *precursor* for the Co(0)_n Ziegler nanoclusters now proposed as the active catalyst [113]. Reprinted with permission.

Magnetic measurements of the catalyst solutions appeared to confirm the reduction of transition metals to the zero-valent state. However, as clearly mentioned by the authors, the

presence of low spin Co(II) or Ni(II) complexes exhibiting the same μ_{eff} as Co(0) and Ni(0), could not be ruled out [111]. Furthermore, quantitative analysis of these magnetic susceptibility studies showed that *3–8% of the Co in the sample exists in Co(0)_n particles of up to 100 Å*. Without further information, especially the necessary kinetic studies, it is entirely plausible that the observed Co(0)_n particles are responsible for some or all of the observed catalysis.

Shmidt and coworkers [42] proposed a simple mechanistic scheme for the hydrogenation of olefins using Ziegler–type catalysts. This scheme was very similar to the Sloan et al. [57] and Lapporte [58] schemes, and is shown in Scheme 2.5. The true catalyst was assumed to be a complex metal hydride. The idea of initial reversible olefin π -complex addition was supported by the observation that these catalysts cause olefin isomerization. The final step producing saturated hydrocarbon and regenerating the M–H catalyst was shown as hydrogenolysis of the metal–carbon bond as it was in the previous schemes [57,58]. It is shown in Scheme 2.5 as involving a molecule of H₂, which was a common depiction at the time [38], a mechanism consistent with the kinetic observations that olefin isomerization occurred at a slower rate with increasing H₂ pressure, and that the reaction is first order in H₂ pressure (by both their and other’s data) [42,57,70].

However, it is now understood that such a hydrogenolysis is unlikely as an elementary mechanistic step, at least with late metal homogeneous catalysts. Moreover, such a step is probably better depicted by reductive elimination involving M–H formed by a prior oxidative addition of H₂ to the metal [10,89].



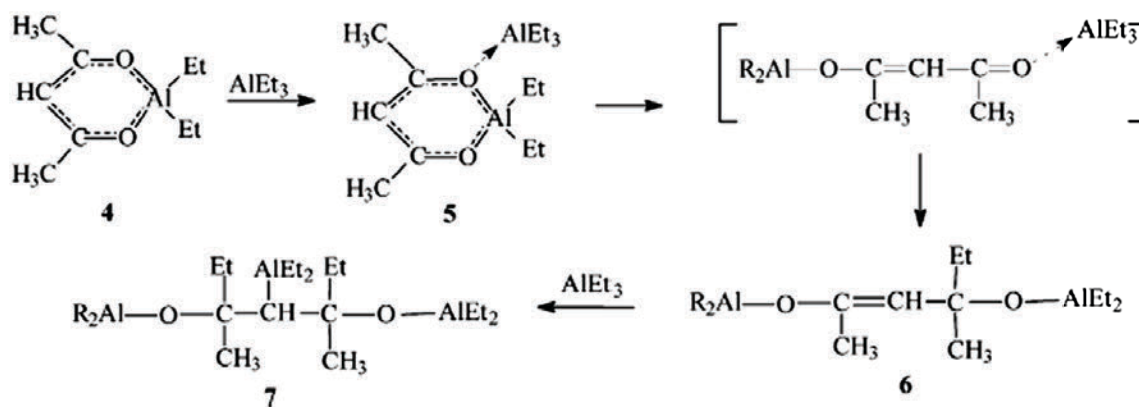
Scheme 2.5. A reproduction of the scheme for catalytic olefin hydrogenation using a Ziegler-type hydrogenation catalyst from Shmidt and coworkers' 1970 paper [42]. Used here with permission.

2.2.2. The “Ziegler-type catalysts are heterogeneous” hypothesis

2.2.2.1. *Systems investigated by Shmidt and coworkers: $\text{Co}(\text{acac})_{2,3}$ [19,113], or $\text{Pd}(\text{acac})_2$ [81,114] plus AlEt_3 .* In 2005 and 2006, Shmidt and coworkers replaced their earlier conclusion of a $\text{Co}(0)$ complex catalyst [109,110,111] with a postulate of catalysis by $\text{Co}(0)_n$ nanoclusters [19,113]. The presence of nanoclusters is consistent with the observation that dark brown solutions formed in both Co and Pd systems upon combination of the precursor components [16]. TEM images of Co samples demonstrated the presence of these clusters, and a particle size histogram displayed two maxima at 2.6 and 5.0 nm. Larger particles of 10–50 nm were thought to be agglomerates of the smaller particles. In the catalyst system prepared from $\text{Pd}(\text{acac})_2$, TEM images exhibited the presence of 4.2 nm particles when $\text{Al/Pd} = 4$. Increasing the Al/Pd ratio to ≥ 8 decreased the particle size to 1–2 nm [81,114].

The Co clusters were shown to be amorphous by XRD, but formed 10 nm crystalline particles after calcination at 450 °C for 4 hours. The $\text{Co}(0)$ complex previously proposed as the catalyst, and based on earlier UV-Visible and EPR spectroscopic results, Figure 2.2 [109,110,111] (*vide supra*), was reinterpreted as being the *precursor* for the $\text{Co}(0)_n$ nanoclusters, something fully consistent with Halpern's Rules (really guidelines) for catalysis [91].⁷ The finely dispersed component observed in the earlier studies was reinterpreted as the 10–50 nm agglomerates of the smaller $\text{Co}(0)_n$ nanoparticles [19,113].

Catalyst formation and the role of AlEt_3 were studied using IR spectroscopy, and analysis of the gaseous and solid products. A reaction scheme based on the IR results was proposed, which showed the reaction of $\text{Et}_2\text{Al}(\text{acac})$ with excess AlEt_3 , Scheme 2.6. The amounts of these species, the stability of the nanoclusters (as judged by the amount and time until precipitate was formed), and their catalytic activity were all found to depend on the Al/M ratio. Activity and stability varied inversely to each other, again consistent with Halpern's Rules, or guidelines, for catalysis [91],⁷ cited earlier.



Scheme 2.6. A scheme proposed for the reaction of $\text{Et}_2\text{Al}(\text{acac})$ with excess AlEt_3 based on the results of IR spectroscopy by Schmidt and coworkers [113]. Reprinted with permission.

Based on their observations, Schmidt and coworkers proposed that the various Al-containing species and arene solvent molecules act as the nanocluster catalyst stabilizers, Figure 2.3. Their difference in binding strengths to the nanocluster surface could explain the ease with which they are replaced by the olefin substrate molecules, and therefore the differences in catalyst stability and activity. AlEt_3 itself was thought to have the highest binding strength, which would explain the observation that increasing excesses of AlEt_3 resulted in increasingly stable, yet decreasingly active catalysts.

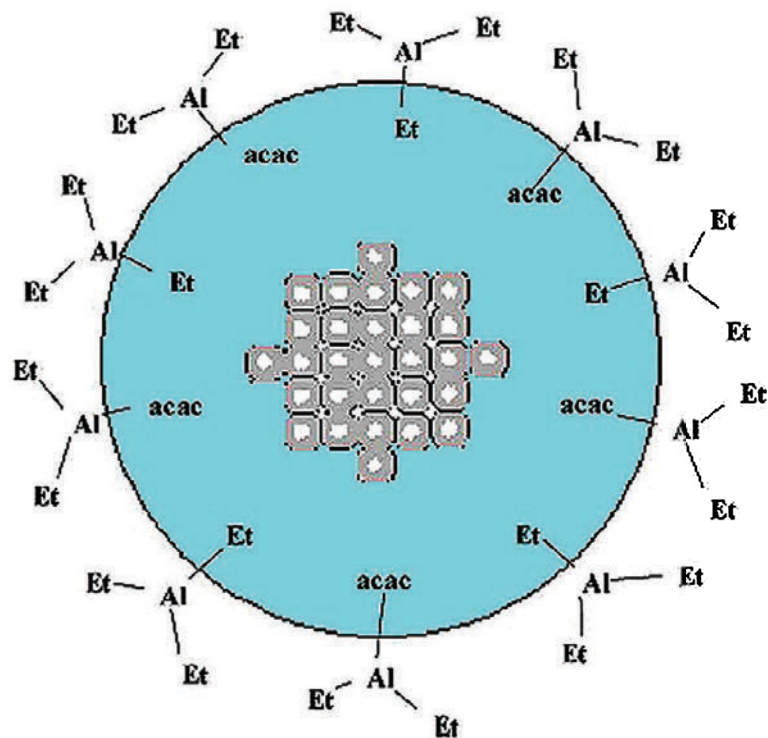


Figure 2.3. A cobalt nanoparticle and the associated organoaluminum stabilizer layer suggested by Schmidt and coworkers [113]. The gray circles in the center are Co atoms in an apparent crystalline array. Reprinted with permission.

The higher catalytic activity and immediate black precipitate formation when precatalysts with crystal H_2O were used were explained by the formation of alumoxane ($\text{R}_2\text{AlOAlR}_2$) oligomers and their acac derivatives. This requires the assumption of *weaker coordination of alumoxane compounds to the nanocluster surface*, and therefore less stabilization compared to the other proposed stabilizers $\text{AlEt}_2(\text{acac})$, AlEt_3 , or their reaction products, a potentially important, more general conclusion. The results from IR and elemental analyses on samples of catalyst precipitates showed the remaining Al compounds were a mixture of species including oligomeric alumoxanes with characteristic Al–O–Al bonding. However, the catalyst precipitates had Al/Co ratios of 1.9–2.2 regardless of whether the initial Al/Co used in their preparation was

2, 4, or 8. The authors suggested that this result indicated that excess AlEt_3 and $\text{AlEt}_2(\text{acac})$ not bound to the catalyst surface were washed away by hexane during sample preparation. However, it is not clear why the purported stronger binding AlEt_3 and $\text{AlEt}_2(\text{acac})$ would wash away instead of the supposed weaker binding alumoxane. Not all aspects of the observed nanocluster and stabilizers from this important study are fully explained [113].

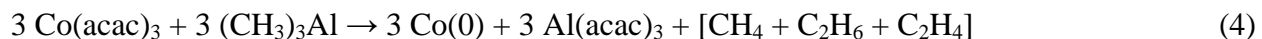
Gas analysis, deuterium labeling, and radical trapping experiments were carried out, the interested reader is referred to the details of those experiments elsewhere [19,113]. The general process of catalyst formation in these studies can be summarized as follows: (i) the anions of the transition metal precatalyst are replaced by R groups from AlR_3 , (ii) the M-alkyl intermediate decomposes during the reduction of M, specifically for Co, the $\text{Co}(0)$ nanocluster precursor complex forms (i.e., the complex previously thought of as the catalyst), and (iii) $\text{M}(0)_n$ nanoclusters then form from that $\text{Co}(0)$ precursor complex, and are stabilized by Al-containing compounds, the details and identities of which depend on the initial Al/M.

This description still lacks a mechanism for formation of nanoclusters from $\text{M}(0)$ complex intermediates. Additionally, and importantly, *in the absence of kinetic evidence, the simple observation of the presence of nanoclusters does not itself necessitate that they are the active catalysts*—although it certainly opens up that hypothesis as a dominant one to try to disprove. Schmidt and coworkers [113] observed Co concentration-dependent turnover frequencies ($\text{TOF} = \text{moles of product}/(\text{moles of catalyst} \times \text{unit time})$ [115]), specifically *lower Co concentrations giving higher TOFs*. Since the TOF would be [Co]-independent for a mononuclear homogeneous catalyst, this indicates that either a $\text{Co}(0)_n\text{L}_x + m\text{L} \rightleftharpoons n\text{Co}(0)\text{L}_{(x/n+m)}$ or related equilibrium is present (see p. 334 elsewhere [16]), that the catalysts are heterogeneous, or possibly some other explanation such as a competing, bimolecular catalyst deactivation pathway.

However, the explanation that catalyst solutions with lower [Co] make less-agglomerated catalysts, with higher TOF's directly contradicts the observation [19,113] that catalyst solutions with *more* agglomeration give higher catalytic rates. These studies do, however, identify kinetics as a function of metal/AlR₃ concentrations as key experiments for future studies. Such studies with a model Ir catalyst have recently been done [52,53,54], as will be briefly described (vide infra).

2.2.2.2. *System investigated by Pasykiewicz et al. [71]: Co(acac)₃ plus 1 AlMe₃ in benzene.*

The 1974 paper by Pasykiewicz et al. investigated the possible reaction pathways and products of the catalyst formation reaction by IR spectroscopy of the reaction mixtures and MS analysis of the gas products. They suggested the following reaction stoichiometry, Equation (4).



The identity of Al(acac)₃ was confirmed by IR, NMR, and elemental analysis. The amount of each of the gaseous products was measured. The yields of the gaseous products were 60–70% based on the number of methyl groups, yet hydrolysis of the products did not result in further gas evolution, which was taken to mean that all the hydrolysable methyl groups had reacted. This leaves 30–40% of methyl groups unaccounted for by the proposed stoichiometry, so that finding the rest of the organic products is a difficult but needed part of understanding Ziegler-type hydrogenation catalyst formation.

Analysis of the solvent after the reaction led to the detection of small amounts of toluene. When benzene-d₆ was used as the solvent 10% of the gas product was CH₃D by MS. These

observations suggested that multiple reactions are probably present (and that not all reactions are on the path to catalyst formation). A mechanistic scheme was proposed containing the following steps: (i) migration of a CH_3 group from Al to Co and simultaneous formation of $\text{Al}(\text{CH}_3)_2(\text{acac})$ and $\text{Co}(\text{acac})_2\text{CH}_3$, (ii) complex formation between the $\text{Co}(\text{acac})_2\text{CH}_3$ intermediate and another molecule of AlMe_3 , leading to (iii) nucleophilic substitution at hydrogen, carbon, or Co atoms, and (iv) further reaction of the intermediates, ultimately resulting in metallic $\text{Co}(0)_n$ thought to be the true catalyst.

The evidence supporting the notion that metallic $\text{Co}(0)_n$ was the true catalyst consisted of: (i) the color of the reaction solution changed to black, (ii) the catalyst residue obtained from solvent evaporation reacted violently with air, methanol, or water, and (iii) reaction of this residue with HCl gave CoCl_2 and H_2 . The problem with this conclusion is that while these results suggest the presence of metallic $\text{Co}(0)$ in the residue, they in no way definitively rule out homogeneous catalysis in solution. The kinetic studies necessary to support or refute the $\text{Co}(0)_n$ catalyst hypothesis remain to be done for this system as well.

2.2.2.3. Systems investigated by Goulon and coworkers: $M(2\text{-ethylhexanoate})_2$ plus AlEt_3 ($M = \text{Co}$ or Ni) [40,116], or $\text{Ni}(\text{acac})_2$ or $\text{Fe}(\text{acac})_3$ plus AlEt_3 [40]. Goulon and coworkers studied Ziegler-type hydrogenation catalysts and their precursors using EXAFS spectroscopy. In their important 1984 paper, they had greater success using the Ni precatalyst than Co because spectra of the Co catalyst solutions were overly affected by their preparation and aging [116]. EXAFS spectra of the Ni catalyst solution obtained at a series of Al/Ni ratios demonstrated Ni-Ni first-neighbors at distances equal to, or slightly larger than, those found in Ni foil. Signals were also detected for Ni-X at shorter distances, where X is C or O. The relative strength of these two signals varied with Al/M, but also with mode of preparation and aging, making truly definitive

conclusions difficult. The Ni–Ni signals expected for the higher metal shells were not observed, arguing, according to one interpretation, against the presence of (extensive amounts of) Ni(0)_n.

These results were interpreted by Goulon and coworkers [116] as consistent with amorphous clusters, but could also have been explained by small Ni(0)_n clusters, $n \approx 4-10$, based on their reported Ni–Ni first shell coordination of 3.8 ± 1 [117,118].¹³ The detection of Ni–X signals by Goulon and coworkers [116] suggests the presence of ligands that may stabilize any small clusters present and is also consistent with the samples showing Ni–Ni distances slightly larger than those found in Ni foil [119,120].¹⁴

A shift observed in the absorption edge supported the hypothesis that Ni species were zero-valent, but incomplete reduction could not be ruled out by EXAFS. The authors pointed out that earlier magnetic susceptibility data, interpreted as ruling out the presence of metal clusters [116], may have been misleading. In light of the definitive EXAFS evidence for the existence of close M–M interactions, the earlier lack of detected ferromagnetism expected for metal clusters could be explained if “carbonaceous ‘screens’...prevent magnetic coupling” [116].

In their subsequent study, Goulon and coworkers [40] used other catalyst precursors in an attempt to avoid the variability problems of the initial study. They again observed EXAFS signals dominated by Ni–Ni first neighbors suggesting the presence of metal clusters. The model of molecular “[Ni,Al]” complexes or clusters was ruled out by the similarity of spectra

¹³ See the references cited [117,118] for an explanation on how the conversion between average coordination number and number of atoms in a cluster is carried out, which is closely related to the method used for estimating number of atoms in a metal cluster of a given diameter [50].

¹⁴ Goulon and coworkers tentatively discounted the data as indicative of small clusters because of the expectation that Ni–Ni distances would be shorter for metal clusters of less than about 10 atoms. However, in a recent study of Rh clusters [119], contraction of M–M distances was expected for metal nanoclusters *without ligands* according to an approximate $n^{-1/3}$ relationship (where n = the number of atoms) [120], whereas in experimentally observed clusters *with ligands*, *larger* Rh–Rh distances were observed. This observation was explained by donation of M–M valence electrons to M–ligand bonds, thereby lengthening the M–M distance.

using GaEt₃ as the cocatalyst, and by Ga K-edge spectra. Interestingly, EXAFS spectra of the Fe(acac)₃ plus 6 AlEt₃ catalyst system were interpreted as ruling out the presence of small Fe metal particles, but were similar to the EXAFS spectra of amorphous iron carbide. When the amorphous metal carbide model was used to fit the Ni sample spectra, the initial results were promising, but not definitive. Formation of clusters in these systems is undeniable, but whether they are small ~4–10 atom clusters, amorphous M or M–carbide clusters, or some combination is still unclear. Furthermore, the question of which species is the predominant catalyst remains open, kinetic studies being required to answer that question.

2.2.2.4. *Systems investigated by Bönemann and coworkers: Ni(acac)₂ plus 3 Al(*i*-Bu)₃ [121], Pt(acac)₂ plus 4 AlMe₃ [121,122,123,124,125], or [(COD)Pt(CH₃)₂] plus 10 AlEt₃, or Al(C₈H₁₇)₃ [126].* Bönemann and coworkers have studied the reaction between Ziegler–type precursors and have worked on characterizing the products. They observed that solutions turned brown or black upon precursor combination in the Ni(acac)₂ plus 3 Al(*i*-Bu)₃ and Pt(acac)₂ plus 4 AlMe₃ systems, which is consistent with the formation of nanoclusters [16].¹⁵ In addition, TEM images of these systems revealed the presence of 3.2 ± 0.8 nm and 2.5 nm Ni and Pt nanoclusters respectively. TEM images alone, however, can be misleading as (i) the technique has been shown to be sensitive to sample preparation, especially with samples of Ziegler–type systems [9], and also (ii) can *cause* particle formation and/or crystallization under the electron beam, especially for the lighter first and second row metals [17,127]. Unlike Schmidt and coworkers who used a minimal beam current and compared images from repeated beam

¹⁵ Bönemann and coworkers use the terms “colloidal nanometals,” “transition metal nanocolloids,” and “nanosized organosols” interchangeably for what we define herein as “Ziegler nanoclusters” (and only for cases where an AlR₃ component is present).

exposures [113], Bönemann and coworkers [121,122,123,124,126] reported no attempt to rule out these potential TEM artifacts.

Bönemann and coworkers focused several of their subsequent studies on the Pt(acac)₂ plus 4 AlMe₃ system. A fit of the EXAFS spectrum taken of the isolated dried colloid gave a Pt–Pt interaction with an average coordination number of 5.0 ± 0.5 , and a lack of longer range Pt–Pt shells. These two observations could be explained by the predominance of clusters with ~8–13 atoms, nanoclusters with an amorphous structure, or a combination of the two. High resolution TEM images and corresponding optical diffractograms showed 1.2 nm amorphous particles. Analysis of the samples by anomalous small-angle X-ray scattering (ASAXS) spectroscopy confirmed the presence of 1.2 nm amorphous nanoclusters. The different sizes of nanoclusters observed in the Pt(acac)₂ plus 4 AlMe₃ system (2.5 nm by TEM vs. 1.2 nm by HRTEM and ASAXS) may be a result of the different methods used, differences in sample preparation, or a combination of the two.

Formation of nanoclusters was monitored as a function of time with in-situ ASAXS, Figure 2.4 [124,125]. The clusters of final 1.2 nm diameter were observed within 1 hour of the start of the reaction, and stayed constant for at least 1000 hours. The constant final size of the nanoclusters, and a fit of the data by an empirical [128], exponential model, Figure 2.4 (bottom), were interpreted as evidence for continuous “nucleation” or “agglomeration” of reduced Pt(0) atoms into 1.2 nm diameter, Pt(0)_{~55} nanoclusters,¹⁶ without any observable contribution from nanocluster “growth” [124]. The identity of the clusters as Pt(0)_{~55} is significant because 55 is the second of the “magic number” series of atoms for icosahedra with a full/closed outer shell,

¹⁶ Bönemann and coworkers discuss the clusters as being comprised of 53 Pt atoms based on an ideal icosahedral structural model and their experimentally determined 1.2 nm diameter. This is actually an approximation since the techniques used show the clusters are amorphous (i.e., not ideally icosahedral) and that a distribution of cluster sizes exists. The clusters have been written here as Pt(0)_{~55} to emphasize these facts according to a convention established in the literature for representing the approximate number of atoms in such (non-monodisperse) nanoclusters [50].

and thus more stable than non-magic number clusters [129]. To the best of our knowledge, Bönemann and coworkers' study is the first that has successfully monitored the in-situ formation of nanoclusters from Ziegler-type precursors, an important contribution.

Some confusion may be created by the terminology used by Bönemann and coworkers for nanocluster formation [124], which is different than the terminology commonly used in the nucleation and growth literature [49,130,131,132]. In a range of systems, and according to a well-precedented nanocluster formation mechanistic model (nucleation $A \rightarrow B$ (rate constant k_1), and autocatalytic growth $A + B \rightarrow 2B$ (rate constant k_2) [130], the term “nucleation” refers only to the k_1 step, which is typically followed by (autocatalytic surface) “growth”, the step with rate constant k_2 . Subsequent increases in size could then proceed by either continued “growth” or by, mechanistically now precedented, particle “agglomeration” (the combination of nanoparticles to form larger agglomerates) [131]. However, in the work by Bönemann and coworkers [124], “nucleation” is used to describe the formation of the final-sized 1.2 nm nanoparticles, “agglomeration” is used to describe a part of the “nucleation” process (the joining of single zero-valent Pt atoms, the other part of the “nucleation” process being the initial precursor decomposition), and “growth” is used to describe an increase in size of the 1.2 nm nanoparticles after “nucleation” has taken place (presumably occurring via continued “agglomeration”). In short, the mechanistic nomenclature used elsewhere [124] is inconsistent with the existing literature [49,130,131,132], and therefore confusing. However, despite the above nomenclature issues, the relatively slow nanoparticle development observed for this system makes it promising—if catalytically competent for hydrogenation, as is expected—for further studies aimed at determining the true nature of the catalyst and the catalyst formation mechanism. In addition, Bönemann and co-workers' studies, along with Goulon's and co-workers' efforts

nearly 20 years earlier [40], promise to be important classic studies in identifying what we term “Ziegler nanoclusters”.

A similar system, $\text{Pt}(\text{acac})_2$ plus 4 AlEt_3 ($[\text{Pt}] = 1.2 \text{ mM}$, solvent = toluene, temperature = $22.0 \text{ }^\circ\text{C}$, initially 40.0 psig H_2 , stirring = 1000 rpm.), has been tested for its ability to catalytically hydrogenate cyclohexene. The results of following the formation of a Ziegler–type hydrogenation catalyst from this system by the cyclohexene hydrogenation reporter reaction method [50,130,133] are shown here for the first time, Figure 2.5 (for complete experimental details see the Supporting Information).¹⁷ The hydrogenation curves show the production of active Ziegler–type hydrogenation catalysts after an induction period, but the curves end abruptly upon total consumption of cyclohexene, and do not have a truly sigmoidal shape. The same, now well precedented nanocluster formation mechanistic model discussed above (nucleation $\text{A} \rightarrow \text{B}$ (rate constant k_1), and autocatalytic growth $\text{A} + \text{B} \rightarrow 2\text{B}$ (rate constant k_2) [130]) was employed, but failed to produce good fits in the latter portions of the curves. A representative hydrogenation curve is shown, and the fitting results are given, Figure 2.5. The different systems and conditions used prohibit direct comparison between these experiments and the findings of Bönemann and coworkers. However, the use of slow-forming catalysts, even if such model systems are not what are desired industrially, appears to be one important way in which new insights could be gained. Hence, the $\text{Pt}(\text{acac})_2$ plus AlR_3 system is one of interest for further studies.

¹⁷ Other systems surveyed for use as model Ziegler–type hydrogenation catalysts are $[(1,5\text{-COD})\text{Ir}(\text{acac})]$, $[(1,5\text{-COD})\text{Rh}(\text{acac})]$, $\text{Rh}(\text{acac})_3$, $\text{Co}(\text{acac})_2$. The results of these previously unpublished hydrogenation survey experiments are also given in the Supporting Information for the interested reader.

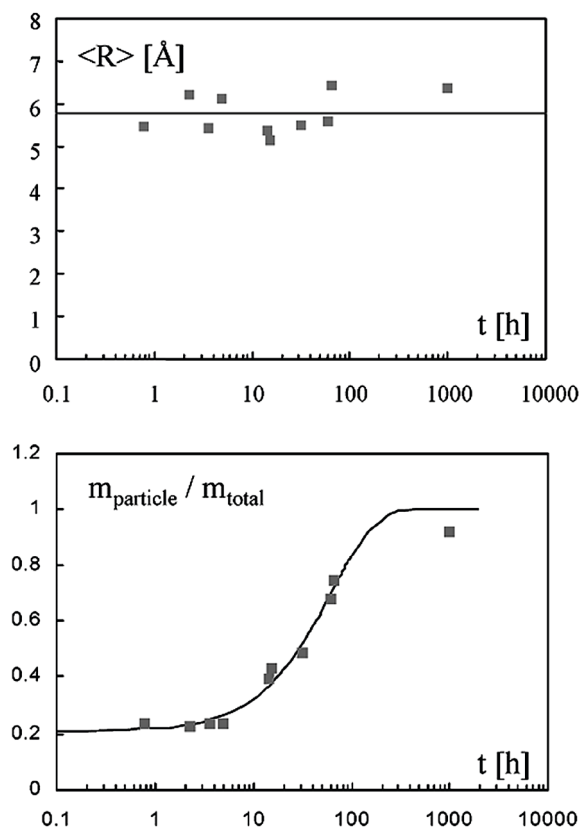


Figure 2.4. The results of in-situ ASAXS to monitor the formation of Pt(0) nanoparticles by Bönemann and coworkers [124]. The mean particle radius (top) remained essentially constant from the time particles were first detected, and up to 1000 hours attesting to particle stability (mean particle diameter = 1.2 nm). The mass fraction ($m_{\text{particle}}/m_{\text{total}}$) of Pt atoms in nanoparticles as a function of time (bottom) fit with an empirical exponential model. Reprinted with permission.

Bönemann and coworkers reported the presence of a binuclear Pt complex $\text{Me}_4\text{Pt}(\mu\text{-AlMe})_2\text{PtMe}_4$ as an intermediate in the formation of Pt nanoparticles [122,123,124]. Its existence and structure were investigated using ^1H and ^{13}C NMR, MS, XPS and EXAFS studies. Decomposition of the binuclear platinum intermediate lead to “nucleation” of the 1.2 nm, $\text{Pt}_{\sim 55}$ nanoparticles. From the in-situ ASAXS experiments, the rate of “nucleation” was found to be linearly proportional to the concentration of the binuclear intermediates. Bönemann and coworkers concluded, therefore, that the rate-determining step in nanocluster formation is the decomposition of the binuclear intermediate. A word and picture mechanism of colloid

formation from the work of Bönemann and coworkers [124] is reproduced below, Scheme 1.7. In the absence of excess AlMe_3 or $\text{AlMe}_2(\text{acac})$, an insoluble “Pt nanopowder” was observed made of 1.4 nm diameter clusters [123].

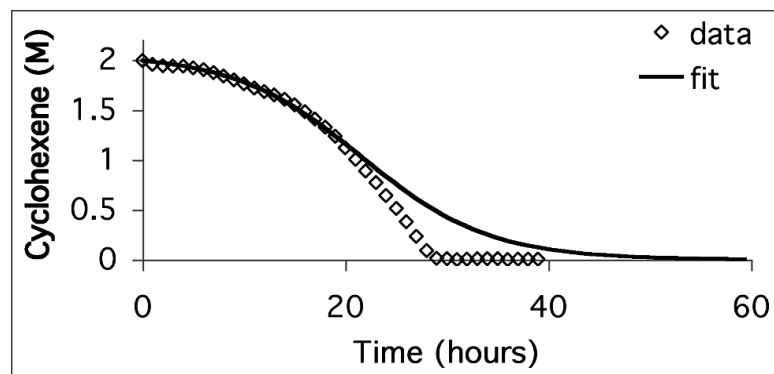


Figure 2.5. A representative reaction of $\text{Pt}(\text{acac})_2$ plus 4 AlEt_3 followed by the cyclohexene hydrogenation reporter reaction method [50,130,133] ($[\text{Pt}] = 1.2 \text{ mM}$, solvent = toluene, temperature = $22.0 \text{ }^\circ\text{C}$, initially 40.0 psig H_2 , stirring = 1000 rpm), and attempted fit of the data using the now well-established $\text{A} \rightarrow \text{B}$ (rate constant k_1), $\text{A} + \text{B} \rightarrow 2\text{B}$ (rate constant k_2) mechanistic model for nanocluster nucleation and autocatalytic growth [130]. The resulting rate constant values taken from 5 such runs are $k_1 = 0.004 \pm 0.002$, and $k_2 = 0.09 \pm 0.03$. All the fits obtained were similarly poor in the last part of the curve, with a range of R^2 values of 0.9491–0.9954.

In the soluble, stabilized nanoclusters, the stabilizer layer has been referred to by Bönemann and coworkers as an “organo-aluminum protecting shell” [121]. In-situ ^1H NMR studies confirmed an exchange reaction between the methyl groups of AlMe_3 and the acac ligands from $\text{Pt}(\text{acac})_2$, resulting in the appearance of $\text{AlMe}_2(\text{acac})$ peaks [122,124]. Protonolysis of a sample of the dry colloid allowed the calculation that 6 active Al–C bonds per Pt atom exist in the stabilizer of Pt nanoclusters. The representation of the resulting stabilized cluster is shown, Scheme 1.7.

Bönemann and coworkers also analyzed the products formed upon the reaction of $[(1,5\text{-COD})\text{Pt}(\text{CH}_3)_2]$ plus 10 AlEt_3 or $\text{Al}(\text{C}_8\text{H}_{17})_3$ [126]. As with other systems studied, the solution became a brown/black color upon the addition of AlR_3 . The presence of $\text{Pt}(0)_{13}$ nanoclusters was

interpretation could be supported by a distinct bimodal size distribution obtained from TEM images. However, this was not provided; the reported size and dispersity do not correlate well with truly monodisperse, precise 13 and 55 Pt atom particles as reported. Truly monodisperse nanoparticle samples are rare: single crystals of thiol-protected Au₁₀₂ nanoparticles are, for example, one case of a *truly* monodisperse nanoparticle sample [134].

The timescale of the reaction varied between 1 hour to more than one month depending on the temperature and whether Al(C₈H₁₇)₃ or AlEt₃ was used. No color change was observed using AlMe₃, implying the absence of nanoclusters in the resulting solution. However, the authors did not mention the temperature or time allowed for observation, so that observation does not rule out possible nanocluster formation with AlMe₃ as the cocatalyst. Bönemann and coworkers [126] believed that β-H elimination was rate-determining in nanocluster formation, yet that explanation is not necessarily consistent with the observation of cluster formation in their own Pt(acac)₂ plus AlMe₃ system [121-125], or with catalyst formation using AlMe₃ in other systems [4,71]. Furthermore, if β-H elimination is rate-determining, one might have expected faster cluster formation with AlEt₃ than with Al(C₈H₁₇)₃, since the former has 50% more β-H's (and if one assumes an equal amount of Al-alkyl is present in each case at the rate determining step). Moreover, β-H elimination is typically very facile in organometallic chemistry and rarely a rate-determining step to our knowledge [10]. Clearly, there are many aspects of the mechanism of formation of Ziegler nanoclusters that require further explanation.

Bönemann and coworkers have several other, valuable publications dealing with interesting topics that are related to Ziegler-type hydrogenation catalysts. Other research on the Pt(acac)₂ plus 4 AlMe₃ system was focused on the characterization of networks formed by the nanoclusters [135,136]. Syntheses starting with Ni(COD)₂ and AlEt₃, and using high

temperatures, resulted in the formation of NiAl_x materials [137,138]. Another system gave ~ 10 nm $\text{Co}(0)_n$ nanoclusters by the combination of $\text{Co}_2(\text{CO})_8$ and AlR_3 [139]. These studies, however, are beyond the scope of this review; the interested reader is referred to those original publications [135,136,137,138,139].

It is still unclear why *cluster* formation is relatively slow in both the $\text{Pt}(\text{acac})_2$ plus 4 AlEt_3 and $[(\text{COD})\text{Pt}(\text{CH}_3)_2]$ plus 10 AlEt_3 , or $\text{Al}(\text{C}_8\text{H}_{17})_3$ systems investigated by Bönemann and coworkers, when *catalyst* formation is rapid in virtually all other systems explored [37]. One possible explanation of this is that the heterogeneous component observed in some systems is the product of catalyst deactivation, as has been observed in a $\text{Ni}(\text{diisopropylsalicylate})_2$ plus AlR_3 system with aromatic solvents [70]. Another conceivable explanation, in light of the studies of Schmidt and coworkers [19,81,113,114] (who showed the presence of nanoclusters in systems of active hydrogenation catalysts) and the results in Figure 2.5, *vide supra*, showing an induction period prior to the catalytic hydrogenation of cyclohexene using a similar $\text{Pt}(\text{acac})_2$ plus 4 AlEt_3 system, is that the slow cluster formation reaction is inherent to the use of these particular precursors, conditions, or both. These studies serve to again illustrate the importance of kinetic experiments in studies attempting to determine the true catalyst. Notable here is that the slow formation of these systems could be exploited in the pursuit of a more detailed investigation into the kinetics and mechanism of Ziegler–nanocluster formation, a key goal in the field of Ziegler–type hydrogenation catalysts.

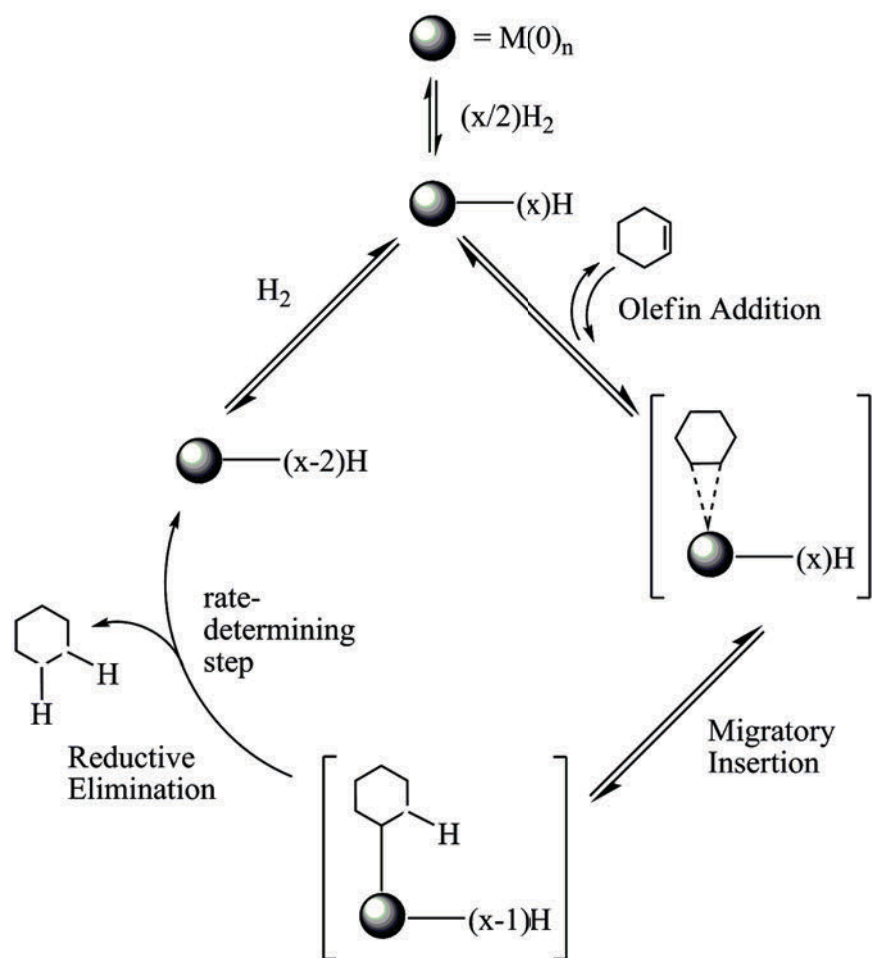
2.2.2.5. *Systems investigated by Alley, Hamdemir, Wang, Frenkel, Li, Yang, Menard, Nuzzo, Özkar, Johnson, and Finke: $[(1,5\text{-COD})\text{Ir}(\mu\text{-O}_2\text{C}_8\text{H}_{15})]_2$ plus AlEt_3 [52,53,54], $\text{Co}(\text{neodecanoate})_2$ plus AlEt_3 [55], and $\text{Ni}(2\text{-ethylhexanoate})_2$ [56] plus AlEt_3 .* Model and industrial Ziegler–type hydrogenation catalyst systems that have recently been under

investigation by the above-noted team include AlEt_3 plus $[(1,5\text{-COD})\text{Ir}(\mu\text{-O}_2\text{C}_8\text{H}_{15})]_2$ [52,53,54], $\text{Co}(\text{neodecanoate})_2$ [55], or $\text{Ni}(2\text{-ethylhexanoate})_2$ [56]. Studies have been carried out using a variety of analytical methods including kinetic measurements, TEM, MALDI MS, EXAFS, XPS, and NMR. Interestingly, the catalytic activity of the Ir model system varies inversely with Ir concentration, similar to the [Co]-dependent TOF results reported by Schmidt and coworkers using their $\text{Co}(\text{acac})_{2,3}$ plus AlEt_3 system already discussed [113]. Some of the other key results thus far appear to be that the precatalyst plus cocatalyst reactions in these Ziegler-type catalyst systems produce a mixture of sub-nanometer *and* amorphous $\text{M}(\text{O})_n$ nanoclusters, and that this result would have gone unrealized without using a combination of analytical methods. This review is one of the necessary first steps of the studies in progress, work currently in various stages of preparation for publication [53,54,55,56].

The above group has also briefly investigated the mechanism of cyclohexene hydrogenation using a Ziegler-type hydrogenation catalyst made from $\text{Co}(\text{neodecanoate})_2$ plus AlEt_3 , $\text{Al/Co} = 3$. A D_2 labeling experiment was used to determine the location of the rate-determining step with regard to the Schmidt mechanism shown back in Scheme 1.5. Based on those results, reported here for the first time, an updated mechanistic scheme is proposed, Scheme 2.8. A full description of the results and experimental details will be found by the interested reader in the Supporting Information. Briefly, the Co-based Ziegler-type hydrogenation catalyst was prepared in cyclohexane, cyclohexene substrate was added, and the vessel containing the solution was pressurized with D_2 . The amount of deuterium incorporation into the resulting hydrogenation product cyclohexane was analyzed by gas chromatography mass spectrometry, Figures SI-A6 and SI-A7, Supporting Information. The observation of a significant amount of cyclohexane containing > 2 deuterium atoms supports the precedented hypothesis, in

line with the accepted mechanism for heterogeneous transition metal catalyzed hydrogenations [140], that reductive elimination, as opposed to migratory insertion [42], is the rate determining step, with prior equilibria existing in the earlier step(s). In fact, this updated mechanism, Scheme 1.8, better explains the previous observation that the reaction becomes zero order in H_2 at pressures above 1.5 atm [42]. A caveat on these studies is that they are not complete as of this writing, so that their full findings and resultant insights remain to be completed.

2.2.2.6. Conclusions for the section on the nature and mechanism of formation of Ziegler–type hydrogenation catalysts. The following results appear to apply across different systems: (i) the exchange of ligands between AlR_3 and the precatalyst has been established by IR and 1H NMR spectroscopy; (ii) for $M(L)_2$ precatalysts plus AlR_3 , the resulting Al species present are $AlR_2(L)$, $AlR(L)_2$, $Al(L)_3$, or some combination of the three depending on the Al/M used, and the presence of additional impurities or additives such as H_2O ; (iii) the formation of alumoxanes (i.e., Al–O–Al complexes) and their contribution to the stabilizer layer of observed nanoclusters also has some precedent, but could still use additional study; and (iv) the most recent studies favor the hypothesis of $M(0)_n$ nanocluster catalysts. In these cases AlR_3 is generally believed to reduce the higher-valent transition metal from the precursor to the zero-valent state, and it or its reaction products are thought to ligate and stabilize the resulting $M(0)_n$ nanocluster catalyst. However, disagreement persists concerning the reaction forming Ziegler–type hydrogenation catalysts, and the nature of the catalysts themselves. Whether or not the catalysts are homogeneous or heterogeneous is still a central remaining issue, as is the composition of the active catalyst(s). In most cases, the kinetic studies required to answer the homogeneous versus heterogeneous catalysis question are lacking.



Scheme 2.8. A schematic catalytic olefin hydrogenation mechanism (shown here for cyclohexene for convenience) using Ziegler-type hydrogenation catalysts. The ball implies a transition metal nanocluster catalyst, but could also represent a monometallic catalyst. The postulated steps are oxidative addition of H_2 , olefin addition, migratory insertion to form an alkyl hydride species, and irreversible, rate-determining reductive elimination yielding the saturated cyclohexane. Evidence for reductive elimination being rate limiting is our observation of multiply deuterated (> 2 deuterium atoms) in the hydrogenation product of cyclohexene (the results and experimental details are given in the Supporting Information for the interested reader). The actual timing of oxidative addition of H_2 versus olefin addition steps is a standard mechanistic ambiguity [38], so that the H_2 activation (first) pathway is shown only for the sake of illustration.

Several factors conspire to make solving the homogeneous or heterogeneous catalysis question especially difficult for Ziegler-type catalyst systems. The high sensitivity of Ziegler-type hydrogenation catalyst systems to factors such as air and water complicates reproducible catalyst preparation, and has probably contributed to the occasional contradictory

characterization results seen for otherwise ostensibly similar systems. There is also the possibility that some Ziegler–type catalyst systems are homogeneous and some are heterogeneous, especially when considering the identities of the catalyst precursor components in different systems. This sentiment was expressed by Breslow and Newburg back in 1959 [23], “It is our belief that there is not one, but a family of Ziegler–type catalysts.” Even given identical systems, the variables of the synthesis procedure affect catalyst activity and may lead to modifications in the nature of the resulting catalyst. This was recognized by Barrault et al. [37], who noted that “the nature of these complexes is largely controlled by differences in preparation.” In other words, despite the narrow definition used herein for Ziegler-type hydrogenation catalysts, the creation of fundamentally different catalysts from similar *or even identical* starting materials may occur because of differences in other variables in the catalyst preparation, or conditions employed during analysis [10,17]. This is a reflection of an insight of Halpern’s from the mechanistic study of organometallic systems [141,142], which “underlines the danger of assuming the mechanisms... or of extrapolating from one system or set of conditions to another (even closely related) one” [141]. Hence, it is certainly possible that small changes may alter the state of the transition metal from single metal complexes to multimetallic nanoclusters, which are quite different species and catalysts.

Despite the conflicting reports that exist concerning the homogeneous or heterogeneous nature of Ziegler–type polymer hydrogenation catalysts, there is good reason to believe that, in many systems and under conditions commonly employed, there is at least a heterogeneous, nanocluster, or possibly sub-nanocluster component to the active catalysts [16]. That early researchers favored the conclusion that Ziegler–type hydrogenation catalysts are homogeneous makes perfect sense. The prior lack of examples of organic-solvent-soluble nanoclusters, and

prior lack of knowledge of the kinetics and mechanism of formation of transition-metal nanoclusters, meant that it simply was not possible to routinely know when soluble nanocluster catalysts were both forming and then serving as the kinetically dominant catalyst [16].¹⁸ The recent observation of Ziegler nanoclusters in some systems is a direct result of characterizations using modern methods such as TEM, XAFS, and ASAXS. The availability and improvement of other, advanced analytical methods may eventually assist in the disproof of the homogeneous or heterogeneous catalyst hypothesis for a given system and set of conditions. Another reasonable hypothesis warranting disproof is that of the simultaneous existence of both homogeneous *and* heterogeneous active catalysts in a single system. Additionally, results from studies under well-documented conditions using *well defined precursor materials* (i.e., and in comparison to the common, but somewhat ill-defined, industrially used Ni and Co precursors) promises to allow generalization of any important findings [52]. Ideally, such studies would simultaneously be able to detect the effects of catalyst preparation variables on both catalyst properties *and* catalyst composition and structure (vide infra).

2.3. A closer look at the more general homogeneous versus heterogeneous catalysis question

2.3.1. The 1994 four-prong methodology

Since it is central to the main unanswered question of industrial Ziegler-type hydrogenation catalysts, namely are they “homogeneous” or “heterogeneous” (or both), we conclude with a last section before the summary on the current methods and approaches to this historically challenging, if not perplexing, research question. In 1994, a *multi-pronged*

¹⁸ Ziegler-type $M(O_2CR)_2/AlR_3$ catalysts were listed in our 2003 review [16] on the “is it homogeneous versus heterogeneous catalysis?” question as systems where heterogeneous catalysis is strongly suspected, but where studies confirming or refuting this suspicion are needed.

approach with kinetic studies at its heart¹⁹ was published [12]. That approach emphasizes using multiple analytical techniques and the requirement that any proposed explanation of the catalyst must satisfy *all* the data [13,16]. The approach has been shown to be successful in addressing the homogeneous versus heterogeneous catalysis question on at least four occasions [12,15,17,18]. The approach was the outgrowth of a painstaking, 5-year study that eventually identified novel, highly stabilized, as well as highly catalytically active $\text{P}_2\text{W}_{15}\text{Nb}_3\text{O}_{62}^{9-}$ polyoxoanion-stabilized $\text{Ir}(0)_{\sim 300}$ nanoclusters as the true catalyst in hydrogenation systems beginning with $[(1,5\text{-COD})\text{Ir} \cdot \text{P}_2\text{W}_{15}\text{Nb}_3\text{O}_{62}]^{8-}$ as precatalyst under H_2 and in the presence of cyclohexene, Figure 2.6.

A more general solution to the homogeneous vs. heterogeneous catalysis problem, diagrammed in a simplified form, Figure 2.7, resulted from that work because the polyoxoanion-stabilized nanoclusters turned out to be the most highly anionically stabilized nanocluster known at the time, and thus very “homogeneous-like” [12]. This extreme-case-developed methodology has since proven able to identify nanoparticle catalysts in at least 3 of 4 systems previously believed to be homogeneous catalysis [12,15,17,18]. The methodology even detected both homogeneous and nanocluster heterogeneous catalysis derived from a Rh-system,

¹⁹ Support for the central importance of kinetic experiments in catalyst studies comes from, as Halpern put it, “the fact that catalysis is, by definition, purely a kinetic phenomenon” [89].

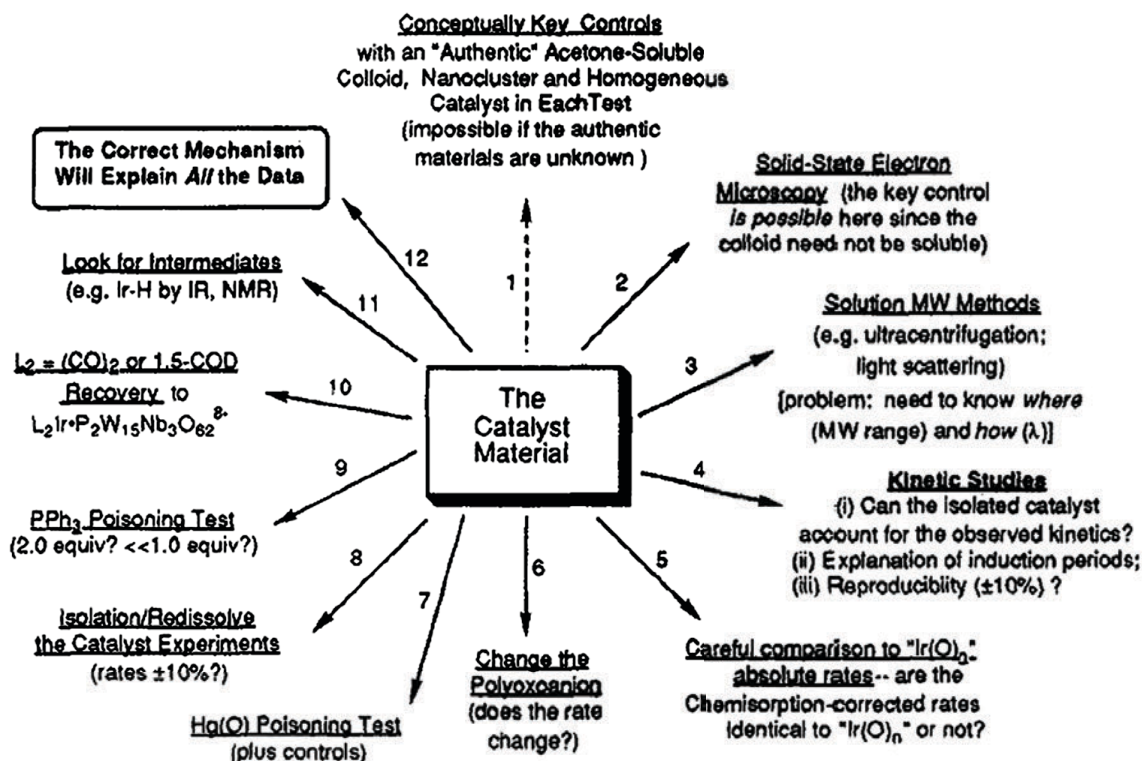


Figure 2.6. The multi-step approach developed for distinguishing homogeneous from heterogeneous catalysis in acetone-soluble Ir(O)_n nanocluster systems formed from a [(1,5-COD)Ir^I•P₂W₁₅Nb₃O₆₂]⁸⁻ catalyst precursor under H₂ in acetone and in the presence of cyclohexene at room temperature [12]. Reprinted with permission.

[Rh(C₅Me₅)Cl₂]₂, in which the nature of the catalyst changed depending on the conditions used [17]. Note that the goal is not to try the impossibility of “proving” that Ziegler–type hydrogenation catalysts are nanoclusters, but rather to have a way to rule out—that is to falsify, to disprove—all but one of the competing hypotheses for the nature of the true catalyst in a given system and for a specific set of conditions [143], leading to a set of data consistent with, and strongly supportive of, ideally one remaining hypothesis regarding the true catalyst(s). Figure 2.8 provides the most current, “6-prong approach” to the “is it homogeneous or heterogeneous catalysis?” question.

Because this methodology ideally involves the use of all relevant techniques with the realization that a proposed answer must explain all the data for a given system, any interpretation

These exist because Ziegler–type hydrogenation catalysts are: (i) notoriously sensitive to both the variables in their preparation (see section 2.1 above), and sensitive to conditions during characterization experiments; (ii) difficult to isolate for the needed kinetic studies; and (iii) prone to giving spurious results in poisoning experiments, especially since *selective* poisons for the AlR_3 -derived component and, separately, for the transition-metal components are needed, but do not exist at present. Efforts to isolate Ziegler–type hydrogenation catalysts in their resting state have often met with failure (e.g., $\text{M}(\text{2-ethylhexanoate})_2$ plus $m \text{ AlEt}_3$, $\text{M} = \text{Ni}$ or Co , $m = 3\text{--}4$, and $\text{Co}(\text{stearate})_2$ plus 2 AlEt_3 systems)[58,67]. Early successful efforts required use of non-Ziegler–type catalyst models such as $[(\alpha,\alpha'\text{-bipyridyl})\text{NiMe}_2]$, [4] or experiments under atypical conditions such as low temperatures [4,58,105]. The 2005 and 2006 work of Schmidt and coworkers [19,81,113], and 1999-2005 work of Bönemann and coworkers [121-124,126], reports successful isolation of the catalyst-related material, and nanocluster materials, respectively. However, the handling procedures required for isolation of these materials, which often involves removal of the solvent under vacuum, washing the residue with hexane, and drying, may influence the nature of the material, the characterization results, or both [146]. This is especially true for the use of TEM, which despite some recent success [19,81,113,121-124,126], has also given results that were highly dependent on the method of sample preparation in some Ziegler–type catalyst systems [9]. Furthermore, and as already mentioned, without checking for artifacts when using TEM (by control experiments and complementary characterization techniques), misleading change in, or damage to, the sample from the electron beam of the TEM may occur and go undetected [17,127]. *This is especially true for TEM of Ziegler–type catalyst samples of the relatively light elements of Ni and Co*, which are more

susceptible to certain types of TEM-beam-induced damage in addition to poor contrast and image quality [147].

Normally, quantitative catalyst poisoning experiments using established poisons such as CS_2 have the potential to give definitive results [148]. Less than 1 equivalent of poison should be needed to completely kill catalyst activity if the catalyst is a particle with only a fraction of transition metal atoms on its surface. However, if a full equivalent of poison is needed it may indicate a molecular homogeneous catalyst [16]. The use of such poisons with Ziegler-type hydrogenation catalysts is problematic because the Lewis acidic AlR_3 component can be expected to compete with the transition metal for the poison—again, ideally two types of selective poisons are needed. Attempts to use alcohol in catalyst poisoning led to contradictory results, as has already been discussed [57,75,114]. Poisoning Ziegler-type hydrogenation catalysts with $\text{Hg}(0)$ —a (non-definitive, but often useful) test of heterogeneous catalyst formation—suffers from the possibility that $\text{Hg}(0)$ might also poison homogeneous complex catalysts or catalyst precursors [16]. Difficulties with the $\text{Hg}(0)$ poisoning test have been discussed elsewhere [90]. Additionally, control experiments to illuminate or rule out these effects would need to take into account the fact that most Ziegler-type hydrogenation catalysts are rapidly pre-formed before use in hydrogenation.

Finally, the requirement that the correct explanation be consistent with all the data is an important, but tall order for Ziegler-type hydrogenation catalysts. A lot of conflicting data on what appears to be comparable systems exists. This requirement is, nevertheless, one that will have to be met before a systematic understanding of Ziegler-type hydrogenation catalyst systems is realized.

2.3.3. *Conclusions for the section on the more general homogeneous versus heterogeneous catalysis question*

Despite the success of the 1994 approach in Figures 2.6 and 2.7, applying it toward determining the true nature of Ziegler–type hydrogenation catalysts is changing and upgrading that approach [53,54,55,56]. However, it must be remembered that the approach in Figures 2.6 and 2.7 is nothing more than a guideline for one’s own, creative thinking and approach for the specific, “true catalyst determination” problem and catalyst at hand. The central tenets of the methodology should still apply: (i) find what form or forms the precursor materials take in a sample of the resting state(s) of the catalyst; (ii) perform kinetic studies from resting state(s) to determine which are the kinetically competent/dominant species; (iii) use all available/applicable techniques; and (iv) eliminate all reasonable alternative hypotheses to arrive at, ideally, a unique catalyst formulation that accounts for all the data.

The ideal goal in this updated approach to the “homogeneous versus heterogeneous catalysis” problem is the *simultaneous spectroscopic and kinetic analysis of a catalyst at the desired or normal operating conditions*, that is, via “operando” spectroscopy (the term “operando” is from the Latin for “working” or “operating”) [149,150,151,152]. This combination overcomes weaknesses of using either kinetic [89, 153] or spectroscopic analysis alone [152], especially if *multiple* spectroscopic techniques are simultaneously used [154]. However, the use of operando spectroscopy requires overcoming difficult challenges in experiment and reactor cell design [154]. Considerable challenges are likely to be encountered in any attempt to analyze Ziegler–type hydrogenation catalysts by operando spectroscopy. The use of an experimental setup, no matter how sophisticated, cannot supplant the importance of using Platt’s method of disproof of all reasonable alternative hypotheses [143].

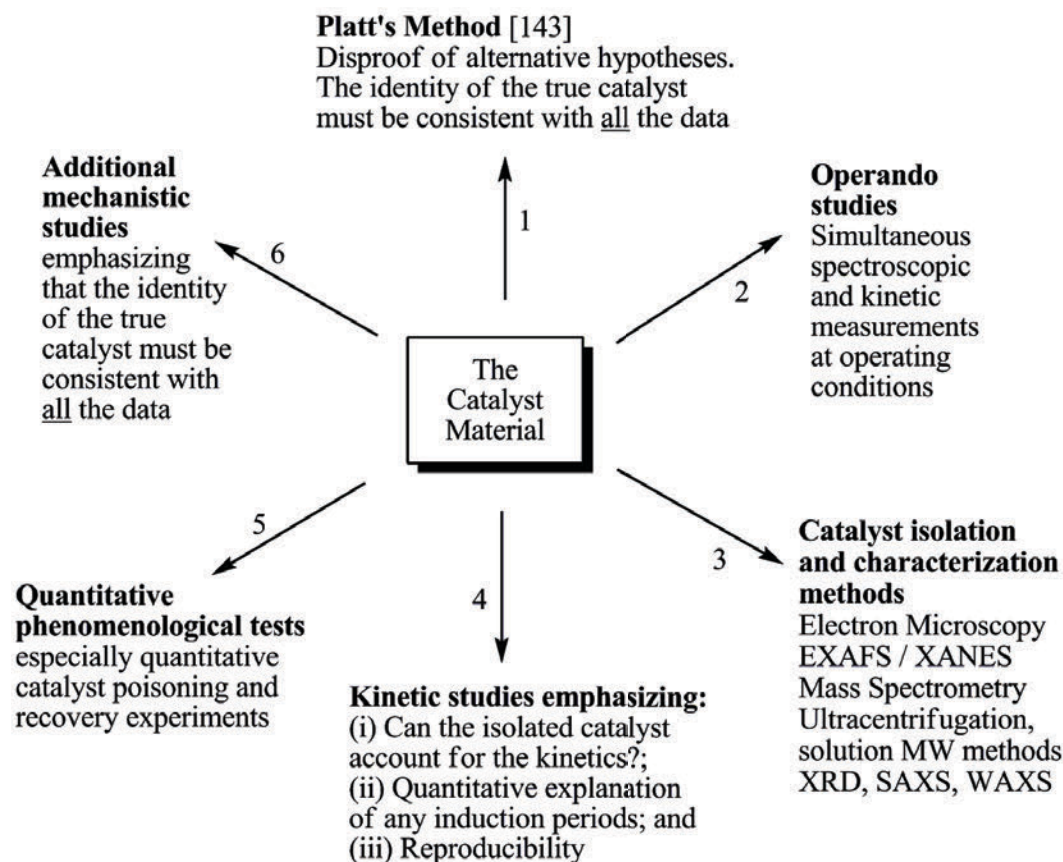


Figure 2.8. The updated “six-prong” approach for distinguishing homogeneous from heterogeneous catalysis, updated to include operando spectroscopy. The basic principles, however, remain the same: (i) find what form or forms the precursor materials take in a sample of the resting form(s) of the catalyst; (ii) perform kinetic studies from resting state(s) to determine which are the kinetically competent/dominant species; (iii) use all available/applicable techniques; and (iv) eliminate alternative hypotheses [143] to arrive at, ideally, a unique explanation that accounts for all the data.

3. Summary

The key points from the introduction section are:

- Ziegler–type hydrogenation catalysts made of group 8–10 transition metal precatalysts, particularly first row metal chelates or carboxylates, and AlR_3 cocatalysts, are important for the industrial hydrogenation of a variety of unsaturated organic compounds, including diene polymers. Ziegler–type *hydrogenation* catalysts should *not* be confused with Ziegler–Natta *polymerization* catalysts, which were not a part of this review.

- Despite their relatively long history of industrial use, there is a need for an improved fundamental understanding of Ziegler–type hydrogenation catalysts. That improved understanding should, in turn, drive further *rationally-directed* synthetic, mechanistic, and industrial improvements.
- The key general areas investigated in the literature can be categorized as: (i) the variables important to catalyst synthesis and their effect on catalyst properties, particularly hydrogenation activity, (ii) the reaction between the transition metal precatalyst and cocatalyst components, (iii) the compositional and structural nature of the active catalyst species, and (iv) the mechanism of catalytic hydrogenation.

The main findings from the section on catalyst preparation variables are:

- The most important variables of catalyst preparation appear to be: (i) the identities of the transition metal precatalyst and the organometallic cocatalyst; (ii) the ratio of these two components and the role of impurities, particularly H₂O; (iii) the solvent; (iv) the identity of the substrate; (v) the details of component addition (such as order and rate, presence of substrate, atmosphere, and temperature); and (vi) the aging of prepared catalyst before use in hydrogenation reactions.
- Catalysts made from Ni or Co precursors are favored by industry. They tend to have the highest activities, and have an advantageous balance of desirable properties, low cost, and relative ease of preparation.
- The anions present are another important aspect of the identity of the precatalysts. Anions such as 2-ethylhexanoate and acac are the most popular for use and study. The activity of catalysts made with these precursors appears to be positively correlated to

their solubility. Some precatalyst anions, especially halogens, reduce catalyst activity, likely by acting as poisons.

- Short chain AlR_3 cocatalysts, particularly AlEt_3 , are most commonly used. The preferred cocatalyst varies with the particular system.
- One of the main variables appears to be the Al/M ratio. Most studies seem to agree that there is an optimum Al/M ratio for most systems. The optimum Al/M ratio has been reported to exist due to incomplete activation at too low Al/M and poisoning by excess AlR_3 at high Al/M. Water and other impurities have been reported to have both beneficial and detrimental effects, depending on the particulars of the system being studied, and appear to affect the optimum Al/M ratio. The optimum Al/M ratio is one of the areas where a greater fundamental understanding of the nature of the catalyst for each given system could help to make sense of the range of results observed in the literature.
- The other variables involved in catalyst preparation (the solvent, the substrate, the order and rate of component addition, the presence or absence of substrate, the atmosphere, the temperature, and catalyst aging before use) are not universally agreed to be important. However, in most cases, they have been reported as having an effect on the activity of the resulting catalyst, but generally less so than the identity of the catalyst precursors, the Al/M ratio, and the amount of H_2O present. Many variables are likely connected to each other in complicated ways, such as the Al/M ratio and the amount of H_2O , but these relationships are incompletely understood.

- Mass transfer limitations should be suspected in many studies for these active catalysts, and unless the control experiments designed to rule out MTL were specifically done and reported in detail. This is especially true for instances where reports claim that certain catalyst preparation variables were not important to catalytic activity, but other reports claim that they are.
- The ability to explain the effects of variables in the preparation of Ziegler–type hydrogenation catalysts is hampered by the fact that the effects themselves are often dissimilar for ostensibly similar, but in fact different systems. Answers as to *how* variables in catalyst synthesis affect catalytic activity are needed and are possible from studies of the ways in which each variable affects the mechanism of formation, composition, and resultant structure of the catalyst. Ultimately being able to connect the variables to catalyst activity, composition, structure and formation mechanism remains a significant challenge.

The main findings from the section on the nature and mechanism of formation of Ziegler–type hydrogenation catalysts are:

- The most important unknowns in Ziegler–type hydrogenation catalysis are the reaction between the catalyst precursors, whether the resulting catalysts are homogeneous or heterogeneous, and the details of the mechanism of catalytic hydrogenation? The most important of these questions is the nature of the true catalyst. Specific questions in this regard include: (i) how is the catalyst formed, (ii) how many transition metal atoms constitute the active catalyst species, (iii) what are their oxidation states, and (iv) what is the composition, structure, and role of the cocatalyst?

- Ziegler assumed early on that the catalyst of the Ni effect took the form of colloidal Ni. Early efforts by Wilke and coworkers attempted to disprove this, and to show that the catalyst could be a homogeneous allyl-complex. That classic work laid the groundwork for subsequent researchers of Ziegler-type *hydrogenation* catalysts to propose homogeneous catalysts for those systems. More recent research, with the aid of much improved instrumentation technology and improved precedent for hydrocarbon-soluble colloids, has obtained results that suggest the true catalysts are heterogeneous, what we have termed herein as “Ziegler nanoclusters.”
- Definitive *kinetic* evidence remains to be reported for many Ziegler-type hydrogenation catalyst systems. Without that data, the homogeneous versus heterogeneous catalysis question cannot be answered.
- It may be that no single type of catalyst results for Ziegler-type hydrogenation catalyst systems. Small but important differences in outwardly similar systems may cause fundamental differences in the type(s) of catalyst(s) present. This, in turn, reveals the importance of using well-defined catalyst precursors, and carefully controlled conditions, in the needed studies attempting to identify the true catalyst(s). Additionally, some Ziegler-type hydrogenation catalyst systems may *simultaneously* contain catalytically active homogeneous *and* heterogeneous components. If so, it will take an extraordinarily careful, comprehensive, and detailed effort, all on the right/“best” system, to definitively support this particular hypothesis.

The key messages from the section taking a closer look at the more general homogeneous versus heterogeneous catalysis question are:

- A multi-pronged approach, demonstrated on multiple occasions to be successful, exists for distinguishing between homogeneous versus heterogeneous catalysis. Explicit application of that approach in addressing the homogeneous versus heterogeneous catalysis question for Ziegler-type hydrogenation catalysts, is proving useful in work underway [53,54,55,56].
- There are special challenges to answering the homogeneous versus heterogeneous catalysis question for Ziegler-type hydrogenation catalysts: (i) they are typically very sensitive to both the variables in their preparation, and conditions during characterization experiments; (ii) they have been difficult to isolate for the needed kinetic studies; and (iii) poisons selective for each of the metal and Al-based components do not currently exist.
- The multi-pronged approach to the homogeneous versus heterogeneous catalysis problem has been updated to include operando spectroscopy for catalyst characterization.

We would like to end by noting that, despite the many challenges summarized in this review, Ziegler-type hydrogenation catalysts hold considerable promise for other applications. Ziegler-type hydrogenation catalysts are, despite the homogeneous versus heterogeneous catalysis question, largely unrecognized as hydrocarbon soluble, readily self-assembled catalysts with neutral charge, high activity, and long lifetime, at least in many of the cases examined herein. Additional catalytic application, fundamental kinetic, spectroscopic, as well as other studies are strongly encouraged, regardless of whether Ziegler nanoclusters are the true catalysts in all, or even selected, cases.

4. Supplementary data

Supplementary data associated with this article can be found, in the online version, at doi: 10.1016/j.molcata.2009.07.007.

Supplementary Tables 2.A

See Tables 2.A.1–2.A.3.

Table 2.A.1. Patent Literature

Authors (Year)	Catalyst Systems	Other Variables in Catalyst Synthesis	Ref.
Breslow and Matlack (1963)	Ti(<i>i</i> -Pr) ₄ , V(<i>n</i> -Bu) ₃ , Cr(acac) ₃ , MoO ₂ (acac) ₂ , Mn(acac) ₃ , Ru(acac) ₃ , Co(acac) ₃ , Fe(acac) ₃ , Ni(acac) ₂ , or Pd(acac) ₂ + Al(<i>i</i> -Bu) ₃	<i>Solvent</i> : <i>n</i> -heptane, or heptanes. <i>Hydrogenation Substrate</i> : Cyclohexene, 1-octene, ethynylbenzene, polyisoprene rubber, 2-methylbutene-2, hexane-1, or tetramethylethylene. <i>Order of addition</i> : cocatalyst added to the precatalyst in both the presence and absence of substrate. <i>Synthesis atmosphere</i> : H ₂ gas at 50 psi, 43 psi, 40 psig, 21 psig, or 35 psig. <i>Synthesis temp</i> : room temp, 40 °C, 50 °C, 30 °C.	59
Laporte, S. (1965)	Ni(acac) ₂ , Fe(acac) ₂ , Ni(benzoate) ₂ , Ni(acac) ₂ , Cr(acac) ₂ , Co(acac) ₂ , or Cu(acac) ₂ + 1–5, 8 or 30 AlEt ₃ or BEt ₃	<i>Solvent</i> : Benzene. <i>Hydrogenation Substrate</i> : Benzene, <i>o</i> -xylene, 1,3-butadiene, 4-vinylcyclohexane, 1,5,9-cyclododecatriene, naphthalene, methyl ethyl ketone, maleic anhydride, cinnamic acid, benzoic acid, dimethyl terephthalate, benzaldehyde, dimethylphthalate, phenol, nitrocyclohexane, isophthalonitrile, pyridine, aniline, nitrobenzene, 3-hexyne. <i>Order of addition</i> : cocatalyst added to precatalyst in the presence of substrate. <i>Synthesis atmosphere</i> : N ₂ ; <i>Synthesis temp</i> : –50 °C to 200 °C	72
Kroll (1968)	Co(acac) ₂ , Fe(acac) _n , Ni(acac) _n , Pt(acac) _n , Cr(acac) _n , V(acac) _n ^a + 4, 6, 8, 10 or 35 Al(<i>i</i> -Bu) ₃ , AlEt ₂ (<i>n</i> -BuO), AlMe ₂ (acac), AlEt ₃ , or AlH(<i>i</i> -Bu) ₂ , Al(<i>i</i> -Bu) ₃ ⁻	<i>Solvent</i> : Heptane, dimethoxyethane, triethylamine, benzene, decane, <i>p</i> -dioxane, <i>p</i> -xylene, pentane, ether, dimethoxyethane. <i>Hydrogenation Substrate</i> : Cyclohexene, <i>cis</i> , <i>trans</i> , <i>trans</i> -cyclododecatriene, benzonitrile, quinoline, cyclopentadiene, benzophenone, 4-vinylcyclohexene, phenylacetylene, 1-hexene, <i>n</i> -methylmorpholine, anisole, diphenylether, cyclododecatriene, octyne-4, dicyclopentadiene,	64

Authors (Year)	Catalyst Systems	Other Variables in Catalyst Synthesis	Ref.
	p-dioxane, AlEt ₂ Cl/AlEtCl ₂	cyclooctadiene, 3-methyl-1-butene, 2-methyl-2-butene. <i>Order of addition:</i> Precatalyst + cocatalyst (substrate is not mentioned). <i>Synthesis atmosphere:</i> N ₂ . <i>Aging:</i> Overnight, or 5 min. Additional notes: “The stability and/or activity of Ziegler-type catalysts is markedly improved by the addition of a third component, i.e., Lewis base such as p-dioxane or SEt ₂ , weak organic acid such as n-butanol or t-butylalcohol, oxygen, to the catalyst system.”	
Yoshimoto et al. (1970)	Ni naphthenate, Co(acac) _n , ^a Fe naphthenate, bis (salicylaldehyde)Ni, Ni cyclohexylcarboxylate, Co octanoate, or Co naphthenate + 3, 4, or 12 AlEt ₃ , MgEt ₂ , (n-Bu)Li, or LiAlH ₄ , Ni benzenesulphonate or Ni p-toluene sulfonate + AlEt ₃	<i>Solvent:</i> Toluene, hexane, tetrahydrofuran, or n-hexane. <i>Hydrogenation Substrate:</i> Butadiene units of styrene butadiene copolymer. <i>Order of addition:</i> Precatalyst and cocatalyst are mixed in the presence of olefinically unsaturated hydrocarbon which does not act as hydrogenation substrate. <i>Synthesis atmosphere:</i> N ₂ or H ₂ . <i>Synthesis temp:</i> 30 °C, 29 °C, 28 °C, 80 °C, 50 °C, -78 °C. <i>Aging:</i> 5 min. Additional notes: An olefinically unsaturated hydrocarbon such as cyclohexene, 1-heptene, dicyclopentadiene, styrene or 1,7-octadiene, is added to the reaction medium to form the, so called, “three components catalyst.” The use of olefinically-unsaturated hydrocarbon becomes increasingly important to the production of an effective and stable catalyst as temperatures are increased from 0–100 °C. Excess unsaturated hydrocarbon causes an, “undesirable induction period due to the auxiliary reaction in the catalyst formation.”	68
Yoshimoto et al. (1970)	Ni naphthenate, Co naphthenate, bis(ethylacetoacetate) Ni, bis(acetylacetone) Ni, Fe naphthenate, Ni 2-ethylhexanoate, or Co 2-ethylhexanoate + 0.6, 1.3, 2.7, 4.0, or 6.7 (n-Bu)Li, or MgEt ₂	<i>Solvent:</i> Toluene. <i>Hydrogenation Substrate:</i> Styrene butadiene copolymer, or polybutadiene. <i>Order of addition:</i> Substrate + H ₂ (gas) + precatalyst and cocatalyst (order of addition of precatalyst or cocatalyst is not given). <i>Synthesis atmosphere:</i> H ₂ . <i>Synthesis temp:</i> 30 °C. <i>Aging:</i> 5 min. Additional notes: Presence or absence of polymer to be hydrogenated is not an important factor in catalyst preparation.	60

Authors (Year)	Catalyst Systems	Other Variables in Catalyst Synthesis	Ref.
Wald and Quam (1971)	Ni acac + 2 AlEt ₃ or Al(i-Bu) ₃	<i>Solvent:</i> Cyclohexane. <i>Hydrogenation Substrate:</i> Polystyrene-polyisoprene-polystyrene block copolymer. <i>Synthesis temp:</i> 40 °C. <i>Aging:</i> >15 min. Additional notes: Selectively hydrogenates the diene portions of block copolymers without hydrogenating the vinyl aromatic portions thereby reducing oxygen sensitivity, and without “appreciable degradation” (chain scission).	65
Wald and Quam (1972)	Ni octoate, or Ni acac + 2, or 3 AlEt ₃	<i>Solvent:</i> Cyclohexane. <i>Hydrogenation Substrate:</i> Polystyrene-poly(styrene/isoprene) copolymer. <i>Order of addition:</i> Substrate + H ₂ (gas) + pre-prepared catalyst (order of addition of precatalyst and cocatalyst is not given), or precatalyst + cocatalyst + substrate. <i>Synthesis temp:</i> 250 °C. <i>Aging:</i> 15 min. Additional notes: Provides selectively hydrogenated block copolymers with improved processability with minimum degradation of the polymers in the form of chain scission by the hydrogenation catalyst.	66
De La Mare (1973)	Ni(octoate) ₂ or Co(2-ethylhexabunoate) ₂ + 2.5 AlEt ₃	<i>Solvent:</i> Isooctane/cyclohexane. <i>Hydrogenation Substrate:</i> Butadiene-2-vinylpyridine copolymer. <i>Order of addition:</i> Substrate + solvent + pre-prepared catalyst (order of addition of precatalyst and cocatalyst is not given) + H ₂ (gas); <i>Synthesis temp:</i> 25 °C, or 170 °C. Additional Notes: Treatment of copolymers containing blocks from polar monomers with 1–3 moles of a Lewis acid, preferably BF ₃ , per polar group facilitates hydrogenation. Without this treatment it is not possible to use these catalysts to hydrogenate polar copolymers.	76
Loveless et al. (1976)	Ni acac, Ni naphthenate, or Fe(acac) ₃ + 0.8, 3.0, 3.3, 6.0 or 10.0 (n-Bu)Li	<i>Solvent:</i> n-heptane, or cyclohexane. <i>Hydrogenation Substrate:</i> Polyisoprene, sulfur vulcanizable elastomers, or 1-octene. <i>Order of addition:</i> Precatalyst + substrate + H ₂ (gas) + cocatalyst. <i>Rate of addition:</i> Cocatalyst is slowly added (i.e. 250 mmoles of (n-Bu)Li is added over 10 min). <i>Synthesis atmosphere:</i> H ₂ . <i>Synthesis temp:</i> room temp. <i>Aging:</i> 10 min. Additional Notes: A phenolic	77

Authors (Year)	Catalyst Systems	Other Variables in Catalyst Synthesis	Ref.
		<p>substance, such as p-nonyl phenol, is added to the precatalyst solution to produce soluble organometallic complex before the addition of other catalyst components. A claim is that this catalyst is superior to previous ones in, "degree and rapidity of hydrogenation which is possible." There is no upper limit to the amount of cocatalyst that can be used, but there is no benefit to using more than the amount prescribed. "The catalyst is not sensitive to small traces of impurities such as water."</p>	
Baumgartner and Balas (1976)	Ni(2-ethylhexanoate) ₂ + 2.5 or 3.0 AlEt ₃	<p><i>Solvent:</i> Cyclohexane. <i>Hydrogenation Substrate:</i> Styrene-isoprene copolymer. <i>Synthesis temp:</i> 80 °C. Additional Notes: Excess AlEt₃ was added after the reduction of the substrate was completed to some extent. This addition interrupted the hydrogenation. The addition of 2-ethylhexanol after the interruption caused the hydrogenation to resume.</p>	82
Ladenberger et al. (1980)	Ni(acac) ₂ + Al(i-Bu) ₃	<p><i>Solvent:</i> Toluene, hexane. <i>Hydrogenation Substrate:</i> Butadiene-styrene copolymer. <i>Synthesis atmosphere:</i> H₂. <i>Synthesis temp:</i> 25 °C to 30 °C. Additional Notes: A more active catalyst is achieved through the addition of H₂O after reaction of the precatalyst, cocatalyst and the substrate. H₂ uptake frequently only starts after the H₂O addition. Aromatics are more readily hydrogenated if a high Al/M is used.</p>	78
Durand et al. (1981)	Two metal chelate compounds: the first of Co or Ni, and the second of another metal Fe, Zn, Zr, Mn, Mo (all preferably acac or carboxylates), + 1.5 to 6 AlEt ₃ , Al(i-Bu) ₃ or LiBu	<p><i>Solvent:</i> Heptane, cyclohexanol, decahydronaphthalene, benzene, diisopropylether. <i>Hydrogenation Substrate:</i> Bis phenol A, phenol, cyclododecatriene, benzene, propionitrile, oleonitrile, adiponitrile. <i>Order of addition:</i> Substrate + pre-prepared catalyst (order of addition of the precatalysts and the cocatalyst is not given), or Substrate + Catalyst 1 (precatalyst 1 + cocatalyst) + Catalyst 2 (precatalyst 2 + cocatalyst). <i>Synthesis temp:</i> 90 °C. Additional Notes: if the metal salts were reacted separately with the same cocatalyst, an inferior catalyst, or even non-active solution will result. The mode of catalyst preparation is not critical, but is preferably carried out in</p>	155

Authors (Year)	Catalyst Systems	Other Variables in Catalyst Synthesis	Ref.
		the absence of substrate in most cases.	
Willis et al. (1990)	Ni 2-ethylhexanoate + 6 or 2.3 (s-Bu)Li or AlEt ₃	<i>Solvent:</i> Cyclohexane, tetrahydrofuran. <i>Hydrogenation Substrate:</i> Two different styrene butadiene block copolymers. <i>Order of addition:</i> Substrate + catalyst (order of addition of precatalyst and cocatalyst is not given). <i>Synthesis temp:</i> 47 °C, room temp. Additional Notes: Water should be present when the precatalyst and the cocatalyst are combined. Catalysts so prepared are suitable for hydrogenating polymers containing acidic functionality when certain other procedures are followed. Without said procedures (the focus of the patent), acidic functional groups interfere with the hydrogenation reaction by catalyst deactivation and/or gelling of the polymer solution.	61
Abraham et al. (1991)	Fe, Co or Ni halides, acetates, or acacs Co(neodecanoate) ₂ or Pd(PPh ₃) ₄ , Pt(PPh ₃) ₄ , or Rh(PPh ₃) ₃ + 4 AIR ₃ where each R = alkyl has 1–4 C atoms	<i>Solvent:</i> Toluene. <i>Hydrogenation Substrate:</i> Butadiene-methacrylate copolymer. <i>Order of addition:</i> Precatalyst + cocatalyst added over substrate. <i>Synthesis atmosphere:</i> N ₂ . <i>Synthesis temp:</i> room temp. <i>Aging:</i> 1 h. Additional Notes: The use of a complexing agent, such as phosphines (R ₃ P) or phosphites ((RO) ₃ P), is necessary in catalysis of hydrogenation of high MW nitrile-butadiene rubber (NBR) random copolymers. Without the complexing agent, gelation occurs due to complexation of the transition metal catalyst to the polar groups on the polymer chains.	44
Hoxmeier and Slaugh (1991)	Nickel 2-ethylhexanoate + 1, 2, 3, 4, 7, or 10 MAO (Methylalumoxane) or EAO (Ethylalumoxane), an equimolar blend of MAO/EAO, or AlEt ₃	<i>Solvent:</i> Cyclohexane. <i>Hydrogenation Substrate:</i> Polystyrene-polybutadiene-polystyrene triblock copolymer. <i>Order of addition:</i> Substrate + catalyst (order of addition of precatalyst and cocatalyst is not given). <i>Synthesis temp:</i> 25 °C. <i>Aging:</i> 30 min. Additional Notes: 0.5 equivalents of H ₂ O is present in the precatalyst solution. Catalysts made in this manner with MAO offer improved control over the extent of hydrogenation in polymers containing both ethylenic and aromatic unsaturation by an initially slower hydrogenation reaction, but compared to similar catalysts made with AIR ₃ , retain	62

Authors (Year)	Catalyst Systems	Other Variables in Catalyst Synthesis	Ref.
		higher activities over longer time spans. However, the catalyst formed with longer alkyl chain alumoxanes (C ₂ –C ₈) are more active for hydrogenation at all times than similar catalysts made with AlR ₃ .	
Coolbaugh et al. (1991)	Ni(octoate) ₂ or Ti(n-Bu) ₄ + 3.6, 2.5, or 6.0 AlEt ₃	<i>Solvent:</i> Cyclohexane. <i>Hydrogenation Substrate:</i> Isoprene-Butadiene-isoprene triblock copolymer. <i>Order and rate of addition:</i> Precatalyst + cocatalyst, 20.80 mL of cocatalyst is added as quickly as possible (i.e. in 15 sec); or solvent + precatalyst and cocatalyst simultaneously added over 25 min. The catalyst solutions prepared as above are added over substrate. <i>Synthesis atmosphere:</i> N ₂ . <i>Aging:</i> 10 min. Additional Notes: The molar ratio of the transition metal compound to the cocatalyst should be kept essentially constant by either simultaneous addition of solutions of the two, or by as rapid addition of the cocatalyst as possible. If added over the course of more than about 15 min a less selective catalyst results, which may also ppt. from solution. The reversal of the addition sequence is likewise detrimental. "Extreme care must be used to exclude air, moisture and other impurities capable of interfering with the delicate chemical balance involved in the synthesis of the catalyst."	63
Goodwin and Willis (1992)	Ni(2-ethylhexanoate) ₂ + 2.6 AlEt ₃	<i>Solvent:</i> Cyclohexane. <i>Hydrogenation Substrate:</i> Polyisoprene, or polybutadiene. Additional Notes: Complete hydrogenation of olefinic unsaturation in low molecular weight diene polymers, particularly those having terminal hydroxyl groups, is achieved (previously not possible using these catalyst systems) by removing fine particles of ionic Li residues such as LiOR and LiOH through filtering or decanting the polymer solutions prior to hydrogenation.	73
Hergenrother et al. (1994)	Ni octoate + 3, 6, 7 Al(i-Bu) ₃ , or AlEt ₃	<i>Solvent:</i> Hexane, toluene. <i>Hydrogenation Substrate:</i> Polybutadiene. <i>Order of addition:</i> Precatalyst + cocatalyst. The catalyst solution added over the substrate.	45

Authors (Year)	Catalyst Systems	Other Variables in Catalyst Synthesis	Ref.
		<p><i>Synthesis atmosphere:</i> H₂. <i>Synthesis temp:</i> -25 °C, or 66 °C. <i>Aging:</i> 1 h. <i>Additional Notes:</i> Cyclohexene is added to precatalyst solution before cocatalyst addition to stabilize the catalyst prior to hydrogenation.</p> <p>Hydrogenation saturation controlled by treating polymers with an arylphosphine in the presence of the hydrogenation catalyst. The order of reagent addition is unimportant with either the precatalyst or the cocatalyst added incrementally throughout the hydrogenation reaction.</p>	
Handlin et al. (1995)	Ni 2-ethylhexanoate + 2.6 AlEt ₃	<p><i>Solvent:</i> Cyclohexane. <i>Hydrogenation Substrate:</i> Polybutadiene. <i>Additional Notes:</i> the catalyst is used to hydrogenate butadiene polymers having terminal functional groups to give low viscosity polymers.</p>	74
Johnson et al. (2002)	Co neodecanoate, or Ni octoate + 2.0, 2.2, or 1.3 AlEt ₃	<p><i>Solvent:</i> Cyclohexane, diethylether. <i>Hydrogenation Substrate:</i> Linear triblock copolymer of styrene and ethylene/butadiene, polystyrene-polybutadiene-polystyrene triblock copolymer, or linear polystyrene-polyisoprene-polystyrene-polyisoprene block copolymer.</p> <p><i>Order and rate of addition:</i> The catalyst is prepared by slowly adding cocatalyst over the precatalyst in the absence of substrate.</p>	46

^a The “n” values of the precatalyst components are not given; they may be the same or different in different transition metal precatalyst compounds.

Table 2.A.2. Nature and Mechanism of Formation of the Catalyst – the “Ziegler-type Catalysts are Homogeneous” Hypothesis

Authors (year)	Catalyst Systems	Results	Ref.
Wilke and coworkers (1973)	Ni(acac) ₂ + AlMe ₃ , AlEt ₃ or Al(<i>i</i> -Bu) ₃	A homogeneous Ni(0) complex formed as a result of the reaction of Ni–olefin π -complex with Al cocatalyst. The resulting complex is proposed to contain multicenter bonds including C, Ni(0), and Al atoms.	4
Sloan <i>et. al.</i> (1963)	Fe(acac) ₃ , Co(acac) ₂ , Co(acac) ₃ , Ni(acac) ₂ , Ru(acac) ₃ , or Pd(acac) ₂ + AlEt ₃ , Al(<i>i</i> -Bu) ₃ , or AlH(<i>i</i> -Bu) ₂	M–H species, given as MHX _{n-1} , are claimed as the active catalyst. The M–H species are proposed to form by alkylation and then hydrogenolysis of the precatalyst.	57
Laporte (1969)	Ni(2-ethylhexanoate) ₂ , or Co(2-ethylhexanoate) ₂ + 3–4 AlEt ₃	Mononuclear H–M(0)–L species, L = labile –H, –R, solvent, olefin, or AlEt ₂ (2-ethylhexanoate), is proposed as the catalyst. However, binuclear M(I) is not ruled out.	58
Klinedinst and Boudart (1973)	Fe(acac) ₃ + 6 AlEt ₃	Mössbauer spectroscopy shows that high spin Fe(II) are the only Fe species present at low temp. Rules out catalysis by (crystalline) metallic Fe particles \geq 1.7 nm in diameter.	105
Alvanipour and Kispert (1988)	Co(stearate) ₂ + 2 AlEt ₃	Homogeneous M(0) species are proposed to form via unstable ethyl–Ni (L ₃ Ni–Et) and/or Ni–H (L ₂ Ni–H–C=C) where L: solvent, CH ₂ =CH ₂ or RCO ₂ AlEt ₂ .	67
Reguli and Stasko (1987)	Ni(3,5-diisopropylsalicylate) ₂ , Ni(acac) ₂ , Ni(stearate) ₂ , or Ni(benzohydraxamate) ₂ + AlEt ₃ , Al(<i>i</i> -Bu) ₃ , or BuLi	Homogeneous diamagnetic Ni(II) formed by alkylation of the transition metal precatalyst is suggested as the active catalyst species. Ni colloid formation is observed in the presence of aromatic compounds.	70
Barrault et al. (1994)	Co(acac) ₂ + AlEt ₃	Co(0) clusters, and Co(0) complexes are simultaneously present, neither of which can be ruled out as active catalyst species.	37
Shmidt and	Co(acac) ₂ , Co(acac) ₃ , Ni(acac) ₂ ,	A paramagnetic homogeneous Co(0) complex,	42,

Authors (year)	Catalyst Systems	Results	Ref.
coworkers (1970, 1979, 1983)	Fe(acac) ₃ or Pd(acac) ₂ + AlEt ₃ , AlMe ₃ , n-BuLi, n-PrMgBr or i- PrMgBr	stabilized by arene solvent, R of AlR ₃ and acac from the Co precatalyst is thought to be the active catalyst. Presence of low spin M(II) is not ruled out. In addition, ≤ 100 Å M(0) particles are observed.	109, 110, 111

Table 2.A.3. Nature and Mechanism of Formation of the Catalyst – the “Ziegler-type Catalysts are Heterogeneous” Hypothesis

Authors (year)	Catalyst Systems	Results	Ref.
Shmidt and coworkers (2005, 2006)	Co(acac) ₂ , Co(acac) ₃ , or Pd(acac) ₂ + AlEt ₃	Observe ferromagnetic β-Co(0) _n or Pd(0) _n nanoparticles (1–5 nm) apparently stabilized by AlEt ₃ , and/or acetylacetonone derivatives of AlEt ₃ including AlEt ₂ (acac) or alumoxanes. The Co(0) complex proposed previously as the active catalyst is reinterpreted as the precursor to Co(0) _n nanoclusters.	19,113, 81,114
Pasynkiewicz et al. (1974)	Co(acac) ₃ + 1 AlMe ₃	A mixture of Co(II), Co(I) complexes and metallic Co(0) are reported. Suggest the true catalyst is metallic Co(0). The other reaction products proposed: [Co(acac) ₂ CH ₃], (CH ₃) ₂ Al(acac), [(acac)Co=CH ₂], [Co(acac)], [(acac)Co(CH ₃) ₂].	71
Goulon and coworkers (1984, 1986)	Ni(acac) ₂ , Ni(2-ethylhexanoate) ₂ , Co(2-ethylhexanoate) ₂ , or Fe(acac) ₃ + AlEt ₃	M(0) _n clusters are proposed as catalysts. However, whether they are small ~4–10 atom clusters, amorphous M or M-carbide clusters, or some combination is unclear.	40,116
Bonnemann and coworkers (1999-2005)	Ni(acac) ₂ + 3 Al(i-Bu) ₃ , Pt(acac) ₂ , + 4 AlMe ₃ , [(1,5-COD)Pt(CH ₃) ₂] + 10 AlEt ₃ or Al (C ₈ H ₁₇) ₃ , and a variety of other systems	M(0) _n amorphous nanoclusters stabilized by an organoaluminum multilayer are observed. Catalytic activities are not tested.	121, 122, 123, 124, 125, 126

REFERENCES

- [1] K. Ziegler, E. Holzkamp, H. Breil, H. Martin, *Angew. Chem.* 67 (1955) 541–547.
- [2] G. W. Parshall, S. D. Ittel, *Homogeneous Catalysis*, second ed., John Wiley & Sons, New York, 1992.
- [3] P. W. Jolly, G. Wilke, *The Organic Chemistry of Nickel*, Vol. II, Academic Press, New York, 1975.
- [4] K. Fischer, K. Jonas, P. Misbach, R. Stabba, G. Wilke, *Angew. Chem. Int. Ed.* 12 (1973) 943–953.
- [5] K. Ziegler, *Nobel Lectures, Chemistry 1963–1970*, Elsevier Publishing Company, Amsterdam, 1972.
- [6] N. T. McManus, G. L. Rempel, *J.M.S. Rev. Macromol. Chem. Phys.* 35 (1995) 239–285.
- [7] M. P. McGrath, E. D. Sall, S. J. Tremont, *Chem. Rev.* 95 (1995) 381–398.
- [8] H. Weiner, A. Trovarelli, R. G. Finke, *J. Mol. Catal. A: Chem.* 191 (2003) 217–252.
- [9] K. A. Johnson, *Polym. Prepr.* 41 (2000) 1525–1526.
- [10] J. P. Collman, L. S. Hegedus, J. R. Norton, R. G. Finke, *Principles and Applications of Organotransition Metal Chemistry*, University Science Books, Mill Valley, 1987.
- [11] J. Schwartz, *Acc. Chem. Res.* 18 (1985) 302–308.
- [12] Y. Lin, R. G. Finke, *Inorg. Chem.* 33 (1994) 4891–4910.
- [13] J. D. Aiken III, Y. Lin, R. G. Finke, *J. Mol. Catal. A: Chem.* 114 (1996) 29–51.
- [14] K. S. Weddle, J. D. Aiken III, R. G. Finke, *J. Am. Chem. Soc.* 120 (1998) 5653–5666.
- [15] J. A. Widegren, M. A. Bennett, R. G. Finke, *J. Am. Chem. Soc.* 125 (2003) 10301–10310.
- [16] J. A. Widegren, R. G. Finke, *J. Mol. Catal. A: Chem.* 198 (2003) 317–341.
- [17] C. M. Hagen, J. A. Widegren, P. M. Maitlis, R. G. Finke, *J. Am. Chem. Soc.* 127 (2005) 4423–4432.
- [18] E. E. Finney, R. G. Finke, *Inorg. Chim. Acta* 359 (2006) 2879–2887.

- [19] L. O. Nindakova, F. K. Shmidt, V. V. Saraev, B. A. Shainyan, N. N. Chipanina, V. A. Umanets, L. N. Belonogova, D.-S. D. Toryashinova, *Kinetics and Catalysis* 47 (2006) 54–63.
- [20] H. Sinn, W. Kaminsky, *Adv. Organomet. Chem.* 18 (1980) 99–149.
- [21] P. Corradini, G. Guerra, L. Cavallo, *Acc. Chem. Res.* 37 (2004) 231–241.
- [22] R. H. Crabtree *The Organometallic Chemistry of the Transition Metals*, fourth ed., John Wiley & Sons, New York, 2005.
- [23] D. S. Breslow, N. R. Newburg, *Org. Bio. Chem.* 81 (1959) 81–85.
- [24] G. Natta, G. Mazzanti, *Tetrahedron* 8 (1960) 86–100.
- [25] W. P. Long, D. S. Breslow, *J. Am. Chem. Soc.* 82 (1960) 1953–1957.
- [26] A. Andresen, H.-G. Cordes, J. Herwig, W. Kaminsky, A. Merck, R. Mottweiler, J. Pein, H. Sinn, H.-J. Vollmer, *Angew. Chem. Int. Ed.* 15 (1976) 630–632.
- [27] L. Resconi, S. Bossi, L. Abis, *Macromolecules* 23 (1990) 4489–4491.
- [28] M. R. Mason, J. M. Smith, S. G. Bott, A. R. Barron, *J. Am. Chem. Soc.* 115 (1993) 4971–4984.
- [29] T. Sugano, K. Matsubara, T. Fujita, T. Takahashi, *J. Mol. Catal.* 82 (1993) 93–101.
- [30] A. R. Barron, *Organometallics* 14 (1995) 3581–3583.
- [31] D. W. Imhoff, L. S. Simeral, S. A. Sangokoya, J. H. Peel, *Organometallics* 17 (1998) 1941–1945.
- [32] A. R. Barron in: J. Scheirs, W. Kaminsky (Eds.), *Metallocene-based Polyolefins*, John Wiley & Sons, New York, 2000, pp. 33–67.
- [33] A. R. Barron, *Macromol. Symp.* 97 (1995) 15–25.
- [34] E. Y.-X. Chen, T. J. Marks, *Chem. Rev.* 100 (2000) 1391–1434.
- [35] A. H. Tullo, *Paying Attention to Activators. Chemical and Engineering News* (Oct 22, 2001) 38–39.
- [36] A. Fischbach, F. Perdih, E. Herdtweck, R. Anwander, *Organometallics* 25 (2006) 1626–1642.
- [37] J. Barrault, M. Blanchard, A. Derouault, M. Ksibi, M. I. Zaki, *J. Mol. Catal.* 93 (1994) 289–304.

- [38] B. R. James, *Homogeneous Hydrogenation*, John Wiley & Sons, New York, 1973.
- [39] S. J. Lapporte, W. R. Schuett, *J. Org. Chem.* 28 (1963) 1947–1948.
- [40] C. Esselin, E. Bauer-Grosse, J. Goulon, C. Williams, Y. Chauvin, D. Commereuc, E. Freund, *J. Phys. Colloques* 47 (1986) C8-243–C8-248.
- [41] W. Keim, *J. Mol. Catal.* 52 (1989) 19–25.
- [42] F. K. Shmidt, V. G. Lipovich, S. M. Krasnopol'skaya, I. V. Kalechits, *Kinetika i Kataliz* 11 (1970) 595–602.
- [43] K. Bronstert, V. Ladenberger, G. Fahrbach, *Catalytic Hydrogenation of Polymers Containing Double Bonds*. U.S. Patent 3,673,281, Jun. 27, 1972.
- [44] T. Abraham, P. H. Starmer, A. H. Jorgensen, *Composition of and a Method for Preparing High-Temperature Oil-Resistant Elastomers from Hydrogenated Butadiene-Acrylate Copolymers*. U.S. Patent 4,994,528, Feb. 19, 1991.
- [45] W. L. Hergenrother, J. M. Doshak, *Process and Catalyst for Producing Partially Hydrogenated Diene Polymers Containing Endo and Exo Chain Trisubstituted Unsaturation*. U.S. Patent 5,310,817, May 10, 1994.
- [46] K. A. Johnson, W. De Jong, D. K. Schisla, *Method for Making Selectively Hydrogenated Block Copolymers of Vinyl Aromatic Hydrocarbons and Conjugated Dienes*. U.S. Patent 7,390,856, June 24, 2008.
- [47] J. F. Haw (Ed.), *In-Situ Spectroscopy in Heterogeneous Catalysis*, Wiley VCH, Weinheim, 2002.
- [48] J. Pérez-Ramírez, E. V. Kondratenko, *Catal. Today* 121 (2007) 160–169.
- [49] R. G. Finke in: D. L. Feldheim, C. A. Foss Jr. (Eds.), *Metal Nanoparticles: Synthesis, Characterization, and Applications*, Marcel Dekker, Inc. New York, 2002, pp. 17–54.
- [50] Y. Lin, R. G. Finke, *J. Am. Chem. Soc.* 116 (1994) 8335–8353.
- [51] A. K. Galwey, *Thermochim. Acta* 413 (2004) 139–183.
- [52] W. M. Alley, C. W. Girard, S. Özkar, R. G. Finke, *Inorg. Chem.* 48 (2009) 1114–1121.
- [53] W. M. Alley, I. K. Hamdemir, Q. Wang, A. Frenkel, L. Li, J. C. Yang, L. D. Menard, R. G. Nuzzo, K. A. Johnson, R. G. Finke, *Ziegler-Type, Industrially Relevant Hydrogenation Catalysts Made from [(1,5-COD)Ir(μ -O₂C₈H₁₅)₂] and AlEt₃: Evidence for the Ir(0)_n species present and for the true catalyst*, submitted for publication.

- [54] I. K. Hamdemir, S. Özkar, K. A. Johnson, R. G. Finke, Ranking the activity and other catalytic properties of Ziegler-Type, industrially relevant hydrogenation catalysts made from $[(1,5\text{-COD})\text{Ir}(\mu\text{-O}_2\text{C}_8\text{H}_{15})_2]$ and AlEt_3 , via a modified five-criteria method, in preparation.
- [55] W. M. Alley, I. K. Hamdemir, Q. Wang, A. Frenkel, L. D. Menard, R. G. Nuzzo, S. Özkar, K. A. Johnson, R. G. Finke, Cobalt Ziegler-Type industrial hydrogenation catalysts made from $\text{Co}(\text{neodecanoate})_2$ and AlEt_3 : evidence for nanoclusters and nanocluster-based catalysis, in preparation.
- [56] W. M. Alley, I. K. Hamdemir, Q. Wang, A. Frenkel, L. Li, J. C. Yang, L. D. Menard, R. G. Nuzzo, S. Özkar, K. A. Johnson, R. G. Finke, Nickel Ziegler-Type industrial hydrogenation catalysts made from $\text{Ni}(2\text{-ethylhexanoate})_2$ and AlEt_3 : evidence for nanoclusters and nanocluster-based catalysis, in preparation.
- [57] M. F. Sloan, A. S. Matlack, D. S. Breslow, *J. Am. Chem. Soc.* 85 (1963) 4014–4018.
- [58] S. J. Lapporte, *Ann. N. Y. Acad. Sci.* 158 (1969) 510–525.
- [59] D. S. Breslow, A. S. Matlack, Hydrogenation of Unsaturated Hydrocarbons. U.S. Patent 3,113,986, Dec. 10, 1963.
- [60] T. Yoshimoto, S. Kaneko, T. Narumiya, H. Yoshii, Hydrogenation Catalysts and a Process for Hydrogenating Polymers by the Use of Them. U.S. Patent 3,541,064, Nov. 17, 1970.
- [61] C. L. Willis, L. A. Pottick, D. E. Goodwin, Method for Hydrogenating Functionalized Polymer and Products Thereof. U.S. Patent 4,970,254, Nov. 13, 1990.
- [62] R. J. Hoxmeier, L. H. Slaugh, Hydrogenation Catalyst and Hydrogenation Process Wherein Said Catalyst is Used. U.S. Patent 5,057,582, Oct. 15, 1991.
- [63] T. S. Coolbaugh, F. C. Loveless, D. N. Mathews, Method of Synthesizing a Selective Olefin Hydrogenation Catalyst. *Eur. Pat. Appl.* 91300316.6, Jan. 16, 1991.
- [64] W. R. Kroll, Hydrogenation Process Employing a Transition Metal Catalyst. U.S. Patent 3,412,174, Nov. 19, 1968.
- [65] M. M. Wald, M. G. Quam, Partially Hydrogenated Block Copolymers. U.S. Patent 3,595,942, July 27, 1971.
- [66] M. M. Wald, M. G. Quam, Selectively Hydrogenated Block Copolymers. U.S. Patent 3,700,633, Oct. 24, 1972.
- [67] A. Alvanipour, L. D. Kispert, *J. Mol. Catal.* 48 (1988) 277–283.

- [68] T. Yoshimoto, S. Kaneko, T. Narumiya, H. Yoshii, Three Component Hydrogenation Catalysts and a Process for Hydrogenating Polymers by the Use of Them. U.S. Patent 3,531,450, Sep. 29, 1970.
- [69] S. Šabata, J. Hetflejš, *J. Appl. Polym. Sci.* 85 (2002) 1185–1193.
- [70] J. Reguli, A. Staško, *Chem. Papers* 41 (1987) 299–310.
- [71] S. Pasynkiewicz, A. Pietrzykowski, K. Dowbor, *J. Organomet. Chem.* 78 (1974) 55–59.
- [72] S. J. Lapporte, Preparation of Complex Organic Metallic Hydrogenation Catalysts and Their Use. U.S. Patent 3,205,278, Sep. 7, 1965.
- [73] D. E. Goodwin, C. L. Willis, Hydrogenation of Unsaturation in Low Molecular Weight Diene Polymers. U.S. Patent 5,166,277, Nov. 24, 1992.
- [74] D. L. Handlin, D. E. Goodwin, C. L. Willis, D. J. St. Clair, J. D. Wilkey, M. J. Modic, C. A. Stevens, Butadiene Polymers Having Terminal Functional Groups. U.S. Patent 5,393,843, Feb. 28, 1995.
- [75] W. R. Kroll, *J. Catal.* 15 (1969) 281–288.
- [76] H. E. De La Mare, Process for Hydrogenation of Polar Copolymers and Complexed Copolymer Compositions. U.S. Patent 3,766,300, Oct. 16, 1973.
- [77] F. C. Loveless, D. H. Miller, Hydrogenation Catalyst. U.S. Patent 3,932,308, Jan. 13, 1976.
- [78] V. Ladenberger, K. Bronstert, G. Fahrbach, W. Groh, Catalytic Hydrogenation of Diolefin Polymers. U.S. Patent 4,207,409 Jun. 10, 1980.
- [79] J. C. Falk, *J. Polym. Sci., Part A: Polym. Chem.* 9 (1971) 2617–2623.
- [80] H. W. Roesky, M. G. Walawalkar, R. Murugavel, *Acc. Chem. Res.* 34 (2001) 201–211.
- [81] L. B. Belykh, T. V. Goremyka, N. I. Skripov, V. A. Umanets, F. K. Shmidt, *Kinetics and Catalysis* 47 (2006) 367–374.
- [82] H. J. Baumgartner, J. G. Balas, Hydrogenation Process. U.S. Patent 3,937,759, Feb. 10, 1976.
- [83] D. R. Lide (Ed.), *CRC Handbook of Chemistry and Physics*, seventy seventh ed., CRC Press, Boca Raton, 1996.
- [84] B. R. James, Y. Wang, C. S. Alexander, T. Q. Hu, *Chem. Ind.* 75 (1998) 233–242.
- [85] J. Aiken III, R.G. Finke, *J. Am. Chem. Soc.* 120 (1998) 9545–9554.

- [86] F. Notheisz, Á. Zsigmond, M. Bartók, Z. Szegletes, G. V. Smith, *Appl. Catal. A: General* 120 (1994) 105–114.
- [87] B. Cornils, W. A. Herrmann (Eds.), *Applied Homogeneous Catalysis with Organometallic Compounds, Vol. 2: Developments*, Wiley VCH, Weinheim, 1996.
- [88] B. A. Steinhoff, S. S. Stahl, *J. Am. Chem. Soc.* 128 (2006) 4348–4355.
- [89] J. Halpern, *Inorg. Chim. Acta* 50 (1981) 11–19.
- [90] N. T. S. Phan, M. Van Der Sluys, C. W. Jones, *Adv. Synth. Catal.* 348 (2006) 609–679.
- [91] C. M. Hagen, L. Vieille-Petit, G. Laurency, G. Süß-Fink, R. G. Finke, *Organometallics* 24 (2005) 1819–1831.
- [92] G. Wilke, G. Herrmann, *Angew. Chem. Int. Ed.* 1 (1962) 549–550.
- [93] G. Wilke, B. Bogdanović, P. Hardt, P. Heimbach, W. Keim, M. Kröner, W. Oberkirch, K. Tanaka, E. Steinrücke, D. Walter, H. Zimmermann, *Angew. Chem. Int. Ed.* 5 (1966) 151–164.
- [94] G. Wilke, G. Herrmann, *Angew. Chem. Int. Ed.* 5 (1966) 581–582.
- [95] B. Bogdanović, H. Bönemann, G. Wilke, *Angew. Chem. Int. Ed.* 5 (1966) 582–583.
- [96] G. Wilke, H. Schott, *Angew. Chem. Int. Ed.* 5 (1966) 583.
- [97] N. Hebben, H.-J. Himmel, G. Eickerling, C. Herrmann, M. Reiher, V. Herz, M. Presnitz, W. Scherer, *Chem.—Eur. J.* 13 (2007) 10078–10087.
- [98] L. Farády, L. Bencze, L. Markó, *J. Organomet. Chem.* 10 (1967) 505–510.
- [99] L. Farády, L. Bencze, L. Markó, *J. Organomet. Chem.* 17 (1969) 107–116.
- [100] J. J. Eisch, M. W. Foxton, *J. Organomet. Chem.* 12 (1968) P33–P36.
- [101] L. Lardicci, G. P. Giacomelli, P. Salvadori, P. Pino, *J. Am. Chem. Soc.* 93 (1971) 5794–5800.
- [102] J. J. Eisch, X. Ma, M. Singh, G. Wilke, *J. Organomet. Chem.* 527 (1997) 301–304.
- [103] H. J. Motulsky, A. Christopoulos, *Fitting Models to Biological Data using Linear and Nonlinear Regression. A practical guide to curve fitting*. GraphPad Software Inc., San Diego, CA, www.graphpad.com, 2003, p. 58.
- [104] J. Halpern, *Homogeneous and Heterogeneous Catalysis: Kinetic and Mechanistic Aspects*. In, *Relations Between Homogeneous and Heterogeneous Catalysis*, Proceedings of the

International Symposium on the Relations between Heterogeneous and Homogeneous Catalytic Phenomena, Lyon, 3–6 Nov. 1977, Centre National de la Recherche Scientifique: Paris, 1978, no. 281, pp. 27–47.

[105] K. A. Klinedinst, M. Boudart, *J. Catal.* 28 (1973) 322–328.

[106] J. M. Greneche, F. Varret, M. Leblanc, G. Ferey, *Solid State Commun.* 61 (1987) 813–816.

[107] G. Kataby, Yu. Koltypin, J. Rothe, J. Hormes, I. Felner, X. Cao, A. Gedanken, *Thin Solid Films* 333 (1998) 41–49.

[108] P.-R. Cha, Yu. C. Kim, K.-B. Kim, H.-K. Seok, E. Fleury, S.-H. Han, *Scr. Mater.* 56 (2007) 609–612.

[109] F. K. Schmidt, V. V. Sarayev, Y. S. Levkovskii, V. G. Lipovich, V. A. Gruznykh, G. V. Ratovskii, T. V. Dmitrieva, L. O. Nindakova, *React. Kinet. Catal. Lett.* 10 (1979) 195–199.

[110] G. V. Ratovskii, T. V. Dmitrieva, L. O. Nindakova, F. K. Schmidt, *React. Kinet. Catal. Lett.* 11 (1979) 121–124.

[111] F. K. Schmidt, G. V. Ratovskii, T. V. Dmitrieva, I. N. Ivleva, Y. G. Borodko, *J. Organomet. Chem.* 256 (1983) 309–329.

[112] J. Klosin, G. R. Roof, E. Y.-X. Chen, K. A. Abboud, *Organometallics* 19 (2000) 4684–4686. Also see reference 22 therein.

[113] F. K. Schmidt, L. O. Nindakova, B. A. Shainyan, V. V. Saraev, N. N. Chipanina, V. A. Umanetz, *J. Mol. Catal. A: Chem.* 235 (2005) 161–172.

[114] L. B. Belykh, Yu. Yu. Titova, V. A. Umanets, F. K. Schmidt, *Russian Journal of Applied Chemistry* 79 (2006) 1271–1277.

[115] B. C. Gates, *Catalytic Chemistry*, John Wiley & Sons, New York, 1992, pp. 385–386.

[116] J. Goulon, E. Georges, C. Goulon-Ginet, Y. Chauvin, D. Commereuc, H. Dexpert, E. Freund, *Chem. Phys.* 83 (1984) 357–366.

[117] A. I. Frenkel, C. W. Hills, R. G. Nuzzo, *J. Phys. Chem. B* 105 (2001) 12689–12703.

[118] J. M. Montejano-Carrizales, J. L. Morán-López, *Nanostruct. Mater.* 1 (1992) 397–409.

[119] J. L. Fulton, J. C. Linehan, T. Autrey, M. Balasubramanian, Y. Chen, N. K. Szymczak, *J. Am. Chem. Soc.* 129 (2007) 11936–11949.

[120] A. L. Ankudinov, J. J. Rehr, J. J. Low, S. R. Bare, *J. Chem. Phys.* 116 (2002) 1911–1919.

- [121] H. Bönemann, W. Brijoux, R. Brinkmann, U. Endruschat, W. Hofstadt, K. Angermund, *Revue Roumaine de Chimie* 44 (1999) 1003–1010.
- [122] H. Bönemann, N. Waldöfner, H.-G. Haubold, T. Vad, *Chem. Mater.* 14 (2002) 1115–1120.
- [123] K. Angermund, M. Bühl, E. Dinjus, U. Endruschat, F. Gassner, H.-G. Haubold, J. Hormes, G. Köhl, F. T. Mauschick, H. Modrow, R. Mörtel, R. Mynott, B. Tesche, T. Vad, N. Waldöfner, H. Bönemann, *Angew. Chem. Int. Ed.* 41 (2002) 4041–4044.
- [124] K. Angermund, M. Bühl, U. Endruschat, F. T. Mauschick, R. Mörtel, R. Mynott, B. Tesche, N. Waldöfner, H. Bönemann, G. Köhl, H. Modrow, J. Hormes, E. Dinjus, F. Gassner, H.-G. Haubold, T. Vad, M. Kaupp, *J. Phys. Chem. B* 107 (2003) 7507–7515.
- [125] H.-G. Haubold, T. Vad, N. Waldöfner, H. Bönemann, *J. Appl. Cryst.* 36 (2003) 617–620.
- [126] F. Wen, H. Bönemann, R. J. Mynott, B. Spliethoff, C. Weidenthaler, N. Palina, S. Zinoveva, H. Modrow, *Appl. Organomet. Chem.* 19 (2005) 827–829.
- [127] C. A. Jaska, I. Manners, *J. Am. Chem. Soc.* 126 (2004) 1334–1335.
- [128] E. E. Finney, R. G. Finke, Fitting and Interpreting Transition-Metal Nanocluster Formation and Other Sigmoidal Kinetic Data: A More Thorough Testing of Empirical, Dispersive Kinetics vs Chemical-Mechanism-Based Equations and Treatments, *Chem. Mater.* in press.
- [129] M. A. Watzky, R. G. Finke, *Chem. Mater.* 9 (1997) 3083–3095.
- [130] M. A. Watzky, R. G. Finke, *J. Am. Chem. Soc.* 119 (1997) 10382–10400.
- [131] (a) C. Besson, E. E. Finney, R. G. Finke, *J. Am. Chem. Soc.* 127 (2005) 8179–8184. (b) C. Besson, E. E. Finney, R. G. Finke, *Chem. Mater.* 17 (2005) 4925–4938.
- [132] (a) A. M. Morris, M. A. Watzky, J. N. Agar, R. G. Finke, *Biochem.* 47 (2008) 2413–2427. (b) M. A. Watzky, A. M. Morris, E. D. Ross, R. G. Finke, *Biochem.* 47 (2008) 10790–10800.
- [133] J. A. Widegren, J. D. Aiken III, S. Özkar, R. G. Finke, *Chem. Mater.* 13 (2001) 312–324.
- [134] P. D. Jadzinsky, G. Calero, C. J. Ackerson, D. A. Bushnell, R. D. Kornberg, *Science* 318 (2007) 430–433.
- [135] L. Beuermann, W. Maus-Friedrichs, S. Krischok, V. Kempter, S. Bucher, H. Modrow, J. Hormes, N. Waldöfner, H. Bönemann, *Appl. Organomet. Chem.* 17 (2003) 268–276.
- [136] F. Wen, N. Waldöfner, W. Schmidt, K. Angermund, H. Bönemann, S. Modrow, S. Zinoveva, H. Modrow, J. Hormes, L. Beuermann, S. Rudenkiy, W. Maus-Friedrichs, V. Kempter, T. Vad, H.-G. Haubold, *Eur. J. Inorg. Chem.* (2005) 3625–3640.

- [137] H. Bönemann, W. Brijoux, H.-W. Hofstadt, T. Ould-Ely, W. Schmidt, B. Waßmuth, C. Weidenthaler, *Angew. Chem. Int. Ed.* 41 (2002) 599–603.
- [138] R. Richards, G. Geibel, W. Hofstadt, H. Bönemann, *Appl. Organomet. Chem.* 16 (2002) 377–383.
- [139] H. Bönemann, W. Brijoux, R. Brinkmann, N. Matoussevitch, N. Waldöfner, N. Palina, H. Modrow, *Inorg. Chim. Acta* 350 (2003) 617–624.
- [140] R. L. Augustine, F. Yaghmaie, J. F. Van Peppen, *J. Org. Chem.* 49 (1984) 1865–1870.
- [141] J. Halpern, *Acc. Chem. Res.* 15 (1982) 332–338.
- [142] M. J. Nappa, R. Santi, J. Halpern, *Organometallics* 4 (1985) 34–41.
- [143] J. R. Platt, *Science* 146 (1964) 347.
- [144] C. A. Jaska, I. Manners, *J. Am. Chem. Soc.* 126 (2004) 9776–9785.
- [145] Y. Chen, J. L. Fulton, J. C. Linehan, T. Autrey, *J. Am. Chem. Soc.* 127 (2005) 3254–3255.
- [146] A. Duteil, G. Schmid, W. Meyer-Zaika, *Chem. Commun.* 1995 31–32.
- [147] D. B. Williams, C. B. Carter, *Transmission Electron Microscopy*, Plenum Press, New York, 1996.
- [148] B. J. Hornstein, J. D. Aiken III, R. G. Finke, *Inorg. Chem.* 41 (2002) 1625–1638.
- [149] J. M. Thomas, G. A. Somorjai, *Top. Catal.* 8 (1999) preface.
- [150] B. M. Weckhuysen, *Chem. Commun.* 2002, 97–110.
- [151] M. O. Guerrero-Pérez, M. A. Bañares, *Chem. Commun.* 2002, 1292–1293.
- [152] F. Meunier, M. Daturi, *Catal. Today* 113 (2006) 1–2.
- [153] J. Halpern, T. Okamoto, A. Zakhariiev, *J. Mol. Catal.* 2 (1976) 65–68.
- [154] S. J. Tinnemans, J. G. Mesu, K. Kervinen, T. Visser, T. A. Nijhuis, A. M. Beale, D. E. Keller, A. M.J. van der Eerden, B. M. Weckhuysen, *Catal. Today* 113 (2006) 3–15.
- [155] D. Durand, G. Hillion, C. Lassau, L. Sajus, *Process for Hydrogenating Unsaturated Compounds*. U.S. Patent 4,271,323, Jun. 2, 1981.

SUPPORTING INFORMATION-A:

ZIEGLER-TYPE HYDROGENATION CATALYSTS MADE FROM GROUP 8-10

TRANSITION METAL PRECATALYSTS AND AlR_3 COCATALYSTS:

A CRITICAL REVIEW OF THE LITERATURE

Hydrogenations using $Pt(acac)_2$ plus $AlEt_3$. Using ASAXS spectroscopy, Bönnemann and coworkers observed the formation of 1.2 nm diameter nanoparticles from a $Pt(acac)_2$ plus $AlMe_3$ system [1]. The relatively slow nanoparticle development observed for this system makes it promising for following the kinetics of catalyst formation en route to determining the true nature of the catalyst. However, in order to do this, it is first necessary to show that the system is indeed catalytically competent for hydrogenation, as expected (i.e., to see if the system forms a Ziegler-type hydrogenation catalyst, an important experiment not reported previously). A similar system tested by us, $Pt(acac)_2$ plus $AlEt_3$, $Al/Pt = 4$, exhibits the ability to catalytically hydrogenate cyclohexene. The results of following the formation of the Ziegler-type hydrogenation catalyst formed from $Pt(acac)_2$ plus $AlEt_3$, $Al/Pt = 4$, by the cyclohexene hydrogenation reporter reaction method [2,3,4] are reported below, Figure SI-A1.

In the drybox, a 9.0 mM toluene solution of $Pt(acac)_2$ precatalyst was prepared by dissolving 0.0668 g of $Pt(acac)_2$ (Strem, 98%) in 18.87 mL of toluene (Aldrich, anhydrous, 99.8%). Using a procedure similar to that employed for the Co catalyst described below, the Pt catalyst solution was prepared in the drybox by adding, in the following order, 1.7 mL of toluene to a new 22 x 175 mm Pyrex borosilicate culture tube containing a new 5/8 x 5/16 inch Teflon-coated magnetic stirbar, followed by 0.4 mL of the Pt precatalyst solution, and with 1000 rpm stirring, 0.4 mL of a 36.0 mM toluene solution of $AlEt_3$, giving $Al/Pt = 4.0$. No color change of the light-yellow solutions was apparent upon the addition of $AlEt_3$. Finally, 0.5 mM of

cyclohexene was added, and the tube was sealed in a Fisher–Porter (FP) bottle. The hydrogenation procedure was also similar to that used for the Co catalyst described below, the only differences being the use of H₂ (General Air, 99.5%) instead of D₂, and the FP bottle was purged with 40 psig of H₂ once every 15 seconds for 3.5 min (15 purges total). The light-yellow solutions gradually changed color to brown during the hydrogenation runs. After pressure data acquisition, data were converted to [cyclohexene] vs. time with MS excel according to the procedure employed with the cyclohexene hydrogenation reporter reaction method [2,3,4].

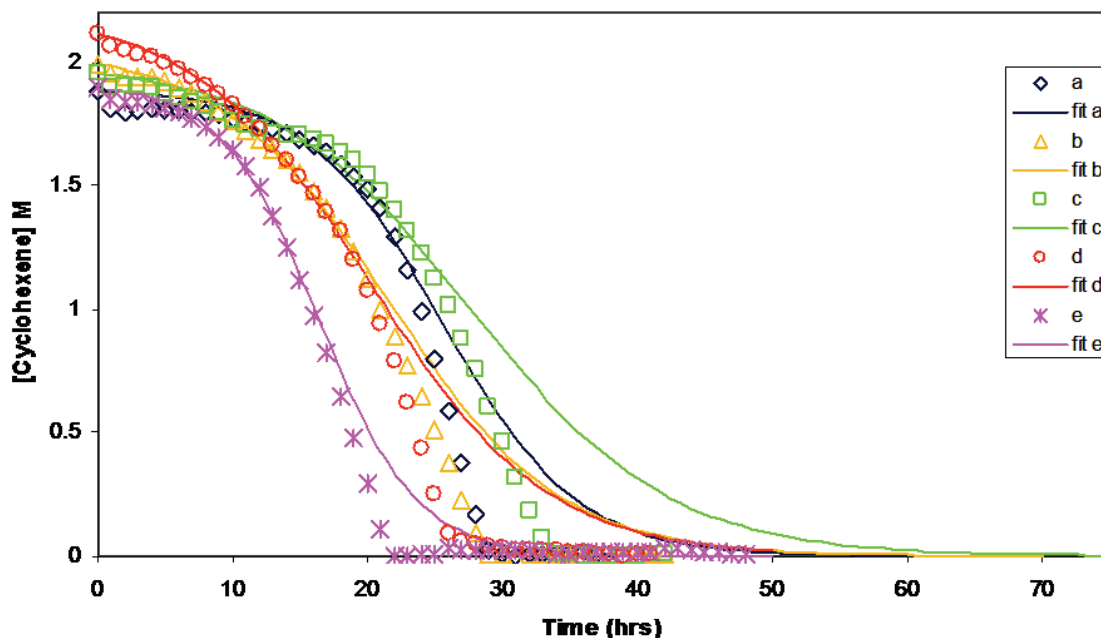


Figure SI-A1. Five catalytic cyclohexene hydrogenation runs using $\text{Pt}(\text{acac})_2 + \text{AlEt}_3$, $\text{Al/Pt} = 4$, $[\text{Pt}] = 1.2 \text{ mM}$, solvent = toluene, temperature = $22.0 \text{ }^\circ\text{C}$, initially 40.0 psig H_2 , stirring = 1000 rpm. Solid lines show the attempted fits by the 2-step mechanism for nanocluster formation [3] consisting of nucleation ($A \rightarrow B$, rate constant k_1) followed by autocatalytic growth ($A + B \rightarrow 2B$, rate constant k_2), giving mean values: $k_1 = 0.004(2) \text{ s}^{-1}$, $k_2 = 0.09(3) \text{ M}^{-1}\text{s}^{-1}$, and a range of R^2 values from 0.9491 to 9954.

The near-sigmoidal-shaped curves, Figure SI-A1, were fit using Origin by the well-precedented, 2-step mechanism of nanocluster formation consisting of nucleation ($A \rightarrow B$, rate constant k_1) followed by autocatalytic growth ($A + B \rightarrow 2B$, rate constant k_2) [3], giving mean values of $k_1 = 0.004(2)$ and $k_2 = 0.09(3)$. The kinetic model fits the initial portions of the curves well, but not the later portions, which deviate from sigmoidal by abruptly ending at the point where all the substrate has been consumed. This implies that changes involving the catalyst(s)—*specifically the evolution of a more active catalyst*—is occurring. These results show that this system, the very similar one investigated by Bönemann and coworkers [1], or another comparable system, are of interest for studies aimed at the mechanism of formation of Ziegler-type hydrogenation catalysts.

Other Survey Hydrogenations En Route to Potentially Useful Ziegler–type Hydrogenation Catalyst Model Systems

A few other precursors were combined with AlEt_3 and the resulting solutions tested for their ability to catalytically hydrogenate cyclohexene, specifically the precursors $[(1,5\text{-COD})\text{Ir}(\text{acac})]$, $[(1,5\text{-COD})\text{Rh}(\text{acac})]$, $\text{Rh}(\text{acac})_3$, and $\text{Co}(\text{acac})_2$. The results are shown below, Figures SI-A2–SI-A5. Catalyst solutions were prepared similarly to as described above. In the drybox, a 3.6 mM in $[\text{Ir}]$ solution of $[(1,5\text{-COD})\text{Ir}(\text{acac})]$ (Strem, 99%) was prepared by weighing out 0.0237 g of $[(1,5\text{-COD})\text{Ir}(\text{acac})]$ and dissolving in 16.48 mL of cyclohexane. The catalyst was prepared in a culture tube by adding in the following order 1.2 mL of cyclohexane, 1.0 mL of the yellow $[(1,5\text{-COD})\text{Ir}(\text{acac})]$ solution, and with 1000 rpm stirring, 0.3 mL of a 36.0 mM AlEt_3 solution in cyclohexane, making $\text{Al}/\text{Ir} = 3$. For $[(1,5\text{-COD})\text{Rh}(\text{acac})]$ (Strem, 98%), 0.292 g were dissolved in 2.3 mL of cyclohexane in a culture tube. Next, 0.20 mL of a 36.0 mM cyclohexane solution of AlEt_3 was then added with 1000 rpm stirring, giving $\text{Al}/\text{Rh} = 2$. For $\text{Rh}(\text{acac})_3$ (Aldrich, 97%), 0.267 g was dissolved in 16.68 mL toluene. Then, 1.4 mL toluene, 0.9 mL of the $\text{Rh}(\text{acac})_3$ solution, and afterwards, with 1000 rpm stirring, 0.2 mL of a 36.0 mM toluene solution of AlEt_3 were added to a culture tube, giving $\text{Al}/\text{Rh} = 2$. For $\text{Co}(\text{acac})_2 \cdot 0.34\text{H}_2\text{O}$ (Strem; H_2O determined by TGA), 0.0386 g were dissolved in 16.3 mL of toluene. Next, 0.4 mL of this solution were added to a culture tube along with 1.7 mL of toluene, and then with 1000 rpm stirring, 0.4 mL of a 36.0 mM toluene solution of AlEt_3 were added, making the $\text{Al}/\text{Co} = 4$. Lastly in each case, 0.5 mL of cyclohexene was added. The hydrogenation procedure, H_2 gas purge cycle, data collection, data conversion, and fitting procedure were all performed the same as described above for experiments using the $\text{Pt}(\text{acac})_2$ precursor. (The data from the $\text{Co}(\text{acac})_2$ system was not converted from psig H_2 to

[cyclohexene] nor fit.) All of the precatalysts tested form active catalysts for the hydrogenation of cyclohexene. However, the most promising Ziegler-type hydrogenation catalyst system for use as a model of industrial catalysts, besides the [(1,5-COD)M(m-O₂C₈H₁₅)]₂ (M = Rh or Ir) + AlEt₃ systems reported elsewhere [5], is the Pt(acac)₂ + AlR₃ system described above.

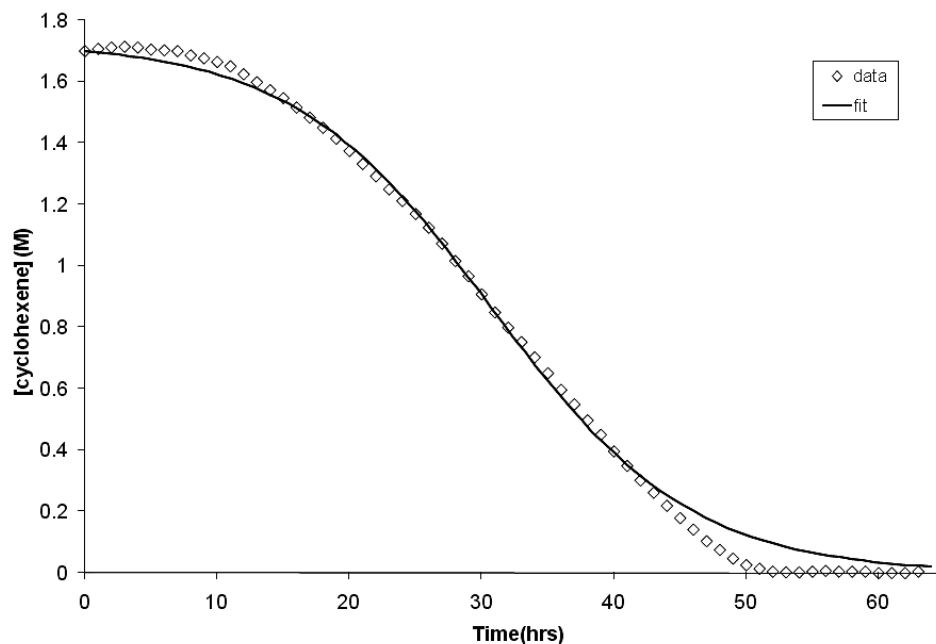


Figure SI-A2. Catalytic cyclohexene hydrogenation using a Ziegler-type hydrogenation catalyst made from addition of AlEt_3 to $[(1,5\text{-COD})\text{Ir}(\text{acac})]$, $\text{Al}/\text{Ir} = 3$, $[\text{Ir}] = 1.2 \text{ mM}$, initially 40.0 psig H_2 , solvent = cyclohexane, temperature = 22.0 °C, stirring = 1600 rpm. The solution changed from yellow to light brown during hydrogenation. The data is reasonably well fit using the well-precedented mechanism for nanocluster formation consisting of nucleation ($\text{A} \rightarrow \text{B}$, rate constant k_1) followed by autocatalytic growth ($\text{A} + \text{B} \rightarrow 2\text{B}$, rate constant k_2) [3], giving $k_1 = 0.0022(1) \text{ s}^{-1}$, $k_2 = 0.077(2) \text{ M}^{-1}\text{s}^{-1}$. However, small amounts of a black solid, presumably bulk Ir metal, were deposited on the stirbar and sides of the culture tube. The shape of the hydrogenation curve and apparently relatively slow catalyst formation show that this system has promise, but the formation of the insoluble black solid is an undesired feature of this system.

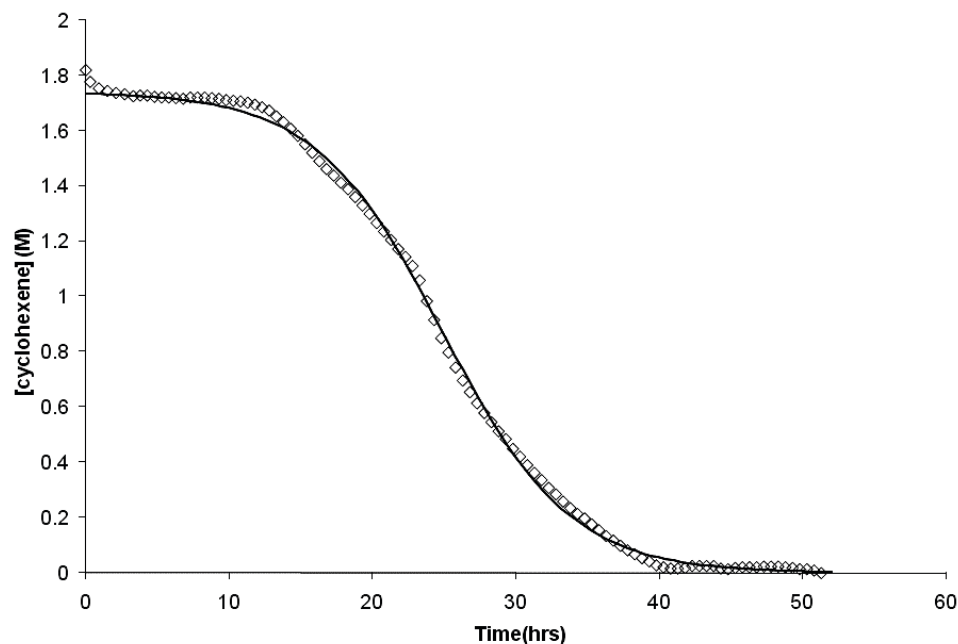


Figure SI-A3. Catalytic cyclohexene hydrogenation using a Ziegler-type hydrogenation catalyst made from addition of AlEt_3 to $[(1,5\text{-COD})\text{Rh}(\text{acac})]$, $\text{Al/Rh} = 2$, $[\text{Rh}] = 1.2 \text{ mM}$, initially 40.0 psig H_2 , solvent = cyclohexane, temperature = 22.0 °C, stirring = 1600 rpm. The data is moderately well fit using the well-precedented mechanism for nanocluster formation consisting of nucleation ($\text{A} \rightarrow \text{B}$, rate constant k_1) followed by autocatalytic growth ($\text{A} + \text{B} \rightarrow 2\text{B}$, rate constant k_2) [3], giving $k_1 = 0.0018(1) \text{ s}^{-1}$, $k_2 = 0.130(4) \text{ M}^{-1}\text{s}^{-1}$. However, the hydrogenation data contain several interesting and unexplained features not well accounted for by the mechanistic model used here, and as a comparison of the above data and solid fit line reveal. In addition, small amounts of a black solid, presumably bulk Rh metal, deposited on the stirbar and sides of the culture tube. The unexplained features of the hydrogenation curve make this system interesting, but the formation of the black solid is an undesired feature. Also, the precatalyst $[(1,5\text{-COD})\text{Rh}(\text{acac})]$ should be stored cold.

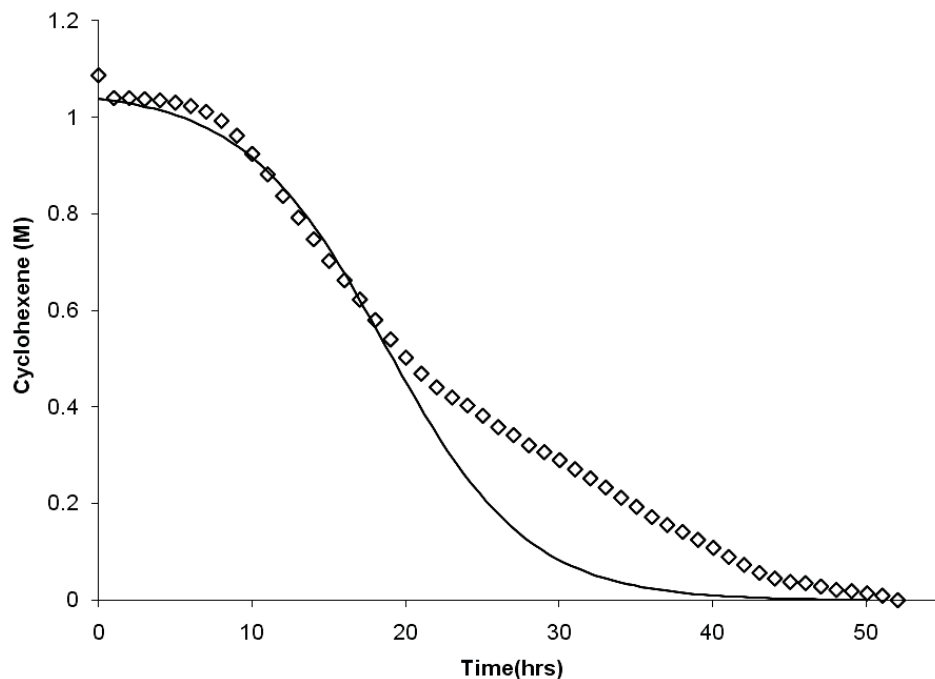


Figure SI-A4. Catalytic cyclohexene hydrogenation using a Ziegler-type hydrogenation catalyst made from addition of AlEt_3 to $\text{Rh}(\text{acac})_3$, $\text{Al/Rh} = 2$, $[\text{Rh}] = 1.2 \text{ mM}$, initially 40.0 psig H_2 , solvent = toluene, temperature = 22.0 °C, and stirring = 1000 rpm. The data are poorly fit using the 2-step mechanism of nanocluster formation consisting of nucleation ($\text{A} \rightarrow \text{B}$, rate constant k_1) followed by autocatalytic growth ($\text{A} + \text{B} \rightarrow 2\text{B}$, rate constant k_2) [3]; the resulting $k_1 = 0.0038(6) \text{ s}^{-1}$ and $k_2 = 0.20(1) \text{ M}^{-1}\text{s}^{-1}$. This system gives an unexplained, and interestingly-shaped hydrogenation curve, but was not pursued further.

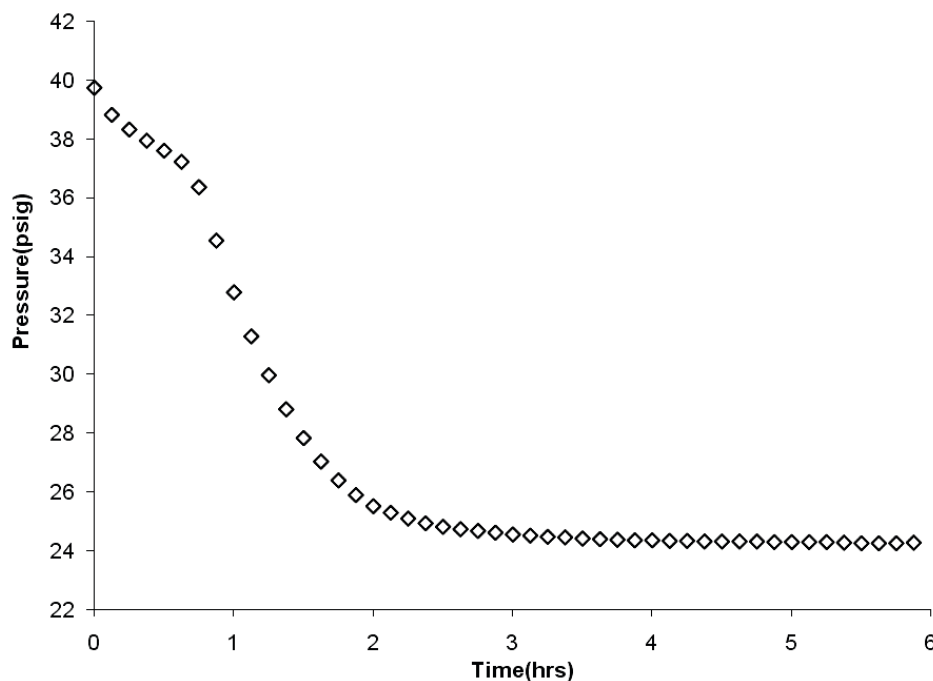
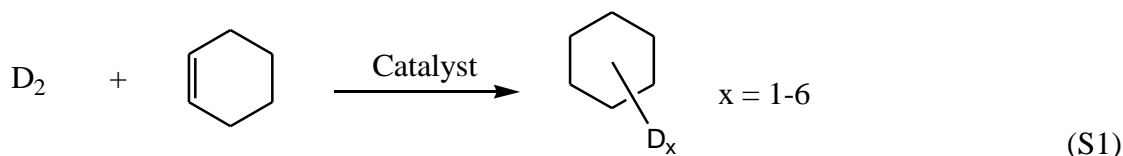


Figure SI-A5. Catalytic cyclohexene hydrogenation using a Ziegler-type hydrogenation catalyst made from addition of AlEt_3 to $\text{Co}(\text{acac})_2 \cdot 0.34\text{H}_2\text{O}$, $\text{Al/Co} = 4$, $[\text{Co}] = 1.2 \text{ mM}$, initially 40.0 psig H_2 , solvent = toluene, temperature = 22.0 °C, and stirring = 1000 rpm. No attempt was made to fit this irregular hydrogenation curve.

A Deuterium Labeling Experiment [6] with a $\text{Co}(\text{neodecanoate})_2$ plus AlEt_3 Catalyst leading to an Updated, Proposed Hydrogenation Mechanism for Ziegler-type Hydrogenation Catalysts

A Ziegler-type hydrogenation catalyst made from combination of $\text{Co}(\text{neodecanoate})_2$ and AlEt_3 , $\text{Al/Co} = 3$, was used to catalytically hydrogenate cyclohexene in a pressurized, Fisher-Porter reaction bottle. When D_2 gas was used, analysis of the resulting products by gas chromatography mass spectrometry (GC-MS) showed significant incorporation of multiple (i.e., > 2) deuterium atoms in the resulting cyclohexane, Equation S1. As stated in the main text, this outcome supports the hypothesis that, at least according to a generally well-accepted mechanism for heterogeneous transition metal catalyzed hydrogenations [7], reductive elimination, as

opposed to migratory insertion [8], is the rate determining step, with prior equilibria existing in the earlier step(s).



Under an N_2 atmosphere in a Vacuum Atmospheres drybox (O_2 levels were maintained at ≤ 5 ppm as monitored by a Vacuum Atmospheres O_2 -level monitor), an 18.0 mM in [Co] cyclohexane (Sigma-Aldrich, anhydrous, 99.5%) solution was prepared from a $Co(neodecanoate)_2$ precatalyst solution (70% $Co(neodecanoate)_2$, 30% mineral spirits) by adding 0.58 ± 0.01 mL to a 100 mL volumetric flask and diluting to the mark. Catalyst solutions were then made individually before use by adding, in the following order, 2.0 ± 0.05 mL of cyclohexane to a new 22 x 175 mm Pyrex borosilicate culture tube containing a new 5/8 x 5/16 inch Teflon-coated magnetic stirbar, followed by 0.200 ± 0.002 mL of the Co precatalyst solution, and with stirring at 1000 rpm, 0.30 ± 0.01 mL of a 36.0 mM cyclohexane solution of $AlEt_3$ (Aldrich, 93%), giving a Al/Co = 3.0 catalyst. $AlEt_3$ was added rapidly resulting in a near instantaneous color change from the indigo Co precursor solution to dark brown. Lastly, 0.50 ± 0.01 mL of cyclohexene (Aldrich, 99%, distilled over Na under an Ar atmosphere) was added to the culture tube. The culture tube was then placed in a Fisher-Porter (FP) bottle, which was sealed and brought out of the drybox in order to attach it to the hydrogenation apparatus [3,4,9]. The F-P bottle was placed in a 22.0 °C recirculating water bath (VWR Scientific) and connected to the apparatus using TFE-sealed Swagelock quick-connects. D_2 gas (Matheson, 99.5%) was purified by passing through an indicating moisture trap (Scott Specialty Gas), a disposable O_2 cartridge (Trigon), and an indicating O_2 trap (Trigon). Stirring at 1000 rpm was started, the bottle was purged with D_2 gas at 40 psig a total 5 times (once every 30 s), set at 40 psig, and

pressure data acquisition was started by means of an Omega PX-624 pressure transducer interfaced to a PC running LabVIEW 7.0.

Pressure in the FP bottle reached a minimum value after 12 min, and after observing a constant value for > 4 min, the sealed FP bottle was detached and brought back into the drybox. Inside the drybox, samples for analysis by GC–MS were prepared by taking 40 μL of the hydrogenation reaction solution in cyclohexane and diluting with 2 mL of acetone (Burdick and Jackson). GC–MS analysis was performed on an Agilent 5973N/GC 6890 instrument equipped with a mass selective detector (70 eV) and an SPB-1, 30 m column. Temperature program: initial temperature, 10 $^{\circ}\text{C}$ (initial time 5.00 min); heating rate, 10.00 $^{\circ}\text{C}/\text{min}$; final temperature, 100 $^{\circ}\text{C}$. The results of analyzing the sample by GC–MS are shown below in Figure S6. The majority of the deuterated product appears at the front of the broad peak in the GC portion (top) of Figure S6. The MS portion (bottom) of Figure S6 is the segment of the GC peak at the retention time of 5.378 min.

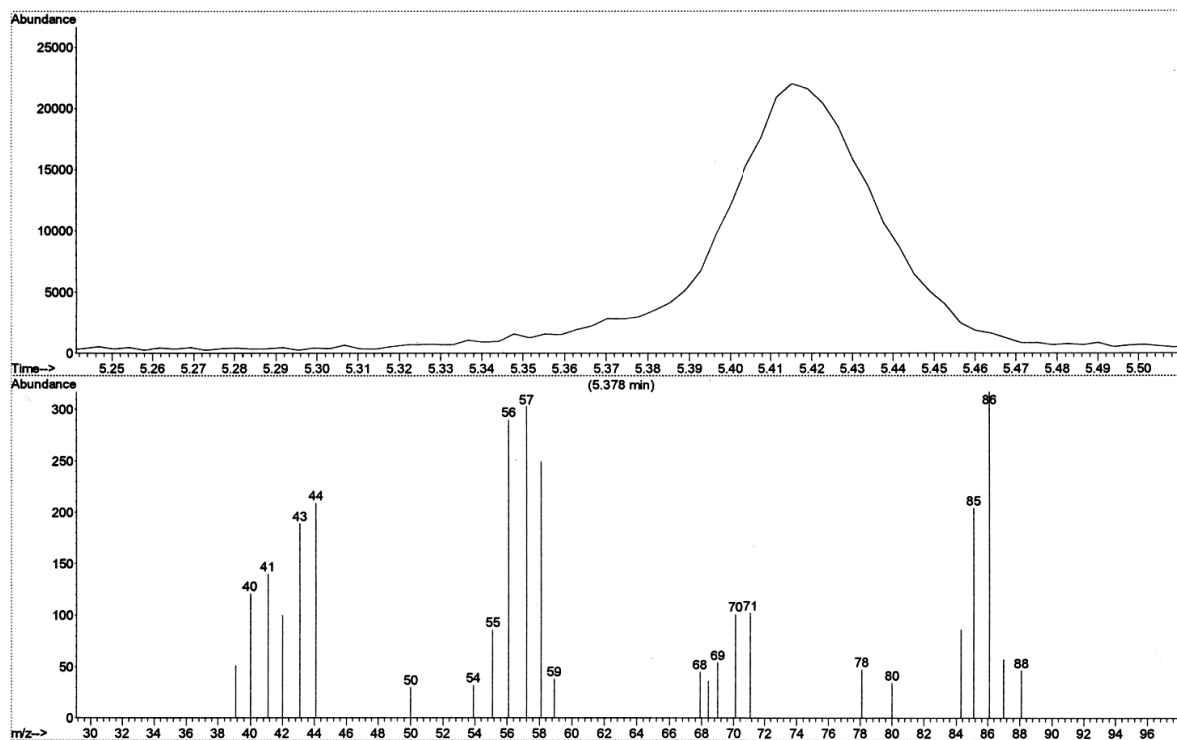


Figure SI-A6. GC MS of a sample from the deuteration of cyclohexene using a $\text{Co}(\text{neodecanoate})_2$ plus AlEt_3 , $\text{Al/Co} = 3.0$, Ziegler-type hydrogenation catalyst. GC (top) shows a single broad peak encompassing both undeuterated cyclohexane (the solvent) and deuterated cyclohexane, the catalytic reaction product. The deuterated cyclohexane is principally found at the leading edge of the peak, evident as the tail on the left. MS (bottom) taken at a retention time of 5.378 min contains significant amounts of multiply (> 2) deuterated cyclohexane ($m/z > 86$).

Peaks of m/z 84 (cyclohexane- d_0) through m/z 88 (cyclohexane- d_4) from individual mass spectra at close time intervals between 5.359min on the leading edge of the peak and the peak maximum at 5.411min were used to calculate the relative amounts of product deuteration, Figure S7. (The m/z – extent of deuterium inclusion correlations were made without regard given to the 1.1% natural abundance of ^{13}C .) On the front edge of the peak there is a significant presence of triply- and quadruply-deuterated cyclohexane (about 60% of the total at 5.359 min). This result supports the hypothesis that reductive elimination is the rate determining step in the proposed cyclohexene hydrogenation mechanism, Scheme 8 of the main text. If migratory insertion was

rate-determining [8], then a maximum of two deuterium atoms per cyclohexane should have been seen.

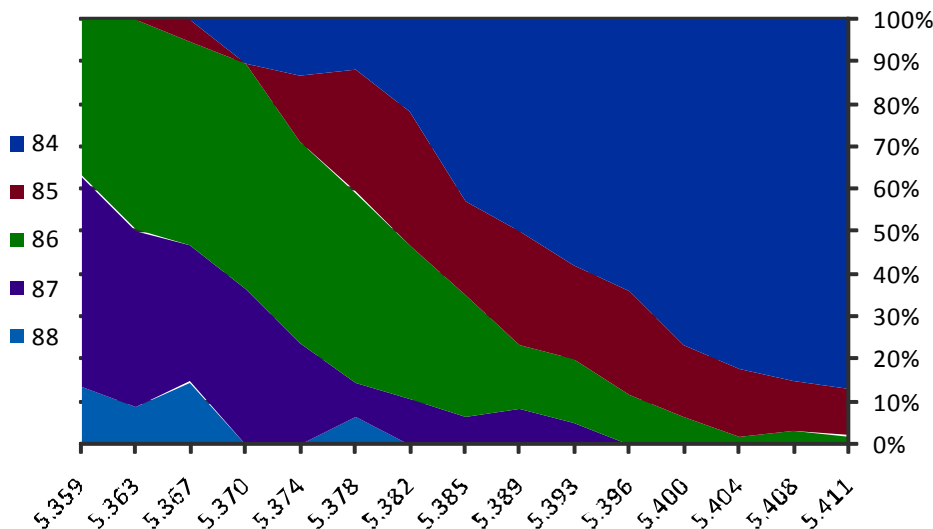


Figure SI-A7. Relative abundances, as a function of retention time, of cyclohexane- d_0 , $m/z = 84$ (dark blue); cyclohexane- d_1 , $m/z = 85$ (red), cyclohexane- d_2 , $m/z = 86$ (green), cyclohexane- d_3 , $m/z = 87$ (purple), and cyclohexane- d_4 , $m/z = 88$ (light blue). The natural 1.1% abundance of ^{13}C has been neglected in calculating these percentages. Triply- and quadruply-deuterated cyclohexane together make up more than 60% of the cyclohexane in the sample at the retention time of 5.359 min, supporting reductive elimination as the rate determining step in the updated cyclohexene hydrogenation mechanism, Scheme 8 of the main text.

Other Experimental Considerations

All materials were stored and used as received in the drybox unless noted otherwise. All glassware was oven-dried at 160 °C overnight and cooled either under vacuum or an atmosphere of N_2 . **Caution!** *Aluminum alkyls such as AlEt_3 are toxic and pyrophoric and must therefore be handled accordingly* [10].

REFERENCES

- [1] K. Angermund, M. Bühl, U. Endruschat, F. Mauschick, R. Mörtel, R. Mynott, B. Tesche, N. Waldöfner, H. Bönemann, G. Köhl, H. Modrow, J. Hormes, E. Dinjus, F. Gassner, H.-G. Haubold, T. Vad, M. Kaupp, *J. Phys. Chem. B* 107 (2003) 7507–7515.
- [2] Y. Lin and R. G. Finke, *J. Am. Chem. Soc.* 116 (1994) 8335–8353.
- [4] M. A. Watzky, R. G. Finke, *J. Am. Chem. Soc.* 119 (1997) 10382–10400.
- [5] J. A. Widegren, J. D. Aiken III, S. Özkar, R. G. Finke, *Chem. Mater.* 13 (2001) 312–324.
- [6] W. M. Alley, C. W. Girard, S. Özkar, R. G. Finke *Inorg. Chem.* 48 (2009) 1114–1121.
- [7] (a) R. L. Burwell, *Acc. Chem. Res.* 2 (1969) 289. (b) K. Schrage, R. L. Burwell, *J. Am. Chem. Soc.* 88 (1966) 4555. (c) J. J. Philipson, R. L. Burwell, *J. Am. Chem. Soc.* 92 (1970) 6125.
- [8] R. L. Augustine, F. Yaghmaie, J. F. Van Peppen, *J. Org. Chem.* 49 (1984) 1865.
- [9] F. K. Schmidt, V. G. Lipovich, S. M. Krasnopol'skaya, I. V. Kalechits, *Kinetika i Kataliz*, 11 (1970) 595–602.
- [10] Y. Lin, R. G. Finke, *Inorg. Chem.* 33 (1994) 4891–4910.
- [11] D. F. Shriver, M. A. Drezdon *The Manipulation of Air-Sensitive Compounds*, second ed., John Wiley and Sons, New York, 1986.

CHAPTER III

HYDROCARBON-SOLUBLE, ISOLABLE ZIEGLER-TYPE Ir(0)_n NANOPARTICLE CATALYSTS MADE FROM [(1,5-COD)Ir (μ-O₂C₈H₁₅)₂] AND 2-5 EQUIVALENTS OF AlEt₃: THEIR HIGH CATALYTIC ACTIVITY, LONG LIFETIME, AND AlEt₃-DEPENDENT, EXCEPTIONAL, 200 °C THERMAL STABILITY

This dissertation chapter contains the manuscript of a paper published in the *ACS Catal.* **2012**, 2, 632-641. This chapter demonstrates the high catalytic activity, long lifetime and unusually high thermal stability of the Ir(0)_n Ziegler nanoparticles formed in the catalyst solution starting with [Ir(1,5-COD)(μ-O₂C₈H₁₅)₂] plus AlEt₃.

All the experiments in the main text were performed by Isil K. Hamdemir. The repeat hydrogenation runs for lifetime measurements were performed by Saim Özkar. Control and survey experiments presented in the Supporting Information (Supporting Information_B) were performed by both Isil K. Hamdemir and Kuang-Hway Yih. The initial complete draft of the paper, subsequent drafts including the final draft and preparation of the document for publication were performed by Isil K. Hamdemir with light editing by Prof. Saim Özkar, Dr. Kuang-Hway Yih, Joseph E. Mondloch and extensive editing by Prof. Richard G. Finke (a 48 hours total).

Synopsis

Hydrocarbon-solvent-soluble, isolable, Ziegler-type $\text{Ir}(0)_n$ nanoparticle hydrogenation catalysts made from the crystallographically characterized $[(1,5\text{-COD})\text{Ir}(\mu\text{-O}_2\text{C}_8\text{H}_{15})]_2$ precatalyst and 2-5 equivs of AlEt_3 (≥ 2 equivs of AlEt_3 being required for the best catalysis and stability, *vide infra*) are scrutinized for their catalytic properties of: (1) their isolability and then redispersibility without visible formation of bulk metal; (2) their initial catalytic activity of the isolated nanoparticle catalyst redispersed in cyclohexane; (3) their catalytic lifetime in terms of total turnovers (TTOs) of cyclohexene hydrogenation; and then also and unusually (4) their relative thermal stability in hydrocarbon solution at 200 °C for 30 minutes. These studies are of interest since $\text{Ir}(0)_n$ nanoparticles are the currently best-characterized example, and a model / analogue, of industrial Ziegler-type hydrogenation catalysts made, for example, from $\text{Co}(\text{O}_2\text{CR})_2$ and ≥ 2 equivalents of AlEt_3 . Eight important insights result from the present studies, the highlights of which are that $\text{Ir}(0)_n$ Ziegler nanoparticles, made from $[(1,5\text{-COD})\text{Ir}(\mu\text{-O}_2\text{C}_8\text{H}_{15})]_2$ and AlEt_3 , are: (i) quite catalytically active and long-lived; (ii) thermally unusually stable nanoparticle catalysts at 200 °C, *vide infra*, a stability which requires the addition of at least 3 equivalents of AlEt_3 ($\text{Al}/\text{Ir}=3$), but where (iii) the $\text{Al}/\text{Ir}=5$ $\text{Ir}(0)_n$ nanoparticles are even more stable, for ≥ 30 minutes at 200 °C, and exhibit 100 000 TTOs of cyclohexene hydrogenation. The results also reveal that (iv) the observed nanoparticle catalyst stability at 200 °C appears to surpass that of any other demonstrated nanoparticle *catalyst* in the literature, those reports being limited to $\leq 130\text{--}160$ °C temperatures; and reveal that (v) AlEt_3 , or possibly surface derivatives of AlEt_3 , along with $[\text{RCO}_2\cdot\text{AlEt}_3]^-$ formed from the 1st equiv of AlEt_3 per $\frac{1}{2}$ equiv of $[(1,5\text{-COD})\text{Ir}(\mu\text{-O}_2\text{C}_8\text{H}_{15})]_2$ are main components of the nanoparticle stabilizer system, consistent with previous suggestions from Schmidt, Goulon, Bönnemann and others. The results therefore also (vi) imply that either

(a) a still poorly understood mode of nanoparticle stabilization by alkyl Lewis acids such as AlEt₃ is present or, (b) that reactions between the Ir(0)_n and AlEt₃ occur to give initially surface species such as (Ir_{surface})_x-Et plus (Ir_{surface})_x-Al(Et)₂Ir, where the number of surface Ir atoms involved, x = 1-4; and (vii) confirm the literature's suggestion that the activity of Ziegler-type hydrogenation can be tuned by the Al/Ir ratio. Finally and perhaps most importantly, the results herein along with recent literature make apparent (viii) that isolable, hydrocarbon soluble, Lewis-acid containing, Ziegler-type nanoparticles are an underexploited, still not well understood type of high catalytic activity, long lifetime and unusually if not unprecedentedly high thermal stability nanoparticles for exploitation in catalysis or other applications where their unusual hydrocarbon solubility and thermal stability might be advantageous.

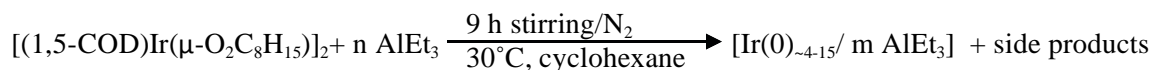
1. Introduction

Ziegler-type, hydrocarbon-solvent-soluble hydrogenation catalysts are formed, by definition [1], from a non-zero valent group 8-10 transition metal precatalyst such as the industrial example [1,2] of Co(neodecanoate)₂ plus a trialkylaluminum cocatalyst, for example AlEt₃. These catalysts are used industrially to produce hydrogenated styrenic block copolymers at a level of ~1.7 × 10⁵ metric tons/year [2,3]. Ziegler-type hydrogenation catalysts made from *third-row elements* of the same column metal (i.e., Ir as an analog of Co Ziegler-type hydrogenation catalysts) are also important,[1] such third-row metals allowing more robust, more easily characterized catalysts [4].

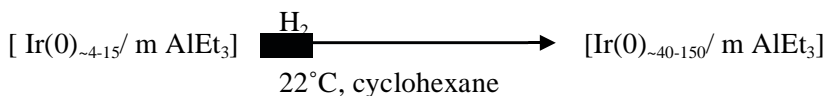
We recently reported high activity Ziegler-type *nanoparticle* hydrogenation catalysts made from the crystallographically characterized [(1,5-COD)Ir(μ-O₂C₈H₁₅)₂] precatalyst [3] plus AlEt₃, Al/Ir=1, 2, 3 or 5 [4], Scheme 3.1. (An Al/Ir=1 catalyst means 1 equivalent of AlEt₃ is added per Ir, i.e., 1 equivalent AlEt₃ is added to 0.5 equivalent of the [(1,5-COD)Ir(μ-O₂C₈H₁₅)₂]

precatalyst dimer). Subsequent studies, using X-ray absorption fine structure spectroscopy (XAFS), Z-contrast scanning transmission electron microscopy (STEM) plus matrix assisted laser desorption ionization mass spectroscopy (MALDI MS), revealed that sub-nanometer particles of an estimated mean-size range of Ir(0)_{~4-15} are formed *initially* as a result of simply mixing [(1,5-COD)Ir(μ -O₂C₈H₁₅)₂] plus AlEt₃ at Al/Ir=1, 2, 3 or 5 (Scheme 3.1, Equation 1). Regardless of the Al/Ir ratio examined (Al/Ir=1-5) or the initial [Ir] concentration ([Ir] = 1.0-7.0 mM), the initially formed Ir(0)_{~4-15} particles were then shown to transform under H₂/cyclohexene hydrogenation catalysis conditions (Scheme 3.1, Equation 2) [4], to Ir(0)_{~40-150} *Ziegler-type nanoparticles* [5,6,7,8] according to XAFS, STEM and MALDI MS characterization results—a new, hydrocarbon soluble, AlR₃-dependent type of catalytically active nanoparticle [1,4], *vide infra*. Concomitant with this transformation to *fcc* Ir(0)_{~40-150} Ziegler nanoparticles, an increase in the catalytic activity in cyclohexene hydrogenation is observed [4]. The combined kinetic, plus XAFS, STEM and MALDI MS characterization, studies both before and after catalysis provide the best evidence to date that Ziegler-type Ir(0)_n nanoparticles both exist and appear to be the fastest catalysts in Ziegler-type hydrogenations [1,4]. The finding of kinetically dominant catalysis by Ziegler nanoparticles is significant since it answers a 50-year old question about the nature of the true catalyst under Ziegler hydrogenation catalysis conditions [1]. Indeed, nanoparticles (or, when these catalysts were first discovered, “colloids”[9,10,11,12,13,14,15,16,17,18,19,20,21]) have been discussed as the possible true catalysts for 50 years now, but definitive demonstration that Ziegler nanoparticles are both present *and* are the most active catalysts in Ziegler-type hydrogenation catalysis [1,2] was previously lacking [1,4].

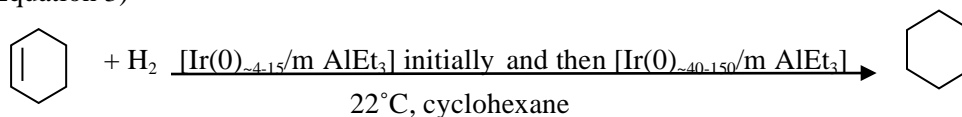
(Equation 1)



(Equation 2)



(Equation 3)



^aConditions for catalyst preparation (eq. 1) are: cyclohexane solvent, [Ir]=1.4 mM, 30°C, N₂ atmosphere. Conditions for cyclohexene hydrogenation (eqs. 2 and 3) are: cyclohexane solvent, [Ir]=1.2 mM (except where noted otherwise), [cyclohexene]_{initial}=1.65 M, 22.0 ± 0.1 °C, 40 ± 1 psig H₂. The side products in Equation 1 include 1,5-COD, O₂C₈H₁₅⁻, and (n-m) AlEt₃ (n≥m) or their combinations.

Scheme 3.1. Ziegler-type hydrogenation catalyst preparation, and subsequent cyclohexene hydrogenation, from [(1,5-COD)Ir(μ-O₂C₈H₁₅)]₂ plus AlEt₃, Al/Ir= 2, 3 or 5.^a

The Ziegler-type nanoparticle catalysts are unusual in that they *are hydrocarbon soluble*. They are further unusual as at least ostensibly an example of “weakly ligated/labile-ligand nanoparticles”[5,6,7,22] in this case nanoparticles in which the only possible ligands are cyclohexane, AlEt₃ Lewis acid (or its nanoparticle surface-derivatives), carboxylates such as C₇H₁₅CO₂⁻ and H₂ (and/or metal hydrides) plus cyclohexene. All these are either relatively weak ligands, or the actual reagents of the desired reaction (H₂ plus cyclohexene hydrogenations), *other than the AlEt₃* (and the combination [C₇H₁₅CO₂•AlEt₃]⁻ for the first equivalent of AlEt₃ per ½[(1,5-COD)Ir(μ-O₂C₈H₁₅)]₂, eq. 1, *vide supra*). Significantly, the high stability of the Ir(0)_n nanoparticles reported herein at ratios ≥2 of AlEt₃ per ½[(1,5-COD)Ir(μ-O₂C₈H₁₅)]₂ would seem to indicate a robust interaction between the Ir(0)_n nanoparticle and the AlEt₃, *vide infra*. Restated,

Ziegler-type nanoparticles appear to be an unusual type of little recognized, and hence underexploited, nanoparticle catalyst, ones used industrially but hidden for a 50-year period due to a lack of knowledge of the probable true catalyst [1,2].

It became, therefore, of significant interest to examine the catalytic activity, lifetime and thermal stability of these hydrocarbon soluble, Ir(0)_n Ziegler-type nanoparticles, as a function of the Al/Ir molar ratio of the AlEt₃ cocatalyst and Ir metal precatalyst [1]. Just how active, long lived and thermally stable are these unusual, hydrocarbon soluble, AlR₃ containing nanoparticles? Relevant here is the previously developed, so-called “five-criteria method” [23,24,25,26] to rank the formation and then stabilizing abilities of various anions, solvents, cations and polymers for catalytically active nanoparticles, a method developed specifically with Ir(0)_n nanoparticles [27].

Herein, a necessarily modified version [28] of the five-criteria ranking method [23,24,25,26,27] is developed and then used to evaluate the catalytic properties of the Ir(0)_n Ziegler-type nanoparticle hydrogenation catalysts made from [(1,5-COD)Ir(μ-O₂C₈H₁₅)₂] plus AlEt₃, as a function of Al/Ir ratios from primarily 2-5 (with 0-1 being examined in control reactions). Those modified evaluation criteria used herein are: (i) the isolability and then redispersibility of the resultant nanoparticle catalyst without visible formation of bulk metal—historically a demanding test of nanoparticle stability [23,24,25,26]; (ii) the initial catalytic activity of the isolated catalyst redispersed in cyclohexane; (iii) the catalytic lifetime; and then also (iv) the thermal stability of the catalyst solution as determined by the ability of the stabilizing species to keep the nanoparticles in solution at 200 °C for 30 minutes without the visible formation of bulk metal. The enhanced (*vide infra*) thermal stability of the Ziegler nanoparticle catalyst solutions is important, since industrial applications of Ziegler-type

hydrogenation catalysts report catalyst preparation temperatures up to 250 °C, and then polymer hydrogenations up to 180 °C [1,29,30]. However, no prior study has examined the thermal stability of a firmly established Ziegler nanoparticle catalyst, in our case an Ir(0)_n catalyst, under controlled conditions.

2. Results and Discussion

*Ir(0)*_{~40-150} “Ziegler Nanoparticle” Catalyst Synthesis and Cyclohexene Hydrogenation: Our review of the literature of Ziegler-type catalysis [1] reveals that the following variables have significant effects on the catalytic activity and other properties of the catalyst [4]: the Al/Ir ratio; the order and rate of addition of the precatalyst and cocatalyst; the solvent used; aging of the initial catalyst material; and whether or not the olefin substrate is present during the initial precatalyst and cocatalyst addition step. Hence, and as detailed in the Experimental section and based on our published experience [4], the Ziegler type Ir(0)_n/AlEt₃ hydrogenation catalysts were prepared from [(1,5-COD)Ir(μ-O₂C₈H₁₅)₂] and AlEt₃, by adding quickly (over 2 sec) a cyclohexane solution of AlEt₃ to a cyclohexane solution of [(1,5-COD)Ir(μ-O₂C₈H₁₅)₂], all while vigorously stirring at 30 °C under N₂. This resultant solution was then aged [1,4] by further stirring for 9 h under N₂ at 30 °C (Scheme 3.1, Equation 1).

Cyclohexene hydrogenation was used as a test reaction to measure the activity and lifetime of [(1,5-COD)Ir(μ-O₂C₈H₁₅)₂] plus AlEt₃, Al/Ir=2, 3 or 5, catalysts, Scheme 3.1, eqs. 2, 3. These catalysts were also tested for their thermal stability by first preparing the catalyst solution in dodecane solvent and then performing a cyclohexene hydrogenation at room temperature. The resulting catalyst solution was then kept at 200 °C for 30 min, followed by a test of cyclohexene hydrogenation activity back at room temperature of the resultant, thermalized nanoparticles. The

transmission electron microscopy (TEM) images of the post catalyst samples were also obtained, *vide infra*.

Redispersibility, Catalytic Activity and Lifetime in Cyclohexane of Ziegler-type Hydrogenation Catalysts made from [(1,5-COD)Ir(μ -O₂C₈H₁₅)]₂ plus AlEt₃, Al/Ir = 2, 3 or 5:

All three catalysts made from [(1,5-COD)Ir(μ -O₂C₈H₁₅)]₂ and AlEt₃, Al/Ir=2, 3 or 5, are isolable as brown/black powders by evaporation of the volatiles under vacuum. The isolated catalysts are then *fully redispersible in cyclohexane* hydrocarbon solvent without visible formation of bulk metal, Figure 3.1 (Table 3.1, entries 1-3, column 3) [31].

For the redispersed catalysts (Al/Ir=2, 3 or 5), hydrogenations start immediately and continue in a slightly sigmoidal fashion until consumption of the cyclohexene is complete, Figure 2, with catalytic activities of 10(3), 7(2) and 3(1) mmol H₂/h [32] for the Al/Ir=2, 3 and 5 catalysts, respectively (Table 3.1, entries 1-3, column 4). The TEM results in Figure 3.1 show that the redispersed Ir(0)_n Ziegler type catalysts for the Al/Ir=2 and Al/Ir=5 ratios are the same size within experimental error as those synthesized as described above and then used in cyclohexene hydrogenation [4]. The Al/Ir=2, 3 or 5 catalysts provide 180 000, 155 000 and 100 000 turnovers over the course of 52 h, 144 h and 150 h, respectively, with average TOF (=TTO/total time before deactivation) of the *rather high values of 3500, 1100 and 700 h⁻¹*, respectively, before deactivation (Table 3.1, entries 1-3, columns 5 and 6).

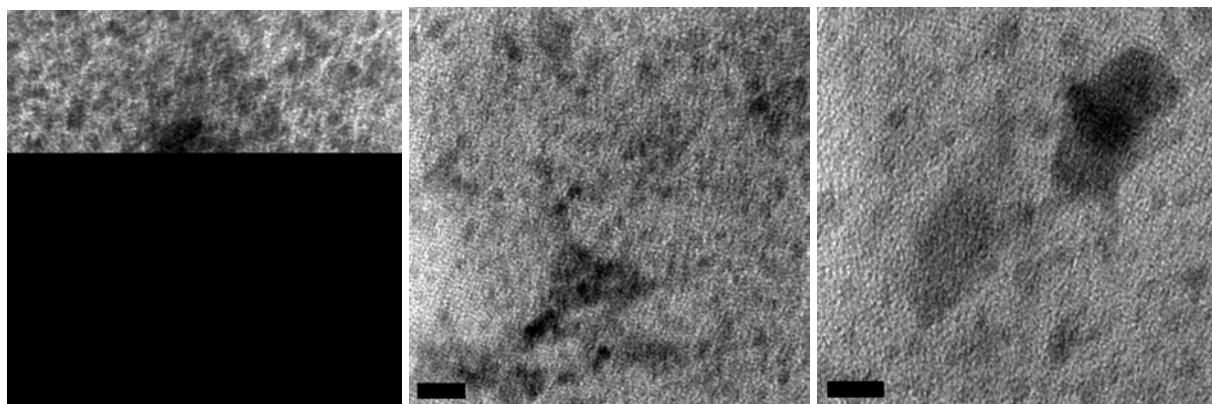


Figure 3.1. Representative TEM images for the Al/Ir=2, 3 and 5 catalysts taken from cyclohexane solutions of initially isolated, but then redispersed, catalysts prepared with [(1,5-COD)Ir(μ -O₂C₈H₁₅)₂] plus AlEt₃, Al/Ir=2 (left), Al/Ir=3 (middle) and Al/Ir=5 (right). The scale bar is 5 nm in each case. The images show nanoparticles with equivalent average sizes within experimental error of: 1.4 ± 0.7 nm (left), 1.5 ± 0.5 nm (middle) and 1.7 ± 0.4 nm (right) for the respective Al/Ir=2, 3 and 5 catalysts.

Comparison to Earlier Literature Ir(0)_n Nanoparticle Catalysis Data: The observed hydrogenation activities of the *redispersed* Al/Ir=2, 3 and 5 catalysts (Table 3.1, entries 1-3) are as high as (and in some cases higher than) any previously reported Ir(0)_n nanoparticle catalysts (Table 3.2, Entries 1-6) [24,25,26,33,34], comparisons made under identical conditions of precatalyst and cyclohexene concentration as well as initial H₂ pressure (but, necessarily, involving a solvent change from cyclohexane for the data in Table 3.1 vs acetone for the data in Table 3.2). In addition, the lifetimes of catalysts made with Al/Ir=2 and Al/Ir=3, 180 000 and 155 000 turnovers, respectively, are longer than those of all other Ir(0)_n nanoparticle catalyst systems previously ranked via the five-criteria method (Table 3.2, Entries 1-6, column 5) [24,25,26,33]. In short, the Ziegler type hydrogenation catalysts made with 2, 3 or 5 equivalents of AlEt₃ are high activity, and longer lifetime, Ir(0)_n nanoparticle catalysts, in comparison to previously reported Ir(0)_n nanoparticle catalysts.

Table 3.1. Compilation of data for the Ziegler-type hydrogenation catalysts made from [(1,5-COD)Ir(μ -O₂C₈H₁₅)₂]₂ plus AlEt₃. Conditions for all hydrogenations are as follows: cyclohexane solvent; [Ir]=1.2 mM; [cyclohexene]_{initial}=1.65 M; 22.0 \pm 0.1 °C; and 40 \pm 1 psig H₂, unless otherwise noted. The catalytic activity data given in the table are the average of three separate hydrogenation runs carried out under identical conditions. For the data shown in the format “x(y)”, x = the average of three separate runs, and y = the standard deviation (1 σ) of those 3 runs.

Entry	Al/Ir ratio	Redispersibility in cyclohexane ^a	Catalytic activity of the redispersed catalyst (mmol H ₂ /h) ^{b,c}	TTO ^{b,d}	TOF _{ave} ^{b,d} (TTO/time) (h ⁻¹)	Appearance after heating at 200 °C	Catalytic activity at 22 °C after heating at 200 °C (mmol H ₂ /h) ^{e,f}	Appearance after hydrogenation of the 200 °C treated catalyst
1	2	Yes	10(3)	180 000	3500	Brown solution, black particles	24(9)	Brown solution, black particles
2	3	Yes	7(2)	155 000	1100	Brown solution, brown particles	5(4)	Brown solution, black particles
3	5	Yes	3(1)	100 000	700	Clear, brown solution	6(4)	<i>Clear, brown solution</i>
Lower Al/Ir ratios—Controls Studying Less Stable Catalysts								
4	1	Partially	19(4)	[370 000] ^g	3600	Colorless solution, black particles	25(5)	Gray solution, black particles
5	0	No	ND ^h	[230 000] ^g	2600	ND	ND	ND

^a “Yes” means all the isolated material dissolved (i.e., no undissolved particles remained in the medium). “Partially” means some visually observable particles are present in the solution after redispersion. ^b Measured in cyclohexane solvent. The reported values are uncorrected for the number of surface atoms and, therefore, are lower limits to the true TTOS and TOFs per available surface active site. ^c Initial rate. ^d A 60-fold lower concentration of Ir ([Ir] = 0.02 mM) was used for the TTO and TOF_{ave} measurements vs the [Ir] = 1.2 mM for catalytic activity or other measurements in columns 4, 7, 8 and 9). Hence, the size and n value of these Ir(O)_n nanoclusters may be somewhat different than those in columns 4, 7, 8 and 9, although our prior work shows that concentrations from [Ir] = 1.0 to 7.0 mM yield Ir(O)_{~40-150} nanoparticles [4]. ^e Maximum catalytic rate observed during the corresponding hydrogenation. ^f Measured in dodecane solvent. ^g The “partial” to “no” redispersibility for these control study entries with 0-1 equivalent of AlEt₃ means that the TTO values are not just for nanoparticles (i.e., reflect significant contributions from bulk metal) and, therefore, are placed in [brackets]. ^h ND: Not determinable.

Table 3.2. A summary of key literature data for Ir(0)_n nanoparticle catalysts in solution.

Entry	Catalyst System	Redispersibility in acetone	Catalytic activity of redispersed catalyst (mmol H ₂ /h)	TTO	Ref
1	[(1,5-COD)Ir(CH ₃ CN) ₂]BF ₄ + [Bu ₄ N] ₂ HPO ₄ + 1 eq. PS ^a	Yes	5(1)	53 000	25
2	[(1,5-COD)Ir(CH ₃ CN) ₂]BF ₄ + [Bu ₄ N] _(8n+1) [P ₂ W ₁₅ (TiOH) ₃ O ₅₉] _n + 1 eq. PS	Yes	2.3(2)	29 000	24
3	[(1,5-COD)Ir(CH ₃ CN) ₂]BF ₄ + [Bu ₄ N]C ₂ H ₃ O ₂	Partial	0.9(2)	[81 000]	24
4	[Bu ₄ N] ₅ Na ₃ [(1,5-COD)Ir•P ₂ W ₁₅ Nb ₃ O ₆₂] + 1 eq. PS	Yes	2.2(2)	68 000	24,33
5	{[(1,5-COD)Ir•HPO ₄]} _n + 1 eq. PS	Yes	0.8(1)	[150 000]	25
6	[(1,5-COD)Ir(CH ₃ CN) ₂]BF ₄ + 1 equiv [Bu ₄ N] ₉ {H[P ₂ W ₁₇ O ₆₁]} + 1 eq. PS	Yes	0.6(1)	71 000	26

^aConditions for all hydrogenations are as follows: acetone solvent; [Ir]=1.2 mM; [cyclohexene]_{initial}=1.65 M; 22.0 ± 0.1 °C; and 40 ± 1 psig H₂ initially. PS: Proton Sponge, 1,8-bis(dimethylamino)naphthalene. TTO values given in [brackets] are upper limits to the TTOS due solely to nanoparticles because of the presence of bulk metal.

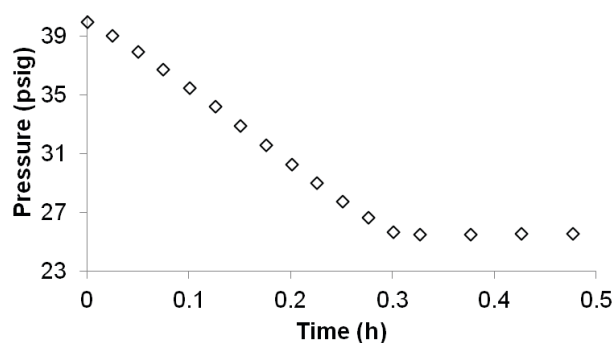


Figure 3.2. Plot of the H₂ pressure vs time data for cyclohexene hydrogenations starting from [(1,5-COD)Ir(μ-O₂C₈H₁₅)₂] plus AlEt₃, Al/Ir=2, catalyst after it was isolated and redispersed in cyclohexane. Conditions for hydrogenations are as follows: cyclohexane solvent; [Ir]=1.2 mM; [cyclohexene]_{initial}=1.65 M; 22.0 ± 0.1 °C; and 40 ± 1 psig H₂.

Thermal Stability in Dodecane at 200 °C: The Ziegler-type hydrogenation catalysts made from [(1,5-COD)Ir(μ -O₂C₈H₁₅)₂] plus AlEt₃, prepared in dodecane [35] (boiling point: 215 °C) and aged in solution for 9 hrs, were tested for their stability against agglomeration at 200 °C for 30 min (see the Supporting Information, Figure SI-B3, for a representative hydrogenation curve using the heat-treated catalyst) [36]. Importantly, using a high Al/Ir ratio up to 5 has a significant effect on the thermal stability of the resulting Ziegler-type hydrogenation catalyst, inhibiting agglomeration *even after heating at 200 °C for 30 min*. In comparison, the Al/Ir = 2 catalyst contained visually observable black bulk metal in a brown solution at the end of 30 min heating at 200 °C (Table 3.1, entry 1, column 7). Cyclohexene hydrogenation [37] with that Al/Ir = 2, 200 °C thermally treated catalyst revealed a still brown solution, but visually observable black bulk (Table 3.1, entry 2, column 9) verified by TEM, Figure 3.3. Heating the Al/Ir=3 catalyst solution at 200 °C results in the appearance of brown Ir(0) particles (as verified by XPS, Figure SI-B5) in a brown solution (Table 3.1, entry 2, column 7), the brown particles being indicative of precipitated Ir(0)_n nanoparticles [38,39]. At the end of the subsequent hydrogenation using the heat-treated Al/Ir=3 catalyst, black Ir(0) bulk is again visually observable in the solution (Table 3.1, entry 2, column 9), a product again verified by TEM, Figure 3.4.

In contrast, *the Al/Ir=5 catalyst remains clear brown both at the end of the 30 min at 200 °C and at the end of the subsequent hydrogenation* (Table 3.1, Entry 3, columns 7 and 9, Figure 3.5). These observations are significant, as they reveal that at a Al/Ir=5 ratio, the AlEt₃ stabilizer (i.e., plus any nanoparticle surface species derived from the AlEt₃) are able to stabilize the Ir(0)_n nanoparticles in solution sufficiently to prevent the formation of bulk metal even after 200 °C heating and subsequent hydrogenation catalysis. The results reveal the high thermal stability of at

least Ir(0)_n Ziegler-type nanoparticle catalysts along with the key role of the higher Al/Ir ratio in achieving that stability. Significantly, the Ir(0)_n/AlEt₃ nanoparticle catalysts appear to be *more thermally stable* [40,41] vs any demonstrated *soluble nanoparticle catalyst* that at least we can find in the current literature. Previous reports of the highest thermal stability of solutions of *claimed* nanoparticle catalysts appear to be limited to the ≤130–160 °C range [42,43,44,45,46,47,48,49,50,51] —although it should be noted that those reports typically *lack* the type of strong evidence provided elsewhere that the Ir(0)_n Ziegler-type nanoparticles studied herein are the true catalysts [4].

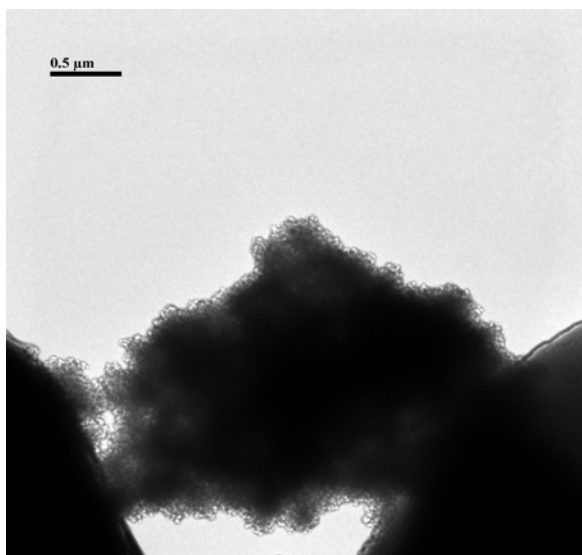


Figure 3.3. A bright-field TEM image on a sample of the Al/Ir=2 Ziegler-type hydrogenation catalyst made from [(1,5-COD)Ir(μ-O₂C₈H₁₅)₂] plus AlEt₃, heat-treated at 200 °C, and then a drop of solution was withdrawn from the reaction’s culture tube at the end of hydrogenation catalysis and placed on a TEM grid. The image shows *bulk Ir metal* (note the 0.5 μm = 500 nm scale bar).

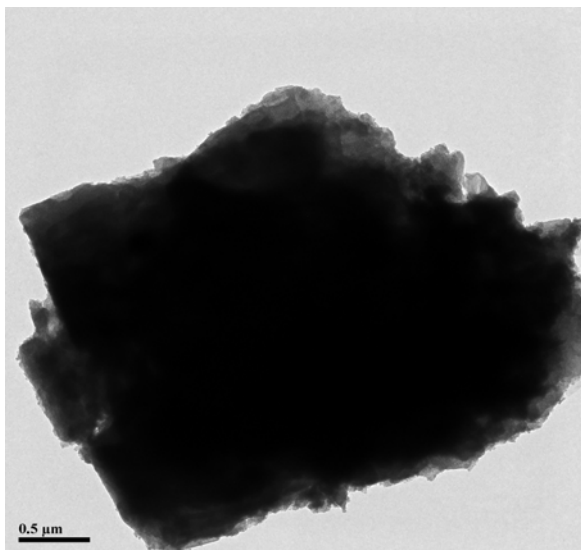


Figure 3.4. A bright-field TEM image on a sample of the $Al/Ir=3$ Ziegler-type hydrogenation catalyst made from $[(1,5-COD)Ir(\mu-O_2C_8H_{15})]_2$ plus $AlEt_3$, heat-treated at $200\text{ }^\circ\text{C}$, and then a drop of solution was withdrawn from the reaction's culture tube at the end of hydrogenation catalysis and placed on a TEM grid. The image shows *bulk Ir metal* (note the $0.5\text{ }\mu\text{m} = 500\text{ nm}$ scale bar).

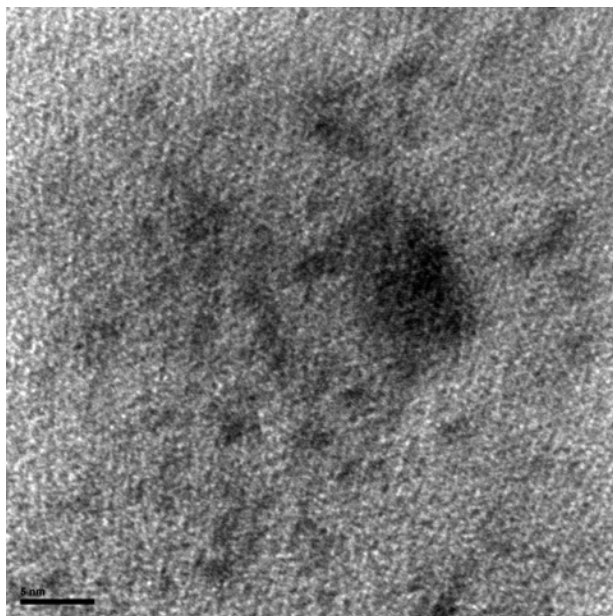


Figure 3.5. TEM image taken from a homogeneously appearing cyclohexane solution of catalyst prepared with $[(1,5-COD)Ir(\mu-O_2C_8H_{15})]_2$ plus $AlEt_3$, $Al/Ir=5$, after hydrogenation with heat-treated catalyst. The image shows nanoparticles of $1.9 \pm 0.3\text{ nm}$, that is, on average Ir_{250} , with no evidence for bulk metal (the scale bar is 5 nm).

Control Studies with the Al/Ir = 1 and Al/Ir=0 Catalysts. The following three observations with an Al/Ir=1 catalyst show that >1 equivalent AlEt₃ per Ir is required to obtain a highly stable catalyst. Specifically, for the Al/Ir=1 catalyst: (i) there are visually observable black particles of bulk Ir(0) in the brown solution and on the stirbar after cyclohexene hydrogenation; (ii) there is only a partial redispersibility in cyclohexane of the isolated catalyst (i.e., isolated by removing the volatiles under vacuum to give a brown suspension, but one with visually observable, bulk-metal particles) (Table 3.1, entry 4, column 3); and (iii) there are visually observable black particles after 30 minutes of heating at 200 °C in dodecane, which also yields a colorless, and therefore nanoparticle-free, solution (Table 3.1, entry 4, column 7). Furthermore, the presence of bulk metal in the post-catalysis solution of the Al/Ir=1 catalyst means that the relatively high TTO value of [370 000] over the course of 104 h at 22.0 ± 0.1 °C contains a significant contribution from bulk metal (see the Supporting Information for a more detailed discussion on the Al/Ir=1 catalyst). Control experiments with the Al/Ir=0 catalyst confirms that the initially formed Ir(0)_n nanoparticles *are unstable against agglomeration in the absence of AlEt₃*: a clear, colorless, and therefore nanoparticle free solution with visually observable black bulk Ir metal results (see the Supporting Information for a more detailed discussion of the Al/Ir=0 catalyst).

The results make clear the stability enhancing effects of added AlEt₃. The ability of Lewis acids to stabilize nanoparticles has general, albeit not well understood, precedent in the studies of Shmidt [52,53,54,55], Goulon [56] and Bönemann [57,58,59,60,61] as detailed on p. 13-17 of our 2010 review [1]. What remains poorly understood, in comparison to what is known in a review of nanoparticle stabilization [22], is why Lewis acids such as AlEt₃—even if in combination with the RCO₂⁻ component of the precatalyst to make the anionic (i.e., DLVO-

theory type [22]) stabilizer $[\text{RCO}_2 \cdot \text{AlEt}_3]^-$ —are any where near as effective a nanoparticle stabilizer as is observed.

The fact that the stabilization is highest at higher (e.g., 5:1) Al/Ir ratios (i.e., 4 equivalents beyond the 1 RCO_2^- present, and thus beyond the consumption of 1 AlEt_3 , to make 1 equiv. of $[\text{RCO}_2 \cdot \text{AlEt}_3]^-$) implies—significantly—*the little appreciated hypothesis that the Lewis acidic AlEt_3 alone appears to be a good stabilizer* [62,63,64], although again Shmidt's pioneering work [52,53,54,55] provides early evidence for this hypothesis if that work is carefully examined (see the discussion on p. 13 elsewhere [1]). It is presently unknown whether the stability enhancing, concomitantly rate decreasing, effects of added AlEt_3 are simply indicating that AlEt_3 is binding at the catalytically active site [65], or if there is some other more complex phenomenon involved (e.g., some structural or compositional change, or both, induced by the added excess AlEt_3 [4,66,67]). Noteworthy here is that one can envisage $\text{Ir}_n \cdot \rightarrow \text{AlEt}_3$ species (where a Al–Et \rightarrow Ir dative bond back to the Ir_n surface may be a key, additional component of that bonding). Also conceivable are the formation of surface species such as $(\text{Ir}_{\text{surface}})_x\text{-Et}$ plus $(\text{Ir}_{\text{surface}})_x\text{-Al(Et)}_2\text{Ir}$ where the number of surface Ir atoms involved could be $x = 1, 2, 3$ or 4, for example, as well as $(\text{Ir}_{\text{surface}})_x\text{-H}$ hydrides from β -H elimination from any putative $(\text{Ir}_{\text{surface}})_x\text{-Et}$. Hence, one important finding of the present work and the work of Shmidt [52,53,54,55], Goulon [56], Bönnemann [57,58,59,60,61] and others discussed elsewhere [1] is that future studies of AlR_3 -stabilized nanoparticles are of considerable interest. The needed studies of the surface composition of Ziegler nanoparticles promise to be challenging, however.

Reflection on the observations uncovered by this research suggests several hypotheses for future research, specifically: (i) that either the expected to be electrophilic, Lewis acidic $\text{Ir}(0)_n$ surface is much more strongly stabilized by the Lewis acidic AlEt_3 than one might have first

expect; or possibly (ii) that reactions with the $\text{Ir}(0)_n$ surface and AlEt_3 occur such as those suggested above. It is also possible (iii) that the true catalyst is a fragment, for example a hydride species (at present we are investigating the catalysis of the combination of AlEt_3 plus the previously unknown [68] $[(1,5\text{-COD})\text{Ir}(\mu\text{-H})_4]$). Our recent XAFS plus kinetic studies argue fairly strongly against the “a fragment is the true catalyst” explanation, however, since faster catalysis is seen when larger $\text{Ir}(0)_n$ nanoparticles are being formed and fewer Ir_4 -sized sub-nanometer particles can be detected [4]. Additional studies of these and other hypotheses are needed and promise to reveal novel insights about nanoparticle stabilization by added AlR_3 or other Lewis acids.

3. Summary and Conclusions

The main conclusions of this study are as follows:

(i) Hydrocarbon soluble, $\text{Ir}(0)_n$ Ziegler nanoparticles made from $[(1,5\text{-COD})\text{Ir}(\mu\text{-O}_2\text{C}_8\text{H}_{15})]_2$ and AlEt_3 are highly active, long-lived and thermally unusually stable—if not unprecedentedly stable—nanoparticle solution catalysts. Their TTO lifetimes are higher than any known $\text{Ir}(0)_n$ nanoparticles, even those of the premier, $\text{P}_2\text{W}_{15}\text{Nb}_3\text{O}_{62}^{9-}$ polyoxoanion, “electrosteric” stabilized [24,33] $\text{Ir}(0)_n$ nanoparticles.

(ii) Thermal stability at 200 °C requires addition of at least 3 equivalents of AlEt_3 and the stability of the resulting catalyst increases at $\text{Al}/\text{Ir}=5$. The addition of ≥ 2 equivalents AlEt_3 is necessary in order to prevent agglomeration of the $\text{Ir}(0)_n$ Ziegler nanoparticles to bulk $\text{Ir}(0)$ metal during room temperature cyclohexene hydrogenation catalysis.

(iii) The $\text{Al}/\text{Ir}=5$ $\text{Ir}(0)_n$ nanoparticles are stable for ≥ 30 minutes at 200 °C, and exhibit 100 000 TTOs of cyclohexene hydrogenation. The observed nanoparticle *catalyst* stability at 200 °C

appears to surpass that of any other demonstrated nanoparticle catalyst that we can find, those literature reports being limited to ≤ 130 - 160 °C temperatures.

(iv) The results strongly suggest that AlEt_3 , or possibly derivatives of it, are a main component of the stabilizer.

(v) The results imply that either (a) a little understood mode of nanoparticle stabilization by alkyl Lewis acids such as AlEt_3 is present (i.e., and in addition to the anionic, DLVO-theory type of stabilization expected for $[\text{RCO}_2 \bullet \text{AlEt}_3]^-$ formed from the first equivalent of added AlEt_3), or (b) that reactions between the $\text{Ir}(0)_n$ and AlR_3 occur to give species such as the $(\text{Ir}_{\text{surface}})_x\text{-Et}$ and $(\text{Ir}_{\text{surface}})_x\text{-Al}(\text{Et})_2\text{Ir}$ detailed earlier. It is also conceivable that (c) some other species is the true catalyst in the reaction, possibly an iridium hydride fragment (which could, then, and for example have a Lewis base / Lewis acid interaction between the Ir-H and the AlEt_3), although the evidence to date argues against this third possibility [4]. Additional studies are, however, warranted and promise to uncover new insights, most likely into the novel stabilization mode of Ziegler-type nanoparticles.

(vi) The results confirm that the activity of Ziegler-type hydrogenation catalysts can be tuned by the Al/Ir ratio, a point apparent in the extant literature [1]. Our results show that, in addition to their catalytic activity, the catalytic lifetime and thermal stability of Ziegler-type hydrogenation catalysts are also strongly influenced by, and thus can be tuned by, the Al/Ir ratio.

(vii) Finally and most importantly, the valuable prior studies of Shmidt [52,53,54,55], Goulon [56], and Bönemann [57,58,59,60,61] plus the results herein and our other, recent publications [4] and critical review [1], make apparent that hydrocarbon soluble, Lewis-acid containing, Ziegler-type nanoparticles are an underexploited type of highly active, long lifetime and

unusually high stability nanoparticle for use in catalysis or other applications where their unusual hydrocarbon solubility and thermal stability might be advantageous.

Overall, the results help confirm the existence of Ziegler nanoparticles, highlight their hydrocarbon solubility, and highlight their high, Al/Ir ratio-tunable catalytic activities and lifetimes while also revealing their exceptionally high thermal stability at 200 °C. It is hoped that these results will open the door to the other possible applications of Ziegler-nanoparticles in catalysis and, possibly, other areas.

In our studies in progress we are concentrating on another historically difficult question in this area [1], namely precisely what happens to the AlEt₃ after mixing [(1,5-COD)Ir(μ-O₂C₈H₁₅)₂] and AlEt₃, as well as any insights that may give about the nature of the true catalyst(s). We are also striving to bring to completion our multi-year studies of the precise form and catalytic properties of other Ziegler-type hydrogenation catalysts made from various combinations of industrial precatalysts [63] such as Co and Ni salts and commonly used cocatalysts such as AlMe₃, Al(*t*-Bu)₃, or alumoxanes and their derivatives.

4. Experimental

Materials, Stock Solutions and Instrumentation. All manipulations were performed under N₂ in a Vacuum Atmospheres drybox (≤5 ppm O₂ as monitored by a Vacuum Atmospheres O₂-level monitor) or using a Schlenk line. All glassware was dried overnight in an oven at 160 °C, cooled under vacuum in a desiccator and then transferred into the drybox while still in the desiccator and under vacuum, since H₂O is known to be detrimental to Ziegler-type hydrogenation catalysts [1]. Cyclohexane (Sigma-Aldrich, 99.5 %, H₂O < 0.001 %) and dodecane (Sigma-Aldrich, anhydrous, ≥99%, water content ≤0.003 %) were dried over activated molecular sieves for 2 days prior to use. Molecular sieves (Acros, 3 Å) were activated by keeping at 200 °C for 8 hours

under vacuum. AlEt₃ (Strem Chemicals, 93%, in 100 g steel cylinder) was used as received. Cyclohexene (Aldrich, 99%) was distilled over Na under N₂(g) and transferred into the drybox under air-free conditions. Silicone oil (Dimethyl Silicone, Thomas Scientific) was used as received. Hydrogen gas (General Air, 99.5%) was passed through an indicating moisture trap (Scott Specialty Gas), a disposable O₂ cartridge (Trigon), and an indicating O₂ trap (Trigon) before use in hydrogenations. [(1,5-COD)Ir(μ-O₂C₈H₁₅)₂] was prepared by W. Morgan Alley in our labs following our previously published procedure [3]. It was characterized, and its purity checked, by ¹H and ¹³C NMR that matched the literature [3].

¹H NMR: The spectra of sample solutions in benzene-d₆ (Cambridge Isotope Laboratories, Inc., 99.5%, w/o TMS) were taken on a Varian Inova 400 instrument and worked out with MestRec software when needed. Observed chemical shifts were referenced to the proton resonance of the benzene-d₆ solvent.

TEM: Sample solutions for TEM were prepared at Colorado State University by first diluting 0.1 mL of a catalyst solution to 0.6 mL using cyclohexane in a 5 mL glass vial. TEM grids (ultrathin carbon film supported by a holey carbon film on a 400 Mesh copper grid, Ted Pella, Inc.) were then immersed into a sample solution, and dried under an N₂ atmosphere in the drybox for ~1 min. The grids were then placed in 5-mL glass vials, double-sealed under N₂ in the drybox, and then sent to Dr. JoAn Hudson at Clemson University for imaging at ≥ 0.5M magnification on a Hitachi H7600T operated at 120 kV.

Procedures and Cautions for Handling the Pyrophoric AlEt₃. CAUTION: AlEt₃ is a well-known pyrophoric reagent. AlEt₃ ignites spontaneously when in contact with air. It, as with all pyrophoric reagents, is more dangerous when flammable solvents are present (e.g., cyclohexane or dodecane, herein). AlEt₃ and solvents are even more dangerous the larger the amounts being employed!

Hence, the required safety considerations were carefully designed followed, including: (i) first reading the MSDS safety sheet on AlEt₃; (ii) working with the minimal amounts of pyrophoric and flammable reagents possible; (iii) using the AlEt₃ only in a drybox or in Fisher-Porter (F-P) bottle under N₂ atmosphere. The F-P bottle was sealed using Swagelock quick-connects before taking it out of the drybox.

AlEt₃ stock solution (36 mM). A stock solution was prepared *in the drybox* by adding neat AlEt₃ (0.529 mL, 0.834 g/mL) using a 1.000 mL gas-tight syringe into 50 mL cyclohexane in a 100 mL volumetric flask. The resulting solution was diluted to 100 mL using cyclohexane.

Hydrogenation Solution Preparation and Catalytic Cyclohexene Hydrogenation with As-prepared Catalysts. Catalyst solutions, 1.44 mM in Ir, were individually prepared in a drybox at 30°C. An example procedure follows for the preparation of catalyst solution with [(1,5-COD)Ir(μ-O₂C₈H₁₅)₂] and AlEt₃, Al/Ir=1: A 1.60 mg portion of [(1,5-COD)Ir(μ-O₂C₈H₁₅)₂] was weighed into a 20 mL screw-cap glass vial and then dissolved in 2.4 mL of cyclohexane forming an orange-red solution. A 5/8 × 5/16 inch Teflon-coated magnetic stir bar was then placed in the 20 mL screw-cap glass vial and the solution was stirred for 1 min at 1.0 × 10³ rpm as measured with a Monarch Instruments Pocket-Tachometer. A AlEt₃ solution (0.1 mL, 36 mM; CAUTION, PYROPHORIC MATERIAL!, *vide supra*, IN COMBINATION WITH FLAMMABLE SOLVENTS!) was then quickly added to the Ir(I) solution within 2 sec using a 0.5 mL gas-tight syringe while vigorously stirring [1]. The original orange-red color of the [(1,5-COD)Ir(μ-O₂C₈H₁₅)₂] solution changed to tawny yellow at the end of AlEt₃ addition. This tawny yellow solution was stirred under N₂ in the drybox for 9 h. At the end of 9 h, the solution appeared clear brown with no visually observable particles. The solution was then transferred into a new 22 × 175 mm Pyrex borosilicate culture tube containing a new 5/8 × 5/16 in. Teflon-coated magnetic stirbar. Cyclohexene (0.5 mL) was added using a 1.0 mL gas-tight syringe and the resulting

hydrogenation solution (1.65 M in [cyclohexene] and 1.2 mM in [Ir]) was stirred for an additional 1 min.

The procedure and apparatus used for catalytic hydrogenations of cyclohexene have been described in detail elsewhere [33,69,70]. Briefly, a culture tube containing the hydrogenation solution was placed in a Fisher-Porter (F-P) bottle, which was then sealed and brought out of the drybox. The F-P bottle was placed in a bath set at 22.0 ± 0.1 °C. Stirring was started at 1000 ± 10 rpm using a Fauske Super magnetic stirplate and the F-P bottle was connected to a pressurized H₂ line using TFE-sealed Swagelok quick-connects. The F-P bottle was purged 15 times (1 purge/15 sec) with H₂ that has passed through an indicating moisture trap (Scott Specialty Gas), a disposable O₂ cartridge (Trigon), and an indicating O₂ trap (Trigon). The pressure in the F-P bottle was then set to 40 psig, and then the data collection was initiated. Hydrogen pressure vs. time data was collected using a pressure transducer (Omega PX 624-100 GSV) interfaced via an Omega D1131 analog to digital converter to a PC running LabVIEW 7.0. Data was subsequently handled using MS Excel. The maximum hydrogenation rate of catalysts before and after catalyst isolation was calculated from each kinetic curve by a linear-least-squares fits to the data points in the highest activity (highest slope) region ($R^2 \geq 0.999$ for the reported data). The maximum hydrogenation rates of redispersed catalysts occur at the beginning of the hydrogenation (i.e., the maximum rate equals the initial rate), so those (maximum) rates were calculated via linear-least-squares fits to the initial, linear regions of the redispersed catalysts hydrogenation curves ($R^2 \geq 0.999$ for the reported data).

For hydrogenations with [(1,5-COD)Ir(μ -O₂C₈H₁₅)₂]₂ plus AlEt₃, Al/Ir=2, 3 or 5, orange-red [(1,5-COD)Ir(μ -O₂C₈H₁₅)₂]₂ (1.60 mg) was dissolved in a total of 2.3 mL, 2.2 mL or 2.0 mL cyclohexane, respectively. Then, 0.2 mL, 0.3 mL or 0.5 mL, respectively, of a stock AlEt₃ solution (36 mM) was added using a 1.0 mL gas-tight syringe. At the end of 9 h aging in the

drybox, all the catalysts made with 1, 2, 3 or 5 equivalents AlEt_3 turn to brown without visually observable bulk metal. At the end of cyclohexene hydrogenation, the catalyst solutions prepared with 2, 3 or 5 equivalents of AlEt_3 are still brown with no visually observable particles in contrast to the $\text{Al/Ir}=1$ catalyst solution which did contain bulk metal particles in the solution and on the stirbar.

Isolation and Redispersion Procedure and Hydrogenation Using Redispersed Catalyst.

After hydrogenation, the F-P bottle was detached from the line and taken inside the drybox. The catalyst solution and the stirbar were then transferred into a new 20 mL screw-cap glass vial. Volatiles were removed under vacuum to yield a black powder which was dried under vacuum for 2 h. Cyclohexane (2.5 mL) was then added to this isolated, black powdered catalyst and the resulting solution was stirred for 2 min. This solution was completely transferred (i.e.; without leaving any observable particles in the glass vial) into a new 22 × 175 mm Pyrex borosilicate culture tube containing a new 5/8 × 5/16 in. Teflon-coated magnetic stirbar. Fresh cyclohexene (0.5 mL) was added using a 1.0 mL gas-tight syringe and the resulting hydrogenation solution (1.65 M in [cyclohexene] and 1.2 mM in [Ir]) was stirred for an additional 1 min.

Catalytic Lifetime Measurements. The catalytic lifetime measurements were performed according to a previously published procedure [23,26]. In the drybox, the orange-red crystals of [(1,5-COD)Ir(μ -O₂C₈H₁₅)] (0.319 mg, 0.72 μ mol) was weighed into a 20 mL screw-cap glass vial. Then, AlEt_3 (20 μ L, 36 mM) was quickly added in one second using a 50 μ L syringe. The resulting solution was stirred for 30 min. The catalyst solution was then diluted with 10 mL cyclohexene and transferred into a new 22 × 175 mm Pyrex borosilicate culture tube containing a new 5/8 × 5/16 in. Teflon-coated magnetic stirbar using a disposable polyethylene pipette. Further cyclohexene (26 mL, to bring the total cyclohexene volume to 36 mL, corresponding to a total of 488 000 total turnovers) was added using a 10 mL syringe while vigorously stirring. The

culture tube containing the hydrogenation solution was placed in a F-P bottle, which was then sealed and brought out of the drybox. The F-P bottle was placed in a water bath set at 22.0 ± 0.1 °C. Stirring was started at 1000 ± 10 rpm using a Fauske Super magnetic stirplate and the F-P bottle was connected to a pressurized H₂ line using TFE-sealed Swagelok quick-connects. The F-P bottle was purged 15 times (1 purge/15 sec) with H₂ that has passed through an indicating moisture trap (Scott Specialty Gas), a disposable O₂ cartridge (Trigon), and an indicating O₂ trap (Trigon). A timer was started and the pressure in the F-P bottle was set to 40 ± 1 psig.

The reaction was monitored by periodically withdrawing 0.1 mL aliquots of the reaction solution and then analyzing that aliquot by ¹H NMR spectroscopy. The aliquots were taken from the reaction solution while the F-P bottle was connected to the H₂ line as follows: the purge valve was opened to air while the H₂ gas at 40 psig pressure was still flowing. A gas-tight syringe with a ~25 cm needle was first purged with H₂ gas by inserting the tip into flowing H₂ gas between Swagelok quick-connects on brass pressure head of F-P bottle. The syringe was filled with H₂ and then emptied while under H₂. This procedure was repeated five times to ensure exclusion of air when the tip of the needle was inserted into the reaction solution. Then 0.1 mL of the reaction solution was withdrawn with the syringe and quickly transferred into an NMR tube including 1.0 mL C₆D₆.

Thermal Stability Experiments. Thermal stability experiments were carried out using dodecane as solvent due to its high boiling point (215 °C vs 81°C for cyclohexane). The catalyst and hydrogenation solutions, except AlEt₃ solution, were prepared in dodecane using the procedure detailed above when cyclohexane was used as the solvent and under the section heading “Hydrogenation Solution Preparation and Catalytic Cyclohexene Hydrogenations”. The AlEt₃ stock solution in cyclohexane (36 mM) (that is, not in dodecane) was used in the thermal stability experiments. A cyclohexene hydrogenation (called initial cyclohexene hydrogenation

hereafter) was carried out as detailed above, but now in dodecane solvent. At the end of the initial cyclohexene hydrogenation the 22 °C water bath was replaced with a silicone oil bath set at $200 \pm 2^\circ\text{C}$. The H_2 pressure in the F-P bottle was decreased to ~ 20 psig and the F-P bottle was placed in silicone-oil bath. The pressure in the F-P bottle was continuously monitored during heating. The solution in the F-P bottle was kept at 200°C for 30 min and then cooled down to room temperature under H_2 . The F-P bottle was then brought into the drybox and 0.5 mL cyclohexene was added. Next, the F-P bottle was taken out of the drybox, connected to H_2 line and purged 15 times (1purge/15 sec) with H_2 that has passed through an indicating moisture trap (Scott Specialty Gas), a disposable O_2 cartridge (Trigon), and an indicating O_2 trap (Trigon). A second cyclohexene hydrogenation was then carried out to test the activity of the 200°C , 30 min, heat-treated catalyst.

5. Supporting Information Available. Detailed experimental procedures for control studies (i) measuring the maximum rate of cyclohexene hydrogenation as a function of cycles of catalyst isolation and then redispersion, (ii) determining the effect of aging the Ziegler-type hydrogenation catalyst made from $[(1,5\text{-COD})\text{Ir}(\mu\text{-O}_2\text{C}_8\text{H}_{15})]_2$ plus AlEt_3 , Al/Ir = 2, in dodecane; and (iii) determining the effect of using Al/Ir=1 and Al/Ir=0 ratios on catalyst activity and stability. Hydrogenation curves with heat-treated Ziegler-type hydrogenation catalyst made from $[(1,5\text{-COD})\text{Ir}(\mu\text{-O}_2\text{C}_8\text{H}_{15})]_2$ plus AlEt_3 , Al/Ir = 2. Control hydrogenations determining the H_2 gas-to-solution, mass-transfer-limited (MTL) rate of the hydrogenation apparatus used in the present work. High resolution XPS spectrum of Ir 4f peaks of brown particles from the Al/Ir = 3 catalyst after heating at 200°C for 30 min. ^1H NMR spectrum of neat AlEt_3 and that of catalyst

solution prepared with [(1,5-COD)Ir(μ -O₂C₈H₁₅)₂] plus AlEt₃, Al/Ir= 5. This material is available free of charge via the Internet at <http://pubs.acs.org/>.

REFERENCES

- [1] W.M. Alley, I.K. Hamdemir, K.A. Johnson, R. G. Finke, *J. Mol. Catal. A. Chem.* 315 (2010) 1-27.
- [2] K.A. Johnson, *Polym. Prepr.* 41 (2000) 1525–1526.
- [3] W.M. Alley, C.W. Girard, S. Özkar, R.G. Finke, *Inorg. Chem.* 48 (2009) 1114-1121.
- [4] W.M. Alley, I.K. Hamdemir, Q. Wang, A. Frenkel, L. Li, J.C. Yang, L.D. Menard, R.G. Nuzzo, S. Özkar, K.A. Johnson, R.G. Finke, *Inorg. Chem.* 49 (2010) 8131-8147.
- [5] E. Bayram, M. Zahmakiran, S. Ozkar, R.G. Finke, *Langmuir* 26 (2010) 12455-12464.
- [6] For definitions of “nanoparticles” vs “nanoclusters” and relevant prior literature discussing these terms see refs 5 and 7.
- [7] Consistent with those definitions [5,6] the nomenclature used herein is “nanoparticles” to define species for which (only) the size distribution is known, but the composition and structure of the nanoparticles are not known. Alternatively, the term “nanocluster” is reserved for atomically precise, compositionally and structurally atomically characterized (nano)clusters.
- [8] The $\text{Ir}(0)_n$ *nanoparticles* studied herein begin in the $\text{Ir}(0)_{\sim 40-150}$ size range [4], and are a bit larger, $\text{Ir}(0)_{\sim 250}$ post the 200 °C heat treatment as demonstrated in Figure 3.5.
- [9] R.G. Finke, In *Metal Nanoparticles: Synthesis, Characterization, and Applications*; Feldheim, D. L., Foss Jr. C. A., Eds.; Marcel Dekker, Inc.; New York, 2002; pp. 17.
- [10] G. Schmid, M. Baumle, M. Geerkens, I. Heim, C. Osemann, T. Sawitowski, *Chem. Soc. Rev.* 28 (1999) 179-185.
- [11] G. Schmid, L. F. Chi, *Adv. Mater.* 10 (1998) 515-526.
- [12] J.H. Fendler, Y. Tian, In *Nanoparticles and Nanostructured Films*; Fendler, J. H., Ed.; Wiley-VCH: Weinheim, 1998; Chapter 18.
- [13] A. Furstner, Ed. *Active Metals: Preparation, Characterization, and Applications*; VCH: Weinheim, 1996.
- [14] J.S. Bradley, In *Clusters and Colloids. From Theory to Applications*; Schmid, G., Ed.; VCH: New York, 1994; pp 459-544.
- [15] G. Schmid, *Chem. Rev.* 92 (1992) 1709-1727.
- [16] G. Schmid, In *Aspects of Homogeneous Catalysis*; Ugo, R., Ed.; Kluwer: Dordrecht, 1990; Chapter 1.

[17] R.P. Andres, R.S. Averback, W.L. Brown, L.E. Brus, W.A. III Goddard, A. Kaldor, S.G. Louie, M. Moscovits, P.S. Peercy, S.J. Riley, R.W. Siegel, F. Spaepen, Y. Wang, J. Mater. Res. 4 (1989) 704-736.

[18] A. Henglein, Chem. Rev. 89 (1989) 1861-1873.

[19] J.M. Thomas, Pure Appl. Chem. 60 (1988) 1517-1528.

[20] P. Jena, B.K. Rao, S.N. Khanna, In *Physics and Chemistry of Small Clusters*; Plenum: New York, 1987.

[21] L.J. de Jongh, Ed. In *Physics and Chemistry of Metal Cluster Compounds*; Kluwer Publishers: Dordrecht, 1994.

[22] L.S. Ott, R.G. Finke, Coord. Chem. Rev. 251 (2007) 1075-1100.

[23] S. Özkar, R.G. Finke, J. Am. Chem. Soc. 124 (2002) 5796-5810.

[24] S. Özkar, R.G. Finke, Langmuir 18 (2002) 7653-7662.

[25] S. Özkar, R.G. Finke, Langmuir 19 (2003) 6247-6260.

[26] C.R. Graham, L.S. Ott, R.G. Finke, Langmuir 25 (2009) 1327-1336.

[27] The original five-criteria method, developed and then applied to rank the efficacy of a given additive (e.g., anions, solvent, cations or polymers) to achieve the kinetically controlled formation and then stabilization and catalytic activity of the resultant nanoparticles, are: (i) the ability to exhibit high level of kinetic control as measured quantitatively by the k_2/k_1 ratio for the nucleation [$A \rightarrow B$ (rate constant k_1)], then autocatalytic surface growth [$A + B \rightarrow 2B$ (rate constant k_2)] mechanism of formation of transition metal nanoparticles under H₂; (ii) the ability to form near-monodisperse ($\leq 15\%$ size dispersion) nanoparticles as evidenced by TEM; (iii) the ability to allow isolation from solution and then complete redispersion without visible formation of bulk metal—a telling test of nanoparticle stability; (iv) the ability of the isolated nanoparticles to exhibit high catalytic activity in cyclohexene hydrogenation once redispersed in the solution; and (v) the ability to allow long catalytic lifetime in the test reaction of cyclohexene hydrogenation as measured by the catalytic total turnovers (TTOs).

[28] The previous 5-criteria method [27] had to be modified somewhat for the present studies since the Ziegler nanoparticles examined herein are preformed quickly upon simple mixing the [(1,5-COD)Ir(μ -O₂C₈H₁₅)₂]₂ with the AlEt₃. This, in turn, means that the kinetic criteria which ranks the ability of the various anions or other ligands and additives (such as polymers) to influence the *nanoparticle formation kinetics* is no longer readily measurable without, for example, stopped-flow kinetics (i.e., kinetic studies not important to the present work whose focal point is nanoparticle catalytic activity, thermal stability and lifetime).

[29] D. Durand, G. Hillion, C. Lassau, L. Sajus, *Process for Hydrogenating Unsaturated Compounds* U.S. Patent 4,271,323, Jun. 2, 1981.

[30] A patent [29] reports that a Ziegler-type hydrogenation catalyst made from $\text{Co}(\text{O}_2\text{CR})$ and $\text{Zn}(\text{O}_2\text{CR})_2$ plus AlEt_3 , prepared at temperatures of 0-200 °C, is a fast, highly efficient catalyst (the hydrogenation of 100 mL of propionitrile is reported to be complete in 11.5 h with a 99.5% conversion to propylamines) Although propionitrile hydrogenation at temperatures from 0 to 300 °C are claimed, the specific examples of hydrogenations (of various substrates) are at only 155, 160 or 180 °C, and not up to 300 °C. In addition, the nature of the active catalyst was not determined, so it is not clear what the true catalyst actually is at these temperatures and in this patent.

[31] Control experiments were performed, on a Ziegler-type hydrogenation catalyst made from $[(1,5\text{-COD})\text{Ir}(\mu\text{-O}_2\text{C}_8\text{H}_{15})_2]$ plus AlEt_3 ($\text{Al}/\text{Ir}=2$) in cyclohexane, to determine the effect of number of catalyst isolation and then redispersion cycles on the hydrogenation rate of the catalyst. Interestingly, the catalyst appears to become slightly more active up to the third cycle of isolation and redispersion (5 ± 2 , 8 ± 1 , and 9 ± 1 mmol H_2/h , respectively, for once-redispersed, two-times-redispersed and three-times-redispersed catalysts), although the results are rigorously the same within a 2σ experimental error (i.e., at 2x the reported 1σ error bars just above). The catalyst retains its activity (~ 9 mmol/h) after redispersion two through eight times (see the Supporting Information for additional details).

[32] Original cyclohexene hydrogenation data is obtained in unit of loss of psig H_2/h . The data in unit of psig H_2/h are then converted as follows to mmol H_2/h using the ideal gas law formula ($PV=nRT$) and the necessary data for our apparatus: $P(\text{psig H}_2)*0.0891*1000/14.7 = n$ (mmol H_2)* $0.082*295$ where $R=0.082 \text{ L}\cdot\text{atm}/\text{mol}\cdot\text{K}$, $T= 295 \text{ K}$ and $1 \text{ atm}=14.7 \text{ psi}$ and $V(\text{volume of F-P bottle used})=0.0891 \text{ L}$.

[33] Y. Lin, R.G. Finke, *Inorg. Chem.* 33(1994) 4891-4910.

[34] J. III Aiken, R.G. Finke, *Chem. Mater.* 1 (11999) 1035-1047.

[35] Control experiments performed on Ziegler-type hydrogenation catalyst made from $[(1,5\text{-COD})\text{Ir}(\mu\text{-O}_2\text{C}_8\text{H}_{15})_2]$ plus AlEt_3 ($\text{Al}/\text{Ir}=2$) in *dodecane* showed that aging the catalyst for 9 h at room temperature appears to decrease slightly the activity of the catalyst (although the results are the same within experimental error if the cited 1σ error bars are expanded by 2x to 2σ values): the catalyst prepared in *dodecane*, and then immediately used for cyclohexene hydrogenation, exhibits a hydrogenation rate of 1.1 ± 0.1 mmol H_2/h , whereas the catalyst aged 9 h has a hydrogenation rate of 0.7 ± 0.1 mmol H_2/h (see the Supporting Information for the corresponding hydrogenation curves). In comparison, the catalyst prepared in *cyclohexane* and aged for 9 h at room temperature is a somewhat faster catalyst compared to the unaged, immediately prepared catalyst [4] (see also the Supporting Information provided with that paper [4]).

[36] Initial survey experiments reveal that an active catalyst is obtained in *dodecane*: (i) when the 9 hr aged was thermally treated and then used for cyclohexene hydrogenation (i.e., without

performing a cyclohexene hydrogenation before the 200 °C thermal treatment); (ii) when the as-prepared catalyst was thermally treated and then used directly for cyclohexene hydrogenation (i.e., without the 9 hrs aging); and (iii) when the catalyst solution is prepared with cyclohexene added before the 200 °C thermal treatment. See the Supporting Information for additional details.

[37] The heat-treated catalyst with an Al/Ir ratio of 2 is highly active for cyclohexene hydrogenation with average maximum rate of 24(9) mmol H₂/h (Table 1 and Figure S3). A fast hydrogenation started immediately in that experiment, and continued with an almost linear rate until the consumption of cyclohexene was complete (Figure S4). The observed linear hydrogenation kinetics reveal that the catalysis has reached the H₂ gas-to-solution mass transfer limited (MTL) rate of even our well-stirred apparatus (~1000 r.p.m. stir-bar stirring)—that is, that H₂ is consumed as fast as it is delivered from the gas phase to solution in our apparatus. Consistent with this interpretation, an independent determination of the H₂ gas-to-solution MTL rate under our reaction conditions, stirring rate and for our specific apparatus revealed that H₂ gas-to-solution MTL occurs at ~20(5) mmol H₂/h for our apparatus (Figure S4). Hence, the true activity of the heat-treated Al/Ir=2 catalyst is greater than or equal to the observed rate of 24(9) mmol H₂/h.

[38] J.D. Aiken III, R.G. Finke, J. Am. Chem. Soc. 121 (1999) 8803-8810 and references therein.

[39] Somewhat analogously, a brown precipitate of Ir(0)_n and Rh(0)_n nanoparticles also settles out of solution during cyclohexene hydrogenation catalysis by Ir(0)₋₃₀₀ nanoparticles [38] formed by placing [Bu₄N]₅Na₃[(1,5-COD)Ir•P₂W₁₅Nb₃O₆₂] or [Bu₄N]₅Na₃[(1,5-COD)Rh•P₂W₁₅Nb₃O₆₂] and cyclohexene under 40 psig H₂, a result that has been ascribed to the conversion of cyclohexene into the somewhat less polar cyclohexane as a result of the hydrogenation reaction. Note, however, that these polar polyoxoanion, P₂W₁₅Nb₃O₆₂⁹⁻-stabilized nanoparticles are expected to have little solubility in non-polar solvents like cyclohexane, at least with Bu₄N⁺ counter-cations.

[40] Y. Lin, R.G. Finke, J. Am. Chem. Soc. 116 (1994) 8335–8353.

[41] For the case of either Ir(0)₋₃₀₀ [33] or Ir(0)₋₉₀₀ [40] nanoparticles stabilized by the “electrosteric”, premier / “Gold Standard” anionic [22], P₂W₁₅Nb₃O₆₂⁹⁻ polyoxoanion stabilizer [22,23,24,25,26] acetone solutions show limited stability and agglomeration to bulk metal above 60 °C. Hence, it is apparent that the thermal stability of Ir(0)_n nanoparticles with added AlEt₃ in hydrocarbon solvents at 200 °C exceeds that of at least these classic, anionically (DLVO-theory [22]) stabilized nanoparticles [33,40].

[42] M. Beller, H. Fischer, K. Kühlein, C.-P. Reisinger, W.A. Hermann, J. Organomet. Chem. 520 (1996) 257-259.

[43] Pd(0)_n nanoparticles *unstable* at 130-140 °C have been reported [42], ones where 490,000-500,000 TTOs of Heck reaction catalysis were obtained by adding preformed Pd(0)_n slowly to the 130-140 °C reaction solution as a way to combat the nanoparticle instability at the 130-140

°C temperatures. Note, however, that the actual catalyst in these reactions was not established and remains controversial.⁴⁴

[44] N. T. Phan, M. Van Der Sluys, C.W. Jones, *Adv. Synth. Catal.* 348 (2006) 609-679.

[45] M.T. Reetz, G. Lohmer, *Chem. Comm.* (1996) 1921-1922.

[46] M.T. Reetz, R. Breinbauer, P. Wedemann, P. Bringer, *Tetrahedron* 54 (1998) 1233-1240.

[47] Two studies [45,46] report nanoparticles stable for at least some (generally unstated) numbers of catalytic turnovers in the 130-160 °C range, and which involve longer chain alkyl-ammonium cations as part of the stabilization system. However, the actual catalyst in these studies was not established.

[48] S. Klingelhöfer, W. Heitz, A. Greiner, S. Oestreich, S. Förster, M. Antonietti, *J. Am. Chem. Soc.* 119 (1997) 10116-10120.

[49] Pd_n nanoparticle stabilities of up to 140 °C for 3 days while undergoing Heck coupling reactions using OAc⁻ plus amphiphilic block copolymers, specifically polystyrene-block-poly-4-vinylpyridine (PS-*b*-P4VP), have been reported [48]. Note, however, that Figures 2 and 3 in this paper show autocatalytic curves. This means that either the PS-*b*-P4VP-stabilized Pd_n nanoparticles are not the true catalyst or that a reaction by-product (the H+X⁻ formed) is involved in the catalytic reaction (e.g., the H+X⁻ by-product should protonate the pyridine in the PS-*b*-P4VP stabilizer, thereby causing it to decoordinate from the metal, in turn giving a more active catalyst, consistent with the observed reaction kinetics).

[50] J.P. Wilcoxon, R.L. Williamson, R. Baughman, *J. Chem. Phys.* 98 (1993) 9933-9951.

[51] A report of Au(0)_n nanoparticles prepared in the presence of various nonionic (such as ethoxylated alcohols), anionic (such as bis(2-ethylhexyl)sulfosuccinate) and cationic (such as didodecyldimethylammonium) surfactants and stable to agglomeration up to 100 °C has appeared, but the Au(0)_n nanoparticles were not shown to be catalysts [50].

[52] L.O. Nindakova, F.K. Shmidt, V.V. Saraev, B.A. Shainyan, N.N. Chipanina, V.A. Umanets, L.N. Belonogova, D.-S.D. Toryashinova, *Kinetics and Catalysis* 47 (2006) 54-63.

[53] F.K. Shmidt, L.O. Nindakova, B.A. Shainyan, V.V. Saraev, N.N. Chipanina, V.A. Umanets, *J. Mol. Catal. A: Chem* 235 (2005) 161-172.

[54] L.B. Belykh, T.V. Goremyka, N.I. Skripov, V.A. Umanets, F.K. Shmidt, *Kinetics and Catalysis* 47 (2006) 367-374.

[55] F.K. Schmidt, G.V. Ratovskii, T.V. Dmitrieva, I.N. Ivleva, Y.G. Borodko, *J. Organomet. Chem.* 256 (1983) 309-329.

[56] J. Goulon, E. Georges, C. Goulon-Ginet, Y. Chauvin, D. Commereuc, H. Dexpert, E. Freund, *Chem. Phys.* 83 (1984) 357-366.

[57] H. Bönemann, N. Waldofner, H.-G. Haubold, T. Vad, *Chem. Mater.* 14 (2002) 1115-1120.

[58] K. Angermund, M. Buhl, E. Dinjus, U. Endruschat, F. Gassner, H.-G. Haubold, J. Hormes, G. Kohl, F.T. Mauschick, H. Modrow, R. Mortel, R. Mynott, B. Tesche, T. Vad, N. Waldofner, H. Bönemann, *Angew. Chem. Int. Ed.* 41 (2002) 4041-4044.

[59] K. Angermund, M. Buhl, U. Endruschat, F.T. Mauschick, R. Mortel, R. Mynott, B. Tesche, N. Waldofner, H. Bönemann, G. Kohl, H. Modrow, J. Hormes, E. Dinjus, F. Gassner, H.-G. Haubold, T. Vad, M. Kaupp, *J. Phys. Chem. B* 107 (2003) 7507-7515.

[60] H. Bönemann, N. Waldofner, H.-G. Haubold, T. Vad, *Revue Roumaine de Chimie* 44 (1999) 1003-1010.

[61] F. Wen, H. Bönemann, R. Mynott, B. Spliethoff, C. Weidenthaler, N. Palina, S. Zinoveva, H. Modrow, *Appl. Organomet. Chem.* 19 (2005) 827-829.

[62] ¹H NMR confirms that intact AlEt₃ (~3 equivalents per Ir) is present in the catalyst solution prepared with [(1,5-COD)Ir(μ-O₂C₈H₁₅)₂] and AlEt₃ when using Al/Ir=5 (see Figures S6 and S7 of the Supporting Information for ¹H NMR spectra of catalyst prepared with [(1,5-COD)Ir(μ-O₂C₈H₁₅)₂] and 5 eq AlEt₃ vs that of pure AlEt₃.)

[63] W.M. Alley, I.K. Hamdemir, Q. Wang, A. Frenkel, L. Li, J.C. Yang, L.D. Menard, R.G. Nuzzo, S. Özkar, K.-H. Yih, K.A. Johnson, R.G. Finke, *Langmuir* 27 (2011) 6279-6294.

[64] Note here that care was taken to minimize the H₂O level to minimize alumoxane (i.e., Al-O-Al compound) production, and controls [63] show that added H₂O to the Al/Co = 2 or 3 catalyst solution prepared with Co(neodecanoate)₂ and AlEt₃ decreases the catalytic activity [63]. Prior studies by Schmidt and coworkers [52,53] show that presence of n = 0.5–1.5 equivalents (per Co) of water of crystallization in a Co(acac)₂•n(H₂O) plus AlEt₃ catalyst system decreases the catalyst stability and increases the amount of precipitate seen attributed to the formation of alumoxanes and their derivatives.

[65] A catalytic inhibiting effect has been observed when the precatalyst {[(1,5-COD)Ir•HPO₄] }_n is examined in the presence of added [Bu₄N]₂HPO₄. The catalytic activity of precatalyst is 1.0(1) mmol H₂/h before the catalyst was isolated and redispersed, while the addition of 1, and then separately [4], equivalents of [Bu₄N]₂HPO₄ to the precatalyst {[(1,5-COD)Ir•HPO₄] }_n lowers the catalytic activity to 0.20(5) and 0.10(5) mmol H₂/h, respectively [25]. It was concluded that "...increasing the concentration of HPO₄²⁻ results in a higher coverage of the Ir(0)_n nanoparticle surface, thereby, inhibiting the catalytic reactions of the Ir(0) active sites..." [25].

[66] An alternative hypothesis for the lower hydrogenation activity at higher AlEt₃ concentrations (i.e.; Al/Ir=2, 3 or 5 when compared to Al/Ir=1) is that a difference in size of the Ir(0)*n* nanoparticles is the main factor behind the different catalytic activities. However, this alternative explanation can be ruled out since the same size nanoparticles are observed within experimental error for each of the Al/Ir=1, 2 and 5 catalysts [4](see also the SI for that paper [4]).

[67] Reactions between AlEt₃ and precatalyst components are known in the literature of Ziegler-type hydrogenation catalysts. For example, when starting with M(acac)₂, where acac: acetylacetonate and M: Co, Pt or Pd, and AlR₃ (R: Me or Et) [54,57,58] the suggested products are: R₂Al-O-C(CH₃)=CH-C(Et)(CH₃)-O-AlR₂, and R₂Al-O-C(Et)(CH₃)-CH(AlEt₂)-C(Et)(CH₃)-O-AlR₂.

[68] K.-H. Yih, I.K. Hamdemir, J.E. Mondloch, E. Bayram, S. Özkar, R. Vasic, A.I. Frenkel, O. Anderson, R.G. Finke, *Inorganic Chemistry* 51 (2012) 3186-3193.

[69] M.A. Watzky, R.G. Finke, *J. Am. Chem. Soc.* 119 (1997) 10382–10400.

[70] J.A. Widegren, J.D. III Aiken, S. Özkar, R.G. Finke, *R. G. Chem. Mater.* 13 (2001) 312–324.

SUPPORTING INFORMATION-B:

HYDROCARBON-SOLUBLE, ISOLABLE ZIEGLER-TYPE Ir(0)_n NANOPARTICLE CATALYSTS MADE FROM [(1,5-COD)Ir(μ-O₂C₈H₁₅)₂] AND 2-5 EQUIVALENTS OF AlEt₃: THEIR HIGH CATALYTIC ACTIVITY, LONG LIFETIME AND AlEt₃-DEPENDENT, EXCEPTIONAL, 200 °C THERMAL STABILITY

Control studies measuring the maximum rate of cyclohexene hydrogenation as a function of the cycles of catalyst isolation and then redispersion: Control hydrogenations performed on Ziegler-type hydrogenation catalyst made from [(1,5-COD)Ir(μ-O₂C₈H₁₅)₂] plus AlEt₃, Al/Ir=2, showed that that the catalyst has the following rates of cyclohexene hydrogenation as it is re-isolated and then re-dispersed for 3 cycles: (5 ± 2, 8 ± 1, and 9 ± 1 mmol H₂/h, respectively, for once-redispersed, twice-redispersed and three-times-redispersed catalyst). The catalyst then retains its activity (~9 mmol/h) after the catalyst is redispersed up through its 8th redispersion.

The *Experimental Procedure* is as follows; note that a different isolation and redispersion procedure is used in this set of experiments vs that given in Experimental section of the main text. Therefore, the cyclohexene hydrogenation data obtained from this set of hydrogenations are not directly comparable to those mentioned in main text.

Catalyst solutions, 1.44 mM in Ir, were individually prepared in a drybox at 30°C. A 1.60 mg portion of [(1,5-COD)Ir(μ-O₂C₈H₁₅)₂] was weighed into a 20 mL screw-cap glass vial and then dissolved in 2.3 mL of cyclohexane forming an orange-red solution. A 5/8 × 5/16 inch Teflon-coated magnetic stir bar was then placed in the 20 mL screw-cap glass vial and the solution was stirred for 1 min at 1.0 × 10³ rpm as measured with a Monarch Instruments Pocket-Tachometer. The AlEt₃ solution (0.2 mL, 36 mM) was then quickly added to the [(1,5-COD)Ir(μ-O₂C₈H₁₅)₂] solution within 2 sec using a 0.5 mL gas-tight syringe while vigorously stirring. The resulting

tawny yellow solution was stirred under N₂ in the drybox for 9 h. At the end of 9 h, the solution appeared clear brown with no visually observable particles. The solution was then transferred into a new 22 × 175 mm Pyrex borosilicate culture tube containing a new 5/8 × 5/16 in. Teflon-coated magnetic stirbar. Cyclohexene (0.5 mL) was added using a 1.0 mL gas-tight syringe and the resulting hydrogenation solution (1.65 M in [cyclohexene] and 1.2 mM in [Ir]) was stirred for an additional 1 min, all in a N₂ atmosphere drybox.

The procedure and apparatus used for catalytic hydrogenations of cyclohexene have been described in detail elsewhere.¹ Briefly, a culture tube containing the hydrogenation solution was placed in a Fisher-Porter (F–P) bottle, which was then sealed and brought out of the drybox. The F–P bottle was placed in a bath set at 22.0 ± 0.1 °C. Stirring was started at 1000 ± 10 rpm using a Fauske Super magnetic stirplate and the F–P bottle was connected to a pressurized H₂ line using TFE-sealed Swagelok quick-connects. The F–P bottle was purged 15 times (1 purge/15 sec) with H₂ that has passed through an indicating moisture trap (Scott Specialty Gas), a disposable O₂ cartridge (Trigon), and an indicating O₂ trap (Trigon). The pressure in the F–P bottle was then set to 40 psig, and then the data collection was initiated. Hydrogen pressure vs. time data were collected using a pressure transducer (Omega PX 624–100 GSV) interfaced via an Omega D1131 analog to digital converter to a PC running LabVIEW 7.0. Data were subsequently handled using MS Excel. The maximum hydrogenation rate of catalysts before and after catalyst isolation was calculated from each kinetic curve by a linear-least-squares fits to the data points in the highest activity (highest slope) region ($R^2 \geq 0.999$ for the reported data). The maximum hydrogenation rates of redispersed catalysts occur at the beginning of the hydrogenation (i.e., the maximum rate equals the initial rate), so those (maximum) rates were

¹ (a) Watzky, M. A.; Finke, R. G. *J. Am. Chem. Soc.* **1997**, *119*, 10382–10400; (b) Widegren, J. A.; Aiken, J. D., III; Özkar, S.; Finke, R. G. *Chem. Mater.* **2001**, *13*, 312–324.

calculated via linear-least-squares fits to the initial, linear regions of the redispersed catalysts hydrogenation curves ($R^2 \geq 0.999$ for the reported data).

After hydrogenation, the F-P bottle was kept connected to the hydrogenation line and volatiles were removed under vacuum to yield a black powder. The F-P was then taken inside the drybox. Cyclohexane (2.5 mL) was then added to this isolated, black powdered catalyst and the resulting solution was stirred for 2 min. Fresh cyclohexene (0.5 mL) was added using a 1.0 mL gas-tight syringe and the resulting hydrogenation solution (1.65 M in [cyclohexene] and 1.2 mM in [Ir]) was stirred for an additional 1 min. The F-P bottle was then sealed and brought out of the drybox. The F-P bottle was placed in a bath set at 22.0 ± 0.1 °C. A cyclohexene hydrogenation was started as detailed above. This procedure was repeated eight times to obtain the 8-times-redispersed catalyst.

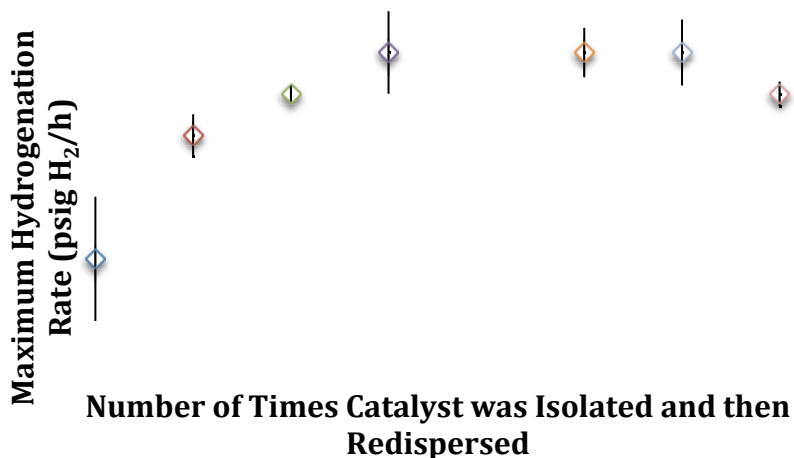


Figure SI-B1. Comparison of the maximum hydrogenation rates of Ziegler-type hydrogenation catalyst made from $[(1,5\text{-COD})\text{Ir}(\mu\text{-O}_2\text{C}_8\text{H}_{15})]_2$ plus AlEt_3 , $\text{Al}/\text{Ir} = 2$, as a function of number of times the catalyst was isolated and then redispersed. Note that we considered if H_2 gas-to-solution mass transfer limitations (MTLs) of our apparatus could be hiding a higher maximum rate and, thereby, hiding some loss of rate at the higher catalyst recycle values. That alternative explanation can be ruled out, however, since the maximum rate of ~ 10 psig /h seen in Figure SI-B1 above is a factor of ~ 8 lower than the MTL of $\sim 80 \pm 20$ psig/h of our apparatus when stirred at 1000 rpm (see Figure SI-B4, *vide infra*).

Control studies to determine effect of aging (9 h at room temperature) the Ziegler-type Hydrogenation Catalyst made from [(1,5-COD)Ir(μ -O₂C₈H₁₅)₂] plus AlEt₃, Al/Ir = 2, in Dodecane: Control experiments, performed on Ziegler-type hydrogenation catalyst made from [(1,5-COD)Ir(μ -O₂C₈H₁₅)₂] plus AlEt₃ in *dodecane*, showed that aging the catalyst for 9 h at room temperature only has a modest effect on the activity of the catalyst. The catalyst prepared in dodecane and then immediately used in cyclohexene hydrogenation exhibits hydrogenation rate of 1.1 ± 0.1 mmol H₂/h whereas the catalyst aged 9 h has hydrogenation rate of 0.7 ± 0.1 mmol H₂/h (Figure SI-B2), values that are not different at a 2σ (i.e., ± 0.2) experimental error in each measurement.

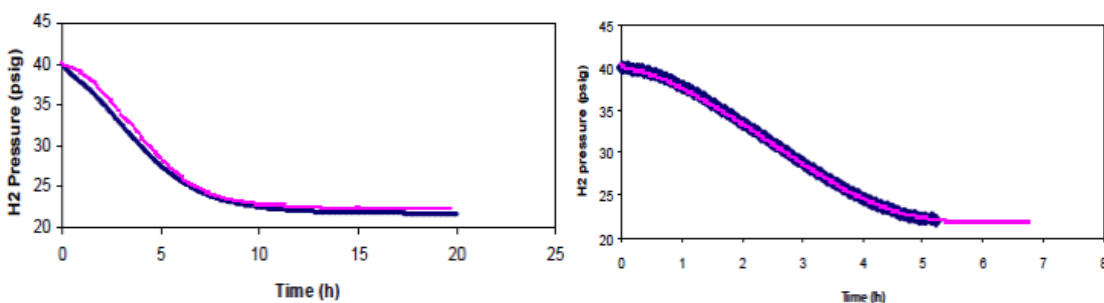


Figure SI-B2. Plot of the H₂ pressure vs time data for cyclohexene hydrogenations with the Ziegler-type hydrogenation catalyst made from [(1,5-COD)Ir(μ -O₂C₈H₁₅)₂] plus AlEt₃, Al/Ir=2, in dodecane solvent. (left) Aged for 9 h at room temperature under N₂ after it was prepared as detailed in experimental section, and (right) used immediately after its preparation. [Ir]=1.2 mM; [cyclohexene]_{initial}=1.65 M; 22.0 ± 0.1 °C; and 40 ± 1 psig H₂.

Other Control or Survey Experiments. The following were done as additional control or survey experiments; the specific experimental details for each are given below, as the experiments below deviate from the catalyst preparation experimental protocols used and reported in the main text in that the studies below do *not* perform a cycle of cyclohexene hydrogenation *before* the 200 °C thermal treatments (i.e., and as was done in the Experimental

section described in the main text). A bottom line of the experiments that follow are that preadding cyclohexene, then heat treatment at 200 °C for 60 minutes (i.e., all without the 9 hrs of room temperature aging), also provides a high activity catalyst.

(i) *Testing the 9 hr aged, then 200 °C thermally, treated catalyst solution in a cyclohexene hydrogenation (i.e., the catalyst prepared without a cyclohexene hydrogenation run after the 9 hr aging, but before the 200 °C thermal treatment):* This survey experiment was performed on the Ziegler-type hydrogenation catalyst made from [(1,5-COD)Ir(μ -O₂C₈H₁₅)₂] plus AlEt₃, Al/Ir=2 as detailed below and without a cyclohexene hydrogenation run before the catalyst is thermally treated. The results shows that the 9 hr aged, then thermally treated catalyst is active with a maximum cyclohexene hydrogenation rate of ~1 mmol H₂/h.

The *Experimental Procedure* is as follows: A 1.60 mg portion of [(1,5-COD)Ir(μ -O₂C₈H₁₅)₂] was weighed into a 20 mL screw-cap glass vial and then dissolved in 2.3 mL of dodecane forming an orange-red solution. A 5/8 × 5/16 inch Teflon-coated magnetic stir bar was then placed in the 20 mL screw-cap glass vial and the solution was stirred for 1 min at 1.0 × 10³ rpm as measured with a Monarch Instruments Pocket-Tachometer. The AlEt₃ solution (0.2 mL, 36 mM, in cyclohexane) was then quickly added to the [(1,5-COD)Ir(μ -O₂C₈H₁₅)₂] solution within 2 sec using a 0.5 mL gas-tight syringe while vigorously stirring. The resulting tawny yellow solution was stirred under N₂ in the drybox for 9 h. At the end of 9 h, the solution appeared clear brown with no visually observable particles. The solution was then transferred into a new 22 × 175 mm Pyrex borosilicate culture tube containing a new 5/8 × 5/16 in. Teflon-coated magnetic stirbar. The culture tube containing the hydrogenation solution was placed in a Fisher-Porter (F–P) bottle, which was then sealed and brought out of the drybox. The F–P bottle was placed in a bath set at 200 ± 2 °C. Stirring was started at 1000 ± 10 rpm using a Fauske Super magnetic

stirplate and the F-P bottle was connected to a pressurized H₂ line using TFE-sealed Swagelok quick-connects. The F-P bottle was purged 15 times (1 purge/15 sec) with H₂ that has passed through an indicating moisture trap (Scott Specialty Gas), a disposable O₂ cartridge (Trigon), and an indicating O₂ trap (Trigon). The pressure in the F-P bottle was then set to ~20 psig and continuously monitored during heating. The solution in the F-P bottle was kept at 200 °C for 30 min and then cooled down to room temperature under H₂. (Note that this procedure differs from that in the main text in that a cycle of cyclohexene hydrogenation was not done prior to the 200 °C thermal treatment.) The F-P bottle was then brought into the drybox and 0.5 mL cyclohexene was added. Next, the F-P bottle was taken out of the drybox, connected to H₂ line and purged 15 times (1purge/15 sec) with H₂ that has passed through an indicating moisture trap (Scott Specialty Gas), a disposable O₂ cartridge (Trigon), and an indicating O₂ trap (Trigon). A room temperature cyclohexene hydrogenation was then carried out to test the activity of the thermally treated catalyst. A maximum hydrogenation rate of ~1 mmol H₂/h was observed.

(ii) *Testing a catalyst solution, prepared with only a 200 °C thermal treatment, in a cyclohexene hydrogenation (i.e., the catalyst prepared without 9 hrs of aging and without a cyclohexene hydrogenation run before the 200 °C thermal treatment):* A survey experiment performed on the Ziegler-type hydrogenation catalyst made from [(1,5-COD)Ir(μ-O₂C₈H₁₅)₂] plus AlEt₃, Al/Ir=2, but without the 9 hr aging step, show that the maximum hydrogenation rates are 11.5 and 12.7 mmol H₂/h for the catalysts kept at 200 °C for 15 or 60 min, respectively.

The *Experimental Procedure* is as follows: A 1.60 mg portion of [(1,5-COD)Ir(μ-O₂C₈H₁₅)₂] was weighed into a 20 mL screw-cap glass vial and then dissolved in 2.3 mL of dodecane forming an orange-red solution. A 5/8 × 5/16 inch Teflon-coated magnetic stir bar was then placed in the 20 mL screw-cap glass vial and the solution was stirred for 1 min at 1.0 × 10³ rpm as measured with

a Monarch Instruments Pocket-Tachometer. A AlEt_3 solution (0.2 mL, 36 mM, in cyclohexane) was then quickly added to the $[(1,5\text{-COD})\text{Ir}(\mu\text{-O}_2\text{C}_8\text{H}_{15})]_2$ solution within 2 sec using a 0.5 mL gas-tight syringe while vigorously stirring. The solution was then transferred into a new 22 × 175 mm Pyrex borosilicate culture tube containing a new 5/8 × 5/16 in. Teflon-coated magnetic stirbar. The culture tube containing the hydrogenation solution was placed in a Fisher-Porter (F-P) bottle, which was then sealed and brought out of the drybox. The F-P bottle was placed in a bath set at 200 ± 2 °C. Stirring was started at 1000 ± 10 rpm using a Fauske Super magnetic stirplate and the F-P bottle was connected to a pressurized H_2 line using TFE-sealed Swagelok quick-connects. The F-P bottle was purged 15 times (1 purge/15 sec) with H_2 that has passed through an indicating moisture trap (Scott Specialty Gas), a disposable O_2 cartridge (Trigon), and an indicating O_2 trap (Trigon). The pressure in the F-P bottle was then set to ~20 psig and continuously monitored during heating. The solution in the F-P bottle was kept at 200 °C for 15 or 60 min and then cooled down to room temperature under H_2 . The F-P bottle was then brought into the drybox and 0.5 mL cyclohexene was added. Next, the F-P bottle was taken out of the drybox, connected to H_2 line and purged 15 times (1purge/15 sec) with H_2 that has passed through an indicating moisture trap (Scott Specialty Gas), a disposable O_2 cartridge (Trigon), and an indicating O_2 trap (Trigon). A cyclohexene hydrogenation was then carried out to test the activity of the thermally treated catalyst. The maximum hydrogenation rates are 11.5 and 12.7 mmol H_2 /h for the catalysts kept at 200 °C for 15 or 60 min, respectively.

(iii) *Testing a catalyst solution prepared with cyclohexene added before the 200 °C thermal treatment (i.e., a catalyst prepared without the 9 hr aging and without a cyclohexene hydrogenation run before the 200 °C thermal treatment, but with cyclohexene added before the thermal treatment):* A survey experiment was performed on the Ziegler-type hydrogenation catalyst made from $[(1,5\text{-COD})\text{Ir}(\mu\text{-O}_2\text{C}_8\text{H}_{15})]_2$ plus AlEt_3 , Al/Ir=2, and as detailed below shows

that this specific catalyst, with cyclohexene added to the catalyst solution before it was thermally treated for 3, 15 or 60 min, is active with maximum hydrogenation rates of 15, 16 and 27 mmol H₂/h, respectively.

The *Experimental Procedure* is as follows: A 1.60 mg portion of [(1,5-COD)Ir(μ -O₂C₈H₁₅)₂]₂ was weighed into a 20 mL screw-cap glass vial and then dissolved in 2.3 mL of dodecane forming an orange-red solution. A 5/8 × 5/16 inch Teflon-coated magnetic stir bar was then placed in the 20 mL screw-cap glass vial and the solution was stirred for 1 min at 1.0 × 10³ rpm as measured with a Monarch Instruments Pocket-Tachometer. A AlEt₃ solution (0.2 mL, 36 mM, in cyclohexane) was then quickly added to the [(1,5-COD)Ir(μ -O₂C₈H₁₅)₂]₂ solution within 2 sec using a 0.5 mL gas-tight syringe while vigorously stirring. Cyclohexene (0.5 mL) was added using a 1.0 mL gas-tight syringe and the resulting hydrogenation solution (1.65 M in [cyclohexene] and 1.2 mM in [Ir]) was stirred for an additional 1 min. The solution was then transferred into a new 22 × 175 mm Pyrex borosilicate culture tube containing a new 5/8 × 5/16 in. Teflon-coated magnetic stirbar. The culture tube containing the hydrogenation solution was placed in a Fisher-Porter (F-P) bottle, which was then sealed and brought out of the drybox. The F-P bottle was placed in a bath set at 200 ± 2 °C. Stirring was started at 1000 ± 10 rpm using a Fauske Super magnetic stirplate and the F-P bottle was connected to a pressurized H₂ line using TFE-sealed Swagelok quick-connects. The F-P bottle was purged 15 times (1 purge/15 sec) with H₂ that has passed through an indicating moisture trap (Scott Specialty Gas), a disposable O₂ cartridge (Trigon), and an indicating O₂ trap (Trigon). The pressure in the F-P bottle was then set to ~20 psig and continuously monitored during heating. The solution in the F-P bottle was kept at 200 °C for 3, 15 or 60 min and then cooled down to room temperature under H₂. A cyclohexene hydrogenation was then carried out. Maximum hydrogenation rates of 15, 16 and 27 mmol H₂/h were observed for the 3, 15 and 60 min thermally treated catalysts, respectively.

Hydrogenation with heat-treated Ziegler-type hydrogenation catalyst made from [(1,5-COD)Ir(μ -O₂C₈H₁₅)₂] plus AlEt₃, Al/Ir=2:

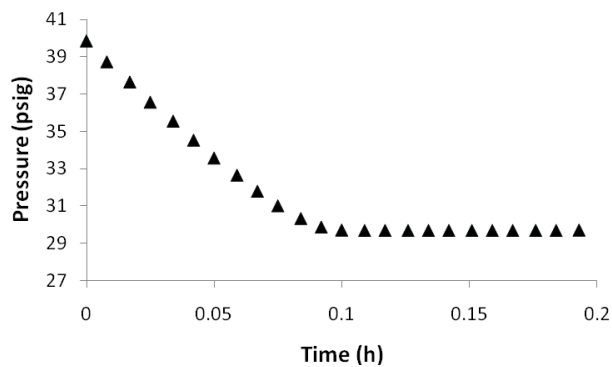


Figure SI-B3. Plot of the H₂ pressure vs time data for cyclohexene hydrogenations with heat-treated Ziegler-type hydrogenation catalyst made from [(1,5-COD)Ir(μ -O₂C₈H₁₅)₂] plus AlEt₃, Al/Ir=2, in dodecane solvent. [Ir]=1.2 mM; [cyclohexene]_{initial}=1.65 M; Hydrogenation temperature: 22.0 \pm 0.1 $^{\circ}$ C; and initial H₂ pressure: 40 \pm 1 psig.

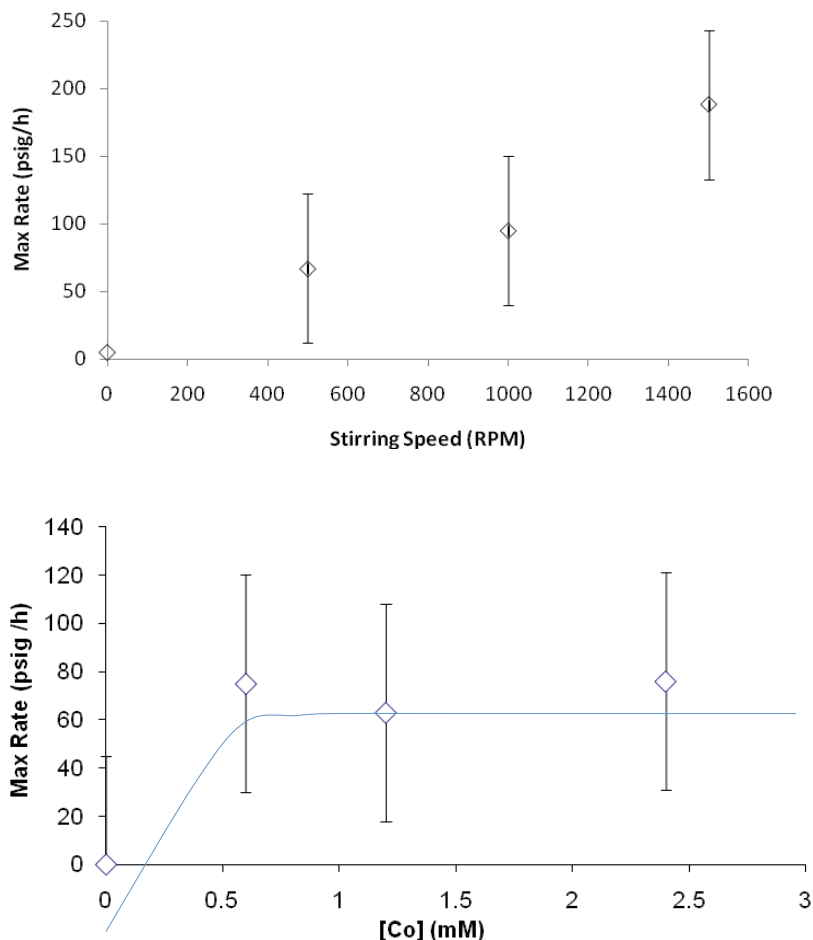


Figure SI-B4. Control hydrogenations catalyzed by $\text{Co}(\text{O}_2\text{C}_{10}\text{H}_{19})_2$ plus AlEt_3 , $\text{Al/Co}=2$, catalyst, studies performed with this superior rate catalyst to determine the H_2 gas-to-solution, mass-transfer-limited (MTL) rate of the hydrogenation apparatus used in the present work and under the specific, Standard Conditions employed (see below). The maximum rates of hydrogenations were calculated as detailed in the main text by linear least-squares fits to the steepest regions of hydrogenation curves. Those maximum rates were then collected as a function of stirring rate (top), and as a function of the $\text{Co}(\text{O}_2\text{C}_{10}\text{H}_{19})_2$ concentration at constant, 1000 ± 300 r.p.m., stirring (bottom). The MTL rate is a function of the hydrogenation apparatus used and the solvent, but will be independent of the metal used (i.e., the bottom of Figure S4). Hence, for the sake of convenience in achieving these fastest rates, the fast cobalt catalyst made from $\text{Co}(\text{O}_2\text{C}_{10}\text{H}_{19})_2$ and AlEt_3 was used. The bottom curve reveals that $\sim 100\%$ MTL has been reached at $\sim 80 \pm 20$ psig/h $\sim 20 \pm 5$ mmol H_2 /h when stirring our apparatus at 1000 ± 300 r.p.m. The top, stirring rate studies confirm that MTL is present (i.e., a stirring rate dependence is seen). The MTL limit is ~ 20 mmol H_2 /h (~ 80 psig H_2 /h) for our particular apparatus, and at the standard conditions used (i.e., for the conditions: solvent = cyclohexane, temp. = 22.0 °C, $[\text{Co}] = 1.2$ mM, $[\text{Cyclohexene}]_{\text{initial}} = 1.65$ M and stirring = 1000 ± 300 r.p.m. as detailed in the main text Experimental section).

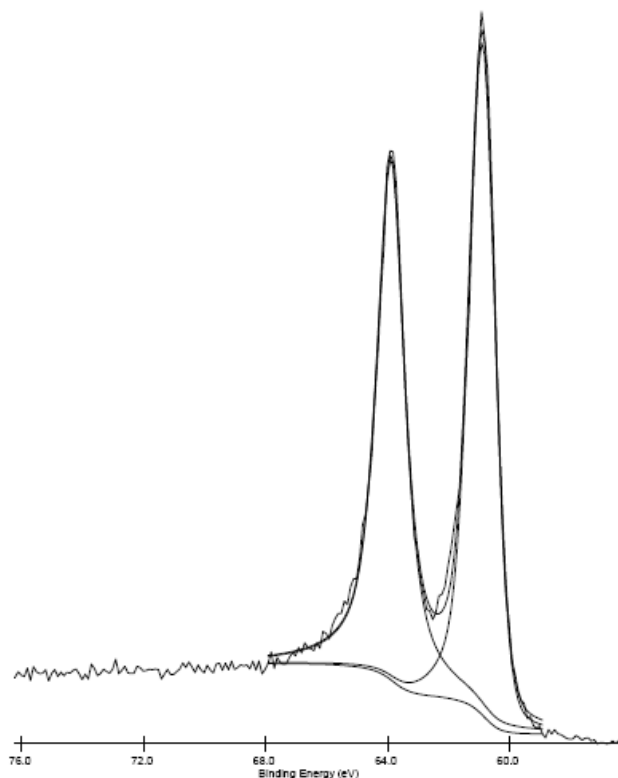


Figure SI-B5. High resolution XPS spectrum showing the Ir 4f peaks of brown particles observed for the Al/Ir=3 catalyst solution after heating at 200 °C for 30 min. The peaks observed at 63.9 eV and 60.9 eV are assigned to Ir(0).

Control Studies with the Al/Ir = 1 Catalyst. While typical industrial conditions employ catalysts with Al/M ratios ≥ 2 , reflection suggested that control experiments with the Al/Ir=1 (as well as the Al/Ir=0 catalyst, *vide infra*) would likely prove of interest in further revealing the effects of the Al/Ir ratio on the catalytic properties. Hence, a control of hydrogenation catalysis using the Al/Ir=1 catalyst was performed.

In that control experiment, the original tawny yellow solution obtained mixing [(1,5-COD)Ir(μ -O₂C₈H₁₅)₂] and AlEt₃ at Al/Ir=1 changes to brown at the end of 9 h of stirring, indicating the presence of Ir(0)_n nanoparticles initially. But, after cyclohexene hydrogenation visually observable black particles of bulk Ir(0) are present in the brown solution and on the stirbar, indicating that the addition of just 1 equivalent AlEt₃ per Ir is insufficient to protect against

agglomeration to bulk Ir(0) metal. Consistent with this, the catalyst isolated by removing the volatiles under vacuum was only partially redispersible in cyclohexane (to give a brown suspension but with visually observable, bulk-metal particles, Table 3.1, entry 4, column 3). Further evidence for the limited thermal stability of the Al/Ir=1 catalyst is that 30 minutes of heating at 200 °C yields a colorless, and therefore largely nanoparticle-free, solution with visually observable black particles (Table 3.1, entry 4, column 7). Use of this Al/Ir=1, thermalized catalyst for hydrogenation yields a gray, turbid solution with visually observable black particles at the end of the catalysis (Table 3.1, entry 4, column 9), and micrometer scale particles by bright-field TEM images, Figure SI-B6. The presence of that bulk metal means that the relatively high TTO value of $TTO = [370,000]$ over the course of 104 h at 22.0 ± 0.1 °C contains a significant contribution from bulk metal, why that TTO value is placed in [brackets] above and in Table 2.1—to indicate that it is an upper limit to the desired TTOs by any nanoparticle component. Overall, this control experiment with the Al/Ir = 1 catalyst system fortifies the results presented in the main text by confirming that higher Al/Ir ratios are required for the most stable catalysts.

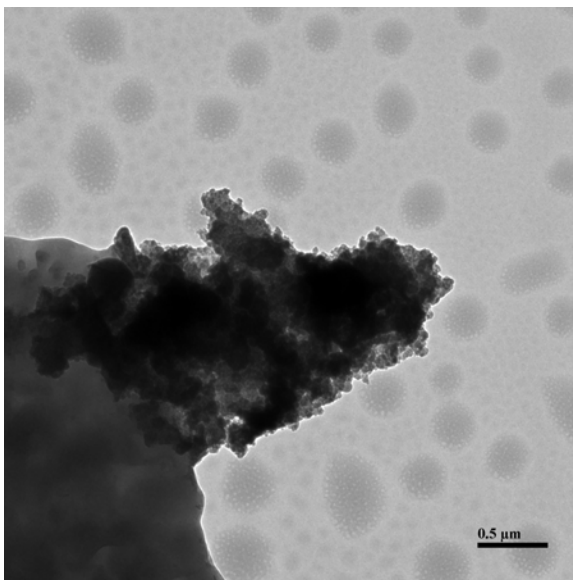


Figure SI-B6. A bright-field TEM image of the $Al/Ir=1$ Ziegler-type hydrogenation catalyst made from $[(1,5-COD)Ir(\mu-O_2C_8H_{15})_2]$ plus $AlEt_3$. The image, taken from the solution withdrawn from the culture tube at the end of cyclohexene hydrogenation catalyzed by the 200 °C-treated catalyst, reveals *micrometer particles of bulk Ir metal* (note the $0.5 \mu m = 500 \text{ nm}$ scale bar).

Control Studies with the $Al/Ir = 0$ Catalysts: The $Al/Ir=0$ catalyst was also briefly examined as a control to reveal the effect of $AlEt_3$ on the activity, lifetime and stability of the resulting hydrogenation catalyst (Table 3.1, Entry 5) that is formally not a Ziegler-type hydrogenation catalyst since it contains no $AlEt_3$. A *clear, colorless, and hence largely nanoparticle free solution*, with visually observable black bulk-metal, results at the end of hydrogenation starting with the $[(1,5-COD)Ir(\mu-O_2C_8H_{15})_2]$ complex with no added $AlEt_3$. (Immediately at the end of the hydrogenation when H_2 consumption ceases, the catalyst solution is the orange, initial color of primarily the unreduced $[(1,5-COD)Ir(\mu-O_2C_8H_{15})_2]$ complex, but with visible black bulk metal on the walls of the culture tube and on the stirbar. Keeping the catalyst solution for an additional ~15 min under H_2 after complete cyclohexene consumption results in formation of the cited colorless solution with visually observable black bulk-metal.) This $Al/Ir=0$ catalyst does

afford [230 000] turnovers of cyclohexene hydrogenation over the course of 90 h at 22.0 ± 0.1 °C ($\text{TOF}_{\text{ave}}=3600 \text{ h}^{-1}$), but this TTO value reflects primarily the visually observable bulk Ir(0) metal that is present on the stir bar after just ~ 1300 turnovers (and, therefore, is again placed in brackets to remind us that the [230 000] is not reflective of just nanoparticle catalysis). The Al/Ir=0 observations are, however, of use in confirming that the initially formed Ir(0)_n nanoparticles *are unstable against agglomeration in the absence of AlEt₃*.

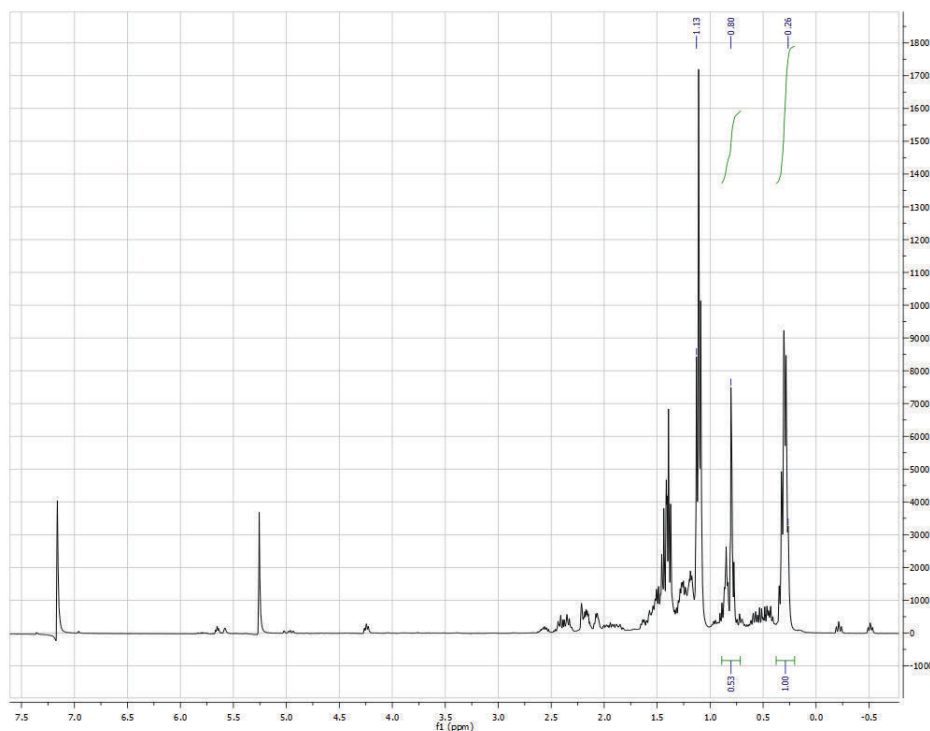


Figure SI-B7. ^1H NMR spectrum of catalyst solution prepared with $[(1,5\text{-COD})\text{Ir}(\mu\text{-O}_2\text{C}_8\text{H}_{15})]_2$ plus AlEt_3 , Al/Ir= 5, in benzene- d_6 . The precatalyst and cocatalyst solutions were prepared under N_2 in a drybox in benzene- d_6 and then mixed in a sealed NMR tube. The spectrum shows that the peaks assigned to unreacted AlEt_3 at 0.26 ppm and 1.13 ppm (see Figure S4) are still present in the solution after mixing with the precatalyst $[(1,5\text{-COD})\text{Ir}(\mu\text{-O}_2\text{C}_8\text{H}_{15})]_2$. Integration of the peaks at 0.26 ppm (assigned to methylene group in AlEt_3) and 0.80 ppm (assigned to methyl in 2-ethylhexanoate of precatalyst) reveals that ~ 3 equivalents per Ir of AlEt_3 remain intact.

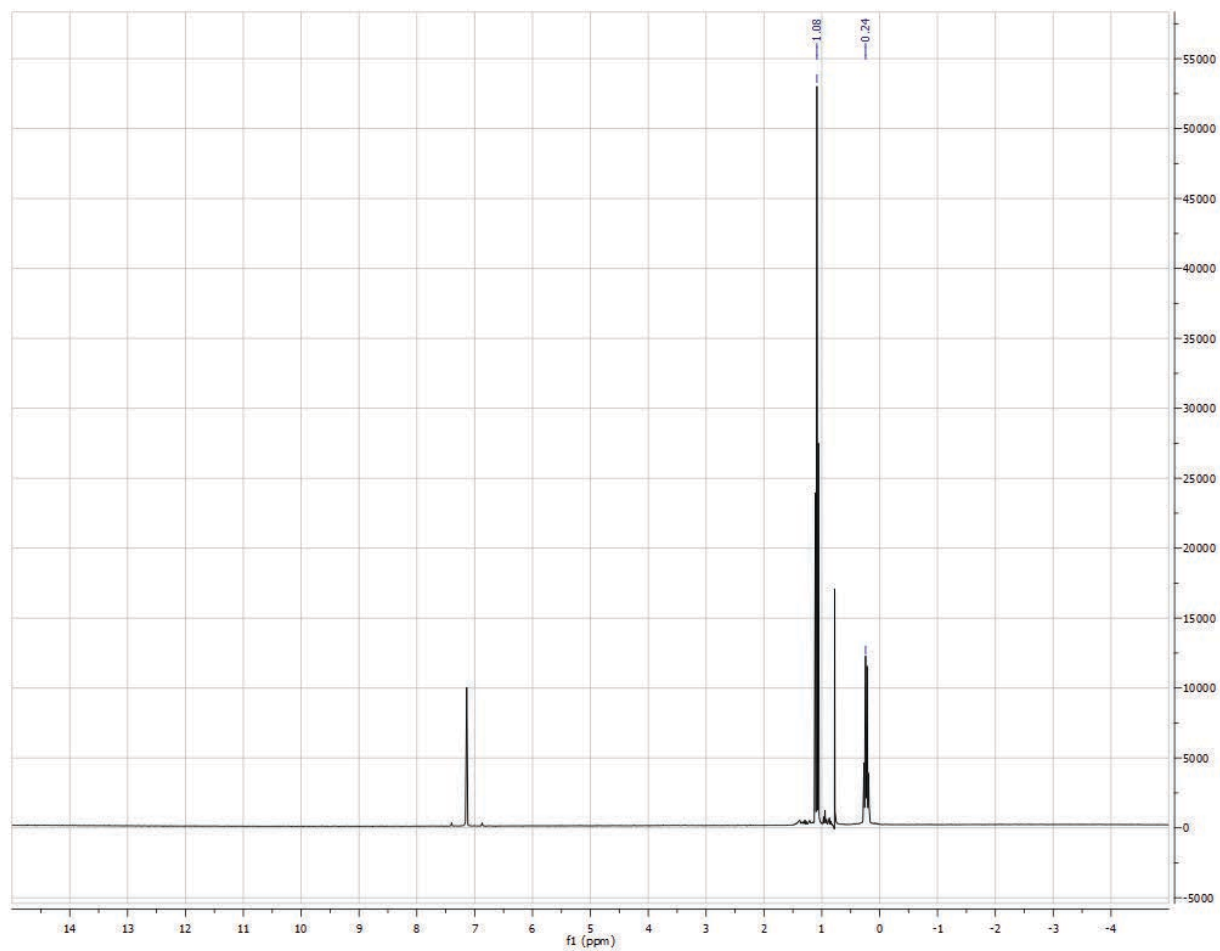


Figure SI-B8. ^1H NMR spectrum of pure AlEt_3 in benzene- d_6 . The peak at 0.24 ppm (quartet) and 1.08 ppm (triplet) are assigned to methylene and methyl signals.

CHAPTER IV

EXCEPTIONALLY THERMALLY STABLE, HYDROCARBON SOLUBLE ZIEGLER-TYPE

$\text{Ir}(0)_n$ NANOPARTICLE CATALYSTS MADE FROM $[\text{Ir}(1,5\text{-COD})(\mu\text{-O}_2\text{C}_8\text{H}_{15})]_2$ PLUS AlEt_3 :

TESTS OF KEY HYPOTHESES FOR THEIR UNUSUAL STABILIZATION

This dissertation chapter presents a manuscript submitted for publication to *J. Mol. Catal.*

A: Chem. This chapter investigates the true nature of the AlEt_3 -derived stabilizer species in the Ziegler-type catalyst solution made from $[\text{Ir}(1,5\text{-COD})(\mu\text{-O}_2\text{C}_8\text{H}_{15})]_2$ plus AlEt_3 using NMR and IR spectroscopic techniques plus catalytic evidence. This study shows that $\text{AlEt}_2(\text{O}_2\text{C}_8\text{H}_{15})$ ($\text{Al}/\text{Ir}=1, 2$ and 3) and free AlEt_3 ($\text{Al}/\text{Ir}=3$) are present in the catalyst solution made with $[\text{Ir}(1,5\text{-COD})(\mu\text{-O}_2\text{C}_8\text{H}_{15})]_2$ plus AlEt_3 . In addition, experimental results of this study helps to rule out the initial, literature-based hypotheses that anionic $[\text{AlEt}_3(\text{O}_2\text{C}_8\text{H}_{15})]^-$ stabilizer exists or that the AlEt_3 -derived stabilizers are Al-O-Al containing alumoxanes.

All the experiments given in the main text were performed by Isil K. Hamdemir. The repeat ^1H and ^{13}C NMR experiments were performed by Saim Özkar. The syntheses of $\text{Al}(t\text{-Bu})_3$, $[(t\text{-Bu})_2\text{Al}(\mu\text{-OH})]_3$ and $[(n\text{-Bu})_4\text{N}](\text{AlEt}_3\text{O}_2\text{C}_8\text{H}_{15})$ were designed in consultation with both Professors Saim Özkar and Richard G. Finke and were performed by Isil K. Hamdemir. The ^{27}Al NMR spectra were obtained by Isil K. Hamdemir with assistance from Prof. Saim Özkar. The ^1H NMR of the $[\text{Ir}(1,5\text{-COD})(\mu\text{-O}_2\text{C}_8\text{H}_{15})]_2$ plus BEt_3 solution was obtained by Saim Özkar. The published synthesis of $[\text{Ir}(1,5\text{-COD})(\mu\text{-H})]_4$ was performed by Kuang-Hway Yih after Isil K. Hamdemir showed that the material existed from an initial low ($\sim 1\%$) yield synthesis. Control experiments starting with $[\text{Ir}(1,5\text{-COD})(\mu\text{-H})]_4$ presented in the Supporting Information (Supporting Information_C) were performed by both Isil K. Hamdemir and Kuang-Hway Yih. The FTIR data for modified-methyl alumoxane sample was obtained by Adam Crooks. XAFS

data (given in Supporting Information (Supporting Information_C), previously published in dissertation by William M. Alley) was obtained, processed, and analyzed by William M. Alley with assistance from Qi Wang, Anatoly I. Frenkel, and Laurent D. Menard. The initial draft of the paper, subsequent drafts including the final draft and preparation of the document in this chapter for publication were performed by Isil K. Hamdemir with light editing by Saim Özkar, and moderate editing by Richard G. Finke (38 hours).

Synopsis

In recent work we showed that Ziegler-type nanoparticles made from $[\text{Ir}(1,5\text{-COD})(\mu\text{-O}_2\text{C}_8\text{H}_{15})]_2$ plus AlEt_3 are an unusually thermally stable (≥ 30 min at 200°C), hydrocarbon-solvent soluble, high catalytic activity nanoparticle catalyst (I.K. Hamdemir, S. Özkar, K.-H. Yih, J.E. Mondloch, R.G. Finke, ACS Catal. 2 (2012) 632-641). As such, they are analogous to—and currently the cleanest and best characterized model system for—Ziegler-type nanoparticles made from Co or Ni precatalysts plus AlEt_3 which are used industrially to hydrogenate $\sim 1.7 \times 10^5$ metric tons of styrenic block copolymers per year (for a review of the area see: W.M. Alley, I.K. Hamdemir, K.A. Johnson, R.G. Finke, J. Mol. Catal. A.Chem. 315 (2010) 1-27). The key question addressed in the present paper is “*What is the nature of the AlEt_3 -derived stabilizer species?*” for the unusually stable and active Ziegler-nanoparticles formed from $[\text{Ir}(1,5\text{-COD})(\mu\text{-O}_2\text{C}_8\text{H}_{15})]_2$ plus AlEt_3 . Specifically tested herein are three primary hypotheses for the AlEt_3 -derived stabilizer(s) in the $\text{Ir}(0)_n$ Ziegler-nanoparticle system: (i) that the key stabilizer is neutral aluminum alkyl carboxylates following precedent from the work of Schmidt and Bönnemann; (ii) that a key stabilizer is the AlEt_3 which reacts with $\text{Ir}(0)_n$ nanoparticle surface; or (iii) that the dominant AlEt_3 -derived stabilizer is Al-O-Al containing alkylalumoxanes formed from any water present.

1. Introduction

Ziegler-type hydrogenation catalysts are formed, by definition [1], from a non-zero valent group 8-10 transition metal precatalyst plus a trialkylaluminum cocatalyst such as AlEt_3 . These catalysts, such as the industrial example [1,2] of $\text{Co}(\text{neodecanoate})_2$ plus AlEt_3 , are used to hydrogenate the double bonds of $\sim 1.7 \times 10^5$ metric tons/year of styrenic block copolymers, thereby removing any allylic C-H bonds greatly increases the stability of the resultant polymer

towards autoxidation [2,3]. A long standing question in this area had been what is the true catalyst when one mixes the precatalysts, such as $\text{Co}(\text{neodecanoate})_2$ or $\text{Ni}(\text{2-ethylhexanoate})_2$, with AlEt_3 cocatalyst? By employing a model, third-row Ziegler-type hydrogenation catalyst made from the crystallographically characterized $[\text{Ir}(\text{1,5-COD})(\mu\text{-O}_2\text{C}_8\text{H}_{15})]_2$ precatalyst [3] plus AlEt_3 , $\text{Al}/\text{Ir} = 1, 2, 3$ or 5 [4], we were recently able to show that sub-nanometer, $\text{Ir}(0)_{\sim 4-15}$ particles are formed initially from mixing $[\text{Ir}(\text{1,5-COD})(\mu\text{-O}_2\text{C}_8\text{H}_{15})]_2$ plus 1, 2, 3 or 5 equivalents of AlEt_3 in cyclohexane. We were also able to show, on the basis of X-ray absorption fine structure spectroscopy (XAFS), Z-contrast scanning transmission electron microscopy (Z-contrast STEM), plus matrix assisted laser desorption ionization mass spectroscopy (MALDI MS), that those initially formed $\text{Ir}(0)_{\sim 4-15}$ particles are then transformed under cyclohexene plus H_2 hydrogenation catalysis conditions to *fcc* $\text{Ir}(0)_{\sim 40-150}$ nanoparticles as the faster catalysts—what we have termed “Ziegler nanoparticles” [1,4]. Post working out the needed methodology using the model $\text{Ir}(0)_{\sim 40-150}$ Ziegler nanoparticles, analogous studies were then published revealing that industrial Ziegler-type hydrogenation catalysts made from $\text{Co}(\text{neodecanoate})_2$ or $\text{Ni}(\text{2-ethylhexanoate})_2$ plus AlEt_3 [5] also yield Ziegler-type nanoparticles, but now a broad distribution of $\text{M}_{\geq 4}$ ($\text{M} = \text{Co}, \text{Ni}$) sub-nanometer to larger particles with a mean diameter of ~ 1 nm.

In another recent publication, the model $\text{Ir}(0)_n$ Ziegler-type nanoparticles with an $\text{AlEt}_3 / \text{Ir}$ ratio of 5 were shown to be highly catalytically active, to exhibit good lifetimes of 100,000 total turnovers of cyclohexene hydrogenation, and to be stable for ≥ 30 min at 200°C [6]. The demonstrated nanoparticle catalyst stability at 200°C appears to surpass that of any other nanoparticle catalyst in the literature [6]. It was concluded that Ziegler-type nanoparticles appear to be an unusual type of little recognized, and hence underexploited, hydrocarbon-soluble and

thermally unusually stable nanoparticle catalysts, ones largely hidden for a 50-year period due to a lack of knowledge that nanoparticles are the true catalyst [1-6].

The “What is the Nature of the Stabilizer?” Question. An important, intriguing but presently ill-understood question is what is the precise nature of the stabilization—the unusually effective, higher temperature stabilization—in Ziegler-type nanoparticle catalysts derived, for example, from $[\text{Ir}(1,5\text{-COD})(\mu\text{-O}_2\text{C}_8\text{H}_{15})]_2$ plus AlEt_3 ? The literature offers some important hints based especially on the pioneering work of Shmidt (aka Schmidt), as well as the valuable studies of Bönemann and co-workers, who provided early evidence for nanoparticle formation, but where the nature of the best, fastest catalyst remained unclear [7,8,9,10,11,12,13,14,15,16,17]. Based on the results of characterization studies on Ziegler-type hydrogenation catalysts made with a metal acetylacetonate precursor $\text{M}(\text{acac})_n$ (M: Fe, Ni, Co, or Pd) plus AlEt_3 cocatalyst [7,8,9,10] (see also part C1.1.1 and Table SI-C1 in the Appendix C), Shmidt and coworkers have suggested a stabilizer layer containing individual molecules of $\text{AlEt}_2(\text{acac})$ [8] as illustrated in Figure 4.1 (and listed in Table SI-C1). Bönemann and coworkers [11,12,13,14] have analyzed the products formed upon the reaction of $\text{Pt}(\text{acac})_2$ with AlMe_3 and have come to conclusion that an “organoaluminum protecting shell” [11] exists and acts as stabilizer around the $\text{Pt}(0)_n$ nanoparticles; they have drawn figures [12] that are largely analogous to that shown in Figure 4.1. The addition of excess amounts of AlEt_3 to $\text{Co}(\text{acac})_{2,3}$ at large Al/Co ratios has been reported to result in the presence of detectable AlEt_3 in the resulting Ziegler-type catalyst solution [8]. The AlEt_3 has been suggested by Shmidt and coworkers as one of the main components of the stabilizer layer on the Ziegler-type nanoparticles catalyst as illustrated in Figure 4.1 [8,9]. In the same reports on Ziegler-type catalyst formed from $\text{Co}(\text{acac})_2 \cdot 1.8\text{H}_2\text{O}$ and AlEt_3 [8,9], Shmidt and coworkers suggest that *alkylalumoxanes* $-(\text{RAl-O})_n-$, acetylacetonate

derivatives of alkylaluminum oxanes ((acac)RAIOAIR(acac)), and their oligomers are formed in the presence of waters of crystallization of the precatalysts (see the Appendix C Section C1.1.2 for a short discussion and additional references on alumoxanes). However, definitive evidence for, much less compositional and structural information about, the proposed alumoxanes is lacking. In short, and as the state of knowledge depicted in Figure 4.1 makes apparent, *much remains to be learned about the precise nature of the stabilizer(s), and their bonding interactions with the surface of the nanoparticles, in Ziegler-type catalysts.* This “What is the nature of the stabilizer?” question takes on added significance given the high catalytic activity *and* exceptional thermal stability of Ziegler-type nanoparticles.

Hence, in the current study we strive to provide some additional insights into the question of “What is the nature of the AlEt₃-derived stabilizer species?” for Ziegler-nanoparticles, in the present case for the system formed from [Ir(1,5-COD)(μ-O₂C₈H₁₅)₂] plus AlEt₃. Specifically, we test herein three key hypotheses for the AlEt₃-derived stabilizer(s) in the Ir(0)_n Ziegler-nanoparticle system: (i) that the key stabilizer is neutral aluminum alkyl carboxylates following the Schmidt and Bönemann precedents noted above; (ii) that a key stabilizer is the free AlEt₃ that reacts with Ir(0)_n nanoparticle surface, perhaps via Ir_{surface}-Et or Ir_{surface}-H groups present there or possibly via formation of Ir-Et and Ir_nAlEt₂ species; or (iii) that the dominant AlEt₃-derived stabilizer is Al-O-Al containing alkylaluminum oxanes. While one does not expect to be able to write

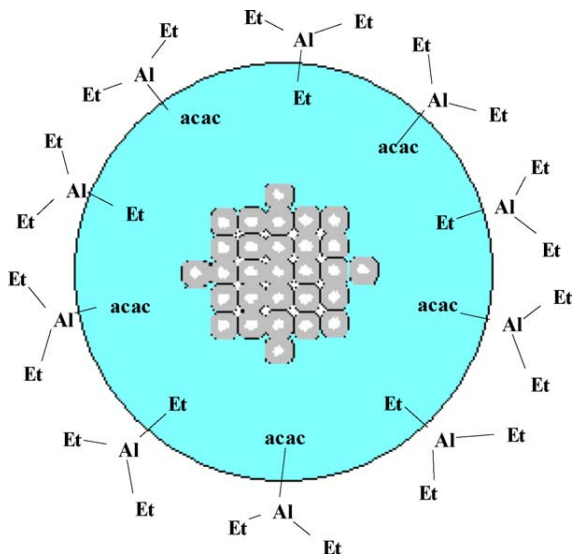


Figure 4.1. A depiction, proposed by Shmidt and coworkers [8], of $\text{Co}(0)_n$ nanoparticles stabilized by a layer of $\text{AlEt}_2(\text{acac})$ and AlEt_3 formed in the Ziegler-type catalyst system made with $\text{Co}(\text{acac})_{2-3}$ plus 2-8 equivalents AlEt_3 . Reprinted with permission.

a precise compositional, much less bonding, picture at this time for these complex nanoparticles (and since even the average, complete composition including all the stabilizers is known for only a handful of transition-metal nanoparticles [29]), the results presented herein do show that (i) $\text{AlEt}_2(\text{O}_2\text{C}_8\text{H}_{15})$ exists in Ziegler-type hydrogenation catalyst solutions made from $[\text{Ir}(1,5\text{-COD})(\mu\text{-O}_2\text{C}_8\text{H}_{15})]_2$ plus AlEt_3 in benzene- d_6 , and (ii) free AlEt_3 is present in the highly thermally stable and long lifetime catalyst solutions at higher Al/Ir ratios (≥ 3 equivalents Al per Ir). In addition, the spectroscopic and catalytic evidence (iii) helps to rule out presence of anionic $[\text{AlEt}_3(\text{O}_2\text{C}_8\text{H}_{15})]^-$, and (iv) shows that when H_2O is deliberately added, to form alkylaluminumoxanes or further hydrolysis products from the AlEt_3 present, a rate decrease is seen. Additionally, (iv) ethane, ethene and free and coordinated 1,5-COD are formed as detectable products upon mixing $[\text{Ir}(1,5\text{-COD})(\mu\text{-O}_2\text{C}_8\text{H}_{15})]_2$ with AlEt_3 .

2. Results and Discussion

The hypothesis that the AlEt₃-derived stabilizers are neutral aluminum alkyl carboxylates: The Ziegler-type catalyst sample made from [Ir(1,5-COD)(μ-O₂C₈H₁₅)₂] plus AlEt₃ at Al/Ir ratios of 1, 2 or 3 were analyzed using ¹H, ¹³C NMR and IR spectroscopies. A necessary change from the previous solvent of cyclohexane to d₆-benzene was used and controls were performed to ensure that the catalyst is still formed and active in benzene (i.e., and as opposed to the cyclohexane solvent otherwise used in these and our prior studies).¹ As detailed in the Experimental section, the Ziegler-type Ir(0)_n hydrogenation catalysts were prepared for NMR analysis from [Ir(1,5-COD)(μ-O₂C₈H₁₅)₂] and AlEt₃, by adding quickly (over 2 sec) a benzene-d₆ solution of AlEt₃ using a gas-tight syringe to a benzene-d₆ solution of [Ir(1,5-COD)(μ-O₂C₈H₁₅)₂] (Al/Ir=1, 2 or 3) at 30 °C under N₂. The initial orange color of the [Ir(1,5-COD)(μ-O₂C₈H₁₅)₂] solution turns to dark-brown immediately after addition of the d₆-benzene solution of AlEt₃, indicating the formation of Ir(0)_n nanoparticles.² The dark-brown catalyst solution was then vigorously shaken for 1 min and then transferred to NMR instrument while still septum-sealed and under N₂. The NMR acquisition was started ca. 1 h after bringing the NMR tube out of the drybox.

¹ As shown in Figure SI-C1 of the Appendix C, a control experiment testing the catalytic activity of [Ir(1,5-COD)(μ-O₂C₈H₁₅)₂] plus AlEt₃ in *benzene* solvent at the standard Al/Ir ratio of 2 reveals an active catalyst with a maximum cyclohexene hydrogenation rate of 5 mmol/h.

² The observation of an immediate color change, in *d₆-benzene solvent for an [Ir] of 25 mM*, from orange to dark-brown is different from the color change from orange to tawny-yellow we previously observed [5] for the [Ir(1,5-COD)(μ-O₂C₈H₁₅)₂] plus AlEt₃ catalyst system at Al/Ir ratios of 1-5 in *cyclohexane at an [Ir] of 0.6 mM*. Characterization in cyclohexane solvent using EXAFS, Z-Contrast STEM and MALDI MS on the tawny-yellow solution showed that the catalyst solution includes Ir₋₄₋₁₅ clusters at this stage. The tawny-yellow catalyst solution in cyclohexane solvent changes its color to dark-brown under cyclohexene hydrogenation conditions. The dark-brown solution contains Ir₋₄₀₋₁₅₀ as confirmed by EXAFS, Z-Contrast STEM and MALDI MS [4].

Since experience shows that simple stoichiometry can be invaluable in comparison to even a host of most powerful physical methods in nano-materials syntheses [18,19,20,21,22], we started our studies by writing a plausible reaction stoichiometry based primarily on the extant literature (Tables SI-C2 and SI-C3) [8,9,10,11,12,14]. That minimal, working stoichiometry of catalyst formation is shown in Scheme 4.1 for $[\text{Ir}(1,5\text{-COD})(\mu\text{-O}_2\text{C}_8\text{H}_{15})]_2$ plus AlEt_3 catalyst at an Al/Ir ratio of 1 (and a more speculative stoichiometry involving a possible $[\text{Ir}(1,5\text{-COD})\text{H}]_4$ intermediate is given in Scheme SI-C2 of the Appendix C).



Scheme 4.1. A proposed, minimal working stoichiometry of catalyst formation based on extant literature and consistent with our experimental data (vide infra) for the Ziegler-type hydrogenation catalyst made from $[\text{Ir}(1,5\text{-COD})(\mu\text{-O}_2\text{C}_8\text{H}_{15})]_2$ plus AlEt_3 at an Al/Ir ratio of 1.

The comparison of ^1H and ^{13}C NMR spectra of Ziegler-type catalyst solution at Al/Ir ratios of 1, 2 and 3 (Figures SI-C1 - SI-C6) to that of independently-synthesized $\text{AlEt}_2(\text{O}_2\text{C}_8\text{H}_{15})$ (Figures SI-C7, SI-C8) clearly shows that $\text{AlEt}_2(\text{O}_2\text{C}_8\text{H}_{15})$ is present in the catalyst solutions. More specifically, the ^1H NMR signals at 0.30, 0.80, 1.18, 1.39, 1.47, 1.57, 2.17 ppm and ^{13}C NMR signals at -0.25, 8.94, 14.33, 23.49, 26.80, 30.10, 32.52, 33.21 and 184.00 ppm in the catalyst solution at Al/Ir ratio of 1 are assigned to $\text{AlEt}_2(\text{O}_2\text{C}_8\text{H}_{15})$. Similar peaks are observed in ^1H and ^{13}C NMR spectra at Al/Ir ratios of 2 and 3 (Figures SI-C3-SI-C6) [23].³ The ^1H and ^{13}C NMR spectra show the presence of additional AlEt_3 -derived species as minor products at Al/Ir ratios of 2 and 3. Ethane, free and coordinated 1,5-COD are observed as additional products in

³ An additional piece of evidence supporting the above peak assignments is the assignment, in a previous publication, of ^1H NMR signals at 0.23, 0.86, 1.0-1.4, 1.30 and 2.03 ppm to $\text{AlEt}_2(\text{octanoate})$ (i.e., to the octanoate-analog of our present $\text{AlEt}_2(2\text{-ethylhexanoate})$) [23].

the NMR spectra upon mixing $[\text{Ir}(1,5\text{-COD})(\mu\text{-O}_2\text{C}_8\text{H}_{15})_2]$ and AlEt_3 at Al/Ir ratios of 1, 2 and 3, again in benzene- d_6 , (see Figures SI-C1-SI-C6 for detailed peak assignments). Our previous XANES study (carried out in cyclohexane) [4] shows that the Ir centers are in zero-valent state in the dark-brown $\text{Ir}_{\sim 40-150}$ nanoparticle solution, consistent with Scheme 4.1.¹

We envisage that the proposed reaction in Scheme 4.1. likely proceeds via an “Ir(1,5-COD)-Et” species (Scheme SI-C2). In order to provide further information on the formation of the putative “(1,5-COD)Ir-Et” species, we performed a control experiment with $[\text{Ir}(1,5\text{-COD})(\mu\text{-O}_2\text{C}_8\text{H}_{15})_2]$ precatalyst, but now *with* BEt_3 , since BEt_3 has a stronger B-Et bond than is present in AlEt_3 . In this experiment, the addition of d_6 -benzene solution of BEt_3 to originally orange-colored $[\text{Ir}(1,5\text{-COD})(\mu\text{-O}_2\text{C}_8\text{H}_{15})_2]$ solution *did not result in any reaction* as confirmed by ^1H NMR spectra (Figure SI-C9). Absence of a reaction between $[\text{Ir}(1,5\text{-COD})(\mu\text{-O}_2\text{C}_8\text{H}_{15})_2]$ and BEt_3 can be explained by the aforementioned, ~74% higher B-C bond dissociation energy (448 kJ/mol) vs that in Al-C (258 kJ/mol) [24,25,26,27,28]. The suggested formation of a “(1,5-COD)Ir-Et” species is consistent with the fact that AlEt_3 , but not BEt_3 , reacts with the $[\text{Ir}(1,5\text{-COD})(\mu\text{-O}_2\text{C}_8\text{H}_{15})_2]$ precatalyst. Also relevant here in a general sense is that AlR_3 compounds are known to be “R-“ donors to sufficiently strong Lewis acceptors, the crystallographically characterized $[\text{Me}_2\text{Al}(\text{OEt}_2)_2]^+[\text{MeB}(\text{C}_{12}\text{F}_9)_3]^-$ from the work of Klosin, Roof and Chen being a compelling case in point [28].

Returning to the AlEt_3 cocatalyst system, for catalyst solutions with Al/Ir ratios of 1, 2 and 3 the ^1H NMR spectra show very low intensity and sharp peaks between -6.3 and -17.8 ppm (see the insets of Figures SI-C2, SI-C4 and SI-C6). These peaks would appear to be hydride resonances, attributable to Ir-H groups of Ir clusters of presumably smaller, but rigorously

unknown size and nature [29,30,31,32,33].⁴ The narrow line widths of the experimentally observed peaks would seem to be inconsistent with their assignment to hydrides on the surface of larger Ir(0)_n nanoparticles [34,35].⁵ IR bands characteristic of carboxylate groups (Figure SI-C11) are observed at 1457 (strong) and 1560 (very weak) cm⁻¹ in cyclohexane solutions of Ziegler-type catalysts at Al/Ir ratios of 1, 2 and 3. Peaks characteristic of monodentate carboxylate groups (1570-1610 cm⁻¹ and 1640-1680 cm⁻¹) [36] are absent in the IR spectra of catalyst solutions in cyclohexane solvent at Al/Ir ratios of 1, 2 and 3. Consequently, the 2-ethylhexanoate group appears to be bidentate, bridging between two Ir, two Al, or Ir/Al metal centers.

An alternative hypothesis here is that *anionic* [AlEt₃(O₂C₈H₁₅)]⁻ is formed and provides stabilization of the type known as DLVO (Derjaugin, Landau, Verwey, and Overbeek)-type, bound-anion-based, Coulombic-repulsion stabilization [37]. However, the comparison of ¹H NMR spectrum of Ziegler-type catalyst made with [Ir(1,5-COD)(μ-O₂C₈H₁₅)₂] plus AlEt₃ in the

⁴ The relevant literature precedent here would seem to be the observation of *sharp hydride peaks* in the ¹H NMR spectrum of mononuclear (e.g., IrH₂LL', where L= P(C₆H₅)₃ and L'= CH₃COCHCOCH₃) [29], binuclear [30], and tetranuclear [31,32] transition-metal hydride complexes. In contrast, a *broad hydride peak* is reported for even the hexanuclear Rh cluster, [RhH₂(*i*-Pr)]₆²⁺ [33].

⁵ Hydrides on the surface of transition-metal nanoclusters are reported to exhibit broad ¹H NMR signals. In a study [34] of a [Pd₄phen(OAc)₂H₄]_n (n≈100) nanocluster (where phen is phenantroline and OAc is acetate), the broad peak observed between -20 and -60 ppm has been assigned to hydrides on the Pd_{~400} nanocluster's surface. Another study [35] reports that, for a 2-3 nm Ru nanoparticles stabilized by hexadecylamine system, "A direct detection of hydrogen bound to Ru failed, probably, because of line broadening due to slow tumbling of the nanoparticles in solution." Hence, the observation of low intensity single and sharp resonances in the metal-hydride chemical shift region at Al/Ir ratios of 1, 2, and 3 is tentatively interpreted as Ir-H resonances due to trace, low nuclearity species. Since our evidence indicates that Ir nanocluster, Ir_n-Et groups are formed that then should undergo facile β-H elimination, we presume that surface hydrides are also present on the Ir(0)_n nanoparticles, although direct evidence for their formation is lacking at present.

non-polar benzene-d₆ solvent (Figure SI-C2) to that of independently synthesized [(*n*-Bu)₄N][AlEt₃(O₂C₈H₁₅)] solution (Figure SI-C12) shows that anionic [AlEt₃(O₂C₈H₁₅)]⁻ does not exist in the catalyst solutions. Hence, the possibility of DLVO-type, [AlEt₃(O₂C₈H₁₅)]⁻ anion-based stabilization of the Ir(0)_{*n*} Ziegler nanoparticles can be ruled. This by itself is an interesting and important result, one which shows that the stabilization mechanism(s) of Ziegler nanoparticles is novel in that they appear to lack the DLVO, anion-based stabilization that is very common for transition-metal nanoparticles [19]. The high solubility of the Ziegler-type nanoparticles herein in non-polar solvents such as cyclohexane is another, simple but telling piece of evidence arguing against the presence of charged, anionic stabilizers in the present Ziegler-type nanoparticles.

The hypothesis that the AlEt₃-derived stabilizer is AlEt₃: The NMR spectra of the Ziegler-type catalyst sample at Al/Ir ratio of 3 in d₆-benzene (Figures SI-C6, SI-C7) includes ¹H NMR signals at 0.30, 1.11 ppm and ¹³C NMR signals at 1.00, 8.77 ppm that are assigned to free AlEt₃ (0.33, 1.11 ppm in ¹H NMR and 1.21, 9.44 ppm in ¹³C NMR, Figure SI-C13, SI-C14). As we have previously reported [6] excess AlEt₃ (Al/Ir ≥ 3) *slows down the hydrogenation rate* by, presumably, it or its derivatives binding close to or at the active site of the Ir(0)_{*n*} Ziegler nanoparticles. Furthermore, the NMR spectra (Figures SI-C6, SI-C7 and [6]), show presence of free AlEt₃ in long-lifetime (≥100,000 total turnovers of cyclohexene hydrogenation) and highly thermally stable (stable for ≥ 30 min at 200 °C) Ziegler-type catalyst solutions made with [Ir(1,5-COD)(μ-O₂C₈H₁₅)₂] and AlEt₃ at Al/Ir ratios of 3 and 5. In short, the presence of detectable AlEt₃, along with its hydrogenation-rate-inhibiting kinetic effect, would seem to provide incontrovertible evidence that AlEt₃, or its products with the Ir(0)_{*n*} nanoparticle surface, bind at or close to the catalytically active site. As such, the evidence seems *strong if not*

compelling that AlEt₃—and/or its possible reaction products with the Ir(0)_n nanoparticle surface, such as Ir_n-Et and IrAlEt₂—are important stabilizers of Ziegler-type nanoparticles.

The hypothesis that the AlEt₃-derived stabilizers are alumoxanes: The studies performed by Shmidt and coworkers [8,9] on Co(acac)_{2,3}•1.8H₂O plus AlEt₃ catalyst system reveals that alumoxanes [38,39,40,41,42,43,44,45,46,47,48] are formed in the catalyst solution under the conditions those workers employed. Importantly, for the Co(acac)_{2,3}•1.8H₂O plus AlEt₃ system Shmidt and coworkers report an *increased catalytic activity, and decreased stability*, in the presence of water (added as *n* waters of crystallization) for their Ziegler-type hydrogenation catalysts made from Co(acac)₂•*n*H₂O (*n*: 0 or 1.8) and AlEt₃ [8,9]. On the surface this would appear to be evidence that alumoxanes such as –[Al(Et)O]_{*n*}– are *not* the best stabilizer of Ziegler-type nanoparticles in comparison to the parent AlEt₃ Lewis acid co-catalyst. However, meriting mention here is that, in our hands (and analogous to the results reported below for the Ir(0)_{*n*} Ziegler-nanoparticle system herein, *vide infra*), we previously reported [5] that increasing the amount of initially added water in Ziegler-type hydrogenation catalyst made with Co(neodecanoate)₂ plus AlEt₃ *decreases* the cyclohexene hydrogenation activity. Open questions, then, regarding the Co system include: (i) if the Co(neodecanoate)₂ vs Shmidt's Co(acac)_{2,3}•1.8H₂O precursors are the source of the difference; (ii) if the different amounts, methods or timing of addition of the water in the two studies are the difference—a real possibility; or (iii) if some other, unknown variable or effect is present and the source of the ostensibly different results in the Co system.

Returning to the Ir system of the present studies, since a version of the somewhat hydrophobic [Ir(1,5-COD)(μ-O₂C₈H₁₅)₂] containing waters of crystallization is not known at present (as a arguably preferred way to selectively add H₂O and form alumoxanes), we strove to

provide at least initial evidence for or against the role of alumoxanes in at least the fastest catalyst formed from $[\text{Ir}(1,5\text{-COD})(\mu\text{-O}_2\text{C}_8\text{H}_{15})_2]$ plus AlEt_3 by the addition of controlled amounts of H_2O . Added water is known to form alumoxanes rapidly when mixed with AlEt_3 [38,39,40,41,42,43,44,45,46,47,48], although a caveat here is that too much water will yield hydrolysis past the $\text{-(RAl-O)}_n\text{-}$ alumoxane stage to even Al_2O_3 . The evidence available at present on the effects of added water and any role of alumoxanes and other AlEt_3 hydrolysis products is as follows: (i) the addition of 2-10 equivalents (per Ir) water, to the Ziegler-type catalyst made from $[\text{Ir}(1,5\text{-COD})(\mu\text{-O}_2\text{C}_8\text{H}_{15})_2]$ and AlEt_3 at Al/Ir ratios of 1 or 2, *decreases* the hydrogenation rate by ~2-10-fold (Figure SI-C15); (ii) the catalyst solution prepared in the presence of 2 equiv of water (per Ir) at an Al/Ir ratio of 1 appears dark-brown without visually observable particles—that is, is still stable with respect to the formation of bulk Ir(0) metal. Indeed, all of the catalyst solutions at an Al/Ir ratio of 2 prepared both without water, and in the presence of 4-10 equiv (per Ir) of water, appear dark-brown without visually observable particles—that is, appear stable; (iii) the formation of the expected Al-O-Al bond-containing products was confirmed by the observation of a broad band between $600\text{-}800\text{ cm}^{-1}$, although this weak band became clear only in the IR spectrum of the $[\text{Ir}(1,5\text{-COD})(\mu\text{-O}_2\text{C}_8\text{H}_{15})_2]$ plus AlEt_3 catalyst (Al/Ir ratio of 2) prepared with 10 equiv H_2O per Ir (which equals 5 equiv of H_2O per Al), Figure SI-C16 of the Appendix C, so that all this may really indicate is the formation of hydrolysis products beyond the $\text{-(RAl-O)}_n\text{-}$ alumoxane level. (iv) A control IR study of commercial modified-methylalumoxane did reveal a broad IR absorption band between $640\text{-}780\text{ cm}^{-1}$ (Figure SI-C17), but (v) the broad absorption between $600\text{-}800\text{ cm}^{-1}$ was not detectable in the IR spectrum (Figure SI-C16) of the $[\text{Ir}(1,5\text{-COD})(\mu\text{-O}_2\text{C}_8\text{H}_{15})_2]$ plus AlEt_3 catalyst prepared without deliberately added water. On the surface, these added water studies would seem to require that AlEt_3 plus

H₂O hydrolysis products do yield a stable, albeit deactivated, Ir(0)_n catalyst, although it seems likely that they may be telling us more about hydrolysis products closer to the final, Al₂O₃ stage of hydrolysis than the -(RAl-O)_n- alumoxane level of hydrolysis.

In order to probe the alumoxane hypothesis via a different approach employing discrete materials, we synthesized Barron's well-characterized, discrete alumoxane (really a "hydroxyl, dialkyl-alumoxane analog"⁶), [(*t*-Bu)₂Al(μ-OH)]₃ [67], and tested it with [Ir(1,5-COD)(μ-O₂C₈H₁₅)₂]. Interestingly, (iii) the maximum catalytic activity of the catalyst made with [Ir(1,5-COD)(μ-O₂C₈H₁₅)₂] plus fresh-made [(*t*-Bu)₂Al(μ-OH)]₃ (Al/Ir=2) is ca. 6-fold lower (max rate of ~1 psig/h, Figure SI-C20) than that made with [Ir(1,5-COD)(μ-O₂C₈H₁₅)₂] plus, now, the parent *t*-Butyl aluminum compound, Al(*t*-Bu)₃ (Al/Ir=2) (max rate of ~6 psig/h, Figure SI-C20, Table SI-C4). Perhaps more importantly, (iv) both catalyst solutions (i.e., that prepared with fresh-made [(*t*-Bu)₂Al(μ-OH)]₃ or with the parent Al(*t*-Bu)₃) appear dark-brown *without visually observable bulk Ir(0) particles* indicating that stable Ziegler nanoparticles did form from these novel precatalyst systems. TEM images (Figures SI-C21, SI-C23, SI-C24 and SI-C26) and MALDI MS spectra (Figure SI-C22 and SI-C25) of the catalysts made with [Ir(1,5-COD)(μ-O₂C₈H₁₅)₂] plus [(*t*-Bu)₂Al(μ-OH)]₃ or Al(*t*-Bu)₃ both before and after cyclohexene hydrogenation catalysis show that the size of the Ir(0)_n particles are the same (~1 nm pre-catalysis and ~2.5 nm post-catalysis) in both catalyst solutions, Figures SI-C21-SI-C26. These

⁶ Note that while even the title of Barron's paper refers to [(*t*-Bu)₂Al(μ-OH)]₃ as an "alumoxane", it does not have the mono-alkyl composition characteristic of common -(RAl-O)_n- alumoxanes. Hence, [(*t*-Bu)₂Al(μ-OH)]₃ is probably better referred to as a "hydroxyl, dialkyl-alumoxane analog" so as to avoid confusion. (We thank Prof. Eugene Chen at Colorado State University for a discussion of this point.) However, note also that this does not detract at all from the interest in using [(*t*-Bu)₂Al(μ-OH)]₃ along with [Ir(1,5-COD)(μ-O₂C₈H₁₅)₂] as catalyst precursors given: (a) the discrete nature of [(*t*-Bu)₂Al(μ-OH)]₃, plus (b) the fact that this "hydroxyl, dialkyl-alumoxane analog" contains a *t*-Bu- group for the reduction of the Ir(I) precatalyst as well as remaining *t*-Bu- group (i.e., enroute to the plausible -(*t*-BuAlO)- plus *t*-Bu• initial products one writes when considering plausible reaction stoichiometries here).

results provide the novel insight that Barron-type, discrete “hydroxyl, dialkyl-alumoxane analogs” can yield stable, reasonably active, ostensibly Ziegler-type Ir(0)_n nanoparticle catalysts.⁷ As such, the above experiments provide probably the best current evidence that alumoxanes, broadly construed, still merit serious consideration as stabilizers of Ziegler-type nanoparticles. For this reason, we have initiated a full, separate, detailed study of the “alumoxane stabilizers of Ziegler-nanoparticles” hypothesis and will report that needed, separate study in due course.

X-Ray Absorption Fine Structure (XAFS) Evidence for an Ir-Al Interaction, at least, In the Smaller Ir_n Subnanometer Clusters Formed Initially From [Ir(1,5-COD)(μ-O₂C₈H₁₅)]₂ plus AlEt₃: It is worth noting here that our recent XAFS studies [4] provided evidence for Ir-Al, possibly Ir-X-Al (X: H or Et), bonding at a distance from Ir of 2.49 (2) to 2.51(1) Å (Table SI-C5) [4], at least in the case of the Ir_n subnanometer clusters formed from just mixing [Ir(1,5-COD)(μ-O₂C₈H₁₅)]₂ with AlEt₃ at Al/Ir ratios between 1.5 and 5.0 and before cyclohexene hydrogenation. Importantly, these Ir-Al distances are within the range of literature crystallographically-characterized Ir-Al distances in [Cp*(PMe₃)IrH₂] \bullet AlPh₃ (2.684 (2) Å) [49] and [Cp*Ir(PMe₃)AlEt]₂ (between 2.456 (1) and 2.459 (1) Å) [50]. Unfortunately, the EXAFS of the larger, on-average, Ir(0)_{~150} was unable to detect such Al-Ir interactions due to the stronger component of Ir-Ir scatterers in the larger nanoparticles which obscures any Ir-Al that are

⁷ A control experiment was performed using MALDI MS with Barron’s well-characterized, discrete alumoxane, [(t-Bu)₂Al(μ-OH)]₃ [59] and the commonly used MALDI MS matrices, dithranol, 2’-4’-6’-trihydroxyacetophenone, 6-aza-2-thiothymine, and graphite. Perhaps not unexpectedly, the spectra (Figure SI-C18) did not show any peaks attributable to [(t-Bu)₂Al(μ-OH)]₃ or any of its plausible fragments, arguably due to reactions between these matrices and the [(t-Bu)₂Al(μ-OH)]₃. Similarly, the MALDI MS spectra of MMAO in 2’-6’-dihydroxyacetophenone or 2’-4’-6’-trihydroxyacetophenone matrices and using Na⁺ or Ag⁺ ionizing agents did not show any peaks that may be assigned to plausible fragments of MMAO. Hence and unfortunately, MALDI MS in at least the matrices tried is not a useful method to test for the presence of such discrete alumoxanes.

present. However, one surmises that such Ir-Al and/or Ir-X-Al contributions are very likely present in the larger Ir(0)_{~150} nanoparticles as well based on the EXAFS of the smaller particles and the other evidence provided in this paper showing that the presence of AlEt₃ influences both the nanoparticle rate and stability. One can also conclude that *Al XAFS* would be a useful, potentially valuable future study so that this, too, is under its own, separate full investigation.

A Pictorial, Working Hypothesis for the Stabilization of Ziegler-type Ir(0)_n Nanoparticles: Scheme 4. presents a minimalistic working hypothesis based on extant literature and experimental evidence (vide supra) for the stabilization of Ziegler-type catalysts made with [Ir(1,5-COD)(μ-O₂C₈H₁₅)₂] plus AlEt₃. The presence of AlEt₃, AlEt₂(O₂C₈H₁₅) and bidentate carboxylates are consistent with the NMR and IR data obtained in the current study (vide supra) [31].⁸ The bidentate carboxylates may be (i) bridging two Al centers, (ii) two Ir atoms, or (iii) one Ir_{surface} and one Al site. In addition, presence of (i) surface species such as (Ir_{surface})_x-Et plus (Ir_{surface})-Al(Et₂)Ir (where x=1-4), and (ii) surface AlEt₃, as well as -Et and -H bridging Ir_{surface} and AlEt_{2,3} centers, are consistent with the rate-decreasing kinetic effects of added AlEt₃ as well as the XAFS of at least the smaller, Ir_{~4} Ziegler nanoparticles. Hence, these structures are shown in Scheme 4.—which again, represents a working hypothesis.

Three primary lines of evidence suggests that the Al centers interact with the Ir sites on the surface of the Ir(0)_n Ziegler nanoparticle surface in Ir(1,5-COD)(μ-O₂C₈H₁₅)₂ plus AlEt₃ catalyst: (i) the XAFS precedent for the Ir_{~4} clusters plus AlEt₃ (Table SI-C5); and (ii) the observation that the cyclohexene hydrogenation activity of the Ziegler-type catalysts made with

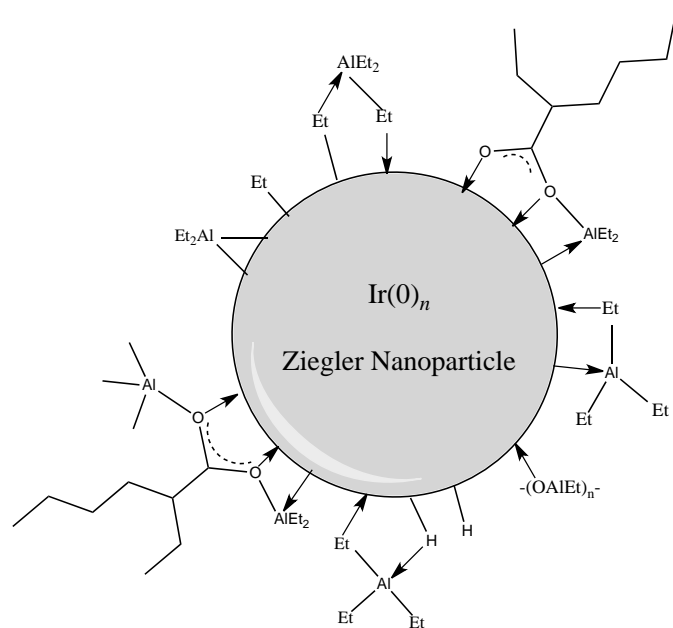
⁸ Interestingly, the solution prepared with the discrete Ir₄H₄ cluster, [(Ir(1,5-COD)(μ-H))₄], [31] as a precatalyst (Table SI-C6) plus premade AlEt₂(O₂C₈H₁₅) is clear and colorless with visually observable black particles at the end of a cyclohexene hydrogenation. This observation shows that AlEt₂(O₂C₈H₁₅) alone is not a sufficient stabilizer of at least any of its nanoparticle products made from [(Ir(1,5-COD)(μ-H))₄].

[Ir(1,5-COD)(μ -O₂C₈H₁₅)₂] and AlEt₃ decreases ~30-fold with increasing Al/Ir ratio of 1 to 5 (Table SI-C7) [4]. Note here that, as we have previously reported [4], the sizes of the Ir(0)_n both in pre- and post-hydrogenation solutions are the same regardless of Al/Ir ratio. Hence, a AlEt₃-derived component, and not a size change of the nanoparticles, has to be the main factor affecting the catalytic activity. Furthermore, (iii) ²⁷Al NMR spectra (Figure SI-C27) shows upfield shift from 170 ppm in neat AlEt₃ sample to 0 ppm at Al/Ir ratio of 1 and at 80 ppm at Al/Ir ratio of 2. These upfield shifts suggests interaction of Al centers with metallic Ir atoms on the surface of Ir(0)_n nanoparticles [51,52,53,54,55,56,57,58,59].^{9,10,11} One should note here that Scheme 4. is admittedly still rather speculative in its structural details. Hence, Scheme 4. *is provided primarily as a pictorial hypothesis for future studies.*

⁹ The upfield or downfield shift in NMR lines in the presence of metallic species is a common phenomenon in the literature. This type of shift is called “Knight Shift”. Sinfelt and coworkers define the Knight shift as “In bulk metals, the polarization of the magnetic moments of conduction electrons gives rise to a shift of the NMR lines called a Knight shift.” [52]. Some references on experimental and theoretical aspects of Knight shift are the following:[53,54,55,56,57,58,59].

¹⁰ Similar upfield Knight shifts (153 and 193 ppm) have been reported previously in ²⁷Al MAS NMR Cu_{0.33}Al_{0.67} and Cu_{0.50}Al_{0.50} alloys when compared to pure Al due to bonding to metallic Cu [53]. The ²⁷Al NMR Knight shift observed from 1639 ppm in aluminum powder to 1486 ppm in Cu_{0.33}Al_{0.67} (i.e., Al/Cu=2) and to 1446 ppm in Cu_{0.50}Al_{0.50} (i.e., Al/Cu=1) alloys [53]. One should note, however, that the ppm values in the present work are from solution NMR studies and not solid-state, magic angle spinning (MAS) NMR. Another example is the observation of 310 ppm downfield Knight shift in ¹³C NMR signal of CO chemisorbed on metallic Pd surface (i.e., Pd particles supported on η -alumina) when compared to metal carbonyl compounds [55]. The shift was attributed in the original publication to “mixing of the Pd conduction band with the CO molecular orbitals.” [55].

¹¹ Alternatively, the signals may be interpreted by considering the effect of coordination number on Al atoms. The signal observed at 0 ppm in ²⁷Al NMR spectrum of Ziegler-type catalyst sample made with [Ir(1,5-COD)(μ -O₂C₈H₁₅)₂] plus AlEt₃ at Al/Ir ratio of 1 (Figure SI-C21) may be due to hexacoordinate environment around Al (hexacoordinate region: -40–20 ppm [60]). The ²⁷Al NMR signals are observed in tetra-coordinate region (reported at 60-110 ppm and 140-180 ppm [60] for the catalyst samples with Al/Ir ratios of 2 and 3 (80 and 170 ppm, respectively, Figure S27).



Scheme 4.2. Working hypothesis representation of $\text{Ir}(0)_n$ Ziegler nanoparticle catalysts formed from $[\text{Ir}(1,5\text{-COD})(\mu\text{-O}_2\text{C}_8\text{H}_{15})_2]$ plus AlEt_3 . The figure has been constructed in the light of extant literature and the experimental results of the present study (*vide supra*). Not shown, but also possible, is an alumoxane component that contains the RCO_2^- carboxylato- moiety. As emphasized in the main text, this schematic is provided primarily as a pictorial working hypothesis to guide the needed future studies designed to further support, or refute, the stabilizers and surface ligands depicted.

Scheme 4. is consistent with, and rationalizes, the hydrocarbon solubility of the $\text{Ir}(0)_n$ Ziegler nanoparticles; *they are overall neutral, with neutral charge stabilizers*, with the lipophilic 2-ethylhexanoate of the $\text{C}_7\text{H}_{15}\text{CO}_2^-$ moiety providing hydrocarbon solubility—as well as steric stabilization [29]. Surface H-, Et-, AlEt_3 and $-\text{X-AlEt}_3$ ($\text{X}=\text{H}, \text{Et}$) components, possible $-(\text{EtAl-O})_n-$ alumoxane as well as possible Ir-bridging, $\text{Et}_2\text{Al-}$ surface species, would, then and in this working hypothesis, provide additional stabilization. As mentioned in the figure caption, not shown, but also possible, is an alumoxane component containing the RCO_2^- carboxylato- moiety, perhaps as a terminating group to an alumoxane chain. We emphasize that this scheme is intended as a proposed working hypothesis for future study about how Ziegler nanoparticles achieve their unusual combination of high stability, hydrocarbon solubility, plus high activity.

A qualitative, but telling, test of Scheme 4.2 is whether or not it can explain why Ir(0)_n Ziegler nanoparticles have the exceptional 200 °C, ≥30 minute stability in dodecane that is observed [6]. The surface ligands and species shown in Scheme 4.2 have the potential to explain the unusual thermal stability of Ziegler-type nanoparticles, perhaps especially the Ir-bridging Et₂Al, any chelating -(EtAl-O)_n- alumoxane present, the surface AlEt₃ and the AlEt₃ with H- or Et-bridging groups, plus all the steric stabilization [37] provided by all the bulky C₈H₁₅O₂- groups. That said, it is still by no means completely obvious why Ir(0)_n Ziegler nanoparticles made from [Ir(1,5-COD)(μ-O₂C₈H₁₅)]₂ and AlEt₃ in cyclohexane solvent have the thermal stability, yet high activity, that they do. Hence, additional tests and studies further testing and refining Scheme 4. are needed and can be anticipated, some of which are continuing in our own research group.

3. Summary and Conclusions.

The present study contributes to the area of Ziegler-type hydrogenation catalysts in that it (i) sheds some light on the intriguing but question of what is the nature of the stabilization, and (ii) provides evidence for the existence of AlEt₂(O₂C₈H₁₅) (Al/Ir=1, 2 and 3) and AlEt₃ (Al/Ir=3) in the catalyst solution in the currently best-understood model Ziegler-type hydrogenation catalyst system, namely that made from [Ir(1,5-COD)(μ-O₂C₈H₁₅)]₂ and AlEt₃ in cyclohexane and used without aging. In addition, the current spectroscopic results (iii) help to rule out the presence of anionic [AlEt₃(O₂C₈H₁₅)]⁻ stabilizer, in turn revealing that classic DLVO-type, Coulombic-repulsion stabilization [19] does *not* appear to be a major contributor to the high stability of these hydrocarbon soluble, high catalytic activity Ziegler-type nanoparticle catalysts. The evidence

provided also (iv) points towards the possibility of alkylaluminumoxanes stabilizers formed under conditions where, for example, 1 equiv of water per otherwise intact AlEt₃ is present. The spectroscopic and catalytic results also (v) show that depending on the initial Al/Ir ratio, additional AlEt₃-derived species, ethane, ethene, free and coordinated 1,5-COD are formed as minor products upon mixing [Ir(1,5-COD)(μ-O₂C₈H₁₅)]₂ and AlEt₃; and (vii) support the expected interaction between Ir(0)_n Ziegler-nanoparticles with Al-centers in the resultant AlEt₃-derived species. Furthermore, in the light of current experimental evidence, we (viii) have proposed a pictorial, working hypothesis for the stabilization of Ziegler-type Ir(0)_n nanoparticles, namely that shown back in Scheme 4.2. It is hoped that the results reported herein will stimulate further studies into the nature of the AlEt₃-derived stabilizer component in especially the industrial Co- and Ni-based Ziegler-type hydrogenation catalysts as a function of the Al/M (M: Co or Ni) ratios and as a function of the precise experimental conditions.

4. Experimental

Materials. All manipulations were performed under N₂ in a Vacuum Atmospheres drybox (≤5 ppm O₂ as monitored by a Vacuum Atmospheres O₂-level monitor) or using a Schlenk line under pre-purified, dried Ar. All glassware were dried overnight in an oven at 160 °C, then cooled under vacuum in the antechamber of the drybox. NMR sample tubes were rinsed with nanopure water and then dried for two days in an oven at 160 °C. They were then transferred into the antechamber of the drybox, cooled down under vacuum for 8 h and then stored in the drybox. Benzene-d₆ (Cambridge Isotope Laboratories, Inc., 99.5%, w/o TMS) was used as received. Benzene (Sigma-Aldrich, anhydrous, 99.8%) was used as received. Cyclohexane (Sigma-Aldrich, 99.5 %, H₂O < 0.001%) was dried over activated (vide infra) molecular sieves for 2

days prior to use. Modified methylalumoxane (MMAO-3A, 2.2 wt% Al in heptane) was purchased from Akzo Nobel. Heptane, (Anhydrous, Sigma-Aldrich, 99%) was degassed under Ar for 30 min before use. Molecular sieves (Acros, 3 Å) were activated by keeping at 200 °C for 8 hours under vacuum ($\leq 10^{-2}$ mmHg). AlEt₃ (Strem Chemicals, 93%, in 100 g steel cylinder) and BEt₃ (Strem Chemicals, 98%, in 100 g steel cylinder) were used as received. *See section 2.2 of the Supporting Information for a detailed discussion of procedures and cautions for handling pyrophoric AlEt₃, Al(*t*-Bu)₃, (*t*-Bu)Li and BEt₃.* The relatively volatile BEt₃ seemed to be the source of spurious reduction chemistry observed for other research samples stored in the drybox, in particular the apparent “autoreduction” of (1,5-COD)IrCl•Al₂O₃ used in a different research project. Hence, the BEt₃ was removed as soon as it was no longer in use (which, in turn, appeared to stop the spurious, otherwise unaccounted for, reduction of (1,5-COD)IrCl•Al₂O₃ stored in the drybox). Al(*t*-Bu)₃ was synthesized as detailed in the Supporting Information. Its purity was determined by ¹H NMR (δ in ppm (multiplicity): 1.10 (s)). Mineral oil (Heavy, Fisher Scientific) was dried under vacuum at 60 °C for 6 h before use. The NaCl windows for solid sample preparation for IR were purchased from Sigma Aldrich (32 mm, round) and used as received. Cyclohexene (Aldrich, 99%) was distilled over Na under N₂(g) and transferred into the drybox under air-free conditions. Hydrogen gas (General Air, 99.5%) was passed through an indicating moisture trap (Scott Specialty Gas), a disposable O₂ cartridge (Trigon), and an indicating O₂ trap (Trigon) before use in hydrogenations. [Ir(1,5-COD)(μ -O₂C₈H₁₅)]₂ was prepared by W. Morgan Alley in our labs following our previously published procedure [3] and its purity was confirmed by ¹H and ¹³C NMR spectra. Crystalline [Ir(1,5-COD)(μ -O₂C₈H₁₅)]₂ was used to prepare a 12.0 mM solution in cyclohexane or a 40.0 mM solution in benzene-d₆. Pentane (Sigma-Aldrich, anhydrous, 99+%, 1 L) was distilled over Na and stored in a 100 mL-round-

bottomed Schlenk flask in the drybox. AlCl_3 (Sigma-Aldrich, Reagent Plus, $\geq 99.9\%$, 1 kg) was sublimed at $\sim 130\text{ }^\circ\text{C}$ under Ar on a Schlenk line using a custom-made sublimation apparatus equipped with a side arm and containing a sublimation chamber for the crude AlCl_3 , plus a cold-finger (i.e., one equipped with a cold water inlet and outlet) to collect the sublimed AlCl_3 . The sublimation mixture was prepared using 40 g AlCl_3 , 4 g NaCl (Fisher, 3 kg) and 1 g Al powder (Al metal, Fisher, finest powder, 500 g) as detailed in the literature [60]. Pure AlCl_3 ($\sim 7\text{ g}$) was collected on the cold-finger after ~ 4.5 hours. A 1.7 M pentane solution of (*t*-Bu)Li (Aldrich, 100 mL brown glass bottle) was used as received. Celite (Sigma, diatomaceous earth, non-washed, $\sim 90\%$ SiO_2) was dried by heating to $200\text{ }^\circ\text{C}$ under vacuum for 8 h and cooled under vacuum. Ultrapure H_2O was prepared using a Barnstead Nanopure system.

Synthesis of $\text{AlEt}_2(\text{O}_2\text{C}_8\text{H}_{15})$: The synthesis was performed in the drybox under N_2 according to a procedure published for $\text{AlEt}_2(\text{acac})$ [61], but using a 6-fold lower concentration of the starting AlEt_3 and $\text{HO}_2\text{C}_8\text{H}_{15}$ solutions than that used in reference 55. A 36 mM solution of AlEt_3 (5 mL) in cyclohexane was transferred using a 5.0 mL gas-tight syringe into a 25 mL glass vial equipped with a $5/8 \times 5/16$ in. Teflon-coated magnetic stirbar. A 5 mL portion of a 36 mM $\text{HO}_2\text{C}_8\text{H}_{15}$ (2-ethylhexanoic acid) was added dropwise (in ~ 10 min) to a AlEt_3 solution in a 25 mL glass vial using a 5.0 mL gas-tight syringe, all while vigorously stirring. Upon removal of the volatiles from the solution under vacuum ($\leq 10^{-2}$ mmHg) at $30\text{ }^\circ\text{C}$ for 8 h, a clear and colorless gel-like liquid was obtained, yield: 0.020 g, 50%. ^1H NMR in benzene- d_6 (δ in ppm): 0.33, 0.80, 1.18, 1.28, 1.39, 1.51, 2.17. ^{13}C NMR in benzene- d_6 (δ in ppm): -1.21, 1.08, 8.90, 13.81, 22.66, 25.72, 29.84, 31.99, 50.21, 185.84.

Synthesis of Al(*t*-Bu)₃: The synthesis of Al(*t*-Bu)₃ was performed under Ar on a Schlenk line. The procedure was adapted from the procedure in a lab notebook provided courtesy of Professor A. R. Barron [62,63].¹² Freshly sublimed pure AlCl₃ (15 g) was transferred into a 500 mL round-bottomed Schlenk flask equipped with a side arm and a 5/8 × 5/16 in. Teflon-coated magnetic stir bar under N₂ in the drybox. The 500 mL round-bottomed flask was sealed under N₂ using two rubber septa, brought out of the drybox, and connected to Ar using a needle tip inserted through the rubber septum. The 500 mL round-bottomed Schlenk flask was then connected a bubbler through its side arm. A 120 mL portion of pentane was added using a cannula through the rubber septum to the 500 mL round-bottomed flask containing AlCl₃, all while vigorously stirring. A 250 mL dropping funnel equipped with a pressure-compensation tube and PTFE-plug was loaded with 200 mL (*t*-Bu)Li under N₂ in the drybox. The dropping funnel was sealed by closing the dropping valve below the liquid chamber and using a rubber septum to seal the glass joint at the top. The dropping funnel was brought out of the drybox while still under N₂ and connected to a flowing Ar stream using a needle tip inserted through the rubber septum. The dropping funnel was left under a flow of Ar for 5 min. The dropping funnel was connected under Ar to the 500 mL round-bottomed Schlenk flask containing AlCl₃ under Ar. The dropping valve of the dropping funnel was opened and (*t*-Bu)Li addition to the AlCl₃ suspension was started while the white suspension of AlCl₃ in pentane was vigorously stirred. The (*t*-Bu)Li addition continued for 4 h. CAUTION: AlCl₃ plus (*t*-Bu)Li yields an exothermic reaction. The (*t*-Bu)Li should be added dropwise while maintaining the solution at room temperature using an ice or cold-water bath as necessary. The resulting bluish-white suspension was stirred for 30 min

¹² The original procedure for synthesis of Al(*t*-Bu)₃ was published in an earlier article [57]. This original procedure by Lehmkuhl *et al.* was not useful, at least in our hands, since many necessary experimental details are not provided in the original publication.

under Ar. CAUTION: A continuous flow of Ar through the 500 mL round-bottomed Schlenk flask will result in evaporation of the pentane from the reaction flask due to its low boiling point (35 °C). Therefore, the valve connecting the 500 mL round-bottomed Schlenk flask to Ar line should be opened once every ~5 min for 2-3 sec and then closed immediately to avoid a continuous Ar flow. The bluish-white suspension in the 500-mL round-bottom Schlenk flask was then allowed to sit without stirring for 30 min to allow solid LiCl to precipitate. A reverse filtration (see Scheme SI-C3) [64]¹³ was then applied to separate the liquid portion containing the desired Al(*t*-Bu)₃ from the gray LiCl precipitate using the following technique. The top of a plastic pasteur pipette was cut and then the cut pipette was stuffed with cotton under air. One end of a cannula was then inserted into the cotton layer through the other end of that cut pipette (i.e., the end not stuffed with cotton, see Scheme SI-C3). The pasteur pipette with the stuffed cotton and the cannula attached was then inserted into the three-necked 500 mL round-bottomed flask containing Al(*t*-Bu)₃ under Ar flow (Scheme SI-C3). Separately, another 500 mL round-bottom Schlenk flask equipped with a side arm was sealed under Ar flow using two rubber septa. The free end of the cannula (i.e., the end not inserted through cut pipette) was inserted through the rubber septum of the Ar filled but otherwise empty 500 mL round-bottomed Schlenk flask. The pasteur pipette was dipped into the cloudy white suspension and then a slight vacuum ($\leq 10^{-2}$ mmHg) was applied through the side arm of the empty 500 mL round-bottomed flask. A clear solution was collected in the 500 mL round-bottomed flask. The 500 mL round-bottomed flask containing the Al(*t*-Bu)₃ solution in pentane was then evacuated, disconnected from the Schlenk line and brought inside the drybox while still under Ar. Next, in the drybox the volatiles were

¹³ Reverse filtration is defined in J. P. Cooke's original publication [58] as "a process of filtration in which the liquid to be filtered is drawn upwards instead of flowing downwards in the usual way."

removed under vacuum ($\leq 10^{-2}$ mmHg) in the drybox and the resultant clear solution was transferred into a 100 mL round-bottomed flask with an O-ring joint on top and equipped with a $5/8 \times 5/16$ in. Teflon-coated magnetic stir bar. While still in the drybox, the 100 mL round-bottomed flask equipped with an O-ring joint was connected using a T-shaped O-ring adapter (with two O-ring joints on sides and one valve on top) to a 50 mL round-bottomed flask equipped with an O-ring joint. The two round-bottomed flasks and the T-shaped O-ring adapter were sealed by closing the valve on top of the T-shaped adapter and brought out of the drybox. The two round-bottomed flasks and the T-shaped adapter were attached to a Schlenk line using the valve on the T-shaped adapter. The 100 mL round-bottomed flask with clear $\text{Al}(t\text{-Bu})_3$ solution while under N_2 was placed in an oil bath at $55\text{ }^\circ\text{C}$. The empty 50 mL round-bottom flask was placed in dry ice/acetone bath at $-78\text{ }^\circ\text{C}$. If condensation on the vacuum line occurred, a heat gun was used to slowly transfer the condensed liquid to 50 mL round-bottomed collection flask. At the end of ~ 3 h, 20 mL clear, colorless $\text{Al}(t\text{-Bu})_3$ was obtained ($\sim 80\%$ yield). Density: 0.978 g/mL . $^1\text{H NMR}$ in benzene- d_6 (δ in ppm, (multiplicity)): 1.10 ppm (s).

Synthesis of $[(t\text{-Bu})_2\text{Al}(\mu\text{-OH})]_3$: This synthesis was performed under Ar on a Schlenk line and, separately, under N_2 in a drybox according to the original published procedure [65], but at a smaller scale ($\sim 1/10$ of original procedure). Briefly, while still in the drybox, 1.59 mL of clear, colorless, liquid $\text{Al}(t\text{-Bu})_3$ liquid was transferred using a 2.50 mL gas-tight syringe into a 100 mL round-bottomed Schlenk flask equipped with a side-arm and a $5/8 \times 5/16$ in. Teflon-coated magnetic stir bar. The 100 mL round-bottomed Schlenk flask was then sealed using a rubber septum and brought out of the drybox while still under N_2 . The 100 mL round-bottomed Schlenk flask was then connected to a Schlenk line through its side arm. Another 100 mL round-

bottomed flask containing pentane distilled over Na was sealed using a rubber septum and brought out of the drybox. A 30 mL portion of pentane was transferred into the 100 mL round-bottomed Schlenk flask containing $\text{Al}(t\text{-Bu})_3$ via cannula through its rubber septum while stirring vigorously. The 100 mL round-bottomed Schlenk flask was placed into an acetone/dry ice bath at -78°C and was let sit for 30 min to reach desired -78°C . Ultrapure H_2O , $97 \pm 1 \mu\text{L}$, was injected in 1 second to $\text{Al}(t\text{-Bu})_3$ solution in 100 mL round-bottom Schlenk flask through the rubber septum using a 100 μL gas-tight syringe. The resulting clear, colorless solution was stirred for 1.5 h at -78°C using an acetone/dry ice bath and then for 2 h at 25°C . The solution was cooled for 8 h at -30°C . At the end of 8 h at -30°C , white crystals were observed in the clear, colorless solution. The white crystals were separated from the liquid portion by transferring the liquid into a different flask using a 1.0 mL gas-tight syringe. The volatiles were removed under vacuum ($\leq 10^{-2}$ mmHg). The white crystals (~ 0.25 g, $\sim 35\%$ yield) were stored at -30°C under N_2 . ^1H NMR (benzene- d_6) (δ in ppm, multiplicity, assignment): 1.10, s, C(CH $_3$) of $[(t\text{-Bu})_2\text{Al}(\mu\text{-OH})]_3$; 2.34, s, OH; 1.071, s, C(CH $_3$) of $\text{Al}(t\text{-Bu})_3$. ^{13}C NMR (benzene- d_6) (δ in ppm): 24.69, 31.08.

Synthesis of $[\text{Ir}(1,5\text{-COD})(\mu\text{-H})]_4$: The synthesis procedure for crystalline $[\text{Ir}(1,5\text{-COD})(\mu\text{-H})]_4$ has been reported in an earlier publication [31]. The identity and the purity of the product was confirmed by ^1H NMR in benzene- d_6 (δ in ppm, (multiplicity, number of H)): -2.89 (s, 1), 1.37 (m, 4), 2.09 (m, 4), 4.14 (m, 4) in line with the values given in earlier publication [31].

Sample Preparation and Instrumentation.

^1H , ^{13}C and ^{27}Al NMR: NMR samples of the Ziegler-type catalyst solution made from $[\text{Ir}(1,5\text{-COD})(\mu\text{-O}_2\text{C}_8\text{H}_{15})]_2$ and AlEt_3 with an Al/Ir ratio of 1.0 were prepared as follows: In the drybox, 50 μL AlEt_3 (340 μmol) was transferred from its stainless steel container using a 50 μL gas-tight syringe to a 2 dram glass vial containing 1.7 mL benzene- d_6 (200 mM AlEt_3 solution). In another 2 dram glass vial, a solution 40 mM in Ir was prepared by dissolving 35.5 mg (80 μmol Ir) of $[\text{Ir}(1,5\text{-COD})(\mu\text{-O}_2\text{C}_8\text{H}_{15})]_2$ in 2.0 mL benzene- d_6 . A 0.5 mL aliquot of 40 mM $[\text{Ir}(1,5\text{-COD})(\mu\text{-O}_2\text{C}_8\text{H}_{15})]_2$ solution was transferred into a NMR sample tube (outer diameter: 5 mm) using a 1.0 mL gas-tight syringe. Next, 0.2 mL of benzene- d_6 was transferred into the same NMR sample tube using a 1.0 mL gas-tight syringe. The NMR sample tube was then sealed by first inserting a precision-seal natural rubber septum (Sigma-Aldrich) through the top of the NMR tube and then folding its flexible sleeve over NMR tube. The AlEt_3 solution in benzene- d_6 (0.1 mL, Al/Ir=1.0) was then injected using a 0.500 mL gas-tight syringe into the septum-sealed NMR sample tube through its septum. The original orange color of the solution in the NMR sample tube (characteristic of $[\text{Ir}(1,5\text{-COD})(\mu\text{-O}_2\text{C}_8\text{H}_{15})]_2$) turned to dark-brown immediately after adding the AlEt_3 solution. The septum sealed NMR sample tube was shaken gently for five minutes and taken out of the dry box while still septum-sealed. ^1H and ^{13}C NMR spectra were taken on a Varian INOVA-400 spectrometer. ^{27}Al NMR spectra were taken on a Varian INOVA-300 spectrometer. Observed ^1H and ^{13}C NMR chemical shifts were referenced to benzene- d_6 solvent. The ^{27}Al NMR spectra were taken by using 14.0 μs 90° pulse-width, 0.06 s relaxation delay and a frequency of 78.221 MHz. The ^{27}Al NMR chemical shifts refer to the $[\text{Al}(\text{H}_2\text{O})_6]^{3+}$ ion in an external capillary containing 25 mM $\text{Al}(\text{NO}_3)_3$ in D_2O by the substitution method. MestReNova LITE-5.2 software was used for data processing.

NMR samples of the catalyst solution with a Al/Ir ratio of 2.0 were prepared following the same procedure as the one given above, but using 0.5 mL of a 40 mM $[\text{Ir}(1,5\text{-COD})(\mu\text{-O}_2\text{C}_8\text{H}_{15})]_2$ solution in benzene- d_6 , 0.2 mL of a 200 mM AlEt_3 solution in benzene- d_6 , and additional 0.1 mL benzene- d_6 to bring the total volume to 0.8 mL. For the preparation of the catalyst solution with Al/Ir ratio of 3.0, 0.5 mL 40 mM $[\text{Ir}(1,5\text{-COD})(\mu\text{-O}_2\text{C}_8\text{H}_{15})]_2$ solution in benzene- d_6 and 0.3 mL 200 mM AlEt_3 solution in benzene- d_6 were combined without any additional benzene- d_6 . An NMR sample of the AlEt_3 solution was prepared using 0.1 mL 200 mM AlEt_3 solution in benzene- d_6 plus 0.7 mL benzene- d_6 . The total volume of the NMR sample solution was 0.8 mL in each case.

IR: IR spectra were taken on a Nicolet Magna-760 FT/IR-Raman Spectrometer.

(i) Preparation of Solution Samples: The catalyst samples for IR analysis were prepared in the drybox using cyclohexane solutions of $[\text{Ir}(1,5\text{-COD})(\mu\text{-O}_2\text{C}_8\text{H}_{15})]_2$ (72.0 mM in Ir) and 36.0 mM AlEt_3 solution in cyclohexane. The $[\text{Ir}(1,5\text{-COD})(\mu\text{-O}_2\text{C}_8\text{H}_{15})]_2$ (72.0 mM in Ir) solution was prepared by first weighing 0.0319 g of solid $[\text{Ir}(1,5\text{-COD})(\mu\text{-O}_2\text{C}_8\text{H}_{15})]_2$ using a weighing boat and then transferring into a 10 mL volumetric flask containing ~5 mL cyclohexane. The resultant solution was diluted to the mark by adding cyclohexane. A stock solution of AlEt_3 in cyclohexane (36 mM AlEt_3) was prepared in the drybox by adding neat AlEt_3 (0.529 mL, 0.834 g/mL) using a 1.000 mL gas-tight syringe into 50 mL cyclohexane in a 100 mL volumetric flask. The resulting solution was diluted to 100 mL mark by adding cyclohexane. A 0.5 mL aliquot of 72.0 mM $[\text{Ir}(1,5\text{-COD})(\mu\text{-O}_2\text{C}_8\text{H}_{15})]_2$ solution was transferred using a 1.0 mL gas-tight syringe into a 4 dram glass vial containing a 5/16 \times 5/16 in. Teflon-coated magnetic stir-bar. Next, 36 mM AlEt_3 solution (0.1 mL, Al/Ir=1.0) was immediately added (in 1 sec) using a 0.5 mL gas-

tight syringe while vigorously stirring. The catalyst solution was then stirred for 30 min under N₂. The IR liquid cell with ZnSe windows was filled with the catalyst solution using a 1.0 mL gas-tight syringe in the drybox and sealed using TEFLON caps. Then, the IR liquid cell was put in a jar, taken out of the drybox while still sealed with TEFLON caps in a jar and carried to the IR facility (~5 min).

IR samples of the catalyst solutions with Al/Ir ratios of 2 and 3 were prepared following the same procedure as the one given above. For the catalyst sample solution with Al/Ir₃ ratio of 2, 0.5 mL of a 72.0 mM [Ir(1,5-COD)(μ-O₂C₈H₁₅)₂] solution and 0.2 mL of a 36 mM AlEt₃ solution were combined in a 4 dram glass vial. The catalyst sample solution with Al/Ir ratio of 3 was prepared by combining 0.5 mL of a 72.0 mM [Ir(1,5-COD)(μ-O₂C₈H₁₅)₂] solution and 0.3 mL of a 36 mM AlEt₃ solution in a 4 dram glass vial, again all in the drybox. IR sample of 360 mM modified methylalumoxane solution was prepared in the drybox by transferring 96 μL of original commercial modified methylalumoxane (MMAO-3A) using a 100 μL gas-tight syringe to 1.5 mL heptane in a 5 mL glass vial.

(ii) Preparation of Solid Samples: The solid catalyst sample at Al/Ir ratio of 2 and with 10 eq of deliberately added water was prepared in the drybox by first removing volatiles under vacuum at 30 °C. The resulting black powder was further dried under vacuum for 8 h. At the end of 8 h, the black powder was transferred on a mortar and ground using a pestle. Next, two drops of mineral oil were added to the fine catalyst powder to obtain a paste. The mineral oil plus black catalyst paste was then transferred onto a polished NaCl plate and the second NaCl plate was placed on top of the first plate with care to keep the paste sandwiched between the two NaCl plates while manually smearing the past into a thin film between the two NaCl plates. The assembled NaCl plates were then placed into a glass vial and sealed under N₂, and the glass vial

in turn place into a desiccator which was sealed, brought out of the drybox and transferred to the IR instrument. Next, the N₂ flow feature for the sample holder compartment of the IR was turned on. After ~5 min of N₂ flow through the sample holder compartment, the glass vial was transferred into the sample holder compartment which was now under a N₂ atmosphere. The sealed glass vial was then opened and the NaCl plate assembly placed onto a sample holder. The door of the compartment was immediately closed and IR spectrum accumulation was started. This procedure was designed to ensure as air- and oxygen-free transfer of catalyst sample to the IR instrument as possible.

TEM, MALDI MS and XAFS: The details of sample preparation and data collection procedures and the instrumentation have been published previously [4]. The Ir-Al bond distances determined by XAFS are reproduced for the interested reader in Table S5.

Hydrogenation Solution Preparation and Catalytic Cyclohexene Hydrogenations. Catalyst solutions, 1.44 mM in Ir, were individually prepared in a drybox. An example procedure follows for the preparation of catalyst solution with [Ir(1,5-COD)(μ-O₂C₈H₁₅)₂] and AlEt₃ with Al/Ir ratio of 1: A 2.1 mL portion of cyclohexane was transferred into a new 22 × 175 mm Pyrex borosilicate culture tube containing a new 5/8 × 5/16 in. Teflon-coated magnetic stirbar. Cyclohexane solution of [Ir(1,5-COD)(μ-O₂C₈H₁₅)₂] (0.3 mL, 12 mM in [Ir]) was transferred into the culture tube using a 1.0 mL gas-tight syringe forming an orange-red solution. The resultant solution was stirred for 1 min at 1.0 × 10³ rpm as measured by a Monarch Instruments Pocket-Tachometer. A AlEt₃ solution (0.1 mL, 36 mM)—CAUTION, PYROPHORIC MATERIAL!, *vide supra*, IN COMBINATION WITH FLAMMABLE SOLVENTS!—was then added quickly (within 2 sec) to the orange-red solution using a 0.5 mL

gas-tight syringe while vigorously stirring. The original orange-red color of the $[\text{Ir}(1,5\text{-COD})(\mu\text{-O}_2\text{C}_8\text{H}_{15})_2]$ solution changed to tawny yellow at the end of AlEt_3 addition. Cyclohexene (0.5 mL) was added using a 1.0 mL gas-tight syringe and the resulting hydrogenation solution (1.65 M in [cyclohexene] and 1.2 mM in [Ir]) was stirred for an additional 1 min.

The procedure and apparatus used for catalytic hydrogenations of cyclohexene have been described in detail elsewhere [66,67]. Briefly, a culture tube containing the hydrogenation solution was placed in a Fisher-Porter (F-P) bottle equipped with Swagelok quick connects, which was then sealed and brought out of the drybox. The F-P bottle was placed in a bath set at 22.0 ± 0.1 °C. Stirring was started at 1000 ± 10 rpm using a Fauske Super magnetic stirplate and the F-P bottle was connected to a pressurized H_2 line using TFE-sealed Swagelok quick-connects. The F-P bottle was purged 15 times with H_2 (1 purge/15 sec) that has passed through an indicating moisture trap (Scott Specialty Gas), a disposable O_2 cartridge (Trigon), and an indicating O_2 trap (Trigon). The pressure in the F-P bottle was then set to 40 psig, and then the data collection was initiated. Hydrogen pressure vs. time data was collected using a pressure transducer (Omega PX 624-100 GSV) interfaced via an Omega D1131 analog to digital converter to a PC running LabVIEW 7.0. Data was subsequently handled using MS Excel. The maximum hydrogenation rate of catalysts was calculated from each kinetic curve by a linear-least-squares fits to the data points in the highest activity (highest slope) region ($R^2 \geq 0.999$ for the reported data).

For hydrogenations with $[(1,5\text{-COD})\text{Ir}(\mu\text{-O}_2\text{C}_8\text{H}_{15})_2]$ plus AlEt_3 , Al/Ir=2, 3 or 5, orange-red $[\text{Ir}(1,5\text{-COD})(\mu\text{-O}_2\text{C}_8\text{H}_{15})_2]$ solution (0.3 mL, 12.0 mM) was combined with a total of 2.0 mL, 1.9 mL or 1.7 mL cyclohexane, respectively. Then, 0.2 mL, 0.3 mL or 0.5 mL, respectively, of 36 mM AlEt_3 solution was added using a 1.000 mL gas-tight syringe. The hydrogenation solution with only-precatalyst was prepared by mixing 0.3 mL of $[\text{Ir}(1,5\text{-COD})(\mu\text{-O}_2\text{C}_8\text{H}_{15})_2]$

solution (12 mM in [Ir]) with 2.2 mL cyclohexane without any AlEt₃. For hydrogenations with [Ir(1,5-COD)(μ-O₂C₈H₁₅)₂] plus Al(*t*-Bu)₃ or [(*t*-Bu)₂Al(μ-OH)]₃, 0.2 mL of 36 mM solutions of Al(*t*-Bu)₃ or [(*t*-Bu)₂Al(μ-OH)]₃ in cyclohexane were used. At the end of cyclohexene hydrogenation, the catalyst solutions prepared with 2, 3 or 5 equivalents of AlEt₃, or 2 equivalents of Al(*t*-Bu)₃ or [(*t*-Bu)₂Al(μ-OH)]₃, were still brown with no visually observable particles. The precatalyst-only solution and the catalyst solution at AlEt₃/Ir ratio of 1 appeared to be clear colorless with visually observable black bulk metal particles in the solution and on the stirbar. For hydrogenations in benzene solvent, a 1.60 mg crystalline [(1,5-COD)Ir(μ-O₂C₈H₁₅)₂] was dissolved in 2.3 mL benzene in a 20 mL glass vial. The resulting orange-red solution was transferred using a 2.5 mL gas-tight syringe into a new 22 × 175 mm Pyrex borosilicate culture tube containing a new 5/8 × 5/16 in. Teflon-coated magnetic stirbar. A 0.2 mL portion of 36 mM AlEt₃ in benzene (Al/Ir=2) was then added quickly (within 2 sec) to the orange-red solution using a 0.5 mL gas-tight syringe while vigorously stirring. The original orange-red color of the [Ir(1,5-COD)(μ-O₂C₈H₁₅)₂] solution changed to tawny yellow at the end of AlEt₃ addition. Cyclohexene (0.5 mL) was added using a 1.0 mL gas-tight syringe and the resulting hydrogenation solution (1.65 M in [cyclohexene] and 1.2 mM in [Ir]) was stirred for an additional 1 min. The hydrogenation was carried out using the procedure given above for cyclohexane solvent.

Hydrogenation Solution Preparation with Added H₂O: For hydrogenations performed with [Ir(1,5-COD)(μ-O₂C₈H₁₅)₂] plus AlEt₃ at Al/Ir ratio of 2 in the presence of 2, 4 or 10 equivalents H₂O (per Ir), the catalyst solutions were prepared in 20 mL batches with an [Ir] of 1.44 mM. First, 16.4 mL of cyclohexane was transferred into a 20 mL glass vial containing a 5/8 × 5/16 in. Teflon-coated magnetic stir bar. Next, 2.0 mL of a [Ir(1,5-COD)(μ-O₂C₈H₁₅)₂] solution in

cyclohexane (14.4 mM) was added. A 2.1, 3.2 or 5.2 μL portion of H_2O was added using a 10 μL gas-tight syringe to the catalyst solutions with $\text{H}_2\text{O}/\text{Ir}$ ratios of 2, 4 and 10, respectively. Stirring (1000 ± 200 rpm) was started, and then 1.6 mL of AlEt_3 solution in cyclohexane (36 mM) was added rapidly (over 2 seconds). The resulting catalyst solution was stirred for 5 min. A 2.5 mL portion of the catalyst solution was transferred using a 2.5 mL gas-tight syringe into a new 22×175 mm Pyrex borosilicate culture tube containing a new $5/8 \times 5/16$ in. Teflon-coated magnetic stirbar. Cyclohexene (0.5 mL) was added using a 1.0 mL gas-tight syringe and the resulting hydrogenation solution (1.65 M in [cyclohexene] and 1.2 mM in [Ir]) was stirred for an additional 1 min. All the catalyst solutions at $\text{H}_2\text{O}/\text{Ir}$ ratios of 2, 4 or 10 appeared dark brown without visually observable black particles both before and after cyclohexene hydrogenation.

Supporting Information-C. Literature tables and related discussion on (i) the nature of AlEt_3 -derived stabilizer of Ziegler-type hydrogenation catalysts, (ii) gaseous side products, and (iii) the stoichiometry of the catalyst formation reaction. Detailed experimental procedures and cautions for handling the pyrophoric AlEt_3 , $\text{Al}(\text{t-Bu})_3$ and $(\text{t-Bu})\text{Li}$. Experimental procedures for synthesis of $[(\text{t-Bu})_4\text{N}](\text{O}_2\text{C}_8\text{H}_{15})$ and $[(\text{t-Bu})_4\text{N}](\text{AlEt}_3\text{O}_2\text{C}_8\text{H}_{15})$. Detailed procedures for preparing catalyst solutions starting with the precatalyst $[\text{Ir}(1,5\text{-COD})(\mu\text{-H})_4]$ and AlEt_3 or $\text{AlEt}_2(\text{O}_2\text{C}_8\text{H}_{15})$. The ^1H , ^{13}C , ^{27}Al NMR and IR spectra for the Ziegler-type catalyst samples made with $[\text{Ir}(1,5\text{-COD})(\mu\text{-O}_2\text{C}_8\text{H}_{15})_2]$ plus AlEt_3 . A more detailed scheme leading to proposed, working stoichiometry of catalyst formation involving a possible $[\text{Ir}(1,5\text{-COD})\text{H}]_4$ intermediate. Cyclohexene hydrogenation curves with Ziegler-type $[\text{Ir}(1,5\text{-COD})(\mu\text{-O}_2\text{C}_8\text{H}_{15})_2]$ plus AlEt_3 plus H_2O catalysts. Control hydrogenations with $[\text{Ir}(1,5\text{-COD})(\mu\text{-O}_2\text{C}_8\text{H}_{15})_2]$ plus AlEt_3 or $\text{Al}(\text{t-Bu})_3$ or $[(\text{t-Bu})_2\text{Al}(\text{OH})]_3$ and precatalyst $[\text{Ir}(1,5\text{-COD})(\mu\text{-H})_4]$ and AlEt_3 catalysts as a function of the Al/Ir ratio. TEM images and MALDI MS spectra of $[\text{Ir}(1,5\text{-COD})(\mu\text{-O}_2\text{C}_8\text{H}_{15})_2]$ plus $[(\text{t-Bu})_2\text{Al}(\mu\text{-OH})]_3$ or $\text{Al}(\text{t-Bu})_3$ catalysts. Table of XAFS-determined Ir-Al distances of Ziegler-

type hydrogenation catalysts made from $[\text{Ir}(1,5\text{-COD})(\mu\text{-O}_2\text{C}_8\text{H}_{15})]_2$ plus AlEt_3 . A schematic representation of the reverse filtration technique. This material is available free of charge via the Internet at <http://pubs.acs.org>.

REFERENCES

- [1] W.M. Alley, I.K. Hamdemir, K.A. Johnson, R.G. Finke, *J. Mol. Catal. A: Chem.* 315 (2010) 1-27.
- [2] K.A. Johnson, *Polym. Prepr.* 41 (2000) 1525–1526.
- [3] W.M. Alley, C.W. Girard, S. Özkar, R.G. Finke, *Inorg. Chem.* 48 (2009) 1114-1121.
- [4] W.M. Alley, I.K. Hamdemir, Q. Wang, A. Frenkel, L. Li, J.C. Yang, L.D. Menard, R.G. Nuzzo, S. Özkar, K.A. Johnson, R.G. Finke, *Inorg. Chem.* 49 (2010) 8131-8147.
- [5] W.M. Alley, I.K. Hamdemir, Q. Wang, A. Frenkel, L. Li, J.C. Yang, L.D. Menard, R.G. Nuzzo, S. Özkar, K.-H. Yih, K.A. Johnson, R.G. Finke, *Langmuir* 27 (2011) 6279-6294.
- [6] I.K. Hamdemir, S. Özkar, K.-H. Yih, J.E. Mondloch, R.G. Finke, *ACS Catal.* 2 (2012) 632-641.
- [7] F.K. Schmidt, G.V. Ratovskii, T.V. Dmitrieva, I.N. Ivleva, Y.G. Borodko, *J. Organomet. Chem.* 256 (1983) 309-329.
- [8] F.K. Shmidt, L.O. Nindakova, B.A. Shainyan, V.V. Saraev, N.N. Chipanina, V.A. Umanetz, *J. Mol. Catal. A: Chem* 235 (2005) 161-172.
- [9] L.O. Nindakova, F.K. Shmidt, V.V. Saraev, B.A. Shainyan, N.N. Chipanina, V.A. Umanets, L.N. Belonogova, D.-S.D. Toryashinova, *Kinetics and Catalysis* 47 (2006) 54-63.
- [10] L.B. Belykh, T.V. Goremyka, N.I. Skripov, V.A. Umanets, F.K. Shmidt, *Kinet.Catalysis* 47 (2006) 367-374.
- [11] H. Bönemann, W. Brijoux, R. Brinkmann, U. Endruschat, W. Hofstadt, K. Angermund, *Revue Roumaine de Chimie* 44 (1999), 1003-1010.
- [12] K. Angermund, M. Bühl, E. Dinjus, U. Endruschat, F. Gassner, H.-G. Haubold, J. Hormes, G. Köhl, F.T. Mauschick, H. Modrow, R. Mörtel, R. Mynott, B. Tesche, T. Vad, N. Waldöfner, H. Bönemann, *Angew. Chem. Int. Ed.* 41 (2002) 4041-4044.
- [13] K. Angermund, M. Bühl, U. Endruschat, F.T. Mauschick, R. Mörtel, R. Mynott, B. Tesche, N. Waldöfner, H. Bönemann, G. Köhl, H. Modrow, J. Hormes, E. Dinjus, F. Gassner, H.-G. Haubold, T. Vad, M. Kaupp, *J. Phys. Chem. B.* 107 (2003) 7507-7515.
- [14] H. Bönemann, N. Waldöfner, H.-G. Haubold, T. Vad, *Chem. Mater.* 14 (2002) 1115-1120.
- [15] W.R. Kroll, W. Naegele, *J. Organomet. Chem.* 19 (1969) 439-443.
- [16] S. Pasykiewicz, K. Dowbor, *J. Organomet. Chem.* 78 (1974) 49-53.

- [17] S. Pasynkiewicz, A. Pietrzykowsky, K. Dowbor, *J. Organomet. Chem.* 78 (1974) 55-59.
- [18] E.E. Finney, R.G. Finke, *J. Coll. Interface Sci.* 317 (2008) 351-374.
- [19] L.S. Ott, R.G. Finke, *Coord. Chem. Rev.* 251(2007) 1075-1100.
- [20] R.G. Finke, S. Özkar, *Coord. Chem. Rev.* 248 (2004) 135-146.
- [21] J.A. Widegren, R.G. Finke, *J. Mol. Catal. A-Chem.* 198 (2003) 317-341.
- [22] J.A. Widegren, R.G. Finke, *J. Mol. Catal. A-Chem.* 191 (2003) 187-207.
- [23] A. Pietrzykowski, S. Pasynkiewicz, J. Poplawska, *Silicon, Germanium, Tin and Lead Compounds* 18 (1995) 651-660.
- [24] T.L. Cottrell, in: *The Strengths of Chemical Bonds*, 2nd ed., Butterworth, London, 1958; vol. 30, pp. 197-218.
- [25] S.W. Benson, *J. Chem. Educ.* 42 (1965) 502-510.
- [26] J.A. Kerr, *Chem. Rev.* 66 (1966) 465-480.
- [27] B. de B. Darwent, in: *National Standard Reference Data Series*, National Bureau of Standards, Washington, 1970; Vol. 31.
- [28] J. Klosin, G. R. Roof, E. Y.-X. Chen, *Organometallics* 19 (2000) 4684-4686.
- [29] A. Aràneo, *J. Inorg. Nucl. Chem.* 32 (1970) 2925-2931.
- [30] Y. Ruiz-Morales, G. Schreckenbach, T. Ziegler, *Organometallics* 15 (1996) 3920-3923.
- [31] K.-H. Yih, I.K. Hamdemir, J.E. Mondloch, E. Bayram, S. Özkar, R. Vasic, A.I. Frenkel, O. Anderson, R.G. Finke, *Inorg. Chem.* 51 (2012) 3186-3193.
- [32] M. Kulzick, R.T. Price, E.L. Muetterties, V. W. Day, *Organometallics* 1 (1982) 1256-1258.
- [33] M.J. Ingleson, M.F. Mahon, P.R. Raithby, A.S. Weller 126 (2004) 4784-4785.
- [34] M.N. Vargaftik, V.P. Zagorodnikov, I.P. Stolarov, I.I. Moiseev, D.I. Kochubey, V.A. Likholobov, A.L. Chivilin, K.I. Zamaraev, *J. Mol. Catal.* 53 (1989) 315-348.
- [35] T. Pery, K. Pelzer, G. Buntkowsky, K. Philippot, H.-H. Limbach, B. Chaudret, *ChemPhysChem* 6 (2005) 605-607.

- [36] C.E. Bethley, C.L. Aitken, C.J. Harlan, Y. Koide, S.G. Bott, A.R. Barron, *Organometallics* 16 (1997) 329-341.
- [37] L.S. Ott, R.G. Finke, *Coord. Chem. Rev.* 251 (2007) 1075-1100.
- [38] A.R. Barron, in: J. Scheirs, W. Kaminsky (Eds.), *Metallocene-based Polyolefins – Preparation, Properties and Technology*, John Wiley and Sons New York, 2000; Vol. 1, pp. 33-69.
- [39] J.N. Pedeutour, K. Radhakrishnan, H. Cramail, A. Deffieux, *Macromol. Rapid Commun.* 22 (2001) 1095-1123.
- [40] H. Sinn, *Macromol. Symp.* 97 (1995) 27-52.
- [41] S. Pasynkiewicz, *Polyhedron* 9 (1990) 429-453.
- [42] I. Tritto, C. Mealares, M.C. Sacchi, P. Locatelli, *Macromol. Chem. Phys.* 198 (1997) 3963-3977.
- [43] E. Zurek, T. Ziegler, *Prog. Polym. Sci.* 29 (2004) 107-148.
- [44] M.R. Mason, J.M. Smith, S.G. Bott, A.R. Barron, *J. Am. Chem. Soc.* 115 (1993) 4971-4984.
- [45] C.J. Harlan, M.R. Mason, A.R. Barron, *Organometallics* 13 (1994) 2957-2969.
- [46] Y. Koide, A.R. Barron, *Organometallics* 14 (1995) 4026-4029.
- [47] Y. Koide, S.G. Bott, A.R. Barron, *Organometallics* 15 (1996) 2213-2226.
- [48] P. Sobota, M.O. Mustafa, J. Utko, T. Lis, *J. Chem. Soc. Dalton Trans.* (1990) 1809-1820.
- [49] J.T. Golden, T.H. Peterson, P.L. Holland, R.G. Bergman, R.A. Andersen, *J. Am. Chem. Soc.* 120 (1998) 223-224.
- [50] K. Isobe, P.M. Bailey, P.M. Maitlis, *J. Chem. Soc. Dalton Trans.* (1981) 2003-2005.
- [51] J.-P. Ansermet, C.P. Slichter, J.H. Sinfelt, *Progress NMR Spectr.* 22 (1990) 401-421.
- [52] Y. Yafet, V. Jaccarino, *Phys. Rev.* 133 (1964) A1630-A1637.
- [53] P.-K. Wang, J.-P. Ansermet, C.P. Slichter, J.H. Sinfelt, *Phys. Rev. Lett.* 55 (1985) 2731-2734.
- [54] S.E. Shore, J.-P. Ansermet, C.P. Slichter, J.H. Sinfelt, *Phys. Rev. Lett.* 58 (1987) 953-956.

- [55] J.-P. Ansermet, P.-K. Wang, C.P. Slichter, J.H. Sinfelt, *Phys. Rev. B: Condensed Matt.* 37 (1988) 1417-1428.
- [56] W.D. Knight, *Phys. Rev.* 76 (1949) 1259-1260.
- [57] M. Cokoja, H. Parala, M.-K. Schroter, A. Birkner, M.W.E. van den Berg, W. Grunert, R.A. Fischer, *Chem. Mater.* 18 (2006) 1634-1642.
- [58] D.R. Torgeson, R.G. Barnes, *J. Chem. Phys.* 62 (1975) 3968-3973.
- [59] J.J. Delpu ech, Chapter 6, *NMR of Newly Accessible Nuclei*, P. Laslo, Ed., 1983, Academic, Press, Inc., New York, pp. 169.
- [60] R.C. Howie, D.W. MacMillan, *Inorg. Nucl. Chem. Lett.* 6 (1970) 399-401.
- [61] W.R. Kroll, W. Naegele, *J. Organomet. Chem.* 19 (1969) 439-443.
- [62] A.R. Barron, personal communication.
- [63] H. Lehmkuhl, O. Olbrysch, H. Nehl, *Liebigs. Ann. Chm.* 9 (1973) 708-714.
- [64] On the Process of Reverse Filtering and Its Application to Large Masses of Material. *Proceedings of the American Academy of Arts and Sciences*; Press of John Wilson and Son: Boston, 1877, Vol. 9, pp. 124-131.
- [65] M.R. Mason, J.M. Smith, S.G. Bott, A.R. Barron, *J. Am. Chem. Soc.* 115 (1993) 4971-4984.
- [66] M.A. Watzky, R. G. Finke, *J. Am. Chem. Soc.* 119 (1997) 10382-10400.
- [67] J.A. Widegren, J.D. Aiken III, S.  zkar, R.G. Finke, *Chem. Mater.* 13 (2001) 312-324.

SUPPORTING INFORMATION-C:

EXCEPTIONALLY THERMALLY STABLE, HYDROCARBON SOLUBLE ZIEGLER-TYPE

$\text{Ir}(0)_n$ NANOPARTICLE CATALYSTS MADE FROM $[\text{Ir}(1,5\text{-COD})(\mu\text{-O}_2\text{C}_8\text{H}_{15})]_2$ PLUS

AlEt_3 : TESTS OF KEY HYPOTHESES FOR THEIR UNUSUAL STABILIZATION

Contents.

C1. Review of the Extant Literature on Ziegler-type Hydrogenation Catalysts

C1.1. A summary of the Literature Relevant to the Nature of the AlEt_3 -derived Stabilizer of Ziegler-type Hydrogenation Catalysts

C1.1.1 The hypothesis that the AlEt_3 -derived stabilizers are neutral aluminum alkyl carboxylates

C1.1.2. The hypothesis that the AlEt_3 -derived stabilizers are alumoxanes

C1.2. Gaseous Side Products and Stoichiometry of the Catalyst Formation Reaction in Ziegler-type Hydrogenation Catalysts

C2. Additional Experimental Details and Procedures

C2.1. Materials

C2.2. Procedures and Cautions for Handling the Pyrophoric AlEt_3 , $\text{Al}(t\text{-Bu})_3$, $(t\text{-Bu})\text{Li}$ and BEt_3

C2.3. Synthesis of $[(t\text{-Bu})_4\text{N}](\text{O}_2\text{C}_8\text{H}_{15})$

C2.4. Synthesis of $[(t\text{-Bu})_4\text{N}](\text{AlEt}_3\text{O}_2\text{C}_8\text{H}_{15})$

C2.5. Hydrogenation Solution Preparation and Catalytic Cyclohexene Hydrogenations with $[\text{Ir}(1,5\text{-COD})(\mu\text{-H})]_4$ plus AlEt_3 or $\text{AlEt}_2(\text{O}_2\text{C}_8\text{H}_{15})$

C3. Experimental Data and Related Discussion

C4. Additional Control Experiments Performed with the Ziegler-type Catalyst Made from $[\text{Ir}(1,5\text{-COD})(\mu\text{-O}_2\text{C}_8\text{H}_{15})]_2$ or $[\text{Ir}(1,5\text{-COD})(\mu\text{-H})]_4$ plus AlEt_3 , $\text{Al}(t\text{-Bu})_3$ or $\text{AlEt}_2(\text{O}_2\text{C}_8\text{H}_{15})$

C1. Review of the Extant Literature on Ziegler-type Hydrogenation Catalysts

C1.1. A summary of the Literature Relevant to the Nature of the AlEt₃-derived Stabilizer of Ziegler-type Hydrogenation Catalysts

The question of “What is the nature of the stabilizer species?” in Ziegler-type hydrogenation catalysts is of significant interest for the reasons mentioned in the main text and discussed in a review [1]. A detailed and intended to be critical analysis of the extant literature on the nature of the AlEt₃-derived stabilizer species is provided in the following paragraphs for the interested reader.

C1.1.1. Aluminum Alkyl Carboxylates Hypothesis: Many studies (Table SI-C1) on Ziegler-type hydrogenation catalysts provide spectroscopic evidence that ligand exchange reaction occurs between M(acac)_n (acac: acetylacetonate) precatalysts and the cocatalyst, AlEt₃. The result of the ligand exchange reaction is an aluminum alkyl acetylacetonate complex. The composition of the resulting aluminum alkyl complex has been found to depend on Al/M ratio initially employed. At Al/M < n (where n is the formal oxidation state of the M), Al(acac)₃ is formed as the main AlEt₃-derived product in catalysts made from M(acac)_n (n=3 for M:Fe, n=2 for M:Ni and n=3 for M:Co) and AlEt₃ [2,3]. In these studies, IR bands at 1261, 1288, 490 and 425 cm⁻¹ are assigned to Al(acac)₃. Furthermore, similarity of UV-Visible spectrum of catalyst solutions to that of separately-synthesized Al(acac)₃ standard suggests the presence of Al(acac)₃ in the catalyst solutions. At Al/M equals n (n=3 for M:Fe, n=2 for M:Ni, n=3 for M:Co, n=3 for M:Cr and n=2 for M:Pd), the only observed reaction product is AlEt₂(acac) in catalyst solutions made from M(acac)_n and AlEt₃. The presence of AlEt₂(acac) is evident by the comparison of the UV-Vis spectrum of the catalyst solutions to that of an individually synthesized Et₂Al(acac)

standard [2]. In the presence of additional AlEt_3 (i.e., at $\text{Al/M} > n$), further reactions are proposed between $\text{R}_2\text{Al}(\text{acac})$ and AlR_3 , R: Et or Me [4,5,6,7,8,9,10,11,12]). These further reactions form additional products, ones denoted in the original publications as $\text{AlEt}_2(\text{acac}) \rightarrow \text{AlEt}_3$, $\text{AlEt}_2(\text{acac-Et})\text{-AlEt}_2$ and $\text{AlEt}_2(\text{Et-acac}(\text{AlEt}_2)\text{-Et})\text{-AlEt}_2$. An FTIR band at 1056 cm^{-1} was assigned to Al-O-C group of the structure $\text{AlEt}_2(\text{acac-Et})\text{-AlEt}_2$ [4]. However, unequivocal evidence for the composition or structure of $\text{AlEt}_2(\text{acac-Et})\text{-AlEt}_2$ or other $\text{AlEt}_2(\text{acac})$ -derived products is often lacking as Table S1 details [4,5,6,7,8,9,10,11,12] despite considerable effort from the authors.

Table SI-C1. Literature Table Detailing the Proposed AlEt₃-derived products in various Ziegler-type Hydrogenation Catalysts

Catalyst System	Proposed Nature of the AlEt ₃ -derived Species and Characterization Methods	Ref.
Ni(acac) ₂ + (0.5-15.0) eq AlEt ₃	AlEt ₂ (acac) and Al(acac) ₃ by UV-Visible	2
Co(acac) _{2,3} + (2-16) eq AlEt ₃	AlEt ₂ (acac) and Al(acac) ₃ are observed by UV-Visible and IR; AlEt ₂ (acac) exists as a dimer as suggested by cryoscopic measurements. Further reaction between AlEt ₂ (acac) and AlEt ₃ is also proposed with a product of Et ₂ Al-O-C(CH ₃)=CH-C(Et)(CH ₃)-O-AlEt ₂ . The FTIR peaks at 600-800 cm ⁻¹ are assigned to Al-O-Al bond of alumoxanes with a degree of oligomerization of 4 to 5.	4,5
Pd(acac) ₂ + n eq. AlEt ₃ , n=1-10	FTIR bands at 1587, 1525, 1284, 1183, 1104, 1047 and 1010 cm ⁻¹ are assigned to AlEt ₂ (acac). These bands are observed in a FTIR spectrum of separately synthesized AlEt ₂ (acac). The broad NMR signals at 1.45 and 0.40 ppm are assigned to Et ₂ Al-O-C(CH ₃)=CH-C(Et)(CH ₃)-O-AlEt ₂ .	6
Pt(acac) ₂ + 4 eq AlMe ₃ , Ni(acac) ₂ + 3 Al(<i>i</i> -Bu) ₃	AlR ₂ (acac) is suggested by IR band at 1600 cm ⁻¹ . Products of further reaction between AlMe ₃ and AlMe ₂ (acac), such as R ₂ AlOC(R) ₂ C(AIR ₂)C(R) ₂ OAlR ₂ are also proposed.	8,10
Co(acac) ₂ + (0.5-1.5) eq AlEt ₃	IR spectra of catalyst samples suggest the presence of Al(acac) ₃ (1533, 1289, 490 cm ⁻¹), AlEt ₂ (acac) (1450, 1295, 1227, 1160, 988, 951 and 905 cm ⁻¹).	13
Co(acac) ₃ + 1 AlMe ₃	Al(acac) ₃ is confirmed by elemental analysis of the solid obtained after removing solvent and obtaining the IR of the catalyst solution (1288, 1261, 490 and 425 cm ⁻¹). AlMe ₂ (acac) is also suggested, although evidence for it is not provided in the original publication.	12
Fe(acac) ₃ + 6 eq AlEt ₃	IR bands observed for AlEt ₂ (acac) and AlEt ₃ are observed in the catalyst solution. Peaks at 1289 and 472 cm ⁻¹ are assigned to Al(acac) ₃ .	14
Co(acac) _{2,3} + (2-16) eq AlEt ₃	The authors suggest that, at Al/Co ratios ≥8, the stabilizer layer consists mainly of AlEt ₃ . No evidence is provided, however.	4,5
Co(acac) _{2,3} + (2-16) eq AlEt ₃	Alkylalumoxanes (R ₂ Al-O-AIR ₂), acetylacetonate derivatives of alkylalumoxanes ((acac)RAIOAIR(acac)), and their oligomers are suggested as the AlEt ₃ -derived stabilizer species on the basis of the IR absorption band at 600-800 cm ⁻¹ (Al-O-Al bond) and the similarity of elemental analysis results to that of oligomeric alumoxanes.	4,5

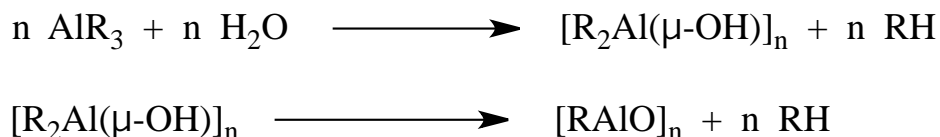
C1.1.2. Alumoxanes and Their Derivatives: A Short Review on the Relevant Alumoxane Literature

The term “alumoxane” is used to describe a molecular species containing at least one oxo group (O^{2-}) bridging (at least) two aluminum atoms, that is, a compound or compounds containing an Al-O-Al subunit [15]. More specifically, a formula of $[(P)Al(O)]_n$ is often used in the literature to denote alumoxanes, where P is the pendant group bonded to aluminum atom and n is the number of repeating units. Alkylalumoxanes, in which the pendant group is an alkyl, $[(R)Al(O)]_n$, are the alumoxanes most commonly employed in the literature. The combination of alumoxanes with metallocenes result in highly active, well-known catalysts used industrially for the polymerization of ethylene and propylene [16,17].

Alumoxanes are synthesized by the reaction of trialkylaluminum compounds (AlR_3) with H_2O (Scheme SI-C1) or species containing reactive oxygen such as CO_2 , PbO , or R_4B_2O (where R is $-Et$ or 1,5-cyclooctadienyl) [18]. Alumoxanes easily undergo: (i) association reactions, yielding di-, tri-, tetra- and oligoalumoxanes [19]; (ii) dissociation reactions, in the presence of strong donors such as 1,4-dioxane or tetrahydrofuran [20,21]; or (iii) disproportionation reactions, in the presence of, for example, excess $AlMe_3$ [22,23] or at high temperatures [24,25]. The highly reactive and complex nature of (mixtures) of alumoxanes has resulted in inconsiderable difficulty historically in attempts to purify, isolate or characterize alumoxanes. Alumoxanes, specifically methylalumoxane, has been called a “black box” [15] due to long-lasting lack of understanding of its precise structure(s) and composition(s).

Barron and coworkers, however, have recently achieved successful isolation and crystallographic characterization of various discrete t-butylalumoxanes [15,26], so that these

molecular complexes (in some cases better described as “hydroxy-alumoxanes”; see the discussion of this point in the main text) were exploited as part of the present work.



Scheme SI-C1. Stoichiometry for the formation of, first, $[\text{RAl}(\mu\text{-OH})]_n$ and then $[\text{RAlO}]_n$ oligomeric alumoxanes starting from AlR_3 and H_2O .

The trimeric *t*-butylalumoxane, $[(t\text{-Bu})_2\text{Al}(\mu\text{-OH})]_3$ (or, again, perhaps better denoted “hydroxy-alumoxane”) was first synthesized by Barron and coworkers [25] via the temperature-controlled reaction of $\text{Al}(t\text{-Bu})_3$ with H_2O . In that study, the crystal structure of $[(t\text{-Bu})_2\text{Al}(\mu\text{-OH})]_3$ was determined by X-ray crystallography [25]. Further characterization was performed with ^{13}C (31.14 ppm), ^1H NMR (2.02 and 1.10 ppm) and IR (3584, 1362, 1043, 998, 936, 815, 635, 506 cm^{-1}) spectroscopies as detailed in the original publication [25].

C1.2. Gaseous Side Products and Stoichiometry of the Catalyst Formation Reaction in Ziegler-type Hydrogenation Catalysts

Mixing transition-metal precatalysts and AlR_3 cocatalyst en route to Ziegler-type hydrogenation catalysts results in production of gaseous products in addition to the M_n nanoparticle. The alkyl group of the cocatalyst (R) determines the nature of the gaseous side products. The major gaseous products obtained are ethane, methane or *i*-butane when R is Et, Me or *i*-Bu, respectively (Table SI-C2) [4,13,22]. The amount of ethane formed is reported to be in the range of 58.0-98.7% of the 1.0 equivalent (100%) expected stoichiometrically for the reaction between AlEt_3 and a Ziegler-type precatalyst such as $\text{Co}(\text{acac})_2$ [4,13], $\text{Co}(\text{acac})_3$ [27], $\text{Fe}(\text{acac})_3$ [28] or metalhalides (MX_n) such as CoCl_2 , CoBr_2 , CuCl , CuCl_2 , NiCl_2 , FeCl_3 or AgCl [29] in non-polar toluene, benzene or cyclohexane solvents. In these catalyst solutions ethylene

is produced at lower amounts (0.3-42.0%) [4,6,13,27,28].¹ The ratio of ethane to ethylene depends on: (i) the initial Al/M ratio [4,13,27,29], (ii) the solvent used [29] and (iii), specifically for MX_a , the anion (X) of the MX_a precatalyst [29]. In most of the Ziegler-type hydrogenation catalyst systems the ethane to ethylene ratio is larger than 1. In addition to ethylene, butane and butylenes gases are detected in minor amounts (0-2.4%) in some Ziegler-type hydrogenation catalyst systems starting with AlEt_3 cocatalyst [4,6,27,29].

A complete and stoichiometrically balanced chemical reaction for formation of any Ziegler-type nanoparticle catalysts is not yet available. Obtaining one will requires the use of a precise composition precatalyst plus detailed knowledge of the nature and composition of the resulting transition metal component, the AlEt_3 -derived stabilizer species and all other products. In the extant literature of Ziegler-type hydrogenation catalysts, many attempted formation stoichiometries contain incompletely characterized and, therefore, vague compounds (e.g., the “ $\text{Me-Al}(\text{acac})\text{-CH}_2$ –“ in entry 1,

Table SI-C3). In many cases, numerous products are proposed without definitive evidence (e.g., $\text{Et}_2\text{AlCH}_2\text{CH}_2\text{AlEt}_2$ or $\text{AlEt}_2(\text{acac})\cdot\text{AlEt}_3$ as in entry 2,

Table SI-C3). In addition, ambiguity still remains currently on the nature and the stoichiometry of the gaseous products formed for many Ziegler-type catalyst systems. For example, Bönnemann’s early studies completely exclude gaseous products from their suggested stoichiometry (entry 5,

Table SI-C3), although this seems unlikely. Some studies include radicals, putatively formed during some intermediate step(s), in their suggested overall reaction stoichiometry (entries 3, 4, 8,

¹ (a) An important point worth mentioning here is that the nature of the major and minor gaseous products is also strongly affected by the solvent used. Ethane is the major gaseous product when the catalyst is formed in most common Ziegler-type catalyst solvents such as benzene, toluene or cyclohexane (vide supra). One study, however, reports that ethylene is formed at higher amounts (52.0-77.5 %) in less commonly used catalyst systems prepared from CoCl_2 precatalyst plus AlEt_3 in the less common solvents 1-hexene, 1-octene, 1-decene or α -methylstyrene [29]. (b) One exception is that ethane is reported [6] in toluene solvent when starting with $\text{Pd}(\text{acac})_2$ plus AlEt_3 . The gaseous products in the $\text{Pd}(\text{acac})_2$ plus AlEt_3 catalyst contain equimolar amounts of ethane and ethylene as evident by ^1H NMR and gas-liquid chromatography data [6].

Table SI-C3). Early studies by Pasynkiewicz and colleagues provide stoichiometrically unbalanced reactions, probably due to lack of information on the AlEt₃-derived and other gaseous products. *In short, the extant literature on Ziegler-type hydrogenation catalysts—including the present study—lack a complete, and stoichiometrically balanced chemical reaction including definitive information on the nature and composition of transition metal, AlEt₃-derived component and other gaseous reaction products.* Hence, an important goal of future work is to achieve a completely balanced stoichiometry for a well-defined system, for example for the precise composition [Ir(1,5-COD)(μ-O₂C₈H₁₅)]₂ precatalyst plus AlEt₃ Ziegler nanoparticle system. Scheme SI-C2 which follows details a working hypothesis for that stoichiometry, one intended solely as a guide to assist the needed, additional studies.

Table SI-C2. Literature Table Summarizing the Gaseous Products of the Reaction between Precatalyst and Cocatalysts en route to Ziegler-type Hydrogenation Catalysts

Catalyst System	Side Products of the Reaction between precatalyst and cocatalyst	Ref.
Co(acac) _{2,3} + (2-16) eq AlEt ₃	<p>Ethane (76%), ethylene (22.3%), butane (1.1%) and isomeric butenes (0.6%) are formed in Al/Co = 4 catalyst solution. An Al/Co ratio of 4 is the most active catalyst.</p> <p>More than 2 mols of gaseous products per 1 mol of Co are observed. The authors state, therefore, that the reaction between the components is NOT a "...simple reduction of Co(+2) to Co(0)..."</p> <p>The amount and ratios of gases formed depends strongly on the Al/Co ratio.</p>	4,5
Pd(acac) ₂ + n eq. AlEt ₃ , n=1-10	Ethane and ethylene , in equimolar amounts, are observed by NMR and GLC	6
Pt(acac) ₂ + 4 eq AlMe ₃	Methane (>90%), ethylene and ethane are observed.	7,10
Co(acac) ₂ + (0.5-1.5) eq AlEt ₃	<p>Ethane (>96%) is the main product as analyzed by GC. Other side products mentioned in the study are: ethylene, methane and higher hydrocarbons (C₃-C₅).</p> <p>The ethylene produced in the medium is believed to coordinate to the Co atoms.</p> <p>The ratio of the gaseous products depends on the Al/M ratio.</p>	13
Co(acac) ₃ + 1 AlMe ₃	<p>Mixtures of methane (72%), ethane (26%) and ethylene (2%) are formed by mass spectrometry.</p> <p>The ratio of the gaseous products depends on the Al/Co ratio.</p>	3

Table SI-C3. Literature Table of the Proposed Stoichiometries of Catalyst Formation in Ziegler-type Hydrogenation Catalyst Systems

Entry	Catalyst System	Proposed Stoichiometry (as given in the original publication)	Notes	Ref
1	Ni(acac) ₂ + 2 AlMe ₃	Ni(acac) ₂ + 2 AlMe ₃ → Ni + [0.25 C ₂ H ₆ + 0.5 AlMe ₂ (acac)] + [1.5 CH ₄ + 1.5 Me-Al(acac)-CH ₂ -]	(None)	28
2	Co(acac) _{2,3} + (2-16) eq AlEt ₃	4 Co(acac) ₂ + 16 AlEt ₃ + C ₇ H ₈ → 4 Co(0) + 3 AlEt ₂ (acac) + 5 AlEt ₂ (acac)•AlEt ₃ + AlEt ₂ C ₇ H ₇ + Et ₂ AlCH ₂ CH ₂ AlEt ₂ + 6 C ₂ H ₆ + 4 C ₂ H ₄	C ₇ H ₈ : Toluene solvent “...the whole process cannot be described by a unified, stoichiometrically balanced reaction.” The net reaction “...does not come to simple reduction of Co(II) to Co(0).”	4
3	Co(acac) ₂ + 2 AlEt ₃	The authors mention that “...the reaction cannot be brought to the reduction of Co ²⁺ to Co(0) in accordance with the (following) equation...” Co(acac) ₂ + 2 AlEt ₃ → Co(0) + 2 AlEt ₂ (acac) + C ₂ H ₆ + C ₂ H ₄ •	“...the (catalyst formation) process occurred without radical escape into the bulk.” It is not clear what “C ₂ H ₄ •” is.	5
4	Pd(acac) ₂ + (<i>I-10</i>) eq. AlEt ₃	Pd(acac) ₂ + 2 AlEt ₃ → Pd(0) + 2 AlEt ₂ (acac) + C ₂ H ₄ + C ₂ H ₆ •	It is not clear what “C ₂ H ₆ •” is.	6
5	Ni(acac) ₂ + 4 Al(<i>i</i> -Bu) ₃ and Pt(acac) ₂ + 4 AlMe ₃	Ni(acac) ₂ + 4 Al(<i>i</i> -Bu) ₃ → Ni _{coll} + Al(<i>i</i> -Bu) ₂ (acac) Pt(acac) ₂ + 4 AlMe ₃ → Pt _{coll} + AlMe ₂ (acac)	The reactions provided are not balanced.	7
6	Pt(acac) ₂ + 4 eq AlMe ₃	2 Pt(acac) ₂ + 6 AlMe ₃ → [Me ₄ PtAl(Me)] ₂ + 4 AlMe ₂ (acac)	The reaction provided yields the formation of [Me ₄ PtAl(Me)] ₂ , not a Pt(0) _n nanoparticle.	8
7	Co(acac) ₃ + 1 AlMe ₃	3 Co(acac) ₃ + 3 AlMe ₃ → 3 Co(0) + 3 Al(acac) ₃ + [CH ₄ + C ₂ H ₆ + C ₂ H ₄]	The reaction provided is not balanced. “...reaction proceeds by more than one route.”	3
8	Co(acac) ₃ + 0.5-2.5 AlEt ₃	Co(acac) ₃ + AlEt ₃ → Co(acac) ₂ + AlEt ₂ (acac) + •Et 2 Co(acac) ₃ + AlEt ₂ (acac) → 2 Co(acac) ₂ + Al(acac) ₃ + 2 •Et Co(acac) ₂ + AlEt ₂ (acac) → Al(acac) ₃ + Co(0) + 2 •Et	The overall stoichiometry is not given in the original publication.	27
9	Fe(acac) ₃ + 6 eq AlEt ₃	Fe(acac) ₃ + AlEt ₃ → Fe(acac) ₂ Et + Al(acac)Et ₂ Fe(acac) ₂ Et → 2Fe(acac) ₂ + H ₂ + 2 C ₂ H ₄ [or + C ₂ H ₆ + C ₂ H ₄]	“...the reaction of Fe(acac) ₃ with AlEt ₃ is limited to a one-electron reduction process.”	14

C2. Additional Experimental Details

C2.1. Materials. All manipulations were performed under Ar using a Schlenk line or under N₂ in a Vacuum Atmospheres drybox (≤ 5 ppm O₂ as monitored by a Vacuum Atmospheres O₂-level monitor). All glassware was dried before they were used in an oven at 160 °C, for 5 days, cooled down to room temperature under vacuum or Ar flow on a Schlenk line or in the antechamber of the drybox. Precatalyst [Ir(1,5-COD)(μ -Cl)]₂ (an orange powder, Strem Chemicals, 99%), LiBEt₃H [as a colorless solution in 1.0 M tetrahydrofuran (THF), Aldrich], 1,5-COD (Aldrich, 99%), toluene (Aldrich, 99.8%, anhydrous), and benzene-d₆ (Cambridge Isotope Laboratories, Inc., 99.5%, w/o tetramethylsilane (TMS)) were used as received. THF (Mallinckrodt Chemicals AR ACS, 500 mL) and *n*-hexane (Sigma-Aldrich, Reagent Plus, 99%, 500 mL) were distilled over sodium/benzophenone under N₂(g) and transferred into the drybox under air-free conditions. Acetone (Burdick and Jackson, >99.9% purity, 0.44% water) and H₂O (Nanopure ultrapure H₂O system, D4754) were degassed by connecting to a Schlenk line and then passing Ar for 5 min through the solution. The [(*t*-Bu)₄N]OH (Acros Organics, 1 M solution in methanol) and 2-ethylhexanoic acid (Aldrich, 99+%) and AlEt₃ (Strem Chemicals, 93%, in 100 g steel cylinder) were used as received.

C2.2. Procedures and Cautions for Handling the Pyrophoric AlEt₃, Al(*t*-Bu)₃, (*t*-Bu)Li and BEt₃: *CAUTION:* AlEt₃, Al(*t*-Bu)₃, (*t*-Bu)Li and BEt₃ are pyrophoric reagents which ignite spontaneously when in contact with air or water. They, as with all pyrophoric reagents, are more dangerous when flammable solvents are present (e.g., the cyclohexane used herein). Combination of pyrophoric reagents and flammable solvents are of course even more dangerous the larger the amounts being employed. Therefore, the amounts used were minimized where

possible and air-free Schlenk [30] and drybox techniques were used in all steps requiring these pyrophoric reagents.

The required safety considerations were carefully designed and followed in Finke Lab [31]², including: (i) first reading the MSDS safety sheet, if available; (ii) working with the minimal amounts of pyrophoric and flammable reagents possible; and (iii) using the pyrophoric reagents only under inert atmosphere such as Ar or N₂ in a drybox or on a Schlenk line. In addition, (iv) once the pyrophoric reagents are outside of the drybox, using them only behind a lowered hood sash all while wearing approved goggles and a face-shield, a flame-resistant lab coat, and proper gloves and shoes (no sandals). A fire extinguisher was placed in close, known proximity (a dry-powder fire extinguisher rather than regular water or air-pressurized water extinguishers; water-based fire extinguishers can make matters worse in a fire involving pyrophoric reagents.). An emergency shower was also available within a ≤5 second, brisk walk. In addition, (v) the use of pyrophoric reagents was performed only when another experienced researcher was present who knew both about the chemistry being done, and about the handling of the pyrophoric reagents, so that help would be immediately available if needed.

The use and handling of AlEt₃ and Al(*t*-Bu)₃ with air-free Schlenk techniques for any non-experienced users was overseen directly by the two most experienced researchers (RGF and SÖ). First, RGF helped design and approved via a walk-through the precise glassware, syringe, and all other steps of the method. Then, a second experienced researcher (SÖ) looked at those steps and procedures, made any comments or suggestions, and the final procedure was then approved by a final walk-through with the first, experienced user (RGF). A key safety rule—the “*Think it*

² Working with pyrophoric reagents requires extreme caution and numerous safety considerations. Failing the required safety rules and regulations can result in serious accidents. One example of a serious laboratory accident happened in 2009 at the University of California Los Angeles in which the research scientist died from injuries incurred during a fire initiated by (*t*-Bu)Li [31].

through ≥ twice, one final time just before you start” rule of one of us (RGF)—was emphasized and followed: namely, that just before one is about to start the procedure, *think it through once more*. Are you completely comfortable with the procedure? Is all safety equipment in place, and are all safety rules being followed? Or, is there some part that you forgot to take care of; some part that means you need to stop, and first do or rethink and redesign some part of the procedure that needs revision to be safe? This simple, but powerful, rule is no different—and no less powerful and important—than looking *once more*, before crossing the street, to be sure that no oncoming traffic is visible!

In the specific case of AlEt_3 , the following methods and safety precautions were also used: (i) AlEt_3 was stored and transferred only in a drybox under N_2 ; (ii) transfer to hydrogen line was done under N_2 in a F–P bottle sealed using Swagelock quick-connects before taking out of the drybox; (iii) transfer to the NMR instrument was done using a NMR sample tube sealed by first inserting a precision-seal natural rubber septum through the top and then folding its flexible sleeve over NMR tube; and (iv) transfer to the XPS instrument was done using a desiccator and a portable glovebag. The catalyst solution including AlEt_3 was transferred onto a sample holder placed in a desiccator. The desiccator was then sealed in the drybox while under N_2 and brought out of the drybox. The desiccator was placed in a glovebag that was already under Ar. The glovebag was then sealed using a sealant tape to the sample exchange window of the XPS instrument and purged three times with Ar. The sample holder was then transferred to the XPS instrument under flowing Ar. (v) The IR liquid cell (ZnSe cell) was filled with the catalyst solution including AlEt_3 using a 1.0 mL gas-tight syringe in the drybox and sealed using TEFLON caps. Then, the IR liquid cell was put in a jar, taken out of the drybox while still sealed with TEFLON caps in a jar and carried to the IR facility.

In the specific case of (*t*-Bu)Li, this pyrophoric reagent was transferred from its original container into a dropping funnel with pressure compensation tube and PTFE-plug while still in the drybox under N₂. The dropping funnel was sealed by (i) first closing the dropping valve below liquid chamber, and then (ii) placing a rubber septum for glass joint at the top. The dropping funnel was brought out of the drybox while still under N₂ and connected to Ar using a needle tip inserted through the rubber septum. Pressure compensation tube on the side of the dropping funnel provided the required vent path; therefore, additional connection to a bubbler was unnecessary. Next, (*t*-Bu)Li was added dropwise to the AlCl₃ solution in 4 h. This procedure avoided any contact with adventitious air or water.

In the case of Al(*t*-Bu)₃, the synthesis was performed under Ar on a Schlenk line or under N₂ in the drybox. All the synthesis steps used either Schlenkware or vacuum flasks with O-ring joints. Transfer of reagents was done either in the drybox or using cannula (double-tipped needle) technique. See the specific synthesis procedure for (*t*-Bu)Li (vide infra) for more detail.

C2.3. Synthesis of [(*n*-Bu)₄N](O₂C₈H₁₅): In the drybox the colorless solution of (*n*-Bu)₄NOH (3mL) was transferred using a 1.0 mL gas-tight syringe into a 20 mL glass vial equipped with a 5/8 by 5/16 in. Teflon-coated magnetic stirbar and stirred for 5 min. Next, 0.476 mL of neat 2-ethylhexanoic acid was added to the vial using a 0.500 mL gas-tight syringe. The resulting colorless solution was stirred for 10 min. The solution was then kept under vacuum at 30 °C for 24 h. A clear, colorless gel was obtained. Yield (0.950 g): 95%. ¹H NMR in benzene-d₆ (δ in ppm, (multiplicity)): 3.18 (t), 2.57 (m), 2.17 (m), 1.77 (m), 1.56 (m), 1.36 (m), 1.05 (t), 0.93 (t).

C2.4. Synthesis of [(*n*-Bu)₄N](AlEt₃O₂C₈H₁₅): In the drybox, 50 μL AlEt₃ (340 μmol) was transferred from its stainless steel container using a 50 μL gas-tight syringe to a 2 dram glass vial containing 1.7 mL benzene-d₆ (200 mM AlEt₃ solution). In another 2 dram glass vial, a 200 mM

$[(n-Bu)_4N](O_2C_8H_{15})$ solution was prepared by dissolving 46.3 mg (120 μ mol) $[(n-Bu)_4N](O_2C_8H_{15})$ in 0.6 mL benzene- d_6 . A 0.1 mL aliquot of 200 mM $[(n-Bu)_4N](O_2C_8H_{15})$ solution was transferred using a 1.0 mL gas-tight syringe into 3 mL benzene- d_6 in an 10 mL glass vial equipped with a 5/8 by 5/16 in. Teflon-coated magnetic stirbar. The resulting solution was stirred for 2 min and then transferred into an NMR tube using a pipette. 1H NMR in benzene- d_6 (δ in ppm, (multiplicity)): 2.72 (t), 2.60 (m), 2.00 (m), 1.85 (t), 1.73 (t), 1.45 (m), 1.15 (m), 1.01 (q), 0.85 (t), 0.53 (q).

C2.5. Hydrogenation Solution Preparation and Catalytic Cyclohexene Hydrogenations with $[Ir(1,5-COD)(\mu-H)]_4$ plus $AlEt_3$ or $AlEt_2(O_2C_8H_{15})$: For the catalysts made with $[Ir(1,5-COD)(\mu-H)]_4$ plus $AlEt_3$, the same procedure was used for the hydrogenation solution preparation and catalytic cyclohexene hydrogenation as given in main text. The only difference was the use of 12 mM $[Ir(1,5-COD)(\mu-H)]_4$ instead of Ziegler-type precatalyst $[[Ir(1,5-COD)(\mu-O_2C_8H_{15})]_2$. Likewise, for the catalyst made with $[Ir(1,5-COD)(\mu-H)]_4$ plus $AlEt_2(O_2C_8H_{15})$, the same procedure was used for the hydrogenation solution preparation and catalytic cyclohexene hydrogenation as given in main text was used. The only two differences were the use of 12 mM $[Ir(1,5-COD)(\mu-H)]_4$ instead of Ziegler-type precatalyst $[[Ir(1,5-COD)(\mu-O_2C_8H_{15})]_2$ and 36 mM $AlEt_2(O_2C_8H_{15})$ instead of $AlEt_3$.

C3. Experimental Data and Related Discussion

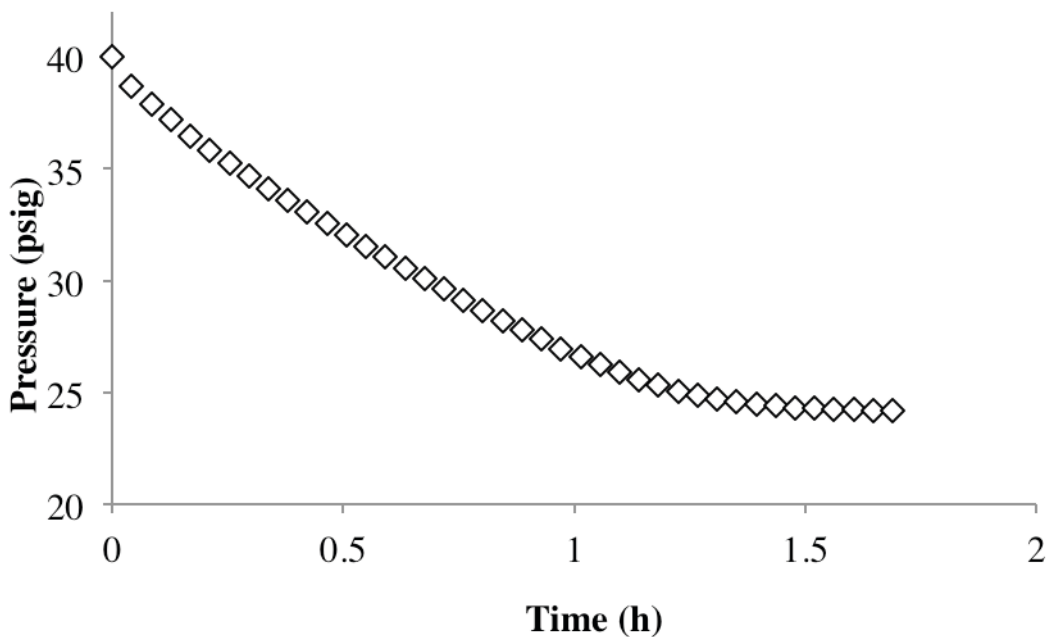


Figure SI-C1. Representative cyclohexene hydrogenation curve (Pressure vs Time) starting with $[\text{Ir}(1,5\text{-COD})(\mu\text{-O}_2\text{C}_8\text{H}_{15})_2]$ plus AlEt_3 catalyst in benzene solvent at Al/Ir ratio of 2. The catalyst was prepared as detailed in the main text. Conditions for hydrogenations are as follows: $[\text{Ir}] = 1.2 \text{ mM}$, benzene solvent, $[\text{cyclohexene}]_{\text{initial}} = 1.65 \text{ M}$, $22.0 \pm 0.1 \text{ }^\circ\text{C}$ and $40 \pm 1 \text{ psig H}_2$. The key point is that the Ziegler-type catalyst made from $[\text{Ir}(1,5\text{-COD})(\mu\text{-O}_2\text{C}_8\text{H}_{15})_2]$ plus AlEt_3 catalyst is active (maximum hydrogenation rate = 5 mmol/h) for cyclohexene hydrogenation in benzene solvent (a control performed since a several of the NMR investigations were performed in $(d_6\text{-})$ benzene solvent).

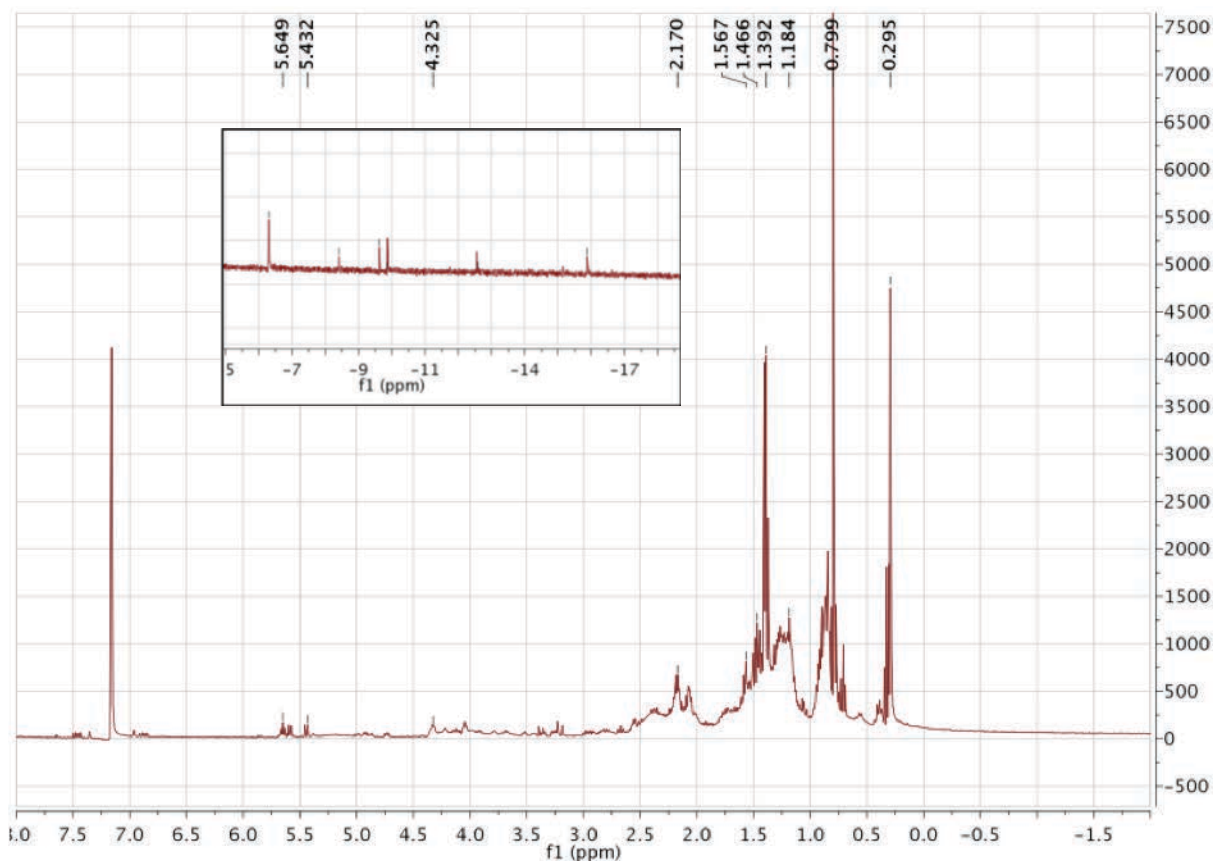


Figure SI-C2. ^1H NMR spectrum of Ziegler-type hydrogenation catalyst made with $[\text{Ir}(1,5\text{-COD})(\mu\text{-O}_2\text{C}_8\text{H}_{15})]_2$ plus AlEt_3 at $\text{Al/Ir}=1$ in benzene- d_6 . The peaks at 0.30, 0.80, 1.18, 1.39, 1.47, 1.57, 2.17 ppm are assigned to $\text{AlEt}_2(\text{O}_2\text{C}_8\text{H}_{15})$. The broad peak between 2.3-2.7 ppm and the peak at 5.65 ppm are due to *uncomplexed, free 1,5-COD*. The olefinic H's of *coordinated 1,5-COD* groups are observed at 4.33 ppm. The peak at 0.80 ppm may have some contribution from *ethane*. **Inset:** A close-up version of Figure S1 showing **Ir-H region**. The narrow peaks observed at -6.31, -8.42, -9.62, -9.85, -12.57 and -15.88 ppm are tentatively assigned to hydrides bonded to Ir atoms in presumably smaller, but rigorously unknown size and nature, Ir clusters (see the main text for additional discussion and references on this point).

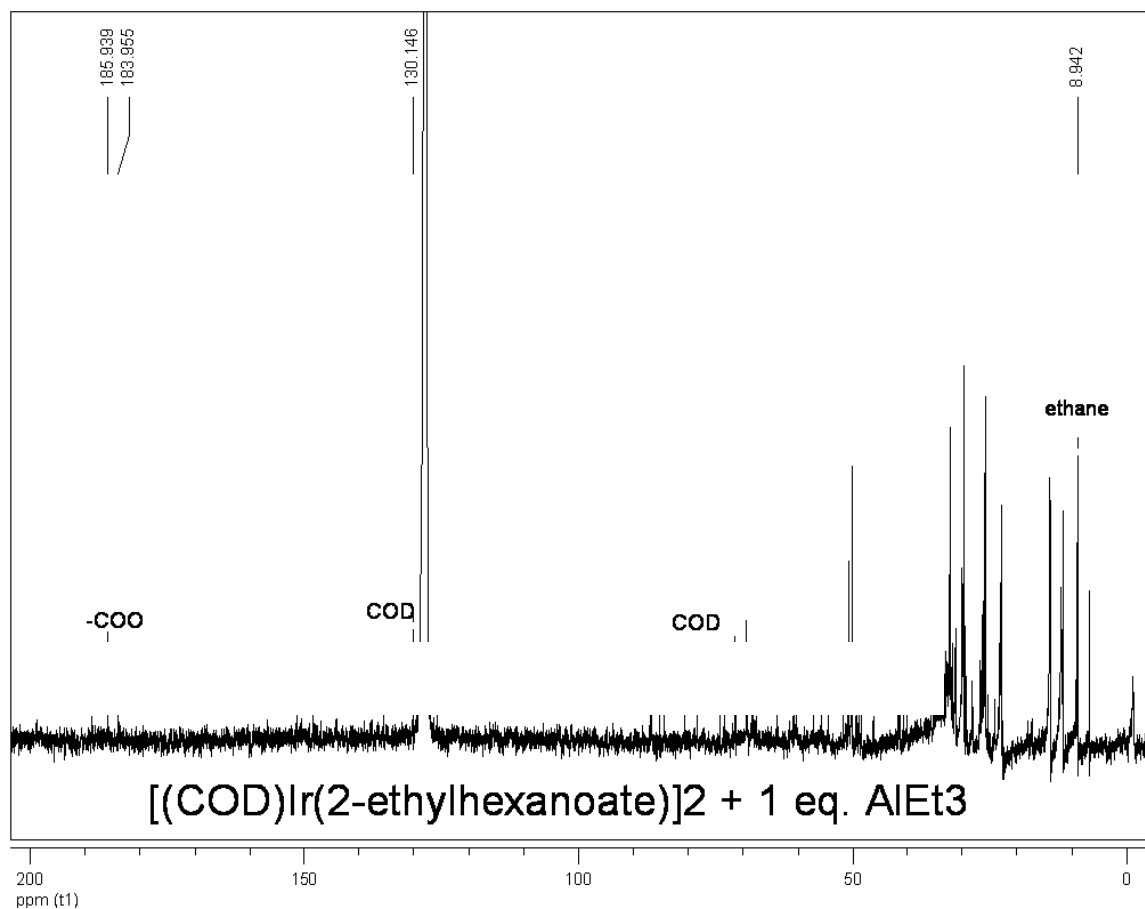


Figure SI-C3. ^{13}C NMR spectrum of Ziegler-type hydrogenation catalyst made from $[\text{Ir}(1,5\text{-COD})(\mu\text{-O}_2\text{C}_8\text{H}_{15})]_2$ plus AlEt_3 at $\text{Al}/\text{Ir}=1$ in benzene- d_6 . The peaks at -0.25 , 8.94 , 14.33 , 23.49 , 26.80 , 30.10 , 32.52 , 33.21 and 184.00 ppm are assigned to $\text{AlEt}_2(\text{O}_2\text{C}_8\text{H}_{15})$. The peak at 130.15 ppm is due to *uncomplexed, free 1,5-COD*. The *coordinated 1,5-COD* groups are observed at 50.00 and 65.01 ppm. The peak at 7.50 ppm is attributed to *ethane*.

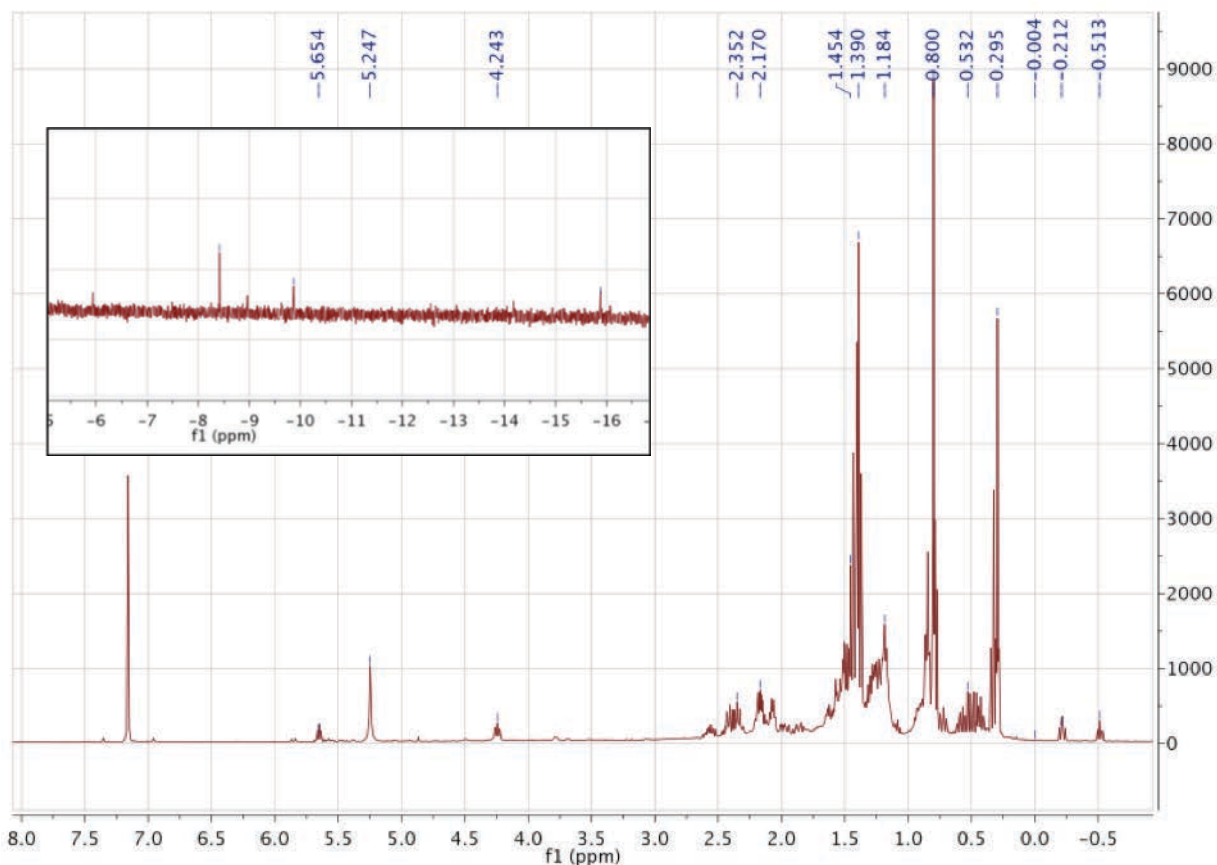


Figure SI-C4. ^1H NMR spectrum of Ziegler-type hydrogenation catalyst made with $[\text{Ir}(1,5\text{-COD})(\mu\text{-O}_2\text{C}_8\text{H}_{15})]_2$ plus AlEt_3 at $\text{Al/Ir}=2$ in benzene- d_6 . The peaks at 0.30, 0.80, 1.18, 1.39, 1.45 and 2.17 ppm are assigned to $\text{AlEt}_2(\text{O}_2\text{C}_8\text{H}_{15})$. The peaks at 0.53, -0.21 and -0.51 ppm are attributed to an $\text{Al}(\text{L}_2)\text{-CH}_x\text{-CH}_2\text{-}$ moiety (L: other ligands present in the medium such as $\text{O}_2\text{C}_8\text{H}_{15}^-$ or $\text{-CH}_2\text{-}$ or -CH_3 , x: 1 or 2) moiety. The signals at 2.35 and 5.65 ppm are due to *uncomplexed, free 1,5-COD*. The olefinic H's of *coordinated 1,5-COD* groups are observed at 4.24 ppm. The peak at 0.80 ppm may have some contribution from *ethane*. The peak at 5.25 ppm is assigned to *ethylene*. **Inset:** A close-up version of Figure S3 showing the putative **Ir-H** region. The narrow peaks observed at -8.42, -9.87 and -15.88 ppm are tentatively assigned to hydrides bonded to Ir atoms in presumably smaller, but rigorously unknown size and nature, Ir clusters (see the main text for additional discussion and references on this point).

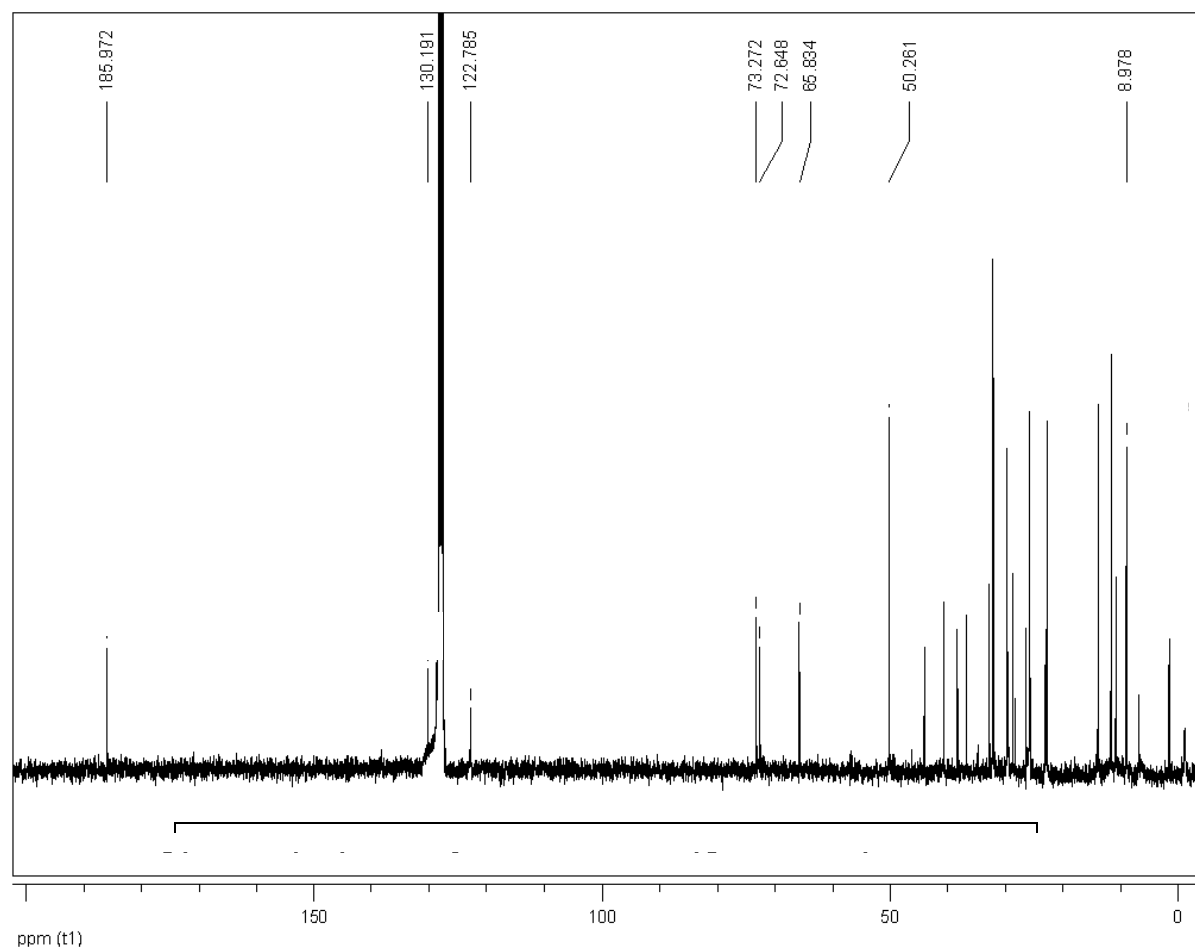


Figure SI-C5. ^{13}C NMR spectrum of Ziegler-type hydrogenation catalyst made from $[\text{Ir}(1,5\text{-COD})(\mu\text{-O}_2\text{C}_8\text{H}_{15})_2]_2$ plus AlEt_3 at $\text{Al/Ir}=2$ in benzene- d_6 . The peaks at -0.20, 8.98, 14.32, 23.485, 26.80, 30.10, 32.52, 33.21 and 185.97 ppm are assigned to $\text{AlEt}_2(\text{O}_2\text{C}_8\text{H}_{15})$. The peak at 130.18 ppm is due to *uncomplexed, free 1,5-COD*. The *coordinated 1,5-COD* groups are observed at 50.28 and 65.83 ppm. The peak at 7.28 ppm is attributed to *ethane*. The peak at 122.79 ppm is assigned to *ethylene*.

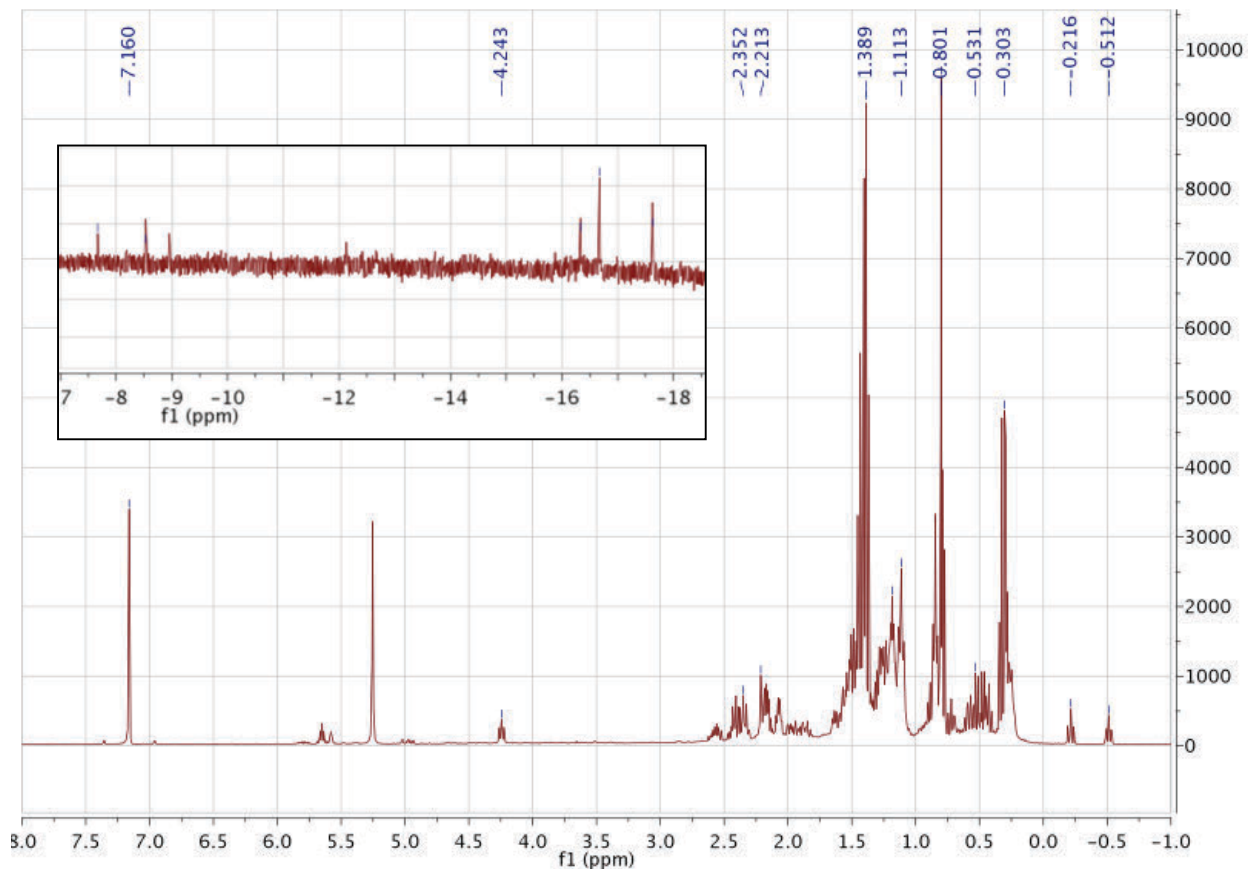


Figure SI-C6. ^1H NMR spectrum of Ziegler-type hydrogenation catalyst made from $[\text{Ir}(1,5\text{-COD})(\mu\text{-O}_2\text{C}_8\text{H}_{15})]_2$ plus AlEt_3 at $\text{Al}/\text{Ir}=3$ in benzene- d_6 . The peaks at 0.30, 0.80, 1.19, 1.39 and 2.21 ppm are assigned to $\text{AlEt}_2(\text{O}_2\text{C}_8\text{H}_{15})$. The peaks at 0.53, -0.22 and -0.51 ppm are attributed to an $\text{Al}(\text{L}_2)\text{-CH}_x\text{-CH}_2\text{-}$ moiety (L: other ligands present in the medium such as $\text{O}_2\text{C}_8\text{H}_{15}^-$ or $\text{-CH}_2\text{-}$ or -CH_3 , x: 1 or 2). The peak at 1.11 ppm is attributed to *uncomplexed, free* AlEt_3 . The signals at 2.35 and 5.65 ppm are due to *uncomplexed, free* 1,5-COD. The olefinic H's of *coordinated* 1,5-COD groups are observed at 4.24 ppm. The peak at 0.80 ppm may have some contribution from *ethane*. The peak at 5.25 ppm is assigned to *ethylene*. **Inset:** A close-up version of Figure S5 showing the putative **Ir-H** region. The narrow peaks observed at -7.67, -8.55, -16.34, -16.68, and -17.63 ppm are tentatively assigned to hydrides bonded to Ir atoms in presumably smaller, but rigorously unknown size and nature, Ir clusters (see the main text for additional discussion and references on this point).

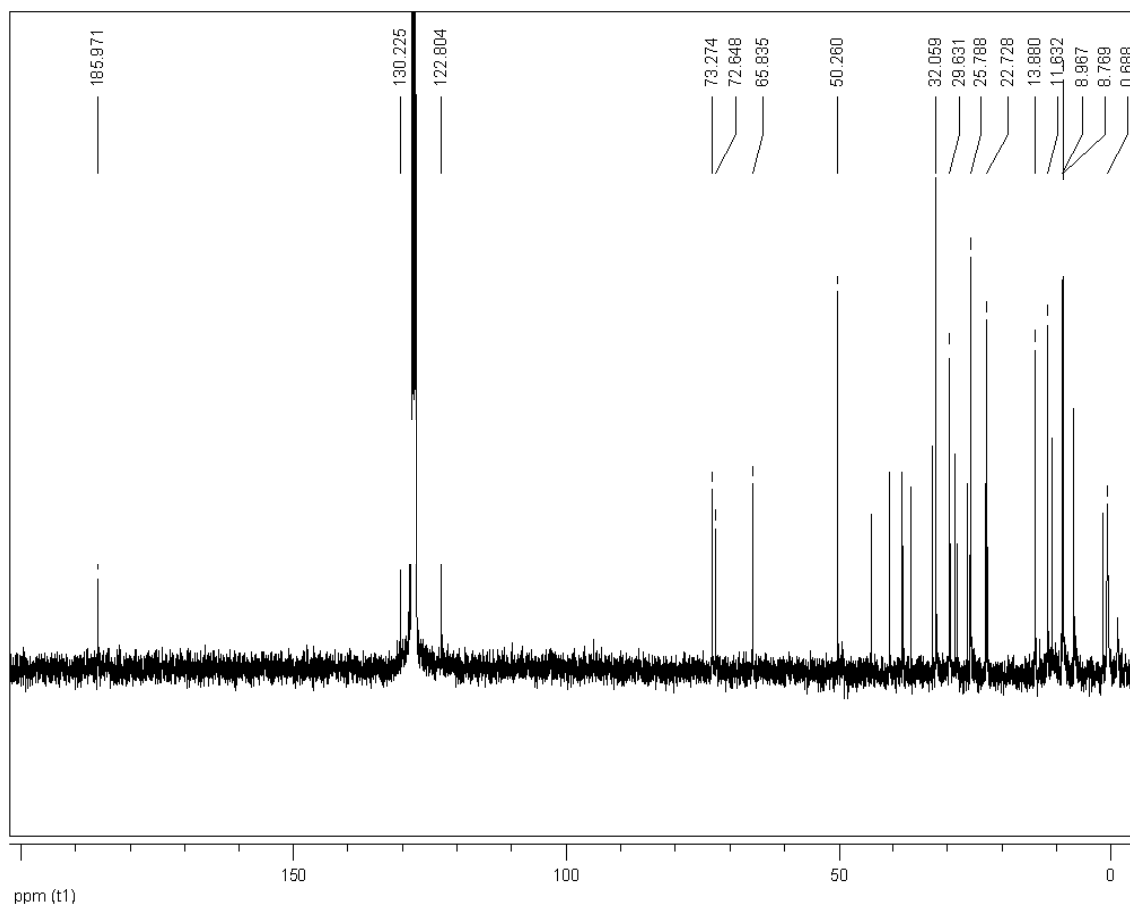


Figure SI-C7. ^{13}C NMR spectrum of Ziegler-type hydrogenation catalyst made from $[\text{Ir}(1,5\text{-COD})(\mu\text{-O}_2\text{C}_8\text{H}_{15})]_2$ plus AlEt_3 at $\text{Al/Ir}=\mathbf{3}$ in benzene- d_6 . The peaks at -0.20, 8.77, 13.80, 22.729, 25.79, 29.63, 32.06 and 185.97 ppm are assigned to $\text{AlEt}_2(\text{O}_2\text{C}_8\text{H}_{15})$. The peaks at 1.00 and 8.77 ppm are attributed to *free* AlEt_3 . The peak at 130.23 ppm is due to *uncomplexed, free* 1,5-COD. The *coordinated* 1,5-COD groups are observed at 50.28 and 65.81 ppm. The peak at 7.50 ppm is attributed to *ethane*. The peak at 122.80 ppm is assigned to *ethylene*.

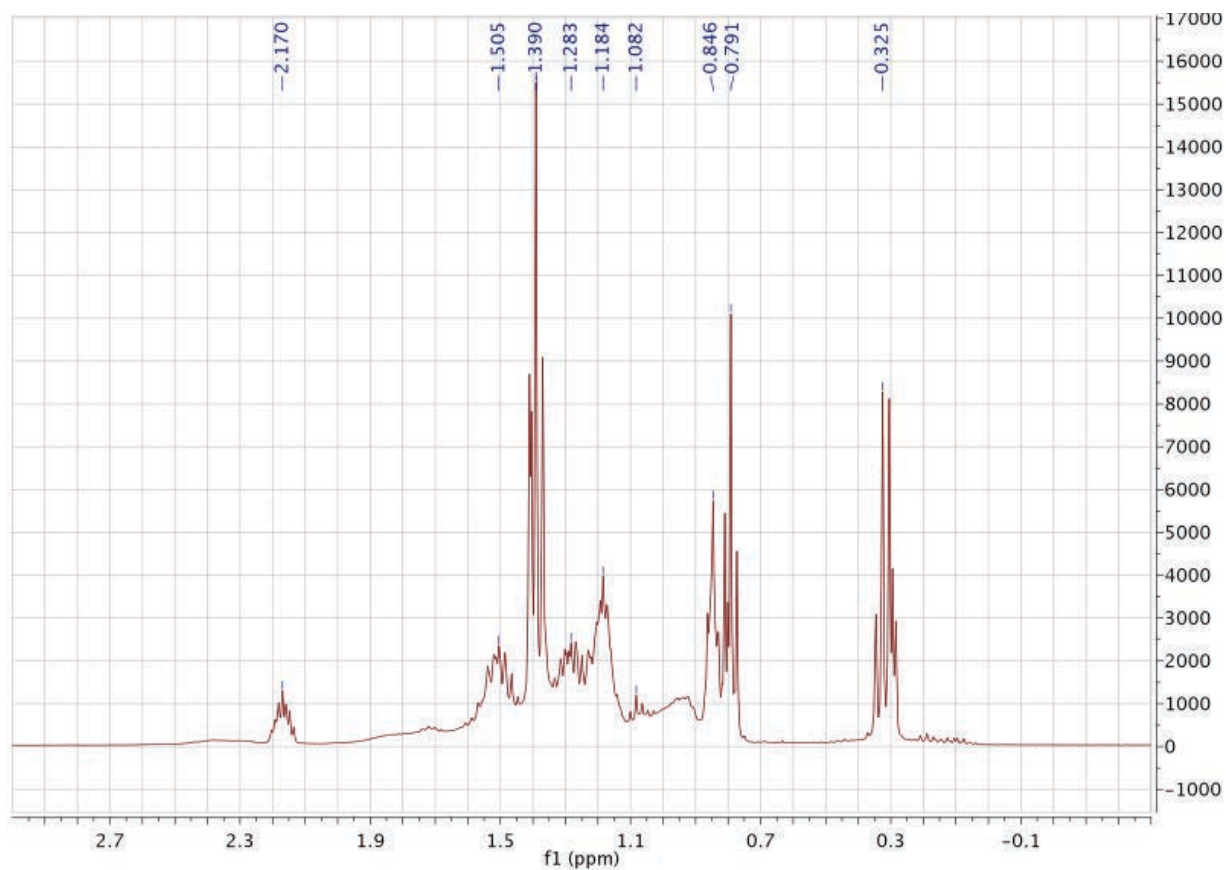


Figure SI-C8. ¹H NMR spectrum of independently synthesized $\text{AlEt}_2(\text{O}_2\text{C}_8\text{H}_{15})$ in benzene- d_6 . The peaks at 0.325 and 1.283 ppm are assigned to *Et*- groups. The peaks observed at 0.79, 1.18, 1.39, 1.51 and 2.17 ppm are due to the 2-ethylhexanoate moiety ($\text{O}_2\text{C}_8\text{H}_{15}$).

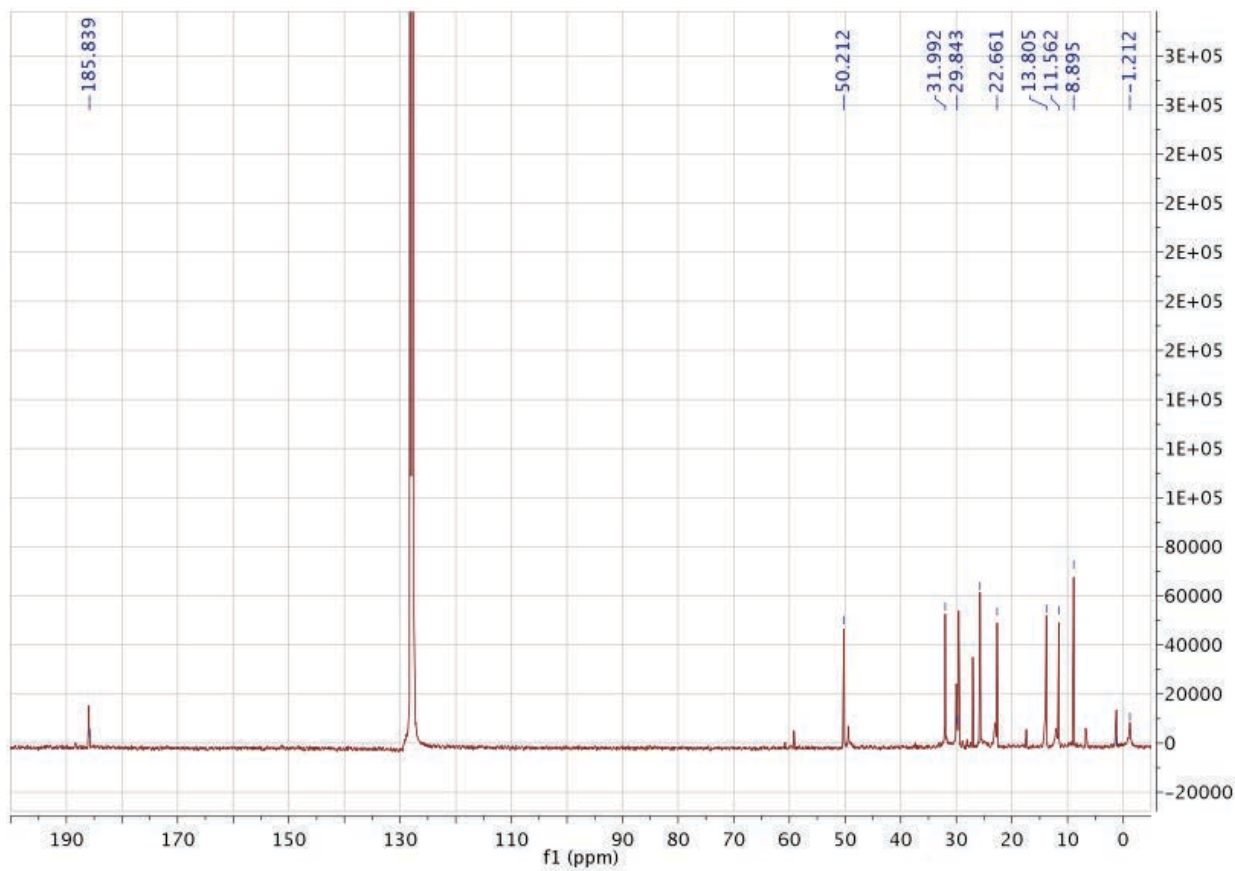
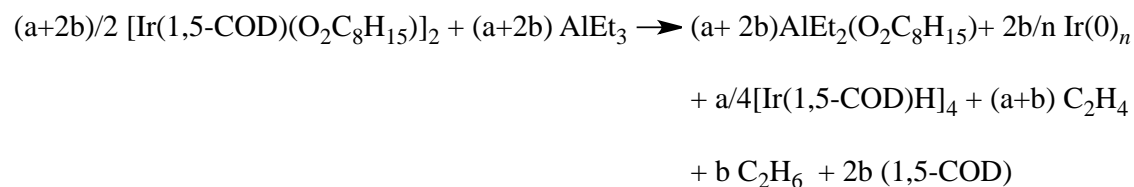
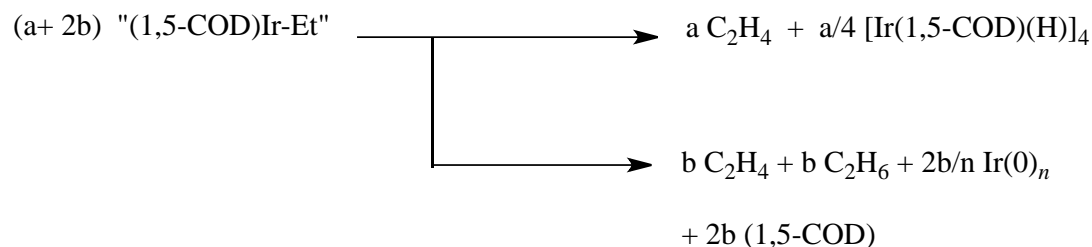


Figure SI-C9. ¹³C NMR spectrum of independently synthesized $\text{AlEt}_2(\text{O}_2\text{C}_8\text{H}_{15})$ in benzene- d_6 . The peaks at -1.21 and 8.90 ppm are assigned to *Et*- groups. The peaks observed at 13.81, 22.66, 25.72, 29.84, 31.99 and 185.84 ppm are due to the 2-ethylhexanoate moiety ($\text{O}_2\text{C}_8\text{H}_{15}$).



Scheme SI-C2. A proposed, working hypothesis for the stoichiometry of catalyst formation for the Ziegler-type hydrogenation catalyst made from $[\text{Ir}(1,5\text{-COD})(\mu\text{-O}_2\text{C}_8\text{H}_{15})]_2$ plus AlEt_3 at an Al/Ir ratio of 1. The scheme shows two proposed individual steps including a plausible “ $\text{Ir}(1,5\text{-COD})\text{-Et}$ ” intermediate and a net reaction (bottom). As noted earlier in this supporting information, the purpose of this hypothesis is to help guide the needed, future studies to unequivocally establish such stoichiometries for the formation of Ziegler-type nanoparticle catalysts from a precise composition precatalyst such as $[\text{Ir}(1,5\text{-COD})(\mu\text{-O}_2\text{C}_8\text{H}_{15})]_2$. Note that H_2 as an initial product, from possible reductive elimination from “ Ir_4H_4 ” or other “ Ir_xH_y ” intermediates, is also possible but has not been included in Scheme S2 simply to keep the scheme below relatively simple. If formed, then possible follow-up reactions of H_2 with olefins like ethylene or 1,5-COD would further complicate the observed stoichiometry.

One positive to date from writing this stoichiometry is that we did predict $[\text{Ir}(1,5\text{-COD})\text{H}]_4$ should exist, and subsequently were able to synthesize it in high yield and crystalline form, followed by its complete and unequivocal characterization [32].

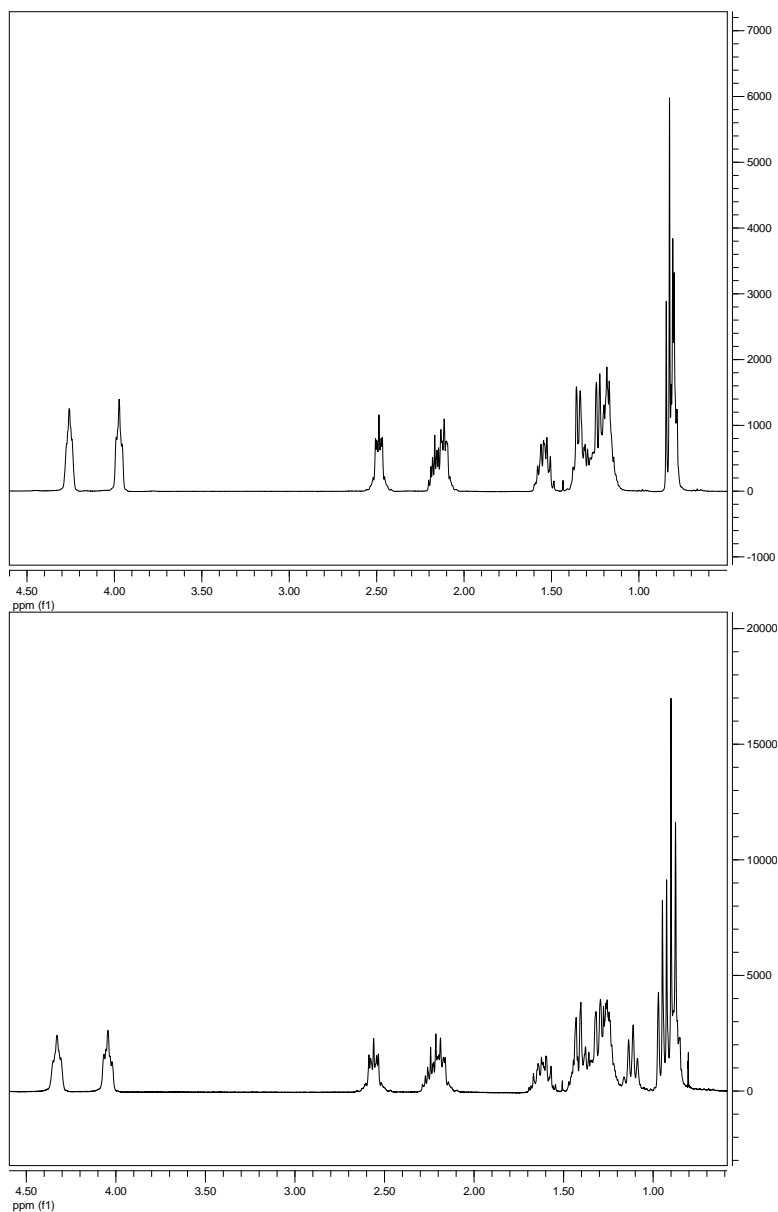


Figure SI-C10. ^1H NMR spectra of (top) Ziegler-type hydrogenation precatalyst, $[\text{Ir}(1,5\text{-COD})(\mu\text{-O}_2\text{C}_8\text{H}_{15})_2]$; (bottom) the catalyst solution made from $[\text{Ir}(1,5\text{-COD})(\mu\text{-O}_2\text{C}_8\text{H}_{15})_2]$ plus BEt_3 at $\text{Al}/\text{Ir}=1$ in benzene- d_6 . The very close correspondence of the two spectra shows that the $[\text{Ir}(1,5\text{-COD})(\mu\text{-O}_2\text{C}_8\text{H}_{15})_2]$ precatalyst and BEt_3 cocatalyst *do not react to any appreciable extent*.

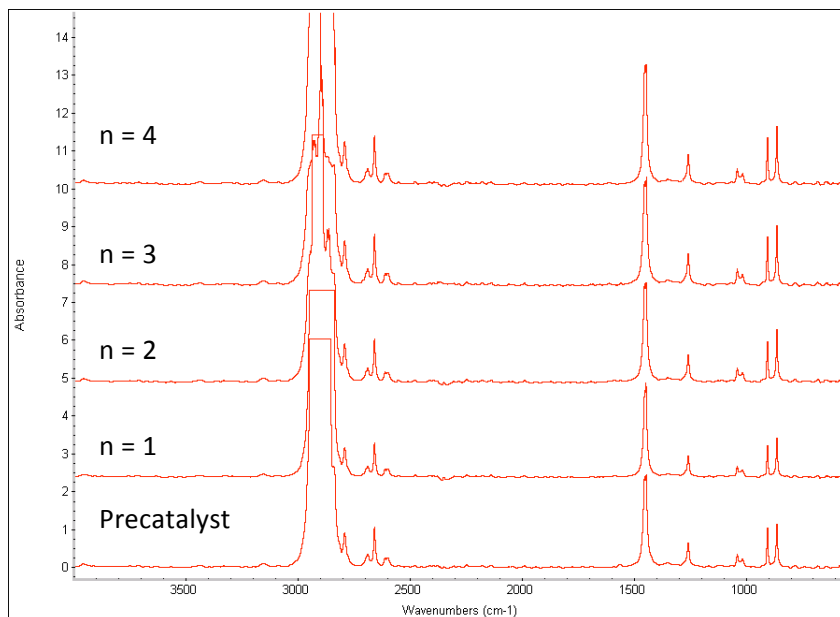


Figure SI-C11. IR spectra of precatalyst, $[\text{Ir}(1,5\text{-COD})(\mu\text{-O}_2\text{C}_8\text{H}_{15})_2]$, (bottom) and $[\text{Ir}(1,5\text{-COD})(\mu\text{-O}_2\text{C}_8\text{H}_{15})_2]$ plus AlEt_3 , $n=\text{Al}/\text{Ir}$, Ziegler-type catalysts in cyclohexane solvent. Spectra show (i) that the 2-ethylhexanoate group appears to be bidentate, bridging between two Ir, or Al, or Ir/Al metal centers; and (ii) that detectable alumoxanes do not exist in the solution, at least, in quantities detectable by IR (at $630\text{-}780\text{ cm}^{-1}$) and under our conditions. See results and discussion section of main text for more information.

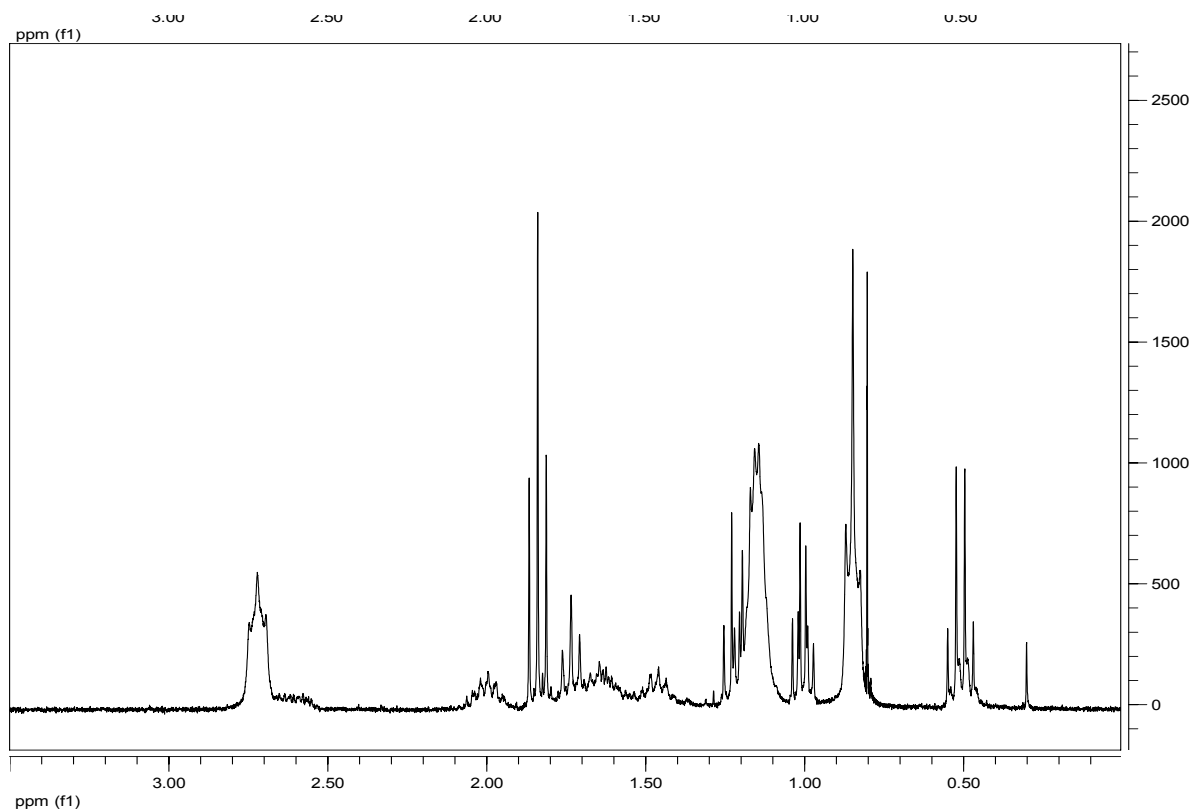


Figure SI-C12. ^1H NMR spectrum of individually-synthesized $[(n\text{-Bu})_4\text{N}][\text{AlEt}_3(\text{O}_2\text{C}_8\text{H}_{15})]$ in benzene- d_6 . Dissimilarity of this spectrum, to that of Ziegler-type catalyst made from $[\text{Ir}(1,5\text{-COD})(m\text{-O}_2\text{C}_8\text{H}_{15})]_2$ plus AlEt_3 at Al/Ir ratio of 1 (Figure SI-C2), rules out the hypothesis *that the AlEt_3 -derived stabilizer is anionic $[\text{AlEt}_3(\text{O}_2\text{C}_8\text{H}_{15})]^-$* .

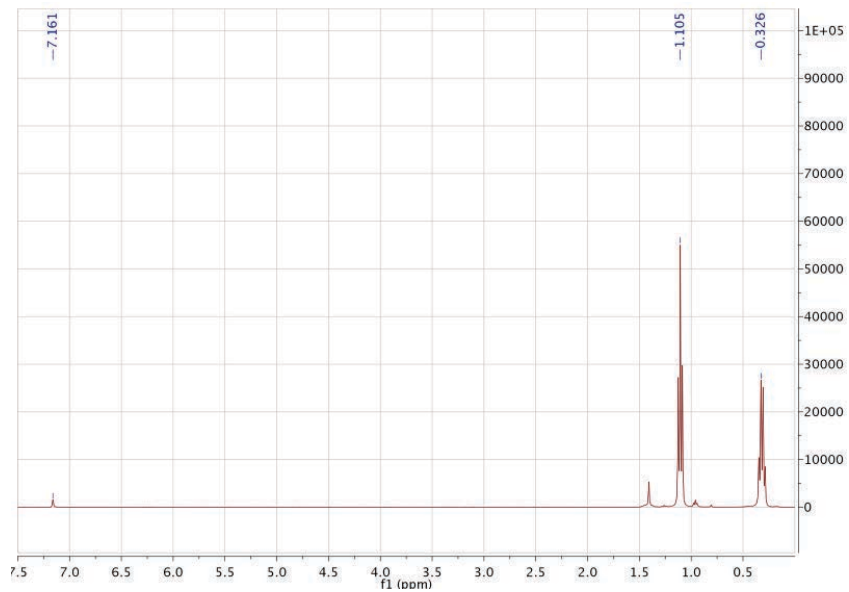


Figure SI-C13. ^1H NMR spectrum of commercially-available neat AlEt_3 (93% purity) in benzene- d_6 . The peaks at 0.33 and 1.11 ppm are assigned to $-\text{CH}_2-$ and $-\text{CH}_3$, respectively.

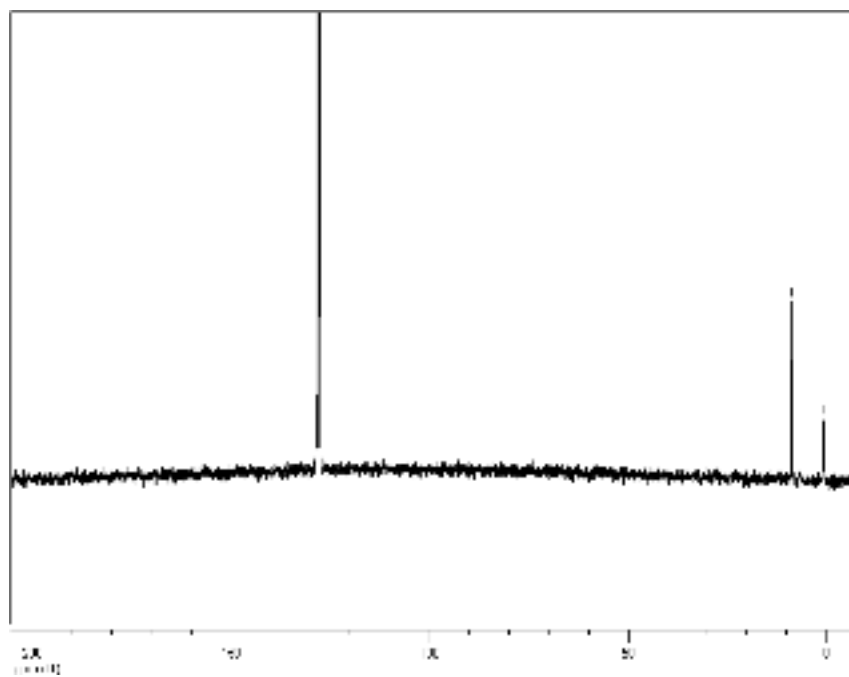


Figure SI-C14. ^{13}C NMR spectrum of commercially available neat AlEt_3 in benzene- d_6 . The peaks at 1.21 and 9.44 ppm are assigned to $-\text{CH}_2-$ and $-\text{CH}_3$, respectively.

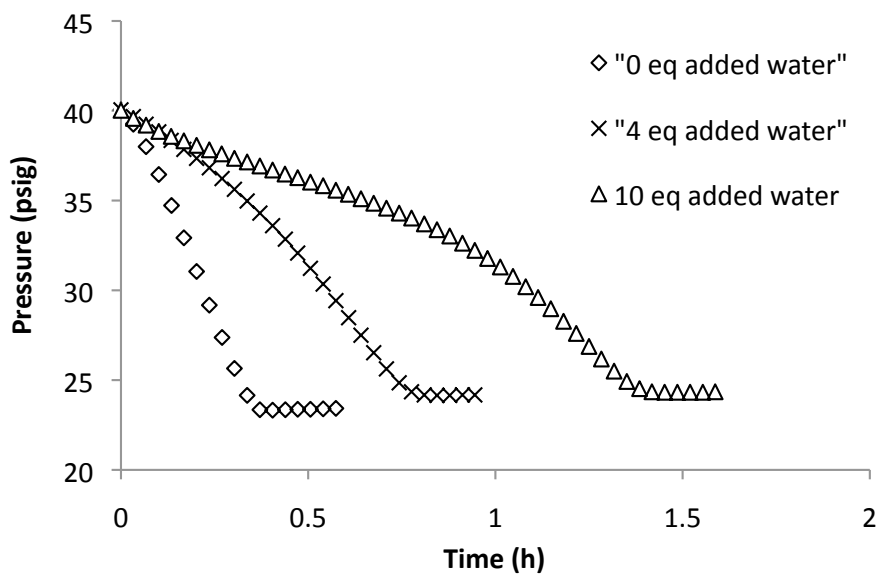
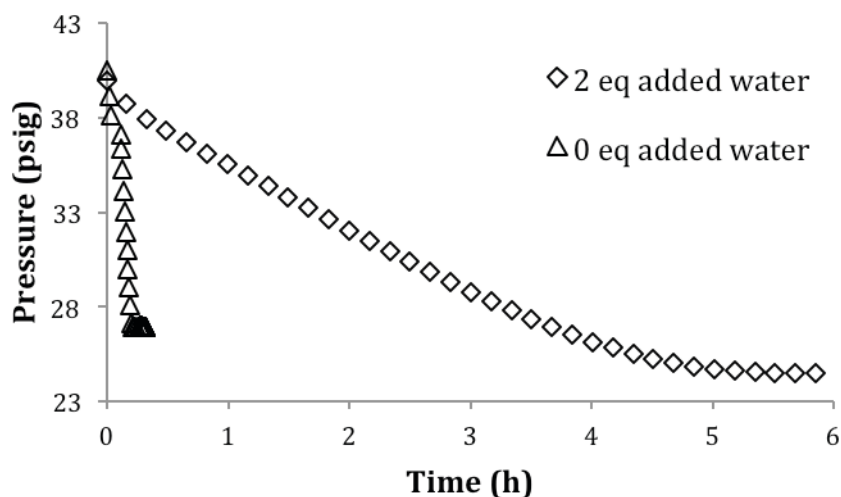


Figure SI-C15. Representative cyclohexene hydrogenation curves (Pressure vs Time) starting with $[\text{Ir}(1,5\text{-COD})(\mu\text{-O}_2\text{C}_8\text{H}_{15})_2]$ plus **1 (top) or 2 (bottom) equivalents AlEt_3 (per Ir) in the presence of 2-10 equivalents of H_2O (per Ir) added to the cyclohexane solution of $[\text{Ir}(1,5\text{-COD})(\mu\text{-O}_2\text{C}_8\text{H}_{15})_2]$ before AlEt_3 was added.** The hydrogenation solutions were prepared in 20 mL batches according to the procedure given in detail in Experimental section of main text under the heading “Hydrogenation Solution Preparation with Added H_2O ”. Conditions for hydrogenations are as follows: $[\text{Ir}] = 1.2 \text{ mM}$, cyclohexane solvent, $[\text{cyclohexene}]_{\text{initial}} = 1.65 \text{ M}$, $22.0 \pm 0.1 \text{ }^\circ\text{C}$ and $40 \pm 1 \text{ psig H}_2$. The results demonstrate rather clearly the rate inhibiting effect of added H_2O and, therefore and presumably, AlEt_3 loss and alumoxane formation (plus any higher hydrolysis products, especially at the higher equivalents of water such as 10 equivs).

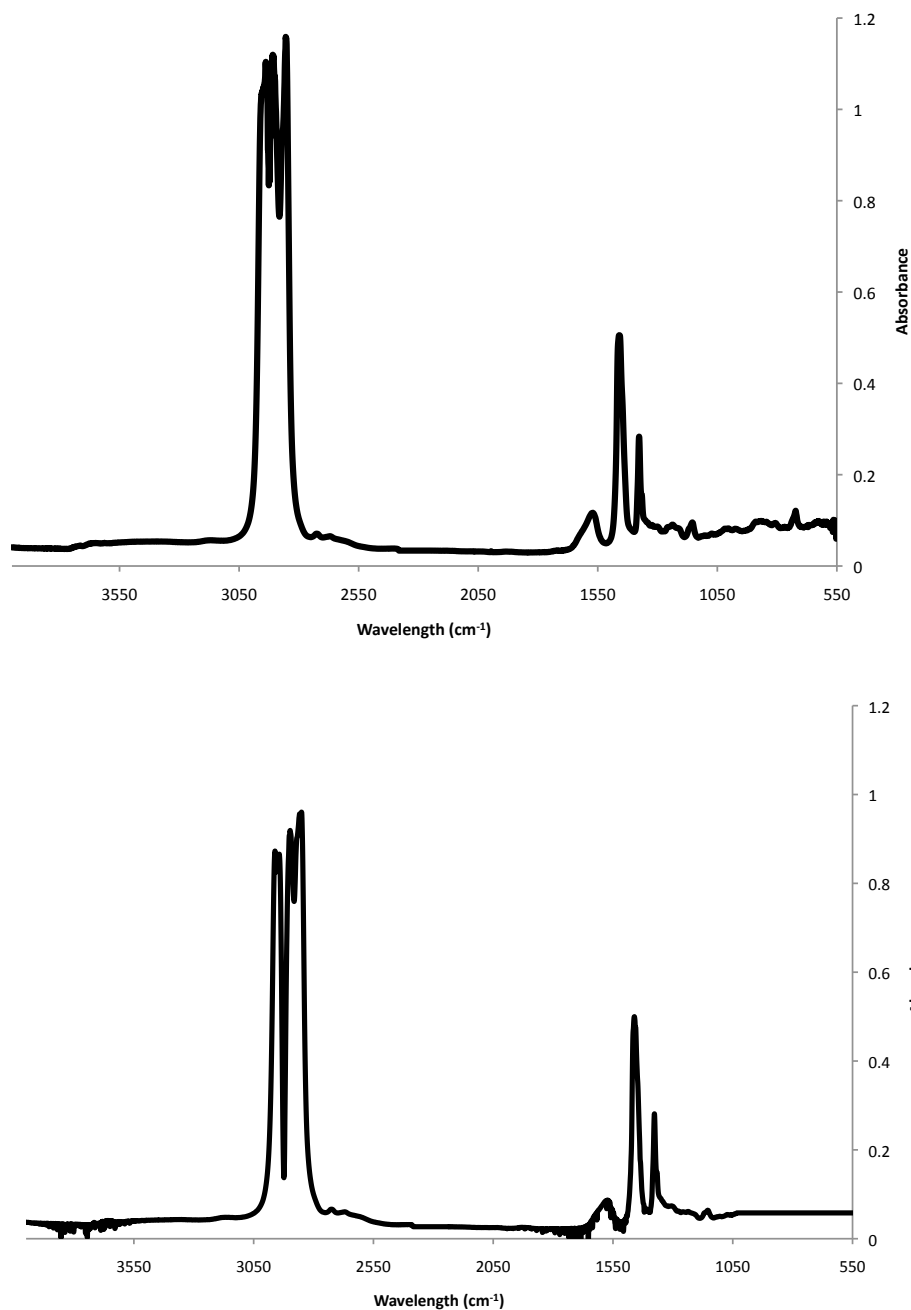


Figure Si-C16. IR spectra of (i) (top) Ziegler-type precatalyst prepared from $[\text{Ir}(1,5\text{-COD})(\mu\text{-O}_2\text{C}_8\text{H}_{15})_2]_2$ plus AlEt_3 at an Al/Ir ratio of 2 prepared in the presence of 10 eq water (per Ir), and (ii) (bottom) the precatalyst prepared from $[\text{Ir}(1,5\text{-COD})(\mu\text{-O}_2\text{C}_8\text{H}_{15})_2]_2$ plus AlEt_3 also at an Al/Ir ratio of 2 prepared without water. The weak absorbance observed in the presence of 10 eq water (top) at $600\text{-}800\text{ cm}^{-1}$ is consistent with the presence of Al-O-Al aluminoxane groups (see also Figure S17). The absence of a similar absorption band at $600\text{-}800\text{ cm}^{-1}$ suggests the absence of IR detectable aluminoxanes in the precatalyst, $[\text{Ir}(1,5\text{-COD})(\mu\text{-O}_2\text{C}_8\text{H}_{15})_2]_2$ plus AlEt_3 solution prepared with an Al/Ir ratio of 2.

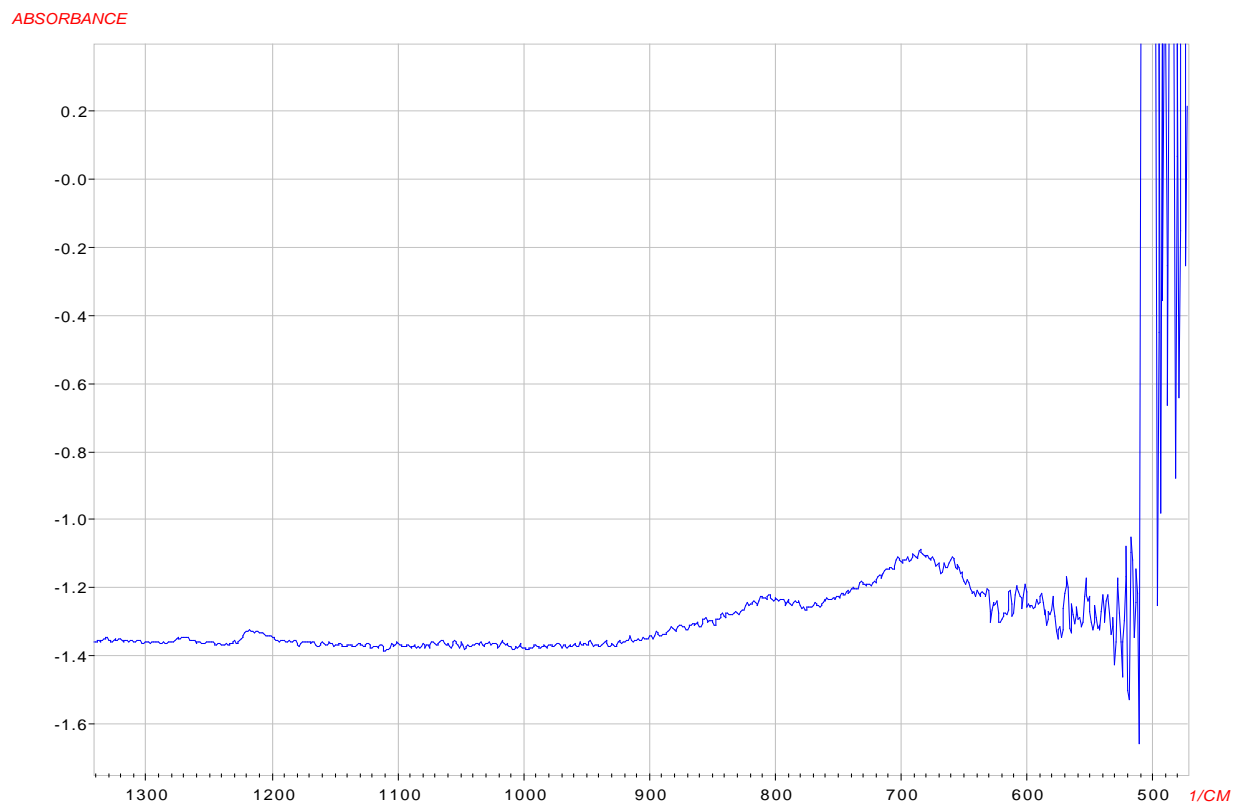


Figure Si-C17. IR spectrum of modified methylalumoxane solution (360 mM in heptane). The broad absorption band observed at $630\text{-}780\text{ cm}^{-1}$ in modified-methylalumoxane solution (right) is due to Al-O-Al groups.

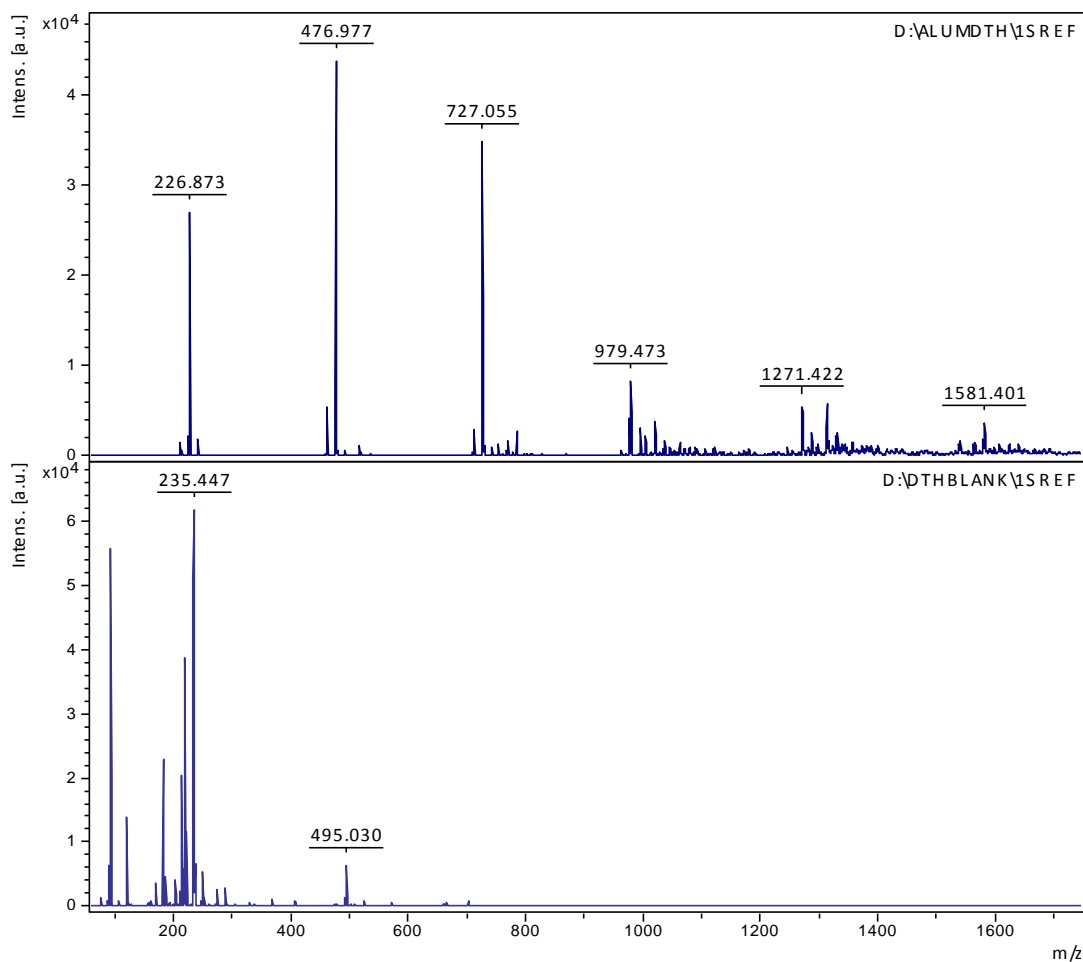


Figure SI-C18. MALDI MS of (top) 36 mM [(*t*-Bu)₂Al(OH)]₃ in cyclohexane taken using dithranol as the matrix and Na⁺ as the ionizing agent and (bottom) dithranol matrix. The observed isotope peak distribution of m/z=476.977 Da peak *does not match* with the theoretical isotope distribution of [(*t*-Bu)₂Al(μ -OH)]₃. The fragment reported at 417 Da in chemical ionization mass spectrum [33] is absent in the MALDI MS of [(*t*-Bu)₂Al(OH)]₃. Therefore, one can conclude that MALDI MS is unsuccessful in characterization of at least this discrete alumoxane while using a dithranol matrix. Similar results were obtained using other commonly used matrices, namely, 2'-4'-6'-trihydroxyacetophenone, 6-aza-2-thiothymine, and graphite. The details of experimental procedure for sample preparation and instrumentation are given in an earlier publication [34].

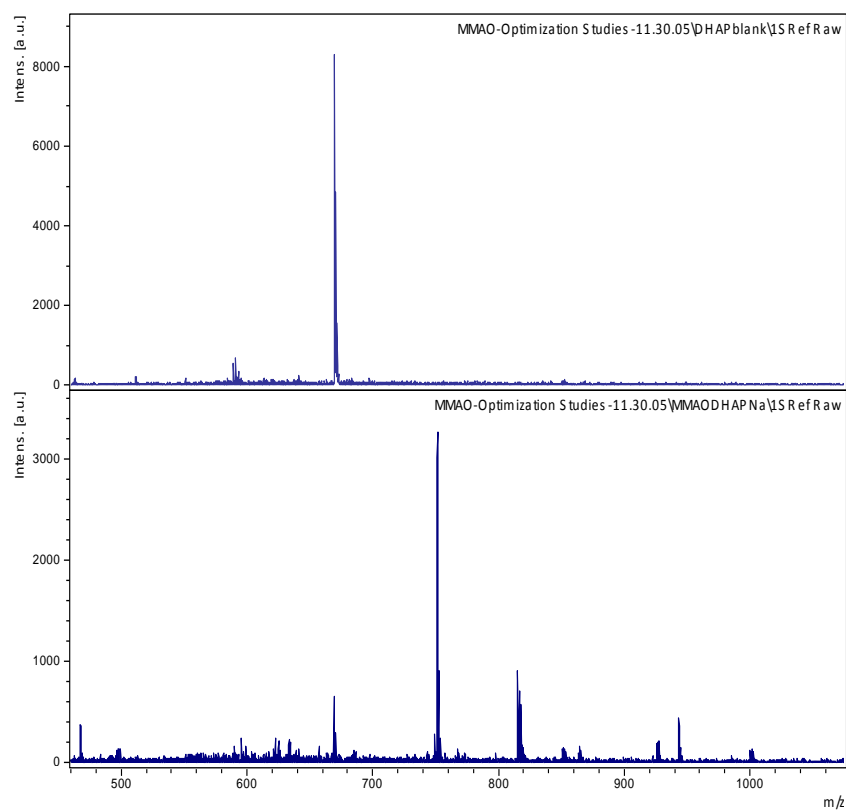


Figure SI-C19. MALDI MS of (top) 2'-6'-dihydroxyacetophenone (DHAP) matrix and (bottom) 36 mM MMAO in cyclohexane taken using DHAP as the matrix and Na⁺ as the ionizing agent. The isotope peak distributions of the observed peaks did not match any plausible MMAO fragments. Therefore, one can conclude that MALDI MS is unsuccessful in characterization of MMAO while using a DHAP matrix. Similar results were obtained using combination of another commonly used matrices, namely, 2'-4'-6'-trihydroxyacetophenone, and the ionizing agent, Ag⁺. The details of experimental procedure for sample preparation and instrumentation are given in an earlier publication [35].

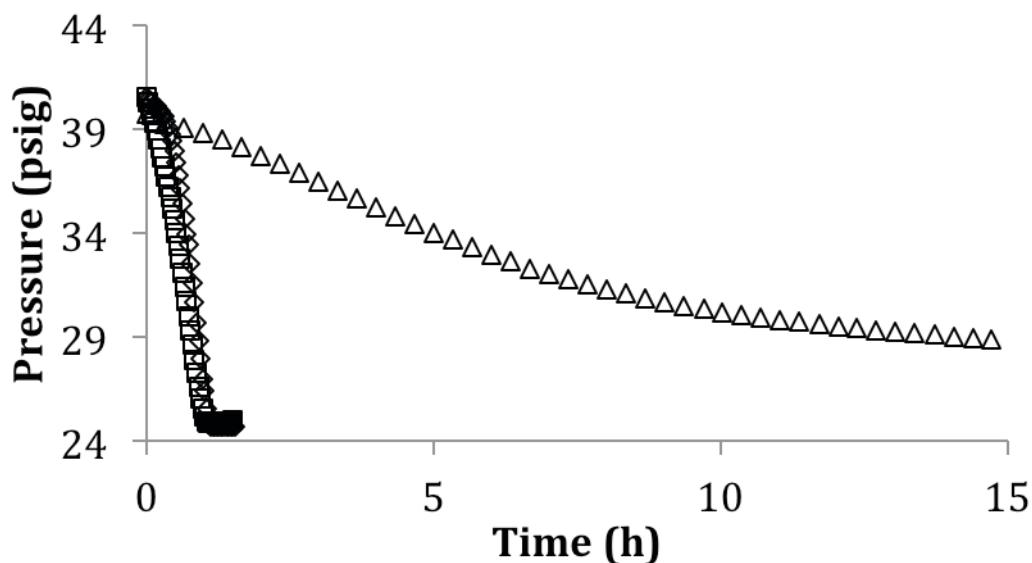


Figure SI-C20. Representative cyclohexene hydrogenation curves (Pressure vs Time) starting with $[\text{Ir}(1,5\text{-COD})(\mu\text{-O}_2\text{C}_8\text{H}_{15})_2]$ plus AlEt_3 (diamonds), $\text{Al}(t\text{-Bu})_3$ (squares) and $[(t\text{-Bu})_2\text{Al}(\text{OH})]_3$ (triangles) catalysts at Al/Ir ratio of 2. The hydrogenation solutions were prepared individually (in 2.5 mL portions) according to the procedure given in detail in Experimental section of main text under the heading “Hydrogenation Solution Preparation and Catalytic Cyclohexene Hydrogenations”. Conditions for hydrogenations are as follows: $[\text{Ir}] = 1.2$ mM, cyclohexane solvent, $[\text{cyclohexene}]_{\text{initial}} = 1.65$ M, 22.0 ± 0.1 °C and 40 ± 1 psig H_2 . A key observation is that the Ziegler-type catalyst made from $[\text{Ir}(1,5\text{-COD})(\mu\text{-O}_2\text{C}_8\text{H}_{15})_2]$ plus $[(t\text{-Bu})_2\text{Al}(\text{OH})]_3$ is less active than those made from $[\text{Ir}(1,5\text{-COD})(\mu\text{-O}_2\text{C}_8\text{H}_{15})_2]$ plus $\text{Al}(t\text{-Bu})_3$ or AlEt_3 .

Table SI-C4. Maximum rates of cyclohexene hydrogenation using $[\text{Ir}(1,5\text{-COD})(\mu\text{-O}_2\text{C}_8\text{H}_{15})]_2$ plus $\text{Al}(t\text{-Bu})_3$ Ziegler-type catalysts at Al/Ir ratios of 1-5. The hydrogenation solutions were prepared individually (in 2.5 mL portions) according to the procedure given in detail in Experimental section of main text under the heading “Hydrogenation Solution Preparation and Catalytic Cyclohexene Hydrogenations”. Conditions for hydrogenations are as follows: $[\text{Ir}] = 1.2$ mM, cyclohexane solvent, $[\text{cyclohexene}]_{\text{initial}} = 1.65$ M, 22.0 ± 0.1 °C and 40 ± 1 psig H_2 .

Al/Ir	Maximum Rate (mmol H_2 /h)
1	12 ± 5
2	6 ± 2
3	2 ± 1
5	2 ± 1

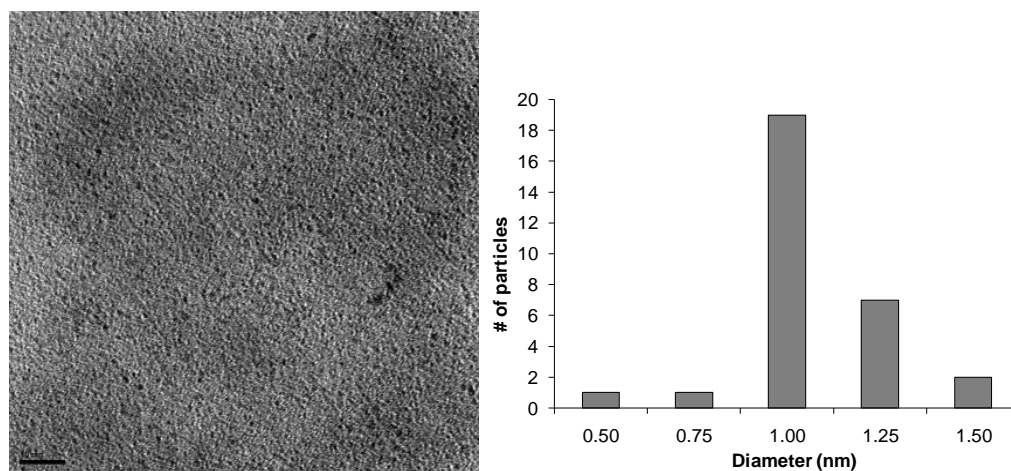


Figure SI-C21. TEM image and corresponding particle size histogram of the Ziegler-type hydrogenation catalyst sample made with $[\text{Ir}(\mathbf{1,5-COD})(\mu\text{-O}_2\text{C}_8\text{H}_{15})_2]$ plus $[(t\text{-Bu})_2\text{Al}(\mu\text{-OH})]_3$ at Al/Ir = 2 **before the catalyst was used in cyclohexene hydrogenation**. The scale bar is 10 nm. Mean diameter from measurement of 30 nanoparticles is 1.1 ± 0.2 nm, corresponding on average to $\text{Ir}_{\sim 50}$.

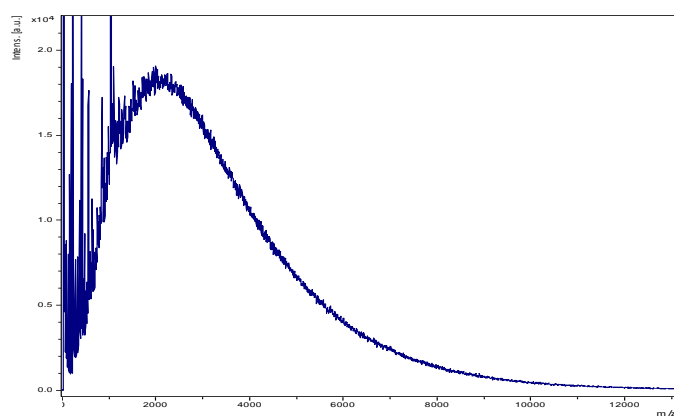


Figure SI-C22. MALDI-TOF MS of the Ziegler-type hydrogenation catalyst made with $[(\mathbf{1,5-COD})\text{Ir}(\mu\text{-O}_2\text{C}_8\text{H}_{15})_2]$ plus $[(t\text{-Bu})_2\text{Al}(\mu\text{-OH})]_3$ at Al/Ir = 2 **before the catalyst was used in cyclohexene hydrogenation**. Using the assumptions (i) that the observed broad peak is composed of only Ir atoms [36,37,38], and (ii) that the ionic charges are +1 [34,36,39], the corresponding diameter for the Ir_n cluster is 0.8 ± 0.3 nm, that is, $\text{Ir}_{\sim 20}$ on average. The details of experimental procedure for sample preparation and instrumentation are given in an earlier publication [33].

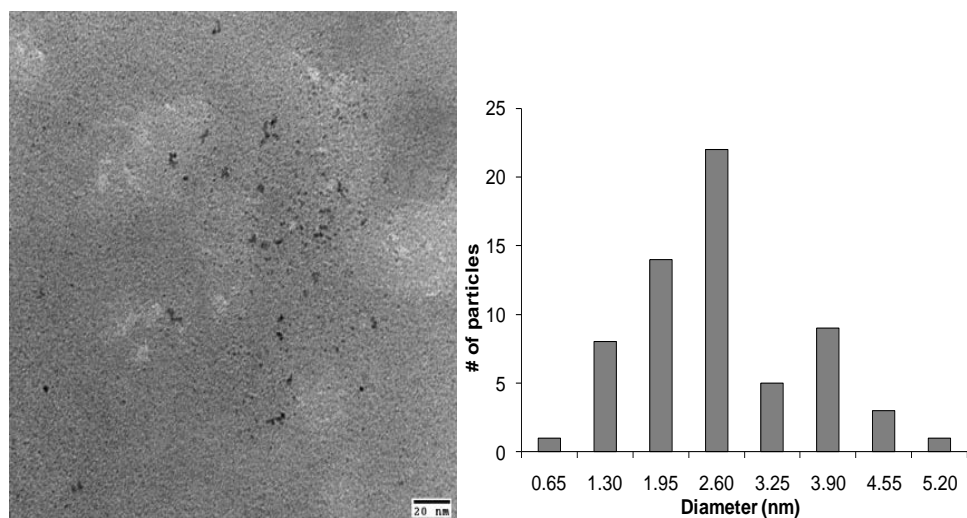


Figure SI-C23. TEM image and corresponding particle size histogram of the Ziegler-type hydrogenation catalyst sample made from $[\text{Ir}(1,5\text{-COD})(\mu\text{-O}_2\text{C}_8\text{H}_{15})_2]$ plus $[(t\text{-Bu})_2\text{Al}(\mu\text{-OH})_3]$ at $\text{Al}/\text{Ir} = 2$ **after the catalyst was used in cyclohexene hydrogenation**. The scale bar is 20 nm. Mean diameter from measurement of 65 nanoparticles is 2.6 ± 1.0 nm, corresponding on average to $\text{Ir}_{\sim 650}$.

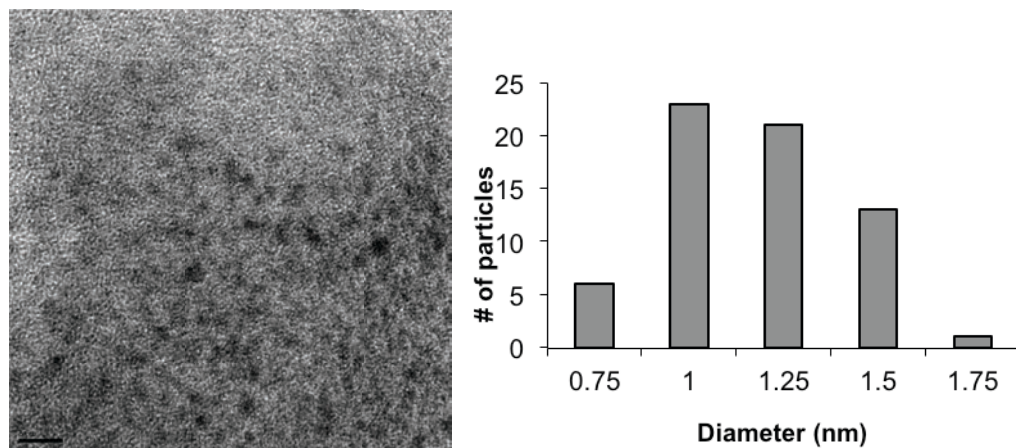


Figure SI-C24. TEM image and corresponding particle size histogram of the Ziegler-type hydrogenation catalyst sample made from $[\text{Ir}(1,5\text{-COD})(\mu\text{-O}_2\text{C}_8\text{H}_{15})_2]$ plus $\text{Al}(t\text{-Bu})_3$ at $\text{Al}/\text{Ir} = 2$ **before the catalyst was used in cyclohexene hydrogenation**. The scale bar is 5 nm. Mean diameter from measurement of 64 nanoparticles is 1.2 ± 0.2 nm correspond on average to $\text{Ir}_{\sim 60}$.

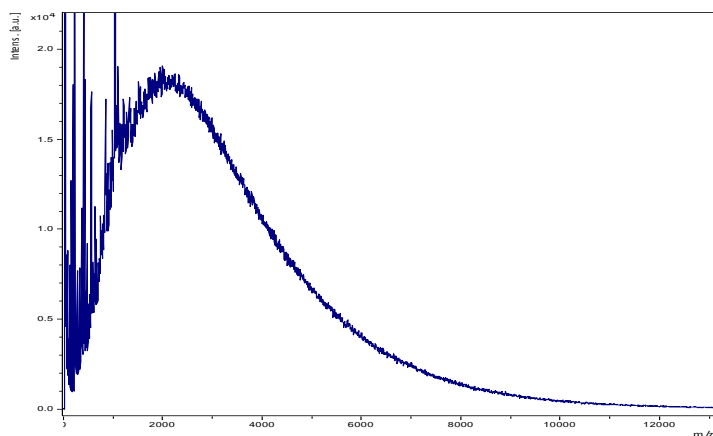


Figure SI-C25. MALDI-TOF MS of the Ziegler-type hydrogenation catalyst made from [(1,5-COD)Ir(μ -O₂C₈H₁₅)₂]₂ plus Al(*t*-Bu)₃ at Al/Ir = 2 before the catalyst was used in cyclohexene hydrogenation. Using the assumptions (i) that the observed broad peak is composed of only Ir atoms [34,35,36], and (ii) that the ionic charges are +1 [34,36,37], the corresponding diameter for the Ir_{*n*} cluster is 0.8 ± 0.3 nm, corresponding on average to Ir₋₂₀. The details of experimental procedure for sample preparation and instrumentation are given in an earlier publication [33].

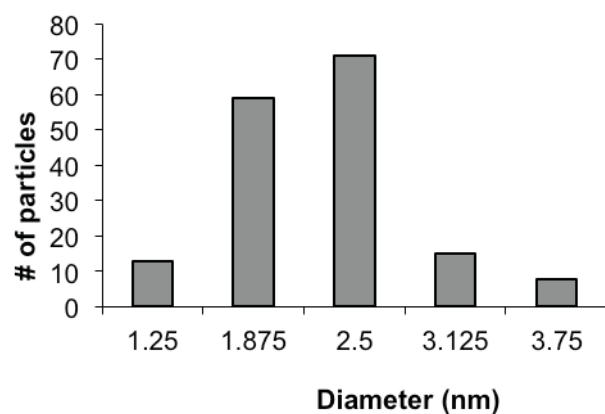
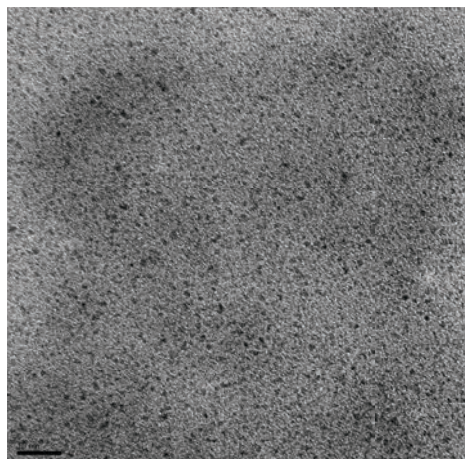


Figure SI-C26. TEM image and corresponding particle size histogram of the Ziegler-type hydrogenation catalyst sample made from $[\text{Ir}(\mathbf{1,5-COD})(\mu\text{-O}_2\text{C}_8\text{H}_{15})_2]$ plus $\text{Al}(t\text{-Bu})_3$ at $\text{Al}/\text{Ir} = 2$ after the catalyst was used in cyclohexene hydrogenation. The scale bar is 10 nm. Mean diameter from measurement of 166 nanoparticles is 2.3 ± 0.6 nm, corresponding on average to $\text{Ir}_{\sim 450}$.

Table SI-C5. Ir-Al bond distances of Ziegler-type hydrogenation catalysts made with [Ir(1,5-COD)(μ -O₂C₈H₁₅)₂ (Ir₂) plus AlEt₃. R: Experimentally determined interatomic distance for the Ir-Al single scattering path, σ^2 :The mean square variation in R due to static and dynamic disorder (Debye-Waller factor), N: Number of Ir or Al atoms in the first single scattering shell

Sample name	$R_{\text{Ir-Al}}$ (Å)	$N_{\text{Ir-Al}}$	$\sigma^2_{\text{Ir-Al}} \times 10^3$ (Å ²)
Ir ₂ + 1.5 AlEt ₃	2.49 ± 0.02	1.0 ± 0.9	7 ± 5
Ir ₂ + 2.0 AlEt ₃	2.51 ± 0.01	1.7 ± 0.8	8 ± 3
Ir ₂ + 2.5 AlEt ₃	2.51 ± 0.01	2 ± 1	8 ± 2
Ir ₂ + 3.0 AlEt ₃	2.51 ± 0.0	3 ± 1	8 ± 3
Ir ₂ + 5.0 AlEt ₃	2.5045*	3 ± 2	8 ± 4

*For this sample, this $R_{\text{Ir-Al}}$ parameter was not varied in the fit.

Table SI-C6. Compilation of visual observations at the end of cyclohexene hydrogenations with $[\text{Ir}(1,5\text{-COD})(\mu\text{-O}_2\text{C}_8\text{H}_{15})_2]$ or $[\text{Ir}(1,5\text{-COD})(\mu\text{-H})_4]$ plus AlEt_3 catalysts at Al/Ir ratios 0-5. The catalysts were used in cyclohexene hydrogenation immediately after they were prepared in cyclohexane solvent.

Initial Catalyst Components	Observations at the End of the Cyclohexene Hydrogenation	Implied Form of the Metal
$[\text{Ir}(1,5\text{-COD})(\mu\text{-H})_4] + 1 \text{ or } 2 \text{ AlEt}_3$	Clear, colorless solution with visually observable black particles	Bulk Ir(0) metal
$[\text{Ir}(1,5\text{-COD})(\mu\text{-H})_4] + 3 \text{ or } 5 \text{ AlEt}_3$	<i>Clear, brown solution</i> with visually observable black particles	<i>Ir_n nanoparticles plus</i> Bulk Ir(0) metal
$[\text{Ir}(1,5\text{-COD})(\mu\text{-H})_4]$	Clear, colorless solution with visually observable black particles	Bulk Ir(0) metal
$[\text{Ir}(1,5\text{-COD})(\mu\text{-H})_4] + 1 \text{ AlEt}_2$ (2-ethylhexanoate)	Clear, colorless solution with visually observable black particles	Bulk Ir(0) metal
$[\text{Ir}(1,5\text{-COD})(\mu\text{-O}_2\text{C}_8\text{H}_{15})_2]$	Orange solution* with visually observable black particles	Bulk Ir(0) metal*
$[\text{Ir}(1,5\text{-COD})(\mu\text{-O}_2\text{C}_8\text{H}_{15})_2] + 1 \text{ AlEt}_3$	Clear, colorless solution, visually observable black particles	Bulk Ir(0) metal
$[\text{Ir}(1,5\text{-COD})(\mu\text{-O}_2\text{C}_8\text{H}_{15})_2] + 2, 3 \text{ or } 5 \text{ AlEt}_3$	<i>Clear, brown solution</i>	<i>Ir_n nanoparticles</i>

* The orange color of the solution implies that there is some unreacted $[\text{Ir}(1,5\text{-COD})(\mu\text{-O}_2\text{C}_8\text{H}_{15})_2]$ precatalyst in the catalyst solution.

Table SI-C7. Maximum cyclohexene hydrogenation rates of the Ziegler-type hydrogenation catalysts prepared with $[\text{Ir}(\text{1,5-COD})(\mu\text{-O}_2\text{C}_8\text{H}_{15})_2]$ plus AlEt_3 at Al/Ir ratios of 1-5 and used in cyclohexene hydrogenation immediately after mixing $[\text{Ir}(\text{1,5-COD})(\mu\text{-O}_2\text{C}_8\text{H}_{15})_2]$ plus AlEt_3 (i.e., the catalysts are *not aged* before their use in hydrogenation).³ The hydrogenation solutions were prepared individually (in 2.5 mL portions) according to the procedure given in detail in Experimental section of main text under the heading “Hydrogenation Solution Preparation and Catalytic Cyclohexene Hydrogenations”

Al/Ir ratio	Maximum Hydrogenation Rate ^a (mmol/h)
1	28 ± 5
2	7 ± 4
3	1 ± 1
5	1 ± 1

^a The H_2 gas-to-solution mass transfer limited rate (MTL) for our apparatus, at 22.0 ± 0.1 °C and 1000 ± 10 rpm stirring rate (see the Experimental section entitled “Hydrogenation Solution Preparation and Catalytic Cyclohexene Hydrogenations” in the main text) is approximately ~ 80 psig/h (20 mmol/h) under the conditions of these experiments. Therefore, the maximum hydrogenation rate for Al/Ir ratio of 1 is under MTL.

³ Similar hydrogenations with $[\text{Ir}(\text{1,5-COD})(\mu\text{-O}_2\text{C}_8\text{H}_{15})_2]$ plus AlEt_3 , Al/Ir=0-5, were previously published [33]. There are some differences in the maximum hydrogenation rates obtained in current study vs those reported previously [33]. Observed differences in catalyst activity are, probably, due to differences in catalyst preparation and hydrogenation procedures used in this study vs those used in previous studies. The catalyst solutions in this study are prepared with [Ir] of 1.2 mM and are immediately used in cyclohexene hydrogenation *without aging*. In comparison, the catalyst solutions in the previous studies were prepared with Ir concentration of 0.6 mM and were aged for 9 h under N_2 atmosphere [33]. The catalyst solutions were prepared individually in this study whereas some of the catalyst solutions were prepared in larger batches (~ 9 -10 times larger in volume) in previous studies. The catalyst preparation procedure and variables are carefully chosen to be as close as possible to those used for NMR characterization studies. However, regardless of the differences between two sets of hydrogenations in this study and those published previously, all the catalysts prepared with $[(\text{1,5-COD})\text{Ir}(\mu\text{-O}_2\text{C}_8\text{H}_{15})_2]$ plus AlEt_3 at Al/Ir ratios of 0-5 are active in cyclohexene hydrogenation.

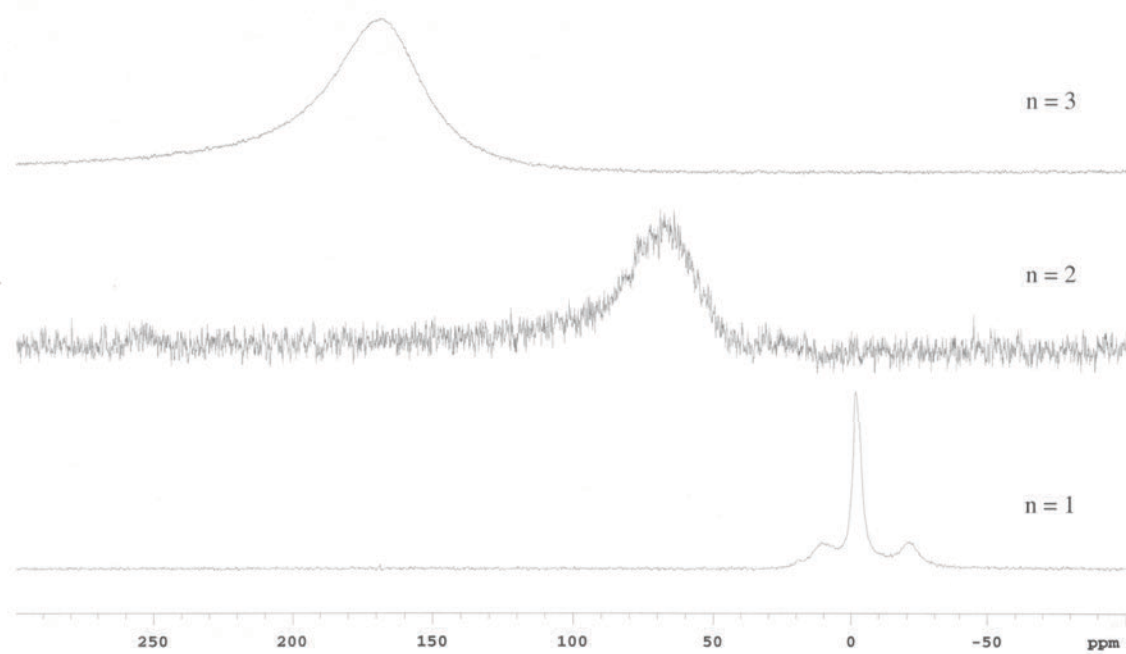
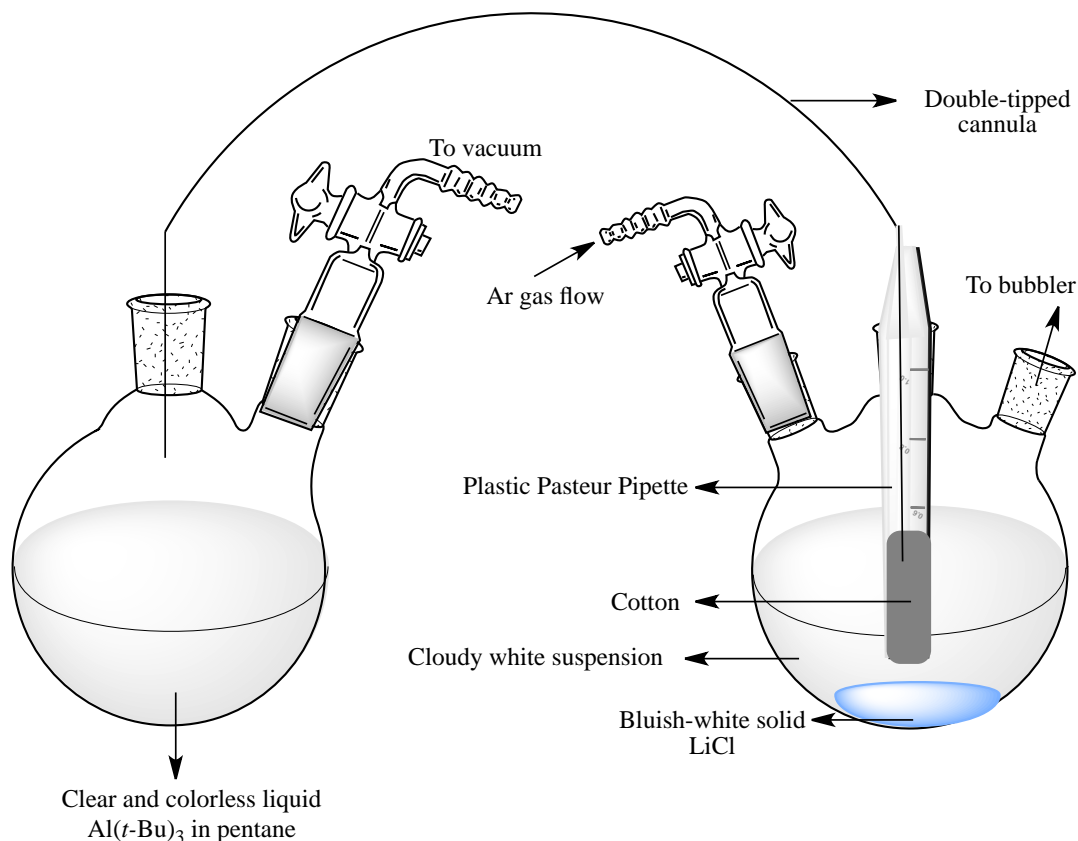


Figure SI-C27. ^{27}Al NMR spectra $[\text{Ir}(1,5\text{-COD})(\mu\text{-O}_2\text{C}_8\text{H}_{15})_2]$ plus AlEt_3 , $n=\text{Al}/\text{Ir}$, Ziegler-type catalysts in benzene- d_6 solvent. The results show that the signal at 170 ppm in neat AlEt_3 sample shifts to 0 ppm at Al/Ir ratio of 1 and at 80 ppm at Al/Ir ratio of 2. These upfield shifts suggest interaction of Al centers with metallic Ir atoms on the surface of $\text{Ir}(0)_n$ nanoparticles as discussed briefly in the main text.



Scheme SI-C3. A schematic representation of the reverse filtration technique. A reverse filtration was applied to separate the liquid portion containing the desired $\text{Al}(t\text{-Bu})_3$ from the bluish-gray LiCl precipitate. The top of a plastic Pasteur pipette was cut and then the cut pipette was stuffed with cotton under air. One end of a cannula was then inserted into the cotton layer through the other end (i.e., the end not stuffed with cotton) of that cut pipette. The Pasteur pipette with the stuffed cotton and the attached cannula was then inserted into the three-necked 500 mL round-bottomed flask containing $\text{Al}(t\text{-Bu})_3$ all while under Ar flow. Separately, another 500 mL round-bottom Schlenk flask equipped with a side arm was sealed under Ar flow using two rubber septa. The free end of the cannula (i.e., the end not inserted through cut pipette) was inserted through the rubber septum of the Ar filled but otherwise empty 500 mL round-bottomed Schlenk flask shown on the left above. The Pasteur pipette was dipped into the cloudy white suspension in the right round bottomed flask and then a slight vacuum ($\leq 10^{-2}$ mmHg) was applied through the side arm of the empty 500 mL round-bottomed flask. A clear solution was collected in the 500 mL round-bottomed flask.

4. Additional Control Experiments Performed with the Ziegler-type Catalyst Made with $[\text{Ir}(1,5\text{-COD})(\mu\text{-O}_2\text{C}_8\text{H}_{15})_2]$ or $[\text{Ir}(1,5\text{-COD})(\mu\text{-H})_4]$ plus AlEt_3 (Figure SI-C25, SI-C27, SI-C28, Table SI-C8) or $\text{Al}(t\text{-Bu})_3$ (Figure SI-C26)

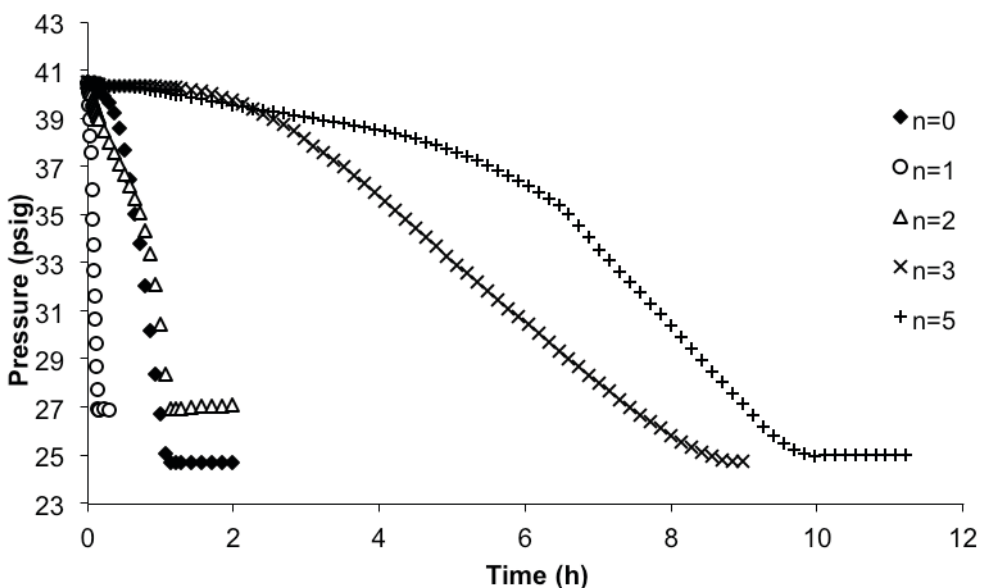


Figure SI-C28. Representative plots of H_2 pressure vs time data for cyclohexene hydrogenations starting with $[\text{Ir}(1,5\text{-COD})(\mu\text{-O}_2\text{C}_8\text{H}_{15})_2]$ plus AlEt_3 catalysts with $\text{Al}/\text{Ir}=0\text{-}5$ ($n=\text{Al}/\text{Ir}$ ratio). The hydrogenation solutions were prepared individually (in 2.5 mL portions) according to the procedure given in detail in Experimental section of main text under the heading “Hydrogenation Solution Preparation and Catalytic Cyclohexene Hydrogenations”. Conditions for hydrogenations are as follows: $[\text{Ir}]=1.2$ mM, cyclohexane solvent, $[\text{cyclohexene}]_{\text{initial}} = 1.65$ M, 22.0 ± 0.1 °C and 40 ± 1 psig H_2 [40]. The catalyst solution appears clear with visually observable black $\text{Ir}(0)$ bulk particles at the end of hydrogenation at Al/Ir ratios of 0 and 1. A clear and dark-brown solution is obtained at the end of hydrogenation at Al/Ir ratios of 2, 3 or 5 indicating $\text{Ir}(0)_n$ nanoparticle formation (Table SI-C7).

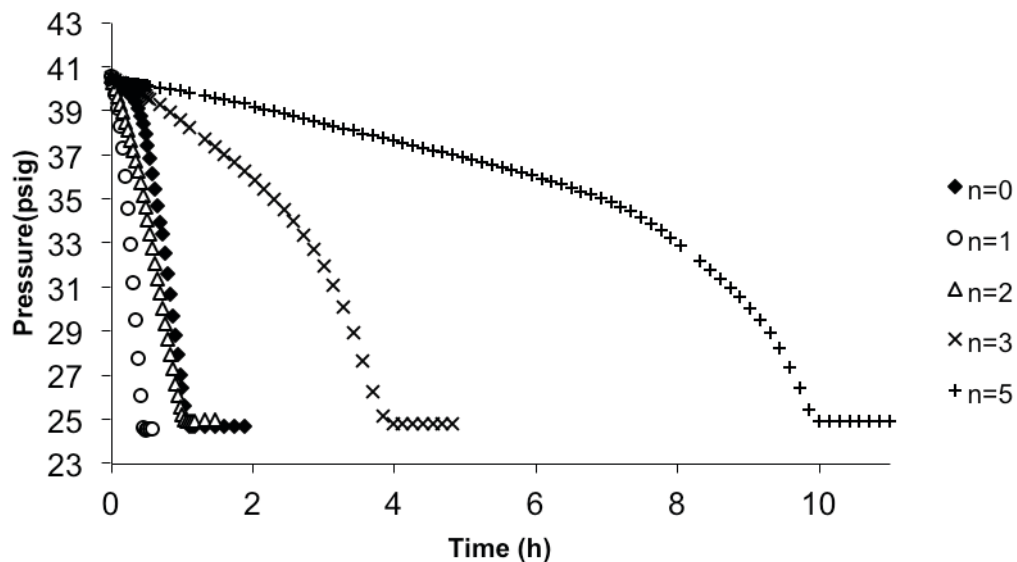


Figure SI-C29. Representative cyclohexene hydrogenation curves (Pressure vs Time) starting with $[\text{Ir}(1,5\text{-COD})(\mu\text{-O}_2\text{C}_8\text{H}_{15})_2]$ plus $\text{Al}(\text{t-Bu})_3$ catalysts at Al/Ir ratios of 0-5 ($n=\text{Al/Ir}$ ratio). Conditions for hydrogenations are as follows: $[\text{Ir}]=1.2$ mM, cyclohexane solvent, $[\text{cyclohexene}]_{\text{initial}} = 1.65$ M, 22.0 ± 0.1 °C and 40 ± 1 psig H_2 . The catalyst solution appears clear with visually observable black Ir(0) bulk particles at the end of hydrogenation at Al/Ir ratios of 0 and 1. A clear and dark-brown solution is obtained at the end of hydrogenation at Al/Ir ratios of 2, 3 or 5 indicating $\text{Ir}(0)_n$ nanoparticles. These observations are similar to those obtained for the catalyst made from $[\text{Ir}(1,5\text{-COD})(\mu\text{-O}_2\text{C}_8\text{H}_{15})_2]$ plus AlEt_3 (Figure SI-C25 and Table SI-C7).

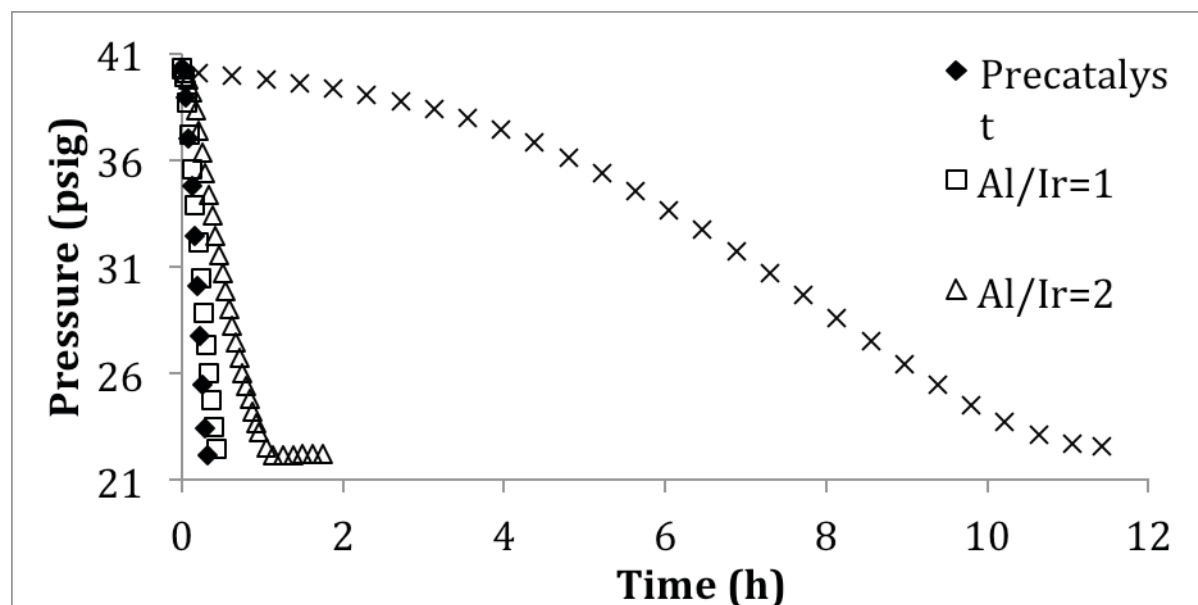


Figure SI-C30. Representative cyclohexene hydrogenation curves (Pressure vs Time) starting with [(1,5-COD)Ir(μ -H)₄] plus AlEt₃ catalysts at Al/Ir ratios of 1-3 and precatalyst [(1,5-COD)Ir(μ -H)₄]. Conditions for hydrogenations are as follows: [Ir]=1.2 mM, cyclohexane solvent, [cyclohexene]_{initial} = 1.65 M, 22.0 \pm 0.1 $^{\circ}$ C and 40 \pm 1 psig H₂. A clear and colorless solution with visually observable black particles, indicative of Ir bulk, is observed at the end of hydrogenation, separately, with the precatalyst and also at Al/Ir ratios of 1 and 2. The catalyst solution appears clear and brown with visually observable black particles at the end of hydrogenation at Al/Ir ratios of 3 or 5. This observation indicates presence of Ir_n nanoparticles in addition to some Ir bulk in the post-catalysis solution at Al/Ir ratios of 3 or 5 (Table SI-C6). The observation of some bulk Ir(0) metal does not rule out [Ir(1,5-COD)H]₄ as a competent intermediate in the formation of Ir(0)_n nanoparticles. In fact, it probably argues the opposite since Ir(0) is so quickly formed from this potential intermediate (i.e., the issue then possibly being one of the relative kinetics of Ir(0)_n nanoparticle stabilization vs agglomeration to bulk Ir(0) metal formation.

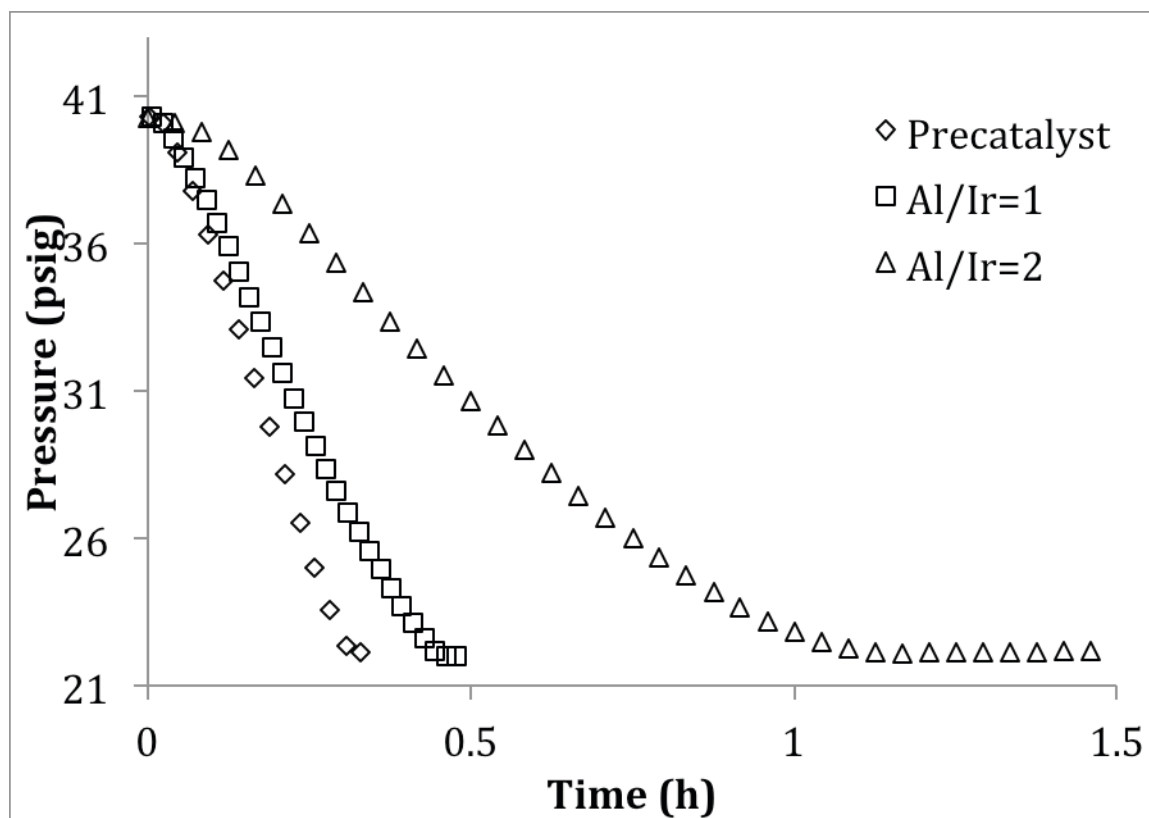


Figure SI-C31. Expanded version of the first 1.5 hours of Figure SI-C25 (above). Representative cyclohexene hydrogenation curves (Pressure vs Time) starting with [(1,5-COD)Ir(μ -H)₄] plus AlEt₃ catalysts at Al/Ir ratios of 1-2 and precatalyst, [(1,5-COD)Ir(μ -H)₄]. Conditions for hydrogenations are as follows: [Ir]=1.2 mM, cyclohexane solvent, [cyclohexene]_{initial} = 1.65 M, 22.0 ± 0.1 °C and 40 ± 1 psig H₂.

Table SI-C8. Maximum rates of cyclohexene hydrogenation using [(1,5-COD)Ir(μ -H)]₄ plus AlEt₃ Ziegler-type catalysts under standard conditions of catalyst preparation and hydrogenation.

Al/Ir ratio	Max Hydrogenation Rate of As-Prepared Catalyst (psig/h)
0 ^{a,d}	60 \pm 6
1 ^a	46 \pm 5
2 ^a	19 \pm 2
3 ^b	2 \pm 1
5 ^b	3 \pm 3
10, 15 or 20 ^c	0

^a A clear and colorless solution with visually observable black particles, indicating bulk Ir is observed at the end of hydrogenation at these Al/Ir ratios (see also Table SI-C5).

^b The catalyst solution appears clear and brown with visually observable black particles at the end of hydrogenation at these Al/Ir ratios. This observation indicates presence of Ir_n nanoparticles in addition to some Ir bulk (see also Table SI-C5).

^c The control experiment with [(1,5-COD)Ir(μ -H)]₄ plus AlEt₃ at Al/Ir ratio of 15 is performed once. The H₂(g) pressure stayed constant at ~40 psig for 10 h.

^d The H₂ gas-to-solution mass transfer limited rate for our apparatus, at 22.0 \pm 0.1 °C and 1000 \pm 10 rpm stirring rate (see the Experimental section entitled “Hydrogenation Solution Preparation and Catalytic Cyclohexene Hydrogenations” in the main text) is approximately ~80 psig/h under the conditions of these experiments.

REFERENCES

- [1] W.M. Alley, I.K. Hamdemir, K.A. Johnson, R.G. Finke, *J. Mol. Catal. A: Chem.* 315 (2010) 1-27.
- [2] F.K. Schmidt, G.V. Ratovskii, T.V. Dmitrieva, I.N. Ivleva, Y.G. Borodko, *J. Organomet. Chem.* 256 (1983) 309-329.
- [3] S. Pasykiewicz, A. Pietrzykowski, K. Dowbor, *J. Organomet. Chem.* 78 (1974) 55-59.
- [4] F.K. Schmidt, L.O. Nindakova, B.A. Shainyan, V.V. Saraev, N.N. Chipanina, V.A. Umanetz, *J. Mol. Catal. A: Chem.* 235 (2005) 161-172.
- [5] L.O. Nindakova, F.K. Schmidt, V.V. Saraev, B.A. Shainyan, N.N. Chipanina, V.A. Umanets, L.N. Belonogova, D.-S.D. Toryashinova, *Kinetics and Catalysis* 47 (2006) 54-63.
- [6] L.B. Belykh, T.V. Goremyka, N.I. Skripov, V.A. Umanets, F.K. Schmidt, *Kinet. Catalysis* 47 (2006) 367-374.
- [7] H. Bönemann, W. Brijoux, R. Brinkmann, U. Endruschat, W. Hofstadt, K. Angermund, *Revue Roumaine de Chimie* 44 (1999) 1003-1010.
- [8] K. Angermund, M. Bühl, E. Dinjus, U. Endruschat, F. Gassner, H.-G. Haubold, J. Hormes, G. Köhl, F.T. Mauschick, H. Modrow, R. Mörtel, R. Mynott, B. Tesche, T. Vad, N. Waldöfner, H. Bönemann, *Angew. Chem. Int. Ed.* 41 (2002) 4041-4044.
- [9] K. Angermund, M. Bühl, D. Eckhard, U. Endruschat, F. T. Mauschick, R. Mörtel, R. Mynott, B. Tesche, N. Waldöfner, H. Bönemann, G. Köhl, H. Modrow, J. Hormes, E. Dinjus, F. Gassner, H.-G. Haubold, T. Vad, M. Kaupp, *J. Phys. Chem. B.* 107 (2003) 7507-7515.
- [10] H. Bönemann, N. Waldöfner, H.-G. Haubold, T. Vad, *Chem. Mater.* 14 (2002) 1115-1120.
- [11] W.R. Kroll, W. Naegele, *J. Organomet. Chem.* 19 (1969) 439-443.
- [12] S. Pasykiewicz, K. Dowbor, *J. Organomet. Chem.* 78 (1974) 49-53.
- [13] J. Barrault, M. Blanchard, A. Derouault, M. Ksibi, M. I. Zaki, *J. Mol. Catal.* 93 (1994) 289-304.
- [14] K.A. Klinedinst, M. Boudart, *J. Catal.* 28 (1973) 322-328.
- [15] A.R. Barron, in: J. Scheirs, W. Kaminsky (Eds.), *Metallocene-based Polyolefins – Preparation, Properties and Technology*, John Wiley and Sons New York, 2000; Vol. 1, pp. 33-69.

- [16] J.N. Pedeutour, K. Radhakrishnan, H. Cramail, A. Deffieux, *Macromol. Rapid Commun.* 22 (2001) 1095-1123.
- [17] H.W. Roesky, M.G. Walawalkar, R. Murugavel, *Acc. Chem. Res.* 34 (2001) 201-211.
- [18] S. Pasynkiewicz, *Polyhedron* 9 (1990) 429-453.
- [19] V.I. Irzhak, T.F. Irzhak, P.E. Matkovski, A.K. Lee, B.G. Song, in *Polymer Yearbook*, Harwood Academic Publishers Singapore, 2000; Vol. 1, pp. 137-145.
- [20] J.N. Pedeutour, K. Radhakrishnan, H. Cramail, A. Deffieux, *Macromol. Rapid Commun.* 22 (2001) 1095-1123.
- [21] H. Sinn, *Macromol. Symp.* 97 (1995) 27-52.
- [22] S. Pasynkiewicz, *Polyhedron* 9 (1990) 429-453.
- [23] I. Tritto, C. Mealares, M.C. Sacchi, P. Locatelli, *Macromol. Chem. Phys.* 198 (1997) 3963-3977.
- [24] E. Zurek, T. Ziegler, *Prog. Polym. Sci.* 29 (2004) 107-148.
- [25] M.R. Mason, J.M. Smith, S.G. Bott, A.R. Barron, *J. Am. Chem. Soc.* 115 (1993) 4971-4984.
- [26] A.R. Barron, *Macromol. Sym.* 97 (1995) 15-25.
- [27] K. Tamai, T. Saito, Y. Uchida, A. Misono, *Bull. Chem. Soc.* 38 (1965) 1575-1580.
- [28] K. Fischer, K. Jonas, P. Misbach, R. Stabba, G. Wilke, *Angew. Int. Ed. Engl.* 12 (1973) 943-1026.
- [29] M.I. Prince, K. Weiss, *J. Organomet. Chem.* 2 (1964) 166-183.
- [30] D.F. Shriver, M.A. Drezdson, *The Manipulation of Air-Sensitive Compounds*, 2nd. Ed.; John Wiley and Sons: New York, 1986.
- [31] J.N. Kemsley, *C. En. News* 87 (2009) 29-31.
- [32] K.-H. Yih, I.K. Hamdemir, J.E. Mondloch, E. Bayram, S. Özkar, R. Vasic, A.I. Frenkel, O. Anderson, R.G. Finke, *Inorg. Chem.* 51 (2012) 3186-3183.
- [33] M.R. Mason, J.M. Smith, S.G. Bott, A.R. Barron, *J. Am. Chem. Soc.* 115 (1993) 4971-4984.
- [34] W.M. Alley, I.K. Hamdemir, Q. Wang, A. Frenkel, L. Li, J.C. Yang, L.D. Menard, R.G. Nuzzo, S. Özkar, K.A. Johnson, R.G. Finke, *Inorg. Chem.* 49 (2010) 8131-8147.

[35] W.M. Alley, I.K. Hamdemir, Q. Wang, A. Frenkel, L. Li, J.C. Yang, L.D. Menard, R.G. Nuzzo, S. Özkar, K.A. Johnson, R.G. Finke, *Inorg. Chem.* 49 (2010) 8131-8147.

[36] R.L. Whetten, J.T. Khoury, M.M. Alvarez, S. Murthy, I. Vezmar, Z.L. Wang, P.W. Stephens, C.L. Cleveland, W.D. Luedtke, U. Landman, *Adv. Mater.* 8 (1996) 428-433.

[37] G.A. Khitrov, G.F. Strouse, *J. Am. Chem. Soc.* 125 (2003) 10465-10469.

[38] T. Kuzuya, Y. Tai, S. Yamamuro, K. Sumiyama, *Chem. Phys. Lett.* 407 (2005) 460-463.

[39] L. Maya, C.H. Chen, K.A. Stevenson, E.A. Kenik, S.L. Allman, T.G. Thundat, *J. Nanoparticle Res.* 4 (2002) 417-422.

[40] W.M. Alley, C.W. Girard, S. Özkar, R.G. Finke, *Inorg. Chem.* 48 (2009) 1114-1121.

CHAPTER V

SYNTHESIS AND CHARACTERIZATION OF [Ir(1,5-CYCLOOCTADIENE)(μ -H)]₄: A TETRAMETALLIC Ir₄H₄-CORE, COORDINATIVELY UNSATURATED CLUSTER

This dissertation chapter contains the manuscript of a paper published in the *Inorg. Chem.* **2012**, *51*, 3186-3193. This chapter describes (i) the synthesis of the previously unavailable [Ir(1,5-COD)(μ -H)]₄ complex in 78% initial, and 55% recrystallized, yield starting from commercially available LiBEt₃H and [Ir(1,5-COD)(μ -Cl)]₂ in the presence of excess 1,5-COD in THF; and (ii) the characterization of the resultant black crystal of [Ir(1,5-COD)(μ -H)]₄ using single-crystal XRD, XAFS, ESI-MS, UV-visible, IR, and NMR.

The initial synthesis attempts resulting in the desired dark-green powder of [Ir(1,5-COD)(μ -H)]₄, in low yield (~1%), were performed by both Isil K. Hamdemir and Ercan Bayram. The black crystal of [Ir(1,5-COD)(μ -H)]₄ in 78% initial, and 55% recrystallized, yield was obtained by Kuang-Hway Yih. The sample of black crystal of [Ir(1,5-COD)(μ -H)]₄ was prepared and then submitted to X-Ray crystallography structure determination were done by Kuang-Hway Yih. The XRD data was interpreted by Isil K. Hamdemir in consultation with Oren P. Anderson. The sample preparation and submission to XAFS analysis were performed by Kuang-Hway Yih. The XAFS data was collected by Relja Vasić and interpreted by Isil K. Hamdemir in consultation with Anatoly I. Frenkel. Additional characterization data (ESI-MS, UV-Visible, IR and NMR) on a black crystal were obtained by Kuang-Hway Yih and interpreted by Isil K. Hamdemir. Initial characterization studies on the initial, ~1% yield dark-green powder using ESI-MS, NMR, IR, UV-Visible and XPS (given in Supporting Information) were performed by Isil K. Hamdemir and were the key results which showed that the desired [Ir(1,5-COD)(μ -H)]₄ had been prepared, albeit in low yield. Control experiments (given in Supporting Information_D), performed to

obtain higher purity and yields were performed by Kuang-Hway Yih. The initial draft of the paper, subsequent drafts including the final draft and preparation of the document for publication were performed by Isil K. Hamdemir with light editing by Saim Özkar, Kuang-Hway Yih, Joseph E. Mondloch and moderate editing by Richard G. Finke (ca. 33 hours).

Synopsis

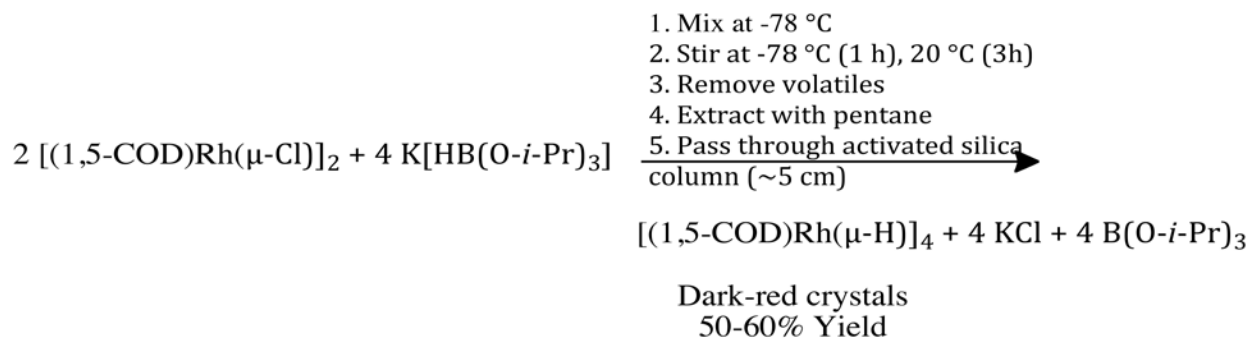
Reported herein is the synthesis of the previously unknown $[\text{Ir}(1,5\text{-COD})(\mu\text{-H})_4]$ (where 1,5-COD = 1,5 cyclooctadiene), from commercially available $[\text{Ir}(1,5\text{-COD})\text{Cl}]_2$ and LiBEt_3H in the presence of excess 1,5-COD in 78% initial, and 55% recrystallized, yield plus its unequivocal characterization via single crystal X-Ray diffraction (XRD), X-ray absorption fine structure (XAFS) spectroscopy, electrospray/atmospheric pressure chemical ionization mass spectrometry (ESI MS) and UV-Visible (UV-Vis), infrared (IR) and nuclear magnetic resonance (NMR) spectroscopies. The resultant product parallels—but the successful synthesis is different than, *vide infra*—that of the known and valuable Rh congener precatalyst and synthon, $[\text{Rh}(1,5\text{-COD})(\mu\text{-H})_4]$. Extensive characterization reveals that a black crystal of $[\text{Ir}(1,5\text{-COD})(\mu\text{-H})_4]$ is composed of a distorted tetrahedral, D_{2d} symmetry Ir_4 core with two long (2.90728(17) and 2.91138(17) Å) and four short Ir-Ir (2.78680(12)-2.78798(12) Å) bond distances. One 1,5-COD and two edge-bridging hydrides are bound to each Ir atom, the Ir-H-Ir span the shorter Ir-Ir bond distances. The XAFS provides excellent agreement with the XRD-obtained Ir_4 core structure, results with both provide considerable confidence in the XAFS methodology and set the stage for future XAFS in applications employing this Ir_4H_4 and related tetranuclear clusters. The $[\text{Ir}(1,5\text{-COD})(\mu\text{-H})_4]$ complex is of interest for at least five reasons, as detailed in the Conclusions section.

1. Introduction

Molecular metal clusters [1] containing four metal atoms, M_4 , are an interesting, increasingly important and evolving area of inorganic, organometallic, catalytic and related sciences. Tetrametallic clusters of Ru, Os, Rh or Ir have been synthesized, fully characterized and used as precatalysts for the catalytic hydrogenation of alkenes, arenes, CO, aldehydes and ketones as

well as in hydroformylation, cyclooligomerization, cyclization and polymerization reactions [2]. Known tetrametallic complexes of group 9 metals including Rh, Ir and Co, and which contain a $[M(\mu-H)]_4$ core, include $[Rh(1,5-COD)(\mu-H)]_4$ [3], $[Ir(CO)(\mu-H)H(PPh_3)]_4$ [4], $[Ir(\eta^5-C_5Me_5)(\mu-H)]_4(BF_4)_2$ [5], $[Co(\eta^5-C_5H_5)Co(\mu-H)]_4$ [6] and $[Co(\eta^5-C_5Me_4Et)(\mu-H)]_4$ [7].

From the above known $[M(\mu-H)]_4$ core complexes, the tetrarhodium complex, $[Rh(1,5-COD)(\mu-H)]_4$, is particularly relevant to the present work. This $[Rh(1,5-COD)(\mu-H)]_4$ complex was first synthesized by Muetterties and coworkers starting with the commercially available $[Rh(1,5-COD)(\mu-Cl)]_2$ complex and $K[HB(O-*i*-Pr)_3]$ as detailed in Scheme 5.1 [3]



Scheme 5.1. A balanced reaction stoichiometry and the reaction conditions for the synthesis of $[Rh(1,5-COD)(\mu-H)]_4$ (adapted from reference 4).

A single crystal structural investigation revealed the Rh_4 core, with 2 long and 4 short Rh-Rh distances. In that publication, hydrides were located using difference Fourier techniques in between two Rh atoms connected by short Rh-Rh distances [3]. The assignment of four short bonds to Rh-H-Rh groups is consistent in a general way with the prior literature [8]. The $[Rh(1,5-COD)(\mu-H)]_4$ proved to be a good precatalyst for the hydrogenation of toluene in cyclohexane- d_{12} [9] and the hydrogenation of carbon dioxide [9]. The active catalyst species is claimed to be rhodium metal under toluene hydrogenation conditions. Kinetic studies performed

on catalytic carbon dioxide hydrogenation system suggested a neutral rhodium(I)hydride species $[\text{Rh}(\text{H})(\text{Ph}_2\text{P}(\text{CH}_2)_4\text{PPh}_2)]_x$, where $x=1$ or $2-4$ as the active catalyst [9c].

Somewhat surprisingly, the Ir-analogue of the above Rh complex, $[\text{Ir}(1,5\text{-COD})(\mu\text{-H})]_4$, has not been previously described, mostly likely because attempted syntheses, analogous to that of the Rh congener, *fail* (yields $\leq 1\%$, vide infra). The net 56 total electron $[\text{Ir}(1,5\text{-COD})(\mu\text{-H})]_4$ complex has a formal 17 electron count at each Ir, and thus is coordinatively unsaturated.

Our recent work on Ir-based models of Ziegler-type industrial hydrogenation catalyst prepared from $[\text{Ir}(1,5\text{-COD})(\mu\text{-O}_2\text{C}_8\text{H}_{15})]_2$ plus AlEt_3 revealed that Ir_4 species are a dominant, initial form of Ir present. [10] Hence, $[\text{Ir}(1,5\text{-COD})(\mu\text{-H})]_4$ with its Ir_4H_4 core (vide infra) is of interest as a new precursor for testing the formation and stabilization mechanisms of such Ziegler-type hydrogenation catalysts [10,11]. More specifically, the new complex $[\text{Ir}(1,5\text{-COD})(\mu\text{-H})]_4$ is of value as a fully compositionally and structurally characterized Ir_4 analog of the on average Co_4 -based, subnanometer clusters identified by XAFS as a dominant species in Co-based Ziegler-type industrial hydrogenation catalysts. Such Ziegler-type industrial hydrogenation catalysts [12] are used industrially to produce styrenic block copolymers at a level of $\sim 1.7 \times 10^5$ metric tons/year [13]. In addition, $[\text{Ir}(1,5\text{-COD})(\mu\text{-H})]_4$ is of considerable interest as a possible, Ir-H containing, tetrametallic Ir_4H_4 intermediate in the nucleation and growth of $\text{Ir}(0)_n$ nanoclusters starting with $(\text{COD})\text{Ir}^+$ precatalysts [14] and with stabilizers such as $[\text{P}_2\text{W}_{15}\text{Nb}_3\text{O}_{62}]^{9-}$, HPO_4^{2-} , and AlEt_3 [10,11,12,15]. Whether or not such polymetallic metal-hydride $(\text{M-H})_n$ species are key intermediates in $\text{M}(0)_n$ nanoparticle formation—rather than the presently assumed $\text{M}(0)_n$ intermediates—remains controversial. The availability of precatalysts and possible intermediates derivable from $[\text{Ir}(1,5\text{-COD})(\mu\text{-H})]_4$ opens up the possibility of QEXAFS and other direct-method tests with such discrete, fully-characterized, Ir_4H_4 core complexes [14].

Herein, we report (i) the 78% initial, and 55% recrystallized, yield synthesis of the previously unknown $[\text{Ir}(1,5\text{-COD})(\mu\text{-H})_4]$ starting from commercially available precursor $[\text{Ir}(1,5\text{-COD})\text{Cl}]_2$ and LiBEt_3H in which *added, excess 1,5-COD* is one key to the improved yield (vs <1% by the literature routes for the Rh congener, vide infra), and then (ii) the complete characterization of the resultant pure, crystalline product by single crystal XRD, XAFS, ESI MS, UV-vis, IR and NMR. There are at least 5 reasons (a couple of which are given above) as to why the present complex is of interest, a full list of which is given as part of the Summary and Possible Future Directions.

2. Experimental.

Materials. All manipulations were performed under N_2 in a Vacuum Atmospheres drybox (≤ 5 ppm O_2 as monitored by a Vacuum Atmospheres O_2 -level monitor) or, where noted, using a Schlenk line. All glassware was dried overnight in an oven at 160°C , cooled under vacuum in a desiccator and then transferred into the drybox while still in desiccator and under vacuum. $[(1,5\text{-COD})\text{Ir}(\mu\text{-Cl})_2]$ (an orange powder, Strem Chemicals, 99%), LiBEt_3H (as a colorless solution in tetrahydrofuran, 1.0 M, Aldrich), toluene (Aldrich, 99.8%, anhydrous) and benzene- d_6 (Cambridge Isotope Laboratories, Inc., 99.5%, w/o TMS) were used as received. Tetrahydrofuran (THF, Mallinckrodt Chemicals AR ACS, 500 mL), *n*-hexane (Sigma-Aldrich, Reagent Plus, $\geq 99\%$, 500 mL) and cyclohexane (Sigma-Aldrich, 99.5 %, $\text{H}_2\text{O} < 0.001\%$) were distilled over Na/benzophenone under $\text{N}_2(\text{g})$ and transferred into the drybox under air-free conditions. Acetone (Burdick and Jackson, $>99.9\%$ purity, 0.44% water) and H_2O (Nanopure ultrapure H_2O system, D4754) were degassed by connecting to a Schlenk line and then passing Ar through the solution for five minutes before transferring into the drybox.

Synthesis of [Ir(1,5-COD)(μ -H)]₄: In the drybox the orange powdered [Ir(1,5-COD)Cl]₂ (1.3434 g, 2 mmol) was weighed out and then transferred into a 100 mL round-bottom Schlenk flask equipped with a side arm and a 5/8 by 5/16 in. Teflon-coated magnetic stirbar. The flask was sealed, removed from the drybox, and placed on a Schlenk line under Ar via its side arm. Next, 70 mL of room temperature THF was added to the flask using a cannula forming an orange solution with some undissolved orange powder. The flask containing the orange solution of [Ir(1,5-COD)Cl]₂ was placed in an acetone/dry ice bath at -78°C and stirred for 15 min. A 2.5 mL gas-tight syringe was purged three times with Ar using a Schlenk line and then used to measure out 4 mL (4 mmol) of LiBEt₃H. The LiBEt₃H was then added dropwise to the orange [Ir(1,5-COD)Cl]₂ solution under an Ar atmosphere while vigorously stirring. The original orange color of the solution changed to dark-brown upon the dropwise addition of the LiBEt₃H. The resulting solution was stirred at -78°C for an additional 10 min and then warmed to room temperature. The solution slowly turned from dark-brown to dark-green within 10 min of additional stirring at room temperature. 1,5-COD (12.3 mL, 25 eq per Ir) was measured out with a 20 mL gas-tight syringe purged with Ar, and then added over 5-10 min to the dark-green solution. The resulting bright-green solution was stirred at room temperature for 24 h and then concentrated to ~5 mL under vacuum at room temperature using Schlenk line. A visually apparent black powder was formed in the bright-green solution. The black powder was separated from bright-green solution under Ar using a medium porosity glass-frit of ca. 16 microns pore size. The open end of the glass-frit was sealed by a rubber septum. The black powder collected on top of the glass-frit was washed with degassed H₂O (5 mL x 2) and then degassed acetone (5 mL x 3) using a gas-tight syringe that was previously purged with Ar. The black powder was then dried overnight under vacuum at room temperature resulting in black

powder (0.471 g, 78% yield) that was transported to the drybox and stored in the glass-frit sealed from the drybox atmosphere via a rubber septum.

Crystallization was accomplished by weighing out 92 mg of the black, powdered $[\text{Ir}(1,5\text{-COD})(\mu\text{-H})_4]$ in the drybox and transferring it into a 15 mL Schlenk tube. The Schlenk tube was then sealed, removed from the drybox, and placed on a Schlenk line under Ar. Next, 2.0 mL of room temperature, *n*-pentane/THF (20/1) mixture was measured out using a gas-tight syringe and then added to the tube. The stopper in the Schlenk tube containing the black powder and THF was black-taped to secure it. The contents of the Schlenk tube were heated to approximately 66 °C using a heat gun while the taped-stopper was held manually to secure it during boiling the minimal boiling. The resulting solution was clear, bright-green and homogeneous with no observable solid or particulate mass. The Schlenk tube was then placed in a -20 °C freezer. Black crystals of $[\text{Ir}(1,5\text{-COD})(\mu\text{-H})_4]$ were obtained in the tube after 4 h at -20 °. At the end of 4 h, the Schlenk tube containing crystals was connected to a Schlenk line, and the liquid portion was removed using a cannula. The tube containing black $[\text{Ir}(1,5\text{-COD})(\mu\text{-H})_4]$ crystals (64 mg, 55% overall yield) was kept under vacuum overnight. The crystalline material was then transported back into the drybox and stored in a 2 mL vial. The $[\text{Ir}(1,5\text{-COD})(\mu\text{-H})_4]$ complex is air-stable in crystalline form. Anal. calcd for $\text{C}_{32}\text{H}_{52}\text{Ir}_4$ (mol. wt. 1205.64 g/mol): C, 31.88; H, 4.35%. Found: C, 31.74; H, 4.28%. ESI MS peaks (*m/z* in Da, assigned ion): 1205.2478, $[\text{C}_{32}\text{H}_{51}\text{Ir}_4]^+$; 1507.3229 $[\text{C}_{40}\text{H}_{66}\text{Ir}_5]^+$. UV-Vis peaks (nm): 476, 626. IR bands (cm^{-1}): 697.90, 766.66, 815.67, 859.46, 866.74, 994.42, 1072.04, 1146.95, 1167.72, 1203.64, 1233.36, 1295.73, 1320.87, 1423.13, 1437.37, 1469.38, 2818.14, 2867.42, 2907.91, 2936.42, 2985.69. ^1H NMR in benzene- d_6 (δ in ppm, (multiplicity, number of H)): -2.89 (s, 1), 1.37 (m, 4), 2.09 (m, 4), 4.14 (m, 4). ^{13}C NMR in benzene- d_6 (δ in ppm): 68.64, 33.29.

Instrumentation and Sample Preparation.

X-Ray Diffraction. Single crystals of $[(1,5\text{-COD})\text{Ir}(\mu\text{-H})_4]$ suitable for X-ray diffraction analysis were grown by recrystallization from 20/1 *n*-pentane/THF using the crystallization procedure detailed above. Diffraction data were collected at 120 K on a Bruker Kappa Apex II diffractometer equipped with graphite-monochromatic Mo $K\alpha$ ($\lambda = 0.71073 \text{ \AA}$) radiation. A suitable single crystal of $[(1,5\text{-COD})\text{Ir}(\mu\text{-H})_4]$ was mounted on a Cryoloop in Paratone-N oil. Initial lattice parameters were determined from 452 reflections harvested from 36 frames. Cell constants and other pertinent crystallographic information is reported in Table S3-S7. The raw intensity data were integrated and corrected for Lorentz and polarization effects; an absorption correction was applied to the data using the program SADABS from the Apex II [16] software package. The structure was solved by direct methods and refined using the SHELXTL [17] software package. The non-hydrogen atoms were refined with anisotropic atomic displacement parameters. Hydrogen atoms bound to carbon were included in their idealized positions and were refined with a riding model using isotropic thermal parameters 1.2 times larger than the U_{eq} value of the atom to which they were bonded. The two unique hydride atoms of the molecular core were located straightforwardly in the difference electron density map and were refined with isotropic atomic displacement parameters.

XAFS Spectroscopy: XAFS experiments were performed at beamline X-19A at the National Synchrotron Light Source (NSLS) at Brookhaven National Laboratory. Energy was swept from 150 eV below to 1528 eV above the Ir L_3 edge (edge energy=11 215 eV) for $[(1,5\text{-COD})\text{Ir}(\mu\text{-H})_4]$ sample. The X-ray absorption coefficient was measured in transmission mode by positioning the sample between the incident beam and transmission beam detectors. Ir(0) black was used as a reference for the X-ray energy calibration and data alignment. The Ir(0) sample

was positioned between the transmission and reference beam detectors, and measured simultaneously with the main sample. The X-ray detectors were gas-filled ionization chambers. A sample solution of initially crystalline $[\text{Ir}(1,5\text{-COD})(\mu\text{-H})_4]$ was freshly synthesized at CSU. The black crystal was transferred into a 5 mL glass vial in a N_2 -filled Vacuum Atmospheres drybox (≤ 5 ppm O_2). The glass vial was then double-sealed under N_2 gas and transported to the National Synchrotron Light Source (NSLS). At the NSLS, the vial was opened in a N_2 -filled MBraun glovebox and in the solution was transferred into a custom-designed airtight XAFS sample holder composed of a stainless steel frame made to press Kapton film windows onto a Teflon block with a ~ 1.5 cm³ sample cavity.

The data processing and analysis was performed using the IFEFFIT package [18]. The EXAFS analysis was done by fitting the theoretical FEFF6 signals to the experimental data in r -space. Theoretical contributions included only the first (Ir-C) and second (Ir-Ir) nearest neighbors (1NN). The passive electron factor, S_0^2 , was found to be 0.84 by fits to the standard Ir(0) black, and then fixed for further analysis of the $[\text{Ir}(1,5\text{-COD})(\mu\text{-H})_4]$. The parameters describing the electronic properties (correction to the photoelectron energy origin) and local structure environment (coordination numbers N , bond lengths R and their mean squared disorder parameters σ^2) around the absorbing atoms were varied during the fitting. There were the total of 13 relevant independent data points and 7 variables in the fit.

3. Results and Discussion

Initial Controls and Attempted Syntheses Based on the Literature

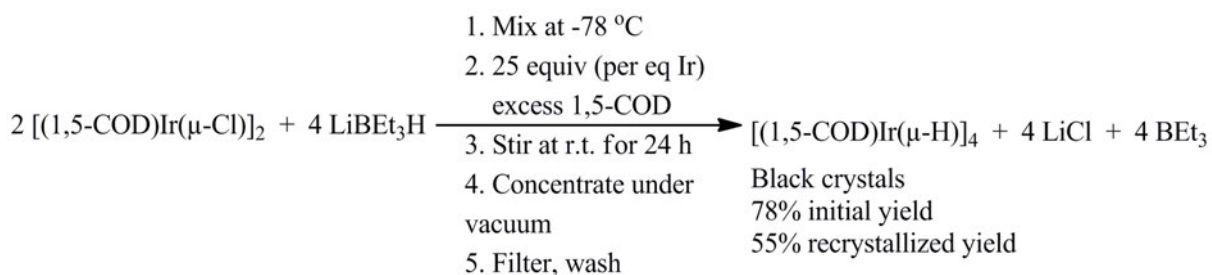
Initially, to calibrate our hands, the known tetrametallic hydride $[\text{Rh}(1,5\text{-COD})(\mu\text{-H})_4]$ was synthesized in two different experimenter's hands using Muetterties' original procedure [3], or

Bönnemann's slightly revised version [3] of Muetterties' original procedure (see the Supporting Information-D for details) [19]. Pleasingly, dark-red crystals of the $[\text{Rh}(1,5\text{-COD})(\mu\text{-H})_4]$ complex were obtained in a 50% yield using both procedures in our hands [20].

Next, the obvious experiments were performed in which we attempted to prepare $[\text{Ir}(1,5\text{-COD})(\mu\text{-H})_4]$ using each of three slightly different procedures published for the $[\text{Rh}(1,5\text{-COD})(\mu\text{-H})_4]$ analog by Bönnemann [3c], Hampden-Smith [3b] and Muetterties [3a] (see the Supporting Information-D for the details of these failed syntheses) [21]. A tiny amount of dark-green powder was obtained in all three trials. The trace, dark-green, Ir-product powder from adapting Muetterties' Rh-congener procedure to the Ir case was characterized using ESI MS, NMR, IR, UV-vis and XPS spectroscopies (as detailed in the Supporting Information-D, results that encouraged us to pursue the superior synthesis reported herein. However, the yield in each case using the adapted literature procedures was extremely low (~1%)—even though we were able to prepare the $[\text{Rh}(1,5\text{-COD})(\mu\text{-H})_4]$ congener in 50% yields (that matched the literature 50-60% yields, *vide infra*) *prior* to the attempted Ir congener syntheses and as control experiments. Moreover, crystallization attempts failed using the small amounts of dark-green, Ir-product powder obtained from each of the three, Muetterties, Bönnemann or Hampden-Smith adapted syntheses. Specifically, solutions cooled down slowly from room temperature to $-76\text{ }^\circ\text{C}$ in hexane, acetone, or ethanol, or cooled from room temperature to $10\text{ }^\circ\text{C}$ in cyclohexane:dichloromethane (1:1) failed to produce single crystals. In addition, dissolving the complex (0.4 mg) in pentane (0.5 mL), adding acetone (pentane:acetone =1:1 by volume) and keeping the resultant slightly cloudy solution at $-78\text{ }^\circ\text{C}$ for 10 h failed to provide single crystals. (The reverse order of solvent addition was also tried.) These initial crystallization studies were

undoubtedly limited by the small amounts of Ir product available from the initial, ~1% yield syntheses. Hence, development of a higher yield synthesis became the next order of business.

Successful Synthesis and Stoichiometry of Formation of [(1,5-COD)Ir(μ -H)]₄: After some trial and error, the successful synthesis of [Ir(1,5-COD)(μ -H)]₄ was discovered, a key of which is *the use of excess 1,5-COD* that was added based on the hypothesis that it might stabilize the product. The successful synthesis is carried out starting with THF solutions of LiBEt₃H [22] and [Ir(1,5-COD)IrCl]₂ at -78 °C (Scheme 5.2). Excess 1,5-COD [23] (25 equivs/equiv Ir) is added slowly over 5-10 minutes post the main reaction and at room temperature, resulting in a solution color change from dark-green to a bright-green (the latter being the characteristic color of solutions when the black-appearing crystals of [Ir(1,5-COD)(μ -H)]₄ are dissolved in THF, for example, vide infra). The resulting black powder is obtained in 78% yield. Following crystallization a *n*-pentane/THF (20/1) solution at -20 °C, a 55% yield of black, crystalline, [Ir(1,5-COD)(μ -H)]₄ was obtained. The black, crystalline [Ir(1,5-COD)(μ -H)]₄ complex dissolves in THF and benzene and is also slightly soluble in diethylether, *n*-pentane, *n*-hexane, acetone, methanol and acetonitrile.



Scheme 5.2. The balanced reaction stoichiometry and reaction conditions of the successful synthesis of [Ir(1,5-COD)(μ -H)]₄.

Single Crystal X-Ray Crystallography Structure: The single-crystal X-ray diffraction structure of $[\text{Ir}(1,5\text{-COD})(\mu\text{-H})_4]$ and the resulting atomic numbering scheme are shown in Figure 5.1. The space group is $Pbcn$ and the lattice constants are $a = 12.5628(3) \text{ \AA}$, $b = 18.4647(5) \text{ \AA}$ and $c = 12.3963(3) \text{ \AA}$. The $[\text{Ir}(1,5\text{-COD})(\mu\text{-H})_4]$ molecule is a diamagnetic, 56 total electron cluster, with formally 17 electrons at each Ir atom (i.e., and unless one would choose to count the two *longer* Ir-Ir bonds as Ir=Ir double bonds as one way to achieve 18 electron counts at each Ir). The $[\text{Ir}(1,5\text{-COD})(\mu\text{-H})_4]$ molecule is composed of a distorted tetrahedral Ir_4 core of D_{2d} geometry. Each Ir center is bonded to two olefinic groups of one 1,5-COD moiety plus two edge-bridging (*vide infra*) hydrides. The resulting Ir_4H_4 core exhibits S_4 geometry. The molecule possesses a crystallographic two-fold symmetry (i.e., the molecule resides on a crystallographic two-fold axis that connects the two halves of the molecule, Ir1 and Ir1A, for example). Selected bond lengths and bond angles are given in Table 5.1 and Table 5.2, respectively. Two Ir-Ir distances are long (2.90728(17) and 2.91138(17) \AA) and four Ir-Ir distances are short (2.78680 (12)-2.78798(12) \AA) [24]. A residual electron-density analysis strongly suggests that the hydrides are located in between two Ir atoms (i.e., are edge-bridging hydrides) connected by short Ir-Ir distances. The hydride positions, from refining the hydride atoms using the procedure detailed in Experimental section, appear reasonable, but may be influenced by Fourier termination errors emanating in the Ir atoms. Hence, *a neutron-diffraction experiment is needed to reveal the true positions of the hydrides* and is planned. That said, the observed short Ir-Ir bond distances are within the range of that of Ir-Ir bonds containing edge-bridging hydrides [4,25]. The longer Ir-Ir bonds correspond to Ir-Ir bonds without bridging hydrides (Ir1-Ir1A and Ir2-Ir2A in Figure 5.1). These long Ir-Ir distances are slightly longer than the literature values for singly bonded Ir-Ir distances (2.65-2.73 \AA) [4,2j]. The observed Ir-

H, Ir–C and C–C bond distances in $[\text{Ir}(1,5\text{-COD})(\mu\text{-H})]_4$ are (1.67 (3) and 1.82 (3) Å, 2.116(2)-2.182(2) Å and 1.407(3) – 1.424(3) Å, respectively) consistent with earlier literature [4,11,26]. The Ir–Ir–Ir angles vary between 58.50 and 62.86° confirming the distorted tetrahedral shape of the Ir₄ core [27]. The H–Ir–H angles (108.2(16)-108.5(15)°) and C–Ir–C angles (88.85(9)-96.88(9)°) are consistent with those previously reported for similar complexes [4].

XAFS Characterization: EXAFS and XANES were collected for two reasons: first, to test whether a minor Ir₅ species, detected by ESI-MS early in the characterization of the crystalline complex, Figure SI-D5 of the Supporting Information, was present in the *bulk sample* of the *crystalline* material (i.e., and in addition to a most abundant peak expected for the Ir₄ species, *vide infra*). Or, as we suspected, is the ESI MS observed Ir₅ species actually formed during the ESI-MS process, and thus an artifact of the ESI MS? Second, EXAFS and XANES were collected on the parent $[\text{Ir}(1,5\text{-COD})(\mu\text{-H})]_4$ complex since these spectroscopies—and, hence, the present study—are expected to be quite valuable in providing a baseline / background study for XAFS characterization of this previously unknown complex in future applications in catalysis and other areas.

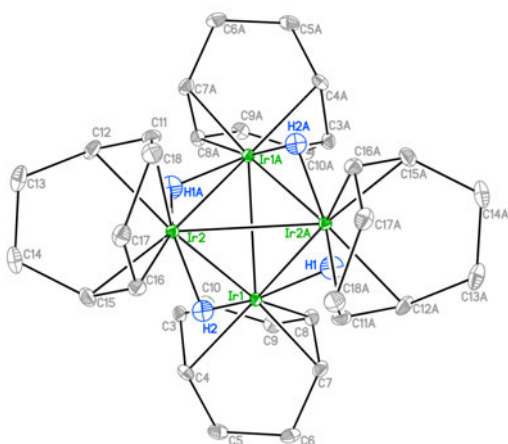


Figure 5.1. Single crystal X-ray structure and atomic numbering scheme for $[\text{Ir}(1,5\text{-COD})(\mu\text{-H})]_4$ at 50% probability.

Table 5.1. Selected bond lengths (Å) in [Ir(1,5-COD)(μ-H)]₄ crystal obtained by XRD structural refinement

Bond	Bond Length	Bond	Bond Length
Ir1-Ir2	2.78680 (12)	Ir1-C7	2.116 (2)
Ir1-Ir2A	2.78798 (12)	Ir1-C8	2.156 (2)
Ir2-Ir1A	2.78797 (12)	Ir2-C11	2.155 (2)
Ir1-Ir1A	2.90728 (17)	Ir2-C12	2.186 (2)
Ir2-Ir2A	2.91138 (17)	Ir2-C15	2.128 (2)
Ir1A-Ir2A	2.78680 (12)	Ir2-C16	2.158 (2)
Ir1-H1	1.71 (3)	C3-C4	1.407 (3)
Ir1-H2	1.82 (3)	C7-C8	1.424 (3)
Ir2-H2	1.67 (3)	C11-C12	1.405 (3)
Ir1-C3	2.156 (2)	C15-C16	1.419 (3)
Ir1-C4	2.187 (2)		

Table 5.2. Selected bond angles (°) in [Ir(1,5-COD)(μ-H)]₄ crystal

Bond	Bond Angle	Bond	Bond Angle
Ir1-Ir2-Ir2A	58.537 (3)	H1-Ir1-H2	108.5(15)
Ir2-Ir1-Ir1A	58.586 (3)	H2-Ir2-H1A	108.2(16)
Ir2-Ir1-Ir2A	62.966 (4)	C3-Ir1-C7	96.88 (9)
Ir2A-Ir1-Ir1A	58.547 (3)	C4-Ir1-C8	88.85 (9)
Ir1-Ir2-Ir1A	62.867 (4)	C11-Ir2-C15	96.77 (9)
Ir1A-Ir2-Ir2A	58.497 (3)	C12-Ir2-C16	87.98 (9)

Hence, a bulk sample of *crystalline* [Ir(1,5-COD)(μ-H)]₄ was examined by EXAFS and XANES spectroscopies. The EXAFS spectrum was analyzed only in the first nearest neighbor

range. Fourier transform (FT) magnitudes of k^3 -weighted Ir-L₃ EXAFS data of the [(1,5-COD)Ir(μ -H)]₄ complex, and its fit using Ir–Ir and Ir–C first nearest neighbor contributions, are shown in Figure 5.2. Two distinct peaks (uncorrected for the photoelectron phase shift) at around 2.5 Å and 1.7 Å are due to the Ir–Ir and Ir–C scattering contributions, respectively. Their real space distances are 2.80 ± 0.01 Å and 2.15 ± 0.01 Å for Ir–Ir and Ir–C, respectively. The Ir–Ir coordination number ($N_{\text{Ir-Ir}}$) of [(1,5-COD)Ir(μ -H)]₄ complex is 3.0 ± 1.2 , as expected for an Ir₄ core. The Ir–C coordination number ($N_{\text{Ir-C}}$) in [(1,5-COD)Ir(μ -H)]₄ crystal is 4.2 ± 0.7 , as expected from one COD attachment to each Ir center. The Ir–Ir and Ir–C bond distances obtained using EXAFS (2.80 ± 0.01 Å and 2.15 ± 0.01 Å, respectively) are consistent with those determined using XRD (2.78680(12)-2.91138(17) Å and 2.116(2)-2.182(2) Å, respectively). The lack of higher order contribution beyond Ir–Ir scatterer at 2.80 Å attests to the homogeneity of the samples and the lack of larger Ir clusters.

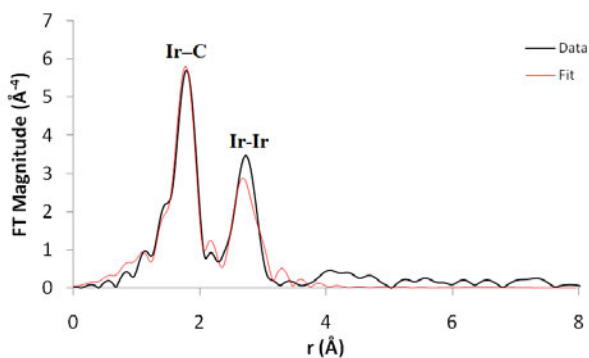


Figure 5.2. FT magnitudes of Ir-L₃ edge EXAFS data for [(1,5-COD)Ir(μ -H)]₄ complex (black) and its associated fit using Ir–C and Ir–Ir contributions (red).

The XANES spectrum of [Ir(1,5-COD)(μ -H)]₄ was obtained and compared to the XANES of both Ir(0) black and crystallographically and EXAFS-characterized [12,10] [Ir(1,5-COD)(μ -O₂C₈H₁₅)₂], Figure 5.3. The position and height of the main absorption peak (white line) at the

Ir-L₃ edge are similar for [Ir(1,5-COD)(μ-H)]₄ and Ir(0) black samples. On the other hand, the Ir-L₃ edge white line is shifted to higher energy and reaches higher normalized absorption coefficient values in [Ir(1,5-COD)(μ-O₂C₈H₁₅)₂] when compared to that of [Ir(1,5-COD)(μ-H)]₄ both of which contain *formally* Ir^I. This observation indicates a higher positive charge on Ir atoms in [Ir(1,5-COD)(μ-O₂C₈H₁₅)₂] complex compared to [Ir(1,5-COD)(μ-H)]₄. Restated, there is greater charge transfer from Ir to surrounding ligands in [Ir(1,5-COD)(μ-O₂C₈H₁₅)₂] in comparison to [Ir(1,5-COD)(μ-H)]₄, so that the XANES-determined, “effective” oxidation state of [(1,5-COD)Ir(μ-H)]₄ is arguably closer to that of bulk Ir⁰ than the *formally* Ir^I in [Ir(1,5-COD)(μ-O₂C₈H₁₅)₂]. However, the overall shape of the XANES spectrum (past the white line) of [Ir(1,5-COD)(μ-H)]₄ is quite similar to that of [Ir(1,5-COD)(μ-O₂C₈H₁₅)₂]. Both [Ir(1,5-COD)(μ-H)]₄ and [Ir(1,5-COD)(μ-O₂C₈H₁₅)₂] spectra lack the post-edge oscillatory behavior seen in the bulk Ir(0) consistent with the small coordination numbers of Ir atoms in both complexes.

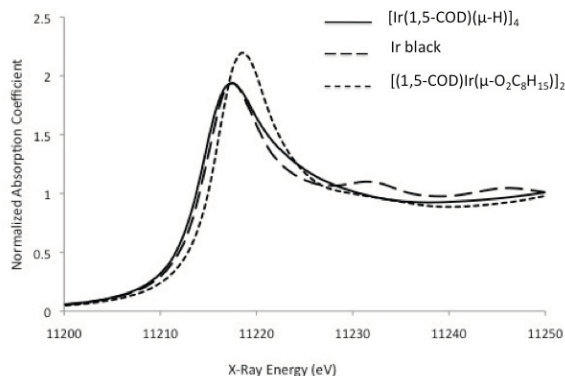


Figure 5.3. XANES of [Ir(1,5-COD)(μ-H)]₄ complex and reference compounds used of formally Ir⁰ black and formally Ir^I [(1,5-COD)Ir(μ-O₂C₈H₁₅)₂] [11].

Additional Characterization using ESI MS, UV-Vis, IR and NMR. The ESI MS [28] of the black $[\text{Ir}(\text{1,5-COD})(\mu\text{-H})_4]$ crystals dissolved in dichloromethane exhibits a most abundant peak located at 1205.2478 Da (Figure SI-D3, SI-D4 and SI-D5). The experimentally observed isotope peak distribution pattern matches the simulated isotopic distribution for $[\text{C}_{32}\text{H}_{51}\text{Ir}_4]^+$, formulated as $[\text{Ir}_4(\text{1,5-COD})_4(\mu\text{-H})_3]^+$. The UV-vis spectrum of the dark-green powder of $[\text{Ir}(\text{1,5-COD})(\mu\text{-H})_4]$ dissolved in THF shows absorption bands at 476 and 626 nm (Figure SI-D6). Of interest is that the experimental observation of two absorption maxima at 476 and 626 nm for $[\text{Ir}(\text{1,5-COD})(\mu\text{-H})_4]$ differ significantly from the UV-vis spectra of formally Ir(0)-containing tetrairidium complexes such as $\text{Ir}_4(\text{CO})_{11}[(\text{OPr})_3(\text{OCH}_2\text{PPh}_2)]$ (278 and 326 nm) [2] or various $\text{Ir}_4(\text{CO})_{12}$ clusters (278, 326 and 430 nm) [29]. Furthermore, the UV-vis spectrum of $[\text{Ir}(\text{1,5-COD})(\mu\text{-H})_4]$ is different from that of formally Ir(I)-containing $[\text{Ir}(\text{1,5-COD})(\mu\text{-O}_2\text{C}_8\text{H}_{15})_2]$ (486 nm), $[(\text{1,5-COD})\text{Ir}(\mu\text{-pyrazole})_2]$ (498, 585 nm) and $[(\text{1,5-COD})\text{Ir}(\mu\text{-6-methyl-2-hydroxypyridine})_2]$ (484 nm) [11,30]. In short, computational assistance will be required before the observed bands at 476 and 626 nm in UV-Vis spectrum of $[\text{Ir}(\text{1,5-COD})(\mu\text{-H})_4]$ can be assigned with confidence.

The IR spectrum of the $[\text{Ir}(\text{1,5-COD})(\mu\text{-H})_4]$ complex is, as expected, similar to that of the well-characterized Rh-analogue (Figure SI-D7) [3]. The ^1H NMR spectrum of crystalline $[\text{Ir}(\text{1,5-COD})(\mu\text{-H})_4]$ dissolved in benzene- d_6 (Figure SI-D8) shows a signal at -2.89 ppm and has the proper integration for the four, Ir-H hydrides [31]. The signals at 4.14, 2.09, and 1.37 ppm are assignable to the olefinic and methylene hydrogen atoms, respectively. The ^{13}C NMR spectrum of crystalline $[(\text{1,5-COD})\text{Ir}(\mu\text{-H})_4]$ dissolved in benzene- d_6 shows signals at 68.64 and 33.29 ppm for the COD ligands (Figure SI-D9), consistent with literature values for similar Ir-

COD complexes (i.e. and within the ranges of 52.6 – 92.6 ppm and 27.0 – 33.4 ppm, respectively) [32].

4. Summary and Possible Future Directions

The synthesis of the previously unavailable $[\text{Ir}(1,5\text{-COD})(\mu\text{-H})]_4$ complex in 78% initial, and 55% recrystallized, yield was accomplished starting with commercially available LiBEt_3H and $[\text{Ir}(1,5\text{-COD})\text{Cl}]_2$ in the presence of excess 1,5-COD in THF. The resultant $[\text{Ir}(1,5\text{-COD})(\mu\text{-H})]_4$ was fully characterized by single-crystal XRD, XAFS, ESI MS, UV-visible, IR and NMR. The $[\text{Ir}(1,5\text{-COD})(\mu\text{-H})]_4$ crystal structure shows distorted tetrahedral, D_{2d} Ir_4 core with one 1,5-COD and what appear to be two edge-bridging hydrides bound to each Ir center. The Ir–Ir, Ir–H, Ir–C distances and Ir–Ir–Ir, H–Ir–H and C–Ir–C bond angles are within the range of those for similar complexes from the extant literature. The EXAFS-determined Ir–Ir and Ir–C bond distances are in good agreement with the XRD results and validate and benchmark EXAFS as a useful method for characterization the $[\text{Ir}(1,5\text{-COD})(\mu\text{-H})]_4$ complex in future applications. The EXAFS results also are of value in that they demonstrate a high degree of homogeneity of the *bulk* $[\text{Ir}(1,5\text{-COD})(\mu\text{-H})]_4$ sample.

As alluded to in the Introduction, there are at least 5 reasons why the previously unknown, tetranuclear, coordinatively unsaturated $[\text{Ir}(1,5\text{-COD})(\mu\text{-H})]_4$ cluster is of interest, the first of which is (i) that $[\text{Ir}(1,5\text{-COD})(\mu\text{-H})]_4$ holds promise of serving as a multipurpose, coordinatively unsaturated, Ir_4 -based precatalyst and organometallic synthon, just as its Rh congener $[\text{Rh}(1,5\text{-COD})(\mu\text{-H})]_4$ has. Our own efforts are focused on employing $[\text{Ir}(1,5\text{-COD})(\mu\text{-H})]_4$: (ii) as a XAFS model/standard and possible Ir_4H_4 intermediate in nucleation and growth studies of $\text{Ir}(0)_n$ nanoclusters starting from $(1,5\text{-COD})\text{Ir}^+$ -based precatalysts—the role of polynuclear M_aH_b

species (M = metal), as opposed to just polynuclear $M(0)_n$ species, in nanocluster nucleation and growth being an important but controversial point at present [14,15]; This new, tetrametallic cluster is also of interest (iii) as a discrete, precise composition tetrametallic Ir_4H_4 complex for possible use in preparing both homogeneous as well as supported, heterogeneous sub-nanometer Ir_4H_4 based catalysts; (iv) as a new precursor for testing the formation and stabilization mechanisms of Ir-based, so-called Ziegler-type industrial hydrogenation model catalysts prepared from (1,5-COD)Ir⁺-based precatalysts and AlEt₃ [10], and (v) as a fully compositionally and structurally characterized Ir_4 analog of the (on-average) Co_4 -based, subnanometer clusters identified by XAFS as a dominant species in Co-based Ziegler-type industrial polymer hydrogenation catalysts [15]. Also noteworthy in conclusion is that the Co member of this class of tetranuclear clusters, $[M(1,5-COD)(\mu-H)]_4$ (M = Ir, Rh, Co) may be preparable as well, although it remains to be synthesized, isolated and unequivocally characterized. Hence, it is hoped that the present synthesis and characterization, of the previously unavailable $[Ir(1,5-COD)(\mu-H)]_4$ will be of value for the above, as well as other, future studies.

5. Supporting Information-D. Instrumentation for, and the experimental procedures behind, the ESI MS, UV-vis, IR and NMR spectroscopic studies. Literature tables for Ir–Ir bond distances and Ir–Ir–Ir bond angles of similar compounds. Crystal data and structure refinement tables with bond distances, bond angles, anisotropic and isotropic displacement parameters, cif file containing the crystal structure data. ESI MS, UV-vis, IR and NMR spectra. Detailed experimental procedures for (i) successful syntheses of $[Rh(1,5-COD)(\mu-H)]_4$, (ii) initial, low yield synthesis attempts for $[Ir(1,5-COD)(\mu-H)]_4$ while following literature procedures for the Rh-congener; and (iii) control experiments performed to decrease the amount of a ¹H NMR-detected impurity. This material is available free of charge via the Internet at <http://pubs.acs.org>.

REFERENCES

[1] Muetterties' 1975 definition of molecular metal clusters is "discrete molecules or molecular ions that contain three or more metal atoms in a bonding interaction" [1a]. Gates has commented that metal clusters are "compounds with metal-metal bonds stabilized by ligands such as carbonyls." [1b]. A few lead references to the extensive literature of molecular metal clusters are given below [1a-1f]. Studies comparing structure, thermochemistry and bonding interactions in molecular metal clusters to those of bulk metal surfaces containing chemisorbed ligands have revealed that one valuable contribution of molecular metal clusters is that they can be reasonable approximations to ligated, bulk-metal surfaces [1e]. (a) E.L. Muetterties, *Bull. Soc. Chim. Belg.* 84 (1975) 959-986. (b) B.C. Gates, *Angew. Chem. Int. Ed. Eng.* 32 (1993) 228-229. (c) P. Chini, *Pure Appl. Chem.* 23 (1970) 489-503. (d) P. Chini, G. Longoni, V.G. Albano, *Adv. Organomet. Chem.* 14 (1976) 285-344. (e) E.L. Muetterties, T.N. Rhodin, E. Band, C.F. Brucker, W.R. Pretzer, *Chem. Rev.* 79 (1979) 91-137. (f) E.L. Muetterties, *Science* 196 (1977) 839-848. (g) P. Chini, *J. Organomet. Chem.* 200 (1980) 37-61. (h) J.C. Calabres, L.F. Dahl, A. Cavalier, P. Chini, G. Longoni, S. Martinen, *J. Am. Chem. Soc.* 96 (1974) 2616-2618. (i) R.G. Vranka, L.F. Dahl, P. Chini, J. Chatt, *J. Am. Chem. Soc.* 6 (1969) 1574-1576. (k) M.D. Morse, *Chem. Rev.* 86 (1986) 1049-1109. (l) R.D. Adams, *Acc. Chem. Res.* 16 (1983) 67-72. (m) R. D. Adams, *Chem. Rev.* 89 (1989) 1703-1712. (n) R.D. Adams, *Polyhedron* 4 (1985) 2003-2025. (o) R.D. Adams, J.E. Babin, M. Tasi, *Inorg. Chem.* 25 (1986) 4514-4519. (p) R.D. Adams, M. Chen, *Organometallics* 30 (2011) 5867-5872. (q) R.D. Adams, M. Chen *Organometallics* 31 (2012) 445-450.

[2] (a) J.-D. Grunwaldt, P. Kappen, L. Basini, B.S. Clausen, *Catal. Lett.* 78 (2002) 13-21. (b) F. Li.; B.C. Gates, *J. Phys. Chem. B* 108 (2004) 11259-11264. (c) G.F. Stuntz, J.R. Shapley, C.G. Pierpont, *Inorganic Chemistry* 17 (1978) 2596-2603. (d) N. Silva, A. Solovyov, A. Katz, *Dalton Trans.* 39 (2010) 2194-2197. (e) J.F. Goellner, J. Guzman, B.C. Gates, *J. Phys. Chem. B* 106 (2002) 1229-1238. (f) F. Li, B.C. Gates, *J. Phys. Chem. B* 107 (2003) 11589-11596. (g) A. Uzun, B.C. Gates, *Angew. Chem. Int. Ed.* 47 (2008) 9245-9248. (h) Z. Xu, F.-S. Xiao, S.K. Purnell, O. Alexeev, S. Kawi, S.E. Deutsch, B.C. Gates, *Nature* 372 (1994) 346-348. (i) A.M. Argo, J.F. Odzak, F.S. Lai, B.C. Gates, *Nature* 415 (2002) 623-626. (j) A.M. Argo, J.F. Odzak, B.C. Gates, *J. Am. Chem. Soc.* 125 (2003) 7107-7115. (k) A. Uzun, B.C. Gates, *J. Am. Chem. Soc.* 131 (2009) 15887-15894. (l) Y. Doi, K. Koshizuka, T. Keii, *Inorg. Chem.* 21 (1982) 2732-2736. (m) Y. Doi, K. Koshizuka, S. Tamura, *J. Mol. Catal.* 19 (1983), 213-222. (n) R.A. Sanchez-Delgado, A. Andriollo, J. Puga, G. Martin, *Inorg. Chem.* 26 (1987) 1867-1870. (o) J.S. Bradley, *J. Am. Chem. Soc.* 101 (1979) 7419-7421. (p) N. Rosas, C. Marquez, H. Hernandez, R. Gomez, *J. Mol. Catal.* 48 (1988) 59-67. (q) R.D. Adams, S.B. Falloon, *Organometallics* 14 (1995) 4594-4600.

[3] (a) M. Kulzick, R.T. Price, E.L. Muetterties, V.W. Day, *Organometallics* 1 (1982) 1256-1258. (b) Z. Duan, M.J. Hampden-Smith, A.P. Sylwester, *Chem. Mater.* 4 (1992) 1146-1148. (c) H. Bonnemann, W. Brijoux, R. Brinkmann, E. Dinjus, R. Fretzen, T. Joußen, B. Korall, *J. Mol. Catal.* 74 (1992) 323-333.

[4] L. Garlaschelli, F. Greco, G. Peli, M. Manassero, M. Sansoni, R. Gobetto, L. Salassa, R.D. Pergola, *Eur. J. Inorg. Chem.* (2003) 2108-2112.

[5] J.A. Cabeza, A. Nutton, B.E. Mann, C. Brevard, P.M. Maitlis, *Inorg. Chim. Acta* 115 (1986) L47-L48.

[6] G. Huttner, H. Lorenz, *Chem. Ber.* 108 (1975) 973-976.

[7] R. Bau, N.N. Ho, J.J. Schneider, S.A. Mason, G.J. McIntyre, *Inorg. Chem.* 43 (2004) 555-558.

[8] (a) V.W. Day, M.F. Fredrich, G.S. Reddy, A.J. Sivak, W.R. Pretzer, E.L. Muetterties, *J. Am. Chem. Soc.* 99 (1977) 8091-8093. (b) R.K. Brown, J.M. Williams, A.J. Sivak, E.L. Muetterties, *Inorg. Chem.* 19 (1980) 370-374. (c) J.S. Ricci, T.F. Koetzle, R.J. Goodfellow, P. Espinet, P.M. Maitlis, *Inorg. Chem.* 23 (1984) 1828-1831.

[9] The tetrarhodium complex $[\text{Rh}(1,5\text{-COD})(\mu\text{-H})]_4$ has also been tested as a precatalyst for toluene hydrogenation after adsorbing it onto silica or onto palladium-supported on silica.^{9a} The hydrogenation of carbon dioxide began with $[\text{Rh}(1,5\text{-COD})(\mu\text{-H})]_4$ and employed $\text{Ph}_2\text{P}(\text{CH}_2)_4\text{PPh}_2$ [9b,9c]. (a) K.J. Stanger, Y. Tang, J. Anderegg, R.J. Angelici, *J. Mol. Catal. A.: Chem.* 202 (2003) 147-161. (b) F. Gassner, E. Dinjus, H. Grls, W. Leitner, *Organometallics* 15 (1996) 2078-2082. (c) W. Leitner, E. Dinjus, F.J. Gassner, *Organomet. Chem.* 475 (1994) 257-266.

[10] (a) W.M. Alley, I.K. Hamdemir, Q. Wang, A. Frenkel, L. Li, J.C. Yang, L.D. Menard, R.G. Nuzzo, S. Özkar, K.A. Johnson, R.G. Finke, *Inorg. Chem.* 49 (2010) 8131-8147.

[11] W.M. Alley, C.W. Girard, S. Ozkar, R.G. Finke, *Inorg. Chem.* 48 (2009) 1114-1121.

[12] By definition, Ziegler-type hydrogenation catalysts are formed from a non-zero valent group 8-10 transition metal precatalyst such as $[\text{Ir}(1,5\text{-COD})(\mu\text{-O}_2\text{C}_8\text{H}_{15})]_2$ plus a trialkylaluminum cocatalyst such as AlEt_3 . For a review of the ~50 year old literature on Ziegler-type hydrogenation catalysts see: W.M. Alley, I.K. Hamdemir, K.A. Johnson, R.G. Finke, *J. Mol. Catal. A. Chem.* 315 (2010) 1-27.

[13] K.A. Johnson, *Polym. Prepr.* 41 (2000) 1525-1526.

[14] (a) J.E. Mondloch, R.G. Finke, *J. Am. Chem. Soc.* 133 (2011) 7744-7756. (b) J.E. Mondloch, Q. Wang, A.I. Frenkel, R.G. Finke, *J. Am. Chem. Soc.* 132 (2010) 9701-9714. (c) E. Bayram, M. Zahmakiran, S. Ozkar, R.G. Finke, *Langmuir* 26 (2010) 12455-12464. (d) M.A. Watzky, E.E. Finney, R.G. Finke, *J. Am. Chem. Soc.* 130 (2008) 11959-11969. (e) L.S. Ott, R.G. Finke, *J. Nanosci. Nanotech.* 8 (2008) 1551-1556. (f) L.S. Ott, S. Campbell, K.R. Seddon, R.G. Finke, *Inorg. Chem.* 46 (2007) 10335-10344. (g) S. Ozkar, R.G. Finke, *J. Organomet. Chem.* 689 (2004) 493-501.

[15] W. M. Alley, I.K. Hamdemir, Q. Wang, A.I. Frenkel, L. Li, J.C. Yang, L.D. Menard, R.G. Nuzzo, S. Özkar, K.-H. Yih, K.A. Johnson, R.G. Finke, *Langmuir* 27 (2011) 6279-6294.

[16] Bruker Analytical X-Ray System, Inc.; Madison, WI, 1999

[17] (a) G.M. Sheldrick, SHELXTL, Version 6.14; Bruker Analytical X-Ray Systems, Inc.: Madison, WI, 1999. (b) A short history of SHELX". Sheldrick, G.M. (2008). *Acta Cryst.* A64,, 112-122

[18] M. Newville, *J. Synchrotron Rad.* 8 (2001) 322-324.

[19] Three main differences between Muetterties' original procedure and Bönemann's synthesis are as follows: (i) Muetterties' procedure starts with 0.02 mmol of $[\text{Rh}(1,5\text{-COD})\text{Cl}]_2$ vs 12.2 mmol in Bönemann's synthesis; (ii) Muetterties and coworkers started with $\text{K}[\text{HB}(\text{O-}i\text{-C}_3\text{H}_7)_3]$ in THF or EtLi in toluene, whereas the hydride source in Bönemann's synthesis is $\text{Na}[\text{BEt}_3\text{H}]$; and (iii) the initial $\text{Rh}(1,5\text{-COD})\text{Cl}_2$ and hydride source are mixed immediately at -78 °C in Muetterties' original synthesis vs over 9 h at room temperature in Bönemann's synthesis.^{3a,3c}

[20] Muetterties' original $[\text{Rh}(1,5\text{-COD})(\mu\text{-H})_4]$ synthesis [3a] reports 50-60% yields when starting with 0.02 mmol of $[\text{Rh}(1,5\text{-CODCl})_2]$. We have obtained a similar yield (~50%) using the same procedure, but when starting with 1.49 mmol $[\text{Rh}(1,5\text{-CODCl})_2]$. However, using Bönemann's, procedure^{3c} we obtain a lower yield (~50%) than those workers report (74%), although our scale of starting with 2 mmols of $[\text{Rh}(1,5\text{-COD})(\mu\text{-H})_4]$ (vs 12.2. mmols in Bönemann's study) is one likely reason for our somewhat lower yield in that synthesis done purely as a control reaction.

[21] Hampden-Smith and coworkers synthesized $[\text{Rh}(1,5\text{-COD})(\mu\text{-H})_4]$ by mixing 1 mmol $[\text{Rh}(1,5\text{-COD})\text{Cl}]_2$ and 2 mmol of LiBEt_3H at 0 °C and obtained a 52% yield. See this reference, as well as reference[20], for a comparison to Muetterties' and Bönemann's syntheses.

[22] The hydride sources $\text{K}[\text{HB}(\text{O-}i\text{-Pr})_3]$ or EtLi used by Muetterties *et al.* [3a] were replaced by LiBEt_3H in our study due to commercial unavailability of the $\text{K}[\text{HB}(\text{O-}i\text{-Pr})_3]$ complex and since Hampden-Smith and coworkers successfully used LiBEt_3H in their $[\text{Rh}(1,5\text{-COD})(\mu\text{-H})_4]$ synthesis [3b]. An attempted synthesis using EtLi was also performed as part of the present work, but failed as detailed in the Supporting Information.

[23] (a) Addition of free 1,5-COD is one key step that differs from Muetterties' original synthesis and which results in a ~78-fold higher yield synthesis $[\text{Ir}(1,5\text{-COD})(\mu\text{-H})_4]$. Another key difference from Muetterties' original synthesis is that dark-green $[\text{Ir}(1,5\text{-COD})(\mu\text{-H})_4]$ is kept in THF solution until filtration step (where as Muetterties synthesis of the Rh-congener evaporates the volatiles under vacuum and then extracts the $[\text{Rh}(1,5\text{-COD})(\mu\text{-H})_4]$ using pentane). (b) Additionally, an impurity detectable as a 12.82 ppm peak in the ¹H NMR is present in the black powder. That impurity can be reduced by: (i) washing the black powder with larger amounts of deoxygenated acetone in a drybox (a total of 250 mL vs 15 mL); (ii) increasing the stirring time from the initial 30 min to 24 h after addition of excess 1,5-COD; or (iii) passing concentrated $[\text{Ir}(1,5\text{-COD})(\mu\text{-H})_4]$ solution in THF through a glass filter (i.e., and without the addition of acetone). See the Experimental section of the Supporting Information for further details and the ¹H NMR spectra (Figures S1 and S2).

[24] Similar to what has been found for $[\text{Ir}(1,5\text{-COD})(\mu\text{-H})_4]$, four short and two long M-M bonds are observed in the crystal structure of the Rh-analogue. The four short bonds (2.802 (0.001) Å) were assigned to bridging hydride, Rh-H-Rh groups [3a] consistent in a general way with the prior literature in which Rh-Rh bond distances varying between 2.610 (0.005) and 2.856 (0.008) Å have been assigned to Rh-H-Rh groups [9a,9b]. On the other hand, the long Rh-Rh distances in $[\text{Rh}(1,5\text{-COD})(\mu\text{-H})_4]$ of 2.971 (0.001) Å are longer than literature values of either singly-bonded Rh-Rh (2.62 – 2.80 Å^{9b}) or Rh-H-Rh distances. (a) R.K. Brown, J.M. Williams, A.J. Sivak, W.R. Pretzer, E.L. Muetterties, *Inorg. Chem.* 19 (1980) 370-374. (b) V.W. Day, M.F. Fredrich, G.S. Reddy, A.J. Sivak, W.R. Pretzer, E.L. Muetterties. *J. Am. Chem. Soc.* 99 (1977) 8091-8093.

[25] The Ir-Ir bond distances for Ir-H-Ir linkages in Ir_n (n=2-4) complexes of between 2.703 and 3.290 Å have been reported: (a) D.M. Heinekey, D.A. Fine, D. Barnhart, *Organometallics* 16 (1997) 2530-2538. (b) K. Fujita, H. Nakaguma, F. Hanasaka, R. Yamaguchi, *Organometallics* 21 (2002) 3479-3757. (c) R. Bau, M.Y. Chiang, C.Y. Wel, L. Garlaschelli, S. Martinengo, T.F. Koetzle, *Inorg. Chem.* 23 (1984) 4758-4761.

[26] Ir-C distances in $[(1,5\text{-COD})\text{Ir}(\mu\text{-H})_4]$ are similar to the Ir-diene distances reported for [26a] $\text{Ir}_4(\text{CO})_5(\text{C}_8\text{H}_{12})(\text{C}_8\text{H}_{10})$ (2.10 – 2.24 Å) and to those previously observed in [11] $[(1,5\text{-COD})\text{Ir}(\mu\text{-O}_2\text{C}_8\text{H}_{15})_2]$. (a) G.F. Stuntz, J.R. Shapley, C.G. Pierpont, *Inorganic Chemistry* 17 (1978) 2596-2603.

[27] Similar M-M-M angles (54.93(11) and 62.53(5) Å) have been seen previously for [27a] $[(\text{C}_5\text{Me}_5)_3\text{Rh}(\mu_3\text{-H})_4]^{2+}$. Table SI-D2 of the Supporting Information contains a comparison of M-M-M bond angles of tetrahedral and butterfly-shaped M_4 complexes [8c].

[28] Many Ir_4 complexes such as $\text{Ir}_4(\text{CO})_5(\text{C}_8\text{H}_{12})_2(\text{C}_8\text{H}_{10})$, $[\text{Ir}_4\text{H}_{10}(\text{PCy}_3)_4(\text{C}_9\text{H}_{11}\text{N})_2](\text{PF}_6)_2$, $[(\eta^5\text{-C}_5\text{Me}_5)\text{IrH}]_4(\text{BF}_4)_2$ and *tert*-butylcalix[4]arene(OPr)₃(OCH₂PPh₂)- $\text{Ir}_4(\text{CO})_{11}$ have been successfully characterized using mass spectroscopy. (a) Y. Xu, M.A. Celik, A.L. Thompson, H. Cai, M. Yurtsever, B. Odell, J.C. Green, D.M.P. Mingos, J.M. Brown, *Angew. Chem. Int. Ed. Eng.* 48 (2009) 582-585. (b) J.A. Cabeza, A. Nutton, B.E. Mann, C. Brevard, P.M. Maitlis, *Inorg. Chim. Acta* 115 (1986) L47-L48.

[29] L.J. Tortorelli, P.A. Flowers, B.L. Harward, G. Mamantov, L.N. Klatt, *J. Organomet. Chem.* 429 (1992) 119-134.

[30] J.L. Marshall, S.R. Stobart, H.B. Gray, *J. Am. Chem. Soc.* 106 (1984) 3027-3029. (b) G.S. Rodman, K.R. Mann, *Inorg. Chem.* 27 (1988) 3347-3353.

[31] For comparison, this -2.89 ppm chemical shift is considerably downfield compared, for example, to hydride peak for $[\text{Rh}(1,5\text{-COD})(\mu\text{-H})_4]$ at ca. -12 ppm. It is also downfield from the hydride signals of previously synthesized tetrahydrido tetrairidium complexes such as $[\text{Ir}(\text{CO})(\text{PPh}_3)(\mu\text{-H})\text{H}]_4$ or $[\text{Ir}(\eta\text{-C}_5\text{Me}_5)(\mu\text{-H})_4](\text{BF}_4)_2$ appear between -12.84 and -18.89 ppm [4,5]. For a broader comparison, the ¹H NMR spectra of various complexes containing M-H-M (M: Ir-Rh or Re) face- or edge-bridging hydrides contain hydride peaks between -4.30 ppm and -

24.00 ppm [31a-e,25a,25b]. Hence, and although one could speculate on the origins of this downfield, hydride chemical shift (using, for example, the Ramsey shielding/deshielding equation^{31f}, or trying to take into account the increased electron density on Ir suggested by the XANES), we choose not to speculate in the absence of a good wave function and subsequent molecular orbital calculation for $[\text{Ir}(1,5\text{-COD})(\mu\text{-H})_4]$. Note here that the needed computations would best come *after* definitive location of the hydrides by neutron diffraction, studies that are planned. (a) B.A. Vaartstra, M. Cowie, *Organometallics* 9 (1990) 1594-1602. (b) T. Hattori, S. Matsukawa, S. Kuwata, Y. Ishii, M. Hidai, *Chem. Comm.* (2003) 510-511. (c) A.M. Mueting, P.D. Boyle, R. Wagner, L.H. Pignolet, *Inorg. Chem.* 27 (1988) 271-279. (d) M.D. Fryzuk, *Organometallics* 1 (1982) 408-409. (e) J.R. Johnson, H.D. Kaesz, *Inorg. Synth.* 18 (1978) 60-62. (f) R.S. Drago, *Physical Methods for Chemists*, Surfside Scientific Publishers: Gainesville, FL, 1977.

[32] (a) C.J. Adams, K.M. Anderson, J.P.H. Charmant, N.G. Connelly, B.A. Field, A.J. Hallett, M. Horne, *Dalton Trans.* (2008) 2680-2692. (b) M.D. Brown, W. Levason, G. Reid, M. Webster, *Dalton Trans.* (2006) 4039-4046. (c) J. Browning, G.W. Bushnell, K.R. Dixon, K. R.W. Hilts, *J. Organomet. Chem.* 452 (1993) 205-218. (d) A.D. Zotto, L. Costella, A. Mezzetti, P.J. Rigo, *Organomet. Chem.* 414 (1991) 109-118.

SUPPORTING INFORMATION-D:

SYNTHESIS AND CHARACTERIZATION OF [Ir(1,5-CYCLOOCTADIENE)(μ -H)]₄: A TETRAMETALLIC Ir₄H₄-CORE, COORDINATIVELY UNSATURATED CLUSTER

Contents

1. Literature Tables

- 1.1. Literature table of Ir-Ir bond distances in various Ir₄ complexes
- 1.2. Literature table of Ir-Ir-Ir bond angles in various Ir₄ and Rh₄ complexes

2. Experiments Determining Conditions Which Decreased the Amount of the ¹H NMR-Detected, 12.82 ppm Impurity

- 2.1. Washing the Black Powder with Acetone
- 2.2. Passing a concentrated THF solution of [(Ir(1,5-COD)(μ -H)]₄ through a glass filter

3. Crystal Structure Data and Tables for [Ir(1,5-COD)(μ -H)]₄

- 3.1. Crystal data and structure refinement
- 3.2. Atomic coordinates and equivalent isotropic displacement parameters
- 3.3. Bond Lengths
- 3.4. Bond Angles
- 3.5. Anisotropic displacement parameters, hydrogen coordinates and isotropic displacement parameters

4. Further Characterization Data for [Ir(1,5-COD)(μ -H)]₄

5. Experimental

- 5.1. Instrumentation and Sample Preparation
- 5.2. Control Experiments Synthesizing [Rh(1,5-COD)(μ -H)]₄ using Muetterties' and Bönemann's procedures

- 5.3. Attempted Synthesis of $[\text{Ir}(1,5\text{-COD})(\mu\text{-H})]_4$ using Bönemann's, Hampden-Smith's and Muetterties' Rh- congener procedures
- 5.4. Characterization of the dark-green powder of $[\text{Ir}(1,5\text{-COD})(\mu\text{-H})]_4$
- 5.5. Control Experiments Performed to Determine the Best Conditions to Decrease the Amount of ^1H NMR-Detected, 12.82 ppm Impurity
- 5.6. Unsuccessful synthesis of $[(1,5\text{-COD})\text{Ir}(\mu\text{-H})]_4$ starting with $[(1,5\text{-COD})\text{Ir}(\mu\text{-Cl})]_2$ and EtLi

1. Literature Tables

Table SI-D1. Literature table of Ir-Ir bond distances in various Ir₄ complexes

Author, year	Complex	Ir-Ir distances (Å)	Method used
Garlaschelli, 2003 ¹	Ir ₄ H ₈ (CO) ₄ (PPh ₃) ₄	2.925 (1) 2.916 (1) 2.906 (1) 2.931 (1) 2.721 (1) 2.732 (1)	XRD
Brown, 2009 ²	[Ir ₄ H ₁₀ (PCy ₃) ₄ (C ₉ H ₁₁ N) ₂] ²⁺	2.7703 (6) 2.6241 (4)	XRD
Brown, 2009 ²	[Ir ₄ H ₁₁ (PMe ₃) ₄ (C ₅ H ₅ N)] ⁺	2.6758 (4) 2.7421 (4) 2.7748 (4) 2.7281 (4) 2.7785 (4)	XRD
Bau and Koetzle, 1984 ³	[HIr ₄ (CO) ₁₁] ⁻	2.712 (1) - 2.800 (1) 2.703 (2) - 2.795 (2)	ND and XRD
Katz, 2010 ⁴	(OPr) ₃ (OCH ₂ PPh ₂)-Ir ₄ (CO) ₁₁	2.708 (1) - 2.786 (1)	XRD
Pierpont, 1978 ⁵	Ir ₄ (CO) ₅ (C ₈ H ₁₂) ₂ (C ₈ H ₁₀)	2.695 (1) - 2.741 (1)	XRD
Gates, 2004 ⁶	Ir ₄ (CO) ₁₂ in zeolite NaY ₂₅	2.71 (1)	XAFS
Gates, 2003 ⁷	Ir ₄ supported on γ-Al ₂ O ₃	2.65	XAFS
Finke, 2012 (This work)	[(1,5-COD)Ir(μ-H)] ₄	2.7869 (2) 2.7881 (2) 2.7881 (2) 2.7869 (2) 2.9072 (3) 2.9112 (3)	XRD
Finke, 2011	[(1,5-COD)Ir(μ-H)] ₄	2.80 (1)	XAFS

¹ Garlaschelli, L.; Greco, F.; Peli, G.; Manassero, M.; Sansoni, M.; Gobetto, R.; Salassa, L.; Pergola, R. D. *Eur. J. Inorg. Chem.* **2003**, 2108-2112.

² Xu, Y.; Celik, M. A.; Thompson, A. L.; Cai, H.; Yurtsever, M.; Odell, B.; Green, J. C.; Mingos, D. M. P.; Brown, J. M. *Angew. Chem. Int. Ed. Eng.* **2009**, *48*, 582-585.

³ Bau, R.; Chiang, M. Y.; Wei, C. Y.; Garlaschelli, L.; Martinengo, S.; Koetzle, T. F. *Inorg. Chem.* **1984**, *23*, 4758-4762.

⁴ Silva, N.; Solovyov, A.; Katz, A. *Dalton Trans.* **2010**, *39*, 2194-2197.

⁵ Stuntz, G. F.; Shapley, J. R.; Pierpont, C. G. *Inorganic Chemistry* **1978**, *17*, 2596-2603.

⁶ Li, F.; Gates, B. C. *J. Phys. Chem. B* **2004**, *108*, 11259-11264.

⁷ Argo, A. M.; Odzak, J. F.; Gates, B. C. *J. Am. Chem. Soc.* **2003**, *125*, 7107-7115.

Table SI-D2. Literature table of Ir-Ir-Ir bond angles in various Ir₄ and Rh₄ complexes

Author, year	Complex	Metal core structure	Ir-Ir-Ir bond angles (°)	Method used
Maitlis, 1984	$[(C_5Me_5)Rh(\mu_3-H)]_4^{2+}$	Tetrahedral	54.93(11) 62.53(5)	ND
Brown, 2009	$[Ir_4H_{10}(PCy_3)_4(C_9H_{11}N)_2]^{2+}$	Butterfly	56.17 (2)	XRD
Brown, 2009	$[Ir_4H_{11}(PMe_3)_4(C_5H_5N)]^+$	Butterfly	57.98 (1) 58.18 (1) 119.70 (1) 122.77 (1)	XRD
Pierpont, 1978	$Ir_4(CO)_5(C_8H_{12})_2(C_8H_{10})$	Butterfly	58.45 (2) 58.70 (2) 59.73 (2) 59.81 (2) 61.49 (2) 61.82 (2) 91.99 (2) 91.88 (2)	XRD
Finke, 2011	$[(1,5-COD)Ir(\mu-H)]_4$	Tetrahedral	62.69 (1) 58.59 (0) 58.55 (0) 62.86 (1) 58.54 (0) 58.50 (0)	XRD

2. Experiments Determining Conditions Which Decreased the Amount of the ^1H NMR-Detected, 12.82 ppm Impurity:

2.1. Washing the Black Powder with Acetone: The impurity/hydride ratio decreased from 1:4 to 1:8 when the black powder was washed with 10×25 mL acetone; see the Experimental Section at the end of this Supporting Information for the details of this specific experiment. (The impurity is labeled an “acid”, but this is not known for certain so that this early / historical experimental nomenclature should be replaced by the more accurate “ ^1H NMR-Detected, 12.82 ppm Impurity”.)

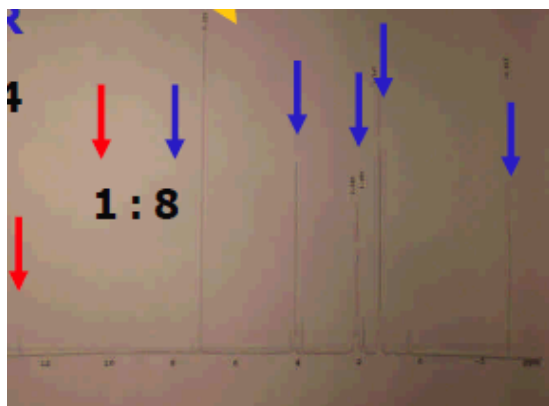
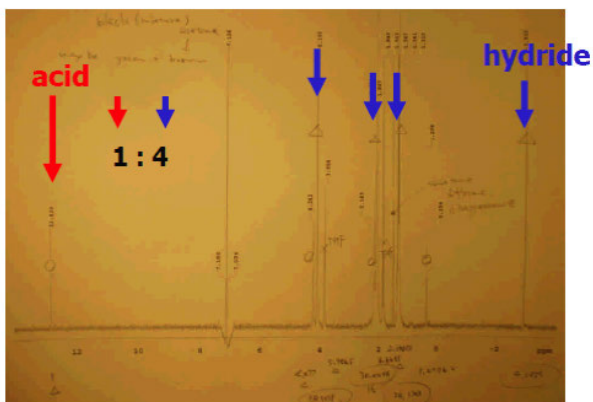


Figure SI-D1. ^1H NMR spectra of the black $[\text{Ir}(1,5\text{-COD})(\mu\text{-H})_4]$ powder in benzene- d_6 (left) and that (right) from a separate synthesis, but in the right-most figure after washing the black powder with 10×25 mL = 250 mL of acetone.

2.2. Passing a concentrated THF solution of $[(\text{Ir}(1,5\text{-COD})(\mu\text{-H}))_4]$ through a glass filter

(i.e., without the addition of 15 mL acetone): The impurity/hydride ratio decreased from 1:4 to 1:12 when the concentrated THF solution of $[(\text{Ir}(1,5\text{-COD})(\mu\text{-H}))_4]$ (without adding 15 mL acetone) was passed through a glass filter (see the Experimental section towards the end of this Supporting Information for details).

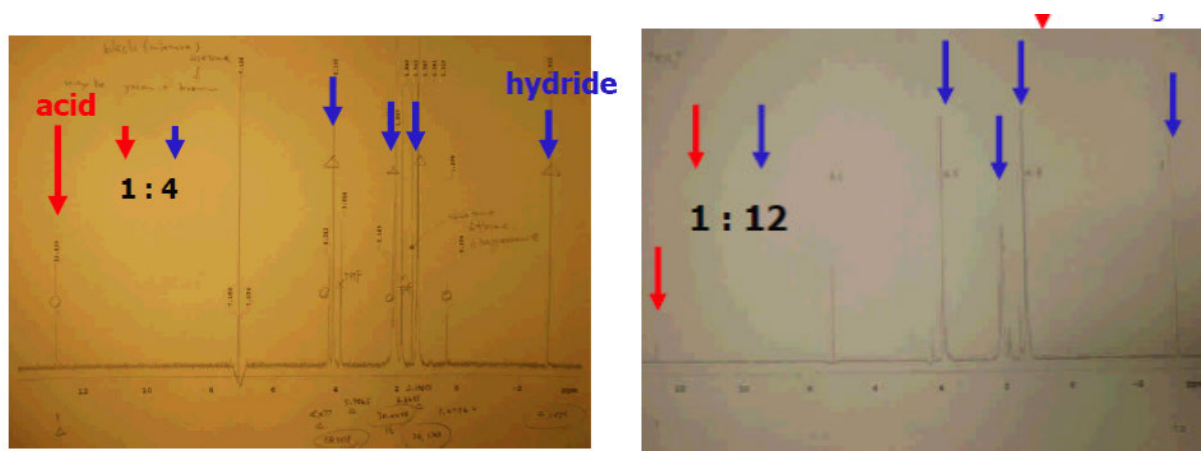


Figure SI-D2. ^1H NMR spectrum in benzene- d_6 of (left) the black $[(\text{Ir}(1,5\text{-COD})(\mu\text{-H}))_4]$ powder obtained by first concentrating the bright-green solution (after excess COD was added) to 5 mL under vacuum, and then adding 15 mL acetone before filtration. In a separate synthesis, the bright-green solution was first concentrated to 5 mL under vacuum and then the resulting mixture was filtered through a glass filter (without addition of acetone), and then (right) its ^1H NMR spectrum in benzene- d_6 was obtained. The spectrum on the left is a reproduction of Figure S1(left) provided for the sake of an easy comparison of the two ^1H NMR spectra.

3. Crystal Structure Data and Tables

3.1. Table SI-D3. Crystal data and structure refinement for $[\text{Ir}(\text{1,5-COD})(\mu\text{-H})]_4$.

Empirical formula	$\text{C}_{32}\text{H}_{52}\text{Ir}_4$	
Formula weight	1205.54	
Temperature	120(2) K	
Wavelength	0.71073 Å	
Crystal system	Orthorhombic	
Space group	Pbcn	
Unit cell dimensions	$a = 12.5628(3)$ Å	$a = 90^\circ$
	$b = 18.4647(5)$ Å	$b = 90^\circ$
	$c = 12.3963(3)$ Å	$g = 90^\circ$
Volume	$2875.55(12)$ Å ³	
Z	4	
Density (calculated)	2.785 Mg/m ³	
Absorption coefficient	18.473 mm ⁻¹	
F(000)	2208	
Crystal size	$0.08 \times 0.08 \times 0.08$ mm ³	
Theta range for data collection	3.19 to 33.17°	
Index ranges	$-19 \leq h \leq 19, -2 \leq k \leq 28, -19 \leq l \leq 18$	
Reflections collected	74947	
Independent reflections	5503 [R(int) = 0.0370]	
Completeness to theta = 33.17°	99.9 %	
Absorption correction	None	
Max. and min. transmission	0.3196 and 0.3196	
Refinement method	Full-matrix least-squares on F ²	
Data / restraints / parameters	5503 / 0 / 171	
Goodness-of-fit on F ²	1.110	
Final R indices [I > 2sigma(I)]	R1 = 0.0151, wR2 = 0.0312	
R indices (all data)	R1 = 0.0183, wR2 = 0.0318	
Largest diff. peak and hole	1.226 and -0.620 e/Å ⁻³	

3.2. Table SI-D4. Atomic coordinates ($\times 10^4$) and equivalent isotropic displacement parameters ($\text{\AA}^2 \times 10^3$) for $[(1,5\text{-COD})\text{Ir}(\mu\text{-H})_4]$. $U(\text{eq})$ is defined as one third of the trace of the orthogonalized U^{ij} tensor.

	x	y	z	U(eq)
Ir(1)	115(1)	1977(1)	8667(1)	9(1)
Ir(2)	1153(1)	959(1)	7384(1)	9(1)
C(3)	1445(2)	2713(1)	8760(2)	13(1)
C(4)	1441(2)	2295(1)	9709(2)	14(1)
C(5)	1094(2)	2580(1)	10807(2)	18(1)
C(6)	-88(2)	2439(1)	11022(2)	17(1)
C(7)	-742(2)	2401(1)	9993(2)	15(1)
C(8)	-722(2)	2939(1)	9170(2)	14(1)
C(9)	-19(2)	3611(1)	9243(2)	16(1)
C(10)	1060(2)	3492(1)	8697(2)	15(1)
C(11)	1167(2)	271(1)	5980(2)	15(1)
C(12)	2121(2)	667(1)	5985(2)	16(1)
C(13)	3188(2)	331(1)	6278(2)	20(1)
C(14)	3463(2)	468(2)	7461(2)	21(1)
C(15)	2482(2)	478(1)	8171(2)	15(1)
C(16)	1652(2)	-43(1)	8125(2)	13(1)
C(17)	1652(2)	-691(1)	7361(2)	16(1)
C(18)	1090(2)	-520(1)	6286(2)	17(1)

3.3. Table SI-D5. Bond lengths (Å) for [(1,5-COD)Ir(μ -H)]₄

Ir1-H1	1.71(3)	C3-C4	1.407(3)	C11-C12	1.405(3)
Ir1-H2	1.82(3)	C3-C10	1.520(3)	C11-C18	1.511(4)
Ir1-C7	2.116(2)	C3-H3A	0.9800	C11-H11A	0.9800
Ir1-C8	2.156(2)	C4-C5	1.524(3)	C12-C13	1.521(3)
Ir1-C3	2.156(2)	C4-H4A	0.9800	C12-H12A	0.9800
Ir1-C4	2.187(2)	C5-C6	1.532(3)	C13-C14	1.528(4)
Ir1-Ir2	2.78680(12)	C5-H5A	0.9700	C13-H13A	0.9700
Ir1-Ir2A	2.78798(12)	C5-H5B	0.9700	C13-H13B	0.9700
Ir1-Ir1A	2.90728(17)	C6-C7	1.519(3)	C14-C15	1.515(4)
Ir1-H1	1.71(3)	C6-H6A	0.9700	C14-H14A	0.9700
Ir1-H2	1.82(3)	C6-H6B	0.9700	C14-H14B	0.9700
Ir2-H2	1.67(3)	C7-C8	1.424(3)	C15-C16	1.419(3)
Ir2-H1A	1.74(3)	C7-H7A	0.9800	C15-H15A	0.9800
Ir2-C15	2.128(2)	C8-C9	1.525(3)	C16-C17	1.526(3)
Ir2-C11	2.155(2)	C8-H8A	0.9800	C16-H16A	0.9800
Ir2-C16	2.158(2)	C9-C10	1.530(3)	C17-C18	1.540(3)
Ir2-C12	2.186(2)	C9-H9A	0.9700	C17-H17A	0.9700
Ir2-Ir1A	2.78797(12)	C9-H9B	0.9700	C17-H17B	0.9700
Ir2-Ir2A	2.91138(17)	C10-H10A	0.9700	C18-H18A	0.9700
Ir2-H2	1.67(3)	C10-H10B	0.9700	C18-H18B	0.9700

3.4. Table SI-D6. Bond angles (°) for [(1,5-COD)Ir(μ -H)]₄

Ir1-H1-Ir2A	108.07(18)	C8-Ir1-Ir2	161.65(6)	C4-Ir1-H1	157.3(11)
Ir1-H2-Ir2	106.1(17)	C3-Ir1-Ir2	95.36(6)	Ir2-Ir1-H1	98.6(12)
Ir2-H1A-Ir1A	108.1(19)	C4-Ir1-Ir2	99.30(6)	Ir2A-Ir1-H1	36.3(12)
Ir1A-H2A-Ir2A	106.1(17)	H1-Ir1-Ir2A	36.3(12)	Ir1A-Ir1-H1	70.4(11)
H1-Ir1-H2	108.5(15)	H2-Ir1-Ir2A	75.0(10)	H1-Ir1-H2	108.5(15)
H1-Ir1-C7	78.0(11)	C7-Ir1-Ir2A	108.75(6)	C7-Ir1-H2	125.7(10)
H2-Ir1-C7	125.7(10)	C8-Ir1-Ir2A	114.33(6)	C8-Ir1-H2	162.9(10)
H1-Ir1-C8	78.3(12)	C3-Ir1-Ir2A	153.24(6)	C3-Ir1-H2	96.5(10)
H2-Ir1-C8	162.9(10)	C4-Ir1-Ir2A	153.08(6)	C4-Ir1-H2	79.2(10)
C7-Ir1-C8	38.93(9)	Ir2-Ir1-Ir2A	62.966(4)	Ir2-Ir1-H2	35.1(10)
H1-Ir1-C3	152.5(12)	H1-Ir1-Ir1A	70.4(11)	Ir2A-Ir1-H2	75.0(10)
H2-Ir1-C3	96.5(10)	H2-Ir1-Ir1A	93.3(10)	Ir1A-Ir1-H2	93.3(10)
C7-Ir1-C3	96.88(9)	C7-Ir1-Ir1A	136.25(7)	H1-Ir1-H2	108.5(15)
C8-Ir1-C3	80.99(9)	C8-Ir1-Ir1A	103.84(6)	H2-Ir2-H1A	108.2(16)
H1-Ir1-C4	157.3(11)	C3-Ir1-Ir1A	97.51(6)	H2-Ir2-C15	78.5(11)
H2-Ir1-C4	79.2(10)	C4-Ir1-Ir1A	131.57(6)	H1A-Ir2-C15	125.8(11)
C7-Ir1-C4	80.20(9)	Ir2-Ir1-Ir1A	58.586(3)	H2-Ir2-C11	154.0(11)
C8-Ir1-C4	88.85(9)	Ir2A-Ir1-Ir1A	58.547(3)	H1A-Ir2-C11	95.4(11)
C3-Ir1-C4	37.80(9)	H2-Ir1-H1	108.5(15)	C15-Ir2-C11	96.77(9)
H1-Ir1-Ir2	98.6(12)	C7-Ir1-H1	78.0(12)	H2-Ir2-C16	80.1(11)
H2-Ir1-Ir2	35.1(10)	C8-Ir1-H1	78.3(12)	H1A-Ir2-C16	162.0(11)
C7-Ir1-Ir2	158.65(7)	C3-Ir1-H1	152.5(12)	C15-Ir2-C16	38.67(9)

C11-Ir2-C16	80.57(9)	C16-Ir2-Ir2A	104.29(6)	C5-C4-H4A	113.9
H2-Ir2-C12	156.9(11)	C12-Ir2-Ir2A	129.22(7)	Ir1-C4-H4A	113.9
H1A-Ir2-C12	78.5(11)	Ir1-Ir2-Ir2A	58.537(3)	C4-C5-C6	111.95(19)
C15-Ir2-C12	79.88(9)	Ir1A-Ir2-Ir2A	58.497(3)	C4-C5-H5A	109.2
C11-Ir2-C12	37.75(9)	H2-Ir2-H2	0(2)	C6-C5-H5A	109.2
C16-Ir2-C12	87.98(9)	H1A-Ir2-H2	108.2(16)	C4-C5-H5B	109.2
H2-Ir2-Ir1	38.8(11)	C15-Ir2-H2	78.5(11)	C6-C5-H5B	109.2
H1A-Ir2-Ir1	73.5(11)	C11-Ir2-H2	154.0(11)	H5A-C5-H5B	107.9
C15-Ir2-Ir1	112.76(7)	C16-Ir2-H2	80.1(11)	C7-C6-C5	112.7(2)
C11-Ir2-Ir1	149.61(6)	C12-Ir2-H2	156.9(11)	C7-C6-H6A	109.1
C16-Ir2-Ir1	118.11(6)	Ir1-Ir2-H2	38.8(11)	C5-C6-H6A	109.1
C12-Ir2-Ir1	151.60(6)	Ir1A-Ir2-H2	101.3(11)	C7-C6-H6B	109.1
H2-Ir2-Ir1A	101.3(11)	Ir2A-Ir2-H2	73.3(11)	C5-C6-H6B	109.0
H1A-Ir2-Ir1A	35.6(11)	C4-C3-C10	124.2(2)	H6A-C6-H6B	107.8
C15-Ir2-Ir1A	160.77(7)	C4-C3-Ir1	72.27(13)	C8-C7-C6	124.0(2)
C11-Ir2-Ir1A	91.44(6)	C10-C3-Ir1	110.28(15)	C8-C7-Ir1	72.07(13)
C16-Ir2-Ir1A	160.56(6)	C4-C3-H3A	114.2	C6-C7-Ir1	113.22(16)
C12-Ir2-Ir1A	96.54(6)	C10-C3-H3A	114.2	C8-C7-H7A	113.6
Ir1-Ir2-Ir1A	62.867(4)	Ir1-C3-H3A	114.2	C6-C7-H7A	113.6
H2-Ir2-Ir2A	73.3(11)	C3-C4-C5	123.9(2)	Ir1-C7-H7A	113.6
H1A-Ir2-Ir2A	93.5(11)	C3-C4-Ir1	69.93(13)	C7-C8-C9	122.3(2)
C15-Ir2-Ir2A	137.33(7)	C5-C4-Ir1	113.76(16)	C7-C8-Ir1	69.00(13)
C11-Ir2-Ir2A	95.04(6)	C3-C4-H4A	113.9	C9-C8-Ir1	113.85(15)

C7-C8-H8A	114.5	C11-C12-C13	122.8(2)	C16-C15-H15A	113.7
C9-C8-H8A	114.5	C11-C12-Ir2	69.92(13)	C14-C15-H15A	113.7
Ir1-C8-H8A	114.5	C13-C12-Ir2	113.68(16)	Ir2-C15-H15A	113.7
C8-C9-C10	111.73(19)	C11-C12-H12A	114.3	C15-C16-C17	123.8(2)
C8-C9-H9A	109.3	C13-C12-H12A	114.3	C15-C16-Ir2	69.54(13)
C10-C9-H9A	109.3	Ir2-C12-H12A	114.3	C17-C16-Ir2	114.04(15)
C8-C9-H9B	109.3	C12-C13-C14	111.2(2)	C15-C16-H16A	113.9
C10-C9-H9B	109.3	C12-C13-H13A	109.4	C17-C16-H16A	113.9
H9A-C9-H9B	107.9	C14-C13-H13A	109.4	Ir2-C16-H16A	113.9
C3-C10-C9	113.25(19)	C12-C13-H13B	109.4	C16-C17-C18	112.10(19)
C3-C10-H10A	108.9	C14-C13-H13B	109.4	C16-C17-H17A	109.2
C9-C10-H10A	108.9	H13A-C13-H13B	108.0	C18-C17-H17A	109.2
C3-C10-H10B	108.9	C15-C14-C13	112.1(2)	C16-C17-H17B	109.2
C9-C10-H10B	108.9	C15-C14-H14A	109.2	C18-C17-17B	109.2
H10A-C10-H10B	107.7	C13-C14-H14A	109.2	H17A-C17-H17B	107.9
C12-C11-C18	123.8(2)	C15-C14-H14B	109.2	C11-C18-C17	112.7(2)
C12-C11-Ir2	72.33(13)	C13-C14-H14B	109.2	C11-C18-H18A	109.0
C18-C11-Ir2	111.48(15)	H14A-C14-H14B	107.9	C17-C18-H18A	109.0
C12-C11-H11A	114.0	C16-C15-C14	124.5(2)	C11-C18-H18B	109.0
C18-C11-H11A	114.0	C16-C15-Ir2	71.79(13)	C17-C18-H18B	109.0
Ir2-C11-H11A	114.0	C14-C15-Ir2	112.14(16)	H18A-C18-H18B	107.8

3.5. Table SI-D7. Anisotropic displacement parameters ($\approx 2 \times 10^3$) for $[\text{Ir}(1,5\text{-COD})(\mu\text{-H})]_4$. The anisotropic displacement factor exponent takes the form: $-2\pi^2 [h^2 a^{*2} U^{11} + \dots + 2 h k a^* b^* U^{12}]$

	U^{11}	U^{22}	U^{33}	U^{23}	U^{13}	U^{12}
Ir(1)	8(1)	9(1)	9(1)	-1(1)	0(1)	-1(1)
Ir(2)	8(1)	9(1)	9(1)	1(1)	1(1)	1(1)
C(3)	10(1)	14(1)	16(1)	-1(1)	0(1)	-3(1)
C(4)	13(1)	15(1)	15(1)	-2(1)	-5(1)	-1(1)
C(5)	23(1)	17(1)	13(1)	-2(1)	-5(1)	-4(1)
C(6)	24(1)	18(1)	10(1)	-2(1)	1(1)	-3(1)
C(7)	14(1)	16(1)	13(1)	-4(1)	4(1)	-1(1)
C(8)	13(1)	13(1)	16(1)	-4(1)	0(1)	1(1)
C(9)	19(1)	12(1)	18(1)	-2(1)	-2(1)	1(1)
C(10)	16(1)	14(1)	16(1)	1(1)	-2(1)	-5(1)
C(11)	18(1)	18(1)	10(1)	-2(1)	0(1)	5(1)
C(12)	17(1)	16(1)	14(1)	2(1)	7(1)	6(1)
C(13)	15(1)	15(1)	29(1)	5(1)	9(1)	4(1)
C(14)	10(1)	18(1)	34(1)	4(1)	0(1)	1(1)
C(15)	12(1)	17(1)	17(1)	1(1)	-3(1)	3(1)
C(16)	15(1)	14(1)	12(1)	4(1)	1(1)	3(1)
C(17)	15(1)	13(1)	19(1)	2(1)	3(1)	2(1)
C(18)	18(1)	15(1)	18(1)	-6(1)	0(1)	2(1)

3.6. Table SI-D8. Hydrogen coordinates ($\times 10^4$) and isotropic displacement parameters ($\text{\AA}^2 \times 10^3$) for $[\text{Ir}(1,5\text{-COD})(\mu\text{-H})_4]$.

	x	y	z	U(eq)
H(3A)	2028	2599	8263	16
H(4A)	2015	1936	9743	17
H(5A)	1229	3097	10840	21
H(5B)	1515	2349	11365	21
H(6A)	-162	1986	11411	21
H(6B)	-367	2823	11477	21
H(7A)	-1443	2178	10093	17
H(8A)	-1405	3017	8807	17
H(9A)	93	3733	9996	20
H(9B)	-379	4015	8902	20
H(10A)	1005	3632	7945	18
H(10B)	1583	3805	9035	18
H(11A)	665	418	5416	18
H(12A)	2162	1043	5429	19
H(13A)	3740	535	5823	24
H(13B)	3163	-187	6146	24
H(14A)	3943	91	7711	25
H(14B)	3830	928	7523	25
H(15A)	2612	668	8897	18
H(16A)	1314	-139	8823	16
H(17A)	1295	-1095	7706	19
H(17B)	2380	-834	7216	19
H(18A)	1406	-810	5719	20
H(18B)	346	-654	6343	20
H(1)	-1170(30)	1767(19)	8330(30)	28(9)
H(2)	900(30)	1148(18)	8670(30)	21(8)

4. Further Characterization Data for $[\text{Ir}(1,5\text{-COD})(\mu\text{-H})_4]$ crystal

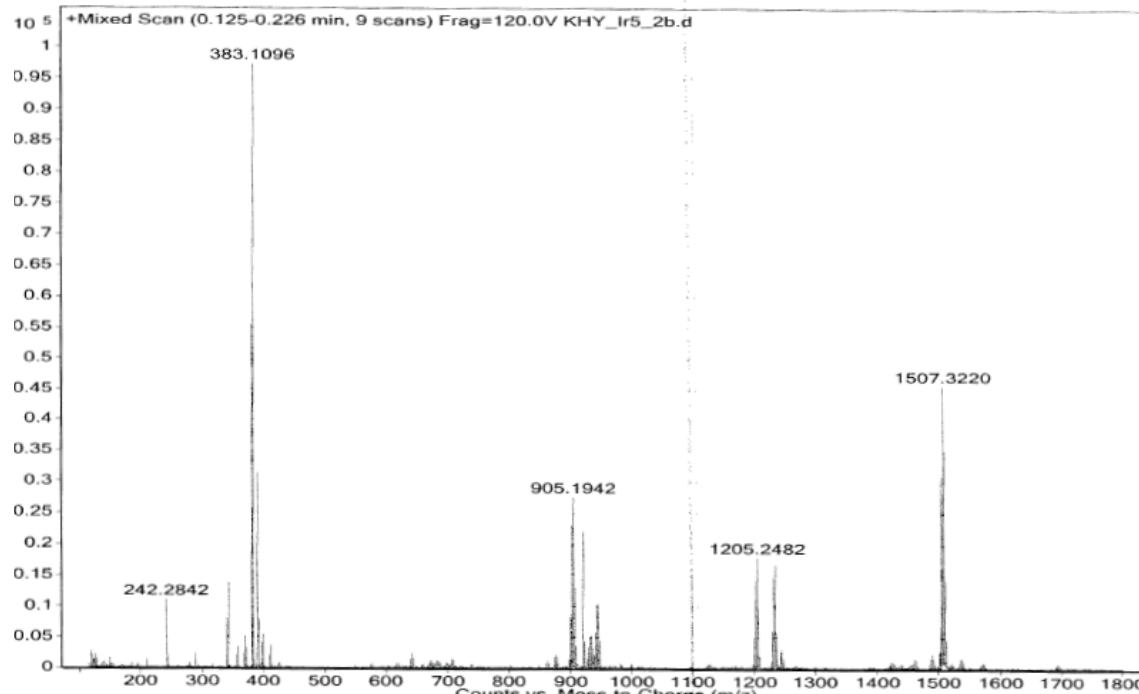


Figure SI-D3. The positive ion ESI MS (counts (y-axis) vs mass-to-charge ratio in Da (x-axis)) of a black $[(1,5\text{-COD})\text{Ir}(\mu\text{-H})_4]$ crystal dissolved in dichloromethane. The peak cluster at 1205.2478 Da is assigned to $[\text{C}_{32}\text{H}_{51}\text{Ir}_4]^+$ (Figure S2). The peak cluster at 1507.3229 Da is assigned to the Ir_5 species, $[\text{C}_{40}\text{H}_{66}\text{Ir}_5]^+$. The absence of an Ir_5 component in XRD or EXAFS analyses (see the main text) rules out the hypothesis that Ir_5 species are present in the initial crystal. Instead, the evidence provided in the main text argues that the Ir_5 species is an artifact of the ESI-MS analysis.

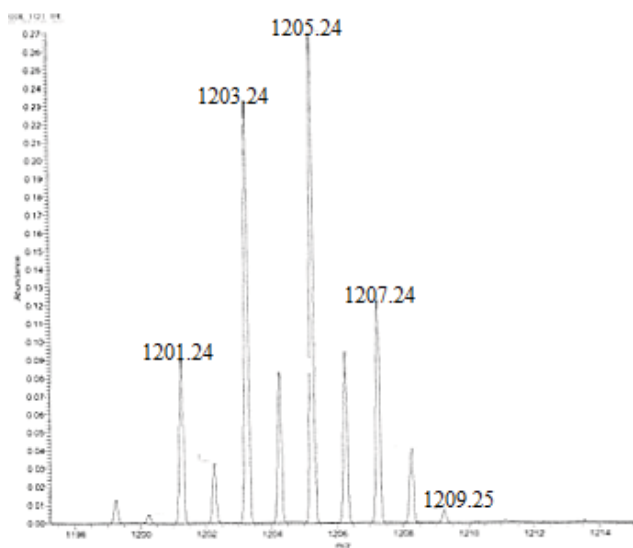
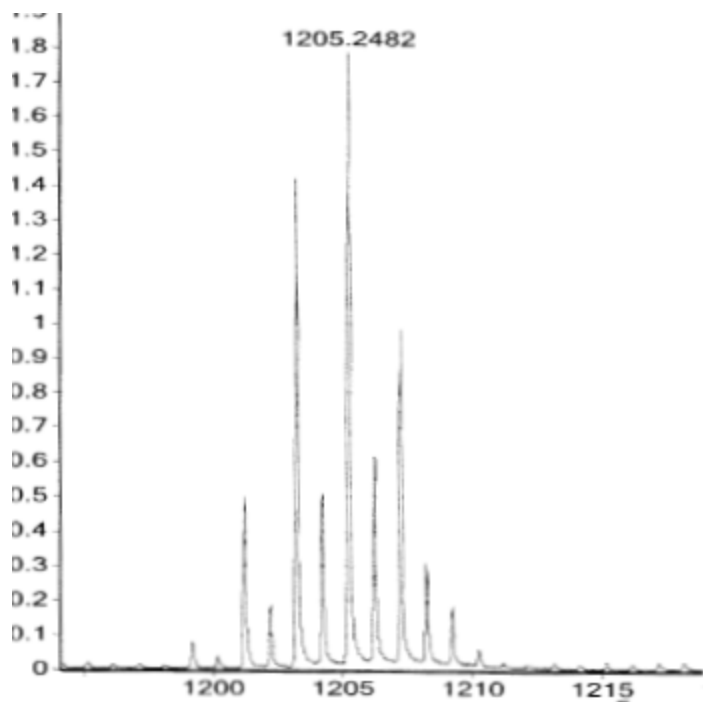


Figure SI-D4. The positive ion ESI MS ((counts (y-axis) vs mass-to-charge ratio in Da (x-axis)) of a black $[\text{Ir}(1,5\text{-COD})(\mu\text{-H})_4]$ crystal dissolved in dichloromethane (top), and most abundant peak at 1205.2478 Da and the simulated isotope peak distribution ((abundance (y-axis) vs mass-to-charge ratio in Da (x-axis)) for $[\text{C}_{32}\text{H}_{51}\text{Ir}_4]^+$ (bottom). A good match is apparent between the experimental (top) and simulated (bottom) spectra.

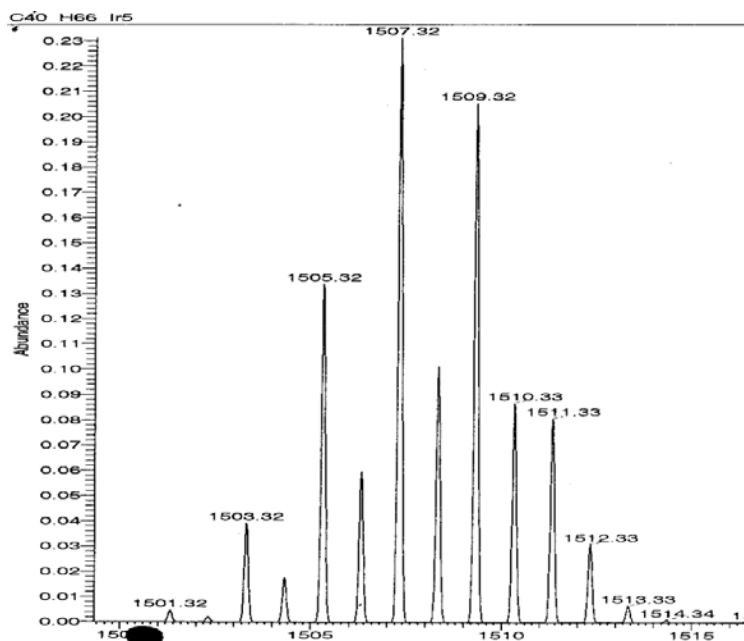
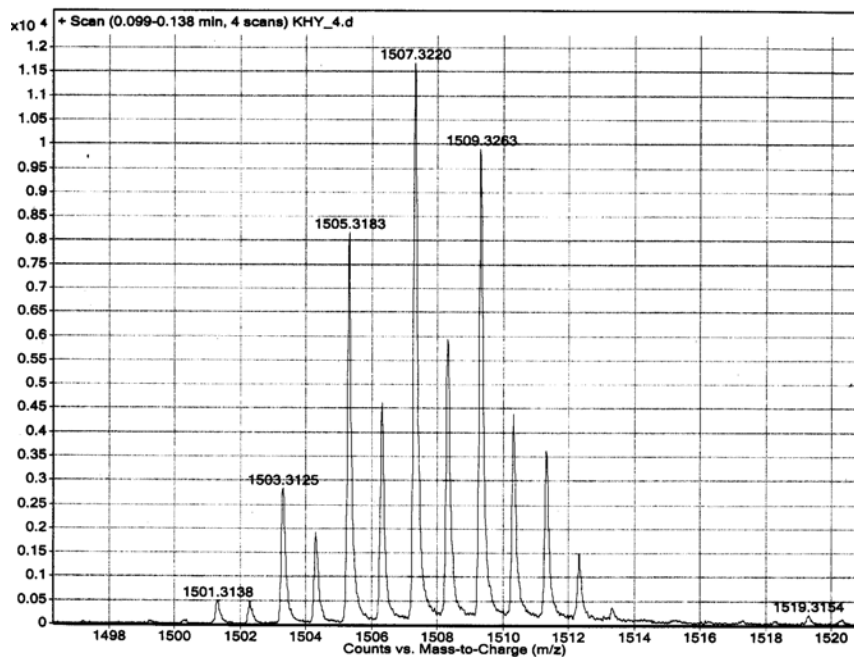


Figure SI-D5. The positive ion ESI MS of a black [Ir(1,5-COD)(μ -H)]₄ crystal dissolved in dichloromethane (top) with its most abundant peak at 1507.3229 Da, and (bottom) the simulated isotope peak distribution for [C₄₀H₆₆Ir₅]⁺. Again, a good match between the experimental (top) and simulated (bottom) spectra is apparent.

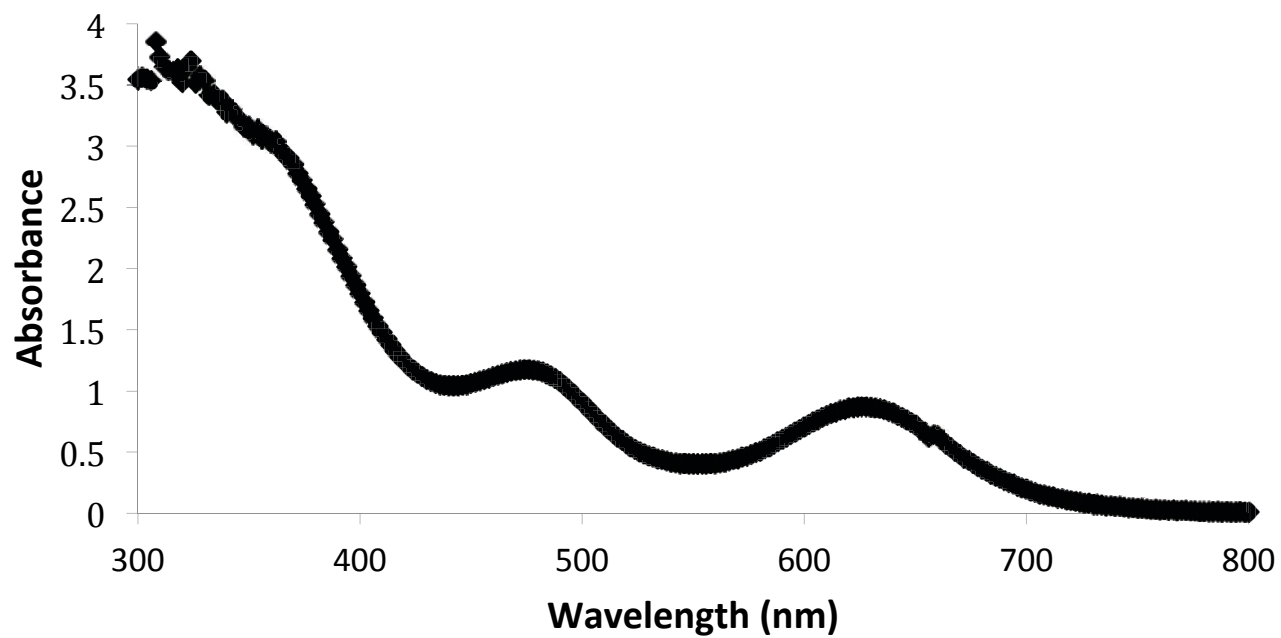


Figure SI-D6. UV-Vis spectrum of crystalline $[(1,5\text{-COD})\text{Ir}(\mu\text{-H})]_4$ dissolved in THF.

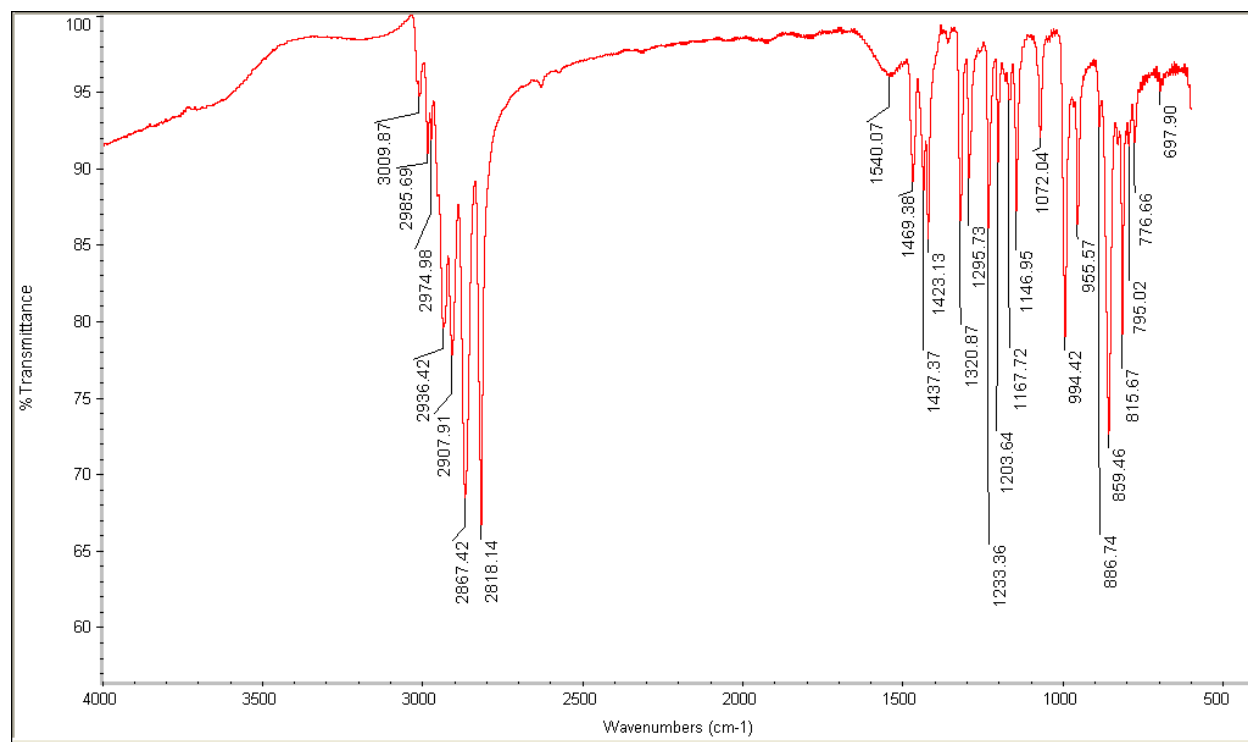


Figure SI-D7. Infrared spectrum of a black [(1,5-COD)Ir(μ -H)]₄ crystal as a KBr pellet. The observed peaks in cm⁻¹ are: 697.90, 766.66, 815.67, 859.46, 866.74, 994.42, 1072.04, 1146.95, 1167.72, 1203.64, 1233.36, 1295.73, 1320.87, 1423.13, 1437.37, 1469.38, 2818.14, 2867.42, 2907.91, 2936.42, 2985.69. For comparison, the signals in IR spectrum of the [(1,5-COD)Rh(μ -H)]₄ complex (see Duan, Z., Hampden-Smith, M. J.; Sylwester, A. P. *Chem. Mater.* 1992, 4, 1146-1148) are observed at: 682.5 cm⁻¹, 753.8 cm⁻¹, 811.8 cm⁻¹, 861.6 cm⁻¹, 880.5 cm⁻¹, 986.0 cm⁻¹, 1072.0 cm⁻¹, 1149.5 cm⁻¹, 1171.0 cm⁻¹, 1210.5 cm⁻¹, 1234.2 cm⁻¹, 1298.3 cm⁻¹, 1326.1 cm⁻¹, 1426.7 cm⁻¹, 1447.4 cm⁻¹, 1473.6 cm⁻¹, 2819.9 cm⁻¹, 2867.3 cm⁻¹, 2908.2 cm⁻¹, 2925.5 cm⁻¹, and 2993.0 cm⁻¹.

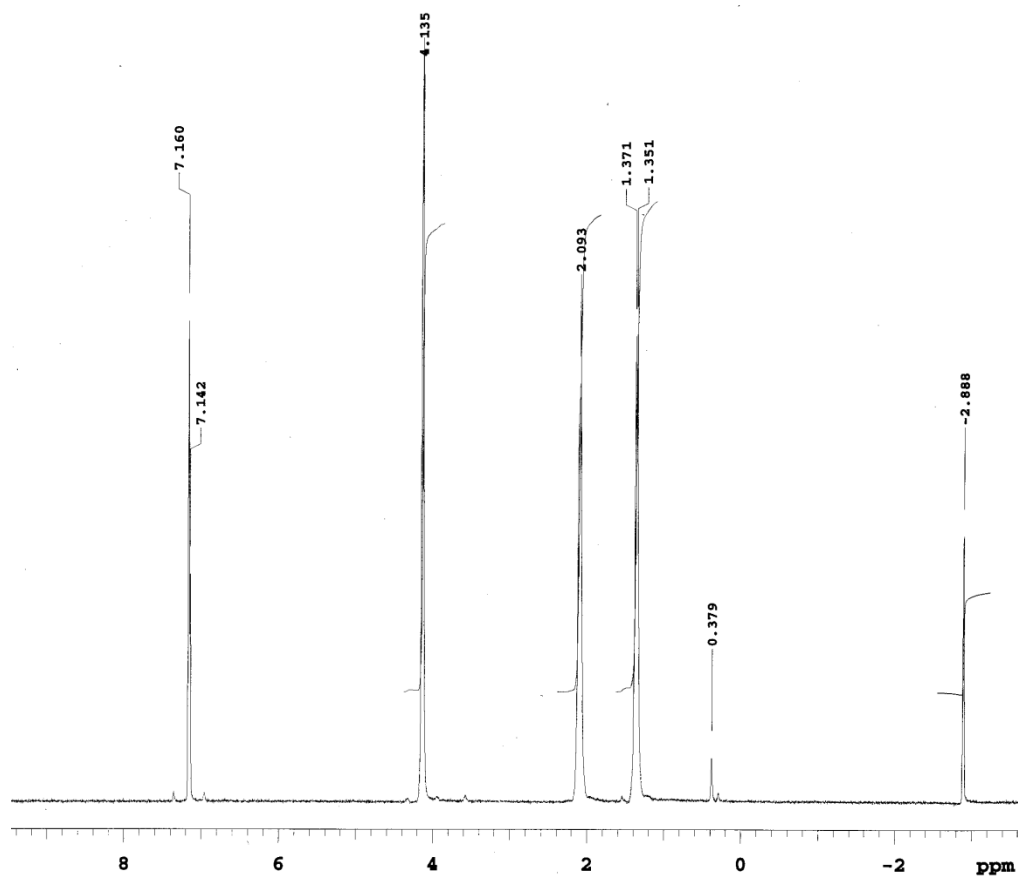


Figure SI-D8. ^1H NMR spectrum of crystalline $[\text{Ir}(1,5\text{-COD})(\mu\text{-H})]_4$ dissolved in benzene- d_6 . The signal at -2.89 ppm is assigned to the 4 hydrides based on its proper integration as 4 H. The signals at 4.14, 2.09, and 1.37 ppm are assigned to the 1,5-COD olefinic and methylene hydrogen atoms, respectively.

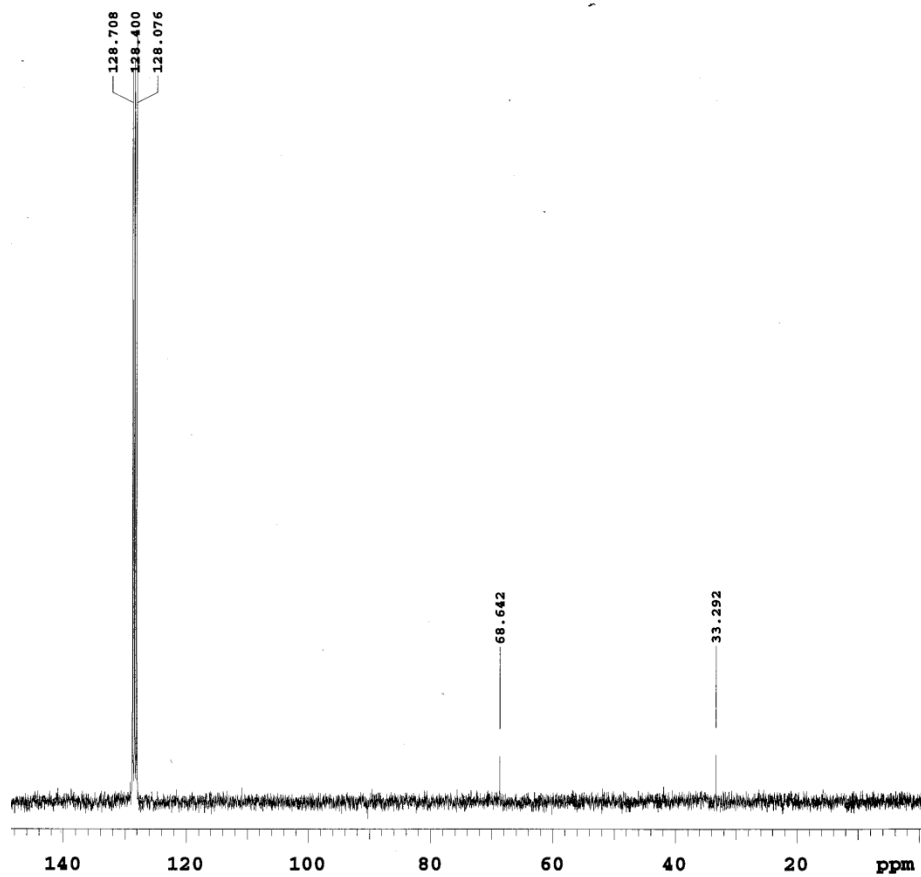


Figure SI-D9. The ^{13}C NMR spectrum of crystalline $[(1,5\text{-COD})\text{Ir}(\mu\text{-H})]_4$ dissolved in benzene- d_6 . The signals at signals at 68.64 and 33.29 ppm are assigned to the 1,5-COD ligands.

5. Experimental.

Instrumentation and Sample Preparation:

(i) *ESI MS:* The mass spectra were taken on a 2001 Agilent GC/MS system consisting of a 5973N Mass Selective Detector, a 6890 Plus Gas Chromatograph, a 7683 Autoinjector and a PC-based data system. The source was operated in mixed mode allowing simultaneous electrospray and atmospheric pressure chemical ionization. The data acquisition and peak assignments were performed using Agilent Mass Hunter Workstation Data Acquisition software. Approximately 0.1 mg of sample was dissolved in 1 mL of dichloromethane and then 0.2 μL of the dissolved sample was analyzed by flow injection with HPLC grade methanol as the carrier solvent. Using a fragmentation voltage of 180 V, the positive ion mass spectrum was recorded.

(ii) *UV-Visible:* The spectra were taken at CSU on a Hewlett-Packard 8452A diode-array spectrophotometer. The sample solutions (in THF) for UV-Visible analysis were prepared in air-free, 3x1x1 cm^3 glass UV-Visible cuvettes and loaded under N_2 atmosphere either inside the drybox or using a Schlenk line. The blank solution was prepared using only THF. The sample solutions were taken from the reaction vessels (3.0 mL, 4×10^{-4} M in [Ir]). The pure [(1,5-COD)Ir(μ -H)]₄ sample solution (4×10^{-4} in [Ir]) was taken from the pure, dark-green powdered [(1,5-COD)Ir(μ -H)]₄ synthesized without using any additional free 1,5-COD.

(iii) *IR spectroscopy:* The spectra was taken on a Nicolet Magna-IR 760 ESP FT-Raman spectrometer that uses a 1064nm Nd:YVO₄ excitation laser, a XT-KBr beam splitter, a He-Ne laser for sample alignment and a InGaAs detector. Samples were prepared in the drybox as KBr pellets, and placed in a ring-shaped steel IR sample holder. Next, the sample holder was placed in a glass vial and sealed under N_2 . The sealed glass vial was then placed in a dry-seal vacuum desiccator and the desiccator was sealed under N_2 . The desiccator with its thereby double-sealed, glass vial

sample was then brought out of the drybox and quickly transferred (i.e., with ~1 sec of air exposure) into the N₂ atmosphere of the IR instrument. (iv) *NMR*: The spectra (¹H and ¹³C) of sample solutions in benzene-d₆ were taken on a Varian Inova 400 instrument and analyzed with MestRec software. Observed chemical shifts were referenced to the proton impurity resonance of benzene-d₆ solvent. Spectral parameters for ¹H NMR (25°C, 400 MHz): Pulse, 31.0 degrees; acquisition time, 2.291 s; relaxation delay, 0.0 s; sweep width, 28000 Hz. Spectral parameters for ¹H NMR (-60°C, 400 MHz): Pulse, 34.0 degrees; acquisition time, 2.728 s; relaxation delay, 1.0 s; sweep width, 24000 Hz. Spectral parameters for ¹³C NMR (25°C, 100 MHz): Pulse, 44.5 degrees; acquisition time, 0.533 s; relaxation delay, 1.7 s; sweep width, 30000 Hz.

Control Experiment Synthesizing [Rh(1,5-COD)(μ-H)]₄ using Muetterties' procedure: In the drybox, an orange powder of [Rh(1,5-COD)Cl]₂ (0.735 g, 1.49 mmol) was dissolved in 50 mL THF in a 100 mL round-bottomed Schlenk flask equipped with side arm and a 5/8 × 5/16 in., Teflon-coated magnetic stirbar. LiBEt₃H (3 mL, 3 mmol) was measured out with a 5 mL syringe and transferred into a 50 mL, side-arm-equipped Schlenk flask. Both flasks were then sealed with a septum and brought out of the drybox. The 50 mL flask containing LiBEt₃H solution was attached to the Schlenk line through its side arm and N₂(g) was passed over the flask for 20 min. The 100 mL round-bottomed Schlenk flask was attached to the Schlenk line through its septum. N₂(g) gas was passed through the flask for 5 min as visually monitored via a bubbler connected through its side arm. The flask containing the orange [Rh(1,5-COD)Cl]₂ solution was placed in an acetone/dry ice bath at -78 °C and stirred for 15 min. The LiBEt₃H solution was then added dropwise to the orange [Rh(1,5-COD)Cl]₂ solution via a cannula under N₂(g). The color of the solution changed to dark-brown immediately after the addition of the first few drops of the

LiBEt₃H solution. The resulting solution was stirred at -78 °C for an additional 10 min and then at room temperature for 4 h. The solution slowly turned from dark-brown to dark-red after 1 h of stirring at room temperature. The volatiles were then removed under vacuum to yield a black residue. The reaction flask was then brought into the drybox and dissolved in 10 mL hexane. Activated silica gel column (height: ~4 cm, diameter: ~2 cm) was prepared in a Pyrex coarse fritted flask using hexane as the solvent. The black extract was passed through activated silica gel column. The dark-red solution (~150 mL) was collected, placed under vacuum and the volatiles removed, all while still at ca. room temperature. Dark-red crystals were obtained in a 50% yield. ¹H NMR in d₈-THF (ppm): 4.6 (singlet, 4H), 2.2 (multiplet, 4H), 1.7 (multiplet, 4H), -11.9 (quintet, 1H).

Control Experiment Synthesizing [Rh(1,5-COD)(μ-H)]₄ using Bönemann's procedure (but at a smaller scale, starting with 2 mmol of [Rh(1,5-COD)Cl]₂ vs 12.2 mmol of Rh-dimer in Bönemann's publication): In the drybox, orange powdered [Rh(1,5-COD)Cl]₂ (1.002 g) was completely dissolved in 33 mL THF in a 100 mL round-bottomed Schlenk flask equipped with side arm and a 5/8 × 5/16 in., Teflon-coated magnetic stirbar. A 10.0 mL portion of NaBEt₃H (Aldrich, 1.0 M solution in THF) solution was diluted with THF to 50 mL using a volumetric flask to obtain a 0.2 M solution. Dilute NaBEt₃H solution (0.2 M, 19 mL) was then transferred into a 50 mL dropping funnel. The dilute NaBEt₃H solution was added dropwise over 80 min to the orange [Rh(1,5-COD)Cl]₂ solution at room temperature, all while still in the drybox. The color of the solution changed to dark-red immediately following the addition of first few drops of NaBEt₃H. The resulting solution was stirred at room temperature under N₂ for 8 h. The volatiles were then removed under vacuum leaving a dark-red residue in the flask. The dark-red residue

was dried at 40 °C for 10 h. The residue was then extracted with 10 × 10 mL pentane. The dark-red extract was filtered through a medium porosity, 10 mL Pyrex fritted filter. A dark-red solution was collected in a 100 mL round bottomed flask. The volatiles were removed under vacuum at room temperature, and black crystals formed. ¹H NMR in d₈-THF (ppm): 4.577, 3.561, 2.441, 2.181, 1.731, -12.073.

Attempted synthesis of [Ir(1,5-COD)(μ-H)]₄ using Bönnemann's Rh-congener procedure: In the drybox, orange powdered [Ir(1,5-COD)Cl]₂ (1.00129 g, 1.5 mmol) was completely dissolved in 25 mL THF in a 200 mL round-bottomed Schlenk flask equipped with side arm and a 5/8 × 5/16 in., Teflon-coated magnetic stirbar. A 10.0 mL solution of NaBEt₃H (Aldrich, 1.0 M solution in THF) was diluted with THF to 50 mL using a volumetric flask. A portion of this diluted NaBEt₃H solution (0.2 M, 14 mL) was then transferred into a 25 mL dropping funnel. The dilute NaBEt₃H solution was added dropwise within 1 h to the orange [Ir(1,5-COD)Cl]₂ solution at room temperature, all while still in the drybox. The color of the solution changed to dark-brown immediately following the addition of first few drops of NaBEt₃H. The resulting solution was stirred at room temperature under N₂ for 8 h. The volatiles were then removed under vacuum leaving a black residue in the flask. The black residue was dried at room temperature for 2 h and then at 40 °C for 7 h. The residue was extracted with 6 × 10 mL pentane. The dark-green extract and black solid on the bottom of the glassware were filtered through a medium porosity 10 mL Pyrex fritted filter. A dark-green solution was collected in a 100 mL round-bottomed flask. The volatiles were removed under vacuum at room temperature; a thin layer of black powder formed on the walls of the flask. ¹H NMR in d₈-THF (ppm): 4.184, 3.560, 2.214, 1.708, 1.538, 1.354, 0.932, 0.087, -3.1333, -7.191.

Attempted Synthesis of [Ir(1,5-COD)(μ -H)]₄ using Hampden-Smith's Rh-congener procedure: In the drybox, orange powdered [Ir(1,5-COD)Cl]₂ (0.67171 g, 1 mmol) was dissolved in 38 mL THF in a 100 mL round-bottomed Schlenk flask equipped with side arm and a 5/8 × 5/16 in., Teflon-coated magnetic stirbar. LiBEt₃H (2 mL, 1.0 M, 2 mmol) was measured out with a 1 mL syringe and transferred into a 3 mL, side-arm-equipped Schlenk flask. Both flasks were then sealed with septa under N₂ and brought out of the drybox. The 3 mL flask containing the LiBEt₃H solution was attached to the Schlenk line through its side arm and N₂(g) was passed over the solution for 20 min. The 100 mL round-bottomed Schlenk flask was attached to a Schlenk line through its septum. Nitrogen gas was passed through the solution for 5 min as visually monitored using a bubbler connected through a side arm. The flask containing the orange solution of [Ir(1,5-COD)Cl]₂ was placed in ice bath at 0 °C and stirred for 15 min. The LiBEt₃H solution was then added dropwise to the orange [Ir(1,5-COD)Cl]₂ solution with a cannula under N₂(g). The color of the solution changed to dark-brown upon addition of the first few drops of the LiBEt₃H solution. The resulting solution was stirred at room temperature for an additional 4.5 h. The dark-brown solution was then brought into the drybox and concentrated to ~10 mL under vacuum at room temperature. An activated silica gel column (height: ~5 cm, diameter: ~2 cm) was prepared in a Pyrex, coarse-fritted filter using pentane as the solvent. The dark-brown solution was passed through the activated-silica-gel column. A dark-green solution was collected in a 100 mL round-bottomed flask. The volatiles were then removed under vacuum at room temperature; a thin layer of dark-green powder formed on the walls of the flask. ¹H NMR in d₆-benzene (ppm): 4.132, 2.100, 1.500, 1.370, 0.935, 0.412, 0.295, -2.884.

Attempted synthesis of [(1,5-COD)Ir(μ -H)]₄ using Muetterties' original Rh-congener procedure: In a drybox, orange powdered [Ir(1,5-COD)Cl]₂ (0.67171 g, 1 mmol) was dissolved in

38 mL THF in a 100 mL round-bottomed Schlenk flask equipped with side arm and a 5/8 ×5/16 in., Teflon-coated magnetic stirbar. LiBEt₃H (2 mL, 2 mmol) was measured out with a 1 mL syringe and transferred into a 3 mL side-arm-equipped Schlenk flask. Both flasks were then sealed with septa and brought out of the drybox. The 3 mL flask containing the LiBEt₃H solution was attached to the Schlenk line through its side arm and N₂(g) passed over the solution for 20 min. The 100 mL round-bottomed Schlenk flask was attached to a Schlenk line through its septum. Nitrogen gas was passed through the solution for 5 min as visually monitored via a bubbler connected through the side arm. The flask containing the orange solution of [Ir(1,5-COD)Cl]₂ was placed in an acetone/dry ice bath at -76°C and stirred for 15 min. The LiBEt₃H solution was then added dropwise to the orange [Ir(1,5-COD)Cl]₂ solution via a cannula under N₂(g). The color of the solution changed to brown/black upon the addition of the LiBEt₃H. The resulting solution was stirred at -78°C for an additional 10 min, and then at room temperature for 4 h. The volatiles were then removed under vacuum and the reaction flask was taken into the drybox. The residue was extracted with 6 × 10 mL hexane. The black extract was concentrated to ~10 mL under vacuum at room temperature. An activated-silica-gel column (height: ~4 cm, diameter: ~2 cm) was prepared in a Pyrex coarse fritted filter using hexane as the solvent. The black extract was passed through the activated-silica-gel column using a total of ~450 mL hexane. A dark-green solution (~150 mL) was collected and concentrated to ~10 mL under vacuum. The resulting solution was kept over dry ice at -76°C for 10 h. The volatiles were then removed under vacuum; a small layer of dark-green powder formed on the walls of the flask. Yield: ~1% based on the starting [Ir(1,5-COD)Cl]₂. ESI/APCI MS (peak m/z, assigned ion⁺) in toluene using MeOH as a mobile phase: 1221.2411 Da, [(1,5-COD)₄Ir₄H₃O]⁺; 933.1572 Da, [(1,5-COD)₄Ir₃O₂]⁺. ¹H NMR (in C₆D₆) (δ in ppm, number of H): 4.144, 4; 2.112, 4; -2.882, 1. ¹³C

NMR (in C₆D₆) (δ in ppm): 68.112, 32.768. IR (cm⁻¹): 486.18, 592.92, 696.76, 815.49, 858.90, 887.15, 955.64, 994.30, 1072.16, 1146.70, 1167.61, 1233.69, 1261.98, 1296.02, 1320.26, 1423.05, 1437.08, 1469.13, 2817.63, 2866.76, 2908.11, 2929.64, 2985.81. UV-Visible peaks (nm): 476, 622.

Characterization of the dark-green powder of [Ir(1,5-COD)(μ -H)]₄ synthesized in ~1% yield using Muetterties' original Rh-congener procedure:

The ESI-MS and other characterization results which follow were on our earliest, ~1% yield sample produced by Muetterties' Rh-congener procedure. In that sense, the results which follow are not crucial to the main text or the conclusions therein. However, the results below have been recorded here for the sake of completeness, and since the unexpected ESI-MS results which follow, in which an O atom is seen in the product, may be of some use to others in the future.

(i) *ESI MS*: The negative-ion ESI MS of the dark-green, powdered, ostensibly [Ir(1,5-COD)(μ -H)]₄ dissolved in toluene, with MeOH used as mobile phase, exhibits a most abundant peak located at 1221.2411 Da (Figure SI-D8). The experimentally observed isotope peak distribution pattern matches exactly the simulated isotopic distribution for an [C₃₂H₅₁Ir₄O]⁻ anion (Figure SI-D8)—*note the presence of the O in this formula*. This peak cluster is assigned to [(1,5-COD)₄Ir₄H₃O]⁻ anion. A fragment ion, with a most abundant peak located at 933.1572 Da, is also observed in the ESI MS (Figure S9) of this material. This peak cluster at 933.1572 Da was assigned to a [(1,5-COD)₃Ir₃O₂]⁻ fragment. The presence of O in the above mentioned anionic

formulas is essential for obtaining a good match between the experimental and simulated mass spectra.⁸

Attachment of O atom(s) to the observed Ir₄ and Ir₃ species have, presumably, occurred during ionization process and accompanied by loss of one or more hydride(s) from the parent molecule.⁹ Presence of O atom in the molecular formulas of detected [(1,5-COD)₄Ir₄H₃O]⁻ and [(1,5-COD)₃Ir₃O₂]⁻ anions raises the question if O is originated from the original sample or if O became attached to the detected anions during the ionization, desorption process in the ESI MS—that is, is the initial compound from the Muttterties' procedure [Ir(1,5-COD)(μ-H)]₄, or conceivably something like [(1,5-COD)₄Ir₄(μ-H)₃(OH)] (with one H⁺ added to the ESI MS-detected [(1,5-COD)₄Ir₄H₃O]⁻ anion) or, possibly, some other molecule containing an Ir₄ core and an O atom? The presence of O in the original, putative [Ir(1,5-COD)(μ-H)]₄, at least in the form of OH or CO and within detection limit of the methods used, is ruled out by ¹H, ¹³C NMR and IR spectra.¹⁰ Despite the fact that the real source of O atom(s) is unknown, the similarity between

⁸ Attachment of a Cs atom to an Ir₄ cluster has been reported in ESI MS analysis of *tert*-butylcalix[4]arene(OPr)₃(OCH₂PPh₂)-Ir₄(CO)₁₁^{1a}, but we were not able to find a prior example of attachment of an O atom to an Ir₄ cluster as a result of ESI-MS. (a) Silva, N.; Solovyov, A.; Katz, A. *Dalton Trans.* **2010**, 39, 2194-2197.

⁹ The O transferred to the [(1,5-COD)Ir(μ-H)]₄ molecule has two possible sources that we can see. (i) First, superoxide anion radical, O₂⁻, produced from atmospheric O₂ is common in APCI sources due to the high electron affinity of O₂ (EA= 0.448 ± 0.06 eV),^{2a} which in turn means that O₂⁻ often exists in atmospheric pressure ion sources of APCI MS.^{2b,2c} (ii) Alternatively, OH⁻ anion produced from MeOH used as mobile phase is a second, at least conceivable source of the observed O atom. Anion attachment has been observed in the literature when anions such as Cl⁻, NO₃⁻, NO₂⁻, acetate, formate or propionate were added to the mobile phase.^{2b,2d,2e} The use of such anion additives, in analysis of compounds that possess low gas-phase acidities or negative electron affinities, have resulted in attachment of one or more anion(s) to the parent or fragment molecules. (a) Ervin, K. M.; Anusiewicz, W.; Skurski, P.; Simons, J.; Lineberger, W. C. *J. Phys. Chem. A* **2003**, 107, 8521-8529. (b) Song, L.; Wellman, A. D.; Yao, H.; Bartmess, J. E. *J. Am. Soc. Mass Spectrom.* **2007**, 18, 1789-1798. (c) Kostianen, R.; Kauppila, T. J. *J. Chromatogr. A* **2009**, 1216, 685-699 and references (151-154) therein. (d) Tannenbaum, H. P.; Roberts, J. D.; Dougherty, R. C. *Anal. Chem.* **1975**, 47, 49-54. (e) Pan, X.; Tian, K.; Jones, L. E.; Cobb, G. P. *Talanta* **2006**, 70, 455-459.

¹⁰ This alternative hypothesis of O present as OH or CO in the original material is ruled out by five lines of evidence from ¹H, ¹³C NMR and IR studies: (i) the absence of a signal in -OH region (~3100-3650 cm⁻¹)¹⁰ in the IR spectrum of powder of ostensibly [(1,5-COD)Ir(μ-H)]₄ (Figure SI-D12) provides evidence against the presence of -OH. In addition, (ii) signals characteristic of -OH groups of carboxylic acids (~10-12 ppm) or alcohols (R-OH, ~1-

experimentally recorded peak clusters and the simulated isotope peak distributions provides clear evidence for the $[\text{C}_{32}\text{H}_{51}\text{Ir}_4\text{O}]^-$ and $[\text{C}_{24}\text{H}_{36}\text{Ir}_3\text{O}_2]^-$ anions. These O-containing anions observed by ESI-MS are, therefore and presumably, formed from $[\text{Ir}(1,5\text{-COD})(\mu\text{-H})]_4$. That said, simple control experiments, in which authentic $[\text{Ir}(1,5\text{-COD})(\mu\text{-H})]_4$ was re-examined by ESI-MS and under the precise toluene/MeOH conditions used above, can be easily done by anyone interested in further insights into the source of O seen in these ESI-MS. These results are, again, included here only for the sake of completeness in reporting even our earliest results en route to the final synthesis and characterization of $[\text{Ir}(1,5\text{-COD})(\mu\text{-H})]_{4\pm}$ reported in the main text.

5 ppm) are absent in the ^1H NMR spectrum of the powdered product (Figure SI-D7). (iii) Integration of ^1H NMR signals shows the theoretically expected atomic ratio (i.e.: olefinic $-\text{H}$ on COD (4.144 ppm): Other $-\text{H}$ on COD (2.112 ppm): Hydride (-2.882 ppm) = 4:4:1). (iv) The IR spectrum of $[(1,5\text{-COD})\text{Ir}(\mu\text{-H})]_4$ complex lacks any peak in carbonyl region ($1550\text{-}1820\text{ cm}^{-1}$)¹⁰, arguing against the presence of $-\text{O}$ in the form of a carbonyl, CO, ligand. Furthermore, (v) ^{13}C NMR spectrum (Figure SI-D13) rules out presence of aldehyde, ketone, carboxylic acid or ester carbonyls confirmed by the absence of peaks between 160-200 ppm region. (a) Socrates, G. In *Infrared and Raman Characteristics Group Frequencies: Tables and Charts*, 3rd Ed.; John Wiley and Sons, Ltd.: New York, 2006. (b) Coates, J. In *Encyclopedia of Analytical Chemistry*; Meyers, R. A., Ed.; John Wiley and Sons Ltd.: Chichester, 2000.

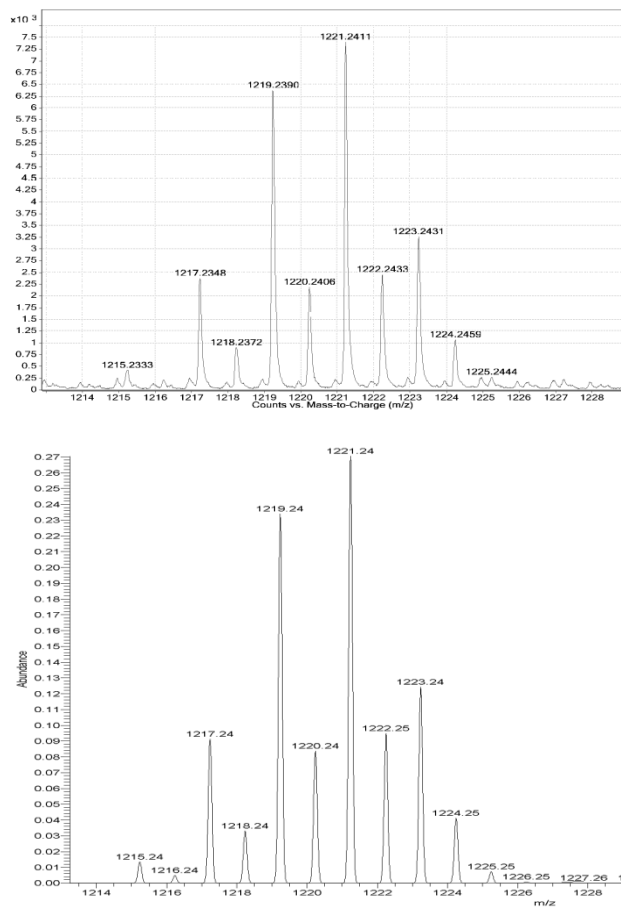


Figure SI-D10. The negative ion ESI/APCI MS, of the powder of [(1,5-COD)Ir(μ -H)₄] from Mutterties' procedure, exhibiting a most abundant peak at 1221.2411 Da when in dissolved in toluene and using MeOH as a mobile phase (top), and simulated isotope peak distribution for [C₃₂H₅₁Ir₄O]⁻ anion (bottom). Note the good match (with a 2.76 ppm mass error as confirmed by Agilent MassHunter software) between the experimental (top) and simulated (bottom) spectra.

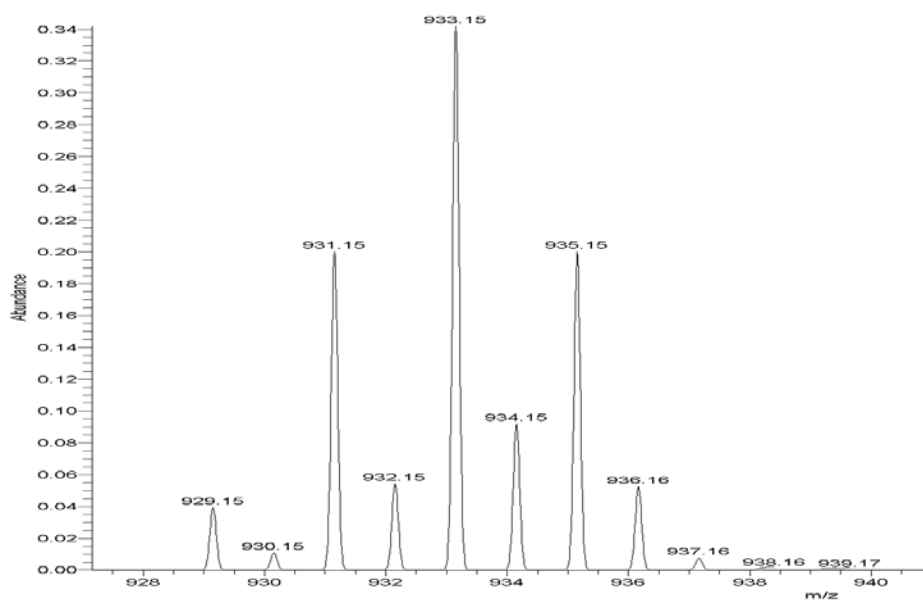
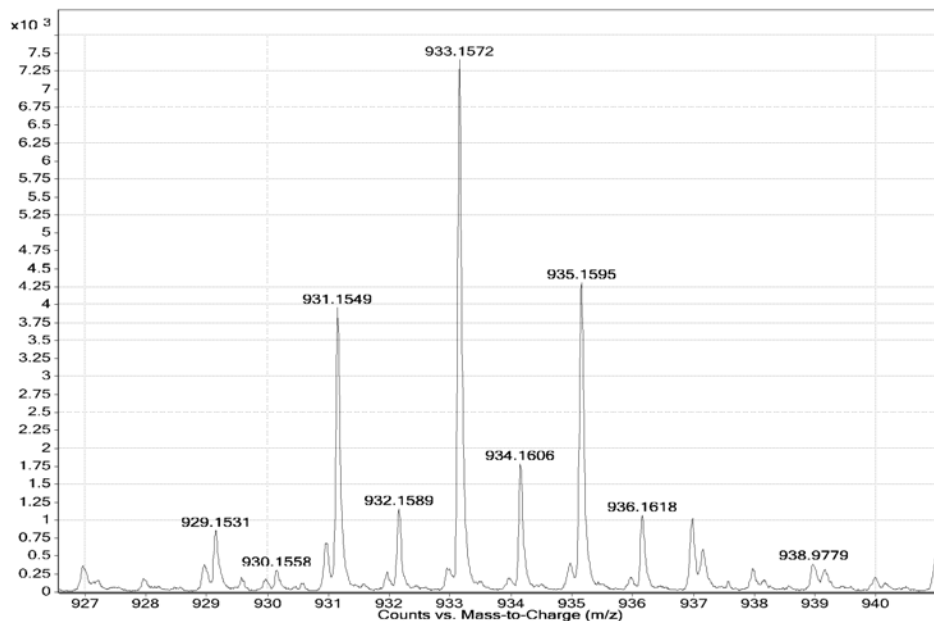


Figure SI-D11. The negative ion ESI MS of the dark-green powder, of $[(1,5\text{-COD})\text{Ir}(\mu\text{-H})_4]$ from Mutterties' procedure, dissolved in toluene with MeOH as a mobile phase exhibiting an abundant peak at 933.1572 Da peak (top), and simulated isotope peak distribution for a $[\text{C}_{24}\text{H}_{36}\text{Ir}_3\text{O}_2]^-$ anion (bottom). Note the good fit (i.e.; 1.53 ppm mass error calculated by Agilent MassHunter software) between the experimental (top) and simulated (bottom) spectra.

(ii) **¹H NMR:** ¹H NMR spectrum of the dark-green powder, of [(1,5-COD)Ir(μ-H)]₄ from Mutterties' procedure, (Figure S12) shows a signal at -2.88 ppm attributed to the hydride, and signals at 4.14, 2.11, and 1.37 ppm assigned to the olefinic and methylene hydrogen atoms, respectively. The signals at 1.37 ppm and 0.300 ppm are due to silica-gel column employed for purification of this low-yield product in the case of the Mutterties procedure. Integration reveals a ratio of peaks of: olefinic -H on COD (4.14 ppm): other (saturated) -H on COD (2.11 ppm): hydride (-2.88 ppm) = 4:4:1 (vs expected 4:8:1).

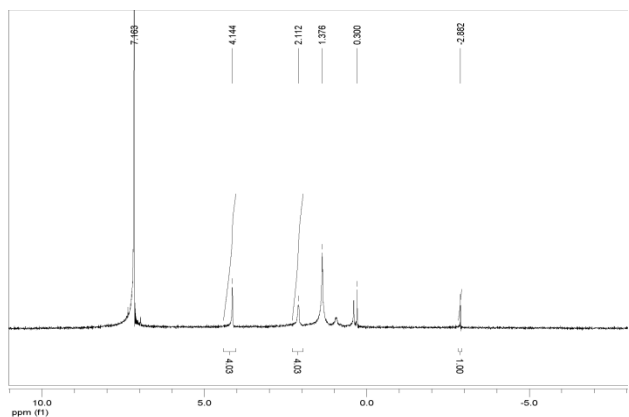


Figure SI-D12. ¹H NMR spectrum of dark-green powder, of [(1,5-COD)Ir(μ-H)]₄ from Mutterties' procedure, in benzene-d₆ and integration values (below the spectrum) of selected peaks.

(iii) **¹³C NMR:** ¹³C NMR spectrum of dark-green powdered [(1,5-COD)Ir(μ-H)]₄ exhibiting signals at 68.11 and 32.76 ppm for the COD ligands (Figure S13).

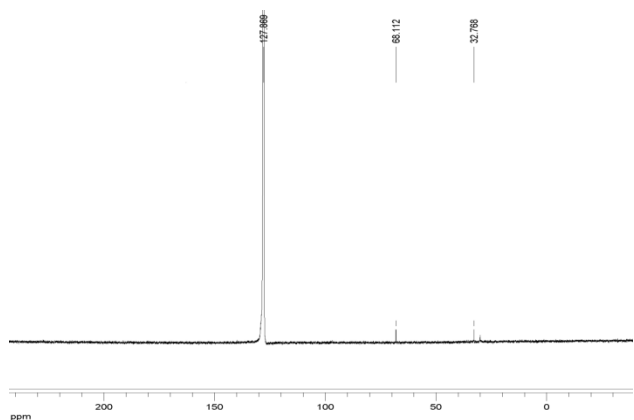


Figure SI-D13. ¹³C NMR spectrum of dark-green powdered [(1,5-COD)Ir(μ-H)]₄ from Mutterties' procedure in benzene-d₆.

(iv) IR Spectrum: The IR spectrum of dark-green powdered [(1,5-COD)Ir(μ -H)]₄ from Mutterties' procedure (Figure SI-D14).

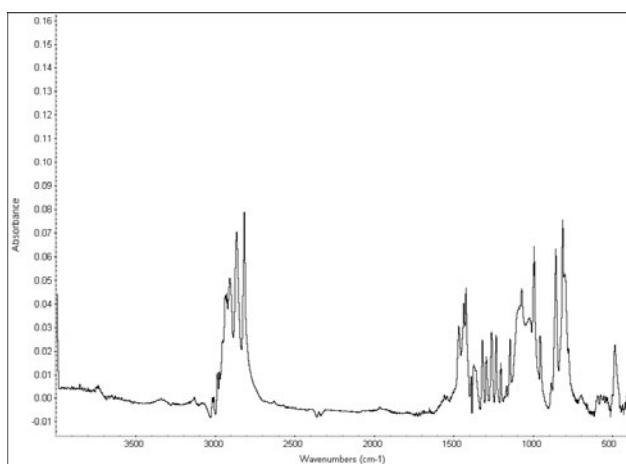


Figure SI-D14. Infrared spectrum of the [(1,5-COD)Ir(μ -H)]₄ powder (KBr pellet). The peaks are observed at 486.18 cm⁻¹, 592.92 cm⁻¹, 696.76 cm⁻¹, 815.49 cm⁻¹, 858.90 cm⁻¹, 887.15 cm⁻¹, 955.64 cm⁻¹, 994.30 cm⁻¹, 1072.16 cm⁻¹, 1146.70 cm⁻¹, 1167.61 cm⁻¹, 1233.69 cm⁻¹, 1261.98 cm⁻¹, 1296.02 cm⁻¹, 1320.26 cm⁻¹, 1423.05 cm⁻¹, 1437.08 cm⁻¹, 1469.13 cm⁻¹, 2817.63 cm⁻¹, 2866.76 cm⁻¹, 2908.11 cm⁻¹, 2929.64 cm⁻¹, 2985.81 cm⁻¹.

(v) *UV-Visible:*

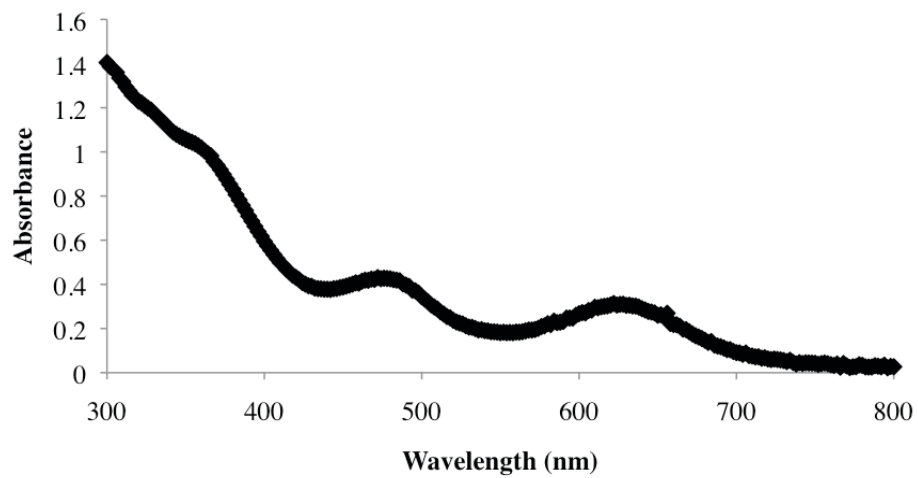


Figure SI-D15. UV-Vis spectra of dark green powder of $[\text{Ir}(1,5\text{-COD})(\mu\text{-H})_4]_4$ from Mutterties' procedure.

(vi) XPS:

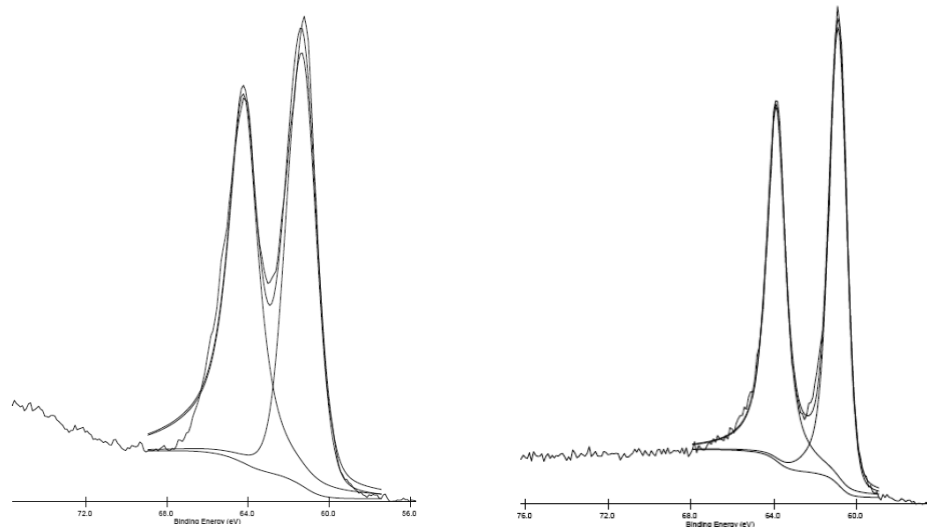


Figure SI-D16. High resolution XPS spectrum of dark-green powder of $[\text{Ir}(1,5\text{-COD})(\mu\text{-H})_4]$ from Muttarties' procedure deposited on a C-film (left). The Ir 4f peaks are located at 64.2 eV and 61.4 eV. Comparison of these peak positions to those of commercially available $\text{Ir}(0)_n$ bulk sample (right) (63.9 eV and 60.9 eV) is consistent with the presence of formally Ir(I) in $[\text{Ir}(1,5\text{-COD})(\mu\text{-H})_4]$ (see, however, the XANES results and discussion in the main text).

Control Experiments Performed to Determine the Best Conditions to Decrease the Amount of ¹H NMR-Detected, 12.82 ppm Impurity:

Control Experiment #1 - Washing the black powder with larger amount (250 mL) of acetone: In the drybox, orange powdered [Ir(1,5-COD)(μ-Cl)]₂ (0.5 mmol) was weighed out and then transferred into a 100 mL round-bottomed Schlenk flask equipped with a side arm and a 5/8 by 5/16 in., Teflon-coated magnetic stirbar. The flask was sealed, removed from the drybox, and placed on a Schlenk line under Ar via its side arm. Next, 20 mL of room temperature THF was added to the flask using a cannula to form an orange solution with some undissolved orange powder. The flask containing the orange solution of [Ir(1,5-COD)(μ-Cl)]₂ was placed in an acetone/dry ice bath at -78°C and stirred for 15 min. A 2.5 mL gas-tight syringe was purged three times with Ar using a Schlenk line. The gas-tight syringe was then used to measure out LiBEt₃H (2.0 mmol). The LiBEt₃H was then added dropwise to the orange [Ir(1,5-COD)(μ-Cl)]₂ solution under an Ar atmosphere with stirring, during which time the solution changed to dark-brown. The resulting solution was stirred at -78°C for an additional 10 min and then warmed to room temperature. The solution slowly turned from dark-brown to dark-green within 10 min of additional stirring at room temperature. Next, 1,5-COD (12.3 mL, 25 eq per Ir) was measured out with a 20 mL gas-tight syringe purged with Ar, and then added over 5-10 min to the dark-green solution. The resulting bright-green solution was stirred at room temperature for 30 min and then concentrated to ~5 mL under vacuum at room temperature by attachment to a Schlenk line. A visually apparent black powder was formed in the bright-green solution upon evaporation of the volatiles under vacuum. A 15 mL portion of acetone was added using a 20 mL gas-tight syringe to the mixture resulting in a black powder plus a bright-green solution. The black

powder was separated from bright-green solution under Ar using a glass-frit-filter Schlenk apparatus in which the open end of the glass filter was sealed by a rubber septum. The black powder collected on top of the glass-frit was washed with degassed H₂O (5 mL x 2) and degassed acetone (25 mL x 10) using a gas-tight syringe that had been previously purged with Ar. The black powder was then dried overnight under vacuum at room temperature resulting in black powder that was transported to the drybox and stored in the glass-frit-filer Schlenk apparatus sealed via a rubber septum. The black powder was then dissolved in benzene-d₆ for ¹H NMR (Figure S1(right), vide supra).

In a control synthesis, 1 mmol of [(Ir(1,5-COD)(μ-Cl))₂] (i.e., twice the scale of the above procedure) was used along with the same procedure as above up to the step of washing the black precipitate (except for 2-fold scaling where necessary). More specifically, the orange powdered [Ir(1,5-COD)(μ-H)]₄ was dissolved in 40 mL of THF. The orange solution was mixed with 4.0 mmol LiBEt₃H and then 24.6 mL 1,5-COD (25 eq per Ir) using the same procedure as given above. Then, the black powder was washed with degassed H₂O (5 mL x 2) and then degassed acetone (5 mL x 3) (i.e., a total of 15 mL acetone in this synthesis vs 250 mL in the above synthesis). The resultant black powder was then dissolved in benzene-d₆ for H NMR (Figure S1(left), vide supra).

Control Experiment #2 - Increasing the stirring time after addition of excess COD: In the drybox orange powdered [Ir(1,5-COD)(μ-Cl)]₂ (0.5 mmol) was weighed out and then transferred into a 100 mL round-bottomed Schlenk flask equipped with a side arm and a 5/8 by 5/16 in., Teflon-coated magnetic stirbar. The flask was sealed, removed from the drybox, and placed on a Schlenk line under Ar via its side arm. Next, 20 mL of room temperature THF was added to the

flask using a cannula forming an orange solution with some undissolved orange powder. The flask containing the orange solution of $[\text{Ir}(1,5\text{-COD})(\mu\text{-Cl})_2]$ was placed in an acetone/dry ice bath at -78°C and stirred for 15 min. A 2.5 mL gas-tight syringe was purged three times with Ar using a Schlenk line. A gas-tight syringe was then used to measure out LiBEt_3H (2.0 mmol). The LiBEt_3H was then added dropwise to the orange $[\text{Ir}(1,5\text{-COD})(\mu\text{-Cl})_2]$ solution under an Ar atmosphere with stirring, during which the original orange color changed to dark-brown. The resulting solution was stirred at -78°C for an additional 10 min and then warmed to room temperature. The solution slowly turned from dark-brown to dark-green within 10 min of additional stirring at room temperature. 1,5-COD (12.3 mL, 25 eq per Ir) was measured out with a 20 mL gas-tight syringe purged with Ar, and then added over 5-10 min to the dark-green solution. The resulting bright-green solution was stirred at room temperature for 24 h and then concentrated to ~ 5 mL under vacuum at room temperature by attachment to a Schlenk line. A visually apparent black powder was formed in the bright-green solution upon evaporation of the volatiles under vacuum. A 15 mL portion of acetone was added to the mixture using a 20 mL gas-tight syringe to obtain a black powder plus a bright-green solution. The black powder was separated from bright-green solution under Ar using a glass-frit-filter in which the open end of the glass-frit-filter Schlenk was sealed via a rubber septum. The black powder collected on top of the glass-frit was washed with degassed H_2O (5 mL x 2) and then degassed acetone (5 mL x 3) using a gas-tight syringe that had been previously purged with Ar. The black powder was then dried overnight under vacuum at room temperature resulting in black powder that was transported to the drybox for storage still in the glass-frit filter apparatus. The black powder was then dissolved in benzene- d_6 for ^1H NMR (Figure S2 (right), vide supra).

Control Experiment #3 - Passing the concentrated $[\text{Ir}(1,5\text{-COD})(\mu\text{-H})_4]$ solution in THF through a glass filter (i.e., without addition of 15 mL of acetone): In the drybox, orange powdered $[\text{Ir}(1,5\text{-COD})(\mu\text{-Cl})_2]$ (0.5 mmol) was weighed out and then transferred into a 100 mL round-bottomed Schlenk flask equipped with a side arm and a 5/8 by 5/16 in., Teflon-coated magnetic stirbar. The flask was sealed, removed from the drybox, and placed on a Schlenk line under Ar via its side arm. Next, 20 mL of room temperature THF was added to the flask using a cannula to form an orange solution with some undissolved orange powder. The flask containing the orange solution of $[\text{Ir}(1,5\text{-COD})(\mu\text{-Cl})_2]$ was placed in an acetone/dry ice bath at -78°C and stirred for 15 min. A 2.5 mL gas-tight syringe was purged three times with Ar using a Schlenk line. A gas-tight syringe was then used to measure out LiBEt_3H (2.0 mmol). The LiBEt_3H was then added dropwise to the orange $[\text{Ir}(1,5\text{-COD})(\mu\text{-Cl})_2]$ solution under an Ar atmosphere with stirring, during which the original orange color changed to dark-brown. The resulting solution was stirred at -78°C for an additional 10 min and then warmed to room temperature. The solution slowly turned from dark-brown to dark-green within 10 min of additional stirring at room temperature. Next, 1,5-COD (12.3 mL, 25 eq per Ir) was measured out with a 20 mL gas-tight syringe purged with Ar, and then added over 5-10 min to the dark-green solution. The resulting bright-green solution was stirred at room temperature for 30 min and then concentrated to ~5 mL under vacuum at room temperature by attachment to a Schlenk line. A visually apparent black powder was formed in the bright-green solution upon evaporation of the volatiles under vacuum. The black powder was separated from bright-green solution under Ar using a glass-frit-filter Schlenk apparatus in which the open end of the glass-frit-filter was sealed via a rubber septum.. The black powder collected on top of the glass-filter was washed with degassed H_2O (5 mL x 2) and degassed acetone (5 mL x 3) using a gas-tight syringe that had been

previously purged with Ar. The black powder was then dried overnight under vacuum at room temperature resulting in black powder that was transported to the drybox and stored in the glass-frit-filter apparatus. The black powder was then dissolved in benzene- d_6 for H NMR (Figure S3 (right), vide supra).

Unsuccessful synthesis of [(1,5-COD)Ir(μ -H)]₄ starting with [(1,5-COD)Ir(μ -Cl)]₂ and EtLi:

In the drybox, orange powdered [(1,5-COD)Ir(μ -Cl)]₂ (1.0 g, 1.49 mmol) dissolved in 500 mL diethylether in a 1000 mL round-bottom Schlenk flask equipped with side arm and a 5/8 × 5/16 in., Teflon-coated magnetic stirbar. The flask was then sealed with septum and brought out of the drybox. The 1000 mL round-bottomed flask was attached to Schlenk line through its side arm and was purged with N₂(g) gas for 5 min. The flask was then placed in an acetone/liquid N₂ bath at -76°C and stirred for 30 min. EtLi (5.96 mL, 2.98 mmol) solution was measured out with a 10 mL syringe, and transferred into a 25 mL side arm equipped Schlenk flask sealed with a septum. The flask containing EtLi solution was attached to the Schlenk line through its side arm and N₂(g) was passed for 5 min. The EtLi solution was then added dropwise to orange [(1,5-COD)Ir(μ -Cl)]₂ solution via a cannula under N₂(g). The color of the solution darkened upon addition. The resulting solution was stirred at -76°C for an additional 3 h and then at room temperature for 4 h. The volatiles were removed under vacuum and the reaction flask was taken into the drybox. The residue was extracted with 6 × 10 mL hexane. An activated silica gel column (height: ~4 cm, diameter: ~2 cm) was prepared in a Pyrex coarse fritted filter funnel using hexane solvent. The black extract was passed through activated silica gel column using hexane. A dark brown solution was collected into a 250 mL round-bottomed flask. The brown color of the filtrate—which is not the expected dark green characteristic of [(1,5-COD)Ir(μ -

H)]₄—confirms that [(1,5-COD)Ir(μ-H)]₄ is not the predominant product when EtLi is utilized as the reductant for [(1,5-COD)Ir(μ-Cl)]₂ and according to the above procedure.

CHAPTER VI

SUMMARY

This dissertation has focused on synthesis, characterization and catalytic evaluation of what is now the currently best-understood Ziegler-type hydrogenation catalyst system, one made from $[\text{Ir}(1,5\text{-COD})(\mu\text{-O}_2\text{C}_8\text{H}_{15})]_2$ plus AlEt_3 . The critical analysis of extant literature, in Chapter II, reveals that the nature of the active catalyst species, and the true nature of the AlEt_3 -derived stabilizer species in Ziegler-type catalyst systems, has a strong dependency on the specific variables of the catalyst system. In Chapter III the high catalytic activity, long lifetime and unusually high thermal stability of the $\text{Ir}(0)_n$ Ziegler nanoparticles formed from $[\text{Ir}(1,5\text{-COD})(\mu\text{-O}_2\text{C}_8\text{H}_{15})]_2$ plus AlEt_3 are demonstrated. The results of this study, then, raises the intriguing question of what is the true nature of the apparently unusual, AlEt_3 -derived stabilizer(s) in Ziegler-type nanoparticle catalysts made from $[\text{Ir}(1,5\text{-COD})(\mu\text{-O}_2\text{C}_8\text{H}_{15})]_2$ plus AlEt_3 ? Chapter IV investigates the nature of the AlEt_3 -derived stabilizer species using spectroscopic techniques and catalytic evidence. The results show that $\text{AlEt}_2(\text{O}_2\text{C}_8\text{H}_{15})$ ($\text{Al}/\text{Ir}=1, 2$ and 3) and free AlEt_3 ($\text{Al}/\text{Ir}=3$) are present in the catalyst solution made with $[\text{Ir}(1,5\text{-COD})(\mu\text{-O}_2\text{C}_8\text{H}_{15})]_2$ plus AlEt_3 . In addition, experimental results of this study helps to rule out the initial, literature-based hypotheses that anionic $[\text{AlEt}_3(\text{O}_2\text{C}_8\text{H}_{15})]^-$ stabilizer exists. Lastly, in Chapter V, a novel $[\text{Ir}(1,5\text{-COD})(\mu\text{-H})]_4$ complex is synthesized in 55% recrystallized yield from commercially available LiBEt_3H and $[\text{Ir}(1,5\text{COD})(\mu\text{-Cl})]_2$ in the presence of excess 1,5-COD in THF. The resultant $[\text{Ir}(1,5\text{-COD})(\mu\text{-H})]_4$ was then fully characterized by single-crystal XRD, XAFS, ESI-MS, UV-visible, IR, and NMR.

There are several potential avenues for future research related to the studies presented herein. For example, useful studies could include: (i) further testing of the catalytic activity,

lifetime and thermal stability of the commercial Co- and Ni-based industrial Ziegler-type hydrogenation catalysts; and (ii) Al XAFS of the stabilizers made in the Ir, Co and Ni catalysts. Also of interest would be (iii) ranking the stabilizing abilities of various Al-containing species, in combination with the $[\text{Ir}(1,5\text{-COD})(\mu\text{-H})]_4$ complex, including separately synthesized $\text{Al}(\text{O}_2\text{C}_8\text{H}_{15})_3$, molecular *t*-butylaluminumoxanes, commercially available aluminumoxanes (such as methylaluminumoxane or ethylaluminumoxane) and Barron's carboxylatoaluminumoxanes. Further studies could also include (iv) investigating the true nature of the stabilizer species in the industrial $\text{Co}(\text{neodecanoate})_2$ or $\text{Ni}(2\text{-ethylhexanoate})_2$ plus AlEt_3 Ziegler-type catalysts using the methods detailed herein. Last, (v) the synthesis, isolation and characterization of the Co analogue of the tetrahydride Ir_4 cluster (i.e., $[\text{Co}(1,5\text{-COD})(\mu\text{-H})]_4$) is another promising area for future research.

APPENDIX A

IRIDIUM ZIEGLER-TYPE HYDROGENATION CATALYSTS MADE FROM [(1,5-COD)Ir(μ -O₂C₈H₁₅)₂ AND AlEt₃: SPECTROSCOPIC AND KINETIC EVIDENCE FOR THE Ir_n SPECIES PRESENT AND FOR NANOPARTICLES AS THE FASTEST CATALYST

This dissertation chapter contains a paper published in *Inorganic Chemistry* **2010**, *49*, 8131–8147 that investigates the nature of the transition metal species in the resulting catalyst solution in the model [Ir(1,5-COD)(μ -O₂C₈H₁₅)₂ plus AlEt₃ Ziegler-type catalyst system. The results of multiple analytical techniques used in this study show that the catalyst solutions contain Ir₄₋₁₅ species before the catalyst was used in hydrogenation. A transformation to Ir(0)₄₀₋₁₅₀ nanoclusters is observed in the [Ir(1,5-COD)(μ -O₂C₈H₁₅)₂ plus AlEt₃ catalyst solution under catalytic cyclohexene hydrogenation conditions.

MALDI MS data was obtained by Isil K. Hamdemir, and interpreted by both Isil K. Hamdemir and William M. Alley. The sample preparation and submission to high resolution and bright field TEM, and electron diffraction imaging were performed by Isil K. Hamdemir. High resolution and bright field TEM, and electron diffraction images were obtained by JoAn Hudson of Clemson University. The bright field TEM images were analyzed by Isil K. Hamdemir. Interpretation of the electron diffraction image was performed by William M. Alley. XPS spectrum was obtained and analyzed by Isil K. Hamdemir. The control experiment with isolated and redispersed catalyst in cyclohexene was performed by Isil K. Hamdemir. The [Ir(1,5-COD)(μ -O₂C₈H₁₅)₂ used in these studies was synthesized by William M. Alley. The sample preparation and submission to Z-contrast STEM imaging were performed by William M. Alley. The Z-contrast STEM images were obtained by collaborator Long Li. The XAFS data was

obtained and interpreted by William M. Alley with assistance from Qi Wang, Anatoly I. Frenkel, and Laurent D. Menard. All other kinetics experiments were performed by William M. Alley.

The complete manuscript was written by William M. Alley using an earlier incomplete draft written by Isil K. Hamdemir which included a detailed analysis of the work she performed. The other coauthors edited and proofread the manuscript. The manuscript was prepared for publication by William M. Alley with moderate editing (43 hours) from Richard G. Finke. The above list of contribution from each coauthor to this chapter agrees well with that given in the dissertation by William M. Alley. A supporting information file is available online for the interested reader at <http://pubs.acs.org>.

Synopsis

Ziegler-type hydrogenation catalysts, those made from a group 8–10 transition metal precatalyst and an AlR_3 cocatalyst, are often used for large scale industrial polymer hydrogenation; note that Ziegler-type *hydrogenation* catalysts are *not* the same as Ziegler–Natta *polymerization* catalysts. A review of prior studies of hydrogenation catalysts (Alley et al. *J. Mol. Catal. A: Chem.* **2010**, *315*, 1–27) reveals that a ~50 year old problem is identifying the metal species present before, during, and after Ziegler-type hydrogenation catalysis, and which species are the kinetically best, fastest catalysts—that is, which species are the true hydrogenation catalysts. Also of significant interest is whether what we have termed “Ziegler nanoclusters” are present and what their relative catalytic activity is. Reported herein is the characterization of an Ir Ziegler-type hydrogenation catalyst, a valuable model (*vide infra*) for the Co-based industrial Ziegler-type hydrogenation catalyst, made from the crystallographically characterized $[(1,5\text{-COD})\text{Ir}(\mu\text{-O}_2\text{C}_8\text{H}_{15})]_2$ precatalyst plus AlEt_3 . Characterization of this Ir model system is accomplished before and after catalysis using a battery of physical methods including Z-contrast scanning transmission electron microscopy (STEM), high resolution (HR)TEM, and X-ray absorption fine structure (XAFS) spectroscopy. Kinetic studies plus $\text{Hg}(0)$ poisoning experiments are then employed to probe which species are the fastest catalysts. The main findings herein are that (i) a combination of the catalyst precursors $[(1,5\text{-COD})\text{Ir}(\mu\text{-O}_2\text{C}_8\text{H}_{15})]_2$ and AlEt_3 gives catalytically active solutions containing a broad distribution of Ir_n species ranging from monometallic Ir complexes to nanometer scale, noncrystalline Ir_n nanoclusters (up to $\text{Ir}_{\sim 100}$ by Z-contrast STEM) with the estimated mean Ir species being 0.5–0.7 nm, $\text{Ir}_{\sim 4-15}$ clusters considering the similar, but not identical results from the different analytical methods; furthermore, (ii) the mean Ir_n species are practically the same regardless of the Al/Ir ratio employed, suggesting that the observed

changes in catalytic activity at different Al/Ir ratios are primarily the result of changes in the form or function of the Al-derived component (and not due to significant AlEt₃-induced changes in initial Ir_n nuclearity). However, (iii) during hydrogenation, a shift in the population of Ir species toward roughly 1.0–1.6 nm, *fcc* Ir(0)_{~40–150}, Ziegler nanoclusters occurs with, significantly, (iv) *a concomitant increase in catalytic activity*. Importantly, and although catalysis by discrete subnanometer Ir species is not ruled out by this study, (v) the increases in activity with increased nanocluster size, plus Hg(0) poisoning studies, provide the best evidence to date that the approximately 1.0–1.6 nm, *fcc* Ir(0)_{~40–150}, heterogeneous Ziegler nanoclusters are the fastest catalysts in this industrially related catalytic hydrogenation system (and in the simplest, Ockham's Razor interpretation of the data). In addition, (vi) Ziegler nanoclusters are confirmed to be an unusual, hydrocarbon-soluble, highly coordinatively unsaturated, Lewis-acid containing, and highly catalytically active type of nanocluster for use in other catalytic applications and other areas.

1. Introduction

Ziegler-type hydrogenation catalysts prepared, by definition, from a nonzero valent, group 8–10 transition metal precatalyst combined with an AlR₃ cocatalyst, such as triethylaluminum (AlEt₃), account for much of the worldwide industrial hydrogenation of styrenic block copolymers (SBCs) [1]. According to one estimate, hydrogenated SBCs are produced at a rate in excess of 1.7×10^5 metric tons annually worldwide [2]. The literature concerning Ziegler-type hydrogenation catalysts has recently been critically reviewed by us [3], leading to the following insights: (i) Improved fundamental understanding of Ziegler-type hydrogenation catalysts is needed so that rationally directed catalyst improvements can be made. (ii) Multiple variables are important in catalyst synthesis, including the specific components used, the cocatalyst/transition

metal ratio (Al/M), the amount of H₂O present (widely observed to be connected to the amount of cocatalyst), and the order of addition of the catalyst components, and (iii) these variables influence the nature of the resulting catalysts and their catalytic properties. Other insights [3] are (iv) a central, unanswered question in the area of Ziegler-type industrial hydrogenation catalysts is whether the true catalyst is a homogeneous (e.g., single metal organometallic) or heterogeneous (e.g., polymetallic M(0)_n nanocluster) catalyst [4], and that (v) the most recent, especially noteworthy prior work—that of Schmidt and co-workers [5] and Bönemann and co-workers [3,6]—is starting to *suggest* that Ziegler-type hydrogenation catalysts are transition metal nanoclusters, what we have coined in our review as “Ziegler nanoclusters” [3]. However, (vi) compelling or even highly suggestive evidence concerning the homogeneous versus heterogeneous catalysis question for Ziegler-type hydrogenation catalysts has remained elusive due to the use of often poorly defined precursors or the lack of application of the best current, previously successful approaches for addressing the historically perplexing “is it homogeneous or heterogeneous catalysis?” question [7]. *Absent in particular are definitive kinetic studies connected to knowledge of the dominant form(s) of the transition metal catalyst.* On the basis of our review of the literature, we reasoned, therefore, that (vii) the use of a well-characterized precatalyst as a model for the industrially favored, but often less well- (or clearly) characterized, Co and Ni precatalysts might allow new insights into Ziegler-type hydrogenation catalyst systems, and (viii) that our previously successful, multipronged, kinetic-containing approach for addressing the homogeneous versus heterogeneous catalysis problem [3,4b,7,8] should be applied to Ziegler-type, industrially relevant hydrogenation catalysts. In addition, (ix) we reasoned that the use of the third row transition metal Ir, where strong Ir–Ir bonds, and for example Ir(0)_n nanoclusters that typically stable under characterization conditions [7a] might

prove very useful—if not necessary—in allowing identification of the dominant species present before and after catalysis without significant artifacts due to the use of *ex situ* or even *in situ* (as opposed to the ideal *operando* [9]) methods.

Herein, we report the characterization of iridium model Ziegler-type hydrogenation catalysts made from the crystallographically characterized precatalyst, [(1,5-COD)Ir(μ -O₂C₈H₁₅)₂] [2], plus AlEt₃ under carefully controlled conditions. The resultant pre- and posthydrogenation catalyst materials are characterized by a variety of analytical techniques including Z-contrast scanning transmission electron microscopy (STEM), high resolution (HR)TEM, X-ray absorption fine structure (XAFS) spectroscopy, and matrix assisted laser desorption ionization mass spectrometry (MALDI MS) [10]. The needed kinetic and Hg(0) poisoning studies round out the work reported herein. The main findings are (i) that combining the catalyst precursors [(1,5-COD)Ir(μ -O₂C₈H₁₅)₂] and AlEt₃ gives catalytically active solutions containing Ir_n clusters with a range of sizes from monometallic Ir complexes to nanometer scale, noncrystalline Ir_n nanoclusters with an estimated mean 0.5–0.7 nm, Ir_{4–15} cluster (considering the similar, but not identical results obtained from the different analytical methods), *but* (ii) that during the hydrogenation process, the development of roughly 1.0–1.6 nm, *fcc* Ir(0)_{40–150} nanoclusters occurs, and (iii) that kinetic studies indicate, importantly, a concomitant *increase in catalytic activity* as the size of the Ir_n nanoclusters increases. In addition, we find (iv) that this size–activity correlation, plus Hg(0) poisoning studies, suggest (as the simplest, “Ockham’s razor” interpretation of the data) that the fastest, kinetically competent catalysts are the larger, roughly 1.0–1.6 nm, Ir(0)_{40–150} nanoclusters rather than the monometallic complexes and 0.5–0.7 nm, Ir_{4–15} clusters initially present (the homogeneous catalyst component alone appears to have about 5% of the activity of the overall catalyst solution, *vide infra*).

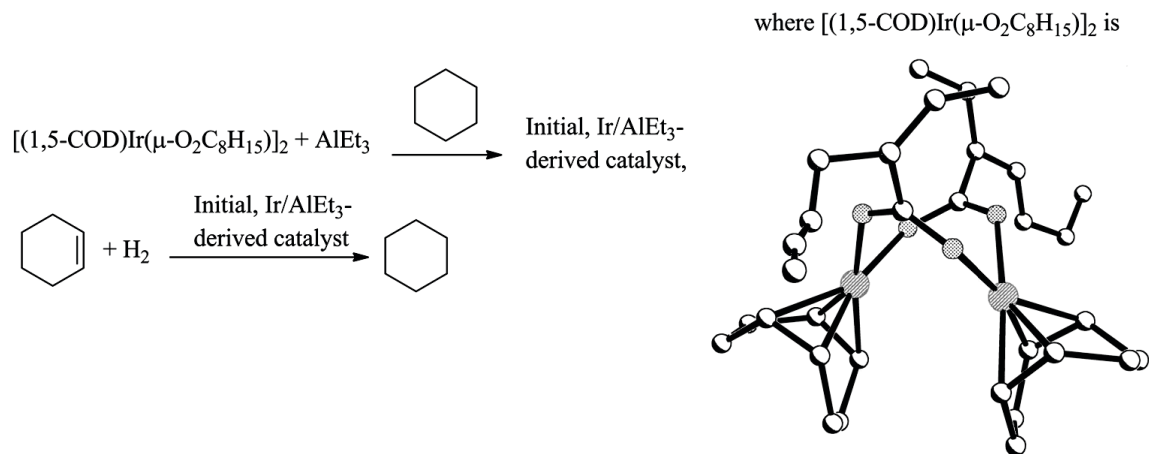
The results are significant in comparison to even the ~50 year history of Ziegler-type hydrogenation catalysts [3] (a) in being the first to show that the transition metal component of the initial catalyst formation reaction is, at least for the present Ir model system, a broadly disperse mixture ranging from mono-Ir complexes to noncrystalline nanoscale clusters, with the estimated mean Ir_n species being 0.5–0.7 nm, Ir_{4-15} clusters; (b) in being the first report of the explicit application of an established, previously successful, multiprong approach for addressing the homogeneous versus heterogeneous catalysis problem in a Ziegler-type hydrogenation catalyst system [3,4b,7,8]; and (c) in providing evidence consistent with and highly supportive of the now dominant hypothesis for future research in the area, namely, that Ziegler nanoclusters appear to be the kinetically dominant catalysts—although we note that the true catalyst in the industrially fastest Co/AlR₃ system remains to be identified and is under investigation. As such, the findings reported herein are both believed to be important fundamentally and are expected to result in practical implications due to the large-scale industrial utilization of Ziegler-type hydrogenation catalysts [11,12,13,14].

2. Results and Discussion

A key insight from our review of the literature of Ziegler-type hydrogenation catalyst [4] is that their catalytic hydrogenation activity is quite sensitive to a number of variables, including the specific conditions and details under which the catalysts are synthesized. Therefore, preliminary catalytic studies were carried out in order to determine appropriate, representative conditions for reliable and reproducible catalyst preparation and subsequent catalytic use as well as to ensure the broadest applicability of the results of the studies which follow.

Catalyst Preparation. Catalyst samples used in olefin hydrogenation were prepared by a combination of $[(1,5\text{-COD})\text{Ir}(\mu\text{-O}_2\text{C}_8\text{H}_{15})_2]$ and AlEt_3 , with Al/Ir ratios of 1.0, 2.0, 3.0, and 5.0. We previously reported the control experiment of using $[(1,5\text{-COD})\text{Ir}(\mu\text{-O}_2\text{C}_8\text{H}_{15})_2]$ for catalytic cyclohexene hydrogenation *without* AlEt_3 [2]. The resulting black, Ir(0) precipitate formed during hydrogenation indicates that the AlEt_3 component is crucial for the stability of the catalyst (and nanoclusters, *vide infra*). A brief summary of those hydrogenation results without AlEt_3 is provided in the Supporting Information (available online at <http://pubs.acs.org>) for the interested reader.

In light of what is known from the literature [], all catalyst solutions were prepared using the same materials from the same sources. Also, the procedures described below and in the Experimental Section were followed exactly for repeat kinetic runs. Specifically, an 18.0 mM cyclohexane solution of AlEt_3 was rapidly added to a cyclohexane solution of the precatalyst, 9.0 mM in [Ir], without the presence of the olefinic substrate, which has been reported to influence these specific catalyst formation reactions in some cases [3]. The addition of AlEt_3 to the cyclohexane solution of $[(1,5\text{-COD})\text{Ir}(\mu\text{-O}_2\text{C}_8\text{H}_{15})_2]$ resulted in an immediate change in color from orange to tawny yellow, regardless of whether an Al/Ir ratio of 1.0, 2.0, 3.0, or 5.0 was used. Catalyst solutions were then used for the catalytic hydrogenation of the model olefin, cyclohexene, as depicted in Scheme A.1.



Scheme A.1. Catalyst Preparation and Hydrogenation of Cyclohexene Plus (shown to the right) the Single-Crystal X-Ray Diffraction Determined Structure of the [(1,5-COD)Ir(μ -O₂C₈H₁₅)₂]₂ Precatalyst (adapted from ref 4, copyright 2009, American Chemical Society).

Cyclohexene Hydrogenation Curves and Catalyst Aging. Example cyclohexene hydrogenation curves obtained by following H₂ pressure loss, and using the [(1,5-COD)Ir(μ -O₂C₈H₁₅)₂]₂ plus AlEt₃ catalysts with Al/Ir ratios of 1.0, 2.0, and 3.0, are shown in Figure A.1. In each case, the Ir/AlEt₃-based catalysts exhibit immediate activity, but the maximum rate is attained later as the reaction proceeds, Figure A.1a and b—that is, either more catalyst or a better catalyst is being formed as the reaction proceeds.

A key factor in the preparation of the catalyst is the time elapsed between mixing the [(1,5-COD)Ir(μ -O₂C₈H₁₅)₂]₂ and AlEt₃ components prior to use of the resultant solution for the test reaction of cyclohexene hydrogenation, hereafter referred to as the *aging time*. Despite the initial reaction between the Ir precatalyst and AlEt₃, hydrogenation activity approaches a maximum value if the initially prepared catalyst solutions are allowed to age by stirring under an atmosphere of N₂ for about 8–24 h before being placed under H₂ (Figure S2, Supporting Information, (available online at <http://pubs.acs.org>)); maximum rates of aged catalysts are ~2–7-fold greater than the maximum rates of their nonaged counterparts, depending on Al/Ir. Without

aging catalyst solutions before their use, the resulting hydrogenation curves exhibit a more distinct transition from a less active—but longer-persisting—initial stage to their maximum rate stage, especially at the Al/Ir ratio of 5.0 (Figure S3, Supporting Information (available online at <http://pubs.acs.org>)). However, even 33 h of aging does not completely eliminate the slower initial rate (Figure S2b of the Supporting Information (available online at <http://pubs.acs.org>)). The maximum rates are ~2–10 times the initial rates in each case, depending on Al/Ir and whether or not catalyst solutions were aged. A table giving the mean initial and maximum rates from multiple runs of both aged and nonaged catalysts samples, and at various Al/Ir ratios, is given in the Supporting Information (available online at <http://pubs.acs.org>). Clearly, evolution of the catalyst is occurring, so that it became important to determine the nature of that evolution, *vide infra*.

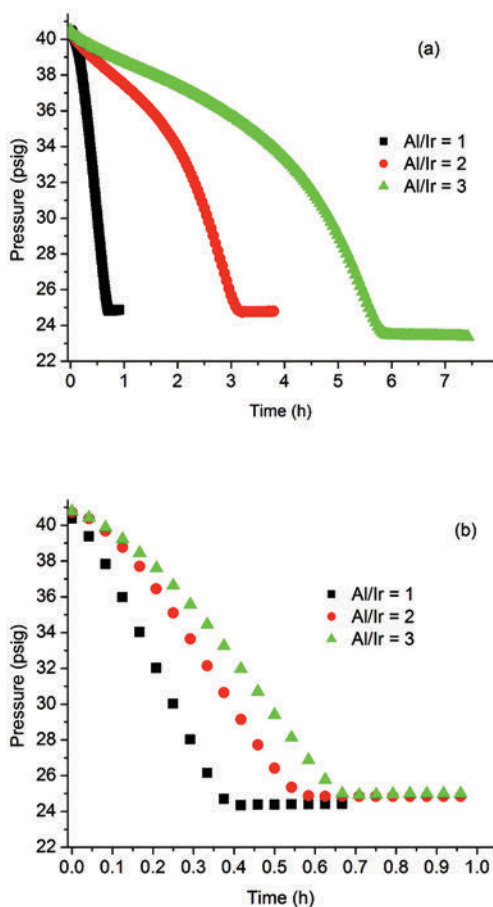


Figure A.1. Catalytic cyclohexene hydrogenations using $[(1,5\text{-COD})\text{Ir}(\mu\text{-O}_2\text{C}_8\text{H}_{15})_2]$ plus AlEt_3 catalysts that were (a) used immediately after preparation or (b) first aged for nine h with stirring under a N_2 atmosphere. Note the ca. 10-fold reduced timescale axis in part b versus that in part a—that is, the aged catalyst is about 2- to 7-fold more active, depending on the Al/Ir ratio, on the basis of the *maximum* hydrogenation rate achieved. In each case, the reaction is fastest just before the end of the catalytic run, despite the normal, rate-slowing decrease in the olefin concentration and H_2 pressure (the max rate is $\sim 2\text{--}10$ times the initial rate of a given run). Also, the effect on the initial rate of the Al/Ir ratio is significantly less when the catalyst solutions are aged before use. Reactions were performed in cyclohexane solutions, 0.6 mM in $[\text{Ir}]$, initially 1.65 M in cyclohexene, at 22.0 °C, and stirred at 1000 ± 10 rpm. Additional catalytic hydrogenation curves, attained using catalysts with an Al/Ir ratio of 5.0, are shown in Figure S3 of the Supporting Information (available online at <http://pubs.acs.org>) of current publication.

As expected from the literature [3], catalyst activity is dependent on the Al/Ir ratio. However, the magnitude of the effect of the Al/Ir ratio on the catalyst activity is diminished when the catalysts are aged. Interestingly, even 33 h of aging of the catalyst solutions does not

result in further color change; yet, in all cases, the reaction solutions change color *during hydrogenation* (i.e., under H₂ and cyclohexene) to darker brown, results that are consistent with further catalyst development to larger Ir(0)_n nanoclusters that have been identified by several physical methods, *vide infra*. Catalyst solutions sometimes give a dark brown/black precipitate within a few days of hydrogenation if the catalyst solution is transferred to a N₂ atmosphere shortly after complete consumption of the substrate. However, a dark brown/black precipitate (Ir(0) by XPS) plus a clear, nearly colorless solution always results if the solutions are left under pressurized H₂ for extended amounts of time after complete consumption of the cyclohexene substrate. The observations of brown-black catalyst solutions plus metal(0) precipitates are strongly suggestive, but by themselves not definitive, evidence for heterogeneous (e.g., nanoparticle) catalysis [4b]. Overall, the increased catalytic activity, color changes, and occasional bulk Ir(0) precipitate after the reaction require *at least one transformation processes of the catalyst, or possibly parallel development of different catalysts, during both the aging stage and the hydrogenation catalysis*. Nanocluster development is strongly implicated by just the color change, although verification of that by several independent methods quickly became the next objective.

The specific objectives for what follows, then, are (i) to determine the nuclearity of the Ir_n species initially present and (ii) to determine the Ir_n species present after the catalyst has entered the maximum rate regime. Those studies presented next comprise the first necessary step en route (iii) to determining the nature of the active catalyst during both the initial and the maximum rate regimes. An important additional goal is to (iv) determine to what extent the rate effect of different Al/Ir ratios is due to AlEt₃-induced changes in the initial Ir component of the catalyst (e.g., does Al/Ir influence initial Ir_n nuclearity?) versus changes in just the AlEt₃-derived

component. Additional studies concerning the challenging problem of the form(s) of the AlEt₃-derived species at varying Al/Ir ratios and their role in catalysis are necessarily addressed elsewhere [13].

Tabulation of the Key Pre- and Posthydrogenation Catalyst Characterization. It will be easier to read what follows if we first summarize in Table A.1 the key results from Z-contrast STEM, XAFS, and MALDI MS, both pre- and postcatalytic hydrogenation runs. The key findings will be that (i) a combination of the catalyst precursors [(1,5-COD)Ir(μ-O₂C₈H₁₅)₂] and AlEt₃ gives catalytically active solutions containing a broad range of Ir_n species spanning from monometallic Ir complexes to noncrystalline Ir_n nanoclusters, with estimated mean 0.5–0.7 nm Ir_{~4-15} clusters. However, (ii) after a catalytic run, the population of Ir_n shifts considerably toward the form of approximately 1.0–1.6 nm, *fcc* Ir(0)_{~40-150}, Ziegler nanoclusters.

Nuclearity of the Ir_n Species in Aged AlEt₃/Ir Catalyst *before* Hydrogenation: Z-contrast Microscopy. A selected Z-contrast STEM image of a [(1,5-COD)Ir(μ-O₂C₈H₁₅)₂] plus AlEt₃, Al/Ir = 2.0, catalyst sample, aged ≥ 2 days and analyzed *before* hydrogenation, shows clusters with a range of diameters, Figure A. 2. The size distribution histogram, also Figure A.2, was constructed by measuring the full width at half-maximum (FWHM) of the intensity profile across 600 particles from images at the same levels of magnification and contrast. Most of the clusters counted in such images are subnanometer in scale. The mean cluster size is 0.5 ± 0.2 nm (a cluster 0.5 nm in diameter corresponds approximately to a theoretical tetrahedral Ir₄ cluster). The smallest Ir species observed appear to be mono-Ir complexes (diameter of Ir in a monometallic compound < 0.3 nm) [15], and the histogram tails off toward larger Ir clusters present in much lower abundance, the largest observed being 1.4 nm in diameter (Ir_{~100}) [16,17,18].

Table A.1. Observed Ir_n Cluster Diameters in the [(1,5-COD)IrO₂C₈H₁₅]₂ Catalyst Both Pre- and Post-Catalytic Runs by Three Different Analytical Methods.

analytical method	precatalysis		postcatalysis			
	range (nm)	mean (nm)	mean Ir _n nuclearity	range (nm)	mean (nm)	mean Ir _n nuclearity
Z-Contrast STEM	0.2–1.4	0.5 ± 0.2	Ir _{~4}	0.4–1.9	1.0 ± 0.3	Ir _{~40}
XAFS	NA ^a	0.5	Ir _{~4}	NA ^a	1.6	Ir _{~150}
MALDI MS	0.5–1.1	0.7 ± 0.2 ^b	Ir _{~15} ^b	0.6–1.4	0.8 ± 0.2 ^b	Ir _{~20} ^b

^a Determination of the range of Ir_n clusters present is not possible by this method. ^b An underestimate due to the irregular shape of the peak, which includes a high *m/z* tail (vide infra). See the discussion which follows for issues with the less reliable MALDI-MS in comparison to the Z-Contrast STEM and XAFS.

An Ir model Ziegler-type hydrogenation catalyst was chosen for the present studies in part because prior TEM experiments and controls have shown that the (third-row metal) Ir nanoclusters and precursor compounds generally have greater stability than lighter transition metal nanoclusters or precursors in TEM electron beams [19,20,21]. Moreover, it has been observed previously that at least first-row metal, Ni Ziegler-type hydrogenation catalysts are highly sensitive to sample preparation required by electron microscopy, specifically, the drying of catalyst samples on grids [1]. Z-contrast STEM cannot overcome the issue of sample drying but does offer the benefit of *scanning* TEM, so that potential sample damage can be minimized by using a small electron probe, low beam current, and minimum time of sample exposure to the electron beam [22]. In this case, the sizes and shapes of Ir spots in the images were continually monitored during image acquisition; no evidence of artifacts or modification of the sample as a result of the microscopy itself was observed, as expected for the third-row Ir system chosen in part for such superior TEM properties [7a,16]. In addition, *the greater resolving power of the Z-contrast method over conventional bright field TEM has permitted detection of the subnanometer clusters* [22,23,24,25], which are important results. To summarize, Z-contrast microscopy indicates that aged catalyst samples before hydrogenation consist of a broad distribution of Ir_n

species ranging from mono-Ir complexes to 1.4 nm, Ir_{~100} Ziegler nanoclusters. Significantly, subnanometer Ir_n clusters are the most abundant species present, and the mean Ir cluster diameter of 0.5 ± 0.2 nm corresponds to Ir_{~4} cluster compounds.

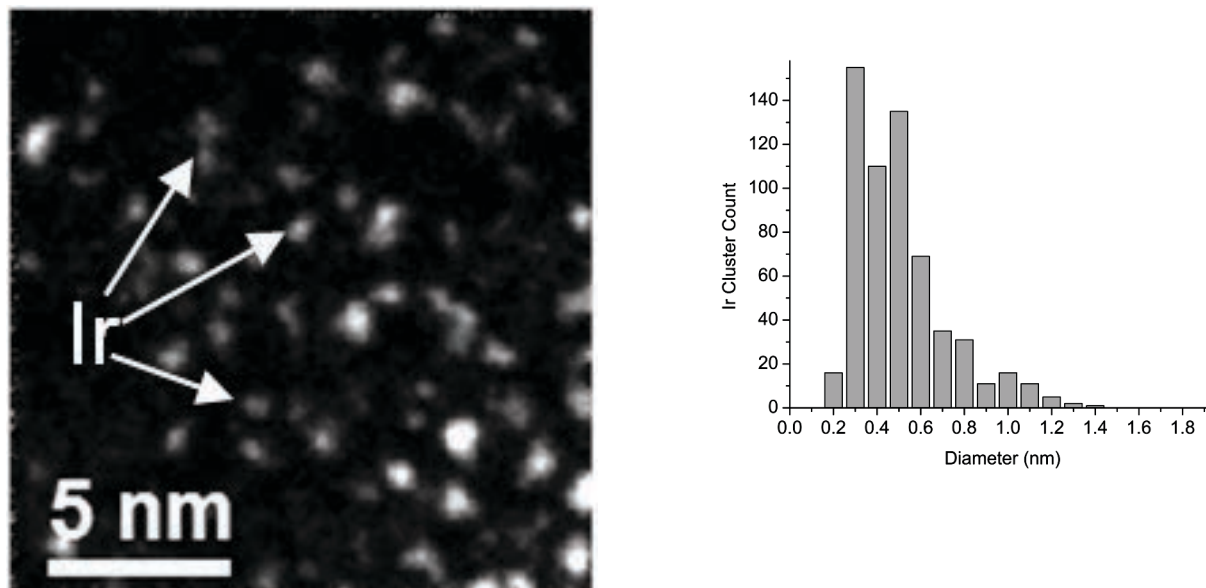


Figure A.2. Representative Z-contrast STEM image of a [(1,5-COD)Ir(μ -O₂C₈H₁₅)₂] plus AlEt₃ catalyst sample with an Al/Ir ratio of 2.0. Ir appears as white spots on a dark background. A diameter measurement of 600 clusters gives an overall distribution ranging from monometallic Ir complexes to 1.4 nm, Ir_{~100}, clusters and a mean cluster diameter of 0.5 nm (Ir_{~4}) \pm 0.2 nm.

Identification of the Ir-Containing Species in Aged AlEt₃/Ir Catalyst before Hydrogenation: XAFS Spectroscopy. XAFS data were first acquired for four reference samples: (i) an Ir black standard, (ii) HPO₄-stabilized *fcc* Ir(0)_n nanoclusters [26], (iii) Ir₄(CO)₁₂, and (iv) the precatalyst [(1,5-COD)Ir(μ -O₂C₈H₁₅)₂]. XAFS data were then acquired for seven different samples of the initial, [(1,5-COD)Ir(μ -O₂C₈H₁₅)₂] plus AlEt₃ catalyst solutions aged ≥ 2 days, and before their use in hydrogenation: catalysts prepared with Al/Ir ratios of 0.5, 1.0, 1.5, 2.0, 2.5, 3.0, and 5.0. Six main results from the XAFS spectroscopy of aged catalyst samples *before hydrogenation* are that (i) all samples lack longer-range coordination shells (in r-space) that are characteristic of ordered nanoclusters. (ii) Spectra from the Al/Ir ≤ 1.0 samples are

satisfactorily fit using a composite model created from an Ir–first-nearest-neighbor (hereafter 1NN) path from [(1,5-COD)Ir(μ -O₂C₈H₁₅)]₂ and the Ir–Ir first-nearest-neighbor (1NN) single scattering path (hereafter SS1) from bulk Ir, but (iii) *modeling the Al/Ir \geq 1.5 samples requires incorporating the contribution of the Ir–Al path*, an important finding. In addition, (iv) small Ir–Ir 1NN coordination numbers (N ; roughly in the range of 2–3, vide infra) correspond to subnanometer Ir cluster sizes. (v) Ir–Ir 1NN distances longer than expected for bulk Ir or ordered Ir nanoclusters indicate valence-electron sharing with ligands, consistent with small, ligated molecular Ir clusters, and (vi) XANES spectra of the Ir catalyst samples differ from bulk Ir but are similar to the precursor [(1,5-COD)Ir(μ -O₂C₈H₁₅)]₂ and Ir₄(CO)₁₂, suggesting formally Ir(I) _{n} or Ir(0) _{n} molecular clusters of few Ir atoms ligated by relatively strongly electron-withdrawing groups. The only sources of ligands in the system other than the weakly coordinating cyclohexane solvent are AlEt₃, C₇H₁₅CO₂[−], and possibly Ir–H (given that the 1,5-COD is hydrogenated to cyclooctane in the reaction), so that the list of possible, dominant species present that could be ligands is actually rather short, primarily, AlEt₃, C₇H₁₅CO₂AlEt₃[−], and possibly Ir–H–AlEt₃ (among a few others such as any Al–O–Al containing alumoxanes formed by trace water present, water that our experimental efforts and conditions have strived to minimize; see the Experimental Section). In short, the XAFS studies reveal that *initial catalyst solutions lack ordered Ir(0) _{n} nanoclusters and contain, on average, molecular Ir _{n} , 0.5 nm clusters ligated by electron-withdrawing groups that are likely derived from the short list of ligands listed above.*

Fourier transform (FT) magnitudes of the background-subtracted XAFS signals for the Al/Ir-dependent sample series are shown in Figure A.3. FT magnitude data of selected reference samples and a catalyst sample with an Al/Ir ratio of 2.0 are shown together in Figure

A.4. For single scattering paths (SS1, SS2, etc.), the positions of isolated peaks in FT plots correspond to the distance between the absorber and its neighbors, albeit shorter than the actual distances due to the photoelectron phase shifts [27,28,29]. The first important observation is that in the FT magnitude sample spectra, Figure A.3, there is a lack of distinct peaks in the 3–6 Å range expected for SS2–5 paths, whereas such peaks are visible in the FT magnitude plots of Ir black, Figure A.4 and Figure S10, Supporting Information (available online at <http://pubs.acs.org>). The lack of these peaks indicates that before hydrogenation there is not an appreciable amount of Ir nanoclusters with ordered, periodic, atomic structures in the catalyst. Restated, the *aged catalyst samples before hydrogenation lack the XAFS longer r-range contribution expected if ordered nanoclusters were present*. Hence, the relatively few nanometer-sized clusters that are present before hydrogenation according to Z-contrast STEM (as well as bright field TEM; see the Supporting Information (available online at <http://pubs.acs.org>)) appear to have significantly *disordered atomic structures* (this finding and its significance are discussed in further detail below) [30,31,32,33,34,35,36,37].

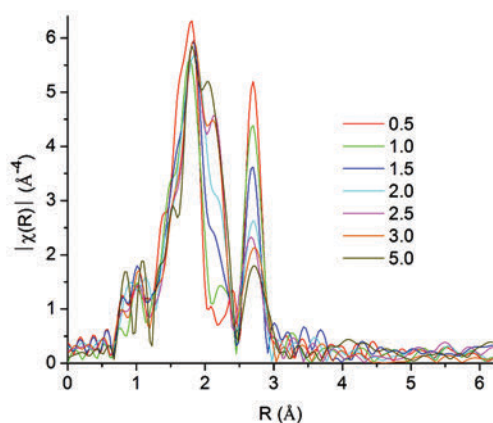


Figure A.3. A k^3 -weighted FT magnitude plot of a series of catalyst samples made from the combination of $[(1,5\text{-COD})\text{Ir}(\mu\text{-O}_2\text{C}_8\text{H}_{15})_2]$ and AlEt_3 ($\text{Al}/\text{Ir} = 0.5, 1.0, 1.5, 2.0, 2.5, 3.0, 5.0$) before their use in hydrogenation. The lack of peaks in the 3–6 Å region indicates the absence of crystalline Ir particles. The large peak on the left at ~ 1.8 Å represents Ir–C and/or Ir–O backscattering contributions (hereafter, “Ir–X”, since XAFS cannot distinguish between C and O backscatterers in catalyst samples, *vide infra*). The shoulder at ~ 2.2 Å on the right of the larger, Ir–X peak that grows in with increasing Al/Ir ratio is well-modeled by single scattering due to Al atoms. The narrow peak at ~ 2.7 Å represents single scattering from the first Ir–Ir nearest neighbor shell. R values are uncorrected for photoelectron phase shifts.

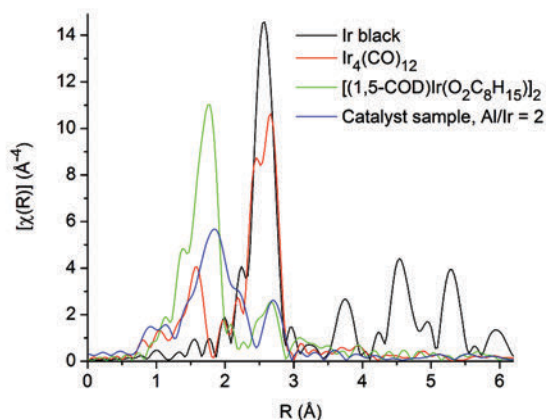


Figure A.4. A plot of FT magnitude of the k^3 -weighted XAFS data for Ir black (scaled by $\frac{1}{4}$ for ease of comparison), $\text{Ir}_4(\text{CO})_{12}$ (scaled by $\frac{1}{2}$ for ease of comparison), $[(1,5\text{-COD})\text{Ir}(\mu\text{-O}_2\text{C}_8\text{H}_{15})_2]$, and a catalyst sample, with an Al/Ir of 2.0, for comparison. The peaks in the 3–6 Å range, seen here only in the spectrum of Ir black, are diagnostic of an ordered Ir phase.

Fitting Results for Catalyst Samples before Hydrogenation. XAFS spectra of Ir black,

HPO_4 -stabilized *fcc* Ir(0) nanoclusters, $\text{Ir}_4(\text{CO})_{12}$, and $[(1,5\text{-COD})\text{Ir}(\mu\text{-O}_2\text{C}_8\text{H}_{15})_2]$ were fit using

theoretical models based on the crystal structures of bulk *fcc* Ir, Ir₄(CO)₁₂ [38], and [(1,5-COD)Ir(μ-O₂C₈H₁₅)₂], respectively [2]. Fits of these standards and reference compounds are shown in Figures S10–S14, Supporting Information (available online at <http://pubs.acs.org>), and the fitting results are summarized in Tables S2–S5, Supporting Information, for the interested reader. The peaks in the spectra of Ir₄(CO)₁₂, and [(1,5-COD)Ir(μ-O₂C₈H₁₅)₂] at about 1.6 Å and 1.8 Å, Figure A.4, correspond to Ir–C and Ir–X first nearest neighbors (again abbreviated 1NN), respectively (X represents both C and O atoms, which were nondistinguishable by XAFS in [(1,5-COD)Ir(μ-O₂C₈H₁₅)₂], Figure S13, Supporting Information (available online at <http://pubs.acs.org>), and in the catalyst samples). The peaks in the spectra of Ir black, HPO₄-stabilized Ir nanoclusters and Ir₄(CO)₁₂ at about 2.5 Å correspond to Ir–Ir 1NN positions. Comparing the spectra in Figures E.3 and E.4, the peaks in the catalyst samples near 1.8 Å and 2.7 Å correspond, roughly, to scattering contributions from Ir–X and Ir–Ir, respectively. Therefore, scattering paths for Ir–X and Ir–Ir were used to model the catalyst sample data.

Fits of the catalyst sample data using a model created from the Ir–X path in [(1,5-COD)Ir(μ-O₂C₈H₁₅)₂] and the Ir–Ir SS1 path in Ir black gave physically reasonable results only for the Al/Ir = 0.5 and 1.0 samples. For the Al/Ir ≥ 1.5 samples, the model was adapted by taking into account backscattering by Al atoms in close proximity to the absorbing Ir. This modified model better accounted for the shoulder on the right side of the leftmost (Ir–X) peak that grows in with the 1.5 and higher Al/Ir ratio samples, Figure A.3. However, attempts to use the model incorporating Al to fit the Al/Ir = 0.5 and 1.0 sample data gave unreasonable results. Fits to the Al/Ir = 1.0 and 2.0 sample data using the model that neglects Al and the model that incorporates Al, respectively, are shown in Figure A.5. The fitting results for all samples are

summarized in Table A.2. Additional spectra of the data and theoretical fits are shown in Figures S15–S21, Supporting Information (available online at <http://pubs.acs.org>).

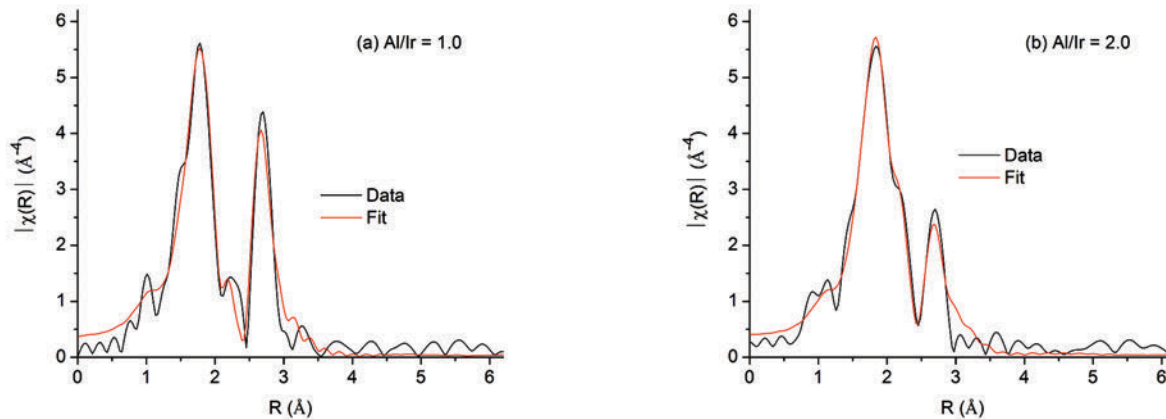


Figure A.5. FT magnitude spectra and fits for the Al/Ir = 1.0 (a) and 2.0 (b) catalysts. The model used to fit the Al/Ir = 1.0 sample was created from the Ir–X path in $[(1,5\text{-COD})\text{Ir}(\mu\text{-O}_2\text{C}_8\text{H}_{15})_2]$ and the Ir–Ir SS1 path in Ir black. The Al/Ir = 2.0 sample was fit by the same model but modified to account for backscattering by Al atoms in close proximity to the absorbing Ir.

Table A.2. Fitting Results for the [(1,5-COD)Ir(μ -O₂C₈H₁₅)₂] Plus AlEt₃ Catalyst Samples before Their Use in Hydrogenation.

sample Al/Ir	Ir black	0.5	1.0	1.5	2.0	2.5	3.0	5.0
$N_{\text{Ir-Ir}}$	12 ^c	1.8 ± 0.4	2.8 ± 0.6	2.1 ± 0.6	3 ± 1	3 ± 1	3 ± 1	3 ± 3
$N_{\text{Ir-X}}$		6.0 ± 0.6	5.8 ± 0.6	5.4 ± 0.8	5.0 ± 0.7	4.7 ± 0.8	4.8 ± 0.8	5 ± 1
$N_{\text{Ir-Al}}$				1.0 ± 0.9	1.7 ± 0.8	2 ± 1	3 ± 1	3 ± 2
$R_{\text{Ir-Ir}} (\text{\AA})^a$	2.711 ± 0.001	2.799 ± 0.005	2.797 ± 0.005	2.803 ± 0.007	2.826 ± 0.007	2.84 ± 0.01	2.849 ± 0.008	2.86 ± 0.02
$R_{\text{Ir-X}} (\text{\AA})^a$		2.149 ± 0.007	2.162 ± 0.008	2.18 ± 0.01	2.19 ± 0.01	2.19 ± 0.02	2.19 ± 0.01	2.20 ± 0.03
$R_{\text{Ir-Al}} (\text{\AA})^a$				2.49 ± 0.02	2.51 ± 0.01	2.51 ± 0.01	2.51 ± 0.01	2.5045 ^c
$\sigma^2_{\text{Ir-Ir}} (\text{\AA}^2)^b$	3.5 ± 0.1	5.2 ± 0.7	7.0 ± 0.7	7 ± 1	10 ± 1	10 ± 2	10 ± 2	11 ± 4
$\sigma^2_{\text{Ir-X}} (\text{\AA}^2)^b$		6.4 ± 0.9	8 ± 1	7 ± 1	7 ± 1	8 ± 2	8 ± 1	9 ± 3
$\sigma^2_{\text{Ir-Al}} (\text{\AA}^2)^b$				7 ± 5	8 ± 3	8 ± 2	8 ± 3	8 ± 4

^a R is the experimentally determined interatomic distance for the Ir–X, Ir–Al, and Ir–Ir single scattering paths. ^b σ^2 , the Debye-Waller factor, is the mean square variation in R due to static and dynamic disorder. The values shown are $\times 10^3$. ^c For this sample only, this parameter was defined to be the value shown and not varied in the fit.

From the fit of the Al/Ir = 2.0 sample data, the 1NN Ir–Ir N of 3 ± 1 indicates an Ir_{~4} cluster, which, in turn, corresponds to an Ir cluster roughly 0.5 nm in diameter. Results for catalyst samples at all AlEt₃/Ir ratios tested *are similar*, giving subnanometer, Ir_{~4}, clusters. Significantly, *XAFS and Z-contrast microscopy fortify one another in finding the same mean cluster size* within experimental error. Recall that Z-contrast STEM also reveals a broad dispersity of Ir cluster sizes in catalyst samples before hydrogenation. XAFS, on the other hand, gives ensemble-average results for local structure; it does *not* provide information regarding *distribution* of Ir cluster sizes [35]. In light of the larger clusters observed by electron microscopy (the tail in the histogram of Figure A.2 showing some Ir_{*n*} clusters with nanometer scale diameters), possible explanations for the XAFS results are that the nanoscale Ir clusters could (i) have considerably disordered structures [31], (ii) actually be groups of tightly associated Ir_{~4} clusters that also exist in solution [36,37], or (iii) simply be artifacts brought about by the ex situ technique itself, with the ex situ observed clusters not existing in the

solutions used in cyclohexene hydrogenation and examined by XAFS spectroscopy. However, the similar Ir cluster sizes and distributions obtained by *both* Z-contrast STEM and MALDI MS (vide infra), and the XAFS-determined Ir–Ir bond lengths and bond length disorders larger than those observed in bulk Ir (see Table A.2, and the text below), make the *presence* of highly disordered nanoscale Ir clusters—along with a majority of subnanometer, Ir_n clusters—a preferred explanation. The key finding by XAFS, then, is that *initial, precatalytic hydrogenation solutions are composed, on average, of Ir_n, 0.5 nm clusters.*

Significantly, the *R* values for Ir–Ir 1NNs in all samples are *larger* than the theoretical values from bulk Ir, Table A.2. If transition metal nanoclusters were the dominant species present, then the M–M distances should have been *smaller* (and as we will see posthydrogenation, vide infra), distances contracted in order to minimize the surface free energy (the surface free energy of small metal clusters is elevated due to the unsatisfied bonding requirements and too-low coordination number of the surface metals) [31,39]. However, the observed, longer Ir–Ir distances are fully consistent with subnanometer, Ir_n cluster compounds [36,40,41,42] coordinated to any available ligands such as those listed earlier, namely, AlEt₃, C₇H₁₅CO₂AlEt₃[−], and possibly Ir–H–AlEt₃. The possibility of Ir–Al bonding (or possibly Ir–X–Al, X = H or Et, bonding) is consistent with the XAFS data; fits of samples with Al/Ir ratios from 1.5–3.0 reveal Al at a distance from Ir of 2.5 Å, which is within the range found for γ-Al₂O₃-supported Ir₄ and Ir₆ clusters [43]. Additionally, the Ir to Al atom-pair distance of ca. 2.5 Å obtained by XAFS is close to crystallographically determined distances 2.456(1) Å and 2.459(1) Å in (Cp*(PMe₃)IrAlEt)₂, which possesses an Ir–Al–Ir bridging motif but is shorter than the Ir–H–Al bond distance of 2.684(2) in Cp*(PMe₃)Ir(H)₂AlPh₃ [44]. These results are of

considerable significance in addressing likely ligands derived from the AlEt_3 and $\text{C}_7\text{H}_{15}\text{CO}_2^-$ components of the catalyst, and under the reaction conditions [13].

The three main results from fitting the XAFS spectra, then, are (i) samples with Al/Ir ratios ≥ 1.5 are best fit using a model incorporating backscattering from Al; (ii) low Ir–Ir first-nearest neighbor coordination numbers imply, on average, $\text{Ir}_{\sim 4}$, 0.5 nm clusters; (iii) Ir–Ir distances longer than expected for bulk Ir were found, consistent with Ir ligated by the ligands present in species such as Ir–X–Al or possible direct Ir–Al interaction. Significantly, the Z-contrast STEM and XAFS results *are consistent, giving $\text{Ir}_{\sim 4}$, 0.5 nm clusters as the mean Ir_n clusters*. The identical mean cluster size results from Z-contrast STEM and XAFS argue strongly against artifacts introduced by either method, including the ex situ STEM, which in turn suggests that the *$\text{Ir}_{\sim 4}$, 0.5 nm clusters are, as the Z-contrast STEM reveals, a major part of a broad distribution of Ir_n clusters*.

The X-ray absorption near-edge structure (XANES) was used to probe the oxidation state of the initial catalyst solutions. The XANES regions of Ir black, $\text{Ir}_4(\text{CO})_{12}$, and $[(1,5\text{-COD})\text{Ir}(\mu\text{-O}_2\text{C}_8\text{H}_{15})]_2$ are shown in Figure A.6 alongside those for the Al/Ir = 1.0 and 2.0 catalyst samples before hydrogenation. The XANES spectra of the catalyst samples are similar to the $[(1,5\text{-COD})\text{Ir}(\text{I})(\mu\text{-O}_2\text{C}_8\text{H}_{15})]_2$ precursor and $\text{Ir}(0)_4(\text{CO})_{12}$ standard (formally Ir(I) and Ir(0), respectively) but unlike the Ir(0) black standard. This is the case regardless of the Al/Ir ratio of the sample and suggests that the Ir species present are formally Ir(I) or Ir(0) ligated by the previously listed ligand possibilities.

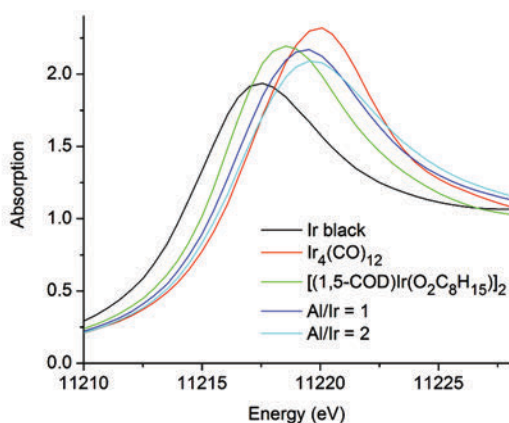


Figure A.6. XANES portions of the normalized $\mu(E)$ spectra for Ir black (black line), $\text{Ir}_4(\text{CO})_{12}$ (red), the $[(1,5\text{-COD})\text{Ir}(\mu\text{-O}_2\text{C}_8\text{H}_{15})_2]$ precatalyst (green), and the $\text{AlEt}_3/\text{Ir} = 1.0$ and 2.0 samples before hydrogenation (blue and light blue). The catalyst samples before hydrogenation are comparable to the formally Ir(I) and Ir(0) $[(1,5\text{-COD})\text{Ir}(\mu\text{-O}_2\text{C}_8\text{H}_{15})_2]$ precatalyst and $\text{Ir}_4(\text{CO})_{12}$ standard, respectively.

A sample of the $[(1,5\text{-COD})\text{Ir}(\mu\text{-O}_2\text{C}_8\text{H}_{15})_2]$ plus AlEt_3 catalyst, Al/Ir of 2.0, was analyzed by XPS to distinguish whether the Ir species in the catalyst before hydrogenation are Ir(I) or Ir(0); experimental XPS spectra and literature reference data are given in the Supporting Information (available online at <http://pubs.acs.org>). The Ir 4f peak positions at 64.30 and 61.33 eV in the experimental XPS spectrum can be attributed to Ir(I) [45] but are also consistent with (i.e., indistinguishable from) $\text{Ir}(0)_n$ Ziegler nanoclusters exhibiting a final-state relaxation effect [46,47,48,49,50,51,52,53]. Therefore, both XANES and XPS results of catalyst samples before their use in hydrogenation are consistent with Ir(I) species as well as $\text{Ir}(0)_n$ Ziegler nanoclusters (or both), but cannot unambiguously distinguish these.

To summarize the observations from XAFS spectroscopy on the aged catalyst samples, but before hydrogenation, (i) longer range scattering peaks, expected for ordered nanoclusters, are not seen; (ii) successful fitting of the Al/Ir ≥ 1.5 catalyst sample spectra requires a model that includes the backscattering from Al atoms in close proximity to Ir atoms; (iii) small Ir–Ir N

values are obtained that correspond to subnanometer cluster sizes; (iv) Ir–Ir bonds longer than expected for bulk or Ir(0)_n nanoclusters, but consistent with ligated Ir_n subnanometer clusters, are seen; (v) XANES spectra are different than those of bulk Ir but are comparable to the [(1,5-COD)Ir(μ-O₂C₈H₁₅)₂]₂ precursor and Ir₄(CO)₁₂. These observations suggest that the initial catalyst samples, regardless of the Al/Ir ratio, are composed on average of Ir(I) or Ir(0) subnanometer, molecular Ir_n clusters shielded from agglomeration by coordinated ligands [54,55,56,57,58,59]. The observations made here by XAFS on catalyst *solutions* are also fully consistent with and supported by the results from (the ex situ, solid state) Z-contrast STEM, which indicates that catalyst samples before hydrogenation are composed of a broad range of cluster sizes from mono-Ir molecules to nanometer scale noncrystalline Ir_n clusters, the most abundant being subnanometer Ir clusters, and the mean clusters being Ir_n, 0.5 nm. The use of these complementary methods and their agreement is important; the results argue strongly against significant sample preparation and method-specific (and ex situ versus in situ) artifacts. The results confirm our design criteria of using the more-stable, third-row Ir precatalyst (i.e., with its stronger Ir–Ir bonds and resultant greater cluster and nanocluster stability) as a needed, but previously little investigated, Ziegler-type hydrogenation catalyst model system.

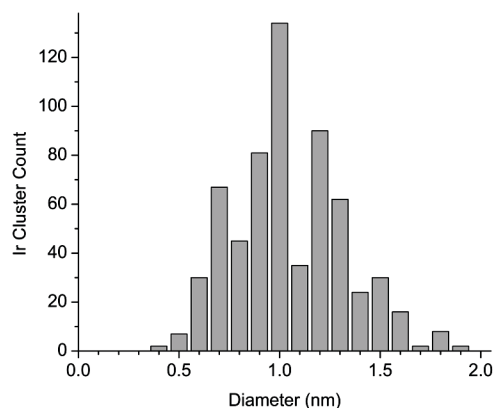
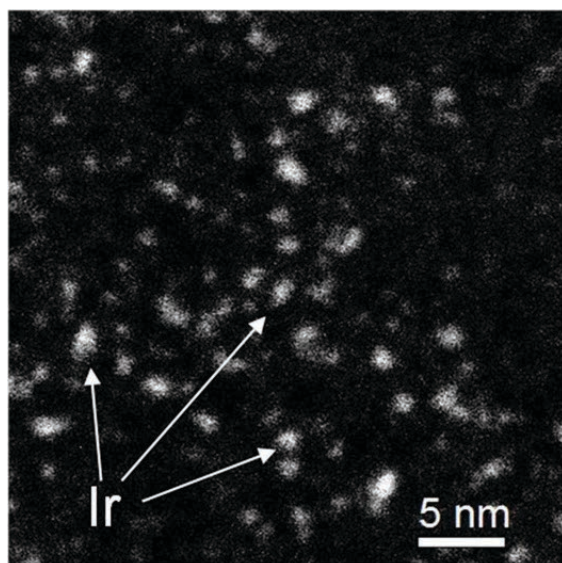
Nuclearity of the Ir_n Species in AlEt₃/Ir Catalyst *before* Hydrogenation: MALDI MS. Despite the agreement between the Z-contrast STEM and XAFS results, an additional method was used in order to further probe the Ir_n cluster size and distribution—as well as to “calibrate” that matrix assisted laser desorption ionization mass spectrometry (MALDI MS) method in this instance; is this ex situ method reliable? Initial catalyst samples, before their use in hydrogenation but without aging, were analyzed. The experimental methods are discussed in greater detail in the Supporting Information (available online at <http://pubs.acs.org>) for the

interested reader, and spectra are shown there as well. Briefly, the ex situ MALDI MS on dried, solid samples reveals a broad Ir-containing peak centered at about 2800 m/z . The FWHM ranges from 1000–5000 m/z , and the peak tails off towards the higher m/z values. With the necessary *assumptions* that the broad peak observed in the full mass spectrum is composed of only Ir atoms [60,61,62] and that the ionic charges are +1 [60,62,63], the peak maximum corresponds to Ir_{~15}, 0.7-nm-diameter clusters [18]. Likewise, the FWHM of the peak corresponds to Ir_{~5-26}, 0.5–0.9-nm-diameter clusters (used to estimate the mean Ir_{*n*} cluster size at 0.7 ± 0.2 nm), and the high m/z tail gives indication of larger clusters present in relatively few numbers. The high m/z tail at one-fourth maximum intensity of the broad peak is positioned at 6000 m/z , which corresponds to Ir_{~30}, 0.9–1.0 nm clusters. The high m/z region of the spectrum continues to tail off indicating the presence of Ir nanoclusters, but in a much lower abundance—for example, Ir_{~50}, 1.1 nm-diameter-clusters at one-eighth the maximum peak intensity (and used as the maximum range limit reported in Table A.1).

The quite different MALDI MS method proved useful in that it provides independent evidence for *similar* (albeit not identical) sizes and size distributions of Ir_{*n*} clusters. The difference between the *estimated* mean Ir_{~15}, 0.7 nm clusters from MALDI MS and the mean Ir_{~4}, 0.5 nm clusters indicated by both Z-contrast STEM and XAFS may be the result of (i) factors due to the differences of the methods, (ii) imperfection in the assumptions necessary for this interpretation of MALDI MS, (iii) the fact that the sample analyzed by MALDI MS was not aged whereas the Z-contrast STEM and XAFS samples were aged, or (iv) some combination thereof. Regardless, the significance here is that MALDI MS confirms, in general, the results of Z-contrast STEM by giving independent evidence that the [(1,5-COD)Ir(μ-O₂C₈H₁₅)₂] plus AlEt₃ catalyst sample, with an Al/Ir ratio of 2.0, *before* hydrogenation, is composed of a broad

distribution of Ir_n clusters, which are primarily subnanometer Ir_n clusters, but include, to a lesser extent, Ir_n nanoclusters. The generally similar results argue against *significant* artifacts caused by these three very different physical methods. The main point is that in catalyst samples before hydrogenation there is a distribution in Ir_n species centered on subnanometer Ir_n clusters, and that the *estimated* mean cluster sizes are 0.5–0.7 nm, $\text{Ir}_{\sim 4-15}$.

Identification of the Ir-Containing Species in the AlEt_3/Ir Catalyst after Hydrogenation: Z-Contrast and HRTEM Microscopy. The size and size distribution of Ir clusters, in a $[(1,5\text{-COD})\text{Ir}(\mu\text{-O}_2\text{C}_8\text{H}_{15})]_2$ plus AlEt_3 catalyst sample with an Al/Ir ratio of 2.0 and *after* its use for cyclohexene hydrogenation, were analyzed using Z-contrast microscopy. Sample Z-contrast images and a histogram are shown in Figure A.7. Measurement of 635 Ir clusters resulted in a mean diameter of 1.0 ± 0.3 nm, with observed Ir_n cluster diameters spanning from 0.4 to 1.9 nm (two additional Ir nanoclusters, with larger diameters of 3.1 and 3.8 nm, were also observed).



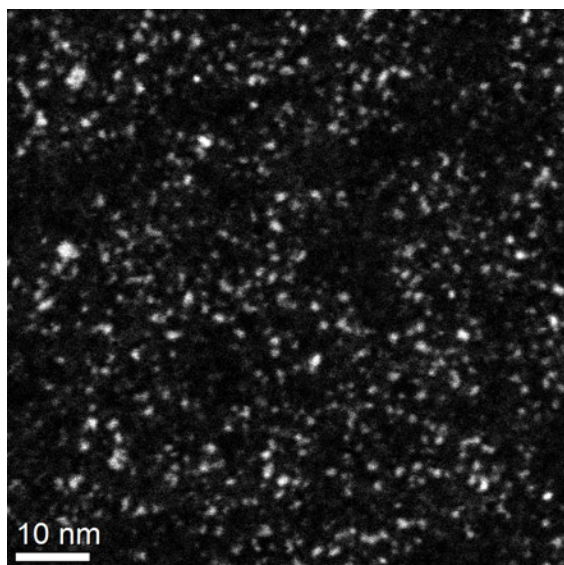


Figure A.7. Example Z-contrast images of the $[(1,5\text{-COD})\text{Ir}(\mu\text{-O}_2\text{C}_8\text{H}_{15})_2]$ plus AlEt_3 , $\text{Al}/\text{Ir} = 2.0$, catalyst sample *after hydrogenation*. The Ir cluster histogram from the diameter measurement of 635 Ir clusters is also shown. The mean Ir cluster diameter is 1.0 ± 0.3 nm, which corresponds to $\text{Ir}(0)_{\sim 40}$ clusters. Two larger Ir nanoclusters with diameters of 3.1 and 3.8 nm are also observed, presumably the result of well-precedented nanocluster aggregation processes [64,65].

Also obtained were HRTEM images of $[(1,5\text{-COD})\text{Ir}(\mu\text{-O}_2\text{C}_8\text{H}_{15})_2]$ plus AlEt_3 catalyst samples after hydrogenation, with Al/Ir ratios of 1.0, 2.0, and 5.0 [66]. An example HRTEM image of the sample with an Al/Ir ratio of 2.0, Figure A.8, shows distinct lattice fringes in the Ir particles. This result is general to all Al/Ir ratios tested; crystalline Ir Ziegler nanoclusters are observed in all HRTEM images obtained for the samples with Al/Ir ratios of 1.0, 2.0, and 5.0 (other images are shown in Figures S27–S30, Supporting Information (available online at <http://pubs.acs.org>)). Electron diffraction shows that these Ziegler nanoclusters after hydrogenation are *fcc* Ir, at least under the conditions of the electron beam (Figure S31, Supporting Information (available online at <http://pubs.acs.org>)). The key result, then, of the combined Z-contrast and HRTEM microscopy is that the mean Ir_n clusters postcatalysis are

larger, crystalline 1.0 ± 0.3 nm, $\text{Ir}_{\sim 40}$ nanoclusters.

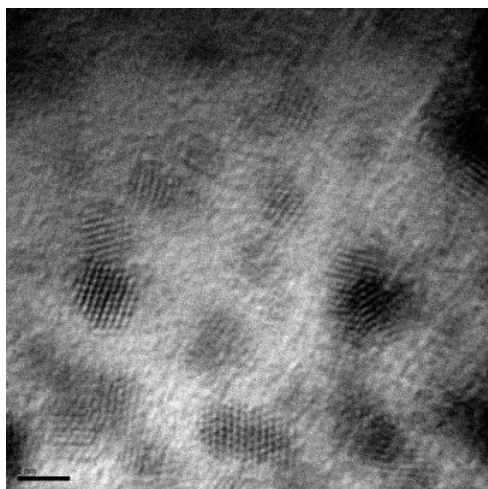


Figure A.8. An example HRTEM image of the $[(1,5\text{-COD})\text{Ir}(\mu\text{-O}_2\text{C}_8\text{H}_{15})_2]$ plus AlEt_3 catalyst, Al/Ir is 2.0, after its use in cyclohexene hydrogenation (scale bar is 2 nm). The distinct lattice fringes show that the Ir particles after use in hydrogenation possess a crystalline structure under the HRTEM observation conditions. Crystalline particles are observed for all Al/Ir values tested, 1.0, 2.0, and 5.0.

Identification of the Ir-Containing Species in the AlEt_3/Ir Catalyst after Hydrogenation: XAFS Spectroscopy. A of the $[(1,5\text{-COD})\text{Ir}(\mu\text{-O}_2\text{C}_8\text{H}_{15})_2]$ plus AlEt_3 catalyst, with an Al/Ir ratio of 1.0, after its use in cyclohexene hydrogenation was analyzed by XAFS spectroscopy. Peaks in the 3–6 Å range of the FT magnitude spectrum reveal that the sample is composed of Ir_n particles with ordered internal atomic structures, Figure A.9, consistent with the microscopy results (vide supra). A fit of the Fourier transform magnitude spectrum, also shown in Figure A.9, gives an Ir–Ir 1NN coordination of 9.0 ± 0.4 . The mean coordination number, obtained from fitting the Ir–Ir 1NN contribution, was used to estimate cluster sizes using a theoretical mean coordination number–particle diameter correlation curve [16,27,67] (Supporting Information, available online at <http://pubs.acs.org>). An Ir–Ir 1NN coordination of 9.0 ± 0.4 according to XAFS corresponds to, on average, 1.6 nm, crystalline *fcc*

$\text{Ir}(0)_{-150}$ clusters. Additionally, the Ir–Ir 1NN distance of $2.688 \pm 0.001 \text{ \AA}$ is now *shorter* than that in bulk Ir, as one would expect for nanometer-sized, contracted surface clusters. Full fitting results are given in Table S.8, Supporting Information (available online at <http://pubs.acs.org>).

The XANES portion of the sample spectrum is essentially identical to the XANES spectra of Ir black, Figure A.10. This shows convincingly that the oxidation state of the Ir in the sample is Ir(0). XPS confirms the predominance of Ir(0) in a catalyst sample with an Al/Ir ratio of 2.0, after hydrogenation. Additionally, the XANES result, especially with corroboration by XPS independently performed on a different sample (Supporting Information (available online at <http://pubs.acs.org>)), shows definitively that the sample analyzed by XANES and XAFS was not contaminated by atmospheric oxygen. In short, the XAFS plus XANES and XPS of post hydrogenation catalyst samples shows the presence of, on average, approximately 1.6 nm, *fcc* $\text{Ir}(0)_{-150}$, nanoparticles.

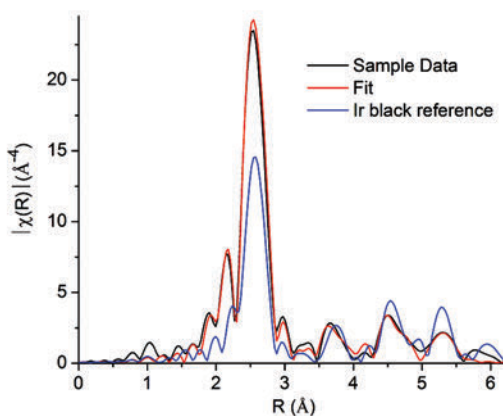


Figure A.9. Fourier transform (FT) magnitudes of the data (black curve) and fit (red) of a powder sample of the Al/Ir = 1.0 catalyst after its use in hydrogenation. The longer range scattering peaks in the 3–6 Å range are expected for Ir nanoclusters with ordered internal structures. The Ir–Ir 1NN coordination number obtained from the fit, 9.0 ± 0.4 , corresponds to, on average, approximately 1.6 nm, crystalline *fcc* $\text{Ir}(0)_{-150}$ clusters, according to XAFS. The FT magnitude spectrum of the Ir black reference, scaled by one-fourth, is shown for comparison (blue).

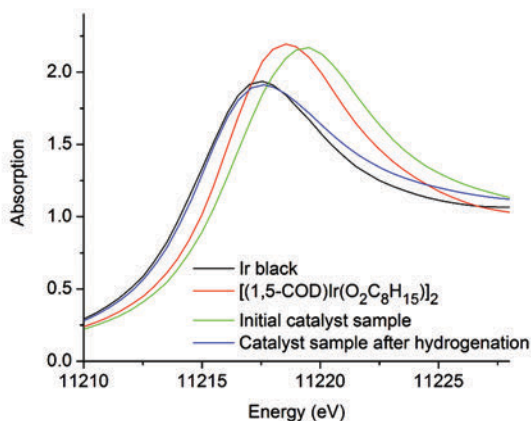


Figure A.10. XANES spectra of Ir black (black line), the precatalyst $[(1,5\text{-COD})\text{Ir}(\mu\text{-O}_2\text{C}_8\text{H}_{15})_2]$ (red), the initial $[(1,5\text{-COD})\text{Ir}(\mu\text{-O}_2\text{C}_8\text{H}_{15})_2]$ plus AlEt_3 catalyst (green), and the same catalyst sample after its use in the catalytic hydrogenation of cyclohexene (blue). The similarity of the Ir black and after-hydrogenation catalyst curves is compelling evidence for an Ir(0) oxidation state in the after-hydrogenation catalyst.

The difference in mean Ir cluster sizes measured by Z-contrast STEM versus those approximated by XAFS spectroscopy for the after-hydrogenation samples is possibly due to the XAFS data being collected on a powder sample. In a control experiment, precipitated catalyst material was collected after an initial cyclohexene hydrogenation run and isolated as a powder. It was then redispersed in cyclohexane, cyclohexene was added, and run in a second hydrogenation (see the Experimental Section for more details). Catalytic cyclohexene hydrogenation begins immediately using redispersed precipitate for a second run, Figure A.11, and at a similar rate to the maximum rate achieved toward the end of an initial run, Figure A.1. In short, this control experiment confirms that a highly active hydrogenation catalyst is retained following the procedures used to analyze the catalyst sample by XAFS and XANES. Add to this the observation, mentioned previously, that catalyst solutions sometimes precipitate after a cyclohexene hydrogenation run under standard conditions, and the combined results argue strongly that the postcatalysis Ir cluster characterization results from XAFS are representative of

the nature of the Ir species postcatalysis (although analysis of the precipitate, likely the result of well-precedented nanocluster aggregation processes, probably gives a larger Ir particle size than what exists in solution before precipitation occurs). The key point is that *fcc* Ir(0)_n Ziegler nanoclusters are increasing in size and abundance postcatalysis. Moreover, they likely are the fastest, best catalysts in this system (on the basis of the results of this control experiment, the increase in the rate of cyclohexene hydrogenation as catalysis proceeds, Figure A.1, and also based on catalyst poisoning studies, *vide infra*).

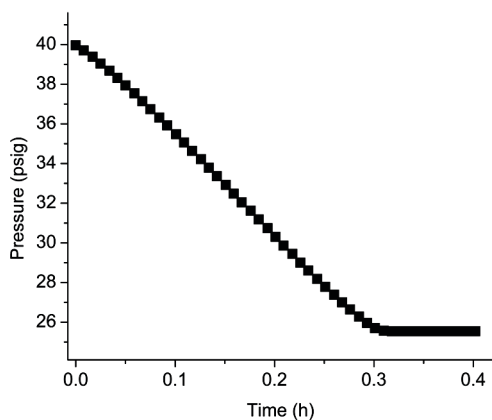


Figure A.11. A second cyclohexene catalytic run following collection and isolation of a precipitate from a first run, and redispersion of it in cyclohexane. The initial hydrogenation rate in this experiment is 47 psig/h, and the maximum rate is 50 psig/h. Both rates are similar to the maximum hydrogenation rate observed from aged catalyst solutions during an initial run.

Identification of the Ir-Containing Species in the AlEt₃/Ir Catalyst *after*

Hydrogenation: MALDI MS. The [(1,5-COD)Ir(μ -O₂C₈H₁₅)₂] plus AlEt₃, Al/Ir = 2.0, catalyst, after its use in cyclohexene hydrogenation, was analyzed using MALDI MS (the spectrum is shown in the Supporting Information (available online at <http://pubs.acs.org>)). Similar to the MALDI MS results from the sample analyzed before hydrogenation, a broad peak representing a range of Ir_n species exists in the ≥ 1000 *m/z* region, with a maximum at about

3000 m/z corresponding to $\text{Ir}_{\sim 16}$, approximately 0.8-nm-diameter clusters. However, this posthydrogenation peak has a significant shoulder at about 5500 m/z , which indicates $\text{Ir}_{\sim 30}$, 0.9 nm clusters, and the FWHM of the peak corresponds to $\text{Ir}_{\sim 8-40}$, 0.6–1.0 nm diameter clusters (the FWHM was used to estimate mean cluster diameter, Table A.1, although it is an underestimation even more so than with the prehydrogenation sample because of the irregular peak shape). In addition, the curve tails off toward higher m/z values considerably less steeply than in the prehydrogenation sample spectrum—it reaches one-quarter max intensity at about 11500 m/z , which corresponds to $\text{Ir}_{\sim 60}$, 1.2 nm clusters (nearly double the ~ 6000 m/z at one quarter intensity in the prehydrogenation spectrum, *vide supra*), and falls to one-eighth the maximum intensity at ~ 19500 m/z , which corresponds to $\text{Ir}_{\sim 100}$, 1.4 nm clusters (again, about double the m/z value at one-eighth maximum intensity in the prehydrogenation sample that corresponds to $\text{Ir}_{\sim 50}$, 1.1 nm clusters).

A broad range of Ir_n cluster sizes is again observed using MALDI MS, but compared to the prehydrogenation sample, the posthydrogenation catalyst includes even larger Ir_n nanoclusters, and a significantly greater quantity of these larger Ir_n species. Again, MALDI MS gives results that are similar, but not identical, to those from Z-contrast STEM; the possible reasons may be any combination of the factors listed previously, and an additional factor may be the difference in transit time between completion of a catalytic run and analysis of the sample [68]. The key point that remains, regardless of the differences in Ir_n cluster sizes obtained using the three methods, is that Z-contrast STEM, XAFS, and MALDI MS *all show a distinct trend toward a greater population of larger, nanoscale Ir_n clusters in the posthydrogenation catalyst sample.* On the basis of the combined results of these three methods (Z-contrast giving mean 1.0 ± 0.3 nm, $\text{Ir}_{\sim 40}$ clusters; XAFS indicating mean 1.6 nm, $\text{Ir}_{\sim 150}$,

clusters; and MALDI MS also showing a shift in the population if Ir_n species towards larger, nanometer scale clusters) we refer to these nanoscale, crystalline $\text{Ir}(0)_n$ clusters herein as *fcc* $\text{Ir}(0)_{40-150}$ Ziegler nanoclusters.

The Before-Hydrogenation-to-After-Hydrogenation Changes of Aged Catalysts: A Summary. The first step in the approach used herein to address the “is it homogeneous or heterogeneous catalyst?” question for the present catalyst system [3,4b,7,8], is identification of the form(s) (e.g., Ir_n cluster nuclearity) that the observable catalyst mass takes. A combination of analytic techniques has revealed that catalyst solutions before their use in hydrogenation contain a broadly dispersed range of Ir_n clusters extending from mono-Ir compounds to Ir_n nanoclusters with significantly disordered internal atomic structures, and with an estimated average of 0.5–0.7 nm, $\text{Ir}(0)_{4-15}$ clusters. *The Ir_n species present are nearly the same regardless of the Al/Ir ratio employed*, an important finding in its own right which, in turn, suggests *that the observed changes in catalytic activity at different Al/Ir ratios are primarily the result of changes in the form and function of the Al-derived component(s) of the catalyst* (i.e., the Al/Ir ratio not causing significant changes in the Ir_n nuclearity) [13]. During the use of these solutions in hydrogenation, a conversion toward roughly 1.0–1.6 nm, *fcc* $\text{Ir}(0)_{40-150}$ Ziegler nanoclusters takes place [69], consistent with the color change of the catalyst solutions from tawny yellow to darker brown as hydrogenation proceeds and the precipitation often seen a few days after the conclusion of a catalytic run. The conversion toward these 1.0–1.6 nm, $\text{Ir}(0)_{40-150}$ Ziegler nanoclusters is independently evidenced by the results of Z-contrast STEM, XAFS spectroscopy, and MALDI MS, which show shifts in the range of Ir_n clusters present toward larger Ir_n clusters and increases in the mean observed clusters sizes and mean Ir_n nuclearities. A key to obtaining these insights is our use of a third-row Ir system where, the evidence argues, its

more stable Ir–Ir bonds mitigate against artifacts due, for example, to sample preparation and ex situ Z-contrast STEM.

Additional Kinetics-Based Experiments Probing the Active Catalyst. Kinetics data are key to determining whether the observed catalytic activity using $[(1,5\text{-COD})\text{Ir}(\mu\text{-O}_2\text{C}_8\text{H}_{15})]_2$ plus AlEt_3 catalysts is homogeneous (e.g., defined here as proceeding via mono-Ir compounds or subnanometer $\text{Ir}_{\sim 4-15}$ cluster catalysts) or heterogeneous (e.g., defined here as proceeding via $\text{Ir}(0)_{\sim 40-150}$ Ziegler nanoclusters) [3,4b,7,8]. We have already shown that catalytic cyclohexene hydrogenation curves obtained using the $[(1,5\text{-COD})\text{Ir}(\mu\text{-O}_2\text{C}_8\text{H}_{15})]_2$ plus AlEt_3 catalyst with an Al/Ir ratio of 2, both with and without prior aging of the catalyst solutions for 9 h, give a maximum hydrogenation rate ($-\text{d}[\text{H}_2]/\text{dt}$) that is *not* the initial rate (i.e., that is faster than the initial rate). Instead, the hydrogenation rate increases concomitant with the increase in cluster size (and corresponding structural change) from $\text{Ir}_{\sim 4-15}$ to *fcc* $\text{Ir}(0)_{\sim 40-150}$. This rate increase is quite pronounced when using catalyst solutions immediately after their preparation (see the switch in activity at ~ 2 h in Figure A.12b) but is more modest when the catalyst solutions have been aged, Figure A.12a. The observed increase in the rate of hydrogenation during catalysis, plus the above studies showing (i) the *presence* of larger $\text{Ir}(0)_{\sim 40-150}$ Ziegler nanoclusters post catalysis and also (ii) *high catalytic activity* when these nanoparticles are collected as a precipitate, redispersed in cyclohexane and used for a second catalytic run, strongly suggests, in the simplest (Ockham's razor) interpretation of the data, *that the fastest, best catalysts are the larger fcc Ir(0)_{~40-150} Ziegler nanoclusters.*

To further test this hypothesis that the larger *fcc* $\text{Ir}(0)_{\sim 40-150}$ Ziegler nanoclusters are the kinetically dominant catalyst, Hg(0) poisoning experiments were utilized (Hg(0) being known to poison most heterogeneous catalysts [3,4b,70,71,72]). Specifically, Hg(0) was added to the

catalyst solutions after the cyclohexene consumption had proceeded about halfway (i.e., and once the catalytic rate had entered the maximum activity regime). The catalysis was poisoned *immediately and completely* by the Hg(0) addition, regardless of whether the initial catalyst solution was aged for 9 h prior to use (Figure A.12a) or used immediately without aging (Figure A.12b). This result provides additional evidence that the catalyst at the most active stage is what we defined earlier as heterogeneous—that is, due to the *fcc* Ir(0)_{~40-150} Ziegler nanoclusters observed post hydrogenation.

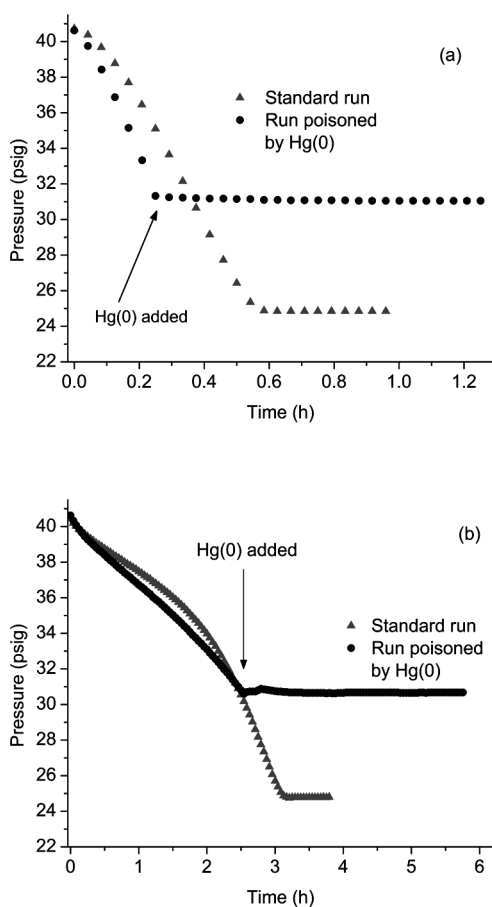


Figure A.12. Cyclohexene hydrogenation curves for $[(1,5\text{-COD})\text{Ir}(\mu\text{-O}_2\text{C}_8\text{H}_{15})]_2$ plus AlEt_3 catalysts with Al/Ir ratios of 2.0, for (a) catalyst solutions aged 9 h, or (b) not aged, alongside hydrogenation runs poisoned by addition of Hg(0) under otherwise identical conditions. The variation in the hydrogenation runs prior to Hg(0) addition is typical for this system. For runs poisoned by Hg(0), the catalytic hydrogenation of cyclohexene was allowed to proceed until the maximum rate regime was reached. Then, the solution was transferred to the drybox where \geq

300 equivalents of Hg(0) per Ir was added and allowed to stir at 1000 rpm before putting it back on the hydrogenation line. The *subsequent* part of the hydrogenation curve shows *immediate and total* poisoning of the catalyst.

As a control experiment, Hg(0) was added to catalyst solutions, both with and without aging, *before* the start of catalytic cyclohexene hydrogenation (i.e., before being exposed to H₂ gas). Near-immediate poisoning of the catalyst, Figure A.13, suggests that the kinetically competent, fastest catalysts, even at the initial stage, are heterogeneous (i.e., larger Ir_n nanoclusters, *not* the initially present mono-Ir complexes and Ir_{~4-15} clusters, although one cannot rule out that Hg(0) is poisoning active Ir_{~4-15} subnanoclusters). However, and interestingly, although ~95% of the activity is poisoned, there is ~5% activity initially, non-Hg(0)-poisoned activity that implies a residual, *apparently* homogeneous catalyst, albeit one that accounts for only ~5% of the catalysis [73]. Whether Hg(0) will or will not poison subnanometer, molecular Ir_n clusters remains an open question, one that will require the synthesis and characterization of, for example, authentic Ir₄ clusters and attempts to poison their expected catalysis with Hg(0). If, for example, the present prehydrogenation Ir clusters are actually of nominal composition Ir(I)₄H₄ (i.e., Ir(I)₄ and not Ir(0)₄), then that would be one *possible* explanation for their insensitivity to Hg(0). Nevertheless, the Hg(0) poisoning experiments provide additional support for the hypothesis—now the dominant hypothesis for further studies in the area of Ziegler-type hydrogenation catalysis—that the *most active, kinetically competent catalysts* at the point of the maximum hydrogenation rate are *heterogeneous Ziegler nanoclusters analogous to the present Ir(0)_{~40-150}*. This is an important, previously unavailable finding. It presages an area of catalysis by hydrocarbon-soluble, Lewis-acid-containing, and thus presumably unusually coordinatively unsaturated—and certainly extremely catalytically active, industrially utilized—“Ziegler nanocluster” catalysts.

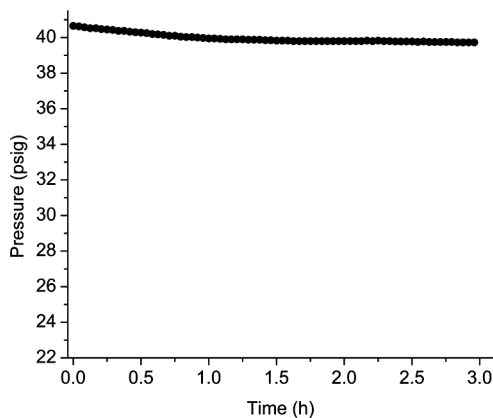


Figure A.13. Near-immediate poisoning of the catalyst. Hg(0), ≥ 300 equivalents per Ir, was added to the catalyst solution after its preparation and 9 h of aging in the drybox. Sufficient mixing was ensured by stirring of the Hg(0)-containing catalyst solution for 24 h at 1000 rpm. Poisoning is 95% complete, but a small, residual, ca. 5% activity (i.e., 5% of the H₂) is still consumed, mostly early in the experiment.

3. Summary

The main findings of this study, then, are as follows:

- The initial [(1,5-COD)Ir(μ -O₂C₈H₁₅)₂] plus AlEt₃ Ziegler-type hydrogenation catalyst solutions, *before*-hydrogenation, are (by Z-contrast STEM, XAFS, and MALDI MS) a broad range of Ir_n complexes from mono-Ir compounds to noncrystalline Ir_n Ziegler nanoclusters, with the estimated mean Ir_n clusters being 0.5–0.7 nm, Ir_{~4-15} subnanometer clusters. The agreement among the results, regardless of whether ex situ solid state Z-contrast imaging or in situ, solution XAFS/XANES is employed, argues against artifacts caused by these methods or the associated sample handling or preparation. Our use of MALDI MS as an additional method yielded estimated mean Ir cluster size and nuclearity results that are similar to those obtained by Z-contrast STEM and XAFS, but not identical—results that we view as a calibration of the less

useful MALDI-MS method in the present case. Nevertheless, the results all yield a consistent picture of the catalyst before hydrogenation as consisting of a broad range of Ir_n species dominated by subnanometer Ir_n clusters.

- According to XAFS, the Ir_n nuclearity results are largely unchanged regardless of the Al/Ir ratio employed. This important observation indicates that differences in catalytic activity, as a function of Al/Ir ratios, must be due just to the form or function of the Al-derived component(s) [13], and not to any Al/Ir- controlled or -dependent nuclearity of the initial Ir_n species present.

- At the end of their use in hydrogenation, the population of Ir_n clusters in the samples has shifted toward larger, 1.0–1.6 nm, *fcc* $\text{Ir}(0)_{\sim 40-150}$ Ziegler nanoclusters. The average sizes of these larger nanoclusters, as determined by Z-contrast STEM, HRTEM, and XAFS/XANES, are similar, but not identical, depending on the technique (and associated sample preparation) used. However, the *trend* toward larger, $\text{Ir}(0)_{\sim 40-150}$ Ziegler nanoclusters in posthydrogenation samples is verified by each method (i.e., is method-independent).

- Significantly, the development of *fcc* $\text{Ir}(0)_{\sim 40-150}$ nanoclusters correlates with both a change in solution color (that also signals nanocluster formation) and an increase in the rate of cyclohexene hydrogenation. Furthermore, a precipitate can be collected from the catalyst solutions and, when redispersed in cyclohexene, displays immediate high activity for the hydrogenation of cyclohexene comparable to the maximum activity observed toward the end of an initial cyclohexene hydrogenation run. The evidence is consistent with and highly supportive of the now-dominant hypothesis for future research in the area, that the larger *fcc* $\text{Ir}(0)_{\sim 40-150}$ Ziegler nanoclusters are the fastest Ziegler-type hydrogenation catalysts attained in at least the present Ir Ziegler-type catalyst system. That said, catalysis of a ~2- to 10-fold slower

rate (depending on the Al/Ir ratio and whether an aged or nonaged catalyst was used) is seen initially, when the estimated mean Ir species present are 0.5–0.7 nm, Ir_{~4-15} clusters.

- Consistent with the above “Ziegler nanocluster catalysis hypothesis”, Hg(0) added to catalyst solutions after the catalysts have entered their maximum rate regime stops the catalytic activity immediately and completely. This further supports evidence that the fastest catalysts found in this system are the *fcc* Ir(0)_{~40-150} Ziegler nanoclusters (i.e., that “heterogeneous catalysis” [3,4] is present). However, it is worth noting that in solutions with Hg(0) added at the prehydrogenation stage, residual catalysis, presumably effected by unpoisoned homogeneous catalyst(s) such as monometallic Ir complexes or 0.5–0.7 nm, Ir_{~4-15} clusters, results in ~5% of the normal total H₂ consumption. Although significant catalysis by discrete subnanometer Ir species is not unequivocally ruled out by this study, the overall simplest interpretation of the data is that the larger, *fcc* Ir(0)_{~40-150} nanoclusters are the more effective catalysts.

- Successfully investigating the problem of the composition and structure of a Ziegler-type hydrogenation catalyst has depended on the approach used herein: (a) the use of a third-row Ir-system with its strong Ir–Ir bonds and, therefore, more robust Ir_n species that are less sensitive to various analytical methods and associated sample preparations, (b) the development [2] and use of the well characterized [(1,5-COD)Ir(μ-O₂C₈H₁₅)₂] precatalyst, and (c) the use of a combination of multiple, complementary analytical techniques *and* kinetic studies plus poisoning studies. That said, additional, ideally operando studies are desirable in this area [3,9], and it is now possible to design them rationally and effectively.

- To our knowledge, this is the first report for a Ziegler-type hydrogenation catalyst where identification of the Ir_n species present using multiple complementary techniques has been coupled to kinetic evidence to show that the best, fastest catalysts are, in all probability

[20,74,75] the larger, *fcc* Ir(0)_{~40–200} Ziegler nanoclusters. Nor has evidence been previously reported that a Ziegler-type hydrogenation catalyst can initially contain a homogeneous component (ca. 5% of the activity) and transition to heterogeneous catalysis during hydrogenation. That said, we wish to emphasize once again (*vide supra*; the Introduction) the important, recent contributions of, especially, Shmidt [5] and co-workers and Bönemann and co-workers [3,6] that also provide evidence for the presence of nanoclusters under Ziegler-type hydrogenation catalysis conditions.

- Further investigation of this prototype Ir Ziegler-type hydrogenation system through additional kinetic studies [12], and evidence for the forms and roles of the AlR₃-derived component of the catalyst, will be reported elsewhere [13]. Those studies include an interesting inverse relationship between the maximum TOF and [Ir] concentration, intriguing findings which have required their own, separate study [12]. In addition, the results of studies analogous to those herein using the Co and Ni systems commonly employed by industry for olefin and polymer hydrogenation will be reported in due course [14].

Our comprehensive review of the literature of Ziegler-type hydrogenation catalyst [4] shows the above insights (*i.e.*, into the products of the precatalyst and cocatalyst reaction, how those products develop with use in a hydrogenation reaction, and the relative activities of those (metal)_n products) are at the state-of-the-art for a Ziegler-type hydrogenation catalyst—despite the industrial use of Ziegler-type hydrogenation catalysts for ~50 years to hydrogenate, currently, around 1.7×10^5 metric tons of styrenic block copolymers annually [2]. One of our hopes is that the present demonstration, that at least Ir_n “Ziegler-type nanoclusters” both exist and are also the kinetically dominant, highly active catalysts, will prompt the community to

begin to make use of these and other highly coordinately unsaturated, relatively “weakly ligated/labile ligand” [76], hydrocarbon-soluble nanoclusters. Such Ziegler-type nanoclusters are unusual in that RCO_2^- from the starting material, *hydrocarbon* solvent, and Lewis acidic AlEt_3 (plus their expected adducts, e.g., $\text{RCO}_2\text{AlEt}_3^-$ and any Al–O–Al-containing alumoxane from trace H_2O) are the only possible (weakly ligating) ligands present, undoubtedly one reason for the high, industrial-level catalytic activity of Ziegler nanoclusters.

4. Experimental Section

Materials. Unless stated otherwise, all materials were handled and stored under N_2 in a Vacuum Atmospheres drybox, with O_2 levels continuously maintained at ≤ 5 ppm according to a Vacuum Atmospheres O_2 -level monitor. All solution measurements and additions done in the drybox at Colorado State University (CSU) utilized gastight syringes. Glassware was dried in an oven at $160\text{ }^\circ\text{C}$ for ≥ 12 h and cooled under a vacuum or dry N_2 . Cyclohexane (Sigma-Aldrich, 99.5 %, $\text{H}_2\text{O} < 0.001$ %) was kept over activated molecular sieves for ≥ 2 days prior to use. Molecular sieves (Acros, 3 Å) were activated by heating at $200\text{ }^\circ\text{C}$ for 6 hours under vacuum. The precatalyst $[(1,5\text{-COD})\text{Ir}(\mu\text{-O}_2\text{C}_8\text{H}_{15})_2]_2$ was prepared as described [4] and used herein as a solution in cyclohexane, typically 9.0 or 12.0 mM in [Ir]. AlEt_3 (Strem Chemicals, 93%) was also used as a cyclohexane solution, typically 18.0 or 36.0 mM.

Caution! *Alkylaluminums are pyrophoric and should be handled with care using air- and moisture-free techniques [77].*

Cyclohexene (Aldrich, 99%) was distilled over sodium under argon. Both Ar and H_2 gases were passed through moisture (Scott Specialty Gases) and oxygen traps (Trigon Technologies) prior to use. Ir black and $\text{Ir}_4(\text{CO})_{12}$ (Strem, 98%) were used as received. HPO_4^-

stabilized *fcc* Ir(0)_n nanos were synthesized as previously described (details are provided in the Supporting Information (available online at <http://pubs.acs.org>)) [26].

Catalyst Solution Preparation. Catalyst solutions were prepared in the drybox at CSU both in batches and in smaller volumes for individual hydrogenation use (the temperature in the drybox was between 25 and 30 °C). For example, a 20 mL, [Ir] = 1.44 mM, batch of catalyst with an Al/Ir ratio of 2 was prepared by first adding 15.2 mL of cyclohexane to a 20 mL glass vial containing a 5/8 × 5/16 in. Teflon-coated magnetic stir bar. Next, 2.4 mL of a cyclohexane solution of [(1,5-COD)Ir(μ-O₂C₈H₁₅)₂], 12.0 mM in [Ir], was added, making an orange/light red solution. Stirring (1000 ± 200 rpm, measured with a Monarch Instruments Pocket-Tachometer 100) was started, and 1.6 mL of a 36.0 mM AlEt₃ solution was added rapidly.

Catalytic Cyclohexene Hydrogenations. All catalyst solutions for cyclohexene hydrogenation were prepared individually in 22 × 175 mm Pyrex culture tubes containing a new 5/8 × 5/16 in. Teflon-coated magnetic stir bar (both rinsed three times with ultrapure water prior to drying). For example, a 0.6 mM in [Ir], Al/Ir = 2.0, catalyst solution was prepared by adding 0.20 ± 0.01 mL of a 9.0 mM in [Ir] cyclohexane solution of [(1,5-COD)Ir(μ-O₂C₈H₁₅)₂] to a culture tube followed by 0.200 ± 0.002 mL of 18.0 mM AlEt₃ in cyclohexane, added rapidly with 1000 ± 200 rpm stirring to make Al/Ir = 2.0. Cyclohexane was added to bring the total volume to 2.5 mL, and then 0.5 ± 0.01 mL of cyclohexene was added, making 3.0 mL of a Al/Ir = 2 catalyst solution, 0.6 mM in [Ir] and 1.65 M in [cyclohexene].

The procedure and apparatus used for catalytic hydrogenations of cyclohexene were described in detail elsewhere [7a, 78, 79]. Briefly, once the hydrogenation reaction solution

was prepared, the culture tube was placed in a Fisher–Porter (F–P) bottle, which was then sealed. The solution was then allowed to stir at 1000 rpm in the sealed F–P bottle in the drybox, typically for 9 h (see Figure S2, Supporting Information (available online at <http://pubs.acs.org>)). At the end of the aging period, if any, the F–P bottle was then brought out of the drybox and placed in a bath set at 22.0 ± 0.1 °C. Stirring was started at 1000 ± 10 rpm employing a Fauske Super Magnetic Stirrer, and the F–P bottle was connected to a pressurized H₂ line using Swagelock quick-connects. The F–P bottle was purged 15 times (1 purge/15 sec). The pressure in the F–P bottle was set to 40 psig, and data collection was initiated at 4 minutes after the first purge. Hydrogen pressure vs time data were collected using a pressure transducer (Omega PX 624–100 GSV) interfaced via an Omega D1131 analog-to-digital converter connected to a PC running LabView 7.0. Data were subsequently handled using MS Excel and Origin 7. In order to quantitatively compare hydrogenation rates, and because of their shapes (i.e., more rapid H₂ pressure loss later in the hydrogenation, as opposed to initially), the initial and maximum rate portions of the curves were fit separately by polynomial and linear expressions, respectively (for an example, see Figure S1 of the Supporting Information (available online at <http://pubs.acs.org>)).

Catalyst Poisoning by Hg(0). All catalyst solutions were first prepared in the drybox as described above with [Ir] = 0.6 mM, Al/Ir = 2.0, and an initial cyclohexene concentration of 1.65 M. Each poisoning experiment used ≥ 300 equivalents of Hg(0) per Ir added in the drybox. Thorough contact of the insoluble Hg(0) and the catalyst in solution was ensured by stirring at 1000 rpm in the sealed FP bottle in the drybox for 24 h. For poisoning after a partially completed hydrogenation run, the hydrogenation reaction was quenched by filling and

purging with 40 psig of Ar gas five times (once every five seconds). The FP bottle was then transferred back into the drybox where Hg(0) was added. After the 24 h mixing period, the sealed FP bottle was again removed from the drybox, and hydrogenation was resumed according to the procedure already described. Time and pressure values then collected have been corrected to fit with the initial portion of the data, Figure A.12. Control experiments show that 24 h of mixing the catalyst solution with Hg(0) is necessary and sufficient for catalyst poisoning (Figure S35, Supporting Information (available online at <http://pubs.acs.org>)) and that the experimental procedure itself is not the cause of the loss of catalytic activity. Another control experiment showed that, for poisoning of the initial catalyst, before a hydrogenation run was started, removal of the Hg(0) from the catalyst solution made no difference in the result.

Z-Contrast Microscopy. Samples of the [(1,5-COD)Ir(μ -O₂C₈H₁₅)]₂ plus AlEt₃ catalyst (3.00 mL, 1.00 mM in [Ir], with an Al/Ir ratio of 2.0) were collected for Z-contrast microscopy both before and after use in cyclohexene hydrogenation, double-sealed airtight, and shipped to the Center for Microanalysis of Materials (CMM), University of Illinois at Urbana–Champaign (UIUC) for imaging. Grid preparation for Z-contrast microscopy was conducted in a glovebag filled with dry N₂ at > 1 atm and located in the TEM room. The solution sample was diluted with cyclohexane to twice its original volume. Next, 2–3 drops were dispersed onto a TEM grid with an ultrathin carbon film on a holey carbon support (Ted Pella, Inc.) and dried at room temperature under N₂ for \geq 10 min. Once dried, a TEM grid was transferred quickly into the TEM column to reduce oxidation of the sample. Images were acquired using a field-emission JEM 2010 (scanning) transmission electron microscope operated at 200 kV. The samples were first treated with a high-intensity electron beam (electron beam shower) for ~15 min each time

in the TEM column (with vacuum better than 3×10^{-6} Torr) to assist in high quality imaging. The high-angle scattering electrons were collected with a JEOL ADF detector at a camera length of 8 cm, with a 0.2 nm (nominal) diameter probe. High-angle annular dark-field (HAADF) images were collected at 2 M (million) magnification and were 1024×1024 pixels in dimension. Cluster diameters were measured at the full width at half-maximum (FWHM) of the intensity profile across ≥ 600 clusters from images at the same levels of magnification and contrast (an example intensity profile is shown in the Supporting Information (available online at <http://pubs.acs.org>)).

XAFS Spectroscopy. Sample solutions were prepared at CSU in 6.0 mL batches at 5.0, 6.0, or 7.2 mM in [Ir]. Containers were double-sealed airtight and transported to the National Synchrotron Light Source (NSLS) at Brookhaven National Laboratory (BNL), Upton, NY (two days transit time). At the NSLS, all catalyst samples were handled and stored in a N_2 atmosphere glovebox maintained at ≤ 10 ppm O_2 . Solution samples were loaded into a custom-designed airtight sample cell composed of a stainless steel frame made to press Kapton film windows onto a Teflon block with a ~ 1.5 mL sample cavity. The samples were loaded using glass pipettes into threaded ports in the Teflon block, which were then sealed using Teflon screws. Airtight seals in the threaded ports and windows were ensured by using Kalrez o-rings.

A portion of the Al/Ir = 1.0 catalyst sample was used for catalytic hydrogenation of cyclohexene and then collected for XAFS analysis. The brown solution had precipitated as a dark brown powder in transit to the NSLS where the XAFS experiments were performed. This is not unusual however because, as already noted, catalyst solutions kept in the drybox sometimes precipitate within a few days after completion of a catalytic run. The powder was

isolated by centrifugation followed by evaporation in vacuo. The powder was then brushed onto the adhesive side of a strip of Kapton tape. The tape was then folded repeatedly and held in place with additional Kapton tape to ensure an airtight seal. Reference samples of Ir black and $\text{Ir}_4(\text{CO})_{12}$ powders were prepared in this manner; however, preparation of Ir black was done outside the drybox. As already mentioned, a lack of contamination by atmospheric O_2 during posthydrogenation XAFS analysis was confirmed from the XAFS, XANES, and independently performed XPS results, all showing that the sample consisted of Ir(0). Control experiments were performed to test whether the treatment of catalyst material necessary for analysis by XAFS and XANES *after* use in cyclohexene hydrogenation affects its activity. Samples of the catalyst after their use for cyclohexene hydrogenation were collected by bringing the F-P bottle back into the drybox after the H_2 consumption had ceased and removing the cyclohexane solvent under a vacuum. This provided isolated catalyst powder analogous to that analyzed by XAFS and XANES. The powder was then redissolved in 2.5 mL of cyclohexane and transferred into a new culture tube in a F-P bottle followed by 0.5 mL of cyclohexene. A second cyclohexene hydrogenation performed following this treatment gave the activity results shown in Figure S.11.

XAFS experiments were performed on a bending magnet beamline, X18b of the NSLS, which uses a Si(111) channel-cut monochromator. X-ray absorption data were collected at room temperature. Samples were mounted and positioned at 45° in the beam path with the help of a motorized sample stage. Gas ion chamber detectors were used for incident, transmitted, fluorescence, and reference channels. Absorption edge calibration was performed prior to XAFS scans using an Ir black standard, for which energy was swept from 150 eV below to 1800 eV above the Ir L3 edge (11215 eV). Energy was swept from 150 eV below to 2000 eV above the Ir L3 edge for all other samples, except in the case of data collection on the [(1,5-COD)Ir(μ -

$\text{O}_2\text{C}_8\text{H}_{15})_2$ precatalyst, when the energy was swept to 1800 eV above the L3 edge. Reference spectra were obtained simultaneously in the transmission mode for all sample scans using the Ir black standard. The number of scans performed was 2, 29, 6, and 9 for Ir black, HPO_4 -stabilized Ir nanoclusters, $\text{Ir}_4(\text{CO})_{12}$, and $[(1,5\text{-COD})\text{Ir}(\mu\text{-O}_2\text{C}_8\text{H}_{15})_2]$, respectively. For the Al/Ir = 0.5, 1.0, 1.5, 2.0, 2.5, 3.0, and 5.0 catalyst samples before hydrogenation, 5, 5, 10, 10, 10, 3, and 6 scans were performed, respectively. Three scans were performed on an Al/Ir = 10.0 sample, but the data were excessively noisy (Figure S22, Supporting Information (available online at <http://pubs.acs.org>)), precluding reliable analysis and fitting. For the Al/Ir = 1.0 sample after hydrogenation, 17 scans were performed. Fluorescence data were deemed inferior in quality to the transmission data and therefore disregarded.

Data processing was accomplished using IFEFFIT [80]. The reference spectra were used for scan alignment. The threshold energy (E_0) was assigned a value that corresponded to approximately half the normalized edge step, 11213 eV, and multiple scans of a single sample were merged (averaged). The range of data deemed to have a sufficient signal-to-noise ratio was selected using a Hanning window function for Fourier transforms (FTs), Figures S10–S21 of the Supporting Information (available online at <http://pubs.acs.org>).

A drift in the scans of the Al/Ir = 1.5, 2.0, and 2.5 catalysts before hydrogenation was observed, Figure S24, Supporting Information (available online at <http://pubs.acs.org>). A control experiment performed in an attempt to rule out possible sample damage caused by the X-ray beam suggests that no beam damage was occurring, Figure S25, Supporting Information (available online at <http://pubs.acs.org>). The reason for the observed drift is not apparent, but to lessen its effect on the analysis, the first two scans in each case were merged, and the others were discarded.

5. Supporting Information Available: Additional experimental information and control experiments for cyclohexene hydrogenations. Bright-field TEM images, corresponding particle size histograms, and images from TEM and HRTEM control experiments. MALDI mass spectra and results of associated control experiments. XAFS spectra with fits, tables of fitting results, and associated XAFS control experiments. Survey and high-resolution XPS spectra. HR and other TEM images of catalysts after hydrogenation. XAFS-determined coordination number-particle diameter correlation curve. Hg(0) poisoning control experiments. A full list of the authors of reference 6d. This material is available free of charge via the Internet at <http://pubs.acs.org>.

REFERENCES

- [1] K. A. Johnson, *Polym. Prepr.* 41 (2000) 1525–1526.
- [2] W.M. Alley, C.W. Girard, S. Özkar, R.G. Finke, *Inorg. Chem.* 48 (2009) 1114–1121.
- [3] W.M. Alley, I.K. Hamdemir, K.A. Johnson, R.G. Finke *J. Mol. Catal. A: Chem.* 315 (2010) 1–27.
- [4] (a) J.P. Collman, L.S. Hegedus, J.R. Norton, R.G. Principles and Applications of Organotransition Metal Chemistry; University Science Books: Mill Valley, CA, 1987. (b) J. Widegren, R.G. Finke *Mol. Catal. A: Chem.* 198 (2003) 317–341. (c) J. Schwartz *Acc. Chem. Res.* 18 (1985) 302–308.
- [5] (a) F.K. Shmidt, L.O. Nindakova, B.A. Shainyan, V.V. Saraev, N.N. Chipanina, V.A. Umanetz *J. Mol. Catal. A: Chem.* 235 (2005) 161–172. (b) L.B. Belykh, Yu. Yu. Titova, V.A. Umanets, F.K. Shmidt *Russ. J. Appl. Chem.* 79 (2006) 1271–1277. (c) L.O. Nindakova, F.K. Shmidt, V.V. Saraev, B.A. Shainyan, N.N. Chipanina, V.A. Umanets, L.N. Belonogova, D.-S. D. Toryashinova *Kinet. Catal.* 47 (2006) 47, 54–63. (d) L.B. Belykh, T.V. Goremyka, N.I. Skripov, V.A. Umanets, F.K. Shmidt, *Kinet. Catal.* 47 (2006) 367–374.
- [6] (a) H. Bönemann, W. Brijoux, R. Brinkmann, U. Endruschat, W. Hofstadt, K. Angermund *Rev. Roum. Chim.* 44 (1999) 1003–1010. (b) H. Bönemann, N. Waldöfner, H.-G. Haubold, T. Vad, *Chem. Mater.* 14 (2002) 1115–1120. (c) K. Angermund, M. Bühl, E. Dinjus, U. Endruschat, F. Gassner, H.-G. Haubold, J. Hormes, G. Köhl, F.T. Mausnick, H. Modrow, R. Mörtel, R. Mynott, B. Tesche, T. Vad, N. Waldöfner, H. Bönemann, *Angew. Chem., Int. Ed.* 41 (2002) 4041–4044. (d) K. Angermund, *et al.* *J. Phys. Chem. B* 107 (2003), 7507–7515. (e) H.-G. Haubold, T. Vad, N. Waldöfner, H. Bönemann *J. Appl. Crystallogr.* 36 (2003) 617–620. (f) F. Wen, H. Bönemann, R.J. Mynott, B. Spliethoff, C. Weidenthaler, N. Palina, S. Zinoveva, H. Modrow *Appl. Organomet. Chem.* 19 (2005) 827–829.
- [7] (a) Y. Lin, R.G. Finke, *Inorg. Chem.* 33 (1994) 4891–4910. (b) J.D. III Aiken, Y. Lin, R.G. Finke, *J. Mol. Catal. A: Chem.* 114 (1996) 29–51. (c) J.A. Widegren, M.A. Bennett, R.G. Finke, *J. Am. Chem. Soc.* 125 (2003) 10301–10310. (d) C.M. Hagen, J.A. Widegren, P.M. Maitlis, R.G. Finke, *J. Am. Chem. Soc.* 127 (2005) 4423–4432. (e) E.E. Finney, R.G. Finke, *Inorg. Chim. Acta* 359 (2006) 2879–2887.
- [8] (a) C.A. Jaska, I. Manners, *J. Am. Chem. Soc.* 126 (2004) 1334–1335. (b) C.A. Jaska, I. Manners, *J. Am. Chem. Soc.* 126 (2004) 9776–9785. (c) M. Zahmakiran, S. Özkar, *Inorg. Chem.* 48 (2009) 8955–8964.
- [9] For lead references to operando studies of catalysis and their importance, see: (a) J.M. Thomas, G.A. Somorjai, *Top. Catal.* 8 (1999)(preface). (b) B.M. Weckhuysen, *Chem. Commun.* 2002, 97–110; (c) M.O. Guerrero-Pérez, M.A. Bañares, *Chem. Commun.* 2002, 1292–1293. (d) F. Meunier, M. Daturi, *Catal. Today* 113 (2006) 1–2.

[10] We were made aware of XAFS as a potentially highly valuable analytical technique for the study of Ziegler-type hydrogenation catalyst systems by the following excellent early studies: (a) J. Goulon, E. Georges, C. Goulon-Ginet, Y. Chauvin, D. Commereuc, H. Dexpert, E. Freund, *Chem. Phys.* 83 (1984) 357–366. (b) C. Esselin, E. Bauer-Grosse, J. Goulon, C. Williams, Y. Chauvin, D. Commereuc, E. Freund, *J. Phys. Colloques* 47 (1986), C8–243–C8–248.

[11] Further analysis of this catalyst system using additional kinetic studies reveals an *increase* in catalyst turnover frequency with *decreasing* [Ir] concentration and will be reported elsewhere [12]. Another important remaining question, one beyond the scope of this work, is what happens to the AlEt₃ cocatalyst; that is, what are the forms and roles of the AlR₃-derived component in the catalysis? That work is also currently underway and will be addressed in a separate paper [13]. Also addressed elsewhere is the question of the true active catalyst species in industrial Co and Ni Ziegler-type hydrogenation catalyst systems.¹⁴

[12] W.M. Alley, L. Li, J.C. Yang, S. Özkar, R.G. Finke, Manuscript in preparation.

[13] I.K. Hamdemir, S. Özkar, K.A. Johnson, R.G. Finke, Manuscript in preparation.

[14] W.M. Alley, I.K. Hamdemir, L. Li, J.C. Yang, Q. Wang, A. Frenkel, L.D. Menard, R.G. Nuzzo, S. Özkar, K.A. Johnson, R.G. Finke, Manuscript in preparation.

[15] B. Cordero, V. Gómez, A.E. Platero-Prats, M. Revés, J. Echeverría, E. Cremades, F. Barragán, S. Alvarez, *Dalton Trans.* 2008, 2832–2838.

[16] Y. Lin, R.G. Finke, *J. Am. Chem. Soc.* 116 (1994) 8335–8353.

[17] CRC Handbook of Chemistry and Physics, 77th ed.; D.R. Lide, H.P.R. Frederikse, Eds.; CRC Press: Boca Raton, FL, 1996.

[18] With the simplifying assumption of fcc clusters, the number (n) of atoms in a transition metal nanocluster of diameter D can be estimated according to $n = (N_0\rho(4/3)\pi(D/2)^3)/W$,¹⁶ where $N_0 = 6.022 \times 10^{23} \text{ mol}^{-1}$, ρ = the room temperature density of the pure bulk metal, and W = atomic weight of the transition metal. For Ir, $\rho = 22.5 \text{ g/cm}^3$ and $W = 192.22 \text{ g/mol}$.¹⁷ According to this estimate, the largest, 1.4-nm-diameter Ir clusters are Ir(0)_{~100}.

[19] L. Starkey Ott, M.L. Cline, M. Deetlefs, K.R. Seddon, R.G. Finke, *J. Am. Chem. Soc.* 127 (2005) 5758–5759.

[20] C.M. Hagen, L. Vieille-Petit, G. Laurency, G. Süss-Fink, R.G. Finke, *Organometallics* 24 (2005) 1819–1831.

[21] D.B. Williams, C.B. Carter, *Transmission Electron Microscopy*; Plenum Press: New York, 1996.

[22] W.D. Pyrz, D.J. Buttrey, *Langmuir* 24 (2008) 11350–11360.

[23] L.D. Menard, S.-P. Gao, H. Xu, R.D. Twisten, A.S. Harper, Y. Song, G. Wang, A.D. Douglas, J.C. Yang, A.I. Frenkel, R.G. Nuzzo, R.W. Murray, *J. Phys. Chem. B* 110 (2006) 12874–12883.

[24] The results of bright field TEM used to analyze the initial [(1,5-COD)Ir(μ -O₂C₈H₁₅)₂] plus AlEt₃ catalyst samples, before their use in hydrogenation, are shown and discussed in the Supporting Information (available online at <http://pubs.acs.org>). An image obtained before hydrogenation of an Al/Ir = 2.0 catalyst sample shows 1.1 ± 0.3 nm diameter Ziegler nanoclusters. This larger mean diameter is a consequence of the inability of bright-field TEM to detect the $\leq \sim 1.0$ nm Ir clusters. In addition, an image of the [(1,5-COD)Ir(μ -O₂C₈H₁₅)₂] precatalyst alone as a control experiment contains dark spots that are likely artifacts of the image background. Hence, the bright-field TEM results were deemphasized in this study. HRTEM was also used to image catalyst samples before hydrogenation. However, images of reasonable quality were not obtained. A sample image and an explanation of the findings are given in the Supporting Information (available online at <http://pubs.acs.org>).

[25] E.E. Finney, R.G. Finke, *J. Colloid Interface Sci.* 317 (2008) 351–374. Also see refs 45–49 therein.

[26] (a) S. Özkar, R.G. Finke, *J. Organomet. Chem.* 689 (2004) 493–501. (b) S. Özkar, R.G. Finke, *Langmuir* 19 (2003) 6247–6260.

[27] A.I. Frenkel, C.W. Hills, R.G. Nuzzo, *J. Phys. Chem. B* 105 (2001) 12689–12703.

[28] In *X-ray Absorption: Principles, Applications, Techniques of EXAFS, SEXAFS, and XANES*; D.C. Koningsberger, Prins, R., Eds.; Wiley: New York, 1988.

[29] E.A. Stern, S.M. Heald, In *Handbook on Synchrotron Radiation*; E.E. Koch, Ed.; North-Holland: New York, 1983; Vol. 1.

[30] The atomic-scale structure of transition metal nanoclusters is a topic of interest in the literature [31–34]. Theoretical and experimental studies have predicted and observed, respectively, the internal atomic structures of transition metal clusters from a variety of different systems [31], including supported clusters [32]. It is found from such studies that nanoscale clusters can possess an assortment of internal structures and exhibit large degrees of structural disorder, or an amorphous-like nature, even while maintaining some signatures of periodicity [31f]. However, precise determination of the internal atomic structures at the nanoscale is a non-trivial problem [33], especially since examples of systems that are amenable to such structural analysis are rare [34].

[31] (a) D.G. Duff, A.C. Curtis, P.P. Edwards, D.A. Jefferson, B.F.G. Johnson, D.E. Logan, *J. Chem. Soc., Chem. Commun.* 1987, 1264–1266. (b) A.L. Ankudinov, J.J. Rehr, J.J. Low, S.R. Bare, *J. Chem. Phys.* 116 (2002) 1911–1919. (c) L.L. Garzón, J.A. Reyes-Nava, J.I. Rodríguez-Hernández, I. Sigal, M.R. Beltrán K. Michaelian, *Phys. Rev. B* 66 (2002) 073403–1–073403–4. (d) V. Petkov, T. Ohta, Y. Hou, Y. Ren, *J. Phys. Chem. C* 111 (2007) 714–720. (e) S.I. Sanchez, M.W. Small, J.-M. Zuo, R.G. Nuzzo, *J. Am. Chem. Soc.* 131 (2009) 8683–8689. (f) V. Petkov, N. Bedford, M.R. Knecht, M.G. Weir, R.M. Crooks, W. Tang, G. Henkelman, A.I. Frenkel, *Phys. Chem. C* 112 (2008) 8907–8911. (g) Y. Sun, L. Zhuang, J. Lu, X. Hong, P. Liu, *J. Am. Chem. Soc.* 129 (2007) 15465–15467. Interestingly these authors also see that larger (Pt) nanoparticles have an increased activity, and that the smaller ≤ 1 nm Pt nanoparticles are amorphous (perhaps due to Pt–O or other surface ligands).

- [32] (a) F. Vila, J.J. Rehr, J. Kas, R.G. Nuzzo, A.I. Frenkel, *Phys. Rev. B* 78 (2008) 121404–1–121404–4. (b) S.I. Sanchez, L.D. Menard, A. Bram, J.H. Kang, M.W. Small, R.G. Nuzzo, A.I. Frenkel, *J. Am. Chem. Soc.* 131 (2009) 7040–7054.
- [33] (a) B. Gilbert, F. Huang, H. Zhang, G.A. Waychunas, J.F. Banfield, *Science* 305 (2004) 651–654. (b) S.J.L. Billinge, I. Levin, *Science* 316 (2007) 561–565.
- [34] P.D. Jadzinsky, G. Calero, J.C. Ackerson, D.A. Bushnell, R.D. Kornberg, *Science* 318 (2007) 430–433.
- [35] (a) Y. Sun, A.I. Frenkel, R. Isseroff, C. Shonbrun, M. Forman, K. Shin, T. Koga, H. White, L. Zhang, Y. Zhu, M.H. Rafailovich, J.C. Sokolov, *Langmuir* 22 (2006) 807–816. (b) L.D. Menard, H. Xu, S.-P. Gao, R.D. Twisten, A.S. Harper, Y. Song, G. Wang, A.D. Douglas, J.C. Yang, A.I. Frenkel, R.W. Murray, R.G. Nuzzo, *J. Phys. Chem. B* 110 (2006) 14564–14573. (c) J.M. Soler, M.R. Beltrán, K. Michaelian, I.L. Garzón, P. Ordejón, D. Sánchez-Portal, E. Artacho, *Phys. Rev. B* 61 (2000) 5771–5780.
- [36] J.L. Fulton, J.C. Linehan, T. Autrey, M. Balasubramanian, Y. Chen, N.K. Szymczak, *J. Am. Chem. Soc.* 129 (2007) 11936–11949.
- [37] M. Harada, K. Asakura, N. Toshima, *J. Phys. Chem.* 98 (1994) 2653–2662.
- [38] M.R. Churchill, J.P. Hutchinson, *Inorg. Chem.* 17 (1978) 3528–3535.
- [39] R.G. Finke, S. Özkar, *Coord. Chem. Rev.* 248 (2004) 135–146.
- [40] T. Shido, T. Okazaki, M. Ichikawa, *J. Mol. Catal. A: Chem.* 120 (1997) 33–45.
- [41] S.J. Cho, J. Lee, Y.S. Lee, D.P. Kim, *Catal. Lett.* 109 (2006) 181–187.
- [42] L. Garlaschelli, F. Greco, G. Peli, M. Manassero, M. Sansoni, R. Gobetto, L. Salassa, R.D. Pergola, *Eur. J. Inorg. Chem.* (2003) 2108–2112.
- [43] A.M. Argo, J.F. Odzak, B.C. Gates, *J. Am. Chem. Soc.* 125 (2003) 7107–7115.
- [44] J.T. Golden, T.H. Peterson, P.L. Holland, R.G. Bergman, R.A. Andersen, *J. Am. Chem. Soc.* 120 (1998) 223–224.
- [45] B.D. El-Issa, A. Katrib, R. Ghodsian, B.A. Salsa, S.H. Addassi, *Int. J. Quantum Chem.* 33 (1988) 195–216.
- [46] According to the final-state-relaxation phenomenon, electron photoemission results in a positive charge on the nanocluster surface, which has a lifetime longer than the time scale of the photoemission (10^{-16} s). This results in an electron binding energy that is shifted higher by 0.1–2.0 eV. The final state relaxation phenomenon has been previously observed for Au_n [47,53], Pt_n [48,49,51,52], and Pd_n , [52] nanoclusters 1–10 nm in diameter. Therefore, the ~0.5 eV positive shift of the Ir 4f peaks in the experimental XPS spectrum (at 64.30 and 61.33 eV) with respect to literature values for bulk Ir(0) could be explained by the final state relaxation effect.
- [47] G.K. Wertheim, S.B. DiCenzo, S.E. Youngquist, *Phys. Rev. Lett.* 51 (1983) 2310–2313.

- [48] X. Fu, Y. Wang, N. Wu, L. Gui, Y. Tang, *J. Colloid Interface Sci.* 243 (2001) 326–330.
- [49] W. Tu, K. Takai, K. Fukui, A. Miyazaki, T. Enoki, *J. Phys. Chem. B* 107 (2003) 10134–10140.
- [50] W.A. De Heer, *Rev. Mod. Phys.* 65 (1993) 611–676.
- [51] W. Eberhardt, P. Fayet, D.M. Cox, Z. Fu, A. Kaldor, R. Sherwood, D. Sondricker, *Phys. Rev. Lett.* 64 (1990) 780–783.
- [52] T.T.P. Cheung, *Surf. Sci.* 140 (1984) 151–164.
- [53] T. Ohgi, D. Fujita, *Phys. Rev. B* 66 (2002) 115410.
- [54] The formally Ir(I) “[$(1,5\text{-COD})\text{IrH}_4$]” is one reasonable hypothesis for an actual form of initial “ Ir_4 ” species in this system consistent with the XANES spectra and XPS results (both methods being unable to distinguish unambiguously whether the, mean $\text{Ir}_{.4}$, 0.5 nm species by XAFS are Ir(I) or Ir(0)). In fact, the previously unknown [$(1,5\text{-COD})\text{Ir}(\mu\text{-H})_4$] has recently been prepared [13] by us by analogy to the synthesis for the known, formally Rh(I) compound, [$(1,5\text{-COD})\text{RhH}_4$] [55]. Other known “ Ir_4H_x ” species are [$(\eta^5\text{-C}_5\text{Me}_5\text{Ir})_4\text{H}_4$](BF_4)₂ [56] and [$\text{Ir}_4\text{H}_8(\text{CO})_4(\text{PPh}_3)_4$] [42]. Additionally, M_4H_4 -type clusters have been of interest as catalysts (or catalyst precursors) in other systems, often with the metal being Ru or Os.^{56,57} Noteworthy here is that the formation [58], and hydrogenation activity [59], of oxide-supported, tetrahedral Ir_4 clusters have been studied extensively by Gates and co-workers.
- [55] (a) M. Kulzick, R.T. Price, E.L. Muetterties, V.W. Day, *Organometallics* 1 (1982) 1256–1258. (b) Z. Duan, M.J. Hampden-Smith, *Chem. Mater.* 4(1992) 1146–1148.
- [56] J.A. Cabeza, A. Nutton, B.E. Mann, C. Brevard, P.M. Maitlis, *Inorg. Chim. Acta* 115 (1986) L47–L48.
- [57] (a) P. Frediani, U. Matteoli, M. Bianchi, F. Piacenti, G.J. Menchi, *Organomet. Chem.* 150 (1978) 273–278. (b) J.S. Bradley, *J. Am. Chem. Soc.* 101 (1979) 7419–7421. (c) Y. Doi, K. Koshizuka, T. Keii, *Inorg. Chem.* 21 (1982) 2732–2736. (d) Y. Doi, S. Tamura, K. Koshizuka, *J. Mol. Catal.* 19 (1983) 213–222. (e) R.A. Sánchez-Delgado, A. Andriollo, J. Puga, G. Martín, *Inorg. Chem.* 26 (1987) 1867–1870. (f) S. Bhaduri, K. Sharma, *J. Chem. Soc., Chem. Commun.* (1988) 173–174. (g) S. Bhaduri, K. Sharma, D. Mukesh, *J. Chem. Soc., Dalton Trans.* (1992) 77–81. (h) R.D. Adams, S.B. Falloon, *Organometallics* 14 (1995) 4594–4600.
- [58] (a) J.F. Goellner, J. Guzman, B.C. Gates, *J. Phys. Chem. B* 106 (2002) 1229–1238. (b) F. Li, B.C. Gates, *J. Phys. Chem. B* 107 (2003) 11589–11596. (c) F. Li, B.C. Gates, *J. Phys. Chem. B* 108 (2004) 11259–11264. (d) A. Uzun, B.C. Gates, *Angew. Chem., Int. Ed.* 47 (2008) 9245–9248.
- [59] (a) Z. Xu, F.-S. Xiao, S.K. Purnell, O. Alexeev, S. Kawi, S.E. Deutsch, B.C. Gates, *Nature* 372 (1994) 346–348. (b) A.M. Argo, J.F. Odzak, F.S. Lai, B.C. Gates, *Nature* 415 (2002) 623–626.

- [60] R.L. Whetten, J.T. Khoury, M.M. Alvarez, S. Murthy, I. Vezmar, Z.L. Wang, P.W. Stephens, C.L. Cleveland, W.D. Luedtke, U. Landman, *Adv. Mater.* 8 (1996) 428–433.
- [61] G.A. Khitrov, G.F. Strouse, *J. Am. Chem. Soc.* 125 (2003) 10465–10469.
- [62] T. Kuzuya, Y. Tai, S. Yamamuro, K. Sumiyama, *Chem. Phys. Lett.* 407 (2005) 460–463.
- [63] L. Maya, C.H. Chen, K.A. Stevenson, E.A. Kenik, S.L. Allman, T.G. Thundat, *J. Nanoparticle Res.* 4 (2002) 417–422.
- [64] B.J. Hornstein, R.G. Finke, *Chem. Mater.* 16 (2004) 139–150.
- [65] (a) C. Besson, E.E. Finney, R.G. Finke, *J. Am. Chem. Soc.* 127 (2005) 8179–8184. (b) E.E. Finney, R.G. Finke, *Chem. Mater.* 20 (2008) 1956–1970.
- [66] Images of catalyst samples after their use in hydrogenation were also obtained using bright field TEM. The images can be found in the Supporting Information (available online at <http://pubs.acs.org>).
- [67] J.M. Montejano-Carrizales, J.L. Morán López, *Nanostruct. Mater.* 1 (1992) 397–409.
- [68] MALDI MS experiments were performed directly after the end of catalytic runs, whereas Z-contrast STEM (and XAFS spectroscopy) required ≥ 2 days between the end of the catalytic run and analysis (primarily for transit). This difference in procedures could affect the particle sizes measured, which makes some sense; catalyst samples sometimes precipitate a dark brown powder after the end of a catalytic run under standard conditions anyway. The observation of a precipitate suggests that Ir_n cluster agglomeration or growth processes initiated during catalysis continue post-catalysis. Ultimately, these observations argue against the reliability of precise, *specific* Ir_n cluster sizes as measured by Z-contrast STEM, MALDI MS, and XAFS spectroscopy, but strongly argue *for* the development of *fcc* $\text{Ir}(0)_n$ Ziegler nanoclusters in this system in general.
- [69] The details of this structural transformation are currently unknown in this system, although for a report of a similar phenomenon in rhodium particles upon exposure to H_2 , see: R. Choukroun, D. De Caro, B. Chaudret, P. Lecante, E. Snoeck, *New J. Chem.* 25 (2001) 525–527.
- [70] N.T.S. Phan, M. Van Der Sluys, C.W. Jones, *Adv. Synth. Catal.* 348 (2009) 609–679.
- [71] K.S. Weddle, J.D. Aiken, R.G. Finke, *J. Am. Chem. Soc.* 120 (1998) 5653–5666.
- [72] Catalyst poisoning by $\text{Hg}(0)$ is, by itself, an imperfect test for homogeneity or heterogeneity, as has been pointed out previously [4b,70]. However, it can be useful, especially considering the challenges posed by identifying Ziegler-type hydrogenation catalysts [3]. One concern with the $\text{Hg}(0)$ catalyst poisoning test is that, due to the insolubility of $\text{Hg}(0)$, it may be difficult to thoroughly contact/react the $\text{Hg}(0)$ with all of the catalyst in solution [4b]. This concern was addressed herein by using > 300 equivalents of $\text{Hg}(0)$ per Ir each time, and by a series of control experiments showing the 24 h of mixing time allowed was necessary and sufficient for poisoning of these particular catalysts. That effective procedure was followed for each subsequent $\text{Hg}(0)$ poisoning experiment.

[73] Two of the three trials using catalysts without aging gave poisoning results similar to that in Figure 13 (i.e., nearly complete poisoning after an initial small H₂ pressure loss). Interestingly, however, even with the ≥ 300 equivalents of Hg(0) per Ir used and an identical procedure used in each case, in one of the three trials, the Hg(0) only disturbed the shape of the hydrogenation curve but failed to prevent substrate hydrogenation. The implication is that an initial homogeneous Ir catalyst has at least some resistance to reaction with, or poisoning by, Hg(0) (although, Hg(0) is also believed to be able to poison homogeneous catalysts in some cases [70]). These other Hg(0) poisoning control experiments are shown in the Supporting Information (available online at <http://pubs.acs.org>) for the interested reader.

[74] A.J. Liang, B.C. Gates, *J. Phys. Chem. C* 112 (2008) 18039–18049.

[75] (a) One, of course, never *proves* anything in science, including the form of the catalyst. Bergman's formulation of "Halpern's Guidelines or Rules for Catalysis" apply here—that the observable species are many times not the catalyst [20]. That said, nonpoisoned nanoclusters are a somewhat different case, at least according to all of our knowledge of metal particle catalysis. Restated, any Ir(0)_n nanocluster that is not poisoned by basic ligands is expected to be a (good hydrogenation) catalyst. This is especially true in the present case, the current Ir/AlEt₃ Lewis acid/cyclohexane catalyst system, where the best (~only) ligands are the cyclohexene and H₂ reactants (i.e., AlEt₃ and cyclohexane being poor "Lewis bases"). Hence, the dominant observable form(s) and sizes of the nanoclusters are expected—and assumed herein if you like—to correlate closely with the dominant catalyst for the present *structure insensitive* hydrogenation reactions. One alternative possibility is that the active catalysts are the result of fragmentation of the observed clusters under catalytic conditions. For example, Gates and co-workers have shown that the nuclearity of *oxide-supported* Rh_n and Ir_n species can be reversibly altered on the basis of the composition of an ethylene–H₂ gas mixture to which they are exposed [58d,74]: small M_{2–4} cluster species oxidatively fragment to M₁ under ethylene (i.e., catalytic conditions with substrate present) but can reform under H₂. However, the conditions of those studies (oxide-supported catalysts, gas phase substrate, no solvent) are very different than those employed herein. Another, perhaps more relevant example is the current debate concerning the true catalyst species in Pd-catalyzed coupling reactions such as Suzuki coupling and Heck arylation. There is disagreement as to whether catalysis is affected by the Pd nanoparticles themselves, or by molecular Pd species that fragment from the larger, inactive clusters [70]. In the final analysis, the result of the present study is to present Ir(0)_{~40–150} Ziegler-type nanocluster hydrogenation catalysts as the leading hypothesis for future studies of the true catalyst.

[76] For lead references, see the following and references therein: (a) J.E. Mondloch, Q. Wang, A.I. Frenkel, R.G. Finke, *J. Am. Chem. Soc.* 132 (2010) 9701–9714. (b) E. Bayram, M. Zahmakiran, S. Özkar, R.G. Finke, *Langmuir* 26 (2010) 12455–12464.

[77] D.F. Shriver, M.A. Drezdson, *The Manipulation of Air-Sensitive Compounds*, 2nd ed.; John Wiley and Sons: New York, 1986.

[78] W.A. Watzky, R.G. Finke, *J. Am. Chem. Soc.* 119 (1997) 10382–10400.

[79] J.A. Widegren, J.D. III Aiken, S. Özkar, R.G. Finke, *Chem. Mater.* 13 (2001) 312–324.

[80] (a) M.J. Newville, *Synchrotron Radiat.* 2001, 8, 322–324. (b) B. Ravel, M.J. Newville, *Synchrotron Radiat.* 12 (2005) 537–541.

APPENDIX B

INDUSTRIAL ZIEGLER-TYPE HYDROGENATION CATALYSTS MADE FROM Co(neodecanoate)₂ OR Ni(2-ethylhexanoate)₂, AND AlEt₃: EVIDENCE FOR NANOCLUSTERS AND SUB-NANOCLUSTER OR LARGER ZIEGLER-NANOCLUSTER BASED CATALYSIS

This dissertation chapter contains a paper published in *Langmuir* **2011**, 27, 6279-6294. This chapter reports studies aimed at determining the nature of the transition metal component in the authentic industrial Co- and Ni-based Ziegler-type hydrogenation catalysts. The results demonstrate that, both before and after catalytic cyclohexene hydrogenation, the species present comprise a broad distribution of metal cluster sizes from subnanometer to nanometer scale particles. The estimated mean cluster diameters is about 1 nm for both Co- and Ni-based Ziegler-type catalysts.

The initial control experiments testing the variables of catalyst formation and catalytic cyclohexene hydrogenation were carried out by both Isil K. Hamdemir and William M. Alley. MALDI MS spectra were obtained by Isil K. Hamdemir, and interpreted by both Isil K. Hamdemir and William M. Alley. TEM images including high resolution and bright field TEM were obtained by either JoAn Hudson of Clemson University or Long Li. The sample preparation and submission to high resolution and bright field TEM imaging were performed by Isil K. Hamdemir or William M. Alley, respectively. The bright field TEM images were analyzed by Isil K. Hamdemir. The sample preparation and submission to Z-contrast STEM imaging were performed by William M. Alley. The Z-contrast STEM images were obtained by Long Li. The XAFS data was obtained and interpreted by William M. Alley with assistance from Qi Wang, Anatoly I. Frenkel, and Laurent D. Menard. All other kinetics experiments were performed by William M. Alley.

The complete manuscript was written by William M. Alley using an earlier incomplete draft written by Isil K. Hamdemir which included a detailed analysis of the work she performed. The other coauthors edited and proofread the manuscript. The complete manuscript was written prepared for publication by William M. Alley with light editing (9 hours) from Richard G. Finke. The above list of contribution from each coauthor to this chapter agrees well with that given in dissertation by William M. Alley. A supporting information file is available online for the interested reader at <http://pubs.acs.org>.

Synopsis

Ziegler-type hydrogenation catalysts are important for industrial processes, namely the large scale selective hydrogenation of styrenic block copolymers. Ziegler-type hydrogenation catalysts are composed of a group 8–10 transition metal precatalyst plus an alkylaluminum cocatalyst (and they are not the same as Ziegler-Natta *polymerization* catalysts). However, for ~50 years two unsettled issues central to Ziegler-type hydrogenation catalysis are the nature of the metal species present after catalyst synthesis, and whether the species primarily responsible for catalytic hydrogenation activity are homogeneous (e.g., mono-metallic complexes) or heterogeneous (e.g., Ziegler nanoclusters defined as metal nanoclusters made from combination of Ziegler-type hydrogenation catalyst precursors). A critical review of the existing literature (Alley et al. *J. Mol. Catal. A: Chem.* **2010**, *315*, 1–27) and a recently published study using an Ir model system (Alley et al. *Inorg. Chem.* **2010**, *49*, 8131–8147) help to guide the present investigation of Ziegler-type hydrogenation catalysts made from the industrially favored precursors Co(neodecanoate)₂ or Ni(2-ethylhexanoate)₂, plus AlEt₃. The approach and methods used herein parallel those used in the study of the Ir model system. Specifically, a combination of Z-contrast scanning transmission electron microscopy (STEM), matrix assisted laser desorption ionization mass spectrometry (MALDI MS), and X-ray absorption fine structure (XAFS) spectroscopy are used to characterize the transition metal species both before and after hydrogenation. Kinetic studies including Hg(0) poisoning experiments are utilized to test which species are the most active catalysts. The main findings are that, both before and after catalytic cyclohexene hydrogenation, the species present comprise a broad distribution of metal cluster sizes from subnanometer to nanometer scale particles, with estimated mean cluster diameters of about 1 nm for both Co and Ni. The XAFS results also imply that the catalyst solutions are a mixture of the metal clusters described above, plus unreduced metal ions. The kinetics-based

Hg(0) poisoning evidence suggests that the Ziegler nanoclusters (i.e., $\geq M_4$) are the most active hydrogenation catalysts in the Ni system; the Hg(0) poisoning tests in the Co system proved inconclusive. Overall, the novelty and primary conclusions of this study are: (i) this study examines Co and Ni-based catalysts made from the *actual industrial* precursor materials, which make catalysts that are notoriously problematic regarding their characterization; (ii) the Z-contrast STEM results reported herein represent, to our knowledge, the best microscopic analysis of the industrial Co and Ni Ziegler-type hydrogenation catalysts; (iii) this study is the first explicit application of an established method, using multiple analytical methods and kinetics-based studies, for distinguishing homogeneous from heterogeneous catalysis; and (iv) this study parallels the successful study of an Ir model Ziegler catalyst system, thereby benefiting from a comparison to those previously unavailable findings, although the greater M–M bond energy, and tendency to agglomerate, of Ir versus Ni or Co are important differences to be noted. Therefore, the leading hypothesis to try to refute in future work is that Ziegler-type sub-(i.e., M_4) to larger nanoclusters are the dominant, industrial, Co- and Ni- plus AlR_3 catalysts.

1. Introduction

Ziegler-type hydrogenation catalysts are, by definition, formed from a non-zerovalent group 8–10 transition metal (M) precatalyst such as $Co(\text{neodecanoate})_2$ or $Ni(2\text{-ethylhexanoate})_2$ plus a trialkylaluminum cocatalyst such as triethylaluminum ($AlEt_3$). Ziegler-type hydrogenation catalysts should not be confused, however, with Ziegler–Natta or other common polymerization catalysts, which are not a subject of this study. The relatively inexpensive Co- or Ni-based catalysts made from $Co(\text{neodecanoate})_2$ or $Ni(2\text{-ethylhexanoate})_2$, respectively, are very significant industrially as they are used in the production of $\sim 1.7 \times 10^5$ metric tons of hydrogenated styrenic block copolymers per year [1]. Several important fundamental questions about Ziegler-type hydrogenation catalysts persist despite the use of these catalysts for five

decades [1,2,3]. One of the most important remaining questions is the ~50 year old problem of whether the true nature of Ziegler-type hydrogenation catalysis is homogeneous (e.g., single metal organometallic) versus heterogeneous (e.g., nanoclusters) [1,3,4,5,6].

A recently published critical review of Ziegler-type hydrogenation catalysts includes an examination of the prior evidence concerning their homogeneous versus heterogeneous nature, and finds that the reasons for the longevity of this problem in this class of catalysts include their sensitivity to variables and conditions in their preparation and use, and their resistance to characterization by physical methods and isolation for kinetic studies [2,3]. The literature review [3] led to the suggestion that answering the homogeneous versus heterogeneous catalysis question for Ziegler-type hydrogenation catalysts could be facilitated through the use of a well characterized, third-row transition-metal precatalyst in combination with a multi-pronged, previously successful approach to solving the homogeneous versus heterogeneous catalysis problem in a variety of other catalyst systems [3,6,7,8,9,10,11,12,13,14,15]. The central concepts of this multi-prong approach towards answering the homogeneous versus heterogeneous catalysis question are (i) identification of the potential catalyst species using multiple complementary techniques, and then (ii) kinetic studies to determine the catalytic competency of those species.

Such studies using a Ziegler-type hydrogenation catalyst made from the crystallographically characterized precatalyst, [(1,5-COD)Ir(μ -O₂C₈H₁₅)₂], plus AlEt₃ have been recently published [14]. Among the multiple analytical methods used were Z-contrast scanning transmission electron microscopy (STEM), matrix assisted laser desorption ionization mass spectrometry (MALDI MS), and X-ray absorption fine structure (XAFS) spectroscopy [14]. Since “catalysis is, by definition, a wholly kinetic phenomenon” [16], kinetic studies were

performed as a necessary component of addressing the homogeneous versus heterogeneous catalysis question [3,14]. Those studies revealed that after the initial catalyst preparation (i.e., after the addition of AlEt_3 to $[(1,5\text{-COD})\text{Ir}(\mu\text{-O}_2\text{C}_8\text{H}_{15})]_2$ in cyclohexane), but before use for catalytic cyclohexene hydrogenation (i.e., before exposure to pressurized H_2 gas), the catalyst solutions contain a wide range of Ir species from mono-Ir complexes up to structurally-disordered $\text{Ir}_{\sim 100}$ Ziegler nanoclusters, with an estimated mean of 0.5–0.7 nm, $\text{Ir}_{\sim 4-15}$ clusters [14]. However, after using catalyst solutions for cyclohexene hydrogenation, the Ir present was in the form of *fcc* $\text{Ir}(0)_{\sim 40-150}$ Ziegler nanoclusters [14]. Moreover, poisoning and other kinetic studies suggested that the *fcc* $\text{Ir}(0)_{\sim 40-150}$ Ziegler nanoclusters are the fastest catalysts [14].

The goal of the present study is to repeat the analyses performed on the Ir model Ziegler-type hydrogenation catalyst system with Co- and Ni-based catalysts made from the authentic $\text{Co}(\text{neodecanoate})_2$ or $\text{Ni}(2\text{-ethylhexanoate})_2$ precursor materials used for industrial polymer hydrogenation. As such, this work not only expands on our own previous study using the Ir model system [14], but also on the results of others—notably the valuable studies by Schmidt and co-workers [17], and Bönemann and co-workers [18] that suggest transition metal nanoclusters are the catalysts in the Ziegler-type systems studied by them. Our main hypotheses for the present work are (i) that the approach that proved useful with the homogeneous vs heterogeneous catalysis question in the Ir system [14] will be applicable to the industrial Co- and Ni-based systems, and (ii) that the results will be similar in that the fastest catalysts will be revealed to consist of Co or Ni Ziegler nanoclusters, even if as small as Co_4 or Ni_4 . Many of the same analytical techniques are employed herein, namely, Z-contrast STEM, MALDI MS, XAFS spectroscopy (through its two complementary modifications, x-ray absorption near edge structure, or XANES, and extended XAFS, or EXAFS), and $\text{Hg}(0)$ poisoning kinetics studies.

Analogous to the previous study on the Ir model system [14], the specific objectives entail (i) determining the nuclearity of the M_n species present initially (M is Co or Ni), (ii) establishing what M_n species are present directly after use of the catalysts for cyclohexene hydrogenation, and (iii) using Hg(0) poisoning as a kinetics-based test of the homogeneous vs heterogeneous nature of the active catalyst [3]. The challenging, yet crucial issues of the form(s) taken, and role(s) played by the $AlEt_3$ component in Ziegler-type hydrogenation catalysts are currently being investigated, and will be reported in due course elsewhere [19].

Before the use of catalyst solutions for cyclohexene hydrogenation, the Z-contrast STEM and MALDI MS results, which follow reveal that M_n clusters with a wide range of sizes are obtained from combining $Co(\text{neodecanoate})_2$ or $Ni(2\text{-ethylhexanoate})_2$, and $AlEt_3$, and the average cluster sizes are between 0.9 and 1.4 nm in diameter. The results of the Z-contrast STEM herein are, to our knowledge, the best existing microscopic analysis of *industrial* Co and Ni Ziegler-type hydrogenation catalysts. The XANES spectroscopy results suggest that a combination of nanoclusters and unreduced metal ions exists, with the ratio of the two phases depending, as one might expect, on the Al/M ratio. EXAFS spectroscopic analysis of both Co and Ni catalyst samples gives mean 1NN coordination number (N) values for both metals in the 3–4 range. The most plausible, self-consistent interpretation of the evidence from multiple, complementary techniques is that the transition metal contents of the catalyst solutions are a combination of disordered nanoclusters and unreduced, mono-metallic species. In addition, Z-contrast STEM, MALDI MS, and XAFS all show that the transition metal species in catalyst solutions remain essentially unchanged by their use for cyclohexene hydrogenation. Furthermore, Hg(0) poisoning studies with the Ni system suggest that catalysis is heterogeneous (i.e., occurs via the observed Ni nanoclusters), but the Hg(0) poisoning experiments are inconclusive for the Co catalyst. Through the use of an established approach to distinguish

homogeneous from heterogeneous catalysis [3,6-15], and with the additional advantage of now being able to compare the results to those from a parallel study of an Ir model system, this study provides the best existing evidence suggesting catalysis by what appear to be Ziegler nanoclusters (i.e., $\geq M_4$) in Ziegler-type hydrogenation catalysts made from the *actual* industrial Co and Ni precatalyst materials. Noteworthy here is that since control experiments (vide infra and in the Supporting Information) show that AlEt₃ is required to generate an active catalyst (that XANES shows is reduced from Co(II)), species like Co–Et that can β –hydrogen eliminate to ethylene plus Co–H, and thus plausible species such as Co₄H₄, all become candidates for the true catalyst.

2. Experimental

Materials and Instruments. Material sources used to prepare catalyst solutions were kept consistent in order to obtain reproducible results (vide infra). All materials were stored and handled under a N₂ atmosphere in a Vacuum Atmospheres drybox, unless stated otherwise. Drybox O₂ levels were continuously monitored via a Vacuum Atmospheres O₂-level indicator and maintained at ≤ 5 ppm. Gastight syringes were used to carry out all solution measurements and additions done in the Finke group drybox at Colorado State University (CSU). Procedures used to control the amount of H₂O present were followed consistently to ensure reproducibility (vide infra); glassware was rinsed with nanopure water, dried overnight at 160 °C, and cooled under a vacuum or N₂ atmosphere. Cyclohexane (Sigma-Aldrich, 99.5 %, H₂O < 0.001 %) was kept over molecular sieves (Acros, 3 Å, activated by heating at 200 °C for 6 hours under vacuum) for ≥ 2 days prior to use with the Co catalyst, but used as received with the Ni catalyst (vide infra). Cyclohexene (Aldrich, 99%) was distilled over Na under argon. Precatalysts were obtained from OMG, as solutions in mineral spirits, Co(neodecanoate)₂, 12% wt. Co, and Ni(2-

ethylhexanoate)₂, 8% wt. Ni (product names: 12% Co ten-cem and 8% Ni hex-cem). The industrial precatalyst sources of Co(neodecanoate)₂ or Ni(2-ethylhexanoate)₂ are neither relatively pure nor well-characterized structurally compared to the Ir model [(1,5-COD)Ir(2-ethylhexanoate)]₂ precatalyst, which was characterized via single crystal X-ray diffractometry and used as the pure crystalline starting material for the preparation of catalyst solutions.^{1,14} These Co(neodecanoate)₂ and Ni(2-ethylhexanoate)₂ precatalyst solutions were used after diluting with cyclohexane to 12.0 mM in [M]. AlEt₃ (Strem Chemicals, 93%) was used as a solution in cyclohexane. Both Ar and H₂ gases were passed through moisture (Scott Specialty Gases) and oxygen traps (Trigon Technologies) prior to use. THAP (2'-4'-6'-trihydroxyacetophenone, Aldrich, 98%), used in the MALDI MS experiments as a matrix, was stored and used outside of the drybox, and applied as an aqueous solution.

Catalyst Solution Preparation and Catalytic Cyclohexene Hydrogenations. Previous investigation into both the existing literature [3], and the Ir model system [14] have made it clear that Ziegler-type hydrogenation catalysts are sensitive to the conditions and procedures used in their synthesis. We therefore carried out a variety of initial control experiments—testing the effects of catalyst aging, the Al/M ratio, the volume and concentration of catalyst solution prepared, the amount of H₂O present, temperature, concentration of AlEt₃ used, and order and rate of precursor component combination—all with the goal of ensuring that the characterization results obtained herein would be both reproducible and representative of active Ziegler-type hydrogenation catalysts. The results from these control experiments are summarized here and given in greater detail in the Supporting Information (available online at <http://pubs.acs.org>) for the interested reader. One of the important findings from these control experiments is the presence of gas-to-solution mass transfer limitation (MTL) effects in our current hydrogenation apparatus, which limits the *measurable* hydrogenation uptake rate to the rate of H₂ gas transfer

into solution where the catalytic reaction takes place [20]. However, we have used catalyst preparation methods and conditions for this study that (i) result in catalytic cyclohexene hydrogenation rates that are at least as rapid as we can observe due to the MTL effects present, (ii) are consistent with the most favorable methods and conditions described in the majority of the literature [3], and (iii) are similar to, or the same as those used for the model Ir Ziegler-type hydrogenation catalyst made from [(1,5-COD)Ir(μ -O₂C₈H₁₅)₂] and AlEt₃ [1,14]. In short, the MTL kinetics present for these exceptionally active, industrial Ziegler-type hydrogenation catalysts did not preclude our determination of conditions and procedures for catalyst synthesis necessary to give results that are both reproducible and representative of active Ziegler-type hydrogenation catalysts standardized to that MTL limit.

Once established, the procedures for preparing and using catalyst solutions (referred to hereafter as the *standard conditions*) were followed consistently for repeat experiments unless specified otherwise. Control experiments demonstrate that the presence of (deliberately added) water during catalyst synthesis negatively affects the cyclohexene hydrogenation activity of the resulting catalysts. Therefore, all glassware was carefully dried as was the cyclohexane solvent for use with the Co-based catalyst (cyclohexane drying was not beneficial for the Ni catalysts, see the Supporting Information (available online at <http://pubs.acs.org>)). The catalyst solutions were made under a N₂ atmosphere by combination of a 36.0 mM cyclohexane solution of AlEt₃ with a 12.0mM Co(neodecanoate)₂ or Ni(2-ethylhexanoate)₂ precatalyst stock solution. The ratios Al/Co = 3 and Al/Ni = 2 were used for the standard conditions on the basis of control experiments testing catalysts prepared with a range of Al/M values. Control experiments were performed with an Al/M ratio of zero for both Co and Ni, and it was found that no H₂ gas uptake

occurred without added AlEt_3 , which shows the importance of the alkylaluminum cocatalyst in making active Ziegler-type hydrogenation catalysts.

Synthesis of catalyst solutions in batches up to 20 mL, as opposed to the 2.5 mL of catalyst solution prepared for use in a single hydrogenation run, had no observable effect on catalyst activity. Likewise, batch catalyst preparation at 7.2 mM in [M] had no observable effect on catalyst activity in comparison to the 1.44 mM in [M] catalyst solutions prepared for use in a single hydrogenation run (diluted after preparation to 1.2 mM in [M] with the addition of 0.5 mL of cyclohexene). Therefore, it was possible to prepare catalyst solutions either individually or batchwise as necessary, and at concentrations necessary for the subsequent type of analysis. Catalyst synthesis carried out with solutions heated to 60 °C resulted in catalyst solutions with lower cyclohexene hydrogenation activity (Supporting Information (available online at <http://pubs.acs.org>)); hence, catalyst synthesis at the ambient drybox temperature of ~25 °C was established as a standard condition. For the sake of consistency, and unless noted otherwise, catalyst solutions were prepared by adding the AlEt_3 solution to either the $\text{Co}(\text{neodecanoate})_2$ or $\text{Ni}(\text{2-ethylhexanoate})_2$ solution dropwise but rapidly (at a rate ≥ 1 drop every 5 sec), and with 1000 ± 200 rpm stirring (measured with a Monarch Instruments Pocket-Tachometer 100). As an example of batch catalyst preparation, 20 mL of catalyst solution was prepared by first adding 16.8 mL of cyclohexane to a 20 mL glass vial containing a new $5/8 \times 5/16$ inch Teflon-coated magnetic stir bar. Next, 1.6 mL of a 12.0 mM cyclohexane solution of $\text{Ni}(\text{2-ethylhexanoate})_2$ was added. Stirring was started, followed by addition of 1.6 mL of a 36.0 mM AlEt_3 solution. Stirring in the drybox was continued for 30 minutes, after which aliquots of the catalyst solution were taken for analysis or transferred to a new 22×175 mm Pyrex borosilicate culture tube containing a new $5/8 \times 5/16$ inch Teflon-coated magnetic stir bar for kinetic studies via use in cyclohexene hydrogenation. Since, as noted above, volume and concentration had no effect on

hydrogenation, catalyst solutions were also prepared directly in the culture tubes for individual hydrogenation runs by, for example, first adding 1.9 mL of cyclohexane to a culture tube followed by 0.3 mL of a cyclohexane solution of $\text{Co}(\text{neodecanoate})_2$, 12.0 mM in $[\text{Co}]$. Stirring was started and then 0.3 mL of the 36.0 mM AlEt_3 solution in cyclohexane was added. Cyclohexene, 0.5 mL, was added last. In general, the procedures used in this study were very similar to, and in a number of cases the same as, those used previously for the Ir model system [14].

After combination of the precursor components, cyclohexene was added to catalyst solutions used for catalytic hydrogenation runs. Control experiments show that aging prepared catalyst solutions resulted in *decreased* catalyst activity (Supporting Information (available online at <http://pubs.acs.org>)), so catalysts were used for hydrogenation or otherwise analyzed as soon as possible after preparation. The procedure and apparatus used for catalytic cyclohexene hydrogenation have been described in detail elsewhere [21]. Briefly, the culture tube containing the catalyst solution was placed in a Fisher-Porter (F-P) bottle, sealed, and transferred out of the drybox. The F-P bottle was placed in a temperature regulating bath, stirring was begun, and the F-P bottle was connected to a pressurized H_2 line using Swagelock quick-connects. The F-P bottle was purged 15 times (1 purge/15 s) before setting the pressure to 40 psig. Data collection was then started at 4 min after the first purge. H_2 pressure data as a function of time was collected using an Omega PX 624-100 GSV pressure transducer, which was connected to a PC running LabView 7.0 by an Omega D1131 analog-to-digital converter. Data was subsequently handled using MS Excel and Origin 7. Standard conditions for hydrogenation runs are: solvent = cyclohexane, $[\text{M}] = 1.2 \text{ mM}$, initial $[\text{cyclohexene}] = 1.65 \text{ M}$, temp = 22.0 °C, initial H_2 pressure = 40 psig, and stirring rate = $1000 \pm 10 \text{ rpm}$. The main point is that in both catalyst synthesis and subsequent hydrogenations, variables with the potential to influence the resulting catalytic

activity have been tested and optimized (to the MTL limit), thereby allowing the development of standard conditions for the preparation and use of the highly active Ziegler-type hydrogenation catalysts used herein. This in turn ensures that the subsequent analytical results should be both reproducible and representative of active Ziegler-type hydrogenation catalysts.

Z-Contrast STEM. Catalyst samples were prepared according to standard conditions as described and collected for Z-contrast microscopy both before and after use in cyclohexene hydrogenation. Sample solutions were double-sealed air-tight, and shipped to the University of Pittsburgh for imaging (2–3 days between preparation and analysis). Preparation of samples on TEM grids was carried out in a glove-bag filled with dry N₂ at >1 atm, and located in the TEM room. Sample solutions were diluted with cyclohexane to twice their original volume, and 2–3 drops were dispersed onto a TEM grid with an ultrathin carbon film on a holey carbon support (Ted Pella, Inc.). These were dried at room temperature under N₂ for ≥10 minutes before being transferred into the TEM instrument. Transfer was done quickly to reduce possible oxidation of the sample. Samples were first treated with a high-intensity electron beam (electron beam shower) for ~15 minutes each time in the TEM column (with vacuum better than 3×10^{-6} Torr). Images were acquired using a field-emission JEM 2010 (scanning) transmission electron microscope operated at 200 kV. The high-angle scattering electrons were collected with a JEOL ADF detector at a camera length of 8 cm, with a 0.2 nm (nominal) diameter probe. High-angle annular dark-field (HAADF) images were collected at 2M (million) magnification, and were 1024 × 1024 pixels in dimension. Cluster diameters were measured manually at the full width at half maximum (FWHM) of the intensity profile across ≥ 600 clusters from images at the same levels of magnification and contrast using Gatan Digital Micrograph.

Control experiments were performed to determine whether the metal clusters observed were artifacts of the microscopy itself. Co(neodecanoate)₂, without added AlEt₃, was deposited

on a TEM grid (ultrathin carbon film supported by a lacey carbon film on a 400 Mesh copper grid, Ted Pella), and imaged following the methods noted above (i.e., including the electron beam shower). No Co clusters could be observed suggesting that neither sample preparation procedures nor Z-contrast STEM conditions are responsible for creating the observed clusters in catalyst samples. No Co clusters were observed when this same control experiment was carried out using high resolution (HR)TEM. (The fact that Co in $\text{Co}(\text{neodecanoate})_2$ could not be observed in Z-contrast STEM images *without* Co cluster formation has a bearing on the interpretation of the EXAFS results, *vide infra*, specifically it leaves open the possibility that mono-metallic, unreduced metal ions are present.) Additionally, $\text{Co}(\text{neodecanoate})_2$, without added AlEt_3 , was deposited on special TEM grids with 25 nm thick SiO_2 windows (Dune Sciences) [22]. However, for this sample on the special SiO_2 grids, imaging using bright field TEM, Z-contrast STEM, and HRTEM all revealed the presence of nanometer-scale clusters, ostensibly the result of Co cluster formation under the TEM beam. These control experiments suggest that the clusters observed using Z-contrast STEM to image catalyst samples deposited on ultrathin carbon grids, and measured to construct the cluster size histograms, are not artifacts resulting from the required sample handling or microscopy itself. Images from control experiments and additional microscopy are provided in the Supporting Information (available online at <http://pubs.acs.org>) for the interested reader.

MALDI MS. Catalyst samples were prepared for analysis by MALDI MS in a manner almost identical to that described previously using the Ir model system [14]. A 0.5 μL , 100 mM aqueous NaI ionizing agent solution was hand-spotted on a steel MS sample plate and air-dried, which was followed by 1 μL of 2'-4'-6'-trihydroxyacetophenone (THAP) over the same spot and then also air-dried. The plate was then transferred into the drybox where sample solutions (1 μL , $[\text{M}] = 1.44 \text{ mM}$) were applied onto the spot of deposited ionizing agent and matrix. The plate

was then covered with its plastic capping plate and placed into a desiccator, which was sealed and removed from the drybox. The plate was transferred in air (exposure of ~30 sec) from the desiccator to the vacuum of the MALDI MS instrument, and MALDI MS spectra were taken immediately thereafter. Mass spectra were obtained at CSU on a Bruker Ultraflex TOF-TOF instrument in linear mode, with acceleration voltage at 25 kV, and in positive ion mode. A nitrogen laser ($\lambda = 337$ nm) with a 3 ns pulse width was focused over a 1 mm diameter spot. Data were collected with the highest laser power possible, for a higher S/N, but which still maximized resolution and avoided sample fragmentation. Calibration was done using Bradykinin, Angiotensin_I, Angiotensin_II, Substance_P, Bombesin, Renin_Substrate, ACTH_clip and Somatostatin (purchased as a mixture of all these peptides from Bruker-Daltonics).

XAFS. Procedures for XAFS spectroscopy herein are similar to those used previously for the analysis of the Ir model system [14]. Solution samples of Co(neodecanoate)₂, Ni(2-ethylhexanoate)₂, and catalysts made from these plus AlEt₃ were prepared at Colorado State University, in 6.0 mL batches at 7.2 mM concentration in [M]. Aliquots of catalyst samples were used for cyclohexene hydrogenation in order to obtain both pre- and posthydrogenation catalyst samples. All samples were then sealed air-tight, and transported to the National Synchrotron Light Source (NSLS) at Brookhaven National Laboratory (BNL), Upton NY (2 days transit). At the NSLS, catalyst samples were handled and stored in an N₂ atmosphere glovebox maintained at ≤ 10 ppm O₂. Catalyst samples were loaded, via glass pipette, into a custom-designed, airtight, ~1.5 mL capacity, solution sample cell composed of a stainless steel frame made to press Kapton film windows onto a Teflon block. Threaded ports in the Teflon block allow for sample loading, which were then sealed using Teflon screws. Airtight seals in the threaded ports and windows were ensured by using Kalrez o-rings. XAFS experiments were

performed at room temperature either on beamline X18b or X11a, which are sourced by bending magnets, and employ Si(111) channel-cut monochromators. Samples were loaded into an airtight sample cell, then mounted and positioned at 45° in the beam path. Three 30 cm long ion chambers filled with suitable gas mixtures were employed to record in transmission mode the incident, transmitted, and reference beam. A Lytle detector was used to measure fluorescence data simultaneously with transmission, but the fluorescence spectra were deemed of inferior quality to the transmission spectra and not used in the analysis. Co or Ni foils were used both for absorption edge calibration of the Co (7709 eV) and Ni (8333 eV) K edges prior to XAFS scans. Co and Ni foils were also used to obtain reference spectra simultaneously in transmission mode for all sample scans. Six to eight scans were typically performed for each sample, and during data processing, multiple scans of a single sample were merged (averaged).

Data processing was accomplished using IFEFFIT [23]. For background removal, threshold energy values (E_0) for both Co and Ni were assigned values corresponding to the inflection point in the normalized absorption edges. A Hanning window function was used to select data ranges in k -space with sufficient signal to noise ratio for Fourier Transforms (FTs), Supporting Information (available online at <http://pubs.acs.org>). The passive electron reduction factors (S_0^2) for Co and Ni were acquired from fitting the Co and Ni foil standards, respectively (Supporting Information (available online at <http://pubs.acs.org>)). Parameters including the coordination numbers (N) bond lengths (R) and their disorders (σ^2) were varied in the fitting of catalyst sample spectra, as well as the correction to the photoelectron energy origin (ΔE_0). Details of fitting EXAFS spectra are given in the Supporting Information (available online at <http://pubs.acs.org>).

Hg(0) poisoning. Catalyst solutions for use in Hg(0) poisoning experiments were first prepared in the drybox according to the standard conditions as described with [M] concentration of 1.2 mM (M is Co or Ni), an Al/Co ratio of 3.0, or an Al/Ni ratio of 2.0, and initial cyclohexene concentrations of 1.65 M. Hg(0) was added to the catalyst solutions before cyclohexene hydrogenation catalysis was started and allowed to mix for the specified time. The bottle containing the catalyst solution and Hg(0) was then transferred to the pressurized H₂ to collect pressure data using normal procedures.

In another version of the Hg(0) poisoning experiment, a standard conditions hydrogenation using the Ni catalyst was stopped after about half the cyclohexene had been consumed by filling and purging the F–P bottle five times with Ar gas pressurized to 40 psig. The F–P bottle was then transferred back into the drybox where the Hg(0) was added. The F–P bottle was then reconnected to the hydrogenation line, refilled with H₂ gas using the standard procedure and data acquisition was restarted. Time and pressure values collected after Hg(0) addition were corrected to fit with the data collected before Hg(0) addition.

The results of Hg(0) poisoning control experiments are shown in the (available online at <http://pubs.acs.org>) for the interested reader. Control experiments using various quantities of Hg(0) added to prepared catalyst solutions followed by various mixing times before their use in hydrogenation show that a procedure using ≥ 300 equivalents of Hg(0) per Ni and ≥ 1.5 hours of stirring (at 1000 rpm in a sealed FP bottle in the drybox) is adequate to thoroughly contact the Hg(0) with all of the Ni catalyst in solution; this procedure was then strictly followed.

In the case of the Co catalyst, control experiments showed that using even ~ 1770 equivalents of Hg(0) per Co, plus 24 h of 1000 rpm stirring, are insufficient to completely and immediately poison all of the Co catalyst in solution. Additionally poisoning results are irreproducible (Supporting Information (available online at <http://pubs.acs.org>)). This implies

that the Hg(0) poisoning results with the Co catalyst cannot be interpreted in terms of catalyst homo- or heterogeneity; they are inconclusive. Other control experiments show that both the Ni and Co catalyst solutions retain catalytic activity when subjected to the handling procedures required for Hg(0) addition, but in the absence of Hg(0). Restated, those additional controls show that it is the Hg(0) itself, and not the procedures, that poison the catalysis.

3. Results and Discussion

Initial Observations, Plus an Overview of the Key Pre- and Posthydrogenation Characterization Results. As noted in a review of the literature of the homogeneous versus heterogeneous catalysis problem [6], initial observations of the catalyst solutions alone make industrial Ziegler-type catalysts candidates for study regarding the homogeneous vs. heterogeneous catalysis question. Specifically, dark brown or black solutions are frequently observed in literature catalyst systems now known to involve heterogeneous (e.g., nanoparticle) catalysis, making such an observation, by itself, *suggestive* of heterogeneous catalysis [6]. In the present study, there are several noteworthy observations from the synthesis of the industrial Co- and Ni-based catalysts, especially in comparison with the observations from the Ir model system [14]. For example, addition of the clear and colorless solution of AlEt₃ to the clear, deep-blue Co(neodecanoate)₂ solution results in an immediate change to a *dark brown, almost black solution*. Likewise, addition of the AlEt₃ solution to the clear, light-green solution of Ni(2-ethylhexanoate)₂ causes an immediate change to a *dark brown solution* (but one that is a lighter shade of brown than the Co/AlEt₃ catalyst solution). Unlike with the [(1,5-COD)IrO₂C₈H₁₅]₂ plus AlEt₃ catalyst system, which is a much lighter, yellow-brown after addition of AlEt₃ but darkens during a cyclohexene hydrogenation run, and will occasionally precipitate a dark brown powder a few days after the completion of a hydrogenation run [14], these industrial Co- or Ni-based

catalysts do not exhibit observable color change or insoluble particle formation upon use for, or post, hydrogenation. Using the Ir model catalyst, it was found that H₂ uptake begins initially at a slower rate, then accelerates to achieve its maximum rate after the start of hydrogenation (i.e., the initial rate is not the maximum rate) [14]. Furthermore, this increase in cyclohexene hydrogenation rate during the hydrogenation itself observed using the model Ir catalyst is accompanied by the observation of, on average, Ir₄₋₁₅ clusters prehydrogenation, but *fcc* Ir(0)₄₀₋₁₅₀ clusters posthydrogenation.

In contrast, with the industrial Co-, or Ni-based catalysts, H₂ uptake begins immediately at the apparent H₂ gas-to-solution MTL rate ($\sim 80 \pm 20$ psig/h at 1000 rpm stirring, (available online at <http://pubs.acs.org>)) or at $\sim 30\%$ of the apparent H₂ gas-to-solution MTL rate respectively, Figure B.1. This implies that in the industrial Co- or Ni-based catalysts, very active catalyst species are present initially (or possibly are formed essentially immediately) upon the introduction of H₂ gas. In short, the initial observations from catalyst preparation alone are consistent with the presence of Co and Ni Ziegler nanoclusters in catalyst solutions both initially, and throughout, the hydrogenation process.

These initial observations of just the dark colors of the catalyst solutions explain why the specific objectives herein necessarily entail: (i) determining the nuclearity of the M_n species present *initially*, and (ii) establishing what M_n species are present *directly after* use of the catalysts for cyclohexene hydrogenation. These are the necessary first steps in probing the homogeneous versus heterogeneous nature of the most active catalyst in these industrial systems.

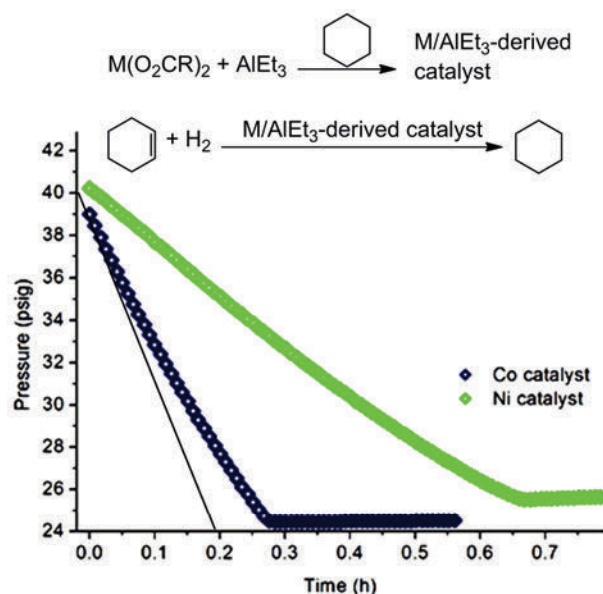


Figure B.1. General steps for the synthesis of Co- or Ni-based Ziegler-type hydrogenation catalyst solutions. $M(O_2CR)_2$ is either of the authentic industrial precatalysts, $Co(\text{neodecanoate})_2$ or $Ni(2\text{-ethylhexanoate})_2$. Catalyst solutions were made by combining a cyclohexane solution of one of the precatalysts, 12.0 mM in $[M]$, with a 36.0 mM cyclohexane solution of $AlEt_3$. Example catalytic cyclohexene hydrogenation curves using standard conditions of solvent = cyclohexane, $[M] = 1.2$ mM, initial $[\text{cyclohexene}] = 1.65$ M, temp = 22.0 °C, and stirring rate = 1000 ± 10 rpm are shown. The apparent MTL value, depicted here as a black line, is $\sim 80 \pm 20$ psig/h in this apparatus and at these conditions (e.g., the 1000 ± 10 rpm stirring rate).

A summary of the results obtained from the analysis of catalyst samples pre- and posthydrogenation by Z-contrast STEM and MALDI MS is given in Table B.1 alongside the results from the Ir model system for comparison. The key findings for both the Co- and Ni-based catalysts are (i) Z-contrast STEM and MALDI MS reveal nanometer-scale clusters for both Co and Ni samples, both before and after hydrogenation, and (ii) the XAFS data indicate that unreduced metal ions are present in solution, depending on the Al/M ratio, with the nanometer-scale Co_n or Ni_n clusters present. In addition, the XAFS shows those Co_n and Ni_n clusters possess disordered atomic structures. In short, disordered transition metal Ziegler nanoclusters appear to be the predominant clusters formed by the industrial Co- and Ni-based precatalysts upon addition of $AlEt_3$, both before and after hydrogenation, yet monometallic (homogeneous) species appear to be present as well. In addition, the ability to directly compare

the results obtained herein to the results from the prior, analogous study of the model Ir system [14], is a valuable, unique feature of the present study.

Table B.1. Summary of results from investigation of metal cluster sizes using Z-contrast STEM and MALDI MS for industrial Ziegler-type hydrogenation catalysts made from Co(neodecanoate)₂ or Ni(2-ethylhexanoate)₂ plus AlEt₃ (Al/Co is 3.0, Al/Ni is 2.0), and for comparison an Ir Ziegler-type hydrogenation catalyst made from [(1,5-COD)Ir(μ-O₂C₈H₁₅)₂] plus AlEt₃ (Al/Ir is 2.0), both before and after use for cyclohexene hydrogenation.

analytical method	precatalysis			postcatalysis			
	range (nm)	average ^a (nm)	average ^a M _n nuclearity	range (nm)	average ^a (nm)	average ^a M _n nuclearity	
Co	Z-contrast STEM	0.6–3.3	1.4	Co _{~130}	0.5–2.5	1.4	Co _{~130}
	MALDI MS	0.8–1.8	1.2	Co _{~80}	0.8–1.8	1.1	Co _{~60}
Ni	Z-contrast STEM	0.4–3.5	1.3	Ni _{~100}	0.6–4.0	1.4	Ni _{~130}
	MALDI MS	0.8–1.7	0.9	Ni _{~34}	0.8–1.6	0.9	Ni _{~34}
Ir ^b	Z-contrast STEM	0.2–1.4	0.5	Ir _{~4}	0.4–1.9	1.0	Ir _{~40}
	MALDI MS	0.5–1.1	0.7	Ir _{~15}	0.6–1.4	0.8	Ir _{~20}

^a The average values are calculated mean cluster diameters from Z-contrast STEM, and estimated mean nuclearities from MALDI MS. Explanations for how these values were determined and how the cluster diameter-nuclearity conversion is performed are given below. ^b Results from a previously published study [14], provided here for comparison.

Nuclearity of M_n Species before Hydrogenation: Z-Contrast STEM. Samples of the Co(neodecanoate)₂ plus AlEt₃ catalyst, with an Al/Co ratio of 3.0, before use for cyclohexene hydrogenation were imaged using Z-contrast STEM. Measurement of 604 clusters shows a range of Co cluster sizes from 0.6 to 3.3 nm in diameter, with a mode and median of 1.3 nm clusters, and a mean Co cluster diameter of 1.4 ± 0.4 nm. These cluster diameters correspond to cluster nuclearities with a range from Co_{~10} to Co_{~1700}, a mode and median of Co_{~100}, and a mean of Co_{~130} [24,25,26]. Figure B.2 shows an example image and the histogram.

Samples of the Ni(2-ethylhexanoate)₂ plus AlEt₃ catalyst, with an Al/Ni ratio of 2.0, before use for cyclohexene hydrogenation were also imaged using Z-contrast STEM. An example image and the histogram are shown in Figure B.3. Measurement of 650 clusters in Z-contrast STEM images reveals a range of Ni cluster sizes from 0.4 nm to 3.5 nm in diameter.

The mode, median, and mean Ni cluster diameters are 1.1 nm, 1.2 nm, and 1.3 ± 0.5 nm, respectively. These diameters correspond to cluster nuclearities ranging from Ni₃ to Ni₂₀₅₀, the mode, median, and mean being Ni₆₀, Ni₈₀, and Ni₁₀₀, respectively [24,25,26].

For both Co and Ni samples, Z-contrast STEM shows the presence of metal clusters with a broad distribution of sizes ranging from sub-nanometer to several nanometers in diameter. Cluster diameter measurements were made using the full width at half-maximum (FWHM) of line intensity profiles across individual clusters. These Z-contrast microscopy results by themselves should not be considered absolutely definitive, however, due to the possibility that the observed clusters are artifacts of the microscopy itself, especially given that lighter (first-row) transition metal clusters and precursors are known to be less stable in TEM electron beams than their heavier (third-row) analogs—a key reason we began our studies with our now-published third-row metal, Ir-model system [14,27,28,29]. More specifically, Ni Ziegler-type hydrogenation catalysts have been observed to be sensitive to electron microscopy sample treatment processes, namely, drying of the Ni catalyst solution on TEM grids [2]. However, the possibility of artifactual results is mitigated herein by the use of *scanning* TEM [30], which diminishes the potential for beam-induced sample damage via a small electron probe, low beam current, and minimal beam exposure time [31]. The images herein were watched during image acquisition for signs of the influence of the TEM beam on the catalyst sample, and no changes in cluster size or shape were observed. In addition, control experiments (described in the Experimental Section, images shown in the Supporting Information (available online at <http://pubs.acs.org>)) suggest that the clusters observed using Z-contrast STEM, and measured to construct the cluster size histograms, are not artifacts. To summarize, Z-contrast microscopy shows that Co and Ni catalyst samples, *before* hydrogenation, each contain a wide range of M_n clusters, 1.4 ± 0.4 nm, Co₁₃₀, and 1.3 ± 0.5 nm, Ni₁₀₀, being the mean cluster size and nuclearity

in each case respectively. To the extent of our knowledge, the results of the Z-contrast STEM herein are the best existing microscopic analysis of *industrial* Co and Ni Ziegler-type hydrogenation catalysts.

Nuclearity of M_n Species before Hydrogenation: MALDI MS. Samples of the Co(neodecanoate)₂ plus AlEt₃ catalyst, with an Al/Co ratio of 3.0, were also analyzed using MALDI MS before their use in cyclohexene hydrogenation. A broad peak is observed with a maximum intensity at ~4500 m/z (Figures are shown in the (available online at <http://pubs.acs.org>)). With the assumptions that the ions forming the broad peaks are composed of only Co atoms [32,33,34], and that the ionic charge is +1 [14,32,34,35], the maximum intensity of the MALDI MS peak at ~4500 m/z corresponds to Co₋₈₀ clusters. This, in turn, corresponds to a diameter approaching ~1.2 nm (used as an estimate of the average Co clusters reported in Table B.1). Furthermore, the broad MALDI MS peak also indicates a wide size dispersity of the Co clusters present, similar to the wide size dispersity of the Co clusters observed using Z-contrast STEM. The FWHM of the broad, asymmetrically shaped MALDI MS peak is from ~2000–9000 m/z , and tails off towards higher m/z values. The peak reaches one-fourth maximum intensity at ~12000 m/z , and one-eighth maximum intensity at ~16000 m/z ; these m/z values correspond to approximately Co₋₃₀₋₁₅₀, Co₋₂₀₀, and Co₋₂₇₀ clusters, respectively, which in turn correspond to approximately 0.9–1.5, 1.6, and 1.8 nm Co clusters, respectively.

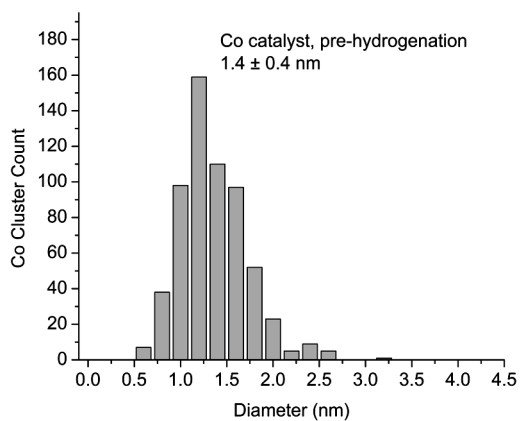
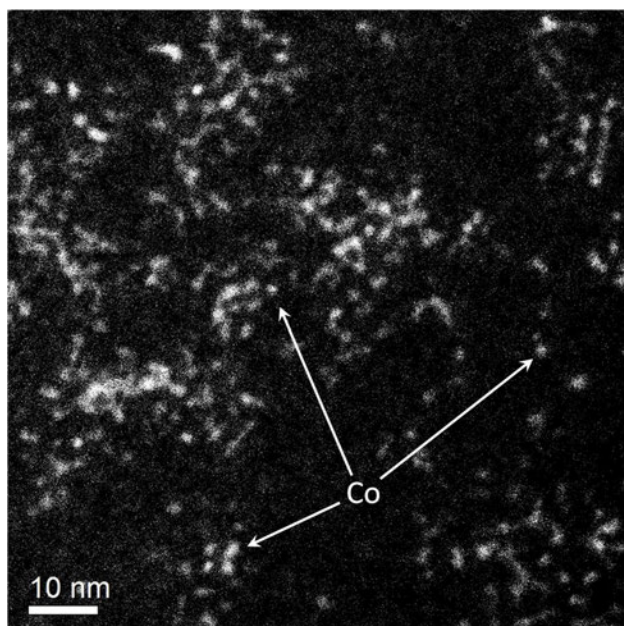


Figure B.2. Example Z-contrast STEM image of the $\text{Co}(\text{neodecanoate})_2$ plus AlEt_3 catalyst, with an Al/Co ratio of 3.0, and before its use for cyclohexene hydrogenation. The histogram from measuring 604 Co clusters reveals an overall range of Co clusters observed from 0.6 to 3.3 nm in diameter, which correspond to $\text{Co}_{\sim 10}$ to $\text{Co}_{\sim 1700}$ clusters. The Co clusters measured have a mode and median of 1.3 nm, and a mean diameter of 1.4 ± 0.4 , corresponding to $\text{Co}_{\sim 100}$ and $\text{Co}_{\sim 130}$ clusters, respectively [24,25,26].

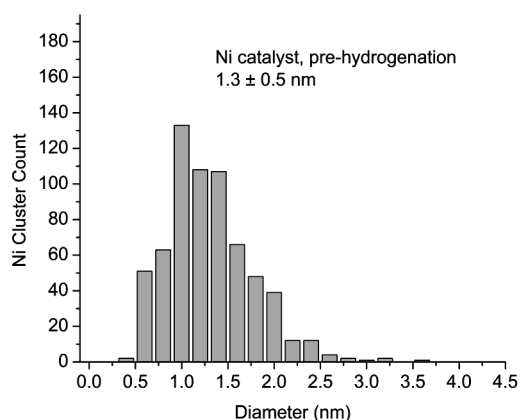
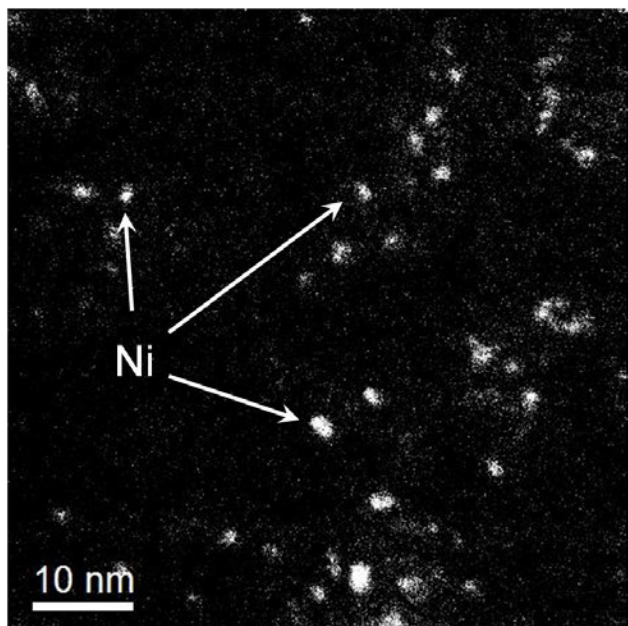


Figure B.3. Example Z-contrast STEM image of the Ni(2-ethylhexanoate)₂ plus AlEt₃ catalyst with an Al/Ni ratio of 2.0, and before use for cyclohexene hydrogenation. The histogram made from measurement of 650 Ni clusters shows Ni cluster sizes ranging from 0.4 to 3.5 nm in diameter, which correspond to Ni_{~3} to Ni_{~2050} clusters. The Ni clusters measured have a mode of 1.1 nm, a median of 1.2 nm, and a mean diameter of 1.3 ± 0.5 nm, corresponding to Ni_{~60}, Ni_{~80}, and Ni_{~100}, respectively [24,25,26].

Samples of the Ni(2-ethylhexanoate)₂ plus AlEt₃ catalyst, with an Al/Ni ratio of 2.0, were also analyzed using MALDI MS before their use in cyclohexene hydrogenation. A broad peak is observed with a maximum intensity at m/z of 2000. However, the presence of Ni atoms in species below 1500 m/z is ruled out by the absence of characteristic Ni isotope peak distributions in that region. In a control experiment, the MALDI MS of a blank sample containing only the

matrix, trihydroxyacetophenone (THAP), and ionizing agent, NaI contains peaks in the 0–1500 m/z range (Supporting Information (available online at <http://pubs.acs.org>)). Therefore, the 0–1500 m/z range was excluded from the mass spectrum region used to calculate number of transition metal atoms (M) in the M_n clusters, and corresponding diameters, for both Co and Ni catalyst samples; the m/z values of 1500–16000 for Co, and 1500–13500 for Ni were used to calculate the cluster diameter ranges reported in BF.1. Using the same assumptions employed for the Co system above, as well as previously in the literature [14,32,33,34,35], the maximum intensity of the broad peak at m/z of ~ 2000 indicates $Ni_{\sim 34}$ clusters, corresponding to ~ 0.9 nm diameter Ni nanoclusters, (used as an estimate of the average Ni clusters reported in Table B.1). Much like the MALDI MS peak of the Co catalyst (and of the Ir model system [14]), the broad, asymmetrically shaped peak of the Ni catalyst also tails off towards higher m/z values reaching ~ 6000 m/z at half maximum intensity, ~ 9000 m/z at one-fourth maximum intensity, and ~ 13500 m/z at one-eighth maximum intensity, which correspond to approximately $Ni_{\sim 100}$, $Ni_{\sim 150}$, and $Ni_{\sim 230}$, respectively. These nuclearities correspond, in turn, to approximately 1.3, 1.5, and 1.7 nm Ni nanoclusters, respectively.

Somewhat as an aside, but interestingly, this study, and the previous one of the Ir model system [14], are unique tests of the value of MALDI MS as an analytical method for measuring the size and size distribution of transition metal nanoclusters in that they obtain MALDI MS data on systems where Z-contrast STEM (and XAFS, *vide infra*) data are available for comparison. Overall, the MALDI MS-determined nanocluster sizes and size distributions for both Co and Ni prehydrogenation catalysts are generally consistent with those determined using Z-contrast STEM in showing cluster sizes in the range of 0.8–1.8 nm for Co, and 0.8–1.7 nm for Ni are present.

Nuclearity of M_n Species before Hydrogenation: XAFS (i.e., XANES plus EXAFS) Spectroscopy. The XANES spectra of both Co and Ni catalysts are compared to those of the corresponding metal foils and catalyst precursors in B.4. In each case, the XANES spectra of the catalyst solution becomes less like the precursor solution and more like the metal foil with higher Al/M ratios. This suggests that, in terms of composite average formal oxidation state, the Co or Ni metals in catalyst solutions become progressively less like their M(II) precatalysts, and progressively more resembling of M(0), as the Al/M ratios increase from 1.0 to 3.0. These results imply that unreduced metal ions are likely present in catalyst solutions in amounts that decrease with additional AlEt₃. Given the M_n nanoclusters observed using both Z-contrast STEM and MALDI MS, these results suggest that catalyst solutions contain a combination of M_n clusters with a wide range of diameters *and* unreduced metal ions, with the proportion of M atoms in the cluster versus ion phases depending on the Al/M ratio used in catalyst preparation.

The potential of EXAFS spectroscopy for the characterization of Ziegler-type hydrogenation catalysts, especially the industrially favored Co and Ni catalysts, was made apparent to us by the valuable prior studies of Goulon and co-workers [36]. Specifically, those authors found Ni–Ni first nearest neighbors indicating the presence of Ni metal clusters [36]. However, additional study using modern EXAFS analysis methods that use *ab initio* theory for the quantitative modeling and analysis of experimental EXAFS spectra proved worthwhile [37], especially when considered alongside results of complementary Z-contrast STEM and MALDI MS techniques used herein, the Hg(0) poisoning studies, and the now possible comparison to the results obtained from the Ir model system [14].

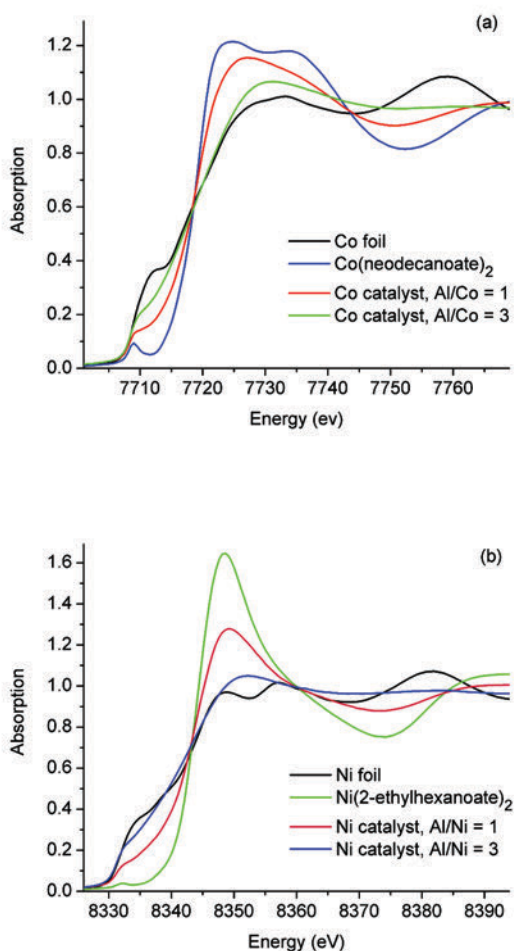


Figure B.4. (a) XANES spectra of Co foil (black) the $\text{Co}(\text{neodecanoate})_2$ catalyst precursor without added AlEt_3 (blue), and $\text{Co}(\text{neodecanoate})_2$ plus AlEt_3 catalysts with Al/Co ratios of 1.0 (red) and 3.0 (green). (b) XANES spectra of Ni foil (black), the $\text{Ni}(\text{2-ethylhexanoate})_2$ catalyst precursor without added AlEt_3 (green), and $\text{Ni}(\text{2-ethylhexanoate})_2$ plus AlEt_3 catalysts with Al/Ni ratios of 1.0 (pink) and 3.0 (blue). In each case, with additional AlEt_3 , the XANES spectra of the catalyst solution becomes less like the precursor solution and more like the metal foil.

First, EXAFS data were collected separately for Co and Ni foils, and cyclohexane solutions of the $\text{Co}(\text{neodecanoate})_2$ and $\text{Ni}(\text{2-ethylhexanoate})_2$ precatalysts, without added AlEt_3 , for use as reference samples (see the Supporting Information (available online at <http://pubs.acs.org>) for the full results, including fits to the data). Solution samples of the catalysts prepared by addition of AlEt_3 , but *before* their use in cyclohexene hydrogenation, were then analyzed by EXAFS. Spectra were collected for catalyst samples with Al/M ratios of 0.5,

1.0, 1.5, 2.0, 2.5, 3.0, and 5.0. However, the EXAFS spectra of many of these samples were of sufficiently poor quality to make fitting and interpretation unreliable. The highest quality spectra were obtained for the Al/M = 1.0 and 3.0 samples; therefore, the spectra and fitting results of the Al/M = 1.0 and 3.0 samples are shown here, but the spectra and fitting results from samples prepared at other Al/M ratios are shown in the Supporting Information (available online at <http://pubs.acs.org>) [38]. For both Co and Ni catalysts, sample spectra show peaks that correspond to the first nearest neighbor (1NN) M–O peak in the precatalyst spectra, and to the 1NN M–M peak in the M foil spectra, Figure B.5. This is analogous to the catalyst spectra of the Ir model catalyst system [14], and so the fitting strategy used herein for the Co- or Ni-based catalysts is analogous to the one employed to fit the EXAFS spectra of the Ir model catalyst samples [14]. The Co and Ni catalyst spectra were fit using composite models created from the 1NN M–O path of the precatalyst and the 1NN M–M path of the bulk metal. Examples of fitting results are shown in Figure B.6, and given in Tables B.2 and B.3.

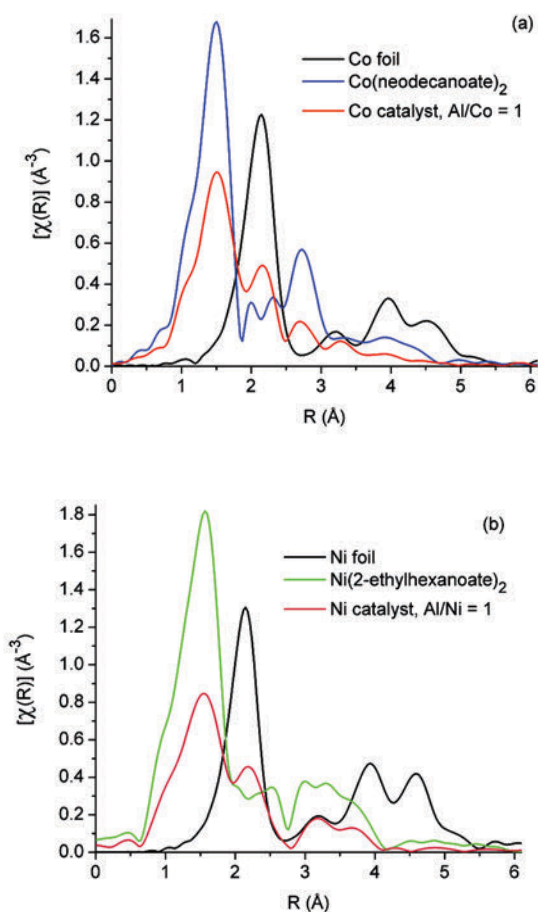


Figure B.5. (a) Fourier transform magnitudes of the k^2 -weighted EXAFS spectra of Co metal foil (black), the $\text{Co}(\text{neodecanoate})_2$ precatalyst without added AlEt_3 (blue), and a sample of the $\text{Co}(\text{neodecanoate})_2$ plus AlEt_3 catalyst with an Al/Co ratio of 1.0 before its use for hydrogenation (red). (b) Fourier transform magnitudes of the k^2 -weighted EXAFS spectra of Ni foil (black), the $\text{Ni}(\text{2-ethylhexanoate})_2$ precatalyst without added AlEt_3 (green) and a sample of the $\text{Ni}(\text{2-ethylhexanoate})_2$ plus AlEt_3 catalyst with an Al/Ni ratio of 1.0 before its use for hydrogenation (pink). Upon addition of AlEt_3 , the Co and Ni catalyst samples still show a peak corresponding to the 1NN, M–O peak of the $\text{Co}(\text{neodecanoate})_2$ and $\text{Ni}(\text{2-ethylhexanoate})_2$ precatalysts, respectively, but also display a peak corresponding to the 1NN, M–M peak from the spectrum of the bulk metal. Also, and significantly, catalyst samples lack peaks in the 3–6 Å range characteristic of ordered, metallic structure. Spectra for Co and Ni foils are shown at one-fourth intensity scale for the purpose of comparison.

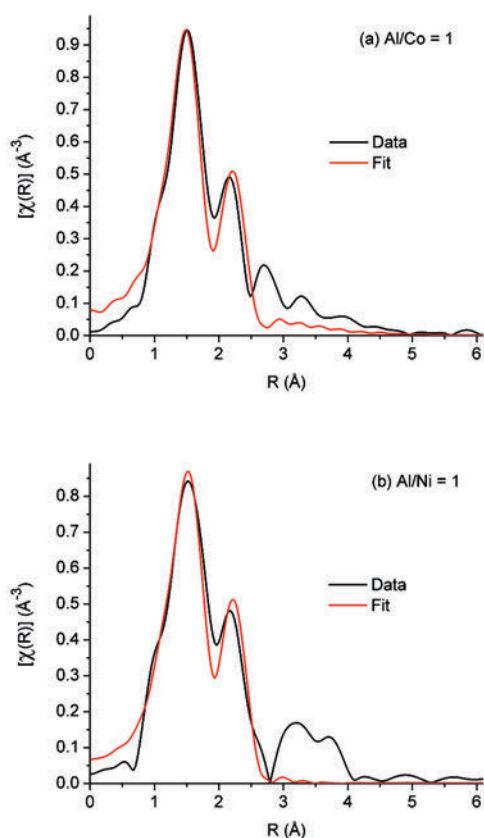


Figure B.6. Data and fits for (a) $\text{Co}(\text{neodecanoate})_2$ plus AlEt_3 catalyst, and (b) $\text{Ni}(\text{2-ethylhexanoate})_2$ plus AlEt_3 catalyst, with an Al/M ratio of 1.0 in each case. The highest quality spectra were obtained for the Al/M = 1.0 and 3.0 samples; the experimental spectra and fits to the Al/M = 1.0 data are shown here as examples—spectra and fitting results from samples prepared at other Al/M ratios are shown in the Supporting Information (available online at <http://pubs.acs.org>).

Table B.2. Fitting results from EXAFS spectroscopic analysis of Co reference samples and $\text{Co}(\text{neodecanoate})_2$ plus AlEt_3 catalyst samples before hydrogenation.

Sample	Co foil	$\text{Co}(\text{O}_2\text{CR})_2^a$	Co catalyst	Co catalyst
Al/Co			1.0	3.0
$N_{\text{Co-Co}}$	12^d		3 ± 2	3.9 ± 0.4
$N_{\text{Co-O}}$		4.7 ± 0.4	3.5 ± 0.9	3 ± 2
$R_{\text{Co-Co}} (\text{Å})^b$	2.492 ± 0.002		2.51 ± 0.02	2.432 ± 0.009
$R_{\text{Co-O}} (\text{Å})^b$		1.959 ± 0.005	1.95 ± 0.02	1.86 ± 0.02
$\sigma_{\text{Co-Co}}^2 (\text{Å}^2)^c$	6.7 ± 0.3		15 ± 6	12 ± 1
$\sigma_{\text{Co-O}}^2 (\text{Å}^2)^c$		4.6 ± 0.7	7 ± 3	20 ± 7

^a $\text{Co}(\text{O}_2\text{CR})_2$ is the catalyst precursor $\text{Co}(\text{neodecanoate})_2$ without added AlEt_3 . The full analysis of $\text{Co}(\text{neodecanoate})_2$ is given in the Supporting Information (available online at <http://pubs.acs.org>). ^b R stands for the interatomic distance corresponding to the single scattering paths. ^c σ^2 represents the mean square variation in R due to both static and dynamic disorder (also known as the EXAFS Debye-Waller factor), and values shown are $\times 10^3$. ^d For Co foil, this parameter was defined as the value shown (i.e., not varied in the fit).

Table B.3. Fitting results from EXAFS spectroscopic analysis of Ni reference samples and Ni(2-ethylhexanoate)₂ plus AlEt₃ catalyst samples before hydrogenation.

Sample	Ni foil	Ni(O ₂ CR) ₂ ^a	Ni catalyst 1.0	Ni catalyst 3.0
N _{Ni-Ni}	12 ^d		3 ± 1	4.4 ± 0.3
N _{Ni-O}		5.8 ± 0.3	2.8 ± 0.5	1.2 ± 0.3
R _{Ni-Ni} (Å) ^b	2.490±0.003		2.51 ± 0.02	2.447±0.006
R _{Ni-O} (Å) ^b		2.035±0.005	2.00 ± 0.02	1.85 ± 0.01
σ ² _{Ni-Ni} (Å ²) ^c	6.9 ± 0.5		13 ± 4	12.4 ± 0.8
σ ² _{Ni-O} (Å ²) ^c		7.4 ± 0.7	8 ± 3	14 ± 5

^a Ni(O₂CR)₂ is the catalyst precursor Ni(2-ethylhexanoate)₂ without added AlEt₃. The full analysis of Ni(2-ethylhexanoate)₂ is given in the Supporting Information (available online at <http://pubs.acs.org>). ^b R stands for the interatomic distance corresponding to the single scattering paths. ^c σ² represents the mean square variation in R due to both static and dynamic disorder (also known as the EXAFS Debye-Waller factor), and values shown are × 10³. ^d For Ni foil, this parameter was defined as the value shown (i.e., not varied in the fit).

The main results from EXAFS are as follows: (i) peaks in the 3–6 Å range in the R-space EXAFS spectra (indicative of ordered metallic structures and evident in the Co and Ni foil reference spectra, Figure B.5), are *absent* for both Co and Ni catalyst samples. This same result was also obtained from previous EXAFS analysis of the Ir model system [14] and the lack of the large distance peaks observed here suggests that Co and Ni catalyst samples are either (a) composed of metal species such as sub-nanometer metal clusters too small to have contributions to that interatomic distance range (b) composed of larger metal nanoclusters with a high degree of atomic disorder, or (c) some combination of the two. (ii) Spectra are fit reasonably well using a composite model analogous to the one employed for the Ir model system [14]. *Significantly, and unlike in the Ir model system, the catalyst samples with an Al/M ratio of 3.0 did not require incorporating a backscattering contribution from M–Al into the model.* Furthermore, the spectra themselves, Figure B.6, lack the feature observed in the spectra of the Ir model system that “grew in” with successively greater Al/M ratios. From fitting the data, (iii) the 1NN M–M coordination numbers observed for Co and Ni samples are, like those observed in the Ir model system studied previously [14], roughly in the 3–4 range, and could point towards the predominance of, on average, sub-nanometer, M_{~4-6}, metal clusters in catalyst solutions before

hydrogenation [39]. Alternatively, low 1NN M–M coordination numbers could signify large degrees of structural disorder in relatively large metal nanoclusters [14,40]. The σ_{M-M}^2 values of the catalyst samples are approximately twice the experimentally determined bulk metal values (Tables B.3 and B.4), which is also suggestive of disordered nanoclusters. Another possibility is that the metal species in catalyst solutions exist as some combination of disordered clusters, and unreduced metal ions.

An additional main result from EXAFS, (iv) the closest M–M distances, given by 1NN R_{M-M} values, overlap within experimental error with the corresponding bulk metals for both Co and Ni samples with Al/M ratios of 1.0, but are *shorter than* the bulk metal M–M distances for both Co and Ni Al/M = 3.0 samples. M–M distances in nanometer scale metal particles with a bulk-like atomic structure are expected to be shorter on average than the corresponding bulk M–M distances due to M–M bond contraction required to counteract (i.e., decrease) the high surface free energy of the small metal clusters [40a-d,41]. Therefore, the implication is that the Co or Ni catalyst materials are becoming *structurally* more like nanoscale metal particles with increasing amounts of AlEt₃, but not to the point that the 1NN N_{M-M} values increase significantly or long range metallic order becomes apparent in the 3–6 Å range in the *R*-space EXAFS spectra (which is also consistent with the changes in the XANES spectra given above).

Interpretation of the EXAFS results from the Co and Ni samples must be carried out in light of the Z-contrast STEM, MALDI MS, and XANES results. For example, the 1NN N_{M-M} values from EXAFS of roughly 3–4 seem, at first take, to imply on average M_{4-6} clusters analogous to the Ir results, but Z-contrast STEM reveals mean Co or Ni cluster diameters of 1.4 or 1.3 nm, respectively, that is M_{130} to M_{100} clusters. Therefore, the most plausible explanation of the results from combining the Z-contrast STEM, MALDI MS, and XAFS (i.e., XANES and

EXAFS) spectroscopy appears to be that a combination of nanoclusters (which are structurally disordered resulting in the absence of peaks at larger distances in the R -space EXAFS spectra, and distorted 1NN N_{M-M} values from fits of the EXAFS spectra [42]) and unreduced metal ions are present, with these two phases of M species both contributing to the mean N_{M-M} value [40i,43]. The possibility of mono-metallic, unreduced metal ions being present is supported by the control experiments for Z-contrast STEM in which no Co was observable when only Co(neodecanoate)₂, without AlEt₃, was on the sample grid. In other words, the metal-containing species in Co and Ni catalyst solutions appear to consist of disordered metal clusters with a broad distribution of sizes, the mean diameters of which are given by Z-contrast STEM and MALDI MS, plus some mono-metallic complexes present as unreduced metal ionic species.

Nuclearity of M_n species after hydrogenation: Z-contrast STEM. The Co(neodecanoate)₂ plus AlEt₃ catalyst, with an Al/Co ratio of 3.0, and *after* its use for cyclohexene hydrogenation was imaged using Z-contrast STEM. Measurement of 614 clusters shows a range of Co cluster sizes 0.5–2.5 nm in diameter. The mode, median, and mean Co cluster diameters are 1.3, 1.4, and 1.4 ± 0.3 nm, corresponding to Co₋₁₀₀ and Co₋₁₃₀, accordingly. Figure B.7 shows an example image and the histogram.

The Ni(2-ethylhexanoate)₂ plus AlEt₃ catalyst, with an Al/Ni ratio of 2.0, *after* its use for cyclohexene hydrogenation was also imaged using Z-contrast STEM. Measurement of 650 clusters in Z-contrast STEM images reveals a range of Ni cluster sizes 0.6–4.0 nm in diameter. The mode and median Ni cluster diameter is 1.4 nm and the mean is 1.4 ± 0.4 nm. These diameters correspond to Ni₋₁₃₀. An example image and the histogram are shown in Figure B.8.

Z-contrast STEM shows that using these Co and Ni Ziegler-type hydrogenation catalysts for cyclohexene hydrogenation does not induce a change in the sizes of the metal cluster species

present in either Co or Ni catalyst samples, at least under the conditions used herein. Although this differs from the distinct increase in metal cluster size and change in structure exhibited by the Ir model system [14], it is consistent with the lack of changes in catalyst solution color, no observation of precipitates in post-hydrogenation solutions (unlike the Ir model system [14]). In short, catalytic cyclohexene hydrogenation induces essentially no changes in size or size distribution of the Co or Ni clusters observed by Z-contrast STEM.

Nuclearity of the M_n species *after* hydrogenation: MALDI MS. Samples of the Co(neodecanoate)₂ plus AlEt₃ catalyst, with an Al/Co ratio of 3.0, were analyzed using MALDI MS *after* their use in cyclohexene hydrogenation (Figures are shown in the Supporting Information (available online at <http://pubs.acs.org>)). MALDI MS of the Co catalyst results in a broad peak with maximum intensity at ~3500 m/z (reported as the average Co cluster in Table B.1), and a shoulder at ~6000 m/z . Using the same necessary assumptions as before, that the broad peaks are composed of only +1 charged ions [14,32,33,34,35], the peak at ~3500 m/z indicates Co_{~60} clusters, corresponding to a diameter of ~1.1 nm. The peak of the post-hydrogenation Co catalyst tails off toward higher m/z values; FWHM of the peak is from ~1500–9500 m/z , the peak reaches one-fourth maximum intensity at ~12000 m/z , and one-eighth maximum intensity at ~17000 m/z (1500–17000 is used to report the range of Co clusters in B.1), which correspond to 0.8–1.5 nm, Co_{~25–160}; 1.6 nm, Co_{~200}; and 1.8 nm, Co_{~290} clusters, respectively—essentially the same as the prehydrogenation results.

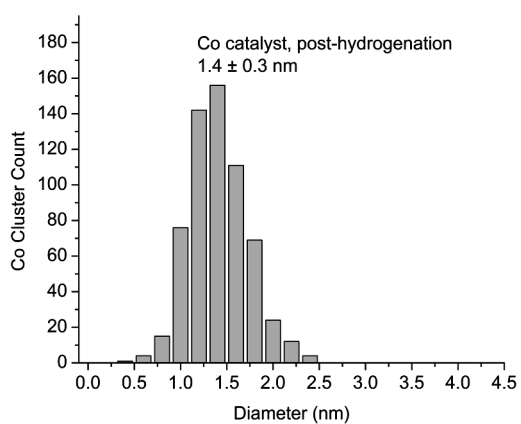
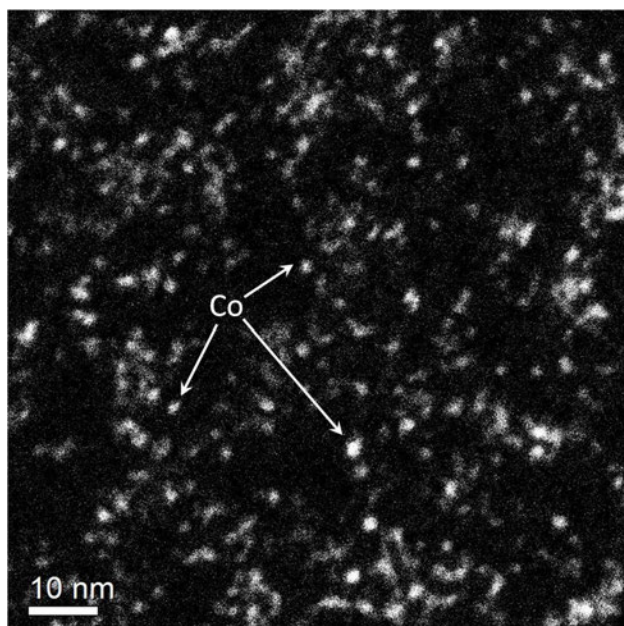


Figure B.7. Example Z-contrast STEM image of a $\text{Co}(\text{neodecanoate})_2$ plus AlEt_3 catalyst sample after its use in hydrogenation. The histogram shows the results from measuring the diameters of 614 Co clusters in such images; measured cluster diameters range from 0.5 to 2.5 nm, which correspond to Co cluster nuclearities from $\text{Co}_{\sim 6}$ to $\text{Co}_{\sim 740}$. The mode, median, and mean diameters of Co clusters are 1.3, 1.4, and 1.4 ± 0.3 nm, corresponding to $\text{Co}_{\sim 100}$ or $\text{Co}_{\sim 130}$ accordingly.

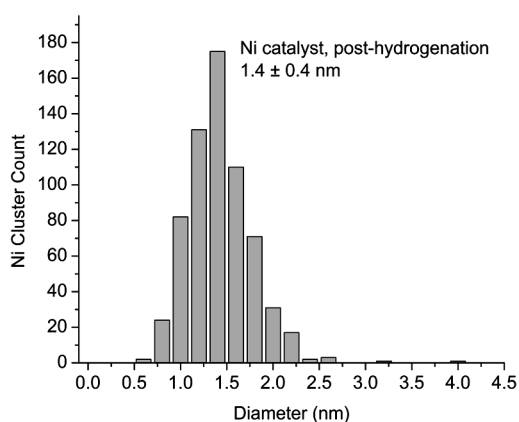
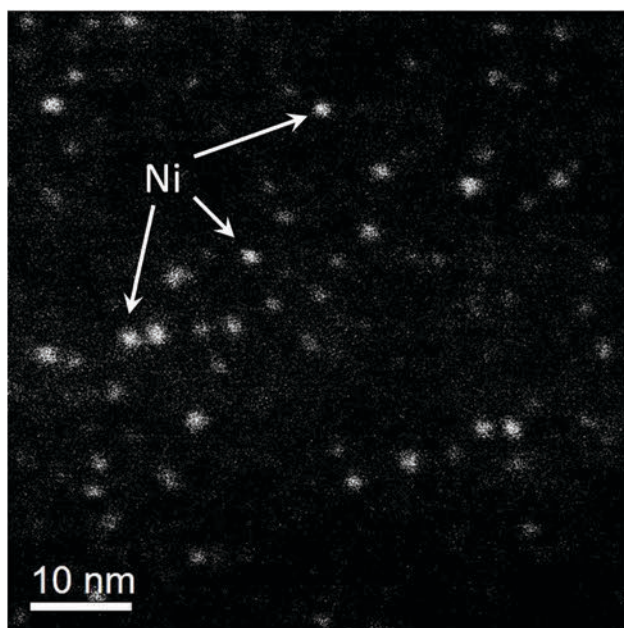


Figure B.8. Example Z-contrast STEM image of a Ni(2-ethylhexanoate)₂ plus AlEt₃ catalyst sample after its use in hydrogenation. The corresponding histogram shows the results from measuring the diameters of 650 Ni clusters in such images, and reveals a range of Ni clusters with diameters from 0.6 to 4.0 nm, corresponding to Ni_{~10} to Ni_{~3060}. The mode and median diameters are 1.4 nm, and the mean is Ni 1.4 ± 0.4 nm, corresponding to mean Ni_{~130} clusters.

The Ni(2-ethylhexanoate)₂ plus AlEt₃ catalyst, with an Al/Ni ratio of 2.0, was also analyzed using MALDI MS *after* it had been used for cyclohexene hydrogenation, giving a broad peak with a maximum intensity at ~2000 *m/z*, which again indicates Ni_{~34} clusters, corresponding to ~0.9 nm diameter Ni nanoclusters (reported as the average cluster size in Table B.1). (As in the catalyst sample before hydrogenation, the presence of Ni atoms in species below

1500 m/z is ruled out by the absence of characteristic Ni isotope peak distributions in that region.) The broad, asymmetrically shaped MALDI MS peak of the catalyst sample *after* hydrogenation also tails off towards higher m/z values, but isn't completely identical to the peak of the sample before hydrogenation; the post-hydrogenation peak displays two slight shoulders at ~ 3000 and ~ 6000 m/z . Nevertheless, the broad peak in the sample after hydrogenation reaches ~ 6500 m/z at half maximum intensity, ~ 8500 m/z at one-fourth maximum intensity, and ~ 11000 m/z at one-eighth maximum intensity (1500–11000 m/z is used to report the range of Ni clusters in Table B.1), which correspond to 1.3 nm, Ni₁₁₀; 1.5 nm, Ni₁₄₅; and 1.6 nm, Ni₁₉₀, respectively. These Ni cluster size and nuclearity values are very similar to those from the prehydrogenation sample. In short, the MALDI MS-determined sizes and size distributions of both Co and Ni clusters in post-hydrogenation samples (i) agree closely with the analysis of posthydrogenation catalyst samples using Z-contrast STEM, and consistent with the Z-contrast STEM, (ii) indicate no significant change in the sizes of the metal clusters present upon their use for the catalytic hydrogenation of cyclohexene.

Nuclearity of M_n species *after* hydrogenation: XAFS (i.e., XANES and EXAFS) Spectroscopy. Solution samples of both Co(neodecanoate)₂ plus AlEt₃, and Ni(2-ethylhexanoate)₂ plus AlEt₃ catalysts, with Al/M ratios of 1.0, were analyzed using XAFS *after* their use in hydrogenation reactions. The XANES spectra of the Co and Ni catalyst solutions posthydrogenation are nearly the same as their prehydrogenation counterparts. XANES spectra collected after hydrogenation are shown and compared to the prehydrogenation spectra in the Supporting Information (available online at <http://pubs.acs.org>)

for the interested reader. For both Co and Ni catalysts, the EXAFS spectra after hydrogenation also appear very similar to the sample spectra before hydrogenation. The spectra

are fit using the same models employed for fitting the catalyst samples before hydrogenation. The results are shown in Figure B.9 and summarized in Table B.3. Complete fit information and additional spectra are in the Supporting Information (available online at <http://pubs.acs.org>).

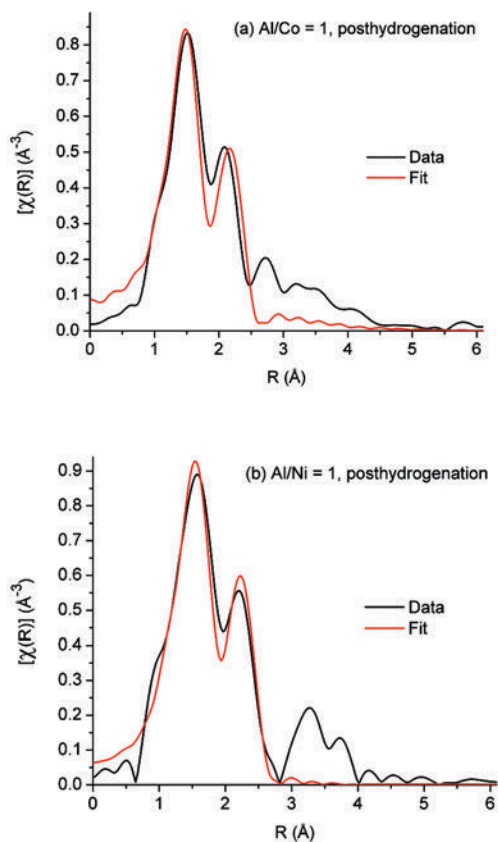


Figure B.9. Data and fits of (a) the $\text{Co}(\text{neodecanoate})_2$ plus AlEt_3 catalyst, Al/Co ratio of 1.0; and (b) the $\text{Ni}(\text{2-ethylhexanoate})_2$ plus AlEt_3 catalyst, Al/Ni ratio of 1.0, both after use for the catalytic hydrogenation of cyclohexene.

The most plausible interpretation of the EXAFS spectra and fitting results is essentially the same for the catalyst samples after hydrogenation as for the samples before hydrogenation. The lack of peaks in the 3–6 \AA range implies that no Co or Ni species with ordered metallic structures on that scale are present, and 1NN single scattering $N_{\text{M-M}}$ values of ~ 3 were obtained for both Co and Ni catalysts. Additionally, the $R_{\text{M-M}}$ values from both Co and Ni samples posthydrogenation are the same as their prehydrogenation counterparts within experimental

error, and are very close to the experimental bulk metal values (within $\leq 0.03 \text{ \AA}$). Recall from the discussion of the prehydrogenation XAFS results that bulk metal-like R_{M-M} values are in contrast to the larger R_{M-M} values expected for subnanometer M_n clusters ligated by Lewis acid species (i.e., AlEt_3 and its derivatives). Lastly, the σ^2_{M-M} values of the catalyst samples are again roughly twice the experimentally determined bulk metal values. Considered in light of the posthydrogenation Z-contrast and MALDI MS results, which reveal a predominance of nanometer scale clusters as part of wide size distributions, the self-consistent interpretation of all measurements (made already for the prehydrogenation samples) is that a combination of disordered nanoclusters and unreduced, mono-metallic species are present in catalyst solutions posthydrogenation. In short, both the XANES and EXAFS spectra confirm that use of catalyst solutions for cyclohexene hydrogenation has a negligible effect on the oxidation state and form of the transition metal catalyst material.

Table B.3. Summary of fit results for posthydrogenation Co and Ni catalyst spectra.

Sample	Co	Ni
N_{M-M}	3 ± 2	3 ± 1
N_{M-O}	3 ± 1	2.7 ± 0.4
$R_{M-M} (\text{\AA})^a$	2.48 ± 0.02	2.52 ± 0.01
$R_{M-O} (\text{\AA})^a$	1.96 ± 0.02	2.02 ± 0.01
$\sigma^2_{M-M} (\text{\AA}^2)^b$	15 ± 7	13 ± 3
$\sigma^2_{M-O} (\text{\AA}^2)^b$	7 ± 4	7 ± 2

^a R stands for the interatomic distance corresponding to the single scattering paths. ^b σ^2 represents the mean square variation in R due to both static and dynamic disorder (the EXAFS Debye-Waller factor), and values shown are $\times 10^3$.

Kinetics Studies: Hg(0) catalyst poisoning. The observation of M_n clusters before and after catalysis does not necessitate that these species are the active hydrogenation catalysts—kinetic studies are required to determine the most active catalyst(s) from sample solutions. Catalyst poisoning by Hg(0) is a useful kinetics-based test for distinguishing homogeneous from heterogeneous Ziegler-type hydrogenation catalysis, as has been shown previously [14]. Hence,

Hg(0) poisoning experiments were utilized to test whether the observed catalytic activity of the industrial Ziegler–type hydrogenation catalysts made from Ni(2-ethylhexanoate)₂ or Co(neodecanoate)₂ and AlEt₃ is “homogeneous” (e.g., via single metal organometallic) or heterogeneous (e.g., via small M₄ or larger nanoclusters), Figure B.10. (Due to the outcomes of the Hg(0) poisoning experiments, the results for Ni are discussed here before those for Co.) One benefit of using Hg(0) poisoning in this case is that the results are not affected by MTL kinetics (vide supra, and in the Supporting Information (available online at <http://pubs.acs.org>)). Hg(0) addition to the Ni catalyst prior to the start of cyclohexene hydrogenation poisons catalysis *immediately and completely*, Figure B.10. When Hg(0) is added to the Ni catalyst solution after about half the cyclohexene had been consumed, the Hg(0) also poisons the catalysis *immediately and completely*. These results suggest that catalysis in the Ni Ziegler–type hydrogenation system, made from authentic industrial Ni(2-ethylhexanoate)₂ precatalyst plus AlEt₃ is heterogeneous (i.e., via the observed sub (~M₄) to larger nanoclusters).

It is known that one potential difficulty with Hg(0) poisoning experiments is that it may be difficult to thoroughly contact the Hg(0) with all of the catalyst in solution due to the insolubility of Hg(0) [44]. Control experiments with the Ni system allowed the determination that a procedure using ≥ 300 equivalents of Hg(0) per Ni and ≥ 1.5 hours of 1000 rpm stirring is adequate to thoroughly contact the Hg(0) with all of the Ni catalyst in solution. However, control experiments show that the degree of poisoning with the Co catalyst is with regard to the amount of Hg(0) used and the length of time it is mixed with the catalyst solution prior to data acquisition, is irreproducible (Experimental Section and Supporting Information (available online at <http://pubs.acs.org>)). Unfortunately, then, the Hg(0) poisoning experiments with the Co catalyst proved inconclusive. Nevertheless, the Hg(0) poisoning results suggest catalysis with

the Ni system is heterogeneous (i.e., proceeds via the observed Ni Ziegler sub-to-higher nanoclusters).

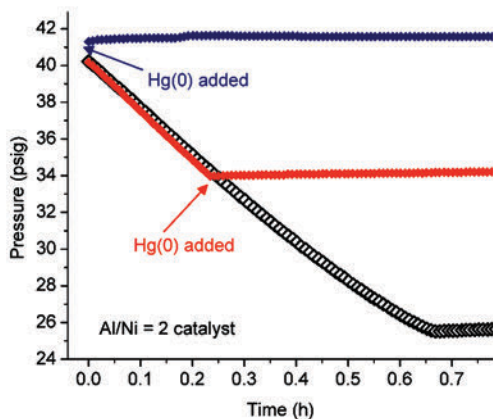


Figure B.10. Poisoning experiments using the Ni(2-ethylhexanoate)₂ plus AlEt₃ catalyst with an Al/Ni ratio of 2.0 are shown next to standard example cyclohexene hydrogenation runs for comparison (black curve). Immediate and complete poisoning of catalysis by addition of Hg(0) after preparation of the catalyst, but before hydrogenation is begun (blue), and partway through a catalytic run (red), suggests that catalysis in the Ni catalyst system is heterogeneous (i.e., via the observed Ni nanoclusters).

4. Conclusions and Needed Future Studies.

Catalysts made from either of the industrial precursors Co(neodecanoate)₂ or Ni(2-ethylhexanoate)₂, plus AlEt₃, were analyzed by Z-contrast STEM, MALDI MS, XAFS (i.e., XANES and EXAFS), and Hg(0) poisoning studies, producing the following observations: (i) Co and Ni Ziegler-type hydrogenation catalyst solutions turn dark brown upon the initial combination of the Co(neodecanoate)₂ or Ni(2-ethylhexanoate)₂ precatalyst solutions with the AlEt₃ solution, and not during hydrogenation catalysis; and (ii) hydrogenation proceeds immediately with the start of data acquisition at, or very near, the maximum observable rate. (iii) Z-contrast STEM reveals, for the prehydrogenation Co sample, a 0.6–3.3 nm range of particle diameters with a mean of 1.4 ± 0.4 nm, which corresponds to Co_{~130}. For the

prehydrogenation Ni sample, Z-contrast STEM reveals a 0.4–3.5 nm range of particle diameters with a mean of 1.3 ± 0.5 nm, which corresponds to Ni_{~100}. (iv) MALDI MS is used to estimate, for the prehydrogenation Co sample, a 0.8–1.8 nm range of particle diameters and an average of 1.2 nm, which corresponds to Co_{~80}. For the prehydrogenation Ni sample, MALDI MS is used to estimate a 0.8–1.7 nm range of particle diameters and an average of 0.9 nm, which corresponds to Ni_{~34}. (v) XANES spectra show that the Co or Ni metals in prehydrogenation catalyst solutions become progressively less like their M(II) precatalysts, in terms of composite average formal oxidation state, and progressively more like the M(0) metal foils as the Al/M ratios increase from 1.0 to 3.0, implying that unreduced metal ions are present in catalyst solutions in amounts that decrease with additional AlEt₃. (vi) EXAFS spectroscopic analysis of prehydrogenation samples reveals a lack of the R-space peaks in the 3–6 Å range indicative of ordered metallic structures. Fitting the spectra of both metals using composite models analogous to that used for the Ir model system [14], gives mean 1NN M–M coordination numbers in the 3–4 range. Fitting the EXAFS spectra also gives 1NN R_{M-M} values that overlap, within experimental error, with the corresponding bulk metals for both Co and Ni samples with Al/M ratios of 1.0, but 1NN R_{M-M} values that are *shorter than* the bulk metal M–M distances for both Co and Ni Al/M = 3.0 samples. Fitting the EXAFS spectra also reveal σ_{M-M}^2 values that are approximately twice the experimentally determined bulk metal values, indicative of disordered metal clusters. In addition, (vii) the Z-contrast STEM, MALDI MS, and XAFS results all show that cyclohexene hydrogenation does not significantly change the transition metal contents of the catalyst solutions. Finally, (viii) Hg(0) poisons the Ni catalyst immediately and completely, regardless of whether the Hg(0) is added before, or in the middle of a hydrogenation run.

The self-consistent interpretation of all results from the complementary techniques used herein is that the transition metal components of catalysts made from either of the industrial precursors $\text{Co}(\text{neodecanoate})_2$ or $\text{Ni}(2\text{-ethylhexanoate})_2$, plus AlEt_3 , consist of a combination of M_n clusters with a broad range of sizes and a large degree of structural disorder, and unreduced, mono-metallic species, the distribution between the two phases depending on the Al/M ratio. Furthermore, the $\text{Hg}(0)$ poisoning in particular suggests that Ziegler nanoclusters are the most active catalysts in the industrial Ni Ziegler-type hydrogenation catalyst system (i.e., that the catalysis is heterogeneous, and if one includes $\geq \text{Ni}_4$ within the definition of heterogeneous). This work expands on the results of others—notably the important studies by Schmidt and co-workers [17], and Bönemann and co-workers [18] which suggest transition metal nanoclusters are the catalysts in the Co, Pd, Ni, and Pt Ziegler-type systems they studied. The combined results present the best evidence to date consistent with the “Ziegler nanocluster hypothesis” as the correct answer to the ~50 year old problem of what is the true nature of the industrial Ni-, and presumably also Co-based catalysts. Hence, the notion that industrial Ziegler-type hydrogenation catalysis proceeds via Ziegler nanoclusters is the leading hypothesis going forward to try to disprove.

Much remains to be done, however. Operando spectroscopy studies of both the formation of, and catalysis by, both the Ni and Co industrial catalyst systems remain to be accomplished [45]. A full kinetic study and rate law determination under non-MTL conditions also remain to be done, and promises to be challenging due to the high rates of these superior catalysts. In addition, the differences regarding the backscattering contribution from M–Al between the EXAFS spectra of the Ir model system (which show the presence of Al) [14], and those of the industrial Co and Ni-based catalysts studied herein (which do not show the presence of Al), are surprising and remain to be explored—could a M_4H_4 type catalyst explain this

discrepancy, for example? Another important difference between the Ir and Co, Ni catalysts is that catalyst aging slows the rates for the Co, Ni catalysts, opposite to what is seen for Ir, so that future studies characterizing the aged Co and Ni catalysts is another, important future objective. Furthermore, specific determination of the form(s) taken, and role(s) played by the AlEt₃ component, both in the initial synthesis of the catalyst and during catalytic cyclohexene hydrogenation, remain to be fully understood [19].

Despite the work remaining to be done, this investigation of the homogeneous versus heterogeneous nature of Ziegler-type hydrogenation catalysts is significant for at least four reasons: (i) this study examines Co and Ni-based catalysts made from the *actual industrial* precursor materials, which make catalysts that are notoriously problematic regarding their characterization [2,3]; (ii) the Z-contrast STEM results reported herein represent, to our knowledge [3], the best microscopic analysis of the industrial Co and Ni Ziegler-type hydrogenation catalysts; (iii) this study is the first explicit application of an established method, using multiple analytical methods and kinetics-based studies, for distinguishing homogeneous from heterogeneous catalysis [3,6-15]; and (iv) this study parallels the successful study of an Ir model Ziegler catalyst system, thereby benefiting from a comparison to those previously unavailable findings [14], although the greater M–M bond energy, and tendency to agglomerate, of Ir versus Ni or Co are important differences to be noted [46]. Overall, the leading hypothesis to try to refute in future work is that Ziegler-type sub-(i.e., M₄) to larger nanoclusters are the dominant, industrial, Co- and Ni- plus AlR₃ catalysts.

6. Supporting Information Available. Experimental information and results of control experiments for cyclohexene hydrogenations used to help establish standard conditions for catalyst preparation and use; additional TEM images; figures showing the MALDI MS results;

EXAFS spectra with fits; Hg(0) poisoning control experiments; and a full list of the authors of reference 18d. This material is available free of charge via the Internet at <http://pubs.acs.org>.

REFERENCES

- [1] W.M. Alley, C.W. Girard, S. Özkar, R.G. Finke, *Inorg. Chem.* 48 (2009) 1114–1121.
- [2] K.A. Johnson, *Polym. Prepr.* 41 (2000) 1525–1526.
- [3] W.M. Alley, I.K. Hamdemir, K.A. Johnson, R.G. Finke, *J. Mol. Catal. A:Chem.* 315 (2010) 1–27.
- [4] J.P. Collman, L.S. Hegedus, J.R. Norton, R.G. Finke, *Principles and Applications of Organotransition Metal Chemistry*; University Science Books: Mill Valley, CA, 1987.
- [5] J. Schwartz, *Acc. Chem. Res.* 1985, 18, 302–308.
- [6] J.A. Widegren, R.G. Finke, *J. Mol. Catal. A: Chem.* 198 (2003) 317–341.
- [7] Y. Lin, R.G. Finke, *Inorg. Chem.* 33 (1994) 4891–4910.
- [8] J.D. III Aiken, Y. Lin, R.G. Finke, *J. Mol. Catal. A: Chem.* 114 (1996) 29–51.
- [9] J.A. Widegren, M.A. Bennett, R.G. Finke, *R. G. J. Am. Chem. Soc.* 125 (2003) 10301–10310.
- [10] C.M. Hagen, J.A. Widegren, P.M. Maitlis, R.G. Finke, *J. Am. Chem. Soc.* 127 (2005) 4423–4432.
- [11] E.E. Finney, R.G. Finke, *Inorg. Chim. Acta* 359 (2006) 2879–2887.
- [12] C.A. Jaska, I.J. Manners, *Am. Chem. Soc.* 126 (2004) 1334–1335.
- [13] C.A. Jaska, I.J. Manners, *J. Am. Chem. Soc.* 126 (2004) 9776–9785.
- [14] W.M. Alley, I.K. Hamdemir, Q. Wang, A.I. Frenkel, L. Li, Y.C. Yang, L.D. Menard, R.G. Nuzzo, S. Özkar, K. Johnson, R.G. Finke, *Inorg. Chem.* 49 (2010) 8131–3147.
- [15] M. Zahmakiran, S. Özkar, *Inorg. Chem.* 48 (2009) 8955–8964.
- [16] J. Halpern, *Inorg. Chim. Acta* 50 (1981) 11–19.
- [17] (a) F.K. Shmidt, L.O. Nindakova, B.A. Shainyan, V.V. Saraev, N.N. Chipanina, V.A. Umanetz, *J. Mol. Catal. A: Chem.* 235 (2005) 161–172. (b) L.B. Belykh, Yu. Yu. Titova, V.A. Umanets, F.K. Shmidt, *Russian Journal of Applied Chemistry* 79 (2006) 1271–1277. (c) L. O. Nindakova, F.K. Shmidt, V.V. Saraev, B.A. Shainyan, N.N. Chipanina, V.A. Umanets, L.N. Belonogova, , D.-S. D. Toryashinova, *Kinetics and Catalysis* 47 (2006) 54–63. (d) L.B. Belykh, T.V. Goremyka, N.I. Skripov, V.A. Umanets, F.K. Shmidt, *Kinetics and Catalysis* 47 (2006) 367–374.

[18] Studies by Bönemann and co-workers do not focus on hydrogenation catalysis using Ziegler-type systems, but do demonstrate the synthesis and identification of nanoclusters from Ni or Pt Ziegler-type systems. (a) H. Bönemann, W. Brijoux, R. Brinkmann, U. Endruschat, W. Hofstadt, K. Angermund, *Revue Roumaine de Chimie* 44 (1999) 1003–1010. (b) H. Bönemann, N. Waldöfner, H.-G. Haubold, T. Vad, *Chem. Mater.* 14 (2002) 1115–1120. (c) K. Angermund, M. Bühl, E. Dinjus, U. Endruschat, F. Gassner, H.-G. Haubold, J. Hormes, G. Köhl, F.T. Mauschick, H. Modrow, R. Mörtel, R. Mynott, B. Tesche, T. Vad, N. Waldöfner, H. Bönemann, *Angew. Chem. Int. Ed.* 41 (2002) 4041–4044. (d) K. Angermund, *et al.* *J. Phys. Chem. B* 107 (2003) 7507–7515. (e) H.-G. Haubold, T. Vad, N. Waldöfner, H. Bönemann, *J. Appl. Cryst.* 36 (2003) 617–620. (f) F. Wen, H. Bönemann, R.J. Mynott, B. Spliethoff, C. Weidenthaler, N. Palina, S. Zinoveva, H. Modrow, *Appl. Organomet. Chem.* 19 (2005) 827–829.

[19] I.K. Hamdemir, S. Özkar, K.A. Johnson, R.G. Finke, manuscript in preparation.

[20] J.D. III Aiken, R.G. Finke, *J. Am. Chem. Soc.* 120 (1998) 9545–9554.

[21] (a) Y. Lin, R.G. Finke, *Inorg. Chem.* 33 (1994) 4891–4910; (b) M.A. Watzky, R.G. Finke, *J. Am. Chem. Soc.* 119 (1997) 10382–10400; and (c) J.A. Widegren, J.D. III Aiken, S. Özkar, R.G. Finke, *Chem. Mater.* 13 (2001) 312–324.

[22] G.J. Kearns, E.W. Foster, J.E. Hutchison, *Anal. Chem.* 78 (2006) 298–303.

[23] (a) M.J. Newville, *Synchrotron Rad.* 8 (2001) 322–324. (b) B. Ravel, M.J. Newville, *Synchrotron Rad.* 2005, 12, 537–541.

[24] Y. Lin, R.G. Finke, *J. Am. Chem. Soc.* 116 (1994) 8335–8353.

[25] *CRC Handbook of Chemistry and Physics*; 77th ed.; D.R. Lide, H.P.R. Frederikse, Eds.; CRC Press, Boca Raton, 1996.

[26] The number of atoms in a transition metal nanocluster (n) may be estimated making the necessary approximation that the nanoclusters have the same close-packed atomic structure as the bulk metal (either face centered cubic (fcc) or hexagonal close packed (hcp)), and using the following formula: $n = (N_0 \rho (4/3) \pi (D/2)^3) / W$.²⁴ According to this approach N_0 is $6.022 \times 10^{23} \text{ mol}^{-1}$, ρ is the room temperature density of the pure bulk metal, D is the measured cluster diameter, and W is the atomic weight of the transition metal. For Ni, ρ is 8.90 g/cm^3 , and W is 58.69 g/mol [25]. For Co, ρ is 8.86 g/cm^3 , and W is 58.93 g/mol [25]. For example, a Ni cluster diameter of 1.3 nm corresponds to Ni~100.

[27] L. Starkey Ott, M.L. Cline, M. Deetlefs, K.R. Seddon, R.G. Finke, *J. Am. Chem. Soc.* 127 (2005) 5758–5759.

[28] C.M. Hagen, L. Vieille-Petit, G. Laurency, G. Süss-Fink, R.G. Finke, *Organometallics* 24 (2005) 1819–1831.

- [29] D.B. Williams, C.B. Carter, *Transmission Electron Microscopy*; Plenum Press: New York, 1996.
- [30] Catalyst samples, both before and after hydrogenation, were also analyzed using bright field and high resolution (HR)TEM as control experiments. Images and a short discussion of those results can be found in the Supporting Information (available online at <http://pubs.acs.org>).
- [31] W.D. Pyrz, D.J. Buttrey, *Langmuir* 24 (2008) 11350–11360.
- [32] R.L. Whetten, J.T. Khoury, M.M. Alvarez, S. Murthy, I. Vezmar, Z.L. Wang, P.W. Stephens, C.L. Cleveland, W.D. Luedtke, U. Landman, *Adv. Mater.* 8 (1996) 428.
- [33] G.A. Khitrov, G.F. Strouse, *J. Am. Chem. Soc.* 125 (2003) 10465.
- [34] T. Kuzuya, Y. Tai, S. Yamamuro, K. Sumiyama, *Chem. Phys. Lett.* 407 (2005) 460–463.
- [35] L. Maya, C.H. Chen, K.A. Stevenson, E.A. Kenik, S.L. Allman, T.G. Thundat, *J. Nanoparticle Res.* 4 (2002) 417.
- [36] J. Goulon, E. Georges, C. Goulon-Ginet, Y. Chauvin, D. Commereuc, H. Dexpert, E. Freund, *Chem. Phys.* 83 (1984) 357–366. (b) C. Esselin, E. Bauer-Grosse, J. Goulon, C. Williams, Y. Chauvin, D. Commereuc, E. Freund, *J. Phys. Colloques* 47 (1986) C8-243–C8-248.
- [37] A.I. Frenkel, C.W. Hills, R.G. Nuzzo, *J. Phys. Chem. B* 105 (2001) 12689–12703.
- [38] Since much of the other data presented herein is for the Al/Ni = 2.0 catalyst, we carefully considered if it was important to have higher quality data from the Al/Ni = 2.0 sample in order to support the conclusions in the present study. We reasoned that such data are not necessary, primarily on the basis of the following four reasons. First, the XANES spectra of these samples show a smooth progression of the samples from the Al/Ni = 1.0 to Al/Ni = 3.0 ratios. Second, there is considerable similarity between the Al/Ni = 2.0 and 3.0 spectra when plotted as $\chi(k)$, and despite the additional noise apparent in the Al/Ni = 2.0 sample (relevant spectra comparisons are given in the Supporting Information (available online at <http://pubs.acs.org>)). Third, these first two observations, together with the similarity between the fitting results from catalyst samples with Al/Ni ratios of 1.0 and 3.0, demonstrate that reliable fitting results for the Al/Ni = 2.0 sample should have values between those obtained from the Al/Ni = 1.0 and 3.0 samples. And fourth, the interpretation of the XAFS data herein, that 1NN M–M coordination numbers are not representative of cluster nuclearity, means that a direct comparison between the results from XAFS and cluster size measurements using other methods such as Z-contrast STEM is not straightforward; this is the case even if higher quality data for the Al/Ni = 2.0 sample were in hand. In short, obtaining higher quality data for the Al/Ni = 2.0 sample is not expected to improve or change any of the conclusions reached in the present study.
- [38] One possible interpretation is that M_{4-6} clusters remain tightly associated (i.e., $(M_{4-6})_n$). (a) J.L. Fulton, J.C. Linehan, T. Autrey, M. Balasubramanian, Y. Chen, N.K. Szymczak, *J. Am. Chem. Soc.* 129 (2007) 11936–11949. (b) M. Harada, K. Asakura, N.J. Toshima, *Phys. Chem.* 98 (1994) 2653–2662.

[40] (a) A.L. Ankudinov, J.J. Rehr, J.J. Low, S.R. Bare, *J. Chem. Phys.* 116 (2002) 1911–1919. (b) V. Petkov, T. Ohta, Y. Hou, Y. Ren, *J. Phys. Chem. C* 111 (2007) 714–720. (c) V. Petkov, N. Bedford, M.R. Knecht, M.G. Weir, R.M. Crooks, W. Tang, G. Henkelman, A.I. Frenkel, *J. Phys. Chem. C* 112 (2008) 8907–8911. (d) Y. Sun, L. Zhuang, J. Lu, X. Hong, P. Liu, *J. Am. Chem. Soc.* 129 (2007) 15465–15467. (e) F. Vila, J.J. Rehr, J. Kas, R.G. Nuzzo, A.I. Frenkel, *Phys. Rev. B* 78 (2008) 121404-1–121404-4. (f) S.I. Sanchez, L.D. Menard, A. Bram, J.H. Kang, M.W. Small, R.G. Nuzzo, A.I. Frenkel, *J. Am. Chem. Soc.* 131 (2009) 7040–7054. (g) B. Gilbert, F. Huang, H. Zhang, G.A. Waychunas, J.F. Banfield, *Science* 305 (2004) 651–654. (h) S.J.L. Billinge, I. Levin, *Science* 316 (2007) 561–565. (i) Y. Sun, A.I. Frenkel, R. Isseroff, C. Shonbrun, M. Forman, K. Shin, T. Koga, H. White, L. Zhang, Y. Zhu, M.H. Rafailovich, J.C. Sokolov, *Langmuir* 22 (2006) 807–816.

[41] R.G. Finke, S. Özkar, *Coord. Chem. Rev.* 248 (2004) 135–146.

[42] A. Yevick, A.I. Frenkel, *Phys. Rev. B* 81 (2010) 115451.

[43] In addition, the explanation of the low XAFS N_{M-M} values involving disordered structure alone requires a degree of N_{M-M} distortion of considerably greater magnitude than reported in the literature [42]. The expected, non-distorted, N_{M-M} value for mean 1.4–1.3 nm Co and Ni clusters (determined by Z-contrast STEM) is approximately 8.6–8.9. The observed values from the XAFS results herein, Tables B.2 and B.3, are decreased by about 50%, as opposed to a disorder-induced decrease in N_{M-M} of 8% calculated in a previous study [42].

[44] (a) The potential weaknesses and pitfalls of Hg(0) as a test for the homogeneous versus heterogeneous nature of a catalyst are discussed elsewhere [6]. (b) Also see, N.T.S. Phan, M. Van Der Sluys, C.W. Jones, *Adv. Synth. Catal.* 348 (2006) 609–679.

[45] (a) J.M. Thomas, G.A. Somorjai, *Top. Catal.* 8 (1999) (preface); (b) B.M. Weckhuysen, *Chem. Commun.* (2002) 97–110; (c) M.O. Guerrero-Pérez, M.A. Bañares, *Chem. Commun.* (2002) 1292–1293. (d) F. Meunier, M. Daturi, *Catal. Today* 113 (2006) 1–2.

[46] (a) The standard heats of formation of Ir, Co, and Ni gases are 159.0, 101.5, and 102.7 kcal/mol, respectively [25]. This means that at least naked, unligated Ir_n clusters have a greater thermodynamic tendency to agglomerate to the thermodynamic minimum of a bulk Ir(0) mirror compared to Co(0) or Ni(0) clusters. The presence of hydrides or surface ligands, such as in a putative $M_4H_4L_y$, mitigates this driving force some, however, since Ir–H and Ir–L bond energies should be stronger than Co or Ni ones. (b) A useful reference on this point is: C. Kilic, *Solid State Communications* 150 (2010) 2333–2336. (c) The difference in aging effects on the catalysts, the Ir system becoming faster, while aging the Co and Ni catalysts for 24 h has either a slight or significant slowing effect, respectively, is noteworthy here, and shows an important difference in the Co and Ni versus Ir samples, which in turn shows that characterization of the Co and Ni samples as a function of aging is an important future goal.

APPENDIX G

GENERAL STATEMENT ON “JOURNALS-FORMAT” THESES

(Written by Professor Richard G. Finke)

The Graduate School at Colorado State University allows, and the Finke Group in particular encourages, so-called journals-format theses. Journals-format theses, such as the present one, consist of a student written and lightly edited literature background section, chapters corresponding (in the limiting, ideal case) to final-form papers either accepted or at least submitted for publication, a summary or conclusions chapter, and short bridge or transition sections between the chapters as needed to make the thesis cohesive and understandable to the reader. The “bridge” sections and summary are crucial so that the thesis fulfills the requirement that the thesis be an entity (an official requirement of most Graduate Schools). All chapters (manuscripts) in a journals-format thesis must of course be written initially by the student, with subsequent (ideally light) editing by the Professor, the student’s committee, and even the student’s colleagues where appropriate and productive.

The advantages for doing a journals-format thesis are several-fold and compelling. Specifically, some of the major advantages are: the level of science (i.e., of refereed, accepted publications) is at the highest level; the student and Professor must interact closely and vigorously (i.e., to bring both the science and the writing to their highest level), hence the student is getting the best education possible and is being at least exposed to (if not held to) the highest standards; the needed clean-up or control experiments that invariably come up have all been identified and completed before the student leaves; there are no further time demands once the student has left the University (since all publications are at least submitted; it is terribly inefficient to try to complete either writing or often specialized experiments once the student has left); and

the American tax payers, who ultimately pay the bill for the research, are getting their money's worth since all the research is published and thus widely disseminated in the highest form, as refereed science. Professorial experience teaches that a student who has achieved a journals-format thesis has indeed received a better education and has learned critical thinking and clear writing skills that will serve them well for a lifetime.

Experience also teaches, however, that much more than light editing is often needed in at least some student theses; it follows, then, that considerable professorial writing and editing might be needed for at least the initial chapters of most journals-format thesis. Indeed, a journals-format thesis is not recommended (and may not even be possible) for less strong students. Hence, the issue arises of exactly how much of the science and the writing, in the final (or submittable) chapters, is due to the student vs. the Professor and whether or not this level of contribution constitutes that acceptable of a new Ph.D. and independent investigator.

To deal with this issue, several recommendations are made. The recommendations are:

(i) That the present pages be enclosed in the thesis until such a time as it is no longer needed (i.e., when the policies and procedures for journals-format theses become routine);

(ii) That for each chapter it is detailed, and to the satisfaction of the committee and the advisor, who made what contributions, both of intellectual substance and writing. [Substantial contributions of other students or Professors should of course be acknowledged. In the case of disagreements, the various drafts (i.e., as their electronic files) can be examined by the committee (in light of a knowledge of who wrote which draft) to easily determine who contributed what. In possible borderline or controversial cases it may even be advisable to keep all (electronic) drafts of the papers as a record];

(iii) That it be specifically stated whether or not all the experimental work is the Ph.D. candidate's [as is usually the case, although the increasing (desirable) collaboration among scientists worldwide makes this a non-trivial point].

(iv) Furthermore, it is recommended that allowances be made for the expectation that a greater degree of involvement of the professorial advisor is likely in a journals-format thesis than in a traditional thesis. That this is reasonable follows from the fact that some Professors write 100% of all their papers; this, unfortunately, robs the student of the valuable experience of participating in the science and the end product as practiced at the highest levels. It also creates an unmanageable writing burden for Professors involved in all but the narrowest of research areas or for Professors involved in more than one competitive research area;

(v) Notwithstanding (iv), there needs to be ideally no more than ca. 40% Professorial writing contribution in a given *early* chapter in the thesis, and there should be a clear evolution in the thesis of a decreasing professorial involvement to, say, a 10-20% direct contribution in the last chapter or two.

(vi) As a further aid towards separating out the candidate's and the professorial (and other) contributions, it is recommended that the Introductory (usually literature background) chapter(s) and at least the final chapter be lightly edited only, so that authentic examples of the student's contributions are documented in an unambiguous form.